School of Civil and Mechanical Engineering
Department of Civil Engineering

Characterisation of Asphalt Mixes with Recycled Asphalt Pavement

Hassan Malekzehtab

This thesis is presented for the Degree of
Doctor of Philosophy
of
Curtin University

October 2016

Declaration

To the best of my knowledge and belief this thesis contains no material previously published by any other person except where due acknowledgment has been made.

This thesis contains no material which has been accepted for the award of any other degree or diploma in any university.

Signature: …….

Date: 25 October 2016……...

Abstract

The use of recycled asphalt pavement (RAP) in hot mix asphalt (HMA) is considered to be one possible solution for reducing the cost of using virgin materials in pavement production as well as reducing the environmental effects. However, to be able to utilise RAPs efficiently the concerns related with this technology need to be considered to prevent lowering the performance of asphalt mixtures. In Australia, the use of RAP is not popular owing to these concerns and there are strict limitations in place for using RAP in asphalt mixtures.

Therefore, in 2011 the Western Australia Main Roads initiated a project through the Western Australia Pavement Asset Research Centre (WAPARC), Australian Road Research Board and Curtin University to characterise the Western Australian HMAs incorporating RAPs. A component of this thesis covers the WAPARC project 2011/0007.

There is currently limited knowledge regarding mixtures containing RAP based on Western Australia specifications and materials; therefore, this research study had the following main objectives:

- To determine how the addition of RAP affects the performance of Western Australian mixtures and binders.
- To determine whether the limits are currently applied in the standards for using RAP in practice are satisfactory.

This thesis reviewed the current status and concerns of using RAP in HMA and then, studied the previous findings on the performance of the RAP contained asphalt mixtures. After the literature review, this thesis presents a comprehensive program has been done in this research for characterising HMA containing RAP. This research was performed using material obtained from an asphalt plant in Western Australia to simulate the asphalt plant product as close as possible. Two typical local HMAs were investigated and redesigned to incorporate four different levels of RAP. These mixtures were grouped into two main groups, 14 and 20 mm nominal sized mixtures. Each group consisted of four mixtures containing 0, 10, 20 and 30% RAP by total

weight of the mixture. Different types of samples were produced from each individual asphalt mixture to determine how the RAP inclusion in the mixture affected their performance. The tests carried out on the samples included maximum density, Marshal stability and flow, resilient modulus, rut resistance, moisture susceptibility, fatigue life and dynamic modulus. The results showed that the RAP presence, has not damage the performance of the mixtures in most of the situations in this study.

The second section of the thesis consists of characterisation of the binders utilised in the research. These binders are virgin C320 binder, aged binder in RAP, aged binder in rolling thin film oven (RTFO) and recovered binders from the mixtures. The performances of the binders were assessed using a dynamic shear rheometer (DSR) apparatus to obtain the complex modulus of the binders in different situations in addition to the penetration test. As predicted, the higher the RAP, the stiffer the binders were in these tests. Furthermore, the level of binder aging occurring in an RTFO was compared to the aging process that occurred in binders during the asphalt mixing procedure. The outcome suggests that the RTFO aging is significantly harsher than oven conditioning the mixture based on the methods used in this study. Next, the correlation of the results obtained from mixtures and binders were investigated.

Moreover, two well-known asphalt mixtures' dynamic modulus prediction models, Hirsch and Al-Khateeb model, were evaluated based on the achieved data in this study. The results provided by these models showed a significant difference to the experimentally obtained values. As the results were not satisfactorily, those models were modified to improve their accuracy to anticipate the dynamic modulus of WA's based asphalt mixtures.

Finally, the results from the study are presented and discussed, and conclusions are drawn on the change of the performance of investigated mixtures regarding the presence of RAP and some recommendations are given for further study.

Acknowledgements

I would like to sincerely acknowledge the Western Australia Main Roads and its Material Engineering Manager, Lez Marchant, who has supported this project by facilitating the required material and funding for this project through the Western Australia Pavement Asset Research Centre (WAPARC).

I also wish to thank Darren Isaac, Pavement Technical Officer at Curtin University's Geomechanics laboratory, whose participation was really appreciated in carrying out laboratory experiments and technical support. Mark Whittaker and Mirzet Sehic, senior technical officer and laboratory technician, for managing the Geomechanics laboratory, its resources and equipment, so this project along with other projects, could be done efficiently.

I would also thank my mother, brother, sisters, Dr. Neville Barber and Dr. Wai Mar Aung whose help and understanding were essential for me to maintain working on this project efficiently.

Finally, I specifically acknowledge my supervisor, Professor Hamid Nikraz, for his continuous efforts, encouragement, support, guidance and precious advice to run this project from the beginning to the end.

Table of Contents

Characterisation of Asphalt Mixes with Recycled Asphalt Pavement

1 Introduction

1.1 Introduction and problem statement

Recycled asphalt pavement (RAP) is a type of asphalt that has been used before in pavement and has been removed usually by cold milling process from the field as part of a maintenance or rehabilitation plan. This material can be utilised again to make fresh hot mix asphalt (HMA) for economic and environmental reasons Al-Qadi, Elseifi, and Carpenter (2007).

Nowadays, increasing interest in reducing environmental impacts and road construction costs has resulted in more attention being focused on the use of recycled materials, especially RAP. For instance, a study by the USA Federal Highway Administration states that using RAP with different percentages (20–50%) in conventional HMA saved between 14 and 34% of the cost (Prithvi S. Kandhal & Mallick, 1997). Furthermore, utilising RAP not only reduces the depletion of natural resources such as virgin aggregates or binders but also helps diminish the need for disposal sites for construction waste materials.

However, there are several issues with fabricating a mix containing RAP that need to be considered. These can be categorised into three groups: binder related, aggregate related, and production and field issues. Binder related issues arise from the fact that the binder utilised in RAP is significantly different from the virgin binder; therefore, the property of the combined binder depends on the properties of each of its components. In addition, there are concerns about these binders ability to blend together, which make the design process more complex (McDaniel, Soleymani, Anderson, Turner, & Peterson, 2000).

The second issue mainly involves the distorted grading of aggregates in RAP as a result of the aging or milling process, which might make it difficult to retain the combined grading within the grading specification (Doyle, 2011), ((Pereira, Oliveira, & Picado-Santos, 2004).

The last issue relates to RAP management in HMA production and field performance, e.g., how an asphalt plant needs to manage their RAP stockpiles or how they need to dry and heat the RAP for mixing (National Asphalt Pavement Association (NAPA), 2007). In addition, field performance monitoring is necessary to ensure that the mix performs well in practice.

In comparison to the USA where recycling of asphalt pavement occurs regularly, in Australia the use of RAP is very limited. To illustrate the increasing asphalt recycling interest in the USA, during 1996 almost 33% of all asphalt pavements were recycled (Sullivan, 1996), with this percentage increasing to 99% by 2012 (Hansen & Copeland, 2013). To illustrate this recycling success, 71.3 million tonnes of RAP was available in 2012 with only 0.2 million tonnes ending up in landfill (Hansen & Copeland, 2013). This increasing trend is depicted in Figure 1-1.

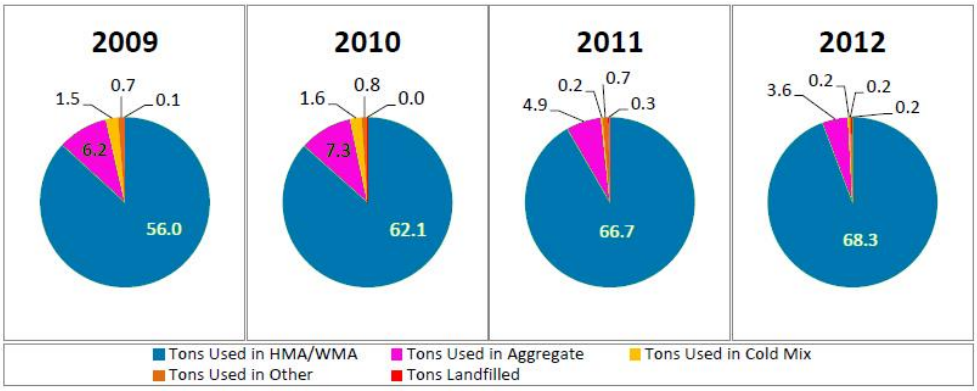

Figure 1-1 RAP usage purpose in the USA between 2009 and 2012 (Hansen & Copeland, 2013)

However, only 6% of asphalt pavements have been recycled in Australia (Kodippily, Holleran, Holleran, Wilson, & Henning, 2014). Moreover, Australian pavement authorities are very conservative in their usage of RAP in HMA, utilising only a very low percentage. For example, Western Australia allows a maximum 10% RAP in only the base layer, and no RAP should be used in the surface layer. The USA allows significantly more

percentage of RAP to be used in HMA, e.g., in 2012, 36 out of 52 states had an average of 15 to 34% of RAP in their HMA production (Hansen & Copeland, 2013).

1.2 Significance of research

The usage of RAP material in asphalt mixtures contains many difficulties, with several of these issues that the present study covers explained in the following paragraphs.

As mentioned before, asphalt recycling is not very common in Australia. One reason for this is that there are few previous studies that have characterised and investigated the performance of Australian asphalt mixtures containing RAP. This is an important issue as Australian asphalt mixtures are not only produced by different resource materials but are also designed based on Australian standards and design criteria, which are quite different to their counterparts from other regions of the world. Even within Australia, each state might follow its own local standards. For instance, in Western Australia, asphalt mixtures are usually designed based on Western Australia Main Roads recommendations, which is a local organisation although there are national standards such as Austroads available. There are many aspects where the standards differ, including mixture conditioning time, the usage of fillers like hydrated lime and volumetric specifications.

In addition, when designing a RAP-containing mixture there is a need to predict the properties of the blended binder. There are different approaches to determine the features of blended binders based on features of the RAP and virgin binder. However, previous studies investigating performances with Western Australian mixtures are limited. Therefore, it is important to verify the accuracy of these methods based on domestic mixtures.

When characterising a binder or mixture, there is an assumption that rolling thin film oven (RTFO) aging of a binder has the same effect as short aging on the binder in the mixture since production until paving. The same assumption is made for conditioning the mixture in the oven after mixing the materials in

the laboratory. Therefore, there a need to verify if both of these methods are equivalent to each other.

Moreover, the dynamic modulus of asphalt mixtures is a very important factor for designing and analysing its behavior. Therefore, it is essential to develop a dynamic modulus prediction model to predict this feature based on several basic properties of the mixture. There are several models available in the literature for this purpose, although their effectiveness and accuracy are not clear for Western Australian asphalt mixtures that might contain RAP.

1.3 Scope and research objectives

The main purpose of this study is to characterise the RAP contained in HMA made by materials available in Western Australia and also designed based on Western Australia Main Road standards to fill the existing knowlegde gap and lead to increasing the usage of RAP in this state. In addition, the study aims to understand whether the current limit of RAP in Western Australian mixtures is appropriate to ensure the RAP has no significant negative effect on the performance of the mixture when no modification is made on the type of binder used.

In the present study, HMA is defined as asphalt concrete that has been mixed and compacted at 150 °C, whereas RAP is defined as a material that has been milled from the previously existing asphalt pavement.

This study attempts to investigate the properties of HMA containing RAP produced in a central plant, not in-situ recycled asphalt. To achieve this, information regarding the job design, aggregates, RAP and bitumen were collected from an asphalt plant so the loose mixture could be replicated in the laboratory.

The investigation aimed to evaluate the following performance features of mixtures with respect to the percentage of RAP:

- Rutting resistance
- Fatigue life
- Moisture susceptibility

- Resilient modulus
- Complex modulus

To characterise the used RAP and the effect of RAP on binder properties, several examination techniques including the penetration test and dynamic shear rheometer (DSR) test were performed on binder properties of each mix and then the effect of binder on the performance of the mixtures were examined. The binders utilised in this study are conventional C320 bitumen binders and a binder that was recovered from the RAP. There were no modifications made to the binders such as adding polymers or other chemicals including rejuvenators.

During the next stage, the performance of the mixture and binders were compared and the correlation between them investigated. Moreover, the different approaches to estimate the properties of blended binder were evaluated based on their accuracy.

Next, the effect of RTFO aging of the binder was compared to oven condition of the mixture to determine if they have the same effect on the binder.

Finally, two popular dynamic modulus prediction methods were evaluated to see if they could predict the dynamic modulus of the mixtures in this study satisfactorily. In the case of inaccurate predictions, modification occurred to improve their estimation.

1.4 Organisation of thesis

This thesis is divided into different chapters. At the beginning of each chapter, an overview will explain how that chapter is organised. The current chapter, Chapter One, provides an introduction to the thesis and contains an introduction, problem statement, scope and research objectives and organisation of thesis. In the next chapter (Chapter Two), background studies are reviewed as a literature review. Chapter Three explains the laboratory evaluation program, which is composed of characterisation of materials utilised in the study, mixture design and procedure and mixture performance tests including asphalt concrete sample tests and binder tests. Chapter Four is a discussion on the data collected from experiments in the previous chapter.

This chapter includes different subchapters on topics such as binder and mixture performance analysis, mixtures and binder's complex modulus master curve construction, evaluation of binder blend properties estimation techniques, the asphalt mixture and binder performance correlation and dynamic modulus prediction models evaluation and modification. Chapter Five provides an overall discussion of all the available data and analysis and includes the conclusion to the study and recommendations for future work.

2 Literature review

2.1 Overview of literature review

To achieve the objectives in this study, it is necessary to review the studies and findings on the RAP usage in HMA. In this chapter, a brief history of usage of recycled asphalt and challenges of incorporating RAP in HMA is introduced, after which the different approaches to manage these problems are summarised. Next, the different laboratory tests and related studies to characterise mixtures containing RAP are explained. Finally, different approaches to predict viscoelastic behavior of mixtures and binders (master curves) over a wide range of temperature and frequencies are introduced. Figure 2-1 illustrates the organisational structure of this chapter.

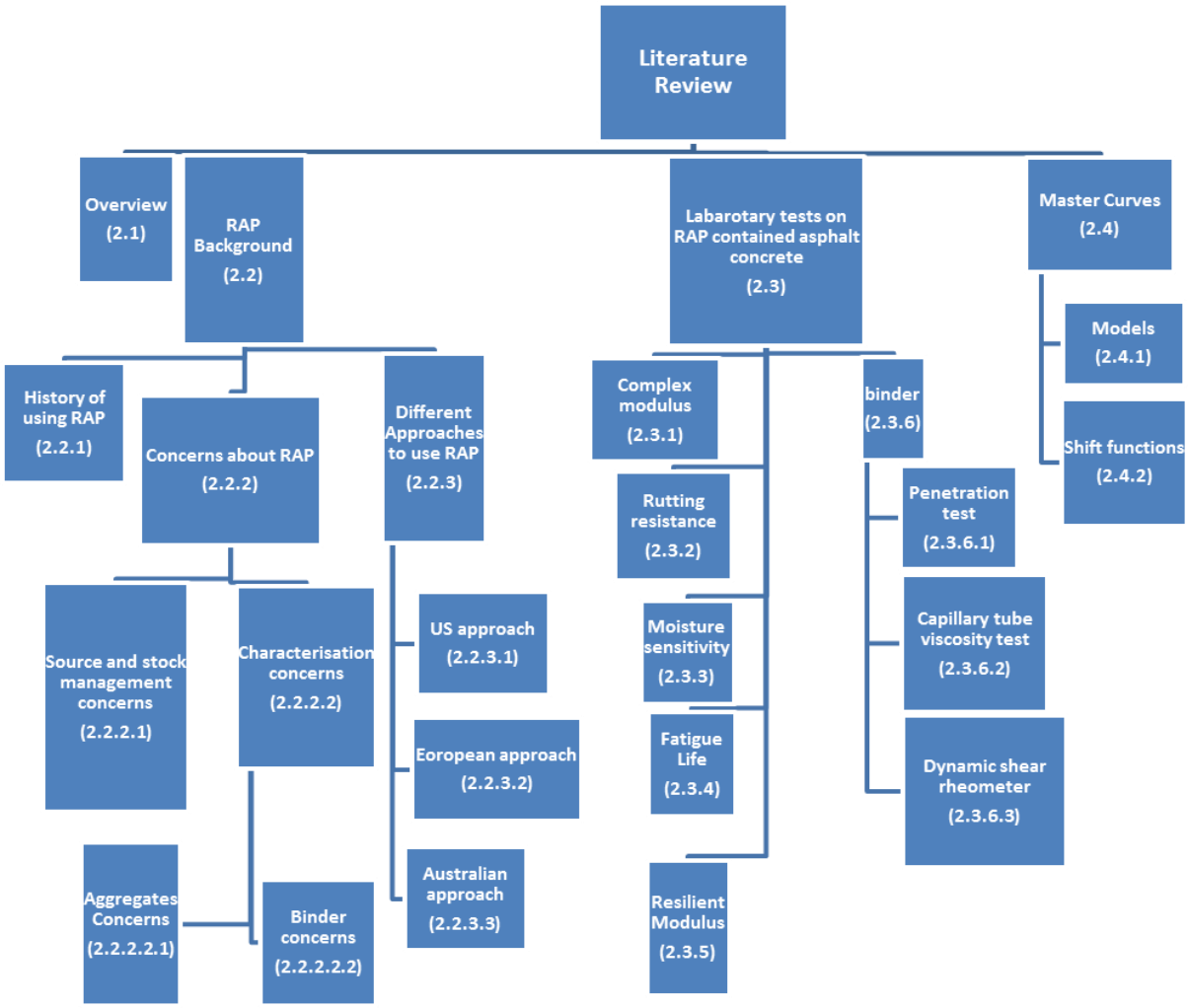

Figure 2-1 Chapter 2 Organisation

2.2 Recycled asphalt pavement background

2.2.1 History of using RAP

Financial issues and recent environmental concerns have encouraged attempts to recycle different types of materials. Many efforts have been focused on RAP owing to the fact that huge amounts of recyclable material is available, which can assist with reducing not only the financial cost but also the environmental effects of asphalt pavement.

There are a few records of HMA recycling from the early 1910s; however, these efforts were limited owing to the relatively low price of materials needed for HMA and a lack of knowledge. For instance, according to Gillespie (1992) in 1915, claimed in the sale brochure of their portable asphalt plant that it heats and uses the existing asphalt pavement to make a new asphalt mix. Warren Brothers also claimed that their plant, achieves to excellent results and is considerably cost effective. Over the next two decades, small recycling practices occurred in urban areas along the east coast of the USA, with the largest hot recycling attempt before the 1970s believed to have been achieved by Allegheny Contracting Industries in Pittsburgh, Pennsylvania, which includes recycling of several thousand tonnes of asphalt in the 1950s and 1960s (Gillespie, 1992).

However, the activities in this field increased dramatically during the 1970s as a result of the oil embargo and increasing price of virgin materials. During this time, there was no tangible information about technology, mix design, pavement design, construction and pavement performance of recycled materials, so many organisations began to study recycled HMA including the National Cooperative Highway Research Program (NCHRP) and Federal Highway Administration (FHWA). The former organisation published one of the first guides based on available data in 1978 and 1980 (Newcomb, Brown, & A.Epps, 2007), while the latter published a report in 1982 on Project No. 39: “Evaluation of a recycled asphaltic concrete pavement” (Missouri Highway And Transportation Department, 1982). These studies have continued, e.g. NCHRP completed significant research (9–12 projects) to integrate the use of RAP in the new HMA mix design procedure, Superpave,

in 2001 (McDaniel & Anderson, 2001). A significant increase in the price of oil products more recently pushed the HMA industry to again utilise more recycled material from 2006. At this time, environment protective aspects of recycling HMA such as conservation of bitumen and aggregate resources and landfill space intensified the recycling demand (Newcomb et al., 2007).

After several decades of study, there still remains great concern about using RAP in HMA, which makes its use limited. In Australia, only 5% of new asphalt material contains RAP. Based on two surveys between 1995 and 2000, RAP is underestimated as an important resource, with only 12% RAP on average was added into the mixtures. In addition, fumes and strict regulations for using uncommon materials prevent wide usage of RAP (Denneman et al., 2013).

Although several Australian states are allowing limited use of RAP, others have prohibited its use or have no regulations regarding its use (Denneman et al., 2013). Furthermore, Western Australia has very strict and limited rules regarding RAP, i.e. it currently allows no RAP in the surface layer (Main Roads Western Australia, 2015), while up to 10% RAP can be used in the intermediate base layer, but only for 14 mm and 20 mm dense graded asphalt (Main Roads Western Australia, 2014). Therefore, this thesis is investigating the RAP containing HMAs in Western Australia to determine their performance and reliability.

2.2.2 Concerns about RAP

There are several concerns regarding RAP, which can be placed into two different groups: RAP production and management concerns, and characterisation of RAP.

2.2.2.1 RAP concerns owing to sources and stock management

Usually, RAP is produced from milling or removing the current asphalt layer while it is cold or softened by heat. The former method involves grinding of the surface layer with a special rotating machine to a specific depth. This method usually results in a product that has minimal post processing requirements before it can be reused because it is already crushed and, if stocked properly, it has almost uniform properties because it comes from the

same source. However, the existing pavement might be removed by loaders or bulldozers to implement a full reconstruction of the area. In this case, an extra process is needed to ensure the RAP is ready for reuse (National Asphalt Pavement Association (NAPA), 2007). Either method is used for producing RAP, with each source having its own specific properties including the level of aging, binder content, gradation and type of materials. Therefore, there are huge amounts of variability between the RAP sources (Harrigan, 2001). One solution is to characterise each source of RAP and store these separately in an appropriate storage system for later use.

However, there are difficulties associated in practise. In many cases, RAP comes from many different sources but in low quantities, which means they will be stocked in the same pile because of not enough room for many stockpiles making the characterisation procedure more complicated. In addition, asphalt plants might consider the waste or extra mix as a RAP as well, which adds more complexity to the RAP characterisation as this material is not aged like other sources of RAP.

In other words, RAP properties are significantly more uncertain than are virgin materials. To resolve this issue, an efficient stock management system is necessary, as well as a characterisation system for the RAP material, unless the usage of RAP is so low that it barely affects the whole mixture.

2.2.2.2 RAP characterisation concerns

RAP consists of aged binders and aggregates that have been exposed to many different factors and finally collected and stored to be used in a new mix. These concerns are allocated into two groups: concerns about aged binders and concerns about aggregates.

2.2.2.2.1 Aged binder concerns

One important benefit of using RAP is the fact that it contains a binder and it can be considered part of the binder needed for the mix. However, the binder from RAP might perform totally different from the virgin binder.

An asphalt layer becomes aged while it is in place during its service life, with this aging process changing its binder properties and making it stiffer; therefore, its mechanical behavior will be changed accordingly.

Generally, the binder hardens rapidly at first and then its hardening rate declines. The aging that occurs rapidly is called short term aging while the aging that occurs over time is called long term aging. The trend of aging against time from different asphalt samples can be seen in Figure 2-2 (difference in penetration test results) and Figure 2-3 (changes in viscosity). The lower the penetration, the higher the viscosity of binder (Newcomb et al., 2007).

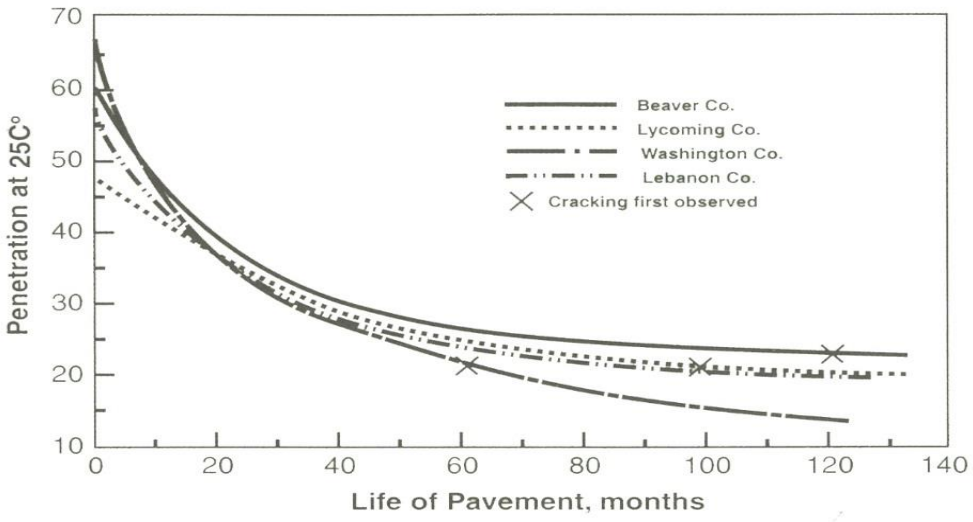

Figure 2-2 Changes in penetration test over time for different samples (Newcomb et al., 2007)

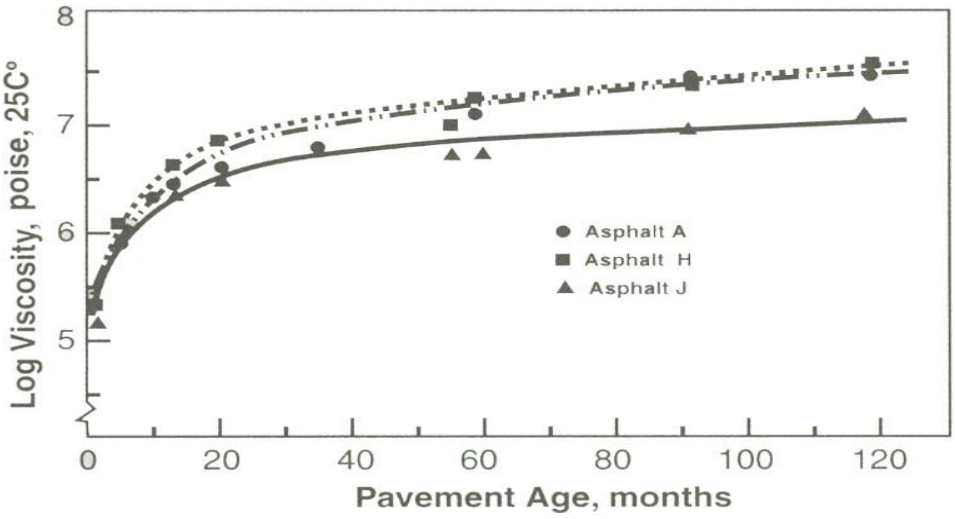

Figure 2-3 Change in viscosity over time for different asphalt samples (Newcomb et al., 2007)

These changes in mechanical behavior are caused as a result of several factors that have been studied extensively. These mechanisms are categorised into six groups in (Al-Qadi et al., 2007), as shown in Figure 2-4:

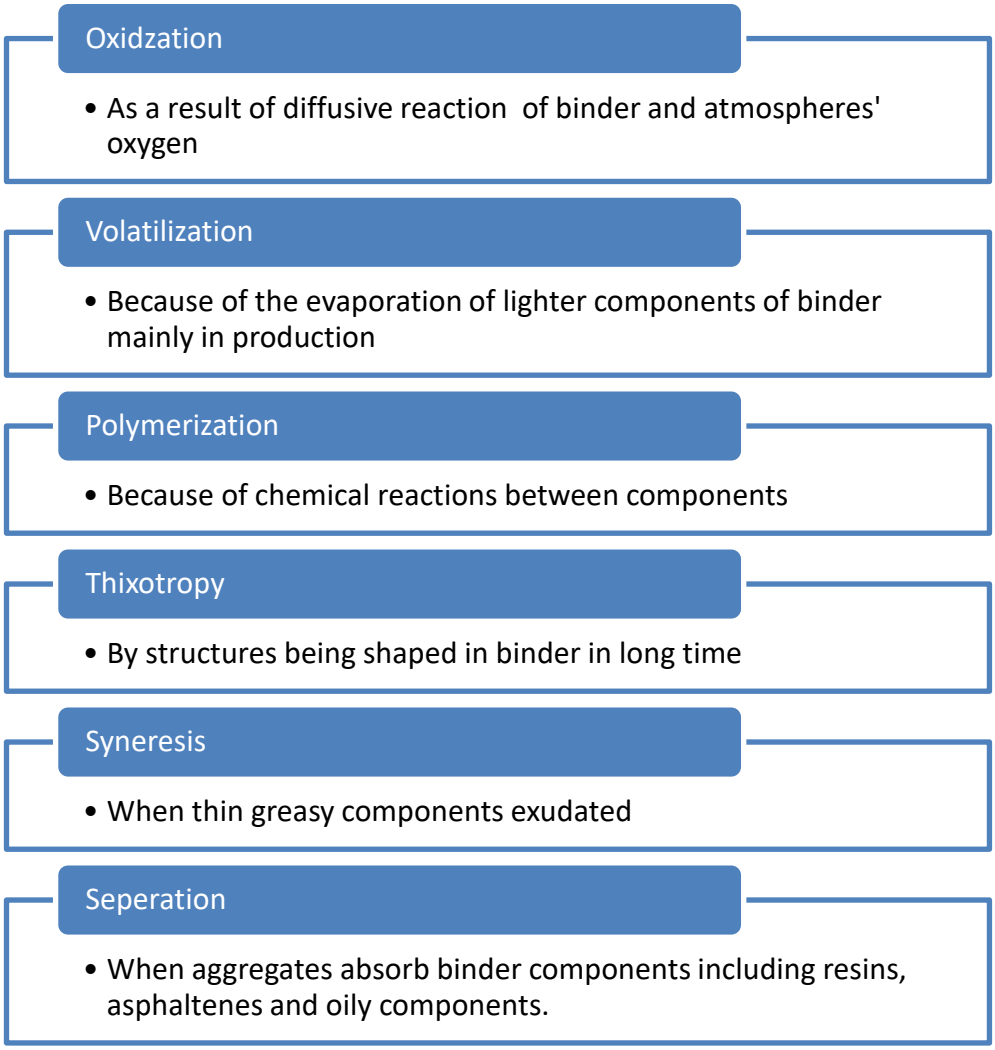

Figure 2-4 Binder aging mechanisms (Al-Qadi et al., 2007)

The main factor is the oxidation of binder molecules over time (Tarbox & Daniel, 2012). Generally, oxidation creates carbonyl compounds by oxidising different types of aromatic compounds such as naphthene, polar aromatics and asphaltene fractions. These extra carbonyl compounds increase the friction coming from asphaltene, and stiffen the whole binder in both elastic modulus and viscosity(Glover et al.). However, oxidation does not occur at a constant rate. Figure 2-5 illustrates the simplified trend of oxidation of a

binder over time when it has an original viscosity of η_0 and there is no oxygen diffusion resistance. In this figure, the viscosity increased to η_{ot} in hot mix plant (simulated by oven test) when it soars in a nonlinear pattern very rapidly (Region A) and then it enters the constant rate region (Region B) and it increases over time.

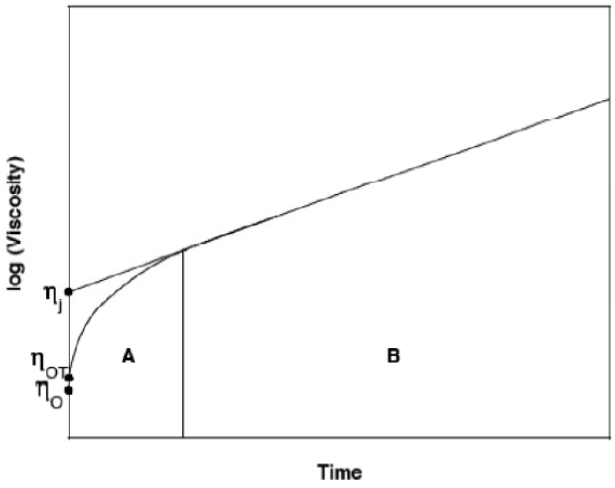

Figure 2-5 Typical oxidation hardening of an unmodified asphalt binder (Glover et al.)

It can be concluded that oxidation is occurring because it is in contact with oxygen but that the rate is declining over time. In reality, this trend is more complicated. One equation that can describe the hardening over time is equation (2-1) below, which is derived from the assumption that almost all the hardening is caused by asphaltene formation:

$$\ln \eta_t = ln\eta_{ot} + \Delta(ln\eta_j)[P] + r_{CA}[T,P].HS[P].t \qquad (2\text{-}1),$$

where, η_t is viscosity over time t, η_{ot} is the viscosity after the oven test (simulating hardening at plant), η_j is the intercept of the linear part of the graph (that is a function of pressure), r_{CA} is the rate of carbonyl area formation in time (that differs by change in temperature and pressure), HS (mainly a function of only pressure) is an almost constant value that represents the impact of increase of asphaltene on the increase of viscosity and also the extent that carbonyl area produces asphaltene and t is time (Glover et al.).

To simulate aging on binder samples for ranking purposes, several tests including rolling thin film oven (RTFO) and pressure air vessel (PAV) have

been developed. The former test approximately mimics the changes of binder in HMA production (CHAFFIN, 1996) via exposing a binder to hot temperature air flow while the latter is utilised to investigate changes over the long term (SHRP, 1994) via keeping a sample in a high temperature and pressure environment. However, there is some debate regarding how close these tests are to in-field aging (JUNG),((Qin, Schabron, Boysen, & Farrar, 2014).

The next crucial debate is to what extent RAP binder will blend with a virgin binder. It is believed that the solubility of two binders is affected by their chemical compatibility, the difference in molecular weights, blending proportion and temperature. Despite some exceptions, RAP binders and virgin binders have no problem blending together in terms of two first parameters because they have the same origin. The mixing temperature should be adequate to soften the RAP binder in an appropriate way as the required temperature is usually well below the asphalt mixture temperature. Therefore, via the use of the correct materials and controlled producing procedure then sufficient blending is feasible. One practical method to check the level of blending is to investigate the dynamic modulus of the blended mix. A significant lower dynamic modulus can be an indication of insufficient blending in the production line (National Asphalt Pavement Association (NAPA), 2009). In general, when two binders are mixed together three cases might occur:

1. RAP acts as black rock–the binder from RAP does not blend with the virgin binder and does not participate in the mixture.
2. Partially mix (actual practice)–RAP binder blends with virgin binder partially.
3. Total blending–RAP binder and virgin binder blend fully and act as a uniform binder.

Different studies have occurred to determine the validity of these views. An extensive research was undertaken in the NCHRP Projects D9-12 to determine the blend ability of RAP and virgin binder. In this study, samples were made containing a different percentage of RAP but the same grading

and total binder content according to the previously mentioned possibilities and based on Superpave standard sample making procedures. To replicate the black rock assumption, RAP binder was extracted before mixing and only RAP aggregates were mixed with virgin binder and aggregates. For simulating the actual practice, RAP and virgin materials were mixed as RAP binder coating was intact. In terms of the total blending case, the binder from RAP was recovered and then mixed with a virgin binder. Afterward, separated RAP aggregates were mixed with virgin aggregates. This followed by adding the blended binder to the mixed aggregate to form the total blended mix. Having made the samples, different types of tests were performed for determining the performance of the mixtures in high, intermediate and low temperatures. These tests included the frequency sweep (FS), simple shear (SS) and repeated shear at constant height (RSCH) for high and intermediate temperature evaluation while indirect tensile creep (ITC) and strength (ITS) tests were utilised to investigate the low-temperature performance of the mixtures. All the tests were repeated three times for each type of sample to minimise any errors (McDaniel et al., 2000). The results revealed that at low percentages of RAP there was no meaningful variation in results for all three cases. Conversely, high and intermediate levels of RAP contained in the samples behaved differently in the three scenarios. In most cases, samples made based on the black rock concept were softer and deformed more in comparison with the samples of the other two cases, while actual practice and total blending samples performed approximately the same. Therefore, it can be concluded that the black rock scenario is not matched with real practise except for when there are low percentages of RAP present, suggesting that the RAP effects of a binder need only be considered when there are low contents of RAP as a result of the negligible effect of RAP in the mixture. It also determined that even though total blending might not be achieved in all cases, partial blending occurs in most of the cases and the effect of RAP binder should be considered specifically on higher percentages of RAP. At intermediate content mixtures, one grade softer binder can be used to cancel the effect of RAP binder in the blend. At high percentages of RAP, specific efforts should be attempted to find a proper grade for a virgin binder or to determine the allowable percentage of RAP (Harrigan, 2001).

Another project that investigated the contribution of RAP binder in the mixture was undertaken by the Illinois University to verify if the assumption of the Illinois Department of Transport was correct owing to the total blending of RAP binder with the virgin binder. To achieve this goal, the following four scenarios were investigated:

1. Intact RAP used with assumption of complete blending (assumption of Illinois Department of Transport)
2. Black rock assumption (no binder from RAP, just recovered aggregates in the mix)
3. Simulating 50% binder blending using recovered binder and aggregates from RAP.
4. Simulating 100% binder blending using recovered binder and aggregates from RAP.

For each set, a group of tests were performed on samples with different percentages of RAP. These tests included dynamic modulus, stripping evaluation, fracture characterisation (direct compact tension and semi-circular bending) in addition to binder characterisation tests and scanning electron microscopy (SEM) imaging. The results indicated that although the idea of complete blending of aged and virgin binder is assumed to be true, it is not fully supported by the data obtained from that study. Based on the minor changes in asphalt content results, it was concluded that the two types of binders had been blended to a high extent. The dynamic modulus results indicate that the greater the percentage of RAP, the higher the dynamic modulus will be. However, for low percentages of RAP (20% in this study), the effects of aged binder on dynamic modulus are not significant, yet it might affect the thermal cracking potential as the results from the fracture energy tests demonstrated. It was also discovered that despite the changes in dynamic modulus owing to RAP, the comparison of dynamic modulus of actual practice and 100% blended binders might not be the correct way to determine the extent of blending between binders. The reason for this is based on the unexpected lower dynamic modulus of samples with 100% blended binder than the actual practice samples where it was expected that they should be equal (if complete blending occurs) or higher (if partial blending occurs). In

addition, this study revealed that SEM images are not sufficient to establish whether the binders are blended well or not. Furthermore, this study challenged the validity of a well-known predictive model for dynamic modulus, the Hirsch model, to back calculate the binder complex modulus of RAP contained asphalt mixtures (Al-Qadi et al., 2009).

Another project by the New York State Department of Transport investigated the level of contribution of the RAP in the mixture by considering 50, 75 and 100% contribution. Different samples were manufactured with identical quantities of RAP but different amounts of virgin binder (to compensate for the different contribution of RAP) to study the dynamic modulus, rutting performance (flow number) and fatigue life (beam fatigue and overlay test). The results indicated that although the stiffness measured from the dynamic modulus test and rutting performance (using flow number) were statistically equal for all samples, there was considerable difference in the results of the other tests (Bennert, 2012). Therefore, monitoring only one parameter, such as the dynamic modulus, might not be the best option to study the contribution of RAP in the mixture.

2.2.2.2.2 Aggregate gradation and particle size distribution concerns

The usage of RAP in a new mixture raises concerns not only about how the blended new and aged binders will perform but also regarding aggregate gradation and the distribution of particle size.

The combination of RAP aggregates and fresh aggregates need to meet the design specifications. Therefore, the size distribution of RAP aggregates should be considered during the mix design process. In this regard, the aggregates remaining after binder extraction from the binder content test can be utilised to determine the particle size distribution (PSD) of the RAP. Another important issue is that RAP production procedures such as milling generally increases the amount of fine aggregates that should be taken into account and the resultant action, e.g. addition of course aggregate might be necessary to keep the combination within the specifications. However, this might not be a serious problem in the asphalt plants that are equipped with

dust removal systems or if the RAP has been screened in different size stockpiles. Moreover, small particles might remain attached together and not blend with other materials, which might also cause some uncertainties in the final mix (Pereira et al., 2004). The RAP aggregate binder absorption might input an error in binder calculation of the whole mix as a result of errors when determining the binder content of the RAP. The absorbed binder might not be able to be extracted completely during the extraction, which results in this error especially if the aggregates have high levels of absorption (Loria-Salazar, 2011).

Although the binder content and PSD are the most important tests that are necessary for investigating RAP, in different cases other tests might also be required. For instance, if the mix has a high percentage of RAP and it is intended for use in surface layers, then the particle shapes/angularity and the hardness/wear test is also necessary. Another method for investigating these properties is to verify the background of the RAP material. However, it should be noted that there are several exceptions. One study has shown that even if the asphalt has been stripped, it might be used successfully as RAP in a new mix even without any modification (Newcomb et al., 2007).

2.2.3 Different approaches to using RAP

In this section, the various solutions that various organisations in different regions, including the USA, Europe and Australia have utilised to manage the design complexity of mixtures containing RAP are introduced. Generally, all these approaches aim to produce a mixture that complies with the specification for HMA whether it includes RAP or not.

2.2.3.1 The USA approach to utilising RAP

In the USA, one of the first suggested procedures to handle designing of RAP contained HMA was provided by the Asphalt Institute in 1981. The procedure developed by this Institute is still being used in several USA states and several other countries including Iran with some modification to design HMA with RAP (Iranian National Standardization Organization, 2013).

In this procedure, after source of each aggregates, i.e. RAP aggregates, reclaimed aggregate material (RAM) and virgin aggregate, is determined for

a specific gradation, then the total binder content that suits that particular gradation can be estimated using the following equation (2-2) (Asphalt-Institute, 1981):

$$P = 0.035a + 0.045b + Kc + F \quad (2\text{-}2)$$

where, P is the estimated asphalt demand for the mixture; and *a*, *b* and *c* are a percentage of aggregates larger than 2.36 mm, between 2.36 and 0.075 mm and smaller than 0.075 mm, respectively. The value of *F* depends on the absorption capability of the aggregates and can be set between 0 and 2, although if there is no data available it is assumed to be equal to 0.7. Finally, the value of *K* is determined based on Table 2-1.

Table 2-1 Values of coefficient K in equation (2-2) for asphalt demand estimation

Value of coefficient K	**Percentage passing 0.075 mm sieve**
0.15	11–15
0.18	6–10
0.20	Equal or less than 5

In the next stage, the percentage of required amount of new binder is approximated based on equation (2-3):

$$P_{nb} = \frac{(100^2 - rP_{sb})P_b}{100(100 - P_{sb})} - \frac{(100 - r)P_{sb}}{100 - P_{sb}} \quad (2\text{-}3)$$

where, P_{nb} is the percentage of the new binder by weight of the total mixture, P_b is the asphalt demand of the mixture, P_{sb} is the asphalt content of RAP (salvaged binder) and r is the ratio of new and recycled aggregates to the total aggregate in the mixture.

After obtaining the percentage of new binder and asphalt demand, the grade of new binder or recycling agent then needs to be determined, so the viscosity of total binder reaches the specific target value.

To achieve this, first, the percentage of new binder to total asphalt content (R) is calculated using equation (2-4), where P_{nb} and P_b are the percentages of new binder and total asphalt demand of mixture, respectively.

$$R = \frac{100P_{nb}}{P_b} \qquad (2\text{-}4)$$

The viscosity of the extracted binder from RAP is then measured at 60 degrees. Second, the target viscosity of the mixture is selected, after which the grade of new binder will be determined using a semi-log blending chart similar to Figure 2-6, from which points A and B are located. Point A demonstrates the viscosity of RAP binder when R is equal to zero, while point B illustrates the target viscosity of the total binder at 60 °C when R is equal to the calculated value in the previous section. Finally, point A is connected to point B using a straight line, which is then stretched until it reaches the point that has an R equal to 100. This point will be called point C and is the viscosity that demonstrates the viscosity of the required new binder at 60 °C.

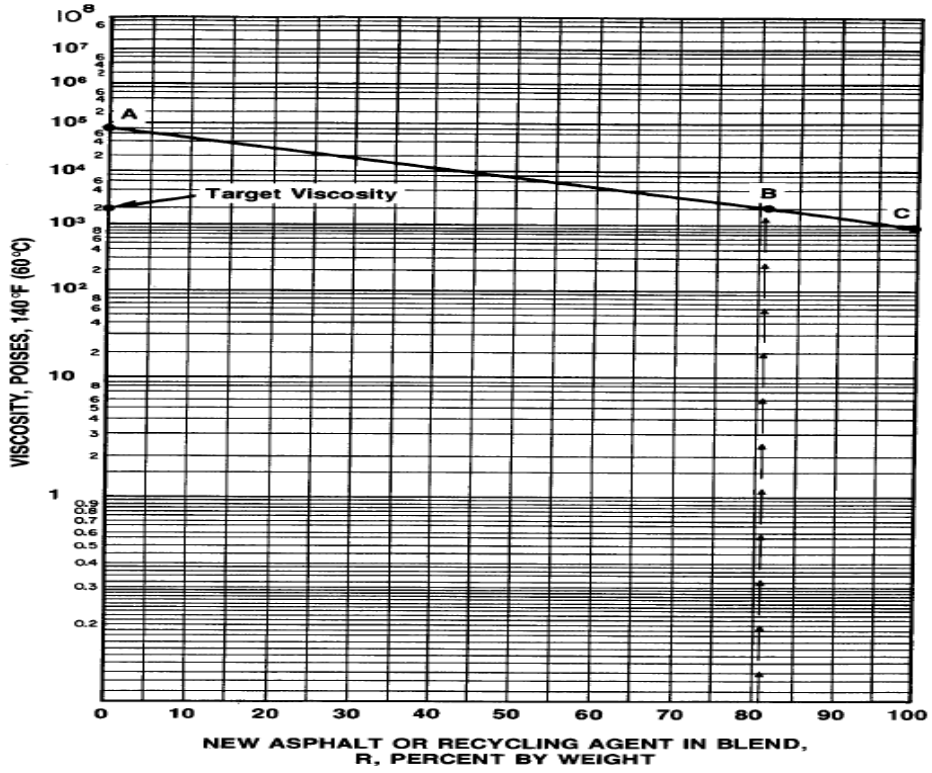

Figure 2-6 Asphalt Institute blending chart (Asphalt-Institute, 1981)

However, the same study is suggested that if the RAP content is lower than 20%, no changes in grading is required, otherwise, not more than one grade should be changed. Finally, trial samples need to be manufactured using these estimations to see if they satisfy the criteria of the Marshal method or whether modifications are required (Asphalt-Institute, 1981).

After development of the Superpave method in the USA for designing HMAs, several other methods have been presented to incorporate designing mixtures containing RAP into HMAs. Basically, in these methods the mixture containing RAP needs to satisfy all the requirements of the Superpave method for mixtures composed of fresh materials. The binder grading in the Superpave method is based on the high, intermediate and low temperature of the asphalt binder.

The high and intermediate temperatures are the temperatures where the complex shear modulus of asphalt binder (explained in Section 2.3.6.3) meets specific requirements in different conditions: virgin, aged by RTFO and aged by RTFO and PAV. The low temperature, however, is defined by the temperature where the binder beam rheometer test results, usually creep stiffness (S value) and m-value (slope) at 60 seconds, are in a specific range of values. Definitions of these critical temperatures are illustrated in Table 2-2 (Prithvi S Kandhal & Foo, 1997).

Table 2-2 Definitions of different temperatures of binder in Superpave method

Temperature	Definition
High	The minimum of temperatures a and b: a) where G*/sin(δ) of virgin binder equals 1 kPa b) where G*/sin(δ) of RTFO aged binder equals 2.2 kPa
Intermediate	Where G*Sin(δ) of RTFO + PAV aged binder equals 5MPa
Low	The maximum of temperatures a, b and c: a) where S = 300 MPa and m < 0.3 b) where (S < 300 MPa, m = 0.3) or (300 MPa < S < 600 MPa, m >= 0.3 c) where failure strain = 1%

Where, the term G*/Sin(δ) and G*.Sin(δ) are factors that are introduced to represent the performance of the binder due to rutting and fatigue (SHRP, 1994). Therefore, these terms can be referred as rut and fatigue factor of the binder. Based on a study by (Prithvi S Kandhal & Foo, 1997), the critical high temperature blending chart, which shows the percentage of new binder against the temperature that G*/sin(δ) equals 1 kPa, is an appropriate tool to

estimate the grading of the combination of RAP and fresh binder based on the percentage of new binder in the mixture. For example, as illustrated in Figure 2-7 if < 33%RAP is used, the grade of combination satisfies the performance grade PG64 and if the percentage of RAP is between 33 and 52%, it meets the condition of PG70 requirements.

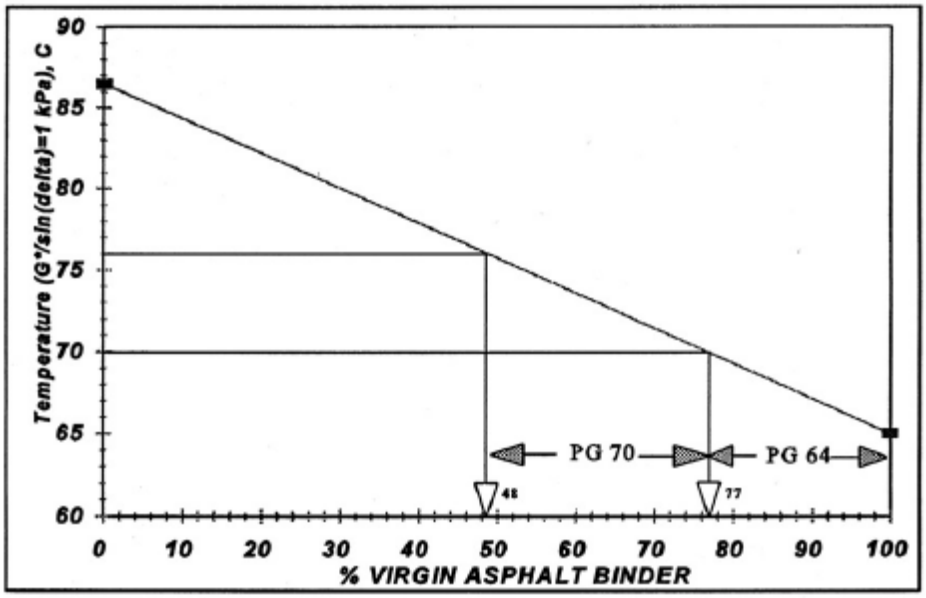

Figure 2-7 An example of Superpave blending chart for determining the PG of blended binder (Prithvi S Kandhal & Foo, 1997)

The same study also indicated that the blending chart of intermediate temperature is not recommended for this purpose. However, constructing such a chart cannot be achieved without great effort as it requires tests performed on different temperatures for the aged and unaged binders. To eliminate this difficulty, this study also suggested the use of a specific grade blending chart. In this chart, the maximum and minimum percentages of RAP that are allowed to be added to the mix can be determined to satisfy the requirements until the total blend can be categorised in a specific grade. In this approach, tests need to be performed only on the critical high temperature of the target grade of virgin binder and aged binder. For example, if the target grade is PG64-22, the tests need to be carried out at 64 °C. Then, the measured values of $G^*/\sin(\delta)$ for virgin binder and RAP binder can be plotted on a graph similar to Figure 2-8, where their horizontal values are 100 and zero, respectively. A straight line can then be drawn between them on the chart.

The intersection of that line with the 1 kPa line determines the maximum virgin binder (minimum RAP binder) while the intersection with 2 kPa line shows the minimum of virgin binder required (maximum RAP binder).

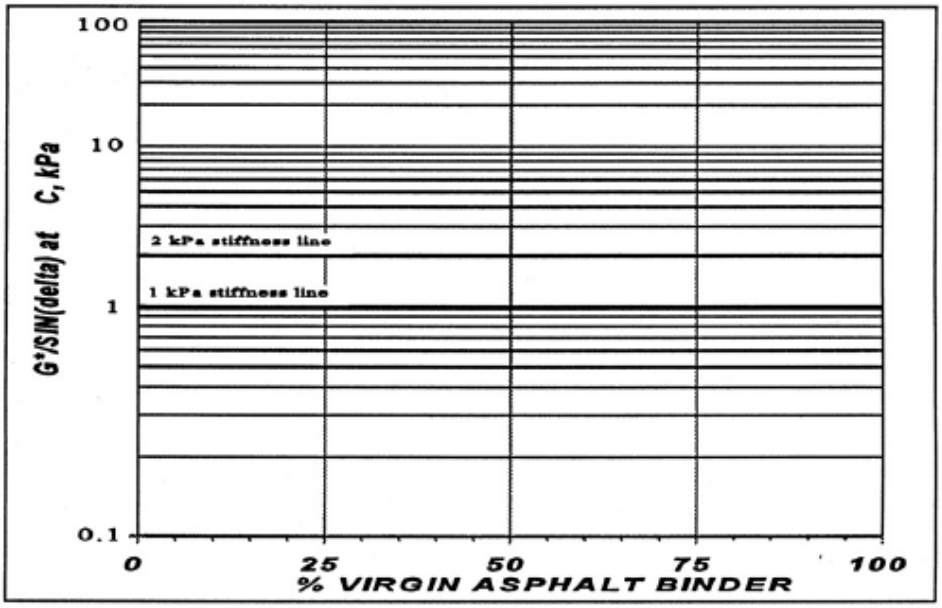

Figure 2-8 Superpave blending chart for a specific grade (Prithvi S Kandhal & Foo, 1997)

Moreover, this study recommends the three-tier system for choosing the grade of the virgin binder with respect to the percentage of RAP in the mixture as described in Table 2-3that are also included in American Association of State Highway and Transportation Officials (AASHTO) M323 that describes the mix design in the Superpave method (AASHTO, 2013).

Table 2-3 Recommendations for selecting PG binder based on (Prithvi S Kandhal & Foo, 1997)

RAP binder (%)	Binder selection
≤ 15	The same grade as specified in the Superpave method
>15 and ≤ 25%	Use a binder with one grade lower on both high and low temperatures of the Superpave specified binder
> 25%	For finding the critical high temperature, a specific blending chart should be used. For low temperature, a binder at least one grade lower should be used.

Similarly, (Harrigan, 2001) and (McDaniel & Anderson, 2001) confirmed the previously mentioned three tier system to determine the binder grade for the

mix; however, these authors suggested different RAP binder limits for different RAP binders as illustrated in Table 2-4.

Table 2-4 Recommendations for selecting PG binder based on the study by (Harrigan, 2001)

	RAP (%)		
	Recovered RAP low temp grade		
How to select virgin binder	**≤–22**	**–16**	**>–10**
Use Superpave specified binder	< 20	< 15	< 10
Choose one grade softer than specified with the Superpave method	20–30	15–25	10–15
Use blending charts as recommended	> 30	> 25	> 15

Furthermore, these two studies provide a procedure in which, although opposite to (Prithvi S Kandhal & Foo, 1997), all the high, intermediate and low temperatures are considered in the suggested mix design procedure. Therefore, high, intermediate and low temperatures of RAP binder should be measured as a virgin binder according to the definitions in Table 2-2, after which this data is utilised to design a mix that the blend satisfies all the requirements for low, intermediate and high temperatures. This procedure is explained in detail in (McDaniel & Anderson, 2001).

In summary, McDaniel and Anderson (2001) investigate two scenarios. The first scenario is when the RAP content is known and the grade of the virgin binder needs to be determined. This might occur when the particle gradation or specifications limit the amount of RAP utilised in the mixture. In this case, after having all the required information regarding the RAP binder and target blend (critical high, intermediate and low temperatures), the required critical low, intermediate and high temperatures of the virgin binder is calculated using equation (2-5) below. Then a grade of virgin binder can be selected that meets or exceed all of the critical temperatures.

$$T_{virgin} = \frac{T_{blend} - (\%RAP \times T_{RAP})}{(1 - \%RAP)} \qquad (2\text{-}5)$$

In the second scenario, the grade of the virgin binder, RAP and the combination of the two is known, while the amount of RAP is unknown. Using equation (2-6) below, the amount of RAP can be determined based on

critical low, intermediate and high temperatures. This equation is basically a reorganised version of equation (2-5):

$$\%\text{RAP} = \frac{T_{Blend} - T_{Virgin}}{T_{Rap} - T_{Virgin}} \qquad (2\text{-}6)$$

In 2011, the majority of the US states used the specifications in Table 2-3 as it was suggested in the standard AASHTO M323. However, 12 of them increased the limit for using softer binder from 15 to 20% (Copeland, 2011). Later, NCHRP published Report No. 752 (West, Willis, & Marasteanu, 2013) that proposed further modifications to the previous studies and standards such as AASHTO M323. At first, it suggested altering the term "RAP content" or "RAP percentage" to "RAP binder ratio". The former terms refer to the ratio of the weight of total RAP to the total blend while the latter is defined as a ratio of RAP binder to the total binder in the mix. The next suggested modification was to remove the middle tier in the three-tier system explained in Table 2-3 and change the limit between the two remaining tiers to 25%. Therefore, for mixtures with less than 25% RAP no changes would be needed, however, for higher RAP contents additional blending charts and tests to characterise the RAP and verify the blend would be required (West et al., 2013). This change in binder grade selection method was supported for two main reasons. First, the middle tier drops the binder grade even in the circumstances that might not be necessary as explained in (Gallivan, 2014). This is the reason some transport departments in the USA have changed this limit themselves and have not encountered any issues. Second, softer binder is not easily available everywhere or its acquisition might place extra burden on construction companies to have extra bitumen tanks and utilities for using a softer binder (Gallivan, 2014).

2.2.3.2 The European approach to utilising RAP

In the European Union, using RAP is allowed under standard EN 13108-1:2006, although local departments might have their own limitations. This standard applies several restrictions on the size of the RAP aggregates according to the size of virgin aggregates and also describes binder selection in mixtures containing RAP as shown in Table 2-5 (NSAI, 2006).

Table 2-5 Recommended procedures to use RAP in mixtures based on EN 13108-1:2006 (NSAI, 2006)

Summary of EN 13108-1:2006	RAP (%)	
	Surface layer	Base/binder layer
No change is needed.	< 10	< 20
Use blend equations in specification (based on softening point/penetration tests)	> 10	> 20

When using blend equations, calculations should demonstrate that the blend meets the specifications of the softening point and penetration test. To calculate the penetration value and softening point of RAP contained mix, equations (2-7) and (2-8) can be applied:

$$a\,log_{Pen_1} + blog_{Pen_2} = (a+b)log_{Pen_{mix}} \quad (2\text{-}7),$$

$$T_{mix} = aT_1 + bT_2 \quad (2\text{-}8)$$

where, Pen_1 and Pen_2 are the measured penetration of recovered binder and added binder, respectively, while Pen_{mix} is the calculated penetration of the total mixture. Similarly, T_1 and T_2 are the measured softening point of recovered binder and added binder, respectively, while T_{mix} is the calculated softening point of the total mixture. Furthermore, the coefficients (a) and (b) are the share of recovered binder and added binder in the total binder, respectively; therefore, the summation of (a) and (b) is always equal to 1.

2.2.3.3 The Australian approach to utilising RAP

In Australia, the Australian Asphalt Pavement Association (AAPA) (2000) published a guide on asphalt mix design that allows addition of RAP to all mixtures (with several conditions) and suggests the use of a three-tier system that has some similarities with the system shown in Table 2-3 Recommendations for selecting PG binder based on (Prithvi S Kandhal & Foo, 1997)(Association, 2000). In this system, equal to or less than 15% RAP is allowed in all mixtures without any special consideration. However, for mixtures that have greater than 15% and less than 30% RAP this guide proposes the use of one of the following procedures:

- One class softer bitumen.
- A specific class of bitumen or amount of rejuvenator based on calculations and tests on samples taken from RAP to adjust the viscosity of combination to the required level.
- No change to the binder.

Furthermore, for mixtures with a higher amount of RAP, the quality and suitability of the mix should be proven by the contractor. In addition, this guide introduces equation (2-9) to calculate the amount of virgin binder or rejuvenator needed to achieve the specific viscosity in the mix:

$$\mathrm{r} = \frac{\log(V+3) - \log(T+3)}{\log(V+3) - \log(R+3)} \qquad \textit{(2-9),}$$

where, r is the ratio of the mass of rejuvenator or virgin binder to the mass of the total binder (including RAP). R, T and V are the logarithms of the following viscosities, respectively: rejuvenating agent or fresh binder, target mixture and binder extracted from RAP. The unit for these viscosities is Pa.s and are all related to the same temperature that should be between 40 and 100 °C (usually either 45 °C or 60 °C).

The target specific viscosity and typical viscosity of the new binder after mixing can be estimated based on its binder class using Table 2-6.

Table 2-6: Recommended values for the viscosity of different classes of virgin binders and target viscosity of mixtures made by each type of binder

Binder Type	Typical viscosity of virgin binder after mixing (log Pa.s)		Target viscosity for blending of binder or rejuvenator (log Pa.s)	
	45 °C	60 °C	45 °C	60 °C
Rejuvenating agent	As provided			
C170	3.8	2.5	3.6–4.1	2.3–2.7
C320	4.2	2.8	4.0–4.5	2.6–3.0
C600	4.6	3.1	4.4–4.8	2.9–3.3

In 2004, Oliver and Luke (2004) published a modifications for Austroads National standards to utilise RAP in the design procedure of asphalt mixtures. Their publication stated that all required RAP properties including grading, binder content and binder viscosity should be measured. The gradation of the combination should comply with the job mix design. In addition, all the RAP binder should be considered in the binder content unless it has already been partially taken into account by the specifications and the usage of RAP should be banned in mixtures containing polymer modified binders.

However, in another Austroad Technical Report in 2006, limits of the RAP proportion in the mix were reported as thresholds of different scenarios, with it reporting that up to 15% or even 20% of RAP has little effect on the mix and no significant change in the production line is required. However, for RAP content between 20 and 40% it suggested compensating the hardening of the binder by using a softer binder or alternative solutions and extra attention should be paid to production issues including heat transfer, emissions. It also stated that the greater amount of RAP used in the mix, the more accurate control on RAP uniformity should occur, and it recommended crushing and screening RAP into different fractions to increase uniformity. Although, this report supports the idea of 100% RAP, it estimated the practical limit of approximately 40–50% of RAP was more realistic in asphalt plants because of their limited heat capacity, emission limits and extra production and quality control costs (Rebbechi, 2006).

The Austroads's 'Guide to Pavement Technology, Part 4B (Asphalt)' incorporates the information needed for usage of RAP in the mix design of HMA, which is almost the same as the proposed procedures by AAPA (2000), as mentioned at the beginning of this section.

Another important practice in Australia related to RAP is the ongoing project by the ARRB group to increase RAP usage in the Australian pavement industry and improve the current guidelines in Austroads standards for using RAP. Two studies have been published, although their outcomes have not been finalised at the time this thesis was written. The first report written by Denneman et al. (2013) discusses binder blend characterisation. In this report,

the DSR test complex modulus result at 1 rad/s is suggested to be utilised to estimate the capillary tube viscosity of binders at 60 °C, which is a standard test to categorise binders in Australia. Therefore, the viscosity of binders can be estimated more easily with a significantly smaller amount of material, which is very important when working with extracted binders as the extraction procedure is very time-consuming and costly. The typical capillary tube viscosities of commonly used binders in Australia are shown in Table 2-7.

Table 2-7 Typical class of binders in Australia based on capillary tube viscosity at 60 °C

Binder Class	Viscosity (Pa.s)
C170	140–200
C320	260–380
C600	500–700

The same study also suggested using a chevron equation similar to equation (2-10), instead of equation (2-9), which has been also suggested by (Austroads, 2015b), to estimate the viscosity of a blend of binders.

$$\mu = 10^{\left(\frac{3VBI_\beta}{1-VBI_\beta}\right)} \qquad (2\text{-}10),$$

where, μ is the viscosity of the blend (centipoise) and VBI_β is the viscosity blending index of the blend that can be calculated using equation (2-11):

$$VBI_\beta = \sum_{i=1}^{n} x_i VBI_i \qquad (2\text{-}11),$$

where, x_i is the volume fraction of the i^{th} component, n is the number of components in the blend and VBI_i is the viscosity blending index of the i^{th} component as described in equation (2-12) that is a function of the viscosity of the i^{th} component (ϑ_i) in centipoise. Although x is a volumetric proportion of a component, it can be assumed that the densities of all the components in the binder blend, virgin binder, RAP binder (and rejuvenator if applicable) are equal. Therefore, the proportion of the masses is used instead. However, if there is a significant difference between the densities of the different materials, the masses proportions cannot be used, instead the volume proportions should be used.

$$VBI_i = \frac{log\vartheta_i}{3 + log\vartheta_i} \qquad (2\text{-}12)$$

Moreover, the same study also proposed the following guidelines for binder blend design for mixtures containing RAP to replicate identical viscosity of typical binders in Australia:

1. If RAP content is greater than 10% of total mass, go to next step, otherwise no specific change in design is needed.
2. Collect samples of RAP.
3. Determine the binder content of samples.
4. Extract RAP binder.
5. Measure complex viscosity of the RAP, fresh binder (and rejuvenator if applicable) using DSR at 60 ° C, at 1 rad/s.
6. Calculate blend viscosity using equation (2-10).
7. If the calculated viscosity was out of the range of the target binder class (Table 2-7), adjust the proportion of the components to bring it back.
8. Check the viscosity of the actual blend using DSR.

In another study by the ARRB group in 2015, the performances of the mixtures containing RAP were investigated in the laboratory. The results were in agreement with the expected performance obtained from the literature. In other words, RAP increased the flexural stiffness and rut resistance while reducing the fatigue life and having no influence on moisture sensitivity. At the completion of this previous study, the guidelines of the first year projects were also confirmed; however, some changes were noted. First, the 10% limit for performing the binder design was altered to 15%, and second, checking the viscosity of the actual blend became optional (J. Lee, Denneman, & Choi, 2015).

Despite the fact that RAP usage has been included in the Australian National Standards, i.e. Austroad, for a long period, local agents in different states are still very conservative about using RAP. The majority of local departments placed a very low limit on the maximum amount of RAP allowed in the asphalt or totally avoided using it in several cases. A summary of the local

regulations for using RAP was collated by (J. Lee et al., 2015), as shown in Table 2-8.

Table 2-8: Regulations in the Australian states for using RAP in pavement.(J. Lee et al., 2015)

State	Surface	Base	Mix types
Victoria	< 20% (< 30% with extra tests)	< 30% (< 40% with extra tests	Not in SMA*, OGA* and PMB*.
New South Wales	< 15% (< 20% with extra tests)	< 15% (< 25% with extra tests)	Not in SMA and OGA. Max 10% for PMB.
Tasmania	< 15% (high RAP, i.e. > 30% can be used if suitable plant and QC is verified)	< 15% (high RAP, i.e. > 30% can be used if suitable plant and QC is verified)	Not in SMA and OGA. Max 15% for PMB.
Queensland	Not allowed	< 15%	Not in SMA, OGA and PMB.
South Australia	Not allowed	< 20%	Not in SMA, OGA and PMB
Western Australia	Not allowed	< 10% (only in intermediate course layer)	Not in SMA, OGA and PMB.
Northern Territory	No regulations	No regulations	No regulations

*SMA: stone mastic asphalt; *OGA: Open graded asphalt; *PMB: Polymer modified binder

2.3 Laboratory tests on mixtures containing RAP

In this section, laboratory tests that have been performed to characterise mixtures containing RAP are introduced, followed by investigation of the outcomes of these tests.

There are different types of tests for characterising asphalt mixtures. In the present thesis, the following tests will be covered:

- Complex modulus;
- Rutting (permanent deformation) resistance;
- Moisture susceptibility;
- Fatigue life;
- Resilient modulus; and
- Binder related.

2.3.1 Complex modulus

This test indicates both the elastic and viscous behavior of the sample when it is loaded in various frequencies and different temperatures. Generally, the sample is placed under a sinusoidal load, which can be compression, tension or compression-tension while, its response is monitored. The results of the test are not expected to be affected by the type of load utilised, as asphalt concrete is supposed to be isotropic (Sondag, Chadbourn, & Drescher, 2002).

Typically this test is preformed on cylindrical shape samples and the load is applied in a uniaxial way, however, several studies have utilised indirect tensile tests to obtain complex modulus with smaller cylinder samples and diametrical loading (H. S. Lee, Kim, & Choubane, 2011; Sondag et al., 2002).

Asphalt concrete can be considered a viscoelastic material; therefore, its schematic response owing to a sinusoidal load is similar to that illustrated in Figure 2-9.

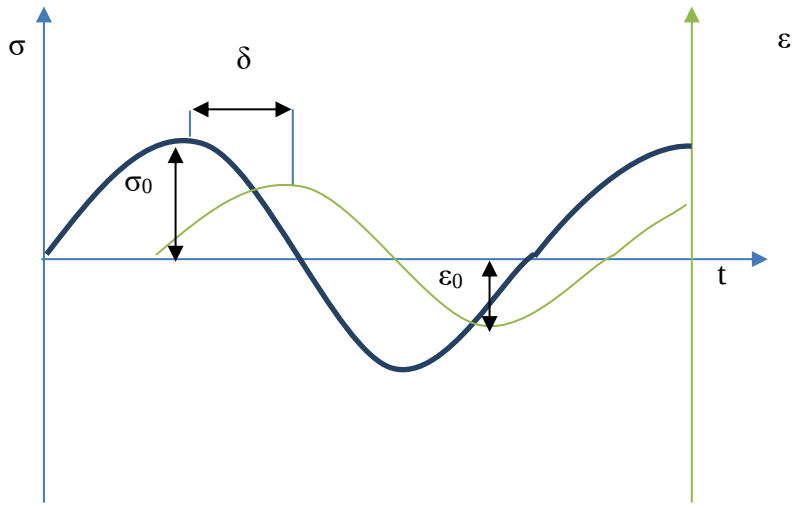

Figure 2-9 Response of viscoelastic material owing to sinusoidal loading

where, σ is an applied stress, ε is a measured strain, σ_0 is the amplitude of applied stress, ε_0 is the amplitude of measure strain and δ is the phase angle. If the material is completely elastic, δ is expected to be 0° while for completely viscous material δ is expected to be equal to 90° (Clyne, Li, Marasteanu, & Skok, 2003).

The complex modulus can be defined as E^*, which is the ratio of stress and strain in complex form, as shown in equation (2-13):

$$E^* = E' + iE^{"} \quad (2\text{-}13),$$

where, E' and E'' are the storage and loss modulus, respectively. The components of complex modulus can be calculated using equations (2-14) and (2-15):

$$E' = \frac{\sigma_0 Cos(\delta)}{\epsilon_0} \quad (2\text{-}14),$$

$$E^{"} = \frac{\sigma_0 Sin(\delta)}{\epsilon_0} \quad (2\text{-}15),$$

The absolute value of the complex modulus is called the dynamic modulus, |E*|, and can be calculated using equation (2-16):

$$|E^*| = \frac{\sigma_0}{\epsilon_0} \quad (2\text{-}16)$$

The dynamic modulus is a very important input parameter in several pavement design methods including the Mechanical-Empirical Pavement design guide in the USA (AASHTO, 2008) (Q. LI, Xiao, Wang, Hall, & Qiu, 2011). As a result of this importance, several methods have been developed to estimate the complex modulus properties of an asphalt sample using different parameters. These predictions can also be used to reduce the amount of laboratory experiments needed to describe the sample's performance by combining experimental and estimated data. For instance, (Bonaquist, 2008) utilised the Hirsch model to estimate the maximum dynamic modulus of samples, which requires measuring with sophisticated equipment in the laboratory, and then combined this information with experimentally acquired data to describe the performance of the samples. There are several methods to estimate the dynamic modulus of the asphalt mixtures in the literature including Witczak 1-37A, Witczak 1-40D, Hirsch model, Al-Khateeb model (also known as mixtures parallel model) as well as artificial intelligence based

methods including the artificial neural network. (Timm & Robbins, 2011), (Al-Khateeb, Shenoy, Gibson, & Harman, 2006), (Kim, Underwood, Sakhaei Far, Jackson, & Puccinell, 2011) (Yousefdoost, Vuong, Rickards, Armstrong, & Sullivan, 2013). Table 2-9 briefly explains each of these methods and their parameters.

Table 2-9 Different predictive models for HMA dynamic modulus

Method		
Witczak 1-37A (Kim et al., 2011)	Model	$$logE^* = -1.249937 + 0.02932\rho_{200} - 0.001767(\rho_{200})^2 - 0.002841\rho_4 - 0.058097V_a - 0.802208\frac{V_{beff}}{V_{beff}-V_a} + \frac{3.871977 - 0.0021\rho_4 + 0.003958\rho_{3/8} - 0.000017(\rho_{3/8})^2 + 00.005470\rho_{3/4}}{1+e^{(-0.603313-0.313351\log(f)-0.393532\log(\eta))}}$$
	Parameters	E^* is dynamic modulus of asphalt sample (psi) ρ_{200}, ρ_4, $\rho_{3/8}$, $\rho_{3/4}$ are percentages of retained aggregates on No. 200, No. 4, 3/8 inch and 3/4 inch sieve, respectively (%) V_a is air voids (% by volume) V_{beff} is effective binder (% by volume) F is loading frequency (Hz) η is the viscosity of binder (10^6poise)
Witczak 1-40D (Kim et al., 2011)	Model	$$logE^* = -0.349 + 0.754(\lvert G_b^*\rvert)^{-0.0052}\times(6.65 - 0.032\rho_{200} + 0.0027(\rho_{200})^2 + 0.011\rho_4 - 0.0001(\rho_4)^2 + +0.006\rho_{3/8} - 0.00014(\rho_{3/8})^2 - 0.08V_a - 1.06\frac{V_{beff}}{V_{beff}-V_a}) + \frac{2.558 + 0.032V_a + 0.713\left(\frac{V_{beff}}{V_{beff}-V_a}\right) + 0.0124\rho_{3/8} - 0.0001(\rho_{3/8})^2 + 0.0098\rho_{3/4}}{1+e^{(-0.7814-0.5785log\lvert G^*\rvert_b+0.8834log\delta_b)}}$$
	Parameters	E^* is dynamic modulus of asphalt sample (psi) ρ_{200}, ρ_4, $\rho_{3/8}$, $\rho_{3/4}$ are percentages of retained aggregates on No. 200, No. 4, 3/8 inch and 3/4 inch sieve, respectively (%) V_a is air voids (% by volume) V_{beff} is effective binder (% by volume) f is loading frequency (Hz) $\lvert G^*\rvert_b$ is dynamic shear modulus of binder (psi) δ_b is phase angle of binder
Hirsch (Kim et al., 2011)	Model	$$\lvert E^*\rvert_m = P_c\left[4200000\left(1-\frac{VMA}{100}\right) + 3\lvert G^*\rvert_b\left(\frac{VFA\times VMA}{10000}\right)\right] + \frac{(1-P_c)}{\frac{\left(1-\frac{VMA}{100}\right)}{4200000} + \frac{VMA}{3\lvert G^*\rvert_b(VFA)}}$$ $$\varphi = -21(logP_c)^2 - 55logP_c$$ $$P_c = \frac{\left(20 + 3\lvert G^*\rvert_b(VFA)/(VMA)\right)^{0.58}}{650 + \left(3\lvert G^*\rvert_b(VFA)/(VMA)\right)^{0.58}}$$

	Parameters	$\|E^*\|_m$ is dynamic modulus of HMA (psi) P_c is aggregate contact volume $\|G^*\|_b$ is dynamic shear modulus of binder (psi) VMA is percentage of voids in mineral aggregates VFA is percentage of void filled with asphalt Φ is phase angle of HMA.
Al-Khateeb (Al-Khateeb et al., 2006)	Model	$\|E^*\|_m = 3\left(\frac{100 - VMA}{100}\right)\left(\frac{\left(90 + 10000\frac{\|G^*\|_b}{VMA}\right)^{0.66}}{1100 + \left(900\frac{\|G^*\|_b}{VMA}\right)^{0.66}}\right)\|G^*\|_g$
	Parameters	$\|E^*\|_m$ is dynamic modulus of HMA (psi) $\|G^*\|_b$ is dynamic shear modulus of binder (psi) VMA is percentage of voids in mineral aggregates $\|G^*\|_g$ is glassy modulus of binder (psi): usually is taken as being equal to 145000 psi
Artificial neural network models (Kim et al., 2011)	Model	Different types of neural network structures.
	Parameters	Different models have been suggested using different types of variables like resilient modulus, binder viscosity or shear modulus, volumetric properties and frequency.

As RAP inclusion in the mixture significantly affects the dynamic modulus results (Shahadan, Hamzah, Yahya, & Jamshidi, 2013), many studies have investigated the performance of HMA containing RAP. In addition, many studies have utilised the dynamic modulus as a dependent variable to study the effects of the different parameters in the mixtures, including the participation of RAP in the total binder. The summary of some of these studies is shown in Table 2-10.

Table 2-10 Summary of complex modulus studies for mixtures containing RAP

Study	Samples	Comments
(Al-Qadi et al., 2009)	Different samples with 0, 20, and 40%of RAP with different assumptions on the RAP binder contribution in the total binder (0, 50 and 100%).	Applied to determine the amount of RAP binder involved in the mix but gives no clear indication. The dynamic modulus increases with higher RAP; however, the 20% RAP has no significant effect.
(Bennert, 2012)	Samples with 100, 75 and 50% RAP binder contribution (total binder contents are 5.3, 5.55 and 5.8%).	This test is utilised to determine how the various percentages of RAP binder contribute to the blend. Results demonstrated that all the stiffness curves were similar for the three different total binders at all temperatures and frequencies.
(Tarbox & Daniel, 2012)	Plant produced mixtures with 0, 20, 30 and 40% RAP aged in 85 °C oven at three levels (2, 4 and 8 days)	To check the long-term oven aging effects on mixtures containing RAP. The results revealed that the mixtures with higher percentages of RAP age less than do the virgin mix or mixtures with less percentages of RAP. The difference is more significant at high temperatures and low frequencies. The phase angle is reduced with aging and makes them behave more elastically.

Table 2-10 Summary of complex modulus studies for mixtures containing RAP (Continued)

Study	Samples	Comments
(West et al., 2013)	30 different mix designs from 0 to 55% RAP.	For checking the stiffness changes and to back-calculate the properties of virgin and RAP material. The results demonstrated that 25% RAP mixtures were between 30 and 43% stiffer than virgin ones were. The largest variances occurred at intermediate temperatures. However, for 55% RAP mixtures, 25 to 60% increases in stiffness were observed in comparison to virgin mixtures. Again, the largest difference was at the intermediate temperatures. For back-calculation purposes, the Hirsch model was utilised; however, this study Was unsuccessful in their aim here.
(Sondag et al., 2002)	Different mixtures with 0, 15, 30 and 40% RAP, three classes of virgin binder and two sources of RAP.	The higher the percentage of RAP, the stiffer the mixture was, especially at high temperatures. At 32 °C, one mix containing 40% RAP contained a triple modulus of the virgin mix. The stiffer binder was observed its dynamic modulus to be more sensitive to addition of RAP, and the phase angle dropped when the RAP content increased.

Table 2-10 Summary of complex modulus studies for mixtures containing RAP (Continued)

Study	Samples	Comments
(Liske et al., 2011)	Field (unconditioned) and laboratory (conditioned for four hours at 135 °C) production of samples with 0, 15and 50% RAP and two types of virgin binders	The dynamic modulus was applied as an indicator of how much damage the freezing-thawing (F-T) cycle or moisture causes on samples with different RAP content. Although after three F-T cycles the final E* in the mixtures containing RAP were still greater than virgin ones, E* decreased more dramatically when RAP was 50%. In addition, for any percentage of RAP, the conditioning time could not replicate the aging in the field production. Moreover, it confirms that no change in the binder is necessary in 15% RAP content.
(J. Li, Zofka, & Yut, 2012)	Different mixtures with 0 and 15% RAP (plant and laboratory-produced) from northeast USA.	This study examined the factors affecting dynamic modulus in addition to verifying prediction models for E* values of the mixtures containing RAP including Hirsh, Andre-Witczak and ENTPE models. All models demonstrated goodness of fit; however, they all showed various advantages and weaknesses.
(Kodippily et al., 2014)	Based on New Zealand specification with 0, 15 and 30% RAP.	The higher the RAP, the stiffer the mix, especially at lower frequencies.

Table 2-10 Summary of complex modulus studies for mixtures containing RAP (Continued)

Study	Samples	Comments
(Colbert & You, 2012)	Several mixtures with 15, 35 and 50% RAP	In contrast with other studies, the dynamic modulus in this study decreased by increasing the RAP percentage
(Silva, Oliveira, & Jesus, 2012)	Conventional mix, 100% RAP with two different additives and without the additive.	100% RAP (no additive) had the highest stiffness and lowest phase angle at all temperatures and frequencies. However, the two different additives performed similarly in that they decreased the stiffness and increased the phase angle, which results in more flexible mixture, especially at higher frequencies or lower temperatures.

2.3.2 Rutting (permanent deformation) resistance

Rutting is one of the most important failure modes of asphalt pavements; therefore, the resistance to this distress is vital for the mix. In this test, the sample is under a repetitive dynamic load while its deformation is being monitored. This procedure continues over a specific number of times or until the sample's deformation reaches a specific value. There are several methods that have investigated the permanent deformation of asphalt samples. One very well documented method is to apply uniaxial compression haversine loads with a rest period between pulses (Witczak, 2005). The rutting resistance can also be estimated under a repeated simple shear at constant height test or accelerated pavement testing simulator (wheel tracking) device. The last method has several advantages as it simulates the traffic load on the surface of the road while recording the rut profile (Fontes, Trichês, Pais, & Pereira, 2010). The schematic loading patterns of the mentioned methods are shown in Figure 2-10.

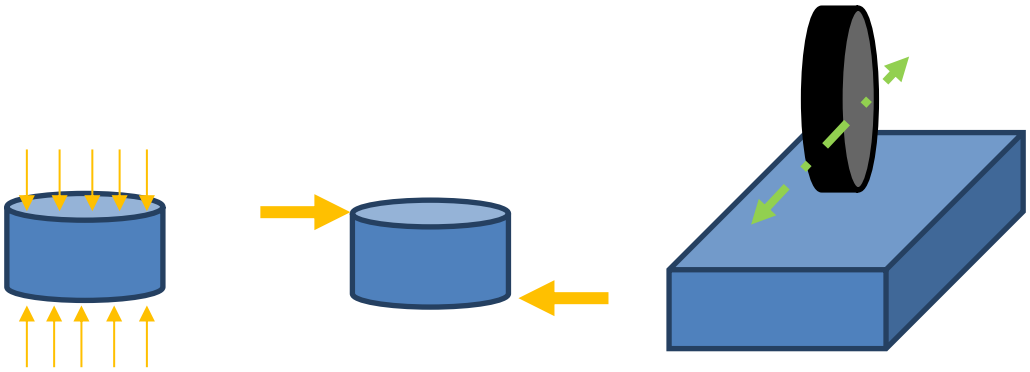

a) Uniaxial compression test b) Repeated simple shear test c) Wheel tracking test

Figure 2-10 Different tests to estimate permanent deformation resistance

It is believed that the increase in rutting depth has two phases. During the first phase, the asphalt mixture is compacted under the load, hence the rut depth increases significantly and the relationship between rut depth and number of loading cycles follows a non-linear regime. During the second phase, however, the rate of rutting decreases and reveals a linear increase in the series of loading cycles. Figure 2-11 illustrates typical changes in rut depth over time while HMA is under repetitive loads (Baghaee Moghaddam et al., 2011).

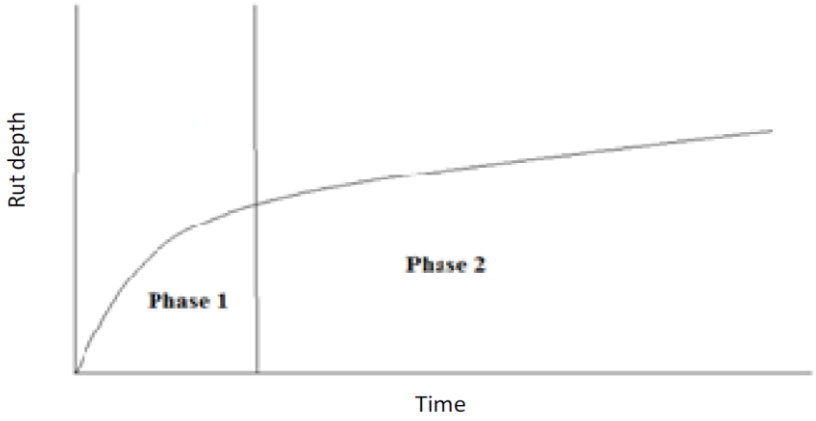

Figure 2-11 Typical change of rut depth over time (Baghaee Moghaddam, Rehan Karim, & Abdelaziz, 2011)

Although results from the uniaxial loading tests have been shown in good correlation with in-field data, they might not completely match the two-phase rutting behavior. For example, the samples under a uniaxial loading method usually present a tertiary non-linear phase after the linear phase two, although this stage of deformation usually will be ignored and only the first two phases

will be considered. A sample of such a response is illustrated in Figure 2-12 (Witczak, 2005).

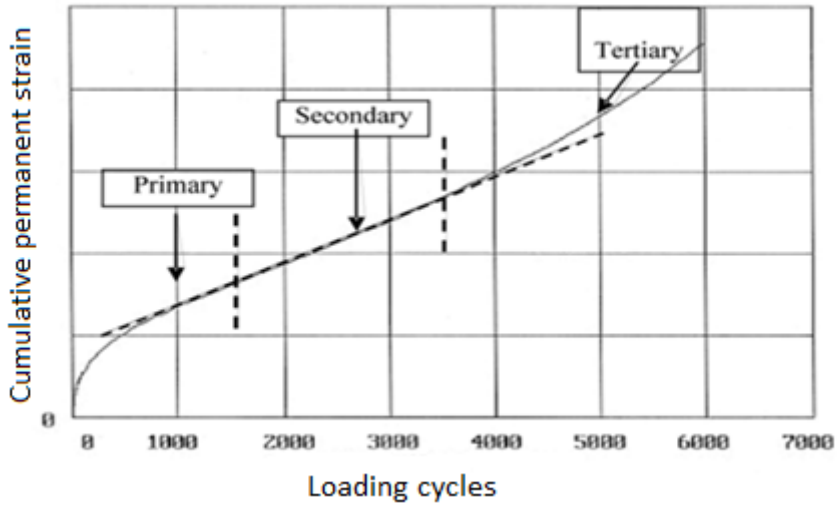

Figure 2-12 Typical response of an HMA sample under uniaxial loading test for rutting

Generally, it is believed that the usage of RAP (with no modification on the original binder) stiffens the mixture, so the rutting resistance is expected to be equal or better than the original mixture with no RAP (Harrigan, 2001; West et al., 2013); however, using softer binder can compensate for the increase in stiffness of the mixture by the addition of RAP and decrease the rutting resistance (Diefenderfer, Diefenderfer, & Apeagyei, 2011). In contrast to these findings, several studies have shown opposite results, e.g. (Widyatmoko, 2008) reported the higher the RAP content, the lower the rutting resistance in the samples. In this study, samples with 10% RAP (no softening oil) and samples with 20 and 30% RAP (with softening oil) showed less resistance to rutting than did the control samples that contained no RAP.

Therefore, many studies have been undertaken to investigate the performance of RAP in rutting resistance, several of which are shown in Table 2-11.

Table 2-11 Summary of rutting resistance studies for mixtures containing RAP (Continued)

Study	Samples	Comments
(Silva et al., 2012)	Conventional mix, 100% RAP with two different additives and without the additive.	100% RAP had much higher resistance to rutting (using wheel tracking device), while the additive contained mixtures had lower performance. However, all the mixtures containing RAP were less susceptible to rutting failure.
(Diefenderfer et al., 2011)	Nineteen plant produced mixtures with 0 to 25% RAP. One grade softer binder was used in the mixture with 25% RAP.	The flow number test was applied. Generally, the 0 and 25% RAP behaved similarly while the 10 and 15% RAP had higher resistance to rutting. The similarity of 25 % RAP to 0% RAP was because of the use of a softer binder in the 25% RAP mixture.
(Widyatmoko, 2008)	Samples with 0, 10, 30 and 50% RAP designed based on UK standards and created in the laboratory for wearing coarse and base course. Softer binder (80/100 pen) and rejuvenator oil added to replicate 60/70 pen binder properties accordingly.	Although the level of rut resistance was at an acceptable level, the mixtures containing RAP had less resistance to rutting.
(Bennert, 2012)	Samples with 100, 75 and 50% RAP binder contribution (total binders were 5.3, 5.55 and 5.8%).	All mixtures showed high rutting resistance in the flow number test and no significant difference was observed between treatments.

Table 2-11 Summary of rutting resistance studies for mixtures containing RAP (Continued)

Study	Samples	Comments
(J. Shen, Amirkhanian, & Tang, 2007)	Samples manufactured with 100% laboratory aged 60/80 pen binder and 0, 2 and 7.4% rejuvenator (the limits that replicate PG64-22 features based on DSR tests and blending charts).	The effect of rejuvenator on rutting was investigated, and it was revealed that by increasing the rejuvenator, the resistance decreased dramatically.
(McDaniel & Shah, 2003)	Samples with 0 to 50% RAP from different sources made in the laboratory. In addition, some plant produced samples were studied.	If the mixture is designed properly, greater percentages of RAP can improve the rutting resistance and stiffness. However, the use of softer binder might change this trend.
(Pereira et al., 2004)	Samples with 50% RAP and different total binder contents (4.5, 5 and 5.5%) were compared with samples that were made with 5% binder content designed by the Marshal method (Portuguese standards).	Repeated shear rate used to determine the rutting resistance of samples and determine whether the Marshal design method is applicable for RAP contained samples by comparing the results of 50% RAP contained samples with samples with no RAP. All samples had better performance than the virgin mix. The lowest binder content had the highest resistance to rutting and permanent deformation.

Table 2-11 Summary of rutting resistance studies for mixtures containing RAP (Continued)

Study	Samples	Comments
(West et al., 2013)	Utilised 30 different mix designs from 0 to 55% RAP	Based on the flow number test, none of the samples showed tertiary deformation and have greater than 5% accumulated strain at 20000 cycles. It was suggested that the results were affected more by mix source and virgin binder rather than RAP content.
(Kodippily et al., 2014)	Based on New Zealand specifications with 0, 15 and 30% RAP	Samples with 15% did not show a significant change in resistance to deformation based on the flow number test, while the 30% RAP mix had a significantly improved performance.
(Hajj, Sebaaly, & Shrestha, 2009)	Samples were created with two binder targets (PG64-22 and PG64-28) and 0, 15 and 30% RAP from the following sources: plant waste materials and 15 and 20-year-old pavement (all rated at PG82-16).	The asphalt pavement analyser (APA) was used to measure the rut depth of four cylinders that were under repeated wheel load. Mixtures targeted with PG64-28 showed better rutting performance. All the mixtures performed adequately except the ones made from plant waste material and target binder of PG64-22.

Table 2-11 Summary of rutting resistance studies for mixtures containing RAP (Continued)

Study	Samples	Comments
(Colbert & You, 2012)	Several samples prepared with 0, 15, 35 and 50% RAP content. The virgin binder used was 58-28 and the RAP high temperature ranked at 88.	The APA was used to measure rut depth. All the mixtures performed better than the control mix by the completion of the test. However, the 35% RAP mix performed worse than the control at the beginning of the experiment, but later regained superiority. The general trend confirmed the common belief that the higher the RAP content, the lower the rut depth.
(Pradyumna, Mittal, & Jain, 2013)	The effect of 20% of RAP in the mixture studied in comparison to control mix. The rejuvenator (10% of RAP binder) was added to replicate the properties of the virgin binder.	It was observed that increasing the amount of RAP decreased the rut depth and stiffened the mixtures.
(J. Lee et al., 2015)	Different mixtures with 0, 15, 30 and 60% RAP and different binders (C170, C320 and rejuvenator).	The higher the RAP, the lower the rut depth. In addition, the target blends produced the expected results with some error.

2.3.3 Moisture sensitivity

The performance of HMA can be very complicated when it is exposed to moisture and water, with comprehensive studies undertaken in the last few decades to investigate this issue.

Generally, tests on compacted samples can be categorised into qualitative and quantitative tests. Several of the methods for the former group include the boiling water test, freeze-thaw test, quick bottle test, rolling bottle method

and so on. Quantitative tests are based on monitoring several of the properties of the mix that are affected by the presence of moisture including the immersion-compression test, indirect tensile strength, Marshal immersion test, double punch method, resilient modulus test and so on. Alternatively, tests can done on the uncompacted samples (loose mixes) as well. These methods have the benefit advantage that they are usually easier and more economical to perform, while they do not consider the traffic, mix mechanical properties and pore pressure. In this regard, the surface energy method, film stripping and surface reaction tests are better examples (Solaimanian, Harvey, Tahmoressi, & Tandon, 2003).

One of the factors that can influence the moisture sensitivity of HMA is the presence of RAP (Al-Qadi et al., 2007). Therefore, it is recommended to test RAP mixtures for moisture sensitivity. For instance, (Copeland, 2011) suggested using either tensile strength ratio (TSR) test or wet wheel tracking to evaluate this issue. A group of efforts and their summaries that have been done to clarify the effect of RAP on moisture susceptibility can be found in Table 2-12.

Table 2-12 Summary of moisture sensitivity studies on RAP mixtures (Continued)

Study	Samples	Comments
(Ghabchi, Singh, & Zaman, 2014)	Samples with 0, 10, 25, 40% RAP using two types of virgin binder (64-28 and 76-28) and two kinds of aggregate.	The surface free energy method was used to evaluate the moisture-induced damage potential of samples.
(West et al., 2013)	Utilised 30 different mix designs from 0 to 55% RAP.	No significant moisture damage was obtained using the TSR (AASHTO 283) method. The high amount of RAP containing no anti-stripping additive ensured the samples did not pass the requirements while addition of an anti-stripping agent rectified this problem.

Table 2-12 Summary of moisture sensitivity studies on RAP mixtures (Continued)

Study	Samples	Comments
(Widyatmoko, 2008)	Samples with 0, 10, 30 and 50% RAP were designed based on UK standards and made in the laboratory for wearing coarse and base course. Softer binder (80/100 pen) and rejuvenator oil added to replicate 60/70 pen binder properties accordingly.	The mechanistic-empirical approach was utilised to evaluate the samples. Indirect tensile stiffness modulus was utilised as a parameter to monitor the before and after water conditioning procedure. The results demonstrated that samples containing RAP were not susceptible to moisture damage.
(Colbert & You, 2012)	Several samples prepared with 0, 15, 35 and 50% RAP content. The virgin binder used was 58-28 and the RAP high temperature ranked at 88.	In this study, the indirect tensile strength of the samples containing RAP was observed to be less affected by moisture than the virgin mix.
(Su, Hachiya, & Maekawa, 2009)	Samples designed to investigate the effect of the addition of RAP in airport pavement using 0, 40 and 70% RAP.	Marshal stability of the samples with RAP improved as the percentage of RAP increased. Similarly, the moisture susceptibility of mixtures increased, which is in conflict with several other studies.

Table 2-12 Summary of moisture sensitivity studies on RAP mixtures (Continued)

Study	Samples	Comments
(Pradyumna et al., 2013)	The effect of 20% of RAP in the mixture studied in comparison to control mix. The rejuvenator (10% of RAP binder) was added to replicate the properties of the virgin binder.	Indirect tensile strength (ASTM D 4867 standard) was utilised to evaluate the performance of samples. The results indicated that RAP decreased the tensile strength slightly while it improved the moisture susceptibility of the mixture slightly
(Sondag et al., 2002)	Different mixtures with 0, 15, 30 and 40% RAP, three classes of virgin binder and two sources of RAP.	The addition of the RAP had no significant influence on the TSR values, which indicates no damage owing to moisture.
(Liske et al., 2011)	Field (unconditioned) and laboratory (conditioned for four hours at 135 °C) production of samples with 0, 15 and 50% RAP and two types of virgin binders.	The tensile strength of laboratory created samples was similar or higher than field-produced ones. However, the mixtures followed the same trend in ranking, so this method is usable for comparing different mixtures. Moreover, there was no significant change in tensile strength owing to the presences of RAP in the mixture.

Table 2-12 Summary of moisture sensitivity studies on RAP mixtures (Continued)

Study	Samples	Comments
(Al-Qadi et al., 2009)	Different samples with 0, 20 and 40%of RAP with different assumptions for binder contribution of RAP in the total binder (0, 50 and 100%).	The tensile strength of two different treatments of the sample were measured, where the first group was maintained in a 60 °C water bath for 24 h while the other group was maintained under dry conditions. As expected, the higher the RAP in the mix, the higher the measured tensile strength. However, for the TSR, the results showed some fluctuations, i.e. the TSR of 20% RAP was higher than that of 0 and 40% RAP.
(Hajj et al., 2009)	Samples were made by RAP material taken from three different sources and two types of binders (PG64-22 and PG64-28). The percentages of RAP in the samples were 0, 15 and 30.	Several fluctuations were seen in the TSR results. One mixture with 15% RAP did not meet the specifications while others passed the minimum TSR limit.
(Diefenderfer et al., 2011)	A total of 19 plants produced mixtures with 0 to 25% RAP. The 25% RAP mixture contained one grade softer binder.	Higher moisture susceptibility was observed in samples with higher RAP content, in comparison with the samples that contained less than 20% RAP.

Table 2-12 Summary of moisture sensitivity studies on RAP mixtures (Continued)

Study	Samples	Comments
(J. Lee et al., 2015)	Different mixtures of 0, 15, 30 and 60% RAP with different binders (C170, C320 and rejuvenator).	The indirect tensile strength of samples showed no meaningful moisture damage in samples and all the samples passed the requirements.

2.3.4 Fatigue life

Asphalt concrete pavements are exposed to repetitive loading during their lifetime, as a result of traffic or environmental factors. These repetitive stresses and strains can cause cracks to grow, which are referred to as fatigue cracking. This deterioration mode is so important that it makes it one of the main criterions in the structural design of a pavement. Generally, in mechanistic pavement design, the tensile strain at the bottom of the asphalt layer is a key parameter to maintain this mode of failure. To evaluate the resistance of each HMA for fatigue cracking, many laboratory tests have been introduced. In loading patterns, four-point bending beam, trapezoidal cantilever (two point beam), simple beam (three point beam), diametral loading and rotating bending are well-known tests that are shown schematically in Figure 2-13.

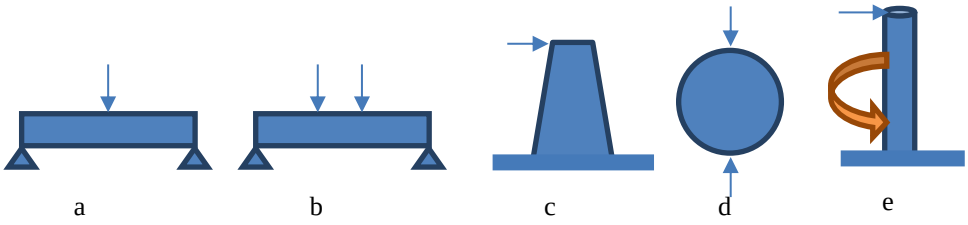

Figure 2-13 Different loading patterns of fatigue life tests

a)three point bending beam b)four-point bending beam c)trapezoidal cantilever beam d)diametral loading e)rotating bending

In terms of loading wave shape, the sinusoidal and haversine loads are the typical loads. However, the load can be applied continuously or by having rest periods and the test can be stress (force) or strain (displacement) controlled (Baburamani, 1999). Several typical load shapes are shown in Figure 2-14 .

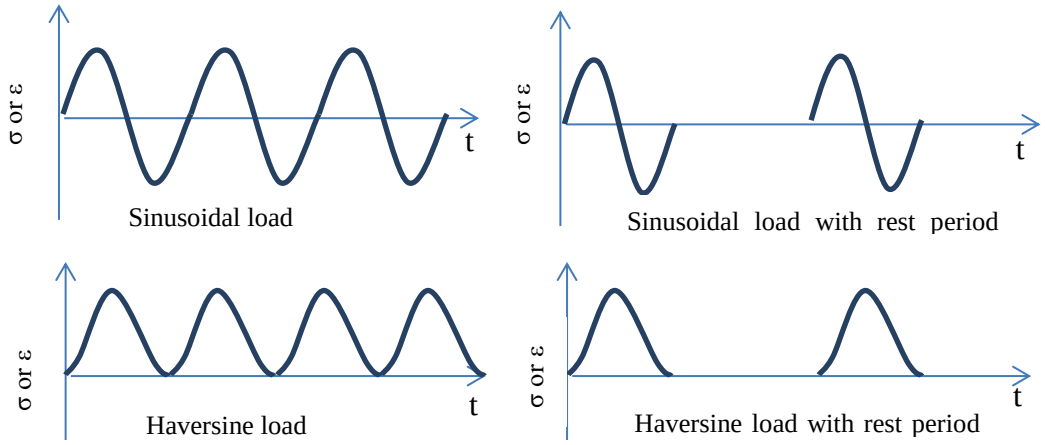

Figure 2-14 Different loading shapes of fatigue life tests

These tests are based on monitoring the change of a specific parameter such as stiffness or dissipated energy (S. Shen, Airey, Carpenter, & Huang, 2006) on the cycles of loading until the predefined termination criterion, for example the maximum number of cycles or value of the monitoring parameter, is reached. It is difficult to directly use the results of these tests to predict the performance of mixtures in the field as these tests are not simulating exactly what occurs in the field; however, they can be utilised to represent how vulnerable the different mixtures are to this phenomenon.

It is generally believed that RAP increases the stiffness of the mixture, so the fatigue cracking resistance of the mixture should be reduced with the addition of RAP. This is one of the reasons why for certain standards the use of softer binders is suggested when the percentage of RAP increases from a specific value, similar to the findings in the NCHRP report (West et al., 2013). However, there are doubts about this hypothesis as studies by several other researchers have demonstrated opposite results. Different definitions of failure of the sample, including obtaining 50% of the initial stiffness or ratio of dissipated energy change (RDEC) might lead to different interpretations of the performance of different mixtures (Shu, Huang, & Vukosavljevic, 2008). Several studies on fatigue performance of RAP contained asphalt concretes are shown in Table 2-13.

Table 2-13 Summary of fatigue life studies for mixtures containing RAP

Study	Samples	Comments
(Shu et al., 2008)	Samples were created from limestone aggregates, PG64-22 binder and 0, 10, 20 and 30% of RAP.	The fatigue resistance of the samples was investigated by the indirect tensile strength tests and four-point bending beams. Former tests helped to measure the dissipated energy and energy ratio. These values indicated that higher RAP content shortens the fatigue life of the samples. However, results from the four-point bending beams were mixed. Using conventional failure criteria (obtaining 50% of the initial stiffness), the RAP actually improved the fatigue cracking resistance while considering other failure criterion (plateau values of RDEC chart) resulted in a similar conclusion as the indirect tensile tests.
(West et al., 2013)	A total of 30 different mix designs from 0 to 55% RAP	Fracture energy calculated from indirect tensile strength was utilised to measure the fatigue performance of the mixtures. The results showed that the higher the RAP content, the lower the fracture energies were. Therefore, higher RAP content increased the likelihood of the mixture getting cracked in a shorter time.
(Pradyumna et al., 2013)	The effect of 20% of RAP in the mixture studied in comparison to the control mix.	The four-point bending beam sample that contained 20% RAP demonstrated higher flexural stiffness than the sample without RAP. Moreover, the presence of RAP increased the number of cycles that is required to halve the initial flexural stiffness significantly.

Table 2-13 Summary of fatigue life studies for mixtures containing RAP

Study	Samples	Comments
(Huang, Shu, & Vukosavljevic, 2011)	The typical surface mixture from the State of Tennessee, USA, was produced using 0, 10, 20 and 30% RAP and two types of aggregate (gravel and limestone). The binders were PG64-22, PG70-22 and PG76-22. Several samples were aged by keeping them in the oven to simulate long and short term aging.	The plateau value results (extracted from the RDEC plot) from both the beam fatigue testing and indirect tensile test suggest that the presence of RAP reduces the fatigue cracking resistance generally, however, this effect varied depending on the type of binder. For example, in this study, the samples with PG64-22 binder affected the most with presence of RAP. Surprisingly, considering the 50% reduction in initial flexural stiffness of the beams as a failure criterion, the mixtures that consisted of higher percentages of RAP performed better in terms of fatigue cracking resistance.
(Silva et al., 2012)	Samples were made with 100% RAP material with or without different kinds of rejuvenators (commercially available ones and used engine oil).	This study examined the feasibility of only using RAP to pave new roads. One of the factors studied was the fatigue performance of such mixtures using the four-point bending beam test. The results showed that all the fully recycled mixtures had improved performance due to fatigue cracking in comparison to the conventional HMAs.

Table 2-13 Summary of fatigue life studies for mixtures containing RAP

Study	Samples	Comments
(Bennert, 2012)	Samples with 100, 75 and 50% RAP binder contribution (total binders were 5.3, 5.55 and 5.8%).	This test was utilised to determine how different percentages of RAP binder contributed to the blend. The results revealed that although the stiffness of the samples did not show a significant variation, the fatigue performance was quite different. While the fatigue life of samples with 100% contribution was lower than other samples at any strain level, the fatigue life of samples with 50 and 75% contribution of RAP had similar results in the lower strain tests, but different results in the higher strain levels. To be more precise, the fatigue life of samples with 50% contribution was higher than the 75% samples.
(Widyatmoko, 2008)	Samples with 0, 10, 30 and 50% RAP were designed based on UK standards and produced in the laboratory for wearing coarse and base course. Softer binder (80/100 pen) and rejuvenator oil were added to replicate 60/70 pen binder properties accordingly.	Indirect tensile fatigue test results revealed that the fatigue life of the samples with RAP inclusion was similar or better than the samples where there was no RAP. This means that the combination of softer binder or rejuvenator could replicate the properties of the target binder in the mix.

Table 2-13 Summary of fatigue life studies for mixtures containing RAP

Study	Samples	Comments
(Pereira et al., 2004)	Samples with 50% RAP and different total binder contents (4.5, 5 and 5.5%) were compared with samples that were produced with 5% binder content designed by the Marshal method (Portuguese standards).	Four-point bending beam test was utilised to check the fatigue performance of samples and to determine whether the Marshal design method was applicable for RAP contained samples by comparing the results of 50% RAP contained samples with samples with no RAP. The performances of RAP included samples were worse than the virgin mix, i.e. the ones having the lowest binder content. Although increasing the binder content from 4.5 to 5%improved the fatigue life, no significant improvements were observed when the binder content was increased from 5 to 5.5%.
(Hajj et al., 2009)	Samples were produced from RAP material taken from three different sources and two types of binders. The percentages of RAP in the samples were 0, 15 and 30.	Four-point bending beam tests were utilised to evaluate the fatigue performance of the samples. Samples with PG64-22 binder demonstrated better performance when they contained 15% RAP. However, with 30% RAP, only samples that were made from 20-year-old RAP represented a better performance; the other samples behaved poorly. The poor fatigue performance observed in both 15 and 30% RAP contained samples that were made with PG64-28 binder.

2.3.5 Resilient modulus

This parameter is one of the key properties of pavement structure and needs to be determined during the mechanistic design approach based on many specifications including those from Main Roads Australia (Main Roads Western Australia, 2010). This test has been utilised by many researchers to

estimate the elastic properties of asphalt samples including ones containing RAP. The typical setup for measuring this parameter is to apply a load diametrically on a cylindrical shape sample, as Figure 2-15 shows, and measure the horizontal deformation of the sample using the appropriate measuring device (LVDT) under the load.

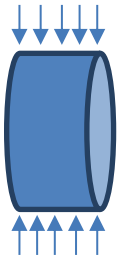

Figure 2-15 Diametrically loading on cylindrical sample for resilient modulus test

The magnitude of the loads in this test is generally 5 and 20% of the indirect tensile strength of the sample; consequently, this test can be considered a non-destructive test. Measuring the magnitude of the force and recovered strain in the sample, the resilient modulus can be calculated using equation (2-17) below (Sondag et al., 2002):

$$M_R = \frac{P(0.27 + v)}{\Delta U t} \qquad (2\text{-}17),$$

where, M_R is the resilient modulus in MPa, P is the applied force in Newtons, ΔU is recovered horizontal deformation in millimetres, t is the sample thickness in millimetres and v is Poisson's ratio.

As mentioned in previous sections, the general belief is that the inclusion of RAP in HMA stiffens the mixture as a result of the aged binder. However, there are still some arguments about the extent of this stiffening. As indicated in one of NCHRP reports, the resilient modulus results are not the best option for evaluating the RAP mixtures because of the uncertainty and inconsistency of the results between different laboratories (McDaniel et al., 2000). Therefore, caution must be taken when interpreting and using results. Table 2-14 shows several of the studies that have investigated the effect of RAP in resilient modulus of the HMA.

Table 2-14 Summary of resilient modulus studies for RAP mixtures

Study	Samples	Comments
(Sondag et al., 2002)	Different mixtures with 0, 15, 30 and 40% RAP, three classes of virgin binder and two sources of RAP.	RAP had less effect on resilient modulus at lower temperatures than at higher temperature. In addition, increased percentage of RAP increased the modulus; however, with a stiffer virgin binder, the increase is less significant than with softer binders. Moreover, the level of increase depends on the stiffness of the aged binder (RAP source).
(Widyatmoko, 2008)	Samples with 0, 10, 30 and 50% RAP were designed based on UK standards and produced in the laboratory for wearing coarse and base course. Softer binder (80/100 pen) and rejuvenator oil added to replicate 60/70 pen binder properties accordingly.	Generally, the samples with replicated binder (virgin binder + RAP + oil) tended to have softer or equal stiffness, except for the base course samples with 10 and 30% RAP. In addition, at different temperatures, the ranking of samples changed.
(Hassan & Tran, 2011)	Samples were produced based on VicRoads (Australia) specifications consisting of 0, 10, 20 and 30% RAP.	The higher the percentage of RAP in the mixture, the stiffer the mixture was.

Table 2-14 Summary of resilient modulus studies for RAP mixtures

Study	Samples	Comments
(Colbert & You, 2012)	Several samples were prepared with 0, 15, 35 and 50 % RAP content. The virgin binder used was 58-28 and the RAP high temperature ranked at 88.	Resilient modulus generally increased by the percentage of RAP. However, at lower and intermediate temperatures (4– 21.3 °C) the samples containing RAP showed less sensitivity to the change of temperature. At 4 °C, the stiffness of all the samples was similar, yet at 21.3 °C the stiffness of samples containing 50% RAP remained the same, but the stiffness of the other samples dropped significantly. This implies that the stiffness of mixtures containing RAP is less sensitive to temperature until it reaches 21.3 °C. However, at 39.2 °C, a dramatic decrease was observed in the stiffness of all samples.
(Pradyumna et al., 2013)	The effect of 20% of RAP in the mixture was studied in comparison to control mix. The rejuvenator (10% of RAP binder) was added to replicate the properties of the virgin binder.	The results of the resilient modulus test of the samples containing RAP were equal or slightly greater than the results of the virgin mixture at all temperatures tested (25, 35 and 45 °C).

Table 2-14 Summary of resilient modulus studies for RAP mixtures

Study	Samples	Comments
(Neumann & Somasundaraswaran, 2014)	Samples were prepared based on Austroads Australian standards with C600 virgin binder and consisting of 0, 15, 30, 45 and 60% RAP. For samples with 30, 45 and 60% RAP, a one grade softer binder (C320) was added to compensate for the effect of the RAP on stiffness.	The 15% RAP sample increased the resilient modulus in comparison to the control samples. However, samples with 30 and 45% RAP were softer than the control mix. Therefore, the softer binder over-compensated for the RAP binder stiffness. Meanwhile, 60% RAP inclusion was observed to produce close results to the control mixture.

2.3.6 Binder related

As explained in Section 2.2.2, the properties of the virgin and aged binder (that might be extracted from the RAP) play a key role in the behavior of the mixture. Therefore, characterising the binders is important during any mixture design. There are many approaches recommended for classifying a binder to use in the asphalt industry including penetration tests, capillary tube viscosity test and DSR. To rank the durability and aging performance of binders other tests such as RTFO and PAV are available.

2.3.6.1 Penetration test

This empirical test was first developed in 1936 and later it was utilised to measure the stiffness of bituminous binders. This method became so popular that the results have been used to standardise and categorise bituminous materials worldwide. However, this method is mainly an empirical method, i.e. it can barely characterise the viscoelastic behaviour of materials (Petersen, Robertson, Branthaver, Harnsberger, Duvall, KIM, Anderson, Christiansen, & Bahia, 1994).

In this test, the stiffness of the material is estimated by measuring how much a standard shaped needle penetrates into the sample under a specific load

(usually 100 g) and specific temperature (usually 25 °C) over a specific period of time (usually 5 s). The results are reported in deci-millimeters, and the higher the penetration result, the softer the sample is (Read & Whiteoak, 2003).

2.3.6.2 Capillary tube viscosity test

In this test, the time that is required for the bitumen to flow through a specific length in a standardised U-shaped glass under gravity (or a known vacuum pressure) is measured and then the kinematic (or dynamic) viscosity of the binder is calculated using the measured time. To adjust the test temperature, this setup is maintained in a temperature controlled environment, usually in a water bath (Read & Whiteoak, 2003).

In Australia, binder grading changed from penetration grading to viscosity grading in 1977. This grading commonly uses capillary tube viscosity at 60 °C to determine the class of bitumen. Common classes of bitumen in Australia are presented in Table 2-15 (Austroads, 2008).

Table 2-15 Typical bitumen classes in Australia

Binder Class	Viscosity at 60 °C (Pa.s)
C-170	140–200
C-320	260–380
C-600	500–700

2.3.6.3 Dynamic shear rheometer (DSR)

This test is designed to measure the complex shear modulus and phase angle of the binder at intermediate or high temperatures (Petersen, Robertson, Branthaver, Harnsberger, Duvall, KIM, Anderson, Christiansen, Bahia, et al., 1994), although recently a study has occurred to investigate the low-temperature performance of binder using DSR (Farrar, Sui, Salmans, & Qin, 2015). The information measured by this test is used to estimate the performance of the binder in different scenarios, for instance, rutting resistance and fatigue life.

In this test, a binder sample is located between two horizontally placed circular-shaped plates, of which the upper one can rotate precisely and apply torque using an electric motor as shown in Figure 2-16.

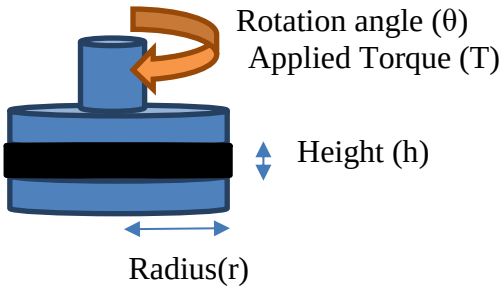

Figure 2-16 Schematic of DSR test

In this test, the torque and rotation movement is monitored via a computer system to calculate the complex shear modulus and phase angle as explained in Figure 2-17.

$$\tau = \frac{2T}{\pi r^3}$$

$$\gamma = \frac{\theta r}{h}$$

$$|G^*| = \frac{\tau_{max}}{\gamma_{max}}$$

$$Phase\ angle(°) = \frac{\delta \times 360}{t}$$

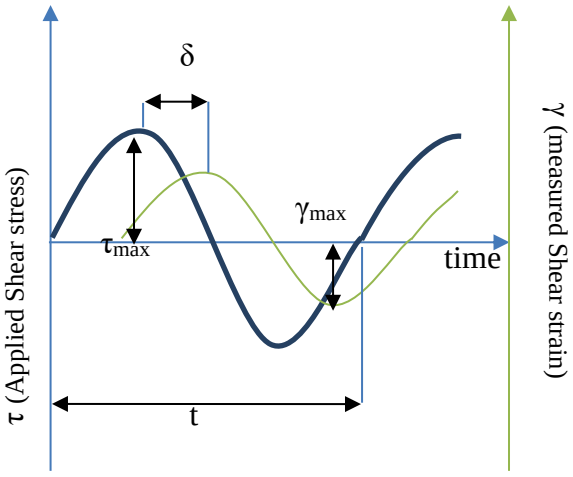

Figure 2-17 Load and response of a bitumen sample in DSR for complex modulus test

where T is applied torque, r is sample's radius, τ is applied shear stress, θ is rotation angle, h is the samples' thickness, γ is shear strain, τ_{max} is the peak of shear stress in loading cycles, γ_{max} is the peak of shear strain in response cycles, G^* is complex shear modulus, t is a cycle period time and δ is the delay time between the peak of stress and strain.

Similar to the dynamic modulus of the asphalt samples in section 2.3.1, the complex shear modulus can be defined as a summation of elastic (storage) modulus and viscous (loss) modulus as equation (2-18) demonstrates (Schramm, 1998):

$$G^* = G' + iG''$$
$$G' = G^* \cos\delta \qquad (2\text{-}18),$$
$$G'' = G^* \sin\delta$$

where, G' is storage modulus, G" is loss modulus and δ is the phase angle. In addition, the complex viscosity of the binder can be defined as equation (2-19) below (Schramm, 1998):

$$\eta^* = \frac{G^*}{i\omega} \qquad (2\text{-}19),$$

where, η^* is complex viscosity and ω is angular velocity. The absolute value of complex viscosity and its components, storage viscosity (elastic component) and dynamic viscosity (viscous component) can be calculated as shown in equation (2-20) below:

$$|\eta^*| = \frac{|G^*|}{\omega}$$
$$\eta' = \frac{G''}{\omega} = \frac{\tau_{max}}{\omega \times \gamma_{max}} \sin\delta \qquad (2\text{-}20),$$
$$\eta'' = \frac{G'}{\omega} = \frac{\tau_{max}}{\omega \times \gamma_{max}} \cos\delta$$

where, η' is storage viscosity and η" is dynamic viscosity (Schramm, 1998). The frequency of oscillation of plates can be adjusted. In the Superpave method, the frequency of 10 rad/s is usually used, which presents the traffic speed of 100 km/h. While looking for performance under slower traffic movement, the lower frequencies can be used and vice versa. For instance, the frequency of 5 rad/s and 1 rad/s can be used for traffic moving at 50 km/h speed and standing traffic, respectively (SHRP, 1994).

2.4 Master curve of complex modulus of binder and mixture

The binder and consequently the asphalt mixture both show a viscoelastic behavior under different loads and temperatures. Therefore, the response of the material depends not only on the amplitude of the load but also on the

frequency of the load and the temperature of the material. In design procedures, the response of the pavement to a wide range of frequencies or temperatures might be required. For example, the MEPDG design guide requires a curve that represents the complex modulus of the mixture over a wide range of frequencies at a reference temperature of 70 °F while designing the pavement (Witczak, 2005). Hence, it is important to estimate the complex modulus of the binder or mixture under the required temperature or frequency. However, laboratory tests can usually only be performed on a limited number of temperatures and frequencies because of experimental limitations. To overcome these limitations, the following procedures can be followed.

If the test is performed within the linear viscoelastic region of the material, the time-temperature superposition principle can be applied to generate the response of the material in a wide range of temperatures and frequencies using available data from laboratory experiments. The linear viscoelastic region is defined as a range of strain levels where the complex modulus shows no changes after altering the strain or stress level (ASTM, 2008). Using the time-temperature superposition principle, the behavior of the material can be predicted for a wide range of frequencies and temperatures using a limited number of tests in particular frequencies and temperatures. Based on this concept, the frequency or temperature of recorded data can be shifted with respect to a reference temperature or frequency (Clyne et al., 2003), i.e. the response of the material at lower temperatures than the reference temperature can be utilised to construct the response of the material at higher frequencies in the reference temperature.

To generate the master curves, a model should be considered for the pattern of complex modulus with respect to frequency (see section 2.4.1 for further explanation on master curve models). After determining the model, a shift function needs to be chosen, which shifts the frequency of data from the test frequency to its equivalent frequency in reference temperature. Generally, models and shift functions have several parameters that can be used to match them with the data; therefore, the parameters need to be adjusted to determine the best fit. This can be achieved by converting this problem to an

optimisation problem, where the adjustable parameters make the search space and the objective function is the error between the data from the experiment and the master curve model. One popular example of such an objective is the summation of square errors (SSE), shown in equation (2-21) below:

$$SSE = \sum \frac{(\log|E_e^*| - \log|E_m^*|)^2}{(\log|E_e^*|)^2} \quad (2\text{-}21),$$

where, E^*_e is the complex modulus of a binder/mixture obtained from the experiment while E^*_m is its counterpart calculated using the chosen master curve model and shift function.

To optimise the parameters, with the objective function likely to be a nonlinear least square function, a capable nonlinear optimisation algorithm should be applied, which can be achieved using nonlinear least square regression tools available in several computer programs.

2.4.1 Master curve models

Generally, the generated curve consisting of shifted data for a wide range of frequencies at a specific temperature is called a master curve. A master curve of a binder or asphalt mixture is considered to be a sigmoidal function similar to equation (2-22) as described in the NCHRP report 547 (Witczak, 2005), NCHRP report 614 (Bonaquist, 2008) and an Austroad report AP-T248 (Denneman, 2013):

$$log\ |E^*| = \delta + \frac{\alpha}{1 + e^{\beta+\gamma(log\omega_r)}} \quad (2\text{-}22),$$

where, E^* is the complex modulus of a binder/mixture, ω_r is the reduced frequency (Hz), δ is the minimum value of $|E^*|$, α is the difference between the maximum and minimum value of $|E^*|$ while β and γ are parameters to adjust the shape of the sigmoidal function. For the binders, the maximum value of E* can be assumed to be the glossy modulus which is the maximum E* that usual bitumen material might have and can be considered to be 1GPa (145000psi). (Bonaquist, 2008). Therefore, for binders, the α can be assumed to be the difference between the glossy modulus of the binder and the δ.

There are other master curve models recommended as well, including generalised logistic sigmoidal (Richards) model, Christensen Anderson (CA) model, Christensen Anderson and Marasteanu (CAM) model and polynomial models (Medani & Huurman; Nur Izzi Md Yusoff, Jakarni, Nguyen, Hainin, & Airey, 2013). Each of these models has its own advantages and disadvantages for describing the behaviour of the viscoelastic materials. For example, the Richards model, as shown in equation (2-23), allows the curve to be non-symmetrical while the sigmoidal model does not allow this (Nur Izzi Md Yusoff et al., 2013):

$$log\,|E^*| = \delta + \frac{\alpha}{[1 + \lambda e^{\beta+\gamma(log\omega_r)}]^{1/\lambda}} \qquad (2\text{-}23),$$

where, λ is an extra adjustment parameter while the other symbols are the same as in equation (2-22).

2.4.2 Shift factor functions

To shift the frequency of the data recorded for temperatures other than the reference temperature to its equivalent frequency on the reference temperature, equation (2-24) can be applied (Nur Izzi Md. Yusoff, Chailleux, & Airey, 2011) (Bonaquist, 2008).

$$a_T = \frac{\omega_r}{\omega} \qquad (2\text{-}24),$$

where, ω_r is the reduced frequency at the reference temperature, ω is the frequency of the data from the experiment and a_T is the shift factor at a temperature of interest T. The equation (2-24) can be reorganised in logarithmic form as shown in equation (2-25):

$$log(\omega_r) = log(\omega) + log[a_T] \qquad (2\text{-}25)$$

Figure 2-18 illustrates how the shift factor helps generate a master curve for complex modulus and phase angle from the data in a limited range of frequencies but at different temperatures for a wider range of frequencies at the reference temperature.

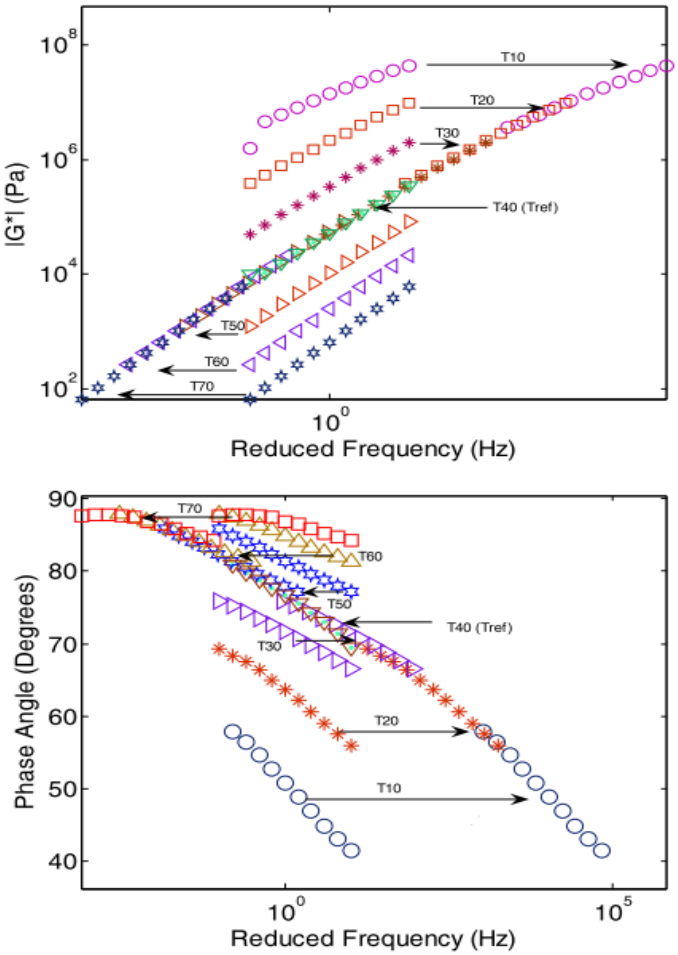

Figure 2-18: Complex modulus and phase angle master curve construction (Nur Izzi Md. Yusoff et al., 2011)

In the literature, several kinds of shift functions have been suggested to be utilised (see Table 2-16 for further information).

Table 2-16 : Several available shift functions from the literature (Nur Izzi Md. Yusoff et al., 2011) and (Witczak, 2005)

Equation	Parameters
Williams, Landel and Ferry (WLF) equation: $$\log a_T = \frac{-C_1(T - T_{ref})}{C_2 + (T - T_{ref})}$$	T: Temperature T_{ref}: Reference temperature C_1, C_2: adjustable constants
Modified Kaelble equation: $$\log a_T = \frac{-C_1(T - T_{ref})}{C_2 + \lvert T - T_{ref}\rvert}$$	Similar to the WLF equation.
Arrhenius Equation:	C: adjustable constant E_a: activation energy that is an adjustable constant and is

$$\log a_T = C\left(\frac{1}{T} - \frac{1}{T_{ref}}\right) = \frac{0.4347E_a}{R}\left(\frac{1}{T} - \frac{1}{T_{ref}}\right)$$	the minimum energy needed for intermolecular movement. R: ideal gas constant (8.314J/mol.K)
Viscosity-Temperature Susceptibility (VTS) equation: $$\log a_T = C\left(10^{A+VTS\log T_R} - 10^{A+VTS\log(T_R)_0}\right)$$	T_R: Temperature (Rankine) $(T_R)_0$: Reference temperature (Rankine) A: regression line intercept of VTS graph VTS: VTS regression line slope
$$\log a_T = aT^2 + bT + c$$	T: Temperature a, b and c: adjustable constants

3 Methodology and laboratory evaluation

3.1 Methodology and laboratory evaluation overview

Although the inclusion of RAP in HMA is allowed to a limited degree in Western Australia by Main Roads, there are still concerns about the performance of these mixtures and a need exists for setting appropriate limits for the amount of RAP that can be utilised. Therefore, to characterise the mixtures containing RAP in Western Australia, a comprehensive research program has been carried out in the Pavement Research Group at Curtin University, which is supported by the Main Roads Western Australia for funding and material supply. In this chapter, the experimental plan of this thesis is briefly explained and then the different stages of laboratory evaluation are introduced and described. These steps can be divided into two main groups: material characterisation and mixture preparation and characterisation. The former section discusses the characterisation of the materials that were used in the study, while the latter describes how the mixtures were designed, created, verified and evaluated.

3.2 Experimental plan

The mixtures studied in this research are typical dense-graded HMA mixtures present in Western Australia with a nominal size of 14 and 20 mm and C320 binder that are designed based on Main Roads specifications for heavy traffic conditions. To produce the mixtures representing the actual material present in the field, material was collected from an asphalt plant and designed to replicate the same mixture as that found out of the asphalt plant. In addition, mixtures were designed to contain 0, 10, 20 and 30% RAP by total weight. In the present study, the RAP content refers to the ratio of the weight of the total amount of RAP (binder and aggregate) to the total weight of the mixture. After characterising and preparation of all the material to be utilised and confirming the mix designs, laboratory samples were produced to investigate the performance of mixtures by completing a variety of tests including complex modulus, rutting resistance, moisture sensitivity, fatigue life and resilient modulus. Moreover, viscoelastic features of the virgin binder added to the mixtures and also the binder extracted from the mixtures were

examined. The workflow of laboratory evaluation is illustrated in Figure 3-1 and is explained in detail in the following sections.

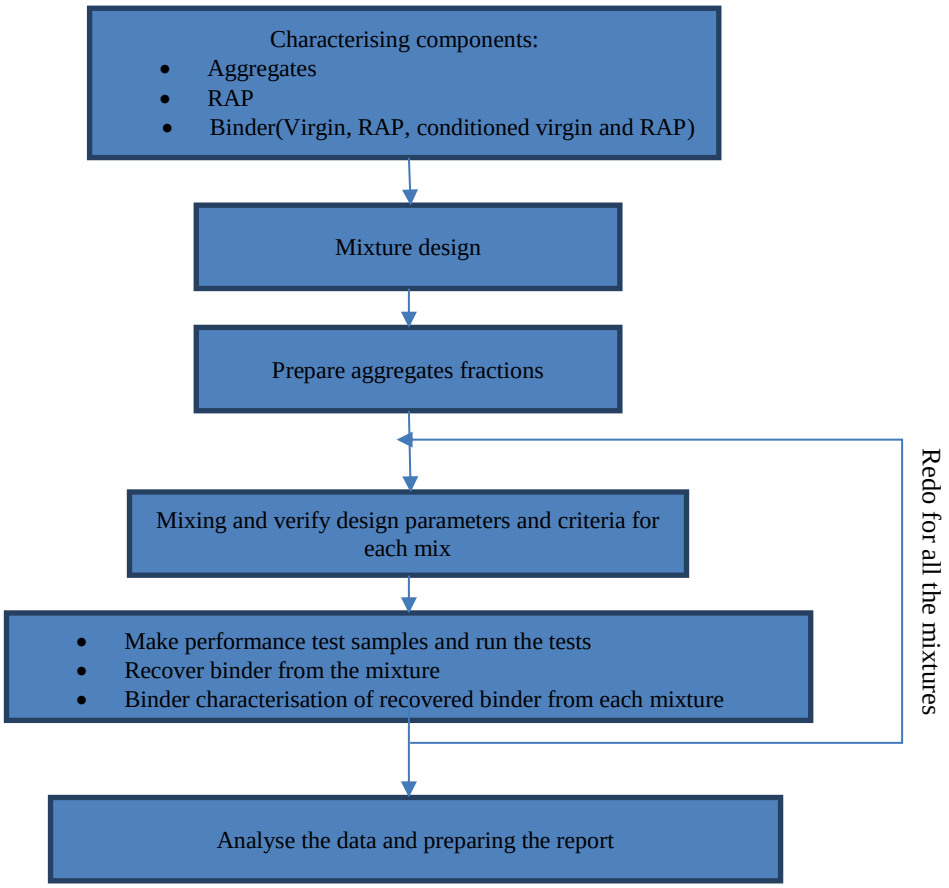

Figure 3-1 Laboratory work flow

A summary of the experimental tests on the materials and HMA mixtures applied in the present study can be found in Table 3-1.

Table 3-1 Summary of experimental tests

Material	Tests
Aggregates	PSD test on each fraction of materials collected from asphalt plant for making DG14 and DG20 (seven types of aggregates)
RAP	Binder content, PSD
Binders	Penetration and complex modulus test (using DSR) on the following binders: virgin, RTFO aged virgin, recovered unconditioned RAP, recovered conditioned RAP and binder recovered from four different DG14 mixtures (a total of eight types of binder).
HMA mixtures	Design verifications tests (binder content, PSD, maximum density, Marshal stability and flow) in addition to performance tests including complex modulus, rutting resistance, moisture sensitivity, fatigue life and resilient modulus on eight different HMA mixtures with four different RAP contents (0,10,20 and 30%) for two dense-graded mixtures with maximum nominal size of 14 and 20 mm.

3.3 Material characterisation

The asphalt mixtures containing RAP in this study consisted of four main components: aggregates, RAP, hydrated lime and virgin binder. To characterise the mixtures accurately, it is important to characterise the main components of the mixtures first. In this section, the method and outcome of the characterization of the aggregates, RAP and hydrated lime are explained. The methods applied to investigate the binder properties will also be described while the outcome of binder characterisation will be analysed and discussed in Chapter 4.

3.3.1 Aggregates

Aggregates utilised in this research are crushed granite obtained from the stockpiles of an asphalt plant as shown in Figure 3-2 based on the (Australian Standard, 2012).

Figure 3-2 Aggregate stockpile in an asphalt plant

These aggregates were categorised in different sizes (Table 3-2) as is typical in asphalt plants

Table 3-2 Aggregate stockpiles in this study

Type	Nominal size range(mm)	Comments
Dust	≤ 2.36	Used for DG14 and DG20
5 mm	≤ 5	Used for DG14 and DG20
7 mm	≤ 7	Used for DG14
7 mm(II)	≤ 7	Used for DG20
10 mm	≤ 10	Used for DG14 and DG20
14 mm	≤ 14	Used for DG14 and DG20
20 mm	≤ 20	Used for DG20

The materials were dried in an oven at 105 °C until a constant mass was achieved, then the material in each group was homogenised by mixing the material from different buckets. Representative samples were taken from each of these aggregates groups using a riffle box as shown in Figure 3-3.

Figure 3-3 Riffle box

Later, each sample was sieved according to AS1152 standard (Australian standard, 1993b) using a nest of sieves and a shaker, similar to Figure 3-4, at least two times, so their PSD could be determined.

Figure 3-4 Sieve shaker

The average results from the PSD tests for each stockpile of aggregates is shown in Table 3-3 and Figure 3-5, while the details of each test can be found in Appendix I.

Table 3-3 PSD result of stockpiles

	Average of % passed through different sized sieves in each stockpile						
Sieve size (mm)	Dust	5 mm	7 mm	7 mm (II)	10 mm	14 mm	20 mm
26.5	100	100	100	100	100	100	100
19.0	100	100	100	100	100	100	95.8
13.2	100	100	100	100	100	88.7	32.4
9.50	100	100	99.5	100	81.8	15.0	8.1
6.70	100	100	86.3	87.8	15.3	2.3	4.3
4.75	99.7	86.5	24.5	29.2	2.6	1.5	3.2
2.36	78.5	19.3	2.10	4.9	1.5	1.3	2.5
1.18	53.60	8.67	1.11	2.94	1.44	1.27	2.22
0.600	36.26	6.18	0.94	2.20	1.36	1.17	2.01
0.300	24.07	5.05	0.86	1.79	1.25	1.04	1.78
0.150	14.94	4.09	0.75	1.43	1.10	0.90	1.51
0.075	9.92	3.13	0.67	1.09	0.90	0.74	1.19

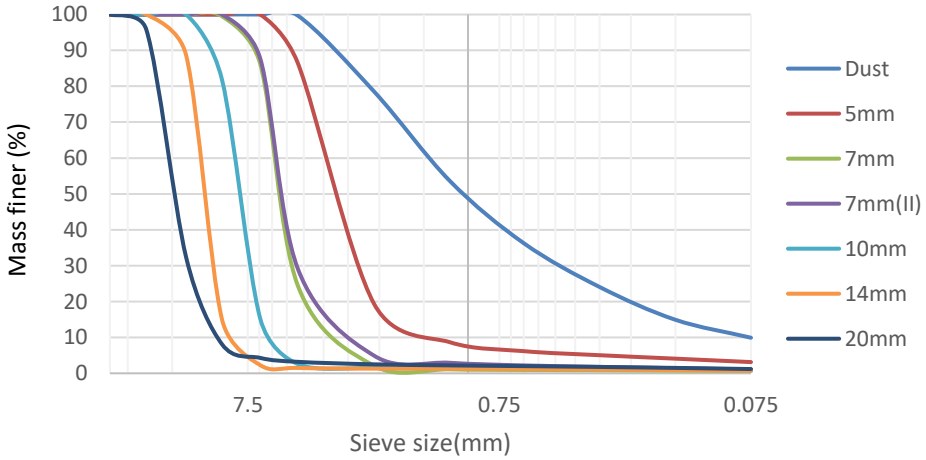

Figure 3-5 Particle size distribution of stockpiles

3.3.2 Recycled asphalt

The recycled asphalt utilised in this study was collected in a similar way to the aggregates from an asphalt plant. The RAP was then homogenised by mixing of the material in the different buckets, and the material was tested for binder content and PSD.

The binder content and PSD of the RAP was determined using the centrifuge method based on Method 730.1 of (Main Roads Western Australia, 2011b). In this standard, a sufficient amount (at least 1 kg in this case) of dried and hot RAP (using a 105 °C oven) was weighed and placed in an extraction bowl. Then, a sufficient amount of solvent to cover the material was added, after which a dried and weighed filter paper was placed on top of the bowl and the lid of the centrifuge closed. The centrifuge was turned on. The speed of the centrifuge was increased gradually (not more than 3600rpm) until the outcome flow of the centrifuge ceased and all the liquid became separated from the aggregates. This process was repeated until the solvent becomes clear. Then, the extracted liquid was homogenised by mixing and two dried centrifuge tubes with known weights were filled with a specific amount of the extracted liquid (usually 50ml each). After centrifuging, the tubes, filter paper and aggregates were dried in the oven until they reach constant mass. The remaining aggregates in the bowl, filter paper and tubes were weighed. Based on the difference of weight of solid particles extracted from the mixture placed in the device initially and the initial weight of the material, the amount of bitumen is estimated. If the remaining aggregates in the bowl were enough to perform a PSD test, this was achieved on the material as explained in section 3.3.1. The PSD report considers not only the material left in the extraction bowl but also the particles stuck on the filter paper and suspended in the extracted liquid. The centrifuges that were utilised for the solvent extraction and separation of the suspended particles from the extracted liquid are shown in Figure 3-6.

(a) (b)

Figure 3-6 a)Solvent extraction centrifuge b)Centrifuge to settle suspended particles in liquid

These tests were performed several times to ensure consistency of results. The average result of binder content of the RAP utilised in this study was found to be 4.1% by weight. The details are shown in Appendix II.

The average PSD of the aggregates recovered from the RAP are shown in Table 3-4 and illustrated in Figure 3-7. Based on (Austroads, 2007a), the grading of the RAP utilised in the present study is similar to the grading specifications of the AC10 dense-graded asphalt concrete, which implies that the RAP in this study is recycled from an AC10 asphalt concrete.

Table 3-4 PSD of aggregates recovered from RAP

Sieve size (mm)	26.5	19.0	13.2	9.50	6.70	4.75	2.36	1.18	0.60	0.30	0.15	0.075
% pass of sieves	100	100	99.9	93.8	77.3	61.6	40.8	31.33	24.6	16.68	9.83	6.24

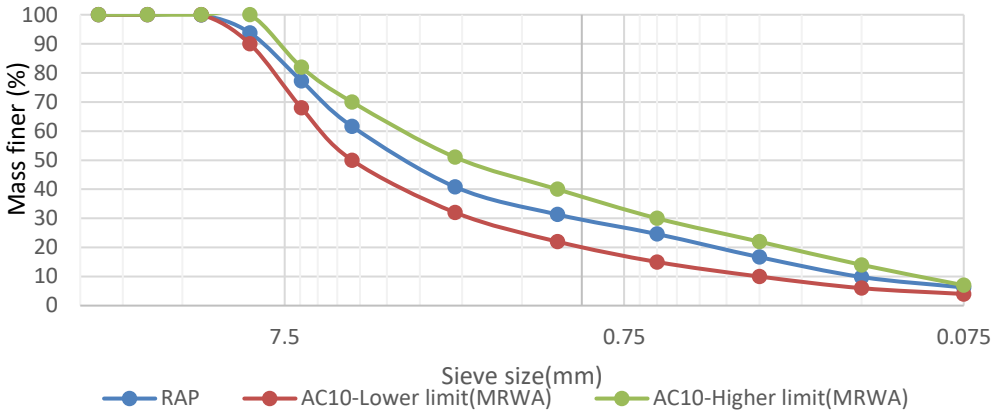

Figure 3-7 PSD graph of aggregates recovered from RAP

3.3.3 Hydrated lime

Based on the specifications in Western Australia, hydrated lime is usually added to the mixture at 1.5% of total weight of aggregates (including RAP aggregates) to reduce the stripping potential of the HMA. As the hydrated lime contributes to the grading of the entire mixture, it is necessary to know the PSD of this component as well as the aggregates and RAP. The PSD is usually provided by the supplier and so there is no need to determine it in the laboratory again. In the present study, the PSD of the hydrated lime is shown in Table 3-5.

Table 3-5 PSD of hydrated lime

	Average of % pass of sieves
Sieve size (mm)	Hydrated lime
26.5	100
19.0	100
13.2	100
9.50	100
6.70	100
4.75	100
2.36	100
1.18	100
0.600	100
0.300	100
0.150	100
0.075	95

3.3.4 Binder characterisation

The investigated binders utilised in the present study are:

- Virgin binder (C320 class)
- Short term aged binders using RTFO
- Recovered binder from conditioned and unconditioned RAP
- Recovered binder from mixtures with 14 mm nominal size

The virgin binder was supplied from the same asphalt plant as that for the mixtures. The virgin binder was exposed to heat and air flow in a RTFO machine to check whether this simulates binder aging since production until paving. The binder from RAP was recovered before and after conditioning in a 150 °C oven for an hour, and the binders from each mixture were extracted from the conditioned mixture and recovered for investigation. The binders from the 20 mm nominal size mixtures were not characterised because of experimental limitation in the present study. Details on the technique utilised to age the binders in the RTFO machine and to recover the binder from the mixtures are described in sections 3.3.4.1 and 3.3.4.2, respectively.

The summary of the Samples taken from different sources for binder testing is shown in Table 3-6.

Table 3-6 Sources of binder samples

Source	Number of samples
C320 virgin	2
RTFO aged C320	1
Recovered unconditioned RAP	2
Recovered conditioned RAP	2
Recovered from DG14	2
Recovered from DG14R10	2
Recovered from DG14R20	1
Recovered from DG14R30	2
Recovered C320 form Toluene solution (for verification purposes)	1

Two main types of tests were performed on the binder samples: the penetration test and complex modulus test. The former test has a long history in the literature for ranking purposes and its results indicate how stiff the binder is under certain conditions. However, the latter test investigates the rheological properties of the binder in different situations and leads to a broader understanding of how the binder behaves. In sections 3.3.4.3 and 3.3.4.4 these tests are explained, respectively.

3.3.4.1 Heat and air effect on binder

The properties of a binder might be changed when subjected to air and heat. Such a scenario is likely especially when a HMA is being transferred from the asphalt plant to the site with it being retained hot until paving. To evaluate the effect of this phenomenon on the mixtures in the laboratory, the mixtures are generally kept in the oven for a certain time after mixing to become conditioned. In the present study, based on Australian standards (Australian/New Zealand Standard, 2014), the conditioning occurred over an hour in a 150 °C oven, in comparison, in the USA standards the samples usually retained in a 135 °C oven for four hours similar to (Liske et al., 2011). To characterise the vulnerability of the binders to heat and air, the binder can be tested in the RTFO as shown in Figure 3-8.

Figure 3-8 Rolling thin film oven

The purpose of this test is to simulate the aging of binder from when the materials are mixed until it paving. It is assumed that the aging that occurs when transporting the mixture has the same effects as the conditioning times in the laboratory (Australian/New Zealand Standard, 2015) (SHRP, 1994)

In the RFTO, a high temperature is maintained, as well as a flow of a hot air hits the thin layer of binder in a bottle that rotates continuously. After the binder is conditioned, any change in its performance can be measured.

In the present study, the Australian standard AS2341.10 (Australian/New Zealand Standard, 2015) was followed to investigate the effect of heat and air on the binder. Based on this standard, 35 g of melted and stirred binder was poured into a specific glass bottle as shown in Figure 3-9. If more conditioned material is required, then more than one bottle can be placed in the machine. Then, the binder is left to become cool.

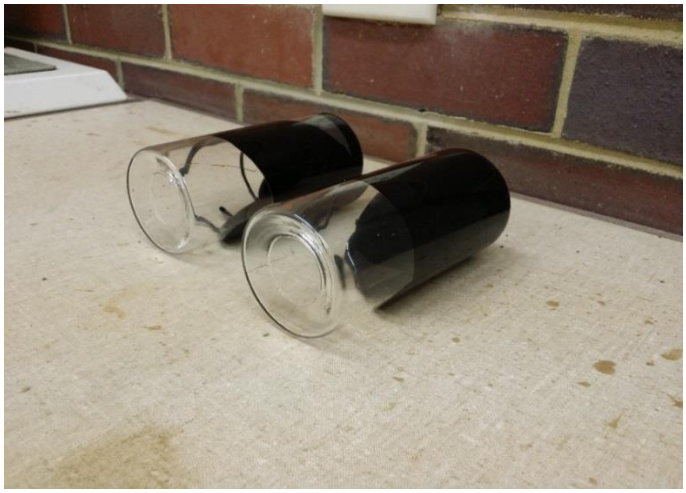

Figure 3-9 Bottles used in RTFO aging process

The oven was preheated until it reached 163 ± 0.5 °C, after which the bottles containing the samples were placed in the carriage in the oven and then the oven closed. The samples were in the carriage with no rotation for 30 ± 1 min and the temperature of the oven was confirmed to be 163 °C. After a waiting period (30 minutes), the carriage and air flow were turned on. The air flow was 4 ± 0.5 L/min while the carriage was rotate 15 ± 0.5 rpm. The carriage setup and hot air flow inside the RTFO machine are illustrated in Figure 3-10.

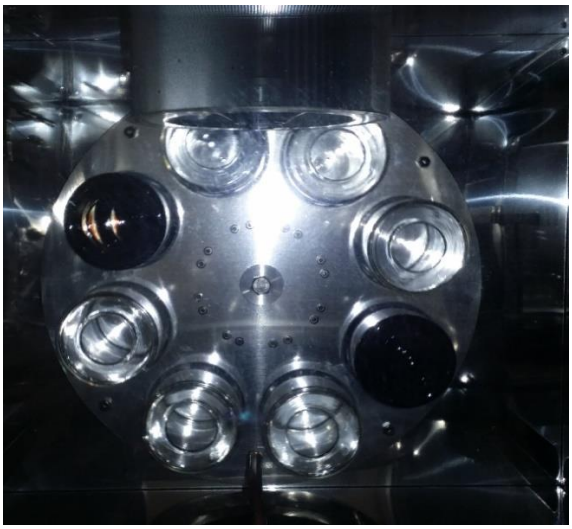

Figure 3-10 Rotating bottle carriage of RTFO

The binders were retained for 60 ± 1 min in the rotating carriage and 163 °C oven, after which the samples were removed and the binder removed from the bottle using a scraper and transferred into an airtight container. The treated binder was tested shortly afterward in the DSR machine after RTFO aging to investigate the differences between the start and the finish of the aging process.

This change was investigated later in the present study by examining the change in properties of the virgin binder after passing through the mixing procedure (including conditioning) and then the recovery procedure to determine whether the assumption in (Bonaquist, 2008), which states that RTFO aging has the same effect as conditioning in the oven during laboratory sample preparation, is true in the present study research or not.

3.3.4.2 Binder recovery

To characterise the binder in the RAP or in mixtures containing RAP, the binder needs to be recovered from the mixture. To recover the bitumen, the European standard EN12697-3 (NSAI, 2013) was followed. Even though using the method M07 developed by ARRB, as described in (Denneman et al., 2013) , for using a RTFO oven to extract the binder from solvent, is common in Australia, this method is not used in this research as this method is only suitable for extracting a small amount of binder. However, in this study, a considerable amount of binder is required to be extracted for

performing a variety of tests including the penetration test and dynamic shear modulus.

In this method, initially the same procedure for determining the binder content of a mix, explained in section 3.3.2, is performed using toluene as a solvent, i.e. the binder is washed from the mixture using an extractor centrifuge. However, for the purpose of binder recovery, the fine particles need to be separated from the resulting solution after the extractor centrifuge. To do this, all the solution is centrifuged again to settle out the fine particles instead of only centrifuging 100 mL of the solution as is the case in the binder content test. Settings are used that assure that the acceleration at the tip of the bottles reaches 15000 m/s^2.

Once the solution is particle free, the solution is then ready bitumen recovery. In this study, based on EN 12697-3 standard, a rotary evaporator, was used to separate the bitumen from the solvent by distillation of the solvent. This procedure involves heating the solution under a vacuum and use of an inert gas (nitrogen). Under specific circumstances, the solvent is evaporated but the binder is left in the container, with the solvent being condensed for further use. In the present study, the Buchi R210 rotary evaporator equipped with an

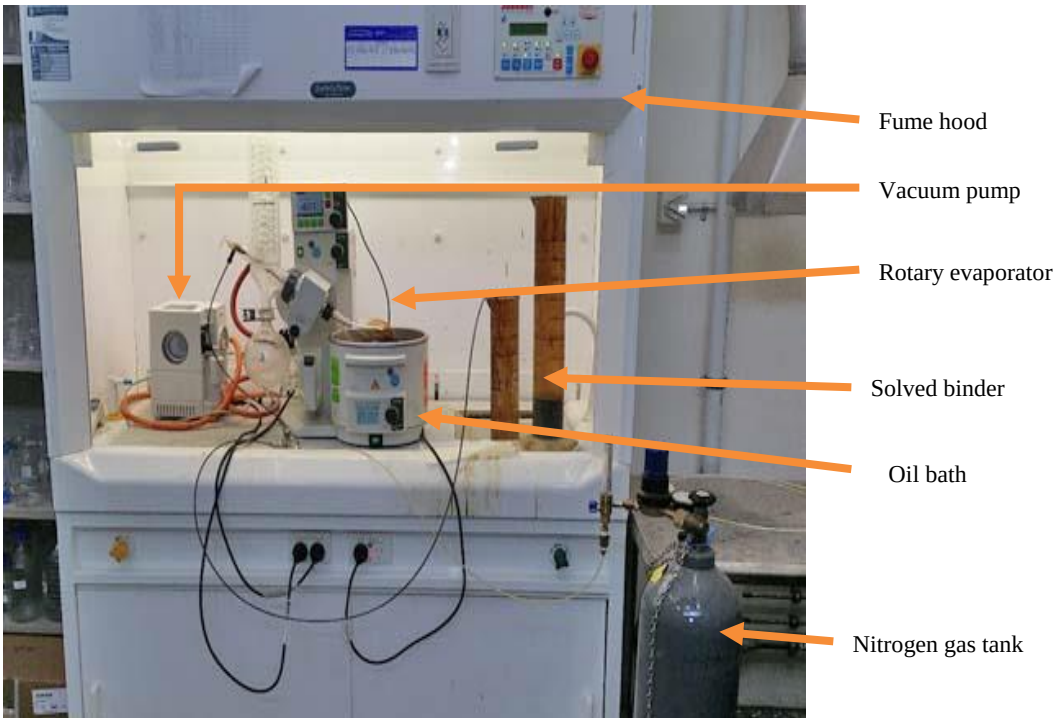

Figure 3-11 Binder recovery setup

oil bath, a vacuum pump and a controller was used. The setup is shown in Figure 3-11.

Based on the standard, to use the rotary evaporator the oil bath was preheated to 110 °C as toluene was used as a solvent. Meanwhile, the cold water flow was allowed to pass through the condenser, and the evaporating flask was lowered into the oil bath and the machine is set to rotate the flask at 75 ± 15 rpm. Subsequently, the pressure in the system was reduced to 40 kPa by adjusting the vacuum controller. Meanwhile, nitrogen gas was allowed into the system to replace the existing air. The induction stopcock was then opened to allow the solution into the evaporating flask gradually. The flow was controlled by adjusting the valve in such a way that the flow in the evaporation flask was almost equal to the rate of distillation in the receiving flask. In addition, the liquid in the evaporation flask did not exceed 400 mL. This process continued until all the solution was passed into the system. It was sometimes necessary to empty the receiving flask during this period. To do so, the vacuum pump was stopped but no air was allowed into the system. Then, the pressure in the system was gradually increased until it reached atmospheric pressure by allowing the nitrogen to move into the system. The solvent in the receiving flask was then emptied using the small valve located at the bottom of the flask. This procedure helps minimise the contact of the distilled bitumen with air.

Once all the solution was in the system, the temperature of the oil bath was raised to 160 ± 5 °C, while the pressure was adjusted slowly to 2 kPa (over 5 min). These conditions were maintained until the distillation process was completed and no bubbles were present in the evaporating flask. To check the bubbling, the rotation could be stopped for a short period. After this step, the receiving flask was emptied as explained previously, after which the pressure was reduced to 2 kPa over 3 min ± 30s that assists with the evaporation of any remaining solvent in the solution. This situation was maintained until the bubbling finished. In the case of very hard bitumen, if after 10 min the bubbling was not finished, the temperature was increased to 185 °C, and this condition maintained until bubbling was finished for a further 10 min. Later, the rotation was stopped and the pressure in the system brought to

atmospheric pressure by letting the nitrogen gas move into the system with no vacuum pump running. Then the flask was wiped and taken out of the apparatus quickly to pour the recovered bitumen into a container with a loose lid. This bitumen was then tested for characterisation. For safety reasons, this recovery process is suggested to be performed under a fume hood.

To determine the minimal effect of the recovery process on the results of the binder tests, a series of tests were conducted on the virgin C320 bitumen and also on the same bitumen that was solved in toluene and then recovered via the procedure mentioned in above.

3.3.4.3 Penetration test

One parameter that can be utilised to describe the stiffness of the bituminous binder is the penetration depth obtained from penetration tests. In the present study, the penetration test was performed based on the Australian standard AS2341.12 (Australian Standard, 1993a), which has a lot of similarities to ASTM D5D5M.

To prepare the samples, binder from each of the mixtures was heated until it became soft and liquid. After stirring the melted binder, it was poured into a conforming container and then left to cool in a 25 °C temperature room for 1 h. Then, it was transferred to a 25 °C water bath to become conditioned for another hour, after which each sample was placed in the penetrometer device while remaining in the transfer dish to maintain the temperature. The setup is shown in Figure 3-12.

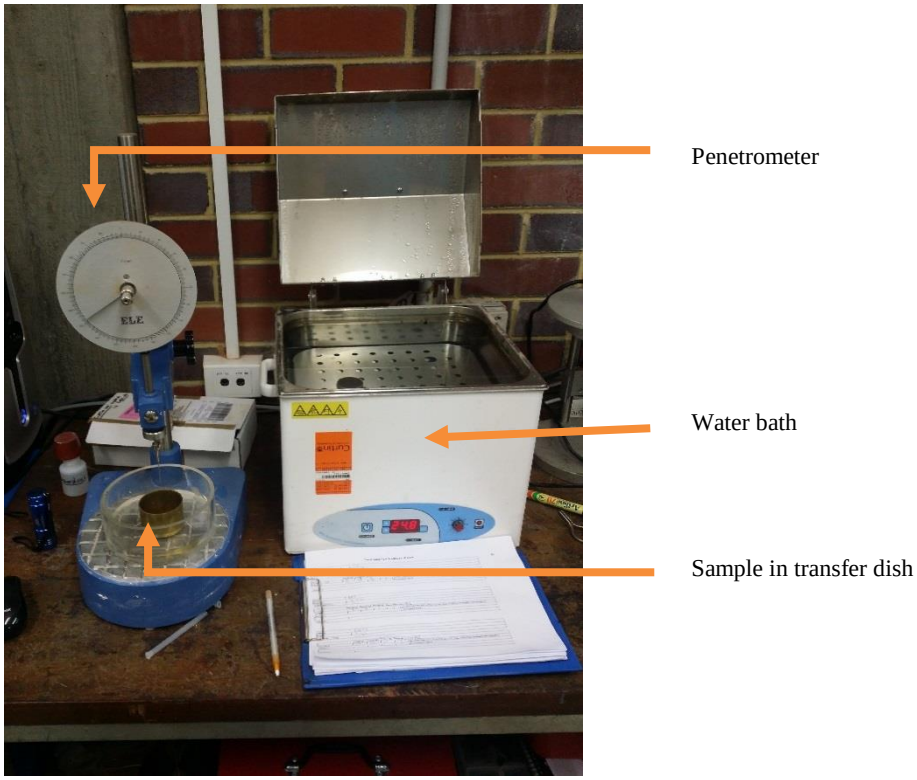

Figure 3-12 Penetration test setup

After securing the sample, the needle of the penetrometer device was adjusted to touch the surface of the sample. The needle and its attached weights have a mass of 100 g. Then, the gauge was set to zero and the needle was released to penetrate the sample under its weight for 5 seconds. After 5 seconds, the needle was fixed back in its place and the penetration depth was read from the gauge to an accuracy of one tenth of a millimeter. The needle was removed, cleaned using a solvent (toluene was used in the present study) and the penetration test was performed another two times on the same sample. The penetration should be performed at a certain distance from previously tested points and the edge of the container. If the results were close enough based on Table 3-7, then the results were considered valid, otherwise, the sample was discarded and the test repeated.

Table 3-7 Penetration results in validity check

Penetration depth (one tenth of a millimetre)	Maximum difference of readings
0–49	2
50–149	4
150–249	6
≥ 250	8

In summary, Table 3-8 presents the penetration tests that were performed in the present.

Table 3-8 Penetration test matrix

Source	Number of penetration tests
C320 virgin	3
RTFO aged C320	3
Recovered unconditioned RAP	3
Recovered conditioned RAP	3
Recovered from DG14	3
Recovered from DG14R10	3
Recovered from DG14R20	3
Recovered from DG14R30	3

3.3.4.4 Complex modulus and viscosity

The complex modulus and viscosity of the binder used in a mixture play vital roles in the behaviour of the mixture. To study the difference of the complex modulus of binders in this study, a DSR was utilised. The ASTM standard D7175(ASTM, 2008) was mainly utilised (with some modifications) for these experiments that were very similar to the Austroad standard AGPT-T192 (Austroads, 2015a). In fact, the ASTM D7175 is one of the references of the previously mentioned Australian standard.

To perform this test, the binder was heated until melting was reached to enable it to be placed on the plates of the DSR machine. Meanwhile, the plates of the DSR machine were preheated as described in the standard being followed. The gap determining the mechanism of the machine was calibrated by closing the gap and setting that position to zero. In the present study, a Kinexus DSR (Malvern Company), shown in Figure 3-13, was utilised. To control the functioning of the machine and to collect and process data, the associated software with the machine, rSpace, was used.

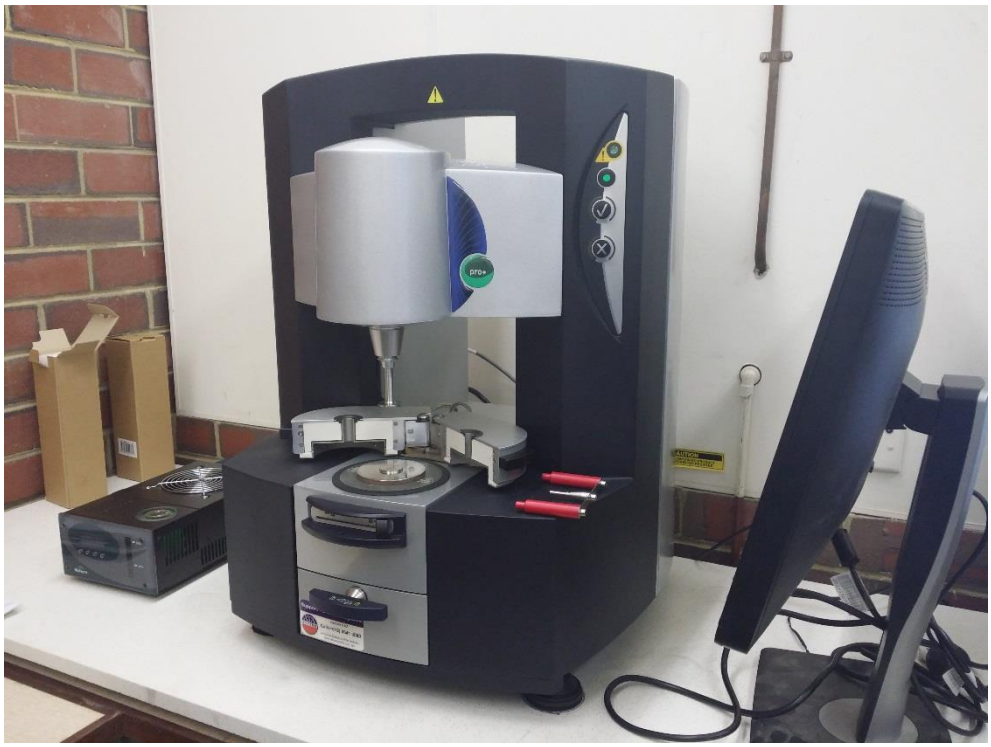

Figure 3-13 Kinexus dynamic shear rheometer

Many types of materials were tested over a wide range of temperatures; therefore, a 25 mm plate was utilised in some cases, whereas an 8 mm plate was used in others Different plate sizes are necessary, because if the sample is very stiff, the machine mechanical capability might not be enough for oscillating the sample in the required way. Moreover, for very soft binders, the amount of torque to oscillate the small plate might be very small, which makes it difficult to measure accurately. Therefore, for the different scenarios investigated in the present study, different size plates were required. To prepare the samples for the 8 mm plate, the stirred melted binder was poured into a silicon mould as shown in Figure 3-14.

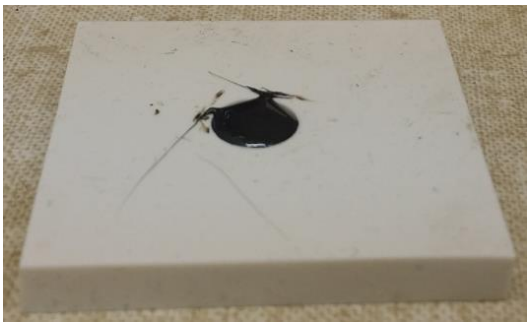

Figure 3-14 DSR sample in a silicon mould

After cooling at room temperature, it was placed on a preheated 8mm plate in the DSR machine. However, for the 25 mm samples, a sufficient amount of the heated and stirred binder was poured directly onto the preheated lower 25 mm plate in the DSR machine as is depicted in Figure 3-15.

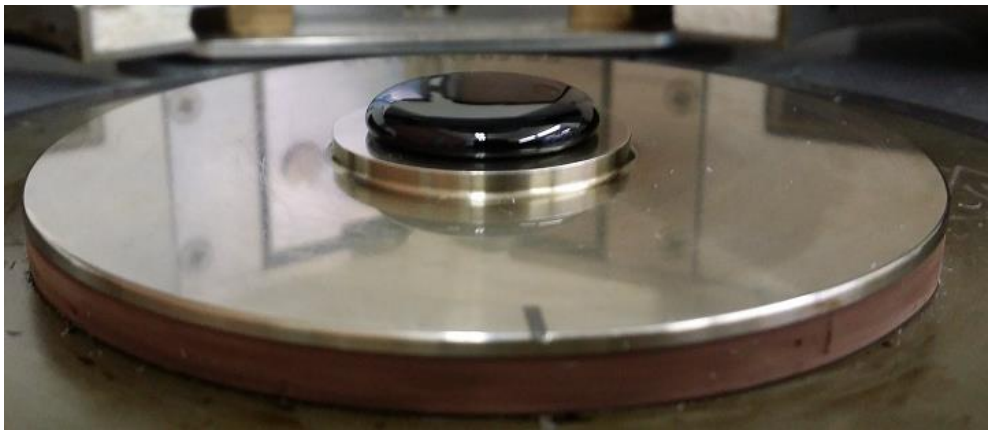

Figure 3-15 DSR sample on a 25 mm plate

After placement of the sample onto the preheated plates in the DSR machine, the top plate was lowered down to a trimming gap. This gap is to a specific height where if the sample was trimmed to that gap, after adjusting the height to the testing gap, the shape of the edge of the sample has a proper bulge as shown in Figure 3-16. The trimming and testing gaps utilised in the present study were 1.05 and 1 mm for 25 mm samples, respectively, while for their 8 mm counterparts, they were 2.1 and 2mm, respectively. These gaps are recommended in the ASTM D7175 standard and it was satisfactorily for using in this research also.

Figure 3-16 Bulge of a DSR sample

For trimming, a heated curved metal thin chemistry spatula was used (Figure 3-17). Then, the gap was set to the testing gap.

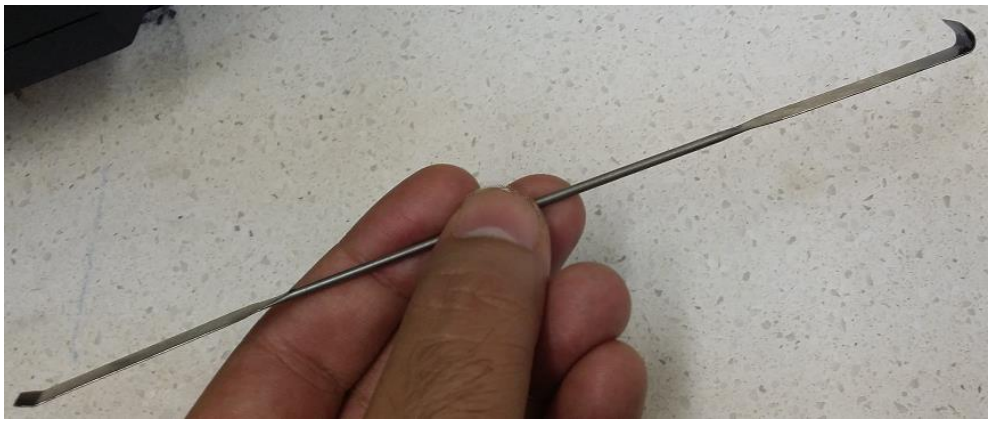

Figure 3-17 Spatula used for trimming DSR samples

At the next step, the temperature controlled chamber was closed and the temperature set to a testing temperature using rSpace software. Then, the sample was left to achieve equilibrium in the testing temperature for at least 10 minutes to prepare it for testing.

To run the test, the sample description was loaded into the rSpace software. Then the specific sequence was executed and the required information was filled in the sequence such as the testing temperature, loading frequency and strain amplitude. The test then began and the system applied a specific torsional load (based on load parameters set by the user) and recorded the behavior of the sample. It also calculated the complex modulus (G^*), elastic modulus (G'), viscous modulus (G''), complex viscosity (η^*) and phase angle automatically based on the collected data and equations explained in section 2.3.1.

In the present study, the master curve of the binder's complex modulus and phase angle was generated, as explained in the next section, to compare the performance of binder more easily. Having the master curve constructed the properties can be conveniently extracted for a given frequency or temperature using temperature-time superposition concept. To characterise the binder in a vast range of temperature and frequency conditions, which is necessary to generate a reliable master curve, the customization capability of Kinexus system was utilized. This system lets the user customise test sequences in

rSpace software to perform several tests with different conditions automatically, consecutively. Thus, a series of sequences were defined to achieve the strain controlled oscillation tests at different frequencies between 0.1 and 10 Hz with a specific logarithmic interval. The used sequence could also change the temperature to different predefined temperatures at the completion of the test and enable conditioning of the sample before it repeated the frequency sweep test again. This feature was utilised to measure the complex modulus and phase angle of binder in a wide range of temperature and frequencies. The details for constructing the master curve are explained in Section 3.3.4.4.1.

3.3.4.4.1 Binder complex modulus/phase angle master curve construction

In the present study, the master curve of the complex modulus and phase angle of each type of binder was produced to enable more convenient comparisons between them, as master curves shape can be interpreted over a wide range of temperatures or frequencies. This also helps with predicting the properties of the binder in a condition that might not be tested experimentally. The model used for the master curve is considered a sigmoidal function and the Arrhenius shift factor function was used. Details of the model and shift factor have been explained in sections 2.4.1 and 2.4.2, respectively. Ensuring the Arrhenius shift factor function is substituted in the sigmoidal shape master curve model results in the master curve equation becoming equation (3-1):

$$log\ |G^*| = \delta + \frac{\alpha}{1 + e^{\beta+\gamma(log\omega+C\left[\left(\frac{1}{T}\right)-\left(\frac{1}{T_r}\right)\right])}} \qquad (3\text{-}1),$$

where, G^* is the complex shear modulus of a binder, ω is the frequency of interest (Hz), δ is the minimum value of $|G^*|$, α is the difference between the maximum and minimum value of $|G^*|$, T is the temperature of interest, T_r is the reference temperature of the master curve, while C, β and γ are parameters to adjust the model. Because the glossy modulus of a binder is the maximum G* it can have, the parameter α is substituted by the glossy modulus minus δ.

The value of the glossy modulus is considered 1 GPa, as this is the value suggested in the literature e.g. (Bonaquist, 2008) for pavement grade binders.

As the minimum and maximum values of G^* were unknown, they were determined during the numerical optimisation stage. Therefore, there were five parameters optimised based on averaged available experimental data for each condition.

In the present study, the temperature reference for binder master curves is considered to be between 20 and 60 °C. In addition, for a reason that will be explained further in section 4.6, the master curves of several binders are constructed between 4 and 40 °C. Based on this approach, the data collected in the complex modulus test by the DSR machine was used to construct a master curve.

To determine the best match of equation to the available data, a SSE function such as equation (3-2) was applied as an objective function to be minimised using a proper optimisation technique by adjusting optimisation parameters; δ, α, C, β and γ. In the present study, Microsoft Excel solver function was applied as an optimisation tool to adjust the optimisation parameters to fit the master curve model:

$$Objective\ function = \sum_{i=1}^{n} \frac{\left(\log(G_{p_i}^*) - \log(G_{m_i}^*)\right)^2}{(\log(G_{m_i}^*))^2} \qquad (3\text{-}2),$$

where, G^*_m is the i_{th} measured complex modulus, G^*_p is the predicted complex modulus from the master curve model for the i_{th} data and n is the number of data records.

3.3.4.4.2 Binder grading

Two approaches were applied to grade the binders as follows.

3.3.4.4.2.1 Performance base grading (Superpave)

To grade the binders using the Superpave method, a similar approach to the techniques explained by (McDaniel & Anderson, 2001) and (Prithvi S Kandhal & Foo, 1997) was followed. However, only the high temperature of

the binders were graded in the present study because (Prithvi S Kandhal & Foo, 1997) recommended that intermediate temperatures were not suitable for predicting the intermediate temperature of the blended binder. To determine the high temperatures from the experimental tests, the method applied in (ASTM, 2008) was utilised, which is similar to the method used in section 2.2.3.1. In this method, the binder was placed between two 25 mm plates and conditioned in a temperature that is equal to or below the high temperature of the binder in the DSR machine. Then the 10 rad/s loading frequency with a specified strain level was applied to the specimen and the value of the complex shear modulus and phase angle was measured and the value of G*/Sin(δ) calculated. The temperature was then increased at specific intervals (usually 6 °C) and the test repeated until the value of G*/Sin(δ) becomes smaller than a specific value. There are two scenarios for this specific value. In the first scenario, the binder is assumed to be virgin, therefore, the value is taken to be equal to 1 KPa, while in the second scenario the binder is considered to be RTFO aged and the value is considered to be equal to 2.2 KPa. Based on interpolation between the last two temperatures for each scenario, the critical high temperature of the binder was obtained by choosing the minimum of the two interpolated temperature. It should be noted that the recommended strain amplitude for virgin binder and RTFO aged binder are recommended to equal 12 and 10 % respectively in the standard.

3.3.4.4.2.2 Viscosity based grading

The complex viscosity of the mixtures can be used to grade the binders as explained in section 2.2.3.3 and Table 2-6. The complex viscosity of the binders were obtained from (Austroads, 2015a) using a DSR apparatus at 60 °C, 1 rad/s and 10% strain. Then, based on the log value of the complex viscosity and the ranges defined in Table 2-6, the grade of the binder was determined.

3.3.4.4.3 Modification of test procedures

While conducting the test, several issues needed to be considered to achieve meaningful results, i.e. the size of the plate used in the DSR machine and the linear region of the material.

3.3.4.4.3.1 Modification of test plate size

An issue related to the size of the plate used in the DSR machine arises from the fact that the binder stiffness changes dramatically with changes in temperature. Therefore, if only one plate size was used during the tests, one of the following situations might occur. If a relatively large plate size is used, although at high temperatures it works adequately, at low temperatures the torque required to oscillate the binder might be outside the capability range of the machine. Conversely, if only a small plate was used, although the machine is capable of providing the torque needed at the lower temperatures, at high temperatures because of the very low stiffness of the sample, the parameters needing to be monitored become too small, which make it difficult for the machine to measure them accurately. Therefore, for different temperatures or binders, different plate sizes should be used. In the present study, the 8mm plate was used for all the binder when the test temperature was lower or equal to 40°C. For test temperatures greater than 40°C, 25mm plate was used for all the binders except the Recovered binders from RAP. For Recovered RAP binders, 8mm plates were used instead. However, for performance grading of the all binders including Recovered RAP binders, 25mm plates were used.

The ASTM (2008) standard recommends the use of a 25 mm plate for the DSR test, with the purpose of this standard being to rank the binders or determine the high/intermediate temperature of binders. Therefore, a relatively large plate is fine for this purpose. However, the present study includes low temperatures as well as high temperatures, so these modifications to the plate sizes were required.

To ensure that the size of the plate does not affect the result of the tests, several tests were completed using both plates with under identical conditions (as explained in section 4.3.1.1.1).

3.3.4.4.3.2 Modification of test strain level and investigation of linear region

In ASTM (2008) it is recommended to use 12, 10 and 1%strain for virgin, RTFO conditioned and PAV conditioned binders, respectively, for

characterisation purposes. However, in Austroads (2015a), 10% shear strain is recommended for RAP binders at 60 °C. In the present study, the majority of the tests were performed by applying 1%t shear strain because it can be used on all the samples at all the studied temperatures, no matter how stiff or soft they were using the Kinexus system. This might be in contrast to what is recommended in the standards; however, the main aim of the present study was to compare the performance of different mixtures. Therefore, all the other parameters were kept constant for the sake of comparison. Although the level of strain was different in the present study than for the standards, an analysis was undertaken to determine whether the material was in its linear region while testing, in order for the results to be used for constructing master curved via linear viscoelastic superposition theory. To do so, a different type of sequence was applied to sweep the strain level of oscillation with recommended frequency by standards in different testing temperatures on the sample. If the results for each binder revealed no significance change, the results were considered to be suitable for use in temperature-time superposition equations. Thus, if the strain amplitude was in the linear region, the results were independent of the level of strain and the material behaviour was in a linear region.

To investigate the linear region of the binders, strain amplitude tests were performed at different temperatures (5, 15, 40 and 70 °C) and changing the strain level in the range of 0.1 to either 12% or the maximum strain level was possible because of the stiffness of the binder and the machine capabilities.

3.3.4.4.4 Binder complex modulus test matrix

Overall, more than 5000 records were collected for the complex modulus tests in the present study. The test matrix of the complex modulus related tests that were conducted are depicted in Table 3-9. The information in the Table is not including the tests were undertaken to determine the critical high temperature of the binders.

Table 3-9 Number of binder complex modulus tests for each temperature-source per source

	Number of tests for each source									
Temperature (°C)	Virgin binder	Recovered Conditioned RAP	Recovered Unconditioned RAP	Recovered from DG14R0	Recovered from DG14R10	Recovered from DG14R20	Recovered from DG14R30	RTFO	Virgin C320 (RV)	Recovered C320(RV*)
5	4-1*	1*	1*	4-1*	4-1*	2-1*	4-1*	2-1*		
15	1*	1*	1*	1*	1*	1*	1*	1*		
20	4	4	4	4	4	2	4	2	1	1
30	4	4	4	4	4	2	4	2		
40	6-1*	4-1*	4-1*	4-1*	4-1*	2-1*	4-1*	2-1*	1	1
50	4	4	4	4	4	2	4	2		
60	4	4-1*	4-1*	4	4	2	4	2	1	1
70	4-1*	4-1*	4-1*	4-1*	4-1*	2-1*	4-1*	2-1*		
80		4	4							
Total Number of tests	31-4*-	28-5*	28-5*	28-4*	28-4*	14-4*	28-4*	14-4*	3	3

(*-fixed frequency-varying strain amplitude)

3.4 Mixture preparation and characterisation

In this section, the mixtures involved in the present study are introduced, and the technique utilised to combine the stockpile of aggregates and other components to produce the grading of the combination matched with the target mixtures' grading are explained. In addition, the method to include RAP in the mixture while maintaining a binder content similar to the target binder content is presented, as is the procedure to make and verify the mixture in the laboratory. Finally, details of how the performance of the mixture is assessed for a variety of tests are provided.

3.4.1 Investigated mixtures

In the present study, eight mixtures were investigated, two typical dense-graded mixtures having four different percentages of RAP added (0, 10, 20 and 30%). The mixtures containing each nominal size had the same grading, binder content and binder type (C320). Therefore, two typical mixtures with

a nominal size of 14 mm, referred to as DG14, and 20 mm, called DG20, were utilised as control mixtures. Different percentages of RAP were added to the mixtures so that the grading and binder content remained the same as the original control mixtures, meaning that any change in performance could be monitored in terms of the presence of RAP. A summary of the properties of the mixtures in the present study are described in Table 3-10.

Table 3-10 Investigated mixtures

Mixture	Type	Nominal size(mm)	RAP content (% of total weight)
DG14	Dense-graded	14	0
DG14R10	Dense-graded	14	10
DG14R20	Dense-graded	14	20
DG14R30	Dense-graded	14	30
DG20	Dense-graded	20	0
DG20R10	Dense-graded	20	10
DG20R20	Dense-graded	20	20
DG20R30	Dense-graded	20	30

The mixtures in the present study were designed based on Main Roads Western Australia (2011d), two typical dense-graded mixtures with a nominal size of 14 and 20 mm for heavy traffic conditions (75 marshal blow/120 gyratory cycles) using C320 binder were utilised as control mixtures. The target PSD of the 14 mm mixture was selected to comply with MRWA specifications while the PSD of 20 mm mixture was given by the supplier to replicate the exact job mix design in the laboratory. The binder content of the conforming DG14 mixture was chosen to be 4.7% by weight, based on Main Roads Western Australia (2013) reccommandation. the binder content of the replicated DG20 mixture was 4.3% by weight, which is approved as the correct binder content obtained from the asphalt plant whose mixture was being replicated. In addition, the target air-void of both mixtures was 5% and the hydrated lime added 1.5% of the weight of aggregates in the mixture based

on (Main Roads Western Australia, 2013). The target PSD of these mixtures are shown in Table 3-11.

Table 3-11 The target PSD of mixtures

	% passes through sieve	
Sieve size (mm)	DG14	DG20
26.5	100.0	100.0
19.0	100.0	99.0
13.2	98.3	82.0
9.50	83.9	71.0
6.70	68.4	55.0
4.75	54.0	45.0
2.36	35.9	33.0
1.18	24.1	23.00
0.600	16.4	17.00
0.300	11.0	12.00
0.150	6.9	8.5
0.075	4.5	4.5

Figure 3-18 and Figure 3-19 illustrate the target PSDs and acceptable range of tolerance of PSD based on specification 510 Main Roads Western Australia (2011a) for 14 mm mixture and approved job mix design of the asphalt manufacturer for 20 mm mixture, respectively.

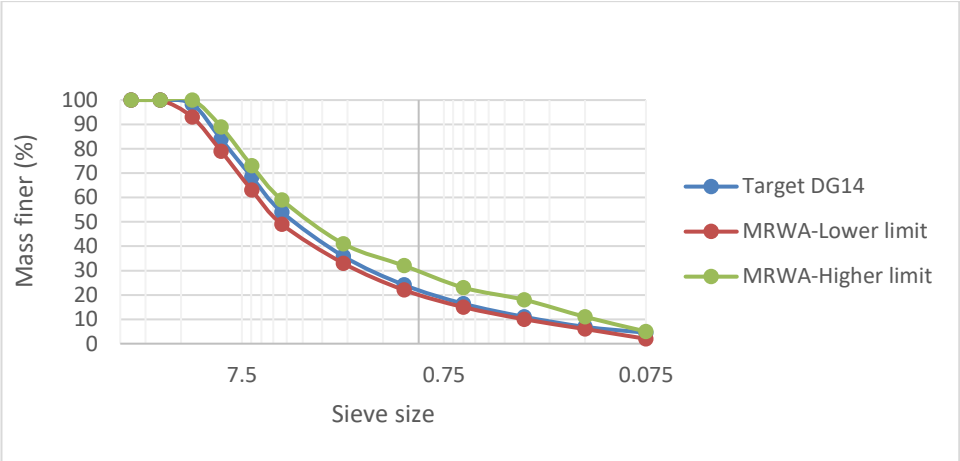

Figure 3-18 The PSD of 14 mm mixtures and the size distribution limits of Main Roads Western Australia (2011a)

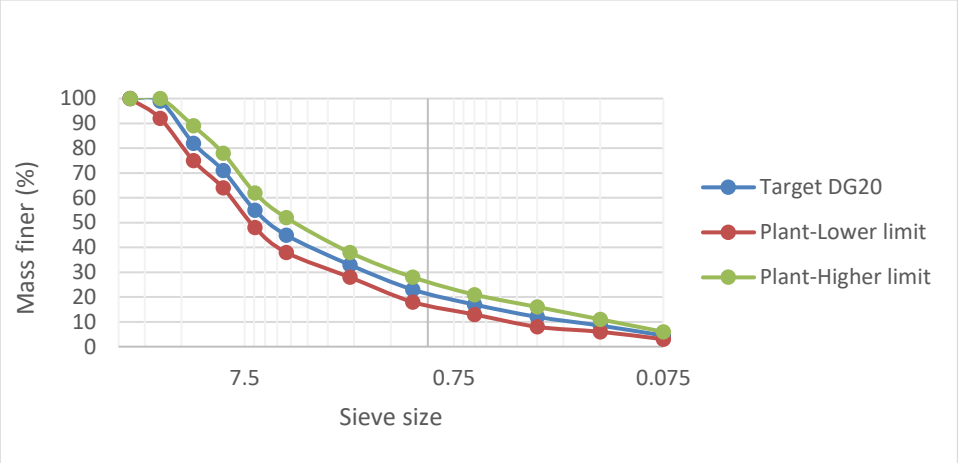

Figure 3-19 The PSD of 20 mm mixtures and the size distribution limits of Main Roads Western Australia (2011a)

3.4.2 Aggregate Combination in the Mixtures

In an asphalt plant, specific amounts of individual aggregates from stockpiles are mixed together to create a specific target grading. Although this approach is appropriate when working with a large amount of material, at smaller scales mixtures produced by this method might show significant amounts of discrepancies in grading. Because the purpose of the present study was to investigate the influence of RAP in the mixture, it was necessary to minimise any changes in any parameters other than RAP. Therefore, to replicate what occurs in an asphalt plant and also ensure the comparison is reliable, the grading from the asphalt plant was replicated for all the mixtures by carrying out the following procedures.

The percentage of each stockpile to produce the mixtures was determined in such a way that, after addition of the appropriate amount of filler and recycled asphalt, the final product had a similar grading to the targeted PSD. Then, the aggregates from the stockpile were mixed with the calculated proportion but with no RAP or hyrated lime. The mixture was then sieved in all fractions used in the PSD analysis and divided into different fractions. These fractions were utilised to replicate precisely the target gradation when batching for the asphalt mixture occurred.

In practice, 8 kg batches were created using stockpile aggregates and appropriate ratios. These batches were sieved using a sieve shaker as shown in Figure 3-20. During the first stage, this material was divided into different sizes including 19, 13.2, 9.5, 6.7, 4.75, 2.36 mm and the sieve pan. During the next stage, the material on the pan from the first stage that had passed through sieve 2.36 mm were sieved again in 2 kg batches and divided into smaller sizes: 1.18, 0.600, 0.300, 0.150, 0.075 mm and the sieve pan.

Figure 3-20 Sieve shaker for aggregate separation

All the divided materials were then washed with water to remove any remaining dust or smaller particles before drying them in the oven until they reached a constant mass as illustrated in Figure 3-21.

Figure 3-21 Setup for aggregate washing

This approach guarantees that the gradation from virgin aggregates is always constant while the fractions are obtained from stockpiles in a similar ratio that occurs in an asphalt plant. To find the share of each stockpile to achieve the target PSD, equation (3-3) can be applied (Austroads, 2007a):

$$P = Aa + Bb + Cc + \cdots \quad (3\text{-}3)$$

where, P is the passing percentage of the combination of aggregates from a specific size sieve, A, B, C, and so on are the passing percentages of each material from a specific size sieve and a, b, c, and so on are the proportion of each material in the combination in percentage. The summation of all lower-case letters is equal to one. The proportion of each material can be found by letting all of them to be zero at the beginning and then adjusting them by try and error, starting from the coefficient related to the finest material.

As the virgin aggregates are sieved after mixing with the appropriate ratio, a portion of the finer materials might get lost in the sieving process. To compensate for this, the combined aggregate used in equation (3-3) is adjusted slightly to produce finer particles. However, the adjustment is expected not to affect the grading accuracy as the mixture is produced by combining all individual fractions to replicate the target PSD.

When adding RAP to a mixture several issues need to be considered, with the procedures that were followed to design the batches utilised in the present study for mixtures with and without RAP explained in the following sections.

3.4.2.1 Design grading for mixtures without RAP

The components of the control mix that had no added RAP were aggregates, hydrated lime and bitumen. To determine the contribution ratio of different stockpiles in these mixtures, equation (3-3) was applied. With this equation, the share of hydrated lime is considered to be 1.5% by weight of total aggregates as the Main Roads Western Australia (2013) standard suggests. The shares of each stockpile were allocated so that the combination of all aggregates included slightly more fine aggregates than the target PSD to compensate for the escape of fine material in later sieving processes. These adjustments were made from observations on the first series of aggregate sieving results. The proportions of each stockpile that were used to reach the adjusted combined aggregates for DG14 and DG20 can be seen in Table 3-12 and Table 3-13, respectively.

Table 3-12 The proportions of stockpiles in the 14 mm control mixture

		% passed for each sieve size (mm)											
Material	**% of proportion**	**26.5**	**19.0**	**13.2**	**9.50**	**6.70**	**4.75**	**2.36**	**1.18**	**0.600**	**0.300**	**0.150**	**0.075**
14 mm	**15.0**	100	100	88.7	15.0	2.3	1.5	1.3	1.3	1.2	1.0	0.9	0.7
10 mm	**16.5**	100	100	100	81.8	15.3	2.6	1.5	1.4	1.4	1.2	1.1	0.9
7 mm	**17.5**	100	100	100	99.5	86.3	24.5	2.1	1.1	0.9	0.9	0.7	0.7
5 mm	**7.0**	100	100	100	100	100	86.5	19.3	8.7	6.2	5.1	4.1	3.1
Dust	**42.5**	100	100	100	100	100	99.7	78.5	53.6	36.3	24.1	14.9	9.9
Hydrated lime	**1.5**	100	100	100	100	100	100	100	100	100	100	100	95.0
Combined PSD		100	100	98.3	84.2	69.0	54.9	37.0	25.5	17.9	12.6	8.6	6.2
Target PSD		100	100	98.3	83.9	68.4	54.0	35.9	24.1	16.4	11.0	6.9	4.5

Table 3-13 The proportions of stockpiles in the 20 mm control mixture

		% passed for each sieve size (mm)											
Material	**% of proportion**	**26.5**	**19.0**	**13.2**	**9.50**	**6.70**	**4.75**	**2.36**	**1.18**	**0.600**	**0.300**	**0.150**	**0.075**
20 mm	**27.0**	100	95.8	32.4	8.1	4.3	3.2	2.5	2.2	2.0	1.8	1.5	1.2
14 mm	**0.0**	100	100	88.7	15.0	2.3	1.5	1.3	1.3	1.2	1.0	0.9	0.7
10 mm	**21.0**	100	100	100	81.8	15.3	2.6	1.5	1.4	1.4	1.2	1.1	0.9
7 mm	**11.0**	100	100	100	100	87.8	29.2	4.9	2.9	2.2	1.8	1.4	1.1
5 mm	**2.0**	100	100	100	100	100	86.5	19.3	8.7	6.2	5.1	4.1	3.1
Dust	**37.5**	100	100	100	100	100	99.7	78.5	53.6	36.3	24.1	14.9	9.9
Hydrated lime	**1.5**	100	100	100	100	100	100	100	100	100	100	100	95.0
Combined PSD		100	98.9	81.8	71.4	55.0	45.2	32.9	23.0	16.3	11.6	8.0	5.8
Target PSD		100	99.0	82.0	71.0	55.0	45.0	33.0	23.0	17.0	12.0	8.5	4.5

The individual stockpiles are then mixed based on the ratios obtained from Table 3-12 and Table 3-13 for the DG14 and DG20 mixtures, respectively. Then the mixtures were divided into all fraction sizes for PSD analysis as explained in Section 3.4.2. Later, for batching asphalt mixtures, these fractions were used to replicate the target PSD mentioned in Table 3-11.

3.4.2.2 Design grading for mixtures containing RAP

In these types of mixtures, the grading of RAP needs to be considered in the grading of the total mixture. Therefore, before determining the share of each stockpile for sieving batches, the target PSD of the virgin aggregates needed to be calculated for each mixture using equation (3-3) to maintain the same grading for the combination as that of the control mixtures.

The proportion of materials, apart from than the binder, for the mixtures DG14R10, DG14R20, DG14R30, DG20R10, DG20R20 and DG20R30 are presented in Table 3-14, Table 3-15, Table 3-16, Table 3-17, Table 3-18, and Table 3-19, respectively.

Table 3-14 The proportion of aggregates, hydrated lime and RAP in DG14R10 mixture

		% passed for each sieve size (mm)											
Material	**% of proportion**	**26.5**	**19.0**	**13.2**	**9.50**	**6.70**	**4.75**	**2.36**	**1.18**	**0.600**	**0.300**	**0.150**	**0.075**
Aggregate	**88.4**	100	100	98.1	82.5	66.9	52.3	34.3	22.0	14.0	8.9	5.0	2.8
Hydrated lime	**1.5**	100	100	100	100	100	100	100	100	100	100	100	95.0
RAP	**10.1**	100	100	99.9	93.8	77.3	61.6	40.8	31.3	24.6	16.7	9.8	6.2
Combined PSD		100	100	98.3	83.9	68.4	54.0	35.9	24.1	16.4	11.0	6.9	4.5
Target PSD		100	100	98.3	83.9	68.4	54.0	35.9	24.1	16.4	11.0	6.9	4.5

Table 3-15 The proportion of aggregates, hydrated lime and RAP in DG14R20 mixture

		% passed for each sieve size (mm)											
Material	**% of proportion**	**26.5**	**19.0**	**13.2**	**9.50**	**6.70**	**4.75**	**2.36**	**1.18**	**0.600**	**0.300**	**0.150**	**0.075**
Aggregate	**78.4**	100	100	97.9	81.0	65.5	51.2	33.4	20.8	12.7	7.9	4.4	2.3
Hydrated lime	**1.5**	100	100	100	100	100	100	100	100	100	100	100	95.0
RAP	**20.1**	100	100	99.9	93.8	77.3	61.6	40.8	31.3	24.6	16.7	9.8	6.2
Combined PSD		100	100	98.3	83.9	68.4	54.0	35.9	24.1	16.4	11.0	6.9	4.5
Target PSD		100	100	98.3	83.9	68.4	54.0	35.9	24.1	16.4	11.0	6.9	4.5

Table 3-16 The proportion of aggregates, hydrated lime and RAP in DG14R30 mixture

		% passed for each sieve size (mm)											
Material	**% of proportion**	**26.5**	**19.0**	**13.2**	**9.50**	**6.70**	**4.75**	**2.36**	**1.18**	**0.600**	**0.300**	**0.150**	**0.075**
Aggregate	**68.4**	100	100	97.6	79.2	63.8	49.6	32.3	19.3	11.0	6.6	3.5	1.8
Hydrated lime	**1.5**	100	100	100	100	100	100	100	100	100	100	100	95.0
RAP	**30.1**	100	100	99.9	93.8	77.3	61.6	40.8	31.3	24.6	16.7	9.8	6.2
Combined PSD		100	100	98.3	83.9	68.4	54.0	35.9	24.1	16.4	11.0	6.9	4.5
Target PSD		100	100	98.3	83.9	68.4	54.0	35.9	24.1	16.4	11.0	6.9	4.5

Table 3-17 The proportion of aggregates, hydrated lime and RAP in DG20R10 mixture

		% passed for each sieve size (mm)											
Material	**% of proportion**	**26.5**	**19.0**	**13.2**	**9.50**	**6.70**	**4.75**	**2.36**	**1.18**	**0.600**	**0.300**	**0.150**	**0.075**
Aggregate	**88.5**	100	98.9	79.7	67.9	51.7	42.2	31.0	20.2	14.2	9.4	6.2	2.7
Hydrated lime	**1.5**	100	100	100	100	100	100	100	100	100	100	100	95.0
RAP	**10**	100	100	99.9	93.8	77.3	61.6	40.8	31.3	24.6	16.7	9.8	6.2
Combined PSD		100	99.0	82.0	71.0	55.0	45.0	33.0	22.5	16.5	11.5	8.0	4.4
Target PSD		100	99.0	82.0	71.0	55.0	45.0	33.0	22.5	16.5	11.5	8.0	4.4

Table 3-18 The proportion of aggregates, hydrated lime and RAP in DG20R20 mixture

		% passed for each sieve size (mm)											
Material	**% of proportion**	**26.5**	**19.0**	**13.2**	**9.50**	**6.70**	**4.75**	**2.36**	**1.18**	**0.600**	**0.300**	**0.150**	**0.075**
Aggregate	**78.5**	100	98.7	77.1	64.6	48.5	39.7	29.7	18.8	12.8	8.5	5.8	2.2
Hydrated lime	**1.5**	100	100	100	100	100	100	100	100	100	100	100	95.0
RAP	**20**	100	100	99.9	93.8	77.3	61.6	40.8	31.3	24.6	16.7	9.8	6.2
Combined PSD		100	99.0	82.0	71.0	55.0	45.0	33.0	22.5	16.5	11.5	8.0	4.4
Target PSD		100	99.0	82.0	71.0	55.0	45.0	33.0	22.5	16.5	11.5	8.0	4.4

Table 3-19 The proportion of aggregates, hydrated lime and RAP in DG20R30 mixture

		% passed for each sieve size (mm)											
Material	**% of proportion**	**26.5**	**19.0**	**13.2**	**9.50**	**6.70**	**4.75**	**2.36**	**1.18**	**0.600**	**0.300**	**0.150**	**0.075**
Aggregate	**68.5**	100	98.5	73.7	60.4	44.2	36.5	28.1	16.9	11.1	7.3	5.2	1.6
Hydrated lime	**1.5**	100	100	100	100	100	100	100	100	100	100	100	95.0
RAP	**30**	100	100	99.9	93.8	77.3	61.6	40.8	31.3	24.6	16.7	9.8	6.2
Combined PSD		100	99.0	82.0	71.0	55.0	45.0	33.0	22.5	16.5	11.5	8.0	4.4
Target PSD		100	99.0	82.0	71.0	55.0	45.0	33.0	22.5	16.5	11.5	8.0	4.4

In summary, the PSD of the virgin aggregates of different mixtures containing RAP to produce the target PSD of the control mixtures when added to other components are shown in Table 3-20.

Table 3-20 The PSD of virgin aggregates combination for mixtures containing RAP

	% passed for each sieve size (mm)											
Mixture	**26.5**	**19.0**	**13.2**	**9.50**	**6.70**	**4.75**	**2.36**	**1.18**	**0.600**	**0.300**	**0.150**	**0.075**
DG14R10	**100**	**100**	**98.1**	**82.5**	**66.9**	**52.3**	**34.3**	**22.0**	**14.0**	**8.9**	**5.0**	**2.8**
DG14R20	**100**	**100**	**97.9**	**81.0**	**65.5**	**51.2**	**33.4**	**20.8**	**12.7**	**7.9**	**4.4**	**2.3**
DG14R30	**100**	**100**	**97.6**	**79.2**	**63.8**	**49.6**	**32.3**	**19.3**	**11.0**	**6.6**	**3.5**	**1.8**
DG20R10	**100**	**98.9**	**79.7**	**67.9**	**51.7**	**42.2**	**31.0**	**20.2**	**14.2**	**9.4**	**6.2**	**2.7**
DG20R20	**100**	**98.7**	**77.1**	**64.6**	**48.5**	**39.7**	**29.7**	**18.8**	**12.8**	**8.5**	**5.8**	**2.2**
DG20R30	**100**	**98.5**	**73.7**	**60.4**	**44.2**	**36.5**	**28.1**	**16.9**	**11.1**	**7.3**	**5.2**	**1.6**

The share of individual stockpiles of virgin aggregates then needed to be determined to achieve the PSD's of the virgin aggregates, with these being determined using equation (3-3) in such a way that it produces finer aggregates to eliminate the effect of lost particles during the sieving procedure. There were no significant differences between PSD's for each group of DG14 or DG20 mixtures (Table 3-20). Therefore, for determining the share of stockpiles for the purpose of sieving the aggregates into fractions, only the PSD of DG14R20 and DG20R20 were considered. The ratio that was calculated for the 20% RAP inclusion (between 10 and 30%) was applied to the 10 and 30% RAP mixtures for both DG14 and DG20. The proportions for each stockpile were calculated as shown in Table 3-21 and Table 3-22 for DG14R20 and DG20R20, respectively. The summary of used proportions is shown in Table 3-23.

Table 3-21 The proportion of stockpiles for 14 mm mixtures containing RAP

		% passed for each sieve size (mm)											
Material	**% of proportion**	**26.5**	**19.0**	**13.2**	**9.50**	**6.70**	**4.75**	**2.36**	**1.18**	**0.60**	**0.30**	**0.150**	**0.075**
14 mm	**19.0**	100	100	88.7	15.0	2.3	1.5	1.3	1.3	1.2	1.0	0.9	0.7
10 mm	**16.0**	100	100	100	81.8	15.3	2.6	1.5	1.4	1.4	1.2	1.1	0.9
7 mm	**18.0**	100	100	100	99.5	86.3	24.5	2.1	1.1	0.9	0.9	0.7	0.7
5 mm	**7.0**	100	100	100	100	100	86.5	19.3	8.7	6.2	5.1	4.1	3.1
Dust	**40.0**	100	100	100	100	100	99.7	78.5	53.6	36.3	24.1	14.9	9.9
Combined PSD		100	100	97.9	80.8	65.4	51.1	33.6	22.7	15.5	10.5	6.7	4.6
Target PSD		100	100	97.9	81.0	65.5	51.2	33.4	20.8	12.7	7.9	4.4	2.3

Table 3-22 The proportion of stockpiles for 20 mm mixtures containing RAP

		% passed for each sieve size (mm)											
Material	**% of proportion**	**26.5**	**19.0**	**13.2**	**9.50**	**6.70**	**4.75**	**2.36**	**1.18**	**0.60**	**0.30**	**0.150**	**0.075**
20 mm	**34.5**	100	95.8	32.4	8.1	4.3	3.2	2.5	2.2	2.0	1.8	1.5	1.2
14 mm	**0.0**	100	100	88.7	15.0	2.3	1.5	1.3	1.3	1.2	1.0	0.9	0.7
10 mm	**20.0**	100	100	100	81.8	15.3	2.6	1.5	1.4	1.4	1.2	1.1	0.9
7 mm(II)	**9.0**	100	100	100	100	87.8	29.2	4.9	2.9	2.2	1.8	1.4	1.1
5 mm	**0.0**	100	100	100	100	100	86.5	19.3	8.7	6.2	5.1	4.1	3.1
Dust	**36.5**	100	100	100	100	100	99.7	78.5	53.6	36.3	24.1	14.9	9.9
Combined PSD		100	98.6	76.7	64.7	48.9	40.6	30.3	20.9	14.4	9.8	6.3	4.3
Target PSD		100	98.7	77.1	64.6	48.5	39.7	29.7	18.8	12.8	8.5	5.8	2.2

Table 3-23 Summary of the share of stockpiles for mixtures containing RAP

	Share of Mixtures (% by weight)	
Material	DG14R10,DG14R20,DG14R30	DG20R10,DG20R20,DG20R30
20 mm	0	34.5
14 mm	19	0
10 mm	16	20
7 mm	18	0
7 mm(II)	0	9
5 mm	7	0
Dust	40	36.5

Later, the individual stockpiles were mixed with the ratios from Table 3-23 for the DG14 and DG20 mixtures, and then they were divided into all fraction sizes of PSD analysis as explained in section 3.4.2. Next, these fractions will be used for batching of asphalt mixtures.

3.4.3 Designing the mixture for the binder

As explained in section 3.4.1, the binder in the control mixtures is only from the added virgin C320 bituminous binder; however, the binder in the mixtures containing RAP is from not only the virgin binder, which is similar to the control mixtures, but also from the RAP.

The binder content in the control mixtures was chosen to be 4.7 and 4.3% by weight for DG14 and DG20 mixtures, respectively, based on MRWA specifications and specific job designs from an asphalt plant. For the mixtures containing RAP, it was assumed that all the binder from RAP would be acting in the mixture. Thus, these mixtures require less virgin binder as a portion of the binder comes from the RAP. The RAP binder content was equal to 4.1% by weight (as discussed in section 3.3.2) and the details of the binder combination in the mixtures were obtained as shown in Table 3-24.

Table 3-24 Binder contribution of virgin binder and RAP in mixtures

	% of binder by weight of total mixture		% RAP binder contribution in total binder
Mixture	From virgin C320	From RAP	
DG14	4.7	0	0
DG14R10	4.29	0.41	8.72
DG14R20	3.88	0.82	17.45
DG14R30	3.47	1.23	26.17
DG20	4.3	0	0
DG20R10	3.89	0.41	9.53
DG20R20	3.48	0.82	19.07
DG20R30	3.07	1.23	28.60

3.4.4 Mixture preparation

To prepare any of previously mentioned mixtures, the following steps were required considering the AS 2891.2.1 standard (Australian/New Zealand Standard, 2014):

- Preparing the batch of aggregates;
- Preparing the RAP;
- Preheating the materials (aggregates, rap, and bitumen); and
- Mixing and conditioning the mixture.

Each of these steps is explained in the following sections.

3.4.4.1 Preparing the batch of aggregates

This section explains how the batch of virgin aggregates were prepared using the aggregates split in all fraction sizes (13 different fractions) and stored in airtight buckets as shown in Figure 3-22.

Figure 3-22 Buckets of separated aggregates in 13 fraction sizes.

To prepare the batch, the size of the required asphalt mixture was determined. This size can be chosen based on the size of the mixer being used in the laboratory and also by the amount of loose asphalt required for preparing different types of samples. For example, in the present study, batches were generally produced to make 7.2 kg of asphalt mixture. Then, the amount of virgin aggregates and hydrated lime required for the chosen weight of asphalt mixture could be calculated by taking the amount of RAP and virgin binder from that weight.

In the next step, the amount of each aggregate size and hydrated lime were determined. To make this procedure easier, the PSD of the virgin materials and the combination of virgin aggregate and hydrated lime were calculated using equation (3-4) (a reorganised version of equation(3-3)) for each particle size and mixture:

$$P = aA + bL \quad (3\text{-}4),$$

where, P is the passing percentage of the combination of aggregates from a specific size sieve, A is the passing percentage of each aggregate from a

specific size sieve taken from Table 3-11 and Table 3-20, L is the passing percentage of hydrated lime from a specific size sieve taken from Table 3-5, and a and b are the proportion of aggregates and hydrated lime, respectively, in the combination of virgin materials in percentage. The results of the calculations are depicted in Table 3-25.

Table 3-25 The share of aggregates and hydrated lime in the combination of only virgin aggregates and hydrated lime in addition to percentage of passed particles for each sieve size in this combination.

	Share in combination of virgin aggregates and lime		% of particles passed for each sieve size (mm) of the combination of virgin aggregates and hydrated lime (batch of virgin material) using equation (3-4)											
Mixture	a%	b%	26.5	19.0	13.2	9.50	6.70	4.75	2.36	1.18	0.600	0.300	0.150	0.075
DG14	98.5	1.5	**100**	**100**	**98.3**	**83.9**	**68.4**	**54.0**	**35.9**	**24.1**	**16.4**	**11.0**	**6.9**	**4.5**
DG14R10	98.33	1.67	**100**	**100**	**98.1**	**82.8**	**67.5**	**53.1**	**35.4**	**23.3**	**15.4**	**10.4**	**6.6**	**4.3**
DG14R20	98.12	1.88	**100**	**100**	**97.9**	**81.4**	**66.1**	**52.1**	**34.7**	**22.3**	**14.3**	**9.6**	**6.2**	**4.0**
DG14R30	97.85	2.15	**100**	**100**	**97.7**	**79.6**	**64.6**	**50.7**	**33.8**	**21.0**	**12.9**	**8.6**	**5.6**	**3.8**
DG20	98.5	1.5	**100**	**99.0**	**82.0**	**71.0**	**55.0**	**45.0**	**33.0**	**23.0**	**17.0**	**12.0**	**8.5**	**4.5**
DG20R10	98.33	1.67	**100**	**98.9**	**80.0**	**68.4**	**52.5**	**43.2**	**32.2**	**21.5**	**15.6**	**10.9**	**7.8**	**4.2**
DG20R20	98.12	1.88	**100**	**98.7**	**77.5**	**65.3**	**49.5**	**40.8**	**31.0**	**20.3**	**14.4**	**10.2**	**7.6**	**3.9**
DG20R30	97.85	2.15	**100**	**98.5**	**74.3**	**61.2**	**45.4**	**37.9**	**29.6**	**18.7**	**13.0**	**9.3**	**7.2**	**3.6**

Once the percentage of passage through each sieve and the weight of the batch was determined, the amount of material from each fraction size could be calculated by multiplying the percentage from Table 3-25 by the total weight of virgin aggregates and hydrated lime in the mixtures. To simplify this procedure, it was assumed that hydrated lime consists of particles finer than 0.075 (i.e. 95% of its particles are finer than 0.075). This assumption does not make any significant difference to the result as the error is only 0.07 percent by weight of the total mixture and only affects the particles retained on the 0.075 mm sieve because all the particles of hydrated lime pass through the next sized sieve, i.e. 0.150mm. This error was calculated as shown in equation (3-5), where, 1.5 and 5 are the percentage shares of hydrated lime and amount of particles larger than 0.075 mm.

$$Error = \frac{1.5}{100} \times \frac{5}{100} \times 100 = 0.07\ \% \qquad (3\text{-}5)$$

Using the procedure explained above, for producing the batch with a weight of 7.2 kg of DG14R10, we required 720 g of RAP (10%) and 308.9 g bitumen (based on Table 3-24). Therefore, the weight of the batch of virgin aggregates and hydrated lime was 6171 g. First, the amount of hydrated lime was calculatedas being 1.67% of the batch, i.e. 1.5% of 90% of the total batch as it contains 10% RAP. This means we needed 103 g of lime. Then, the cumulative mass retained on each sieve was calculated as shown in Table 3-26. To produce the batch, the calculated amount of hydrated lime was poured into a tray (103 g in this case). Then, the material that had passed through the 0.075 mm sieve (Pan) added to the tray so that the total weight became equal to the amount of calculated material passing through the 0.075 mm sieve (in this case 268 g). This procedure was performed for the larger aggregate sizes until the total weight reached the weight of the batch required (in this case 6171 g).

Table 3-26 An example of laboratory batch guide for making 7.2 kg DG14R10 asphalt

Sieve (mm)	Percent Passing	Cumulative Mass Retained
26.5	100.0	
19.0	100.0	6171
13.2	98.1	6171
9.50	82.8	6056
6.70	67.5	5109
4.75	53.1	4163
2.36	35.4	3277
1.18	23.3	2184
0.600	15.4	1438
0.300	10.4	952
0.150	6.6	643
0.075	4.3	406
Pan		268
Lime	1.67	103

The same process can be performed for making batches of different mixtures in any size.

3.4.4.2 Preparing the RAP

For each mixture, the amount of RAP required was calculated by multiplying its RAP content by the amount of asphalt mixture needed. For instance, for

7.2 kg of DG14R10 asphalt mixture, 720 g of RAP (i.e. 10%) was required. To minimise the aging process since the materials were collected, the RAP was retained in airtight non-translucent containers. However, a small amount of moisture might have entered the RAP, therefore, when separating the required RAP, we needed to consider this potential added moisture and thus separate out more material so that after drying the required amount of mixture was left. For example, in the case mentioned above, approximately 800 g of RAP was separated instead of 720 g. However, the exact amount of material (e.g. 720 gin this example) was utilised during the actual mixing process.

In addition, to ensure the grading of the RAP was not disturbed when collecting the amount needed from the buckets of RAP, a riffle box were used to split the material in half. By halving the bucket many times and combining the halves obtained, the required amount of RAP was obtained and poured into a tray for later use.

3.4.4.3 Preheating the materials (aggregates, RAPand bitumen)

For making any HMA, it is essential to preheat the ingredients. Considering Australian Standard AS2891.2 (Australian/New Zealand Standard, 2014) recommendations, to preheat the aggregates they were first stirred a samll amount to homogenise the mixture. Then, the stirred aggregates were placed overnight in an 185 °C oven.

Meanwhile, the RAP was placed in an 105 °C oven overnight for drying, with previous experiments clarifying that drying the RAP overnight (approximately 12–14 hours) in a 105 °C oven totally dries the RAP until it reaches the constant mass. In the morning, approximately two hours before mixing, the RAP was taken out of the 105 °C oven and its weight measured. If necessary, a small amount of the RAP was removed from the tray to adjust the weight so that it precisely equalled the desired amount of RAP in the mixture. Next, it was placed in a 150 °C oven to become preheated for mixing, which was performed within a maximum of two hours, which is necessary to prevent any further aging in the RAP from occurring.

The bitumen that was taken from the asphalt plant was minimally heated until it melted and then decanned into small tins, each of them was enough for one

day's use. Before making asphalt mixture, one of the small bitumen tins was placed in a 150 °C oven with a loose lid for no longer than four hours before mixing. To prevent changes in bitumen properties, the high-temperature heating process was performed only once before mixing and the leftover heated bitumen was disposed of after mixing or four hours of being heated in the oven.

3.4.4.4 Mixing and conditioning the mixture

Before beginning the mixing of ingredients, the mixer bowl and beater were heated to a similar temperature as for the conditioning time, which is 150 °C in the present study based on Australian Standard AS2891.2 (Australian/New Zealand Standard, 2014). After ensuring all the components were heated enough, (150 °C for RAP and bitumen and 185 °C for aggregates), dry components and required amount of virgin binder were poured into a mixing bowl and then, using a mechanical mixer as shown in Figure 3-23, they were mixed until the mixture became uniform and all the aggregates got covered with a thin film of bitumen.

Figure 3-23 Mechanical mixer for asphalt mixing

Mixing for approximately 1 minute was sufficient for this mixing process. The temperature of the mixture was then measured to ensure it had not lost too much heat, i.e. it should not be less than 145 °C. The mixture was then split immediately using a quartering tray, as shown in Figure 3-24, for making different test portions and then all the test portions were transferred to an oven

for conditioning. The quatering tray was sprayed with silicon spray before use to prevent the mixture sticking to it.

Figure 3-24 Quartering the mixed asphalt in a tray

The temperature of the mixtures was maintained at 150 ± 5 °C for one hour to become conditioned in an appropriate oven. After conditioning, the mixture was ready for further tests and might be compacted or kept loose.

3.4.5 Mixture verification and properties

Although every step in the mixture preparing stage was accomplished precisely, it was essential to verify whether the mixture conformed to its design criteria within an acceptable tolerance level. For instance, the grading and binder content of the mixtures are crucial to determine whether the mixture had the same grading and binder content that it was supposed to have. Although aggregates of the mixture were accurately measured during the preparation process, a portion of them might have gotten lost or broken during the mixture preparation stages, which consequently change the grading of the outcome. In addition, the bitumen might stick to the trays, mixing bowl and beater more than expected and affect the binder content dramatically. Thus, it was important to ensure that the outcome of the mixing process was still the mixture as expected or, if different, then this difference was at an acceptable level. Moreover, several of the properties of the mixture needed to be measured as they were required for making the samples, such as maximum density. In the following sections, the methods implemented to verify the

grading and binder content of the mixture and determining the maximum density of the mixture are explained and results presented.

3.4.5.1 Binder content verification

The binder in the mixture arises from two sources: the virgin binder added to the mixture and the aged binder from the RAP. If there is any problem in the evaluation of the binder content of the RAP or exceeding the loss of binder in the mixing process, the binder content of the final product cannot be achieved. To verify whether this process leads to the targeted binder content, for each mixture at least two representative samples were collected from the mixture with the exception of the DG20R0 mixture where only one sample was taken. The binder content test was then performed in a similar way as that described in section 3.3.2 (Main Roads Western Australia, 2011b). The results from this proved that the process maintained the binder content in an acceptable tolerance level to the targeted level. The average bitumen contents for all mixture are shown in Table 3-27, while the details can be found in Appendix III.

Table 3-27 Binder content verification test results

Mixture	Averaged binder content test results %	Targeted binder content %	Variance (shall be <0.1)
DG14	4.6	4.7	-0.1
DG14R10	4.7	4.7	0
DG14R20	4.7	4.7	0
DG14R30	4.7	4.7	0
DG20	4.3	4.3	0
DG20R10	4.3	4.3	0
DG20R20	4.2	4.3	-0.1
DG20R30	4.3	4.3	0

3.4.5.2 Grading verification

To reassess the grading of the mixture, PSD analysis was performed on the extracted aggregates from the mixture using the same method as that used to analyse the PSD of RAP in section 3.3.2. The average passed percentage of

each sieve in PSD analysis are illustrated in Table 3-28 and Table 3-29 for 14 mm and 20 mm nominated size mixtures, respectively. It is obvious that all the variance levels are satisfactory, with only one PSD analysis performed for DG20 mixture. The details of these experiments can be found in Appendix III.

Table 3-28 Grading verification test results of 14 mm mixtures

	14 mm Mixtures												
	DG14 Percent Passing			DG14R10 Percent Passing			DG14R20 Percent Passing			DG14R30 Percent Passing			
Size (mm)	Averaged	Target	Variance	Averaged	Target	Variance	Averaged	Target	Variance	Averaged	Target	Variance	Tolerance
26.5	100.0	100.0	0.0	100.0	100.0	0.0	100.0	100.0	0.0	100.0	100.0	0.0	2.0
19.0	100.0	100.0	0.0	100.0	100.0	0.0	100.0	100.0	0.0	100.0	100.0	0.0	2.0
13.2	97.9	98.3	-0.4	97.6	98.3	-0.7	98.5	98.3	0.2	98.2	98.3	-0.1	2.0
9.50	83.8	83.9	-0.1	84.9	83.9	1.1	84.0	83.9	0.2	82.8	83.9	-1.1	2.0
6.70	68.3	68.4	-0.1	69.3	68.4	0.9	68.7	68.4	0.3	67.5	68.4	-0.9	2.0
4.75	54.6	54.0	0.5	55.0	54.0	0.9	54.4	54.0	0.4	53.3	54.0	-0.8	2.0
2.36	36.7	35.9	0.8	37.1	35.9	1.2	35.9	35.9	0.1	35.3	35.9	-0.6	2.0
1.18	24.6	24.1	0.5	25.1	24.1	0.9	24.5	24.1	0.3	24.2	24.1	0.0	1.0
0.600	17.1	16.4	0.7	17.3	16.4	0.9	17.0	16.4	0.6	16.8	16.4	0.4	1.0
0.300	11.7	11.0	0.7	11.8	11.0	0.8	11.6	11.0	0.6	11.4	11.0	0.4	1.0
0.150	7.1	6.9	0.2	7.3	6.9	0.5	7.3	6.9	0.4	7.3	6.9	0.4	1.0
0.075	4.8	4.5	0.3	4.3	4.5	-0.2	4.8	4.5	0.4	5.0	4.5	0.5	0.5

Table 3-29 Grading verification test results of 20 mm mixtures

	20 mm Mixtures												
	DG20 Percent Passing			DG20R10 Percent Passing			DG20R20 Percent Passing			DG20R30 Percent Passing			
Size (mm)	Averaged	Target	Variance	Averaged	Target	Variance	Averaged	Target	Variance	Averaged	Target	Variance	Tolerance
26.5	100.0	100.0	0.0	100.0	100.0	0.0	100.0	100.0	0.0	100.0	100.0	0.0	2.0
19.0	99.5	99.0	0.5	98.5	99.0	-0.5	99.4	99.0	0.4	99.1	99.0	0.1	2.0
13.2	80.3	82.0	-1.7	81.2	82.0	-0.8	80.9	82.0	-1.1	80.6	82.0	-1.4	2.0
9.50	69.7	71.0	-1.3	72.0	71.0	1.0	71.9	71.0	0.9	71.1	71.0	0.1	2.0
6.70	54.2	55.0	-0.8	55.8	55.0	0.8	55.2	55.0	0.2	56.2	55.0	1.2	2.0
4.75	43.7	45.0	-1.3	45.8	45.0	0.8	45.5	45.0	0.5	45.9	45.0	0.9	2.0
2.36	32.3	33.0	-0.7	33.4	33.0	0.4	33.3	33.0	0.3	33.0	33.0	0.0	2.0
1.18	22.5	23.0	-0.5	22.9	23.00	-0.1	22.9	23.00	-0.1	22.5	23.00	-0.5	1.0
0.600	16.9	17.0	-0.1	17.0	17.00	0.0	16.9	17.00	-0.1	16.6	17.00	-0.4	1.0
0.300	12.0	12.0	0.0	12.1	12.00	0.1	12.1	12.00	0.1	11.9	12.00	-0.1	1.0
0.150	8.1	8.5	-0.4	8.1	8.50	-0.4	8.4	8.50	-0.1	8.2	8.50	-0.3	1.0
0.075	4.7	4.5	0.2	4.9	4.50	0.4	4.9	4.50	0.4	4.9	4.50	0.4	0.5

3.4.5.3 Maximum density of the mixture

The maximum density of the mixture is a property that plays a vital role in determining how much material is needed for each sample when the samples were compacted for the different tests. In the present study, the Rice method was used in accordance with Main Roads Western Australia (2011c) standard.

In this method, a sufficient amount of mixture (1500 grams in the present study was manually separated from the rest of the sample, to ensure that no part of the mixed material is attached together. This was achieved in a tray as shown in Figure 3-25.

Figure 3-25 Separated material for maximum density test on a tray

Then, the material was weighed accurately and poured into a Buchner flask with a small amount of 25 °C water and detergent solution to prevent the particles from sticking together. The flask was topped up with more water so its level covered the material in the flask. Next, the flask was placed under a specific level of vacuum for 20 minutes while the mixture was agitated to remove trapped air using a metal bar in the setup as Figure 3-26 depicts.

Figure 3-26 Vacuum pump and flask setup for maximum density test

After vacuuming, the flask was placed in a 25 °C water bath and weighed precisely under the water. Having the empty flask weighted under water, the maximum density of the mixture can be calculated using equation (3-6):

$$\rho_{max} = \frac{m_2}{m_2 - (m_3 - m_1)} \rho_w \qquad (3\text{-}6,)$$

where, ρ_{max} is the maximum density of the asphalt mixture, ρ_w is the density of water at 25 °C, m_1 is the mass of the Buchner flask under the water, m_2 is the mass of the asphalt mixture in the air and m_3 is the mass of the asphalt mixture and Buchner flask in the water.

This test was performed for all mixtures at least two times each to obtain meaningful results. The average results for all the mixtures in the present study are summarised in Table 3-30, while the details of all the data can be found in section 4.2.1.

Table 3-30 Maximum density test results for all the mixtures

Mixture	Averaged maximum density (t/m^3)
DG14	2.484
DG14R10	2.481
DG14R20	2.496
DG14R30	2.492
DG20	2.505
DG20R10	2.502
DG20R20	2.496
DG20R30	2.507

3.4.6 Mixture performance tests

To characterise the performance of the different mixtures, a comprehensive experiment was planned in the Geo-mechanic and Pavement laboratory at Curtin University. The following tests were conducted on the samples made from all eight mixtures defined previously:

- Marshal stability and flow test;
- Complex modulus test;
- Indirect tensile modulus test;
- Wheel tracking test;
- Four-point bending beam fatigue life test; and
- Tensile ratio tests for investigating moisture sensitivity.

In addition, a new type of sensor was designed and developed by the author to make the in-field investigation more convenient. In the following subsections, each of these tests is explained in detail.

For each of the previously mentioned tests, a specific type of sample needs to be made based on the specifications of the test. One of the parameters used to verify the sample's compaction level and consistency is monitoring of the voids in the sample. The method used to measure the voids in a sample in the present study is based on the MRWA733.1 (2012) standard (Main Roads Western Australia, 2012).

To measure the voids in the samples, the volume of the sample was calculated using equation (3-7) below:

$$V = \frac{m_1 - (m_3 - m_2)}{\rho_w} \quad (3\text{-}7),$$

where, V is the volume of the sample, m_1 is the mass of the sample (g), m_2 is the mass of the device that attached the sample to the scale while immersed in the water bath, m_3 is the mass of the sample and attaching device immersed in the water and ρ_w is the density of water that is 0.997 g/cm^3 in a 25 °C water bath. Then, the bulk density was calculated using equation (3-8):

$$\rho_{bulk} = \frac{m_1}{V} \quad (3\text{-}8)$$

where, ρ_{bulk} is the bulk density of the sample (t/m^3) and the other parameters are as defined in the previous paragraph. Air void and void in mineral aggregates (VMA) could then be calculated following equations (3-17) and (3-10), respectively.

$$AV = \frac{\rho_{max} - \rho_{bulk}}{\rho_{max}} \times 100 \quad (3\text{-}9),$$

$$VMA = AV + \frac{\rho_{max} \times BIT\%}{\rho_{Bit}} \quad (3\text{-}10),$$

where, AV is the air void percentage, ρ_{max} is the maximum density of the mixture as acquired in section 3.4.5.3, ρ_{bulk} is the bulk density as mentioned in the previous paragraph, VMA is the percentage of voids in the mineral aggregate, BIT% is the percentage of bitumen in the mixture and ρ_{bit} is the density of bitumen (t/m^3) at 25 °C, which in the present study is considered to be 1.03 t/m^3.

3.4.6.1 Marshal stability and flow test

This test is incorporated with not only Australian standards but also several other standards as a criterion to validate the mixture. Thus, the mixture has to satisfy several conditions from this experiment to be allowed to be paved on site.

Based on Main Roads Western Australia (2016), Standard 731.1 enough material from a hot asphalt mixture (in the present study at 150 °C ± 5) is poured into a mould to make a cylindrical sample with 100 mm diameter and approximately 64 mm height and then hammered with a Marshal hammer a specified number of times (75 times in the present study) from the top and bottom sides. In the present study, an automated Marshal hammer as shown in Figure 3-27 was used for compaction.

Figure 3-27Automatic Marshal hammer machine

Then, the heights of the samples were measured, and any sample with the height greater than 70 mm or less than 57 mm was discarded. In addition, sample bulk densities were determined based on WA733.1 standard as explained in section 3.4.6, to ensure their air void and VMA were within specifications. In the present study, the specification in MRWA specifications No. 510 (Main Roads Western Australia, 2011d) and job mix design from the asphalt plant were followed. These were the air void of the Marshal samples for 14 mm mixtures should be between 4 and 7%, and between 3.5 and 5% for the 20 mm mixtures. In addition, the minimal VMA was required to be 14% for both sizes of mixtures.

After placing the samples in a 60 °C ± 1 water bath for 30 minutes, each sample was placed in a Marshal testing machine as shown in Figure 3-28.

Figure 3-28 Marshal testing machine

The force was applied with a displacement rate of 51 ± 3 mm/min while the vertical deformation and applied force was monitored by a data acquisition system attached to the machine. The peak force, corrected by multiplying the height factor using equation (3-11), was reported as the stability of the sample and the vertical deformation was reported as its flow.

$$Stability = Peak\ Force \times Height\ correction\ factor \quad (3\text{-}11),$$

where, Peak force is the maximum force applied on the sample in kN and Height correction factor is taken from Table 3-31.

Table 3-31 Height correction factor for stability test

Height of specimen (mm)	Height Correction Factor
57	1.19
58	1.16
59	1.13
60	1.1
61	1.07
62	1.04
63	1.01
64	0.99
65	0.96
66	0.94
67	0.92
68	0.9
69	0.88
70	0.86

For all mixtures except DG20R30, two samples were tested to obtain reasonable results while for DG20R30 three samples were tested.

3.4.6.2 Complex modulus test

This test was performed in accordance with the method suggested in standards NCHRP 9-29 (Bonaquist, 2008) and AASHTO TP 62-07 (AASHTO, 2007). Based on these standards, to produce the samples the conditioned asphalt mixture was poured into a mould having a 150 mm diameter in two layers. After pouring each layer, the mixture was compacted using a heated metal rod. The rod was pushed into the mixture 15 times in the outer areas of the mould and 10 times in the inner parts of the mould. After finishing pouring the material and compacting the mixture manually, the mould was compacted using a Servopac gyratory compactor as Figure 3-29 shows.

Figure 3-29 Servopac gyratory compactor

The compaction settings were adjusted by trial and error so that the final sample had a specific air void (in the present study the target air void was 5 ± 0.5%). After the samples were compacted and cooled to room temperature, a

100 mm core was taken from the compacted material using a drill similar to that shown in Figure 3-30.

Figure 3-30 Drill to make a core from asphalt samples

Later, the top and bottom of the samples were placed in a specific cylindrical sample holder and cut using a IPC global auto saw as shown in Figure 3-31. This process was performed to ensure the height of the sample was approximately 150 mm.

Figure 3-31 Cylindrical sample being cut using IPC global automatic saw

To verify the dimensions and air void of the cut samples, their diameter and height were carefully measured and then their air void was determined with a similar method as explained in section 3.4.6. The dimensions of the samples need to be in an acceptable range as the standard recommends. For example, based on NCHRP 9-29, the height of the sample should be between 147.5 and 152.5 mm. The samples were then left in front of a fan until dry and they had reached a constant mass, at which time they were ready for the complex modulus test.

Once the samples were ready, six knobs were attached to each sample using a two-part epoxy glue and setup as shown in Figure 3-32 to fasten the gauge points.

Figure 3-32 Setup for fastening gauge knobs on sample

a b

Figure 3-33 a) transducers on Complex modulus asphalt sample b)AMPT IPC global machine

This setup restrained the knobs so that three LVDT transducers with 120°gap can be attached to the knobs for the test. The sample was placed in a machine capable of performing dynamic modulus test and transducers were installed between gauge points. In the present study, an AMPT machine (IPC Global) was used (Figure 3-33).

In the next stage, the associated software, UTS 006, for completing the dynamic modulus test in the machine was opened. Then, the transducers were adjusted so that they read a value that was in the middle of their usable reading range. The temperature conditioning chamber was closed and the sample left to become conditioned for the first and lowest testing temperature.

In the present study, the tests were performed at three different temperatures including 4, 20 and 40 °C. The conditioning time for each temperature was different based on the recommendations of the standards. According to TP 62-07 (AASHTO, 2007), the sample was left to be conditioned overnight for the lowest temperature treatment. However, the conditioning time for 20 and 40 °C temperatures was three and two hours, respectively, when the sample was conditioned at a one-level lower temperature, not room temperature.

After conditioning of the sample, information requested by the UTS006 software was filled in, such as a description of the sample, dimensions of the sample, loading frequencies, gauge length and average applied strain level in a screen as shown in Figure 3-34.

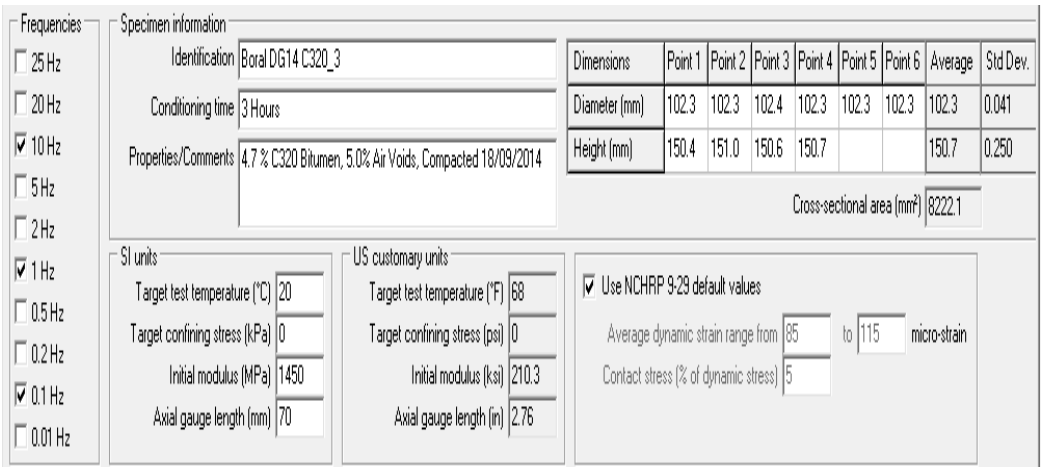

Figure 3-34 Dynamic modulus test input parameters dialogue of UTS006 software

The frequencies used in the present study for each temperature are shown in Table 3-32.

Table 3-32 Loading frequencies for tests at each temperature

Temperatures (°C)	Frequencies (Hz)
4, 20	10, 1, 0.1
40	10, 1, 0.1, 0.01

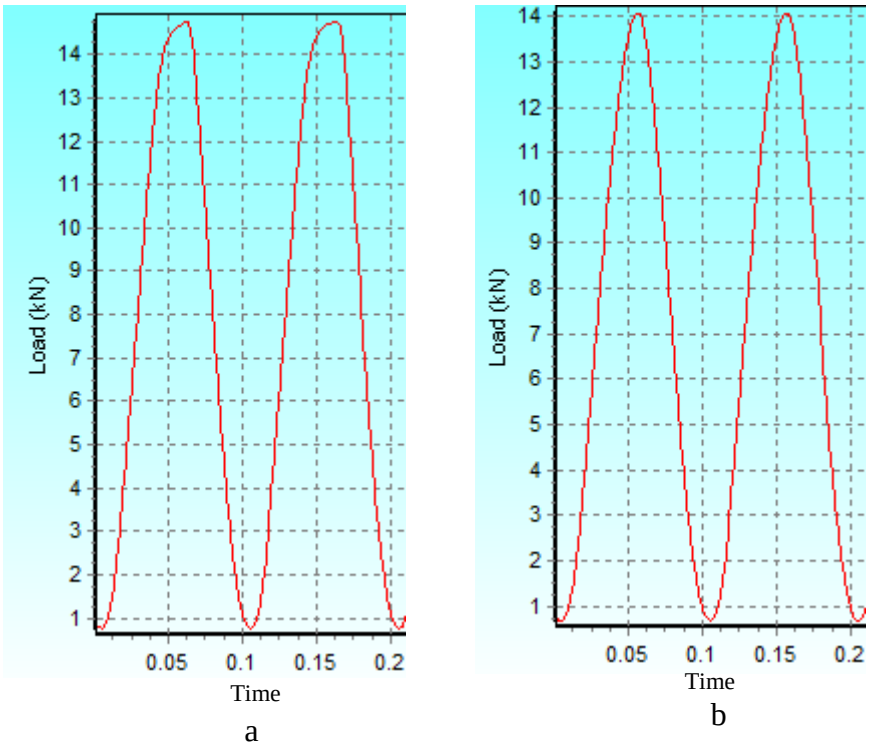

Figure 3-35 Applied Load shapes of DG14R30 sample at 4°c and 10Hz frequency when a) Strain level is set at 100μS b) Strain level is set at 70μS

Whenever possible, the average applied strain was set equal to 100 ± 15 microstrain as NCHRP 9-29 recommends. However, when the sample showed very high stiffness under an applied load, the machine might reach its limit while the strain level is still below the suggested level. This situation can be recognised when the applied load is not a sinusoidal load or the error notification from the software appears. Therefore, in such cases the amount of strain level was set to a lower level so that the shape of the loading on the sample was satisfactorily sinusoidal. For instance, for DG14R30 samples at 4 °C and 10 Hz frequency, the load shapes with 100 microstrain were not sinusoidal, but this is significantly improved when the strain level was reduced to 70 microstrain as illustrated in Figure 3-35. The level of strain, based on TP 62-07 (AASHTO, 2007) cannot be less than 50 microstrains. In the present study, the minimum strain levels used were much higher than 50 microstrains.

For each mixture, three samples were tested at three different temperatures (4, 20 and 40°C) in the frequencies shown in Table 3-32. The software repeats the loading cycles based on the standards to obtain a reasonable result, and it also automatically calculates the dynamic modulus and phase angle based on

the measurements and input data using the equations as described in section 2.3.1. Figure 3-36 shows an example output of the software for each frequency.

	10 Hz	1 Hz	0.1 Hz
Dynamic modulus (MPa)	12250	7767	4180
Phase angle (Degrees)	16.39	22.75	29.86
Average temperature (°C)	20.0	20.0	20.0
Average confining pressure (kPa)	0.2	0.2	0.2
Average micro-strain	95	97	98
Load drift (%)	0.1	0.1	0.0
Load standard error (%)	2.0	0.5	0.2
Average deformation drift (%)	-139.8	-250.6	-357.4
Average deformation standard error (%)	4.2	3.8	4.8
Deformation uniformity (%)	4.4	2.1	1.6
Phase uniformity (Degrees)	0.2	0.2	0.4

Figure 3-36 An example of output of UTS006 software for dynamic modulus testing

The software also calculated the loading error, average deformation error, uniformity error and phase uniformity error, which can be used to evaluate the test results based on standards. For example, NCHRP 9-29 standard recommended an acceptable range for each of these errors as described in Table 3-33.

Table 3-33Acceptable errors in complex modulus of asphalt samples based on NCHRP 9-29

Type of Data	Limit
Load standard error	10%
Deformation standard error	10%
Deformation uniformity	20%
Phase uniformity	3 degrees

Based on NCHRP 9-29 standard (Bonaquist, 2008), in the present study the coefficient of variation for the mean of dynamic modulus of a mixture is 7.5% or less, which test procedures followed appropriately and at least three samples were tested per mixture at different temperatures and loading frequencies to obtain reasonable results. The details of the conditions of the conducted tests are presented in Table 3-34.

Table 3-34 Number of asphalt complex modulus test for different temperatures and load frequencies per mixture

	Temperature (°C)		
Frequency (Hz)	4	20	40
0.01	0	0	3
0.1	3	3	3
1	3	3	3
10	3	3	3

3.4.6.2.1 Asphalt complex modulus master curve construction

In the present study, master curves of the dynamic modulus and phase angle of the mixtures were produced to make the comparison easier between them as the master curves shape can be interpreted over a wide range of temperatures or frequencies. This also helps with predicting the properties of the mixtures in a condition that cannot be tested experimentally. To generate the master curves of the samples, a similar master curve model and shift factor function to the method suggested in the NCHRP report (Bonaquist, 2008) and the method explained in section 3.3.4.4.1 were applied. In the NCHRP report, VTS was suggested to be used as the shift factor function if the viscosity properties of the binder are available before and after the aging process, otherwise the Arrhenius function was recommended. In the present study, as the viscosity of the binders before and after aging was not available for all the mixtures, the Arrhenius shift factor function was used. Details of the model and shift factor have been explained previously in sections 2.4.1 and 2.4.2, respectively. Substituting the Arrhenius shift factor function into the sigmoidal shape master curve model changes the master curve equation to equation (3-12):

$$log\,|E^*| = \delta + \frac{\alpha}{1 + e^{\beta+\gamma(log\omega+C\left[\left(\frac{1}{T}\right)-\left(\frac{1}{T_r}\right)\right])}} \qquad (3\text{-}12),$$

where, E^* is the complex modulus of an asphalt mixture, ω is the frequency of interest (Hz), δ is the minimum value of $|E^*|$, α is the difference between maximum and minimum values of $|E^*|$, T is the temperature of interest, T_r is the reference temperature of the master curve, and C, β and γ are parameters to adjust the model.

To widen the range of available data, as discussed in (Bonaquist, 2008), a maximum dynamic modulus in the master curve model was estimated using the Hirsch model as described in section 2.4.2 with the average volumetric information of the samples. However, in the present study, the maximum dynamic modulus was considered to be one of the optimisation parameters and was discovered during numerical optimisation. The reason for this decision was that even though the Hirsch model is a well-known prediction model for dynamic modulus, it has not been proven as being practical for the mixtures used in the present study and mixtures in Australia in general, as it is mainly established on data from USA asphalt mixtures.

Therefore, there were five parameters to be optimised based on the average available experimental data for each condition. Moreover, the temperature reference was considered to be 20 °C. However, to investigate the behaviour at lower and higher temperatures, the master curves with temperature references of 4 and 40 °C were also generated. Based on this approach, the data collected at 4, 20 and 40 °C and loading frequencies as shown in Table 3-32 were used to construct a master curve.

To determine the best match of equation to the available data, a SSE function similar to equation (3-13) was applied as an objective function to be minimised using a proper optimisation technique by adjusting optimisation parameters; δ, α, C, β and γ. In the present study, Microsoft Excel solver function was applied as an optimisation tool to adjust the optimisation parameters to fit the master curve model.

$$Objective\ function = \sum_{i=1}^{n} \left(\log(E_{p_i}^*) - \log(E_{m_i}^*)\right)^2 \qquad (3\text{-}13),$$

where, E^*_m is the i_{th} measured dynamic modulus, E^*_p is the predicted dynamic modulus from master curve model for the i_{th} data and n is the number of data records.

3.4.6.3 Indirect tensile modulus test

This test was performed based on the Australian standard AS2891.13.1 (Australian/New Zealand Standard, 2013) and conditions of the present study. The conditioned and adequately heated asphalt mixture was poured into a cylindrical mould having 100 mm diameter and was manually compacted using a heated rod. The sample was then compacted using a gyratory compactor. The settings of the compactor were altered through trial and error so that the final product had an air void of 5 ± 0.5%. After the samples were compacted, the air void was measured similarly to section 3.4.6 to ensure the air void was in the acceptable range. Otherwise, the samples needed to be discarded and produced again by tweaking the compaction procedure. The dimensions of the samples were then measured using a pair of Vernier callipers at different locations as the standard describes and the average diameter and height calculated. This was to determine whether the samples sizes were acceptable or not. The maximum error in diameter for the mixtures in the present study was ± 2 mm, and the heights of the samples were required to be between 35 and 70 mm. The UTM25 machine (IPC global) with UTS003 software were utilised to test the resilient modulus of the samples. Figure 3-37 shows the UTM25 machine and the temperature controlled environment used in this test.

Figure 3-37 UTM25 setup and its temperature controlled cabinet

However, because of experimental issues, a component of the tests was completed on the UTM14 machine (IPC global) with UTM16 software.

The samples were placed in a temperature controlled environment to reach the testing temperature of 25 ± 0.5 °C. To ensure correct temperature conditioning of the samples, a dummy sample with an embedded temperature probe was utilised. A sample was then placed in the indirect tensile modulus jig, as shown in Figure 3-38, in the temperature controlled environment and was fixed appropriately as the standard describes.

Figure 3-38 Sample in indirect tensile modulus testing jig

The appropriate software of the testing machine was then opened and the transducers were adjusted to measure the horizontal deformation of the sample correctly. Thus, measurements were read at the middle position of their working range.

The preloading pulses were then applied to the sample vertically and the horizontal deformations monitored. During the preconditioning stage, the load was adjusted so that it took 40 ± 5 ms for the haversine or triangular load to increase from 10% to 90% of its peak, repeated every 3 s. In addition, the sample needed to have 50 ± 20 microstrain recovered horizontal strain. When the loading satisfied these conditions, the pulse was repeated five times to calculate the resilient modulus automatically using equation (2-17) which is described previously in section 2.3.5. The results averaged over the entire five cycles in the associated software. An example of the output of the software (UTS003) is depicted in Figure 3-39.

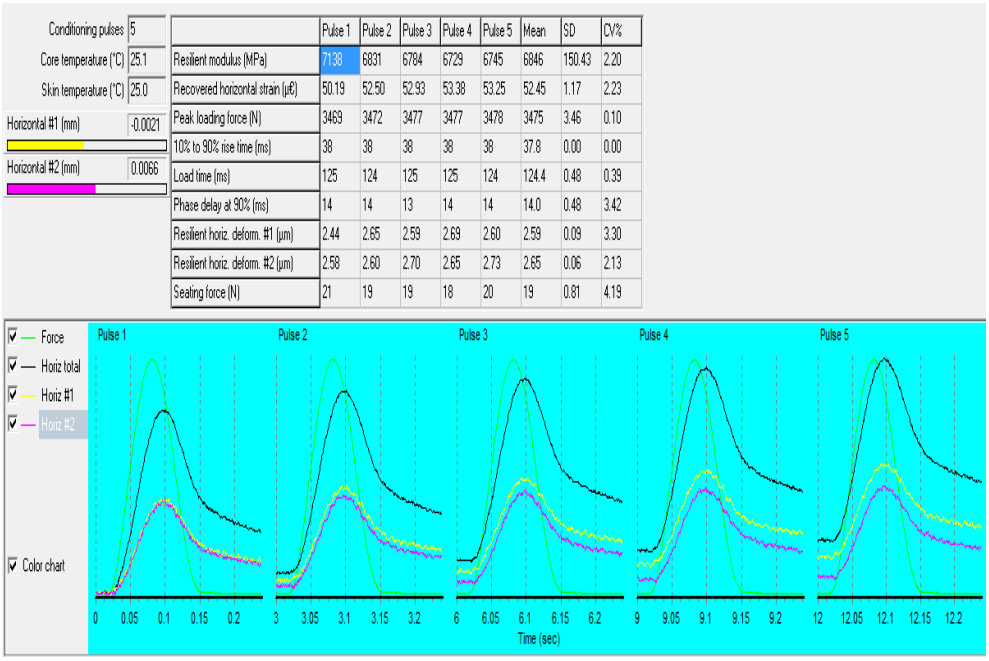

Figure 3-39 An example output of UTS003 software for resilient modulus testing

For each mixture, based on the standard, at least three samples were tested to obtain reasonable results. The details of the number of samples can be found in the test matrix provided in Table 3-35.

Table 3-35 Number of resilient modulus test samples per mixture

Mixture	Number of samples
DG14	8
DG14R10	7
DG14R20	3
DG14R30	4
DG20	4
DG20R10	3
DG20R20	3
DG20R30	4

3.4.6.4 Wheel tracking test

To discover the resistance of the mixture to permanent deformation, the wheel tracking test was performed on slab samples made from the different mixtures. In the present study, slabs were produced according to Austroad standard AG:PT/T220 (Austroads, 2005), and then the test was performed based on Austroad standard AG:PT/T231 (Austroads, 2006a).

To produce the slab for the test, a sufficient amount of conditioned hot asphalt mixture was poured into a 300 × 300 mm mould and distributed uniformly. The amount of material was dependent on the required thickness and air void. The amount of material required was initially determined using the theoretically calculated bulk density of the maximum density of the mixture and targeted air void. This amount was then adjusted by trial and error so that the final product had the required conditions. In the present study, for mixtures with 14 mm nominal size (DG14, DG14R10, DG14R20 and DG14R30) the required thickness was 50 mm, while for the mixtures with 20 mm nominal size (DG20, DG20R10, DG20R20 and DG20R30) size was 75 mm. The target air void for the slabs in all mixtures was 5 ± 1%.

After pouring the HMA into a mould that had been heated previously in a 160 °C oven and had a collar on top to hold the loose material, the mould setup was placed in a roller compactor and the compactor adjusted to handle that size of mould. In the present study, a Cooper roller slab compactor was used as shown in Figure 3-40.

Figure 3-40 Cooper roller slab compactor

The sample was compacted in a series of different loadings so that its height reached the target height after compaction. After the compaction, the direction of the compaction was marked on the sample for later use. After cooling, the bulk density and air void of the sample was measured using a similar method as that explained in section 3.4.6 to assure the value of the air voids conformed to the target values. If the results did not conform, the sample was discarded, the amount of material adjusted accordingly and a new

sample was made. After determining the bulk density and air void, the conforming sample should be placed under the fan until it is dry and has reached a constant mass, for later analysis.

The slab was then placed in the Cooper wheel tracker machine as shown in Figure 3-41. This machine consists of a wheel tracking device that is inside a temperature controlled environment. When placing the slab in the machine, the direction of the movement of the wheel needs to be in the same direction as the slab was compacted and marked previously.

Figure 3-41 Cooper wheel tracker machine

In this machine, the sample needs to be temperature conditioned. To make sure the sample achieved the test temperature, which was 60 ± 1 °C, a small hole was drilled in a corner of the sample, distant from the centre, and a temperature probe was placed in the hole. In addition, a small amount of silicon grease was placed in the hole to improve the contact between the temperature probe and the asphalt slab.

After ensuring the slab had steadily reached the test temperature, the slab was secured to the moving table. Then, the wheel was released and was placed on the sample and the appropriate mass to produce a 700 ± 20N vertical load on

the wheel was hung from the loading arm. The LVDT to measure the vertical displacement of the wheel was also attached to the wheel.

The Cooper wheel tracker software, ENWheelTracker, was launched and the test parameters were set in the software as stated in the Australian standard. For example, the table was set to move in a harmonic manner with an amplitude of 230 ± 5 mm and the speed of movement was set so that there would be 42 ± 0.5 passes per minute. Moreover, the termination condition was set to be either achievement of the number of passes to 10000 or the tracking depth exceeds 15 mm. The same software was utilised to monitor the temperature of the sample and measured rut depth profile during the test. The rut depth profiles were acquired using the data from the LVDT attached to the wheel to measure its vertical movement.

As Austroad standard AG:PT/T231 (Austroads, 2006a) states, the rut depth was calculated based on the mean of rut depth at the centre, ± 7.5, ± 22.5 and ± 37.5 mm from the centre while the locations of the measurements have tolerance limits of ± 2.5 mm. This recording can be achieved during the test or the test can be stopped after a certain number of passes and measuring can proceed manually. This machine is capable of monitoring the data in every pass without disrupting the test, which is more convenient and accurate. However, the software available in the laboratory calculates the rut depth based on EN standard, not Australian standards. Thus, it considers 27 points instead of the 7 points mentioned previously. The considered points in the software utilised during the present study were at centre, ± 4, ± 8, ± 12, ± 16, ± 20, ± 24, ± 28, ± 32, ± 36, ± 40, ± 44, ± 48 and ± 52 mm from the centre. Therefore, the rut depth the machine produces could be different from the rut depth based on the Austroad standard. However, during the data post-processing stage, the rut depth was calculated according to Austroad based on the available recorded data as the machine records the measurements for each point individually in a file. Moreover, in contrary to AG:PT/T231 standard which uses no preconditioning passes, the EN standard uses 10 passes for preconditioning the sample. As the available machine is limited to work based on EN standard, the data after the preconditioning passes is used

in this study. This issue is expected to have no effect on the investigation of the RAP effects in the mixtures as it applies to all the samples.

To monitor the trends occurring throughout the test, the software produces graphs such as shown in Figure 3-42 that illustrates the rut depth over time.

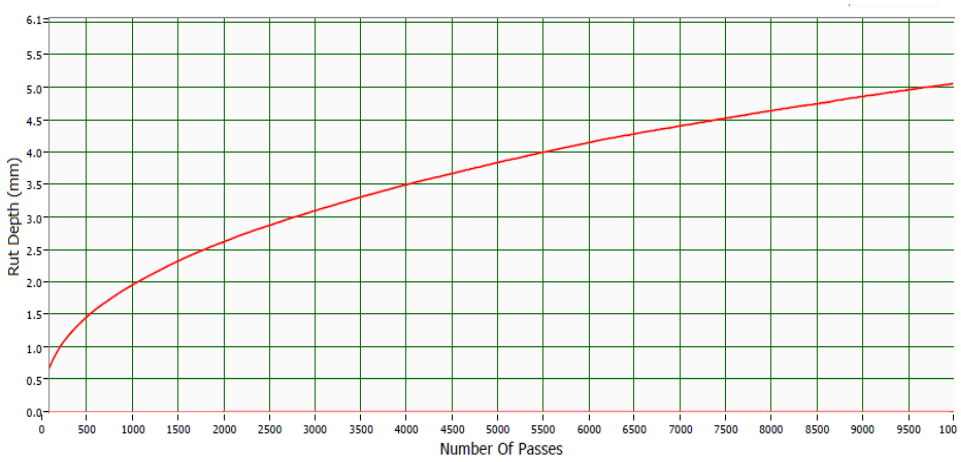

Figure 3-42 Rut depth versus number of passes in the wheel tracking test

For each mixture, based on the standard, at least two samples were tested to obtain reasonable results. The details of the number of samples are found in the test matrix provided in Table 3-36.

Table 3-36 Number of wheel tracking tests per mixture

Mixture	Number of samples(tests)
DG14	3
DG14R10	2
DG14R20	2
DG14R30	2
DG20	2
DG20R10	2
DG20R20	2
DG20R30	2

3.4.6.5 Four-point bending beam fatigue life test

In the present study, the fatigue life of the mixtures was compared using their fatigue life in a four-point loading beam fatigue test. To perform this test, a slab needs to be made using the HMA. The slab making process was achieved according to Austroad standard AG:PT/T220 (Austroads, 2005). Then, the slab was cut and prepared for making the beams for the test and their fatigue life was estimated based on Austroad standard AG:PT/T233 (Austroads, 2006b).

Initially, sufficient HMA was prepared as previously explained and then the mixture was poured into a 400 × 280 mm mould that had been heated in a 160 °C oven and had a collar on top to hold the loose material. The material was then evenly distributed. The amount of material required was determined by trial and error so that the resulting slab has a thickness of 70 mm and the final beams have a target air void of 5 ± 0.5%. However, the required material was estimated using the theoretically calculated target bulk density of the maximum density of the mixture and target air void. If the result was not satisfactorily, the amount could be tweaked to fix the air void and thickness as required. The mould setup was then placed in a Cooper roller slab compactor, as shown in Figure 3-40. The compactor was adjusted for the size of the mould used and then the sample was compacted in series of different loadings so that its height reached the target height after compaction (70 mm in the present study).

After allowing the slab to cool, it was then placed in a specific slab holder instrument and cut in a transverse direction to the compaction direction using an IPC Global auto saw as shown in Figure 3-43.

Figure 3-43 Slab cutting using IPC Global auto saw

The slab needed to be cut to make beams with specific dimensions. In the standard recommendations, the required dimensions were 390 ± 5 mm in

length, 50 ±5 mm in depth and 63.5 ± 5 mm in width. First, the slab was cut in lines as shown in Figure 3-44.

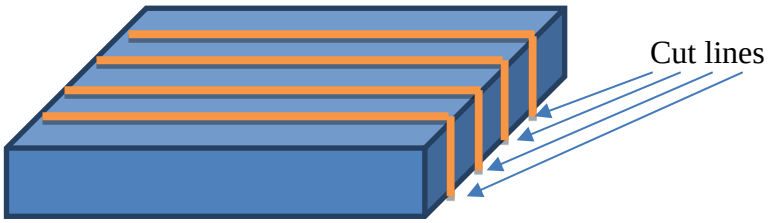

Figure 3-44 Cutting lines on asphalt slab to make four-point bending beam fatigue life samples

The edge sections were discarded. Then, the top and bottom of each section were cut again. This procedure guaranteed that the beams were made using only the middle sections of the compacted material and, thus, the edge effect was expected to be minimum. Thus, more evenly compacted beams were expected to be cut. In addition, when cutting the beams out of the slab, the faces of the beams were smoothed appropriately, which is important for performing the test correctly as stated in the standard. Using this method, from each slab three standard conforming beams were obtained.

In the next step, the bulk density and air void of the beams were determined using a similar technique to that described in section 3.4.6 to ensure they are in the acceptable range (5 ± 0.5% in the present study). If the results did not conform, the sample was discarded and the amount of material for compaction was adjusted accordingly and a new slab and beams were made. After determining the bulk density and air void, the conforming sample should be placed on a completely flat surface under a fan until it dries and reaches a constant mass. The dimensions of the sample were required to be measured in the centre, 20 mm from each end and 90 mm from the centre in both directions. After this stage, the sample could be tested. In the present study, an asphalt standard tester machine (IPC Global) was used for this purpose (Figure 3-45).

Figure 3-45 IPC Global standard tester fitted with four-points bending fatigue life testing jig

The samples were placed in the temperature controlled chamber until their temperature had stabilised at the testing temperature, which was 20 °C based on the Austroad standard used. The sample was then placed in the jig so that the sample was located horizontally and the supports just touched the sample at all four points while applying no load on it. This can be achieved via the associated software, UTS 015. The clamps were then locked to support the sample, while the restraints aligning the supports were removed to let them move freely except in the vertical direction. Then, the sample was left for 30 minutes. Moreover, the transducer was placed on the sample and adjusted to the middle of the travel range. The jig and how the sample was installed in the jig are shown in Figure 3-46.

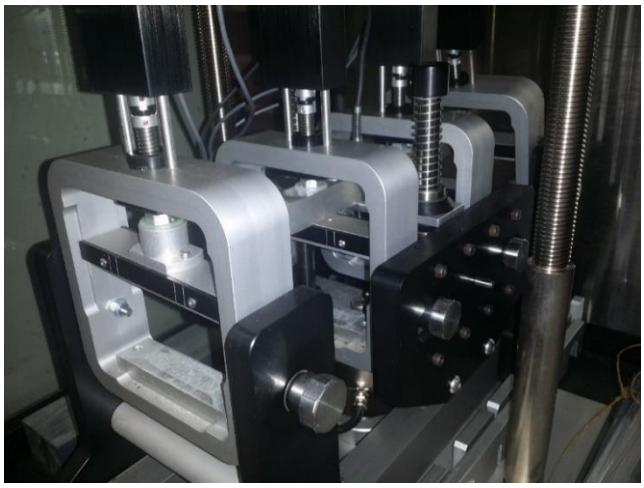

Figure 3-46 Four-points bending beam testing jig for fatigue life investigation

Meanwhile, the information required by the software, UTS015, was entered, including the measured dimensions of the sample, sample description and test parameters. The used test parameters, as recommended by the AG:PT/T233 (Austroads, 2006b), are illustrated in Table 3-37.

Table 3-37 Test parameters used in UTS015 software for four-point bending beam fatigue life testing

Test parameter	Value
Control mode	Strain mode
Load type	Haversine
Load frequency	10 Hz
Peak tensile strain	400 microstrain
Cycle to calculate initial stiffness	50
Poisson ratio	0.4
Termination stiffness	Control mixtures: 50% of initial stiffness Other mixtures: 25% of initial stiffness
Maximum number of cycles	1000000

After the sample was undisturbed for half an hour, the test was begun. The machine applied the load that the user had set in the software and the software calculated the flexural stiffness, modulus of elasticity, phase angle and dissipated energy based on the data received from the transducers. Based on the settings in the present study, the initial stiffness was calculated after

loading the sample 50 times. Then, the test was continued and the software calculated the stiffness during the test using equations (3-14), (3-15) and (3-16):

$$S_{mix} = \frac{1000 \times \sigma_t}{\varepsilon_t} \quad (3\text{-}14),$$

$$\sigma_t = \frac{LP}{wh^2} \times 10^6 \quad (3\text{-}15),$$

$$\varepsilon_t = \frac{108\delta h}{26L^2} \times 10^6 \quad (3\text{-}16),$$

where, S_{mix} is flexural stiffness (MPa), σ_t is peak tensile stress (kPa), ε_t is peak tensile strain (microstrain), L is beam span (356 mm in the present study), P is peak force (kN), w is beam width (mm), h is beam height (mm) and δ is peak displacement (mm).

This procedure was repeated until either the previously set maximum number of cycles or the termination stiffness was reached. During the loading cycles, the software recorded the calculated data and created a graph versus changes in time. An output sample of the software is shown in Figure 3-47.

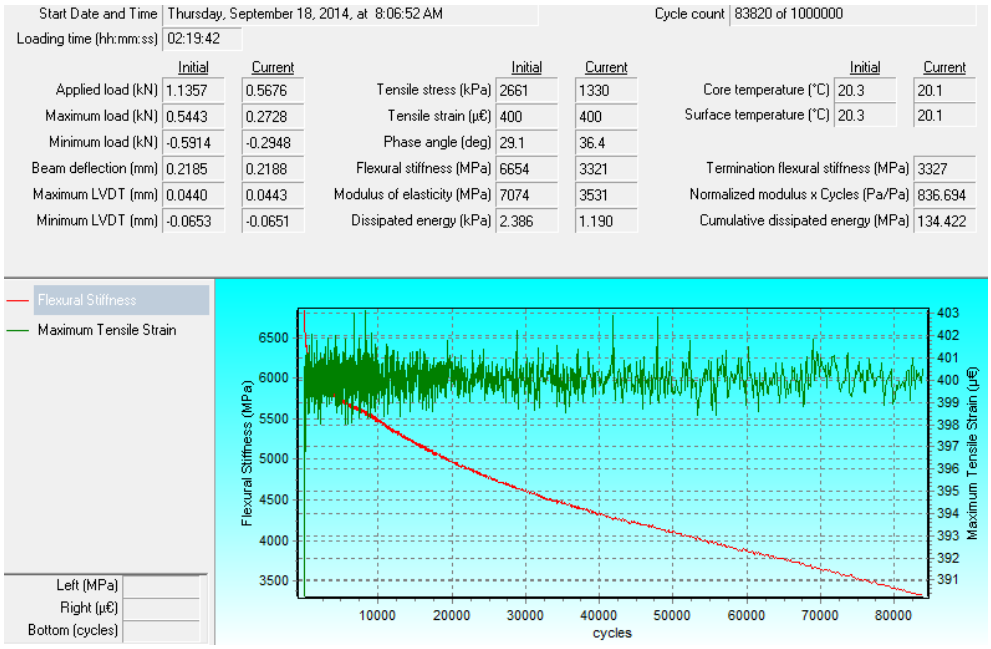

Figure 3-47 Example of the output of UTS015 software for four-points bending beam fatigue life testing

For each mixture, based on the standard, at least six samples were tested to obtain reasonable results. The details of the number of samples are shown in the test matrix provided in Table 3-38.

Table 3-38 Number of samples of four-point bending beam for fatigue life testing per mixture

Mixture	Number of samples(tests)
DG14	7
DG14R10	6
DG14R20	6
DG14R30	8
DG20	6
DG20R10	6
DG20R20	6
DG20R30	6

3.4.6.6 Tensile strength ratio tests

In the present study, the TSR of the samples was considered to be representative of their stripping potential and moisture sensitivity. To perform this test the following procedures as described by the Austroad standard AG:PT/T232 (Austroads, 2007b) were followed.

For this test, at least six samples per mixture were needed to be made using conditioned HMA. The hot mixture was poured into a gyratory mould with 100 mm diameter and compacted appropriately in a way that its height reached 65 ± 1mm. Then, the samples were left to cool and the air void and bulk density measured using a similar method as previously described in section 3.4.6. In addition, the weights and dimensions of all the compacted samples were recorded as required by the standard. The air voids of the samples were required to be 8 ± 1%. If the air voids of the samples were not in this range, they were discarded and new samples with modified amounts of material in the mould made. For the first attempt, the theoretically calculated bulk density of the samples was determined from the maximum density of the mixture and the target air void.

The samples were divided into two groups, in such a way that the average air void of each group was close to the other one (difference less than 0.5 %).

The samples of one group were separated for testing in dry conditions while the other was for testing in wet conditions. The group for wet conditions testing was preconditioned with moisture and then the samples of both groups were tested at the same temperature and using the same method. Thus, the differences that moisture preconditioning could make on the samples could be identified.

To precondition the samples in the wet conditions group, each sample was placed on its side in a vacuum desiccator full of 50 °C water so that the water covers the sample at least 25 mm. A 600 ± 25 mm Hg vacuum was then applied to the desiccator for 10 minutes. The desiccator and vacuum setup is shown in Figure 3-48.

Figure 3-48 Desiccator and vacuum pump setup for TSR test

The sample was removed, wiped with a damp cloth and weighed. The degree of saturation of the sample was calculated using equations (3-17), (3-18) and (3-19):

$$Saturation\ Level(\%) = \frac{m_{ps} - m_d}{V_a} \times 100 \quad (3\text{-}17),$$

$$V_a(cm^3) = \frac{A_v \times V_d}{100} \quad (3\text{-}18),$$

$$V_d(cm^3) = \frac{m_3 - m_2}{F} \quad (3\text{-}19).$$

where, m_{ps} is the mass of partially saturated sample (g), m_d is the mass of dry sample in the air, V_a is the volume of air in the sample (cm^3), A_v is the air void percentage in the sample, V_d is the volume of the dry sample (cm^3), m_3 is the mass of the sample in the saturated surface dry situation in air, m_2 is the mass of the sample in water and F is the density of the water in the test condition. The F is 0.997 in the present study as the tests were performed at 25 °C.

The saturation level required for the test was between 55 and 80%. If the result was less than 55%, the sample was saturated with different water temperatures or vacuum pressures; otherwise, it was discarded. Having a properly partially saturated sample, the sample was wrapped in several layers of cling wrap. Then, it was placed in a plastic bag that contained 10 mL of water, sealed and placed in a –18 ± 3 °C freezer for 18 ± 1 hours. This procedure was repeated for all samples in the wet conditions group (usually three samples). After freeze conditioning the samples, they were unwrapped and placed in a 60 °C water bath for 24 ± 1 hours. The unwrapped frozen samples are shown in Figure 3-49.

Figure 3-49 Frozen TSR test samples

After conditioning the samples in a 60 °C water bath, they were transferred to a 25 °C water bath for a further 2 h ± 5 min. Meanwhile, the samples for dry conditions testing were placed in a temperature controlled environment at 25 ± 1 °C for 2 hours.

Once all the samples were conditioned, their dimensions were recorded. Then, each sample was placed in the specific jig on its side and then loaded into a similar machine as that used for the Marshal stability and flow test that applies a load with a constant displacement rate of 51 ± 3 mm/min. The maximum force applied to the sample was recorded. The loading setup and jig are shown in Figure 3-50.

Figure 3-50 Loading jig and setup for TSR test

The specimen is retained under loading until breaking into two halves. Using the recorded dimensions before and after the conditioning, the change of volume and swell of the samples were determined using equation (3-20):

$$Swell(\%) = \frac{V_{mc} - V_d}{V_d} \times 100 \qquad (3\text{-}20),$$

where, V_{mc} is the volume of a sample after moisture conditioning and V_d is the volume before conditioning (dry condition group).

Using the maximum force recorded, the tensile strength of each sample was determined using equation (3-21):

$$Tensile\ strength(kPa) = \frac{2 \times P}{\pi \times H \times D} \times 10^6 \quad (3\text{-}21),$$

where, P is the maximum force applied on the sample in the test (kN), H is the height of the sample (mm) and D is the diameter of the sample (mm).

After determining the tensile strength for all the samples, the TSR was estimated using equation (3-22).

$$Tensile\ strength\ ratio(\%) = \frac{S_2}{S_1} \times 100 \quad (3\text{-}22),$$

where, S_1 is the average tensile strength of the samples in the dry condition group (unconditioned samples) and S_2 is the average tensile strength of the wet condition samples.

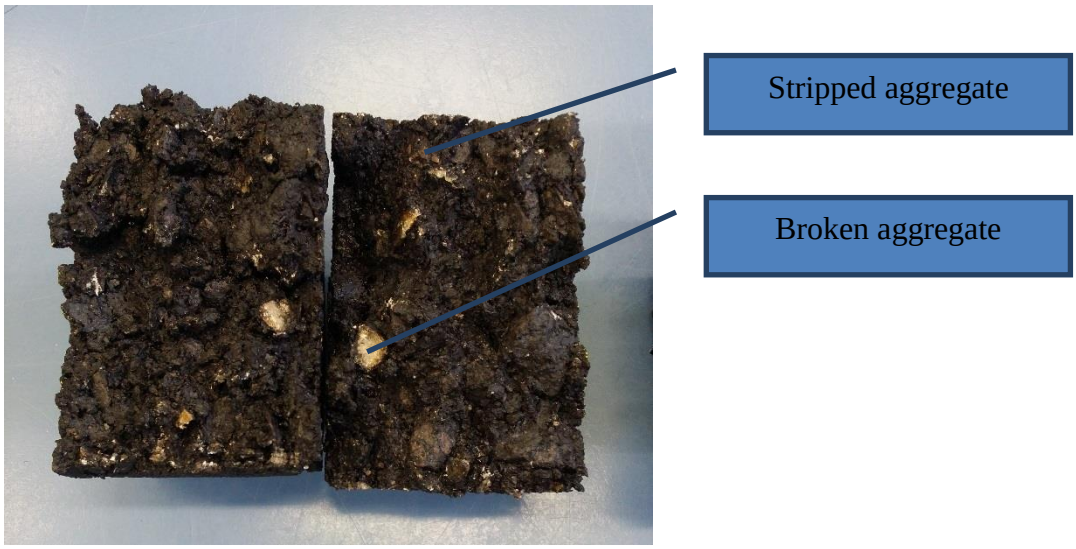

Figure 3-51 Visual assessment of a broken TSR sample after test

Moreover, the broken samples were visually inspected to report the degree of stripping. A picture of broken samples for visual assessment is shown in Figure 3-51.

For each mixture, based on the standard, at least six samples were tested to obtain reasonable results. Details on the number of samples are found in the test matrix provided in Table 3-39.

Table 3-39 Number of tests for TSR test per mixture

Mixture	Number of samples(tests)
DG14	6
DG14R10	6
DG14R20	6
DG14R30	6
DG20	6
DG20R10	6
DG20R20	6
DG20R30	7

3.4.7 In situ simulation and monitoring

The present research study attempted to investigate the performance of HMA containing RAP concrete in the field as well as in conventional laboratory tests. However, the author faced two major problems.

First, in-field evaluation generally takes a significant amount of time and requires a lot of resources. Therefore, it was decided to utilise a brand new accelerated pavement tester machine developed by the IPC Global Company as a tool to simulate the in-field situation. Second was the lack of a monitoring system to investigate the internal mechanical properties of pavement in the field without disturbing the structure of pavement.

In the following subsections, the attempts to deal with these issues are addressed. However, the research resources and unexpected difficulties did not allow the author to accomplish these aims completely. Therefore, there are no results available for these subsections.

3.4.7.1 In-field simulation

In this study, the Austrack accelerated pavement tester machine as shown in Figure 3-52 from IPC Global Company was utilised with the goal to investigate the mixtures performance, including rutting resistance and fatigue life, in a situation closer to the reality in the field.

Figure 3-52 Austrack accelerated pavement tester (picture from Austrack manual; (IPC Global, 2015)

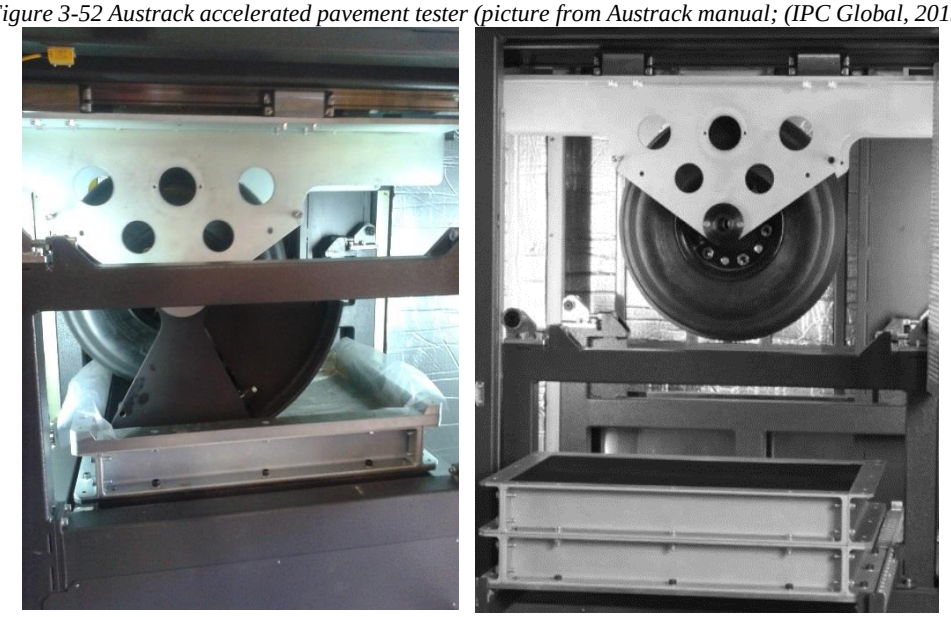

(a) (b)

Figure 3-53 a) Compaction mode b)Wheel tracking mode

This machine is capable of compacting and wheel tracking slabs with dimensions up to 500 mm × 700 mm, while the thickness can be between 50 and 300 mm using modular mould walls and 50 mm packers. Figure 3-53 shows the machine in compaction and wheel tracking mode.

The temperature in the insulated cabinet and the sample can be controlled by two heaters up to 60 °C. This machine can utilise tyres of different sizes including 425 mm diameter × 80 ± 5 mm wide, 550 mm diameter ×110 ± 5 mm wide and 1005 mm diameter ×265 ± 5 mm wide. These wheels are shown in Figure 3-54.

(a) (b) (c)

Figure 3-54 a)Full size tyre (1005 mm dia. × 265 ± 5 mm wide) b)Extra-large tyre (550 mm dia. ×110 ± 5 mm wide) c)Large tyre (425 mm dia. × 80 ± 5 mm wide) from Austrack manual (IPC Global, 2015)

It is also capable of applying loads up to 30 kN to the wheel and the wheel tracking can be performed at a maximum frequency of 1 Hz. This machine is equipped with a tool to measure the rut depth profile under no contact with the sample in different locations using a laser beam in predefined intervals during the wheel tracking test.

Although this machine was very capable, several modifications were required to simulate in-field conditions. For instance, the temperature control cabinet was equipped only with heaters, so the temperature could not be set to normal or low temperatures. Therefore, a customised cooling system was attached to the machine to enable it to perform the tests over a wider range of temperatures. The cooling setup is shown in Figure 3-55.

Figure 3-55 External customised cooling system

Also, the machine was not able to monitor the strain levels at the bottom of the sample, so an external data acquisition system was used to perform this..\ However, to synchronise the data between the data loading of the machine and the external data logger, a trigger switch was installed to the wheel carrier

of the machine that made it possible to see the start of each cycle in the externally recorded data. This trigger switch is shown in Figure 3-56.

Figure 3-56 Installed trigger switch for synchronising data logger with loading data from machine

To prepare the sample, the asphalt mixture was prepared as usual in the laboratory, poured into a preheated mould and then compacted with the machine. In the present study, an asphalt sample with a 50 mm thickness was chosen for investigation. In addition, to minimise the edge effects in the test, the smallest tyre available was used to undertake the wheel tracking test.

(a) (b)

Figure 3-57 Cutting the slab for air void estimation

To ensure the compaction level was satisfactory, initially, a dummy sample was made and compacted with the same setting and amount of material. Then the slab was cut into pieces as illustrated in Figure 3-57 and the air void of each piece was determined as described previously in section 3.4.6. After ensuring the procedure resulted in a proper compaction level, the main slab was made.

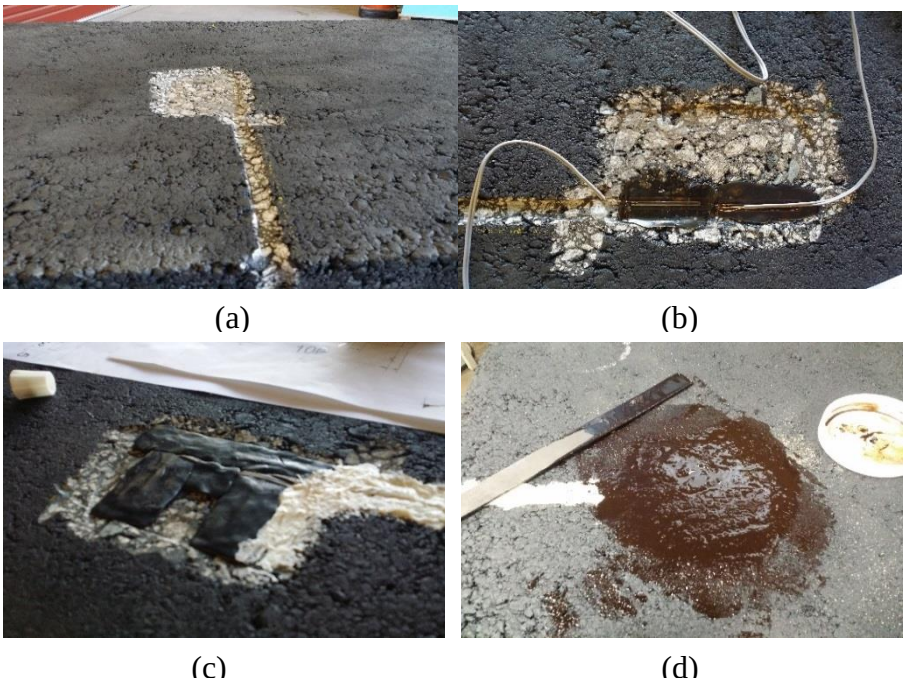

Figure 3-58 a)smoothing the surface for strain gauge installation b) strain gauge installation c)covering the strain gauges with a coating d)covering with emulsion bitumen and stone

After cooling of the slab, the bottom side of the slab was treated to attach strain gauges as depicted in Figure 3-58. Strain gauges were placed to measure tensional strain in two points and two directions (longitudinal and transversal) in the middle of the slab. These were then covered with a special coating and mixture of emulsion bitumen and stone powder to make the surface smooth.

The strain gauges helped monitor the tensile strains at the bottom of the slab during the test.

Furthermore, to simulate the base in the pavement structure, neoprene rubber mat was used as a base of asphalt pavement. To make a bond between these two layers, emulsion bitumen was applied between two layers and left to set under a load. This procedure is illustrated in Figure 3-59.

(a) (b)

Figure 3-59 a) applying emulsion bitumen to asphalt slab and rubber mats b)setting the slab and rubber mats by putting them under a load

Based on results from an approximated numerical model established for this experiment using Abaqus software, the thickness of the rubber was set to 150 mm. In this model, the characteristics of the asphalt were taken from the literature and properties of the rubber were taken from measurements performed under different compression loading conditions (different temperatures and loading frequency) using a UTM14 machine in the laboratory as Figure 3-60 shows.

Figure 3-60 Neoprene rubber under dynamic compression test in UTM14

The final sample for the present study was a 500 mm × 700 mm sample with 150 mm thickness rubber as a base and 50 mm asphalt material on top. The whole sample, cabling for strain gauges and external data acquisition setup can be seen in Figure 3-61.

(a) (b)

Figure 3-61 a) sample ready to test b) data acquisition setup

To monitor the temperature of the sample, a hole was drilled in the corner of the sample and a temperature probe was installed. Then, the sample was conditioned at 20 °C overnight.

Once the sample, machine and data acquisition setup was ready, the initial wheel tracking test was performed. Figure 3-62 shows the temperature probe in the sample while it was testing the samples.

Figure 3-62 Sample under test

The test continued overnight with the data for the strain being recorded for every cycle. When the test was terminated, the sample was taken out for visual inspection, and surprisingly, the sample was deformed dramatically in that all the edges were curved upward (Figure 3-63). This was evidence that the edge effect still existed even when smallest tyre possible was used.

Figure 3-63 Permanent curvature in the sample

After examining the data from the strain gauges, an unexpected pattern was observed in the recorded data as shown in Figure 3-64, with the loading pattern not symmetrical and the tyre travelling in one direction quicker than the other.

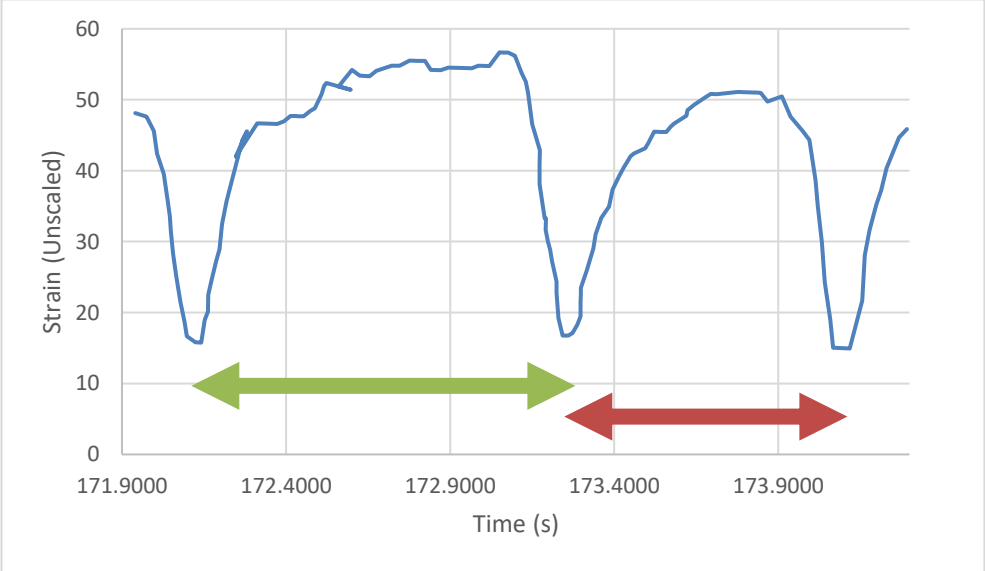

Figure 3-64 Difference in travel time in one direction compared to another direction (green line = the time it takes for the first direction, Red line = the time takes to return from the other side)

This asymmetric pattern was the result of the mechanism used in the machine to move the tyre on the sample and cannot be changed without fundamental changes in the machine. This problem makes the interpretation of the results difficult. Furthermore, as a result of a bidirectional movement of the tyre on the sample, the loading is not the same as in the field.

Observing these issues, the manufacturer was asked to help to with addressing them and this part of the research was put on hold until amendments can be completed on the Austrack setup. Unfortunately, no solution was discovered in the time frame of the present study; therefore, no results can be provided for the simulated in-field behaviour of the investigated mixtures.

3.4.7.2 Developing a system for in situ monitoring of the mechanical behaviour of pavements

To investigate the performance of the mixture in the field, the author discovered a lack of a reliable monitoring platform that can monitor the internal mechanical properties of a mixture in the field without disturbing the pavement. For example, to measure the induced strain in the depth of a compacted mixture in the field when a vehicle passes over the surface of the pavement, there are few options available in the market that can determine this without either disturbing the pavement dramatically or requiring a complex installation procedure. Similarly, there are several difficulties when monitoring the internal temperature of the asphalt. The main causes for these difficulties are that the sensors need a sophisticated cabling from the middle of the pavement to a data acquisition system, which needs to be placed beside the road. Furthermore, to install various types of sensors, the media surrounding them needs to be conditioned by more bitumen or other materials that might affect their reading.

Consequently, as a part of this project, a system is designed to monitor the internal strain and temperature of an asphalt sample with no requirement for cabling, maintenance or even an external data acquisition system installed on the road. Moreover, in the design process, the following criteria were considered:.

- Cost effectiveness.
- Minimal size (tentative dimensions are 6 × 12 ×1 cm) to disturb the pavement to the smallest amount possible and could be utilised in thin asphalt layers.
- Shape is designed, so the sensor engages with the asphalt efficiently.
- Sample rate of 100–200 Hz.

- Tolerates the harsh environment.
- Survives under the compaction loads and hot temperature of the mixture when compacting.

This system has the potential to be used in the field easily with no sophisticated installation and could be very cost effective for monitoring the performance of not only the pavement sections that are paid for research purposes, but also for health monitoring of service roads.

To achieve this goal, this system consisted of battery-free wireless embedded sensors that were installed during the paving of the road and a particular moving vehicle. The potential look of the system is shown in Figure 3-65.

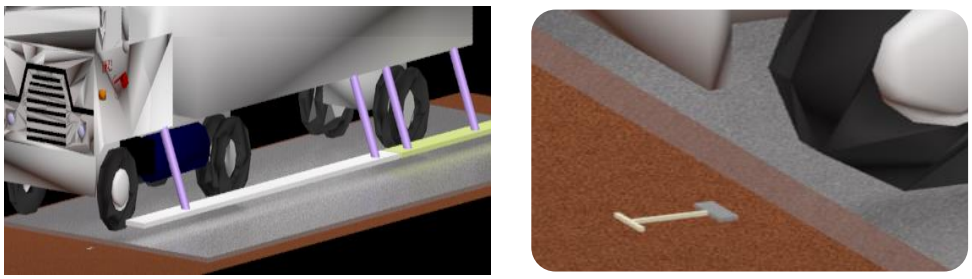

Figure 3-65 Possible look of a developed sensing system in this study

In this system, the sensor would be embedded into the pavement. Then, the specially equipped vehicle passes over the sensor using a specific navigation system that has been specifically designed using GPS and image processing techniques. Equipment on the vehicle then powers the sensor wirelessly by emitting RF energy and the sensor is activated when it receives particular amount of energy. Having the sensor activated, the sensor transmits the data (strain and temperature) wirelessly to the receiver on the vehicle when a known load (such as an axle of the vehicle) with known velocity passes over the surface of the pavement. This procedure is depicted in Figure 3-66.

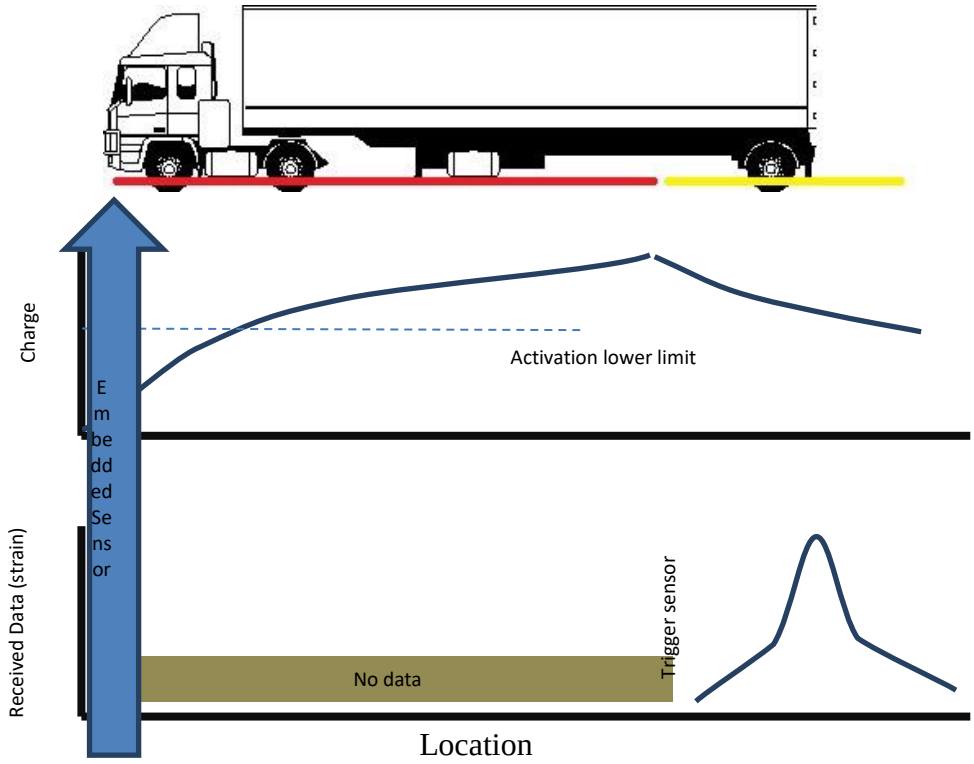

Figure 3-66 Stages of measuring the strain using a developed system in the field

Using such a system, the following benefits could be achieved:

- Measurement of internal mechanical and environmental parameters,
- Cheap, easy to install and widely utilised,
- Almost zero maintenance cost and no vandalism risk of installed equipment.
- Small footprint (negligible disturbance).
- No lane closure needed to monitor (the test occurs when the vehicle is moving).
- Flexible for different uses.

Once the system was designed, manufacturing of the devices began and the prototype of the sensor systems built as illustrated in Figure 3-67.

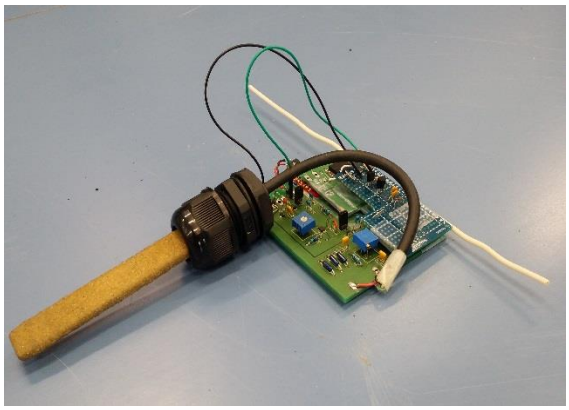

Figure 3-67 A prototype of the embedded sensor developed during this study

Several tests have been completed already to prove the concept of the design. These tests included evaluating the basic transmission capabilities, powering the sensor wirelessly, reading rates and sensitivity.

The results were satisfactory and have proved the feasibility of such a system. However, this project is not completed yet as it requires more resources and support. Therefore, no results are available from this system and in-situ pavement at the moment.

4 Data analysis and discussion

In this chapter, the results of the laboratory experiments for asphalt mixtures and binders are presented while the effect of the RAP will be examined from different facets of the mixtures and binders. Moreover, different approaches to predict the properties of the blended binder made from virgin and RAP binders are investigated. Two common models for prediction of dynamic modulus of the asphalt mixtures are evaluated and then modified to fit the results from the Australian mixtures studied.

4.1 Mixture design verification

Based on Asphalt specification 510 (Main Roads Western Australia, 2011d) and the job mix design utilised in the present study, to ensure that a mixture is valid to be used in the field, the Marshal properties, air voids, VMA, stability and flow test results of an intermediate course mixture should pass a specific criteria as shown in Table 4-1.

Table 4-1 Asphalt mixture requirement by Asphalt specification 510

Nominal size (mm)	Marshal stability (kN)		Marshal flow (mm)		Air Voids (%)		VMA (%)	
	Min	Max	Min	Max	Min	Max	Min	Max
14	8	–	2	4	4	7	14	–
20	8	–	2	4	3.5	5.5	14	–

The tests were performed according to the methods explained in sections 3.4.6 and3.4.6.1 . Results are presented in Table 4-2 and Table 4-3 for 14 and 20 mm mixtures, respectively.

Table 4-2 Marshal properties of 14 mm mixtures

Mixture-Sample	VMA (%)	Air void (%)	Stability (kN)	Flow (mm)	Validity
DG14R0-1	15.52	4.72	14.46	2.45	Valid
DG14R0-2	16.17	5.46	14.38	2.52	Valid
DG14R10-1	16.16	5.46	16.74	2.84	Valid
DG14R10-2	16.03	5.32	18.12	2.92	Valid
DG14R20-1	16.51	5.79	15.93	3.14	Valid
DG14R20-2	15.98	5.18	18.41	2.74	Valid
DG14R30-1	16.22	5.47	20.76	2.99	Valid
DG14R30-2	16.33	5.6	18.16	2.6	Valid

Table 4-3 Marshal Properties of 20 mm mixtures

Mixture-Sample	VMA(%)	AV(%)	Stability (kN)	Flow (mm)	Validity
DG20R0-1	14.2	4.17	16.50	2.93	Valid
DG20R0-2	14.2	4.14	17.61	2.50	Valid
DG20R10-3	14.9	4.67	15.3	3.5	Valid
DG20R10-5	14.8	4.49	21.29	3.3	Valid
DG20R20-1	14.3	4.01	20.68	3.8	Valid
DG20R20-2	14.5	4.24	17.66	3.5	Valid
DG20R30-1	14.6	4.12	21.29	3.9	Valid
DG20R30-3	14.4	4.01	26.36	3.4	Valid
DG20R30-4	14.4	4.06	19.21	4.0	Valid

As can be seen, all the samples passed the criteria in Table 4-1. The changes in Marshal stability and flow due to the percentage of RAP and aggregate nominal size are explained in greater detail in section 4.2.2.

4.2 Mixture performance results

In this section, the properties and performances of the studied asphalt mixtures are evaluated for different aspects, including include maximum density, Marshal stability and flow, indirect tensile modulus, rutting resistance, moisture susceptibility, fatigue life and complex modulus. Using the results from each test, the effects of RAP inclusion in the mixtures can then be studied for the 14 mm and 20 mm aggregate size mixture groups.

4.2.1 Maximum density

The maximum density of the mixtures was measured according to the method explained in section 3.4.5.3. The results for the 14 and 20 mm mixtures are presented and discussed in the following subsections.

4.2.1.1 The 14 mm mixtures

The results of maximum density tests of samples and their average for different percentage of RAP for 14 mm mixtures are presented in Figure 4-1

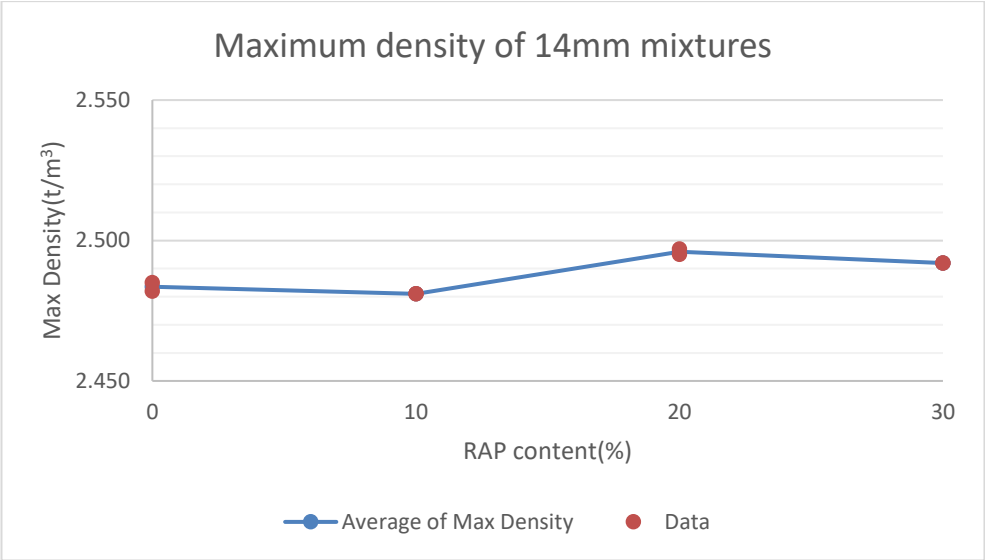

Figure 4-1 Maximum density of 14 mm mixtures versus RAP content

As can be seen from the graph, for each type of mixture, there was little change in the diversity of the samples and the maximum density was not affected dramatically by the amount of RAP included in the mixture. For the mixtures with no RAP or 10% RAP, the maximum density was approximately 2.48 t/m^3, while for mixtures with higher percentages of RAP is the maximum density increased slightly but was still less than 2.50 t/m^3. This trend was expected as the aggregate grading and binder content of the mixtures remained constant between the mixtures although the percentage of RAP changed.

4.2.1.2 The 20 mm mixtures

The results of the maximum density tests in samples and their average for different percentages of RAP in the 20 mm mixtures are presented in Figure 4-2.

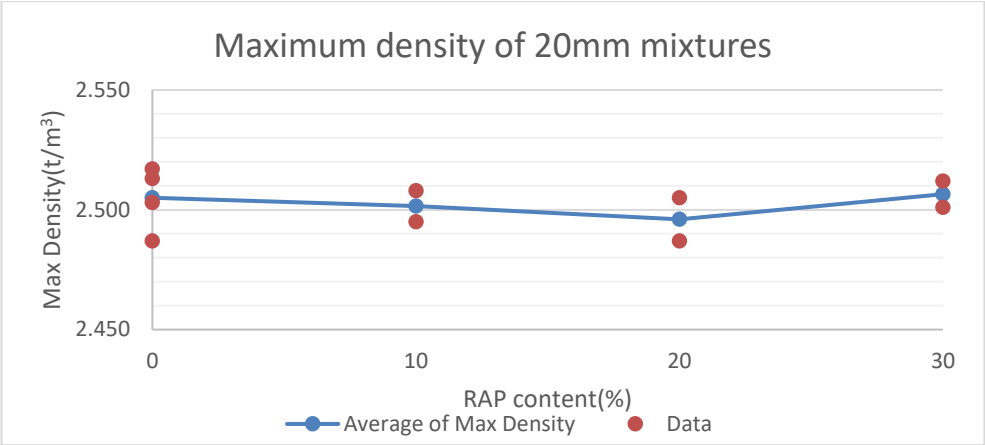

Figure 4-2 Maximum density of 20 mm mixtures versus RAP content

Similar to the 14 mm mixtures, the average maximum density of 20 mm mixtures was not changed significantly by the amount of RAP in the mixture, although in these mixtures the values show larger scattering between samples containing the same amount of RAP than the 14 mm mixtures did. The extra error might arise from the fact that a slight difference in particle distribution of the samples while splitting the mixtures might result in a greater error in density calculation as the mass of larger aggregates are considerably more. For example, having one particle less or more changes the mass to a greater extent when the size of the aggregates is larger.

4.2.1.3 Comparison of 14 and 20 mm mixtures

Figure 4-3 compares the average maximum density of the 14 mm mixtures and the 20 mm mixtures versus their RAP percentages.

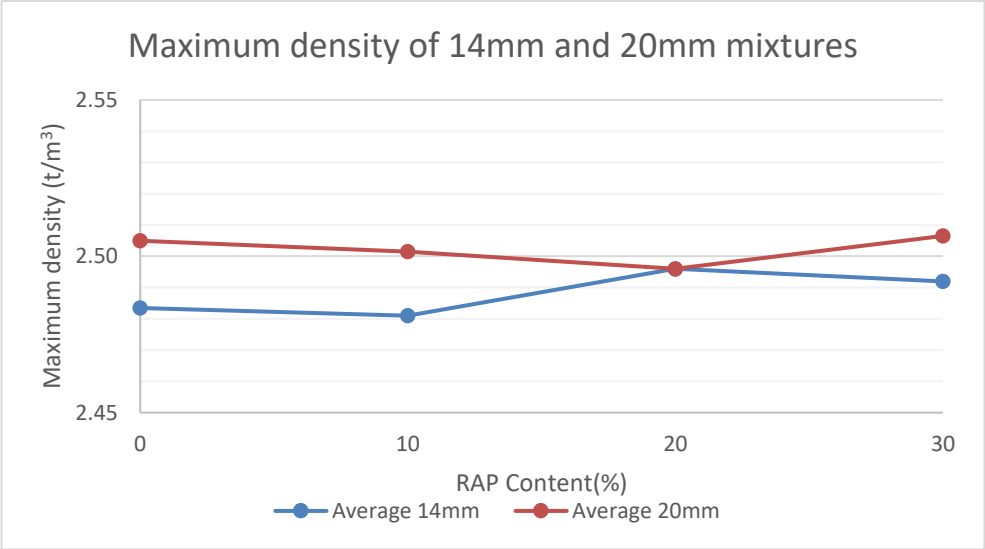

Figure 4-3 Comparison of maximum density of 14 and 20 mm mixtures versus RAP content

It can be seen that the 14 mm mixtures always have less or equal maximum densities to their 20 mm counterparts. The reason for this might be the difference of binder content between the 14 mm and 20 mm mixtures. As 20 mm mixtures have less binder content (4.3%) than the 14 mm mixtures (4.7%), the mass of aggregates will be greater in the same volume of mixture.

4.2.2 Marshal stability and flow

The 14 and 20 mm mixtures were tested according to methods described in section 3.4.6.1 to evaluate their Marshal stability and flow performance.

4.2.2.1 The 14 mm mixtures

The Marshal stability and flow of the 14 mm mixtures are presented in Figure 4-4 and Figure 4-5, respectively.

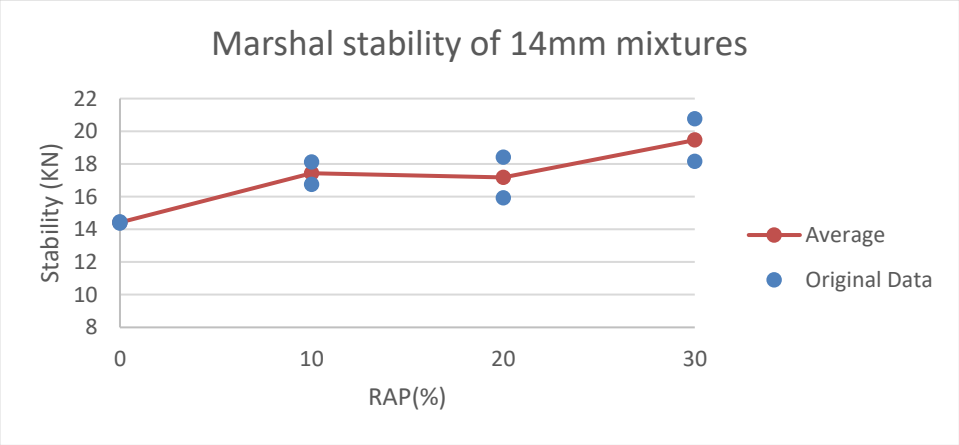

Figure 4-4 Marshal stability of 14 mm mixtures versus RAP content

As expected, Figure 4-4 shows a considerable increase in the stability of the mixtures as the percentage of RAP increases. For instance, 30% RAP resulted in an increase in the stability by approximately 30%. This increase is mainly caused by the binder in the RAP, which is significantly stiffer than the virgin binder used in the control mixture. However, no significant change was observed between the stability of 10% RAP and 20% RAP mixtures.

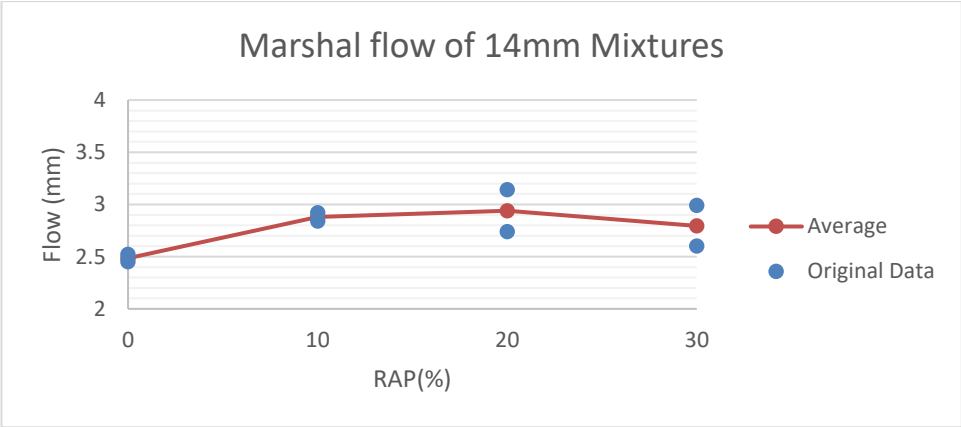

Figure 4-5Marshal flow of 14 mm mixtures versus RAP content

The Marshal flow graph of the 14 mm mixtures in Figure 4-5 demonstrated the increasing trend from 0%RAP to 20%RAP, with this trend becoming smoother when it reaches 20%. However, 30% RAP shows a slight reduction in flow. This decrease in the flow might be caused by experimental errors as the data shows considerable scattering at 20 and 30% RAP.

4.2.2.2 The 20 mm mixtures

The Marshal stability and flow test results of the 20 mm mixtures and their average values are illustrated in Figure 4-6 and Figure 4-7, respectively.

Similar to 14 mm mixtures, the higher the RAP percentage in the mixture, the higher was Marshal stability measured. For example, t 30% RAP in the mixture increased the stability by approximately 30% of its original value.

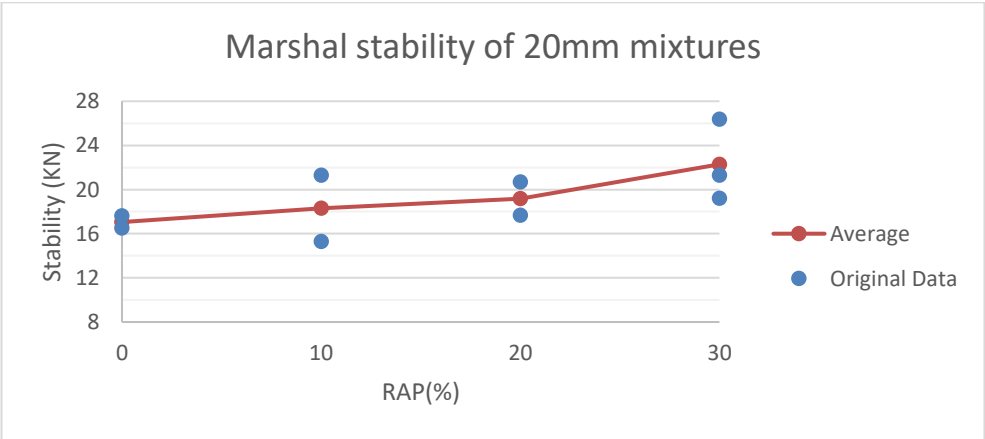

Figure 4-6 Marshal stability of 20mm mixtures versus RAP content

The average Marshal flow trend of the 20 mm mixtures shown in Figure 4-7 also illustrates an increasing trend, with it becoming smoother at higher percentages of RAP, with this trend observed over the averaged data of all available samples.

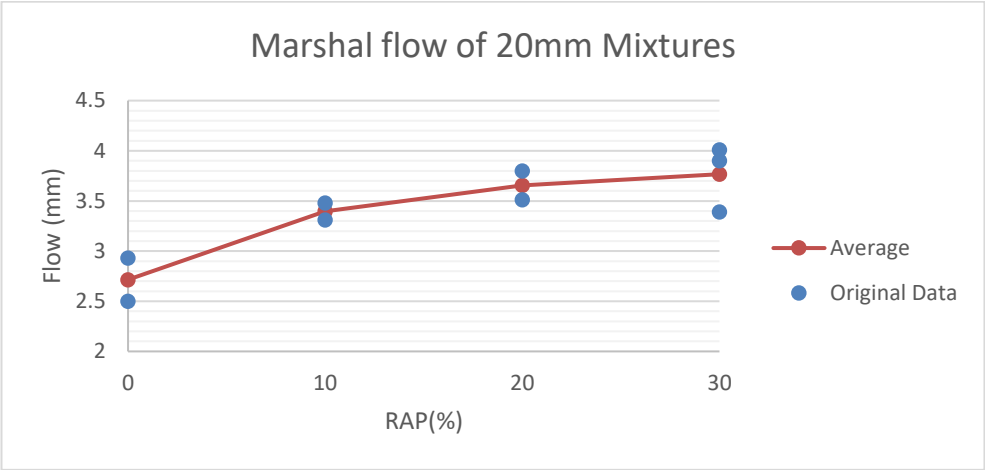

Figure 4-7 Marshal flow of 20 mm mixtures versus RAP content

4.2.2.3 Comparison of 14 and 20 mm mixtures

The stability and flow for both 14 and 20 mm mixtures are illustrated in Figure 4-8 and Figure 4-9, respectively.

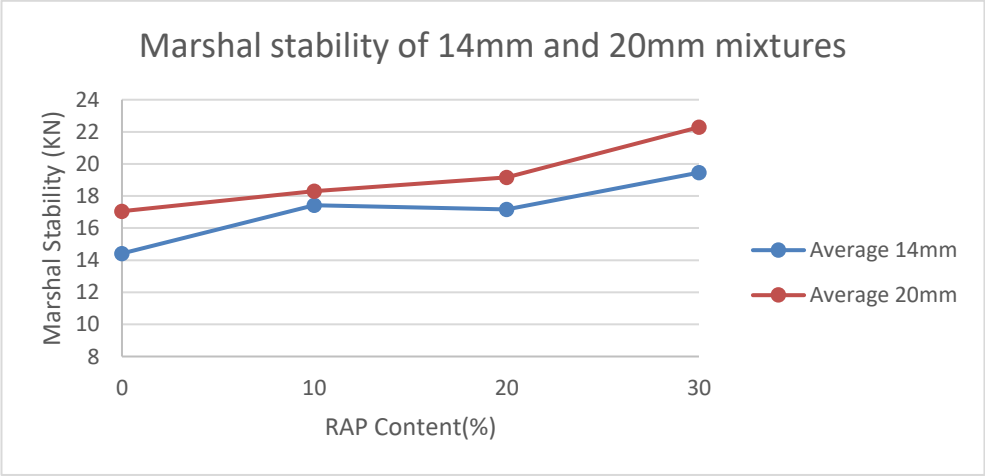

Figure 4-8Comparison of Marshal stability of 14 and 20 mm mixtures versus RAP content

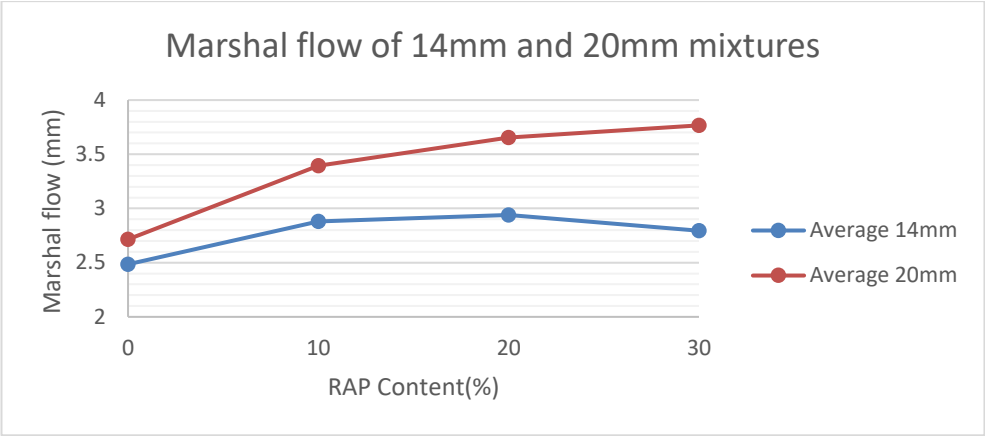

Figure 4-9 Comparison of Marshal flow of 14 and 20 mm mixtures versus RAP content

Comparing the results of the 14 and 20 mm mixtures, it is obvious that both average Marshal stability and flow of all 20 mm mixtures with different percentages of RAP are higher than their 14 mm counterparts while following almost the same trend. The main difference is that, for the flow values, the 20 mm mixtures reveal a steadily increasing trend when the RAP percentage increases, while this increasing trend is only observed up until the 20% RAP in the 14 mm mixtures.

Furthermore, all the mixtures demonstrated far greater stability than 8 kN that is required by the Asphalt specification 510 (Main Roads Western Australia, 2011d), with even the minimum value for stability, which was observed in control mixtures with no RAP, being 14.4 and 17 kN for 14 and 20 mm mixtures, respectively.

Based on the flow results, the average values were in the acceptable range of 2–4 mm for all mixtures. Although the 20 mm mixtures with higher percentages of RAP were on the edge of the higher limits of the flow value, the minimum values for the 14 and 20 mm control mixtures were in the middle of the range (2.4 and 2.7 mm, respectively)

In the present study, Marshal tests were performed to check the validity of the mixtures rather than to investigate the stability and flow of them. To investigate these parameters, more samples are required as the data has a considerable diversity that makes it difficult to interpret the result trends.

4.2.3 Resilient modulus

The resilient modulus of samples was measured using the indirect tensile method according to section 3.4.6.3 for all samples.

4.2.3.1 The 14 mm mixtures

The resilient modulus results for the 14 mm mixtures and their average values for each mixture are shown in Figure 4-10.

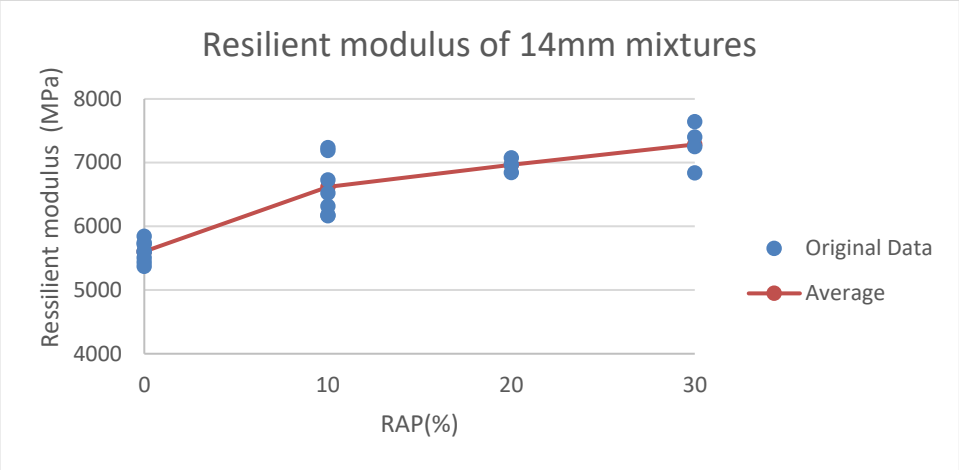

Figure 4-10 Resilient modulus of 14 mm mixtures versus RAP content

In these mixtures, the resilient modulus showed a sudden rise from the average value of 5604 MPa to 6620 MPa with the addition of only 10% RAP to the mixture. This increasing trend continued when higher percentages of RAP were added, although with a much lower, but still consistent, slope. This trend suggests that the resilient modulus of the samples does not have a linear relationship with their RAP content. To investigate this matter further, different linear and nonlinear regression models were built using the original data from the experiments and are presented in Table 4-4

Table 4-4 Regression modelling with resilient modulus of 14 mm mixtures' relationship with RAP content

Regression model	Equation (y = resilient modulus, x = RAP %)	R^2
Linear	$y = 56.718x + 5774.2$	0.7596
2nd order polynomial	$y = -1.9799x^2 + 113.68x + 5621.9$	0.8341
Exponential	$y = 5767.2e^{0.0089x}$	0.756

As Table 4-4 shows, the data has a better fit with the 2nd order polynomial regression model than with the other models.

4.2.3.2 The 20 mm mixtures

The resilient modulus results for the 20 mm mixtures and their average values are shown in Figure 4-11.

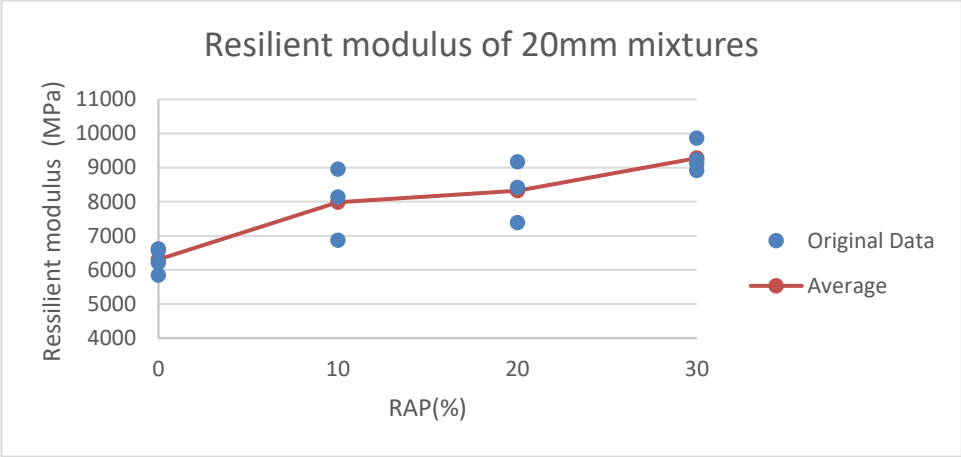

Figure 4-11 Resilient modulus of 20 mm mixtures versus RAP content

The 20 mm mixtures demonstrated a very similar behaviour to the 14 mm mixtures. The higher the percentage of RAP, the higher resilient modulus observed. However, the jump between 0 and 10% RAP was significantly higher than at the other percentage points. To clarify, the average resilient modulus jumped from 6308 to 7984 MPa (1676 MPa difference) between 0 and 10% RAP. However, this jump was only 339 MPa between 10 and 20% RAP.

The shape of the graph and the varying slope between different percentages of RAP for the resilient modulus support the hypothesis that the relationship of the resilient modulus to the RAP content is not linear. This theory is investigated in Table 4-5 by fitting different linear and nonlinear regression models to the original data from the experiments.

Table 4-5 Regression modelling of resilient modulus of 20 mm mixtures relationship with RAP content

Regression model	Equation (y = resilient modulus, x = RAP %)	R^2
Linear	$y = 93.964x + 6538.1$	0.7512
2nd order polynomial	$y = -1.8062x^2 + 148.15x + 6383.3$	0.7707
Exponential	$y = 6527.6e^{0.0122x}$	0.7498

Again, the data has a better fit with the 2nd order polynomial regression model than with the other models.

4.2.3.3 Comparison of 14 mm and 20 mm mixtures

In Figure 4-12, the resilient modulus of the 14 mm mixtures are compared with the resilient modulus of the 20 mm mixtures.

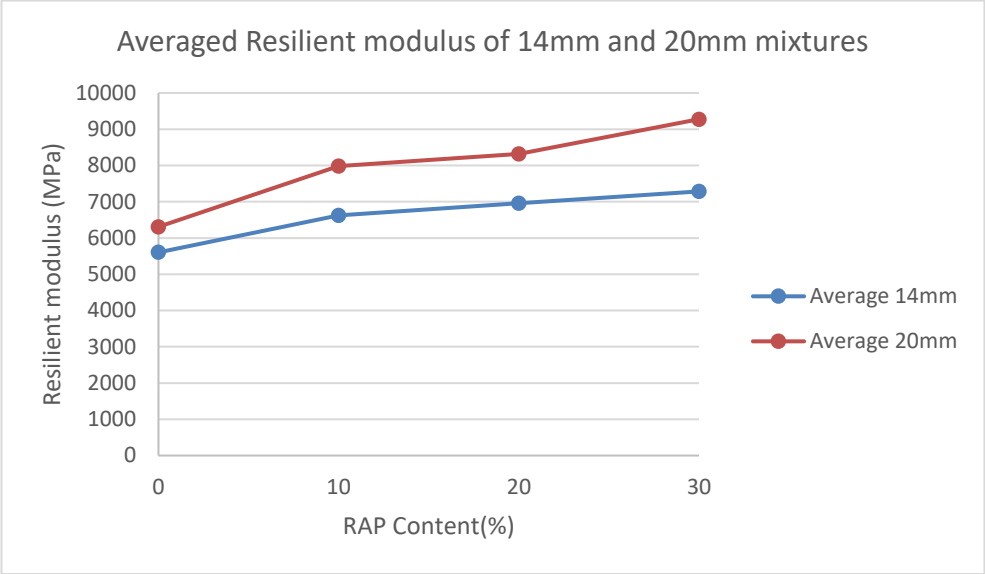

Figure 4-12Comparison of average resilient modulus of 14 and 20 mm mixtures versus RAP content

It is obvious that the 20 mm mixtures generally demonstrated higher values for resilient modulus. For example, the average value for control mixtures with no RAP was 5604 MPa in the 14 mm mixtures, while it was 6308 MPa for its 20 mm counterpart. However, this gap seems to become larger at higher percentages of RAP. For instance, the gap between DG14R10 and DG20R10 mixtures was greater than 1300 MPa in comparison to only approximately 700 MPa difference between both size control mixtures.

4.2.4 Rutting resistance (wheel tracking test)

The rut depth of samples was measured using the indirect wheel tracker method at 60°C under 700N load according to section 3.4.6.4 for all the samples.

4.2.4.1 The 14 mm mixtures

The rut depth resulting from the wheel tracking test for the 14 mm mixtures and their average values are shown in Figure 4-13.

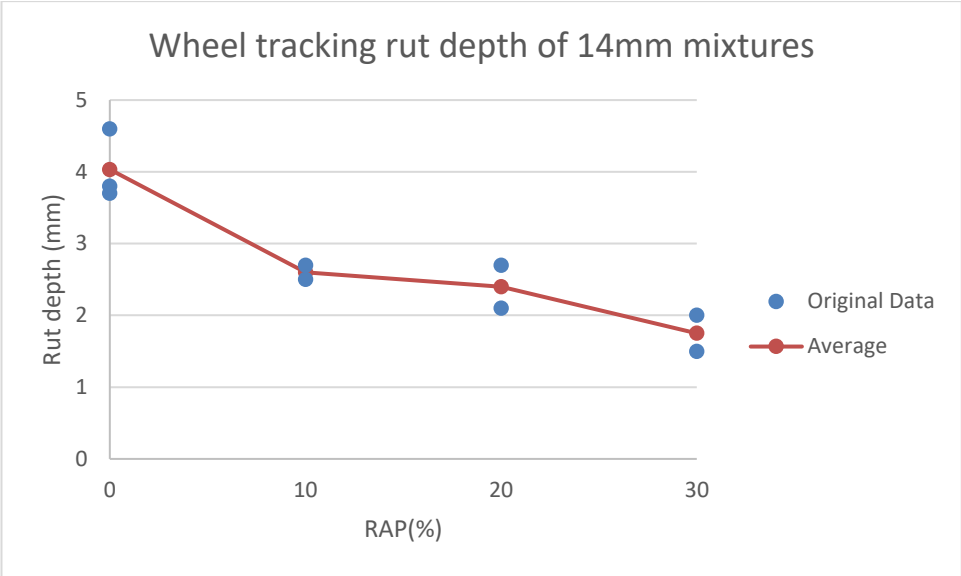

Figure 4-13Rut depth of 14 mm mixtures versus RAP content

As illustrated in Figure 4-13, the rut depth of the averaged 14 mm control mixture was 4 mm. When 10% RAP was added to the mixture, the rut depth dropped significantly (by 35%) to 2.6 mm. However, by adding 20% RAP to the mixture, this parameter only decreased by 0.3 mm, which was followed by another considerable decrease from 2.3 to 1.75 mm when 30% RAP was added.

Generally, it appears there is no considerable effect when the RAP is increased from 10 to 20%in the 14 mm mixtures. This supports the hypothesis that the binder bond is critical for transferring the load in the control mixture. However, having a stiffer binder, the share of aggregates in load carrying will be greater than before, which might be one reason why the slope of the rut depth changed dramatically between different RAP percentage inclusions.

4.2.4.2 The 20 mm mixtures

The rut depth resulting from the wheel tracking test for the 20 mm mixtures and their average values for each mixture are shown in Figure 4-14.

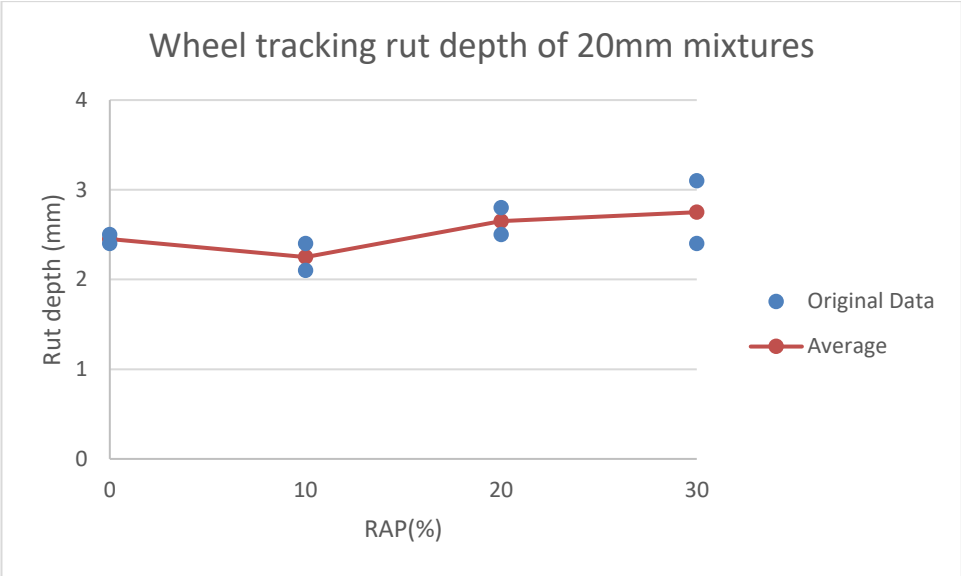

Figure 4-14Rut depth of 20 mm mixtures versus RAP content

Figure 4-14 shows that containing different percentages of RAP did not affect the rut depth dramatically in 20 mm mixtures. The rut depth of the control mixture was measured at 2.45 mm. Adding 10% RAP decreased this parameter slightly to2.25 mm, and the addition of 20% or more RAP increased the rut depth of the samples slightly (2.65 for 20% RAP and 2.75 mm for 30% RAP).

Generally, it can be concluded that the RAP utilised in this study did not have a significant effect on the rut wheel tracking results. The fluctuations in the results might a result of experimental error as the changes are in a very limited range, which indicates that the load is being transferred by aggregate contacting more than the binder binds as a result of having relatively large aggregates. Therefore, the effect of the binder change does not influence the results.

4.2.4.3 Comparison of 14 mm and 20 mm mixtures

Figure 4-15 shows the average rut depth of both 14 and 20 mm mixtures with different percentage of RAP.

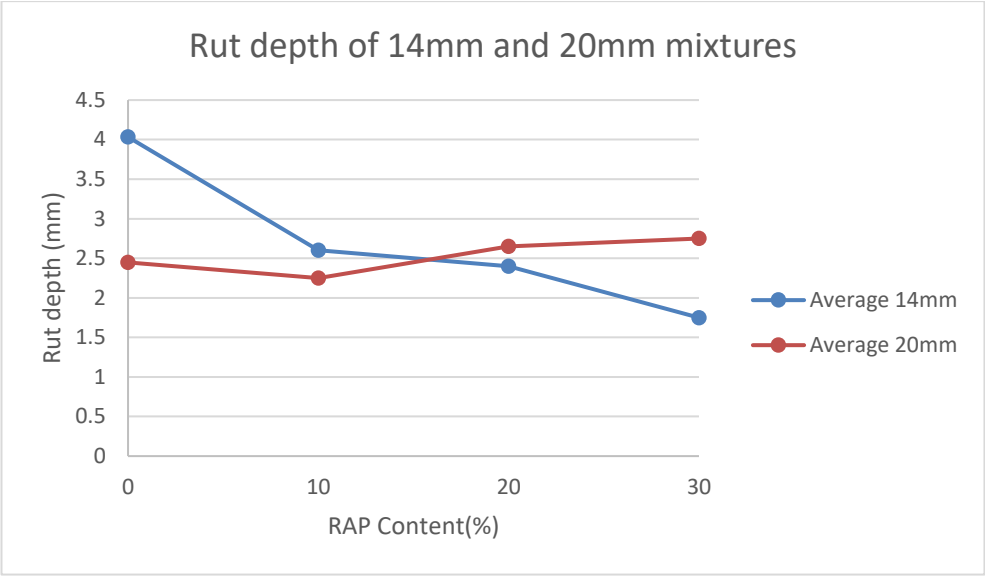

Figure 4-15Comparison of rut depth of 14 and 20 mm mixtures versus RAP content

It is obvious that the effect of RAP was more dramatic in the 14 mm than in the 20 mm mixtures. Having a different percentage of RAP changes the rut depth of the 20 mm mixtures slightly between 2.25 and 2.75 mm, the 14 mm mixtures demonstrate a significant change from 4 to 1.75 mm. As explained before, the reason behind this might be how the binder and aggregates participate in load transferral.

4.2.5 Tensile strength ratio

The moisture sensitivity of samples was evaluated using the TSR between unconditioned and conditioned samples according to the method explained in section 3.4.6.6.

4.2.5.1 The 14 mm mixtures

The tensile strength of unconditioned (dry) and conditioned (wet) 14 mm mixtures are presented in Figure 4-16 and Figure 4-17, respectively. Moreover, the TSRs of the same samples are shown in Figure 4-18.

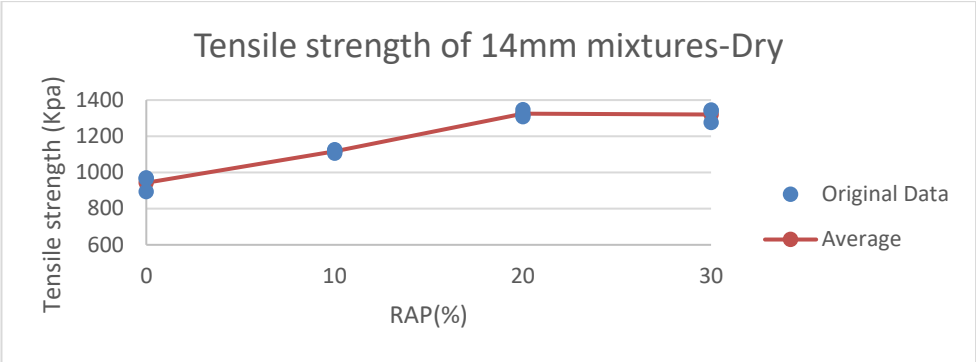

Figure 4-16Tensile strength of unconditioned (dry) 14 mm mixtures versus RAP content

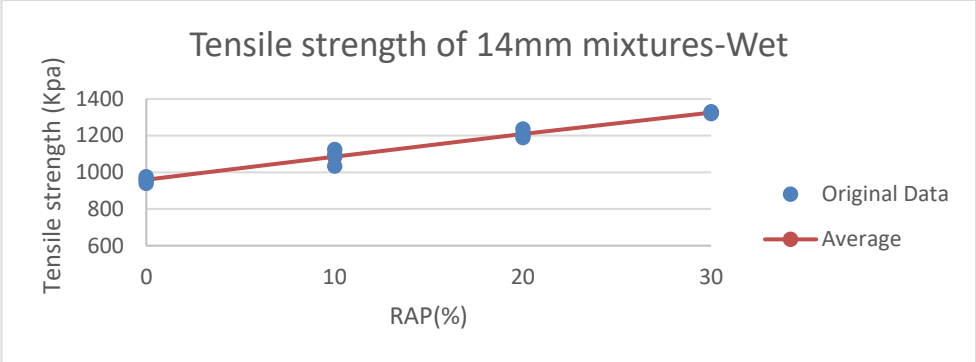

Figure 4-17 Tensile strength of conditioned (wet) 14 mm mixtures versus RAP content

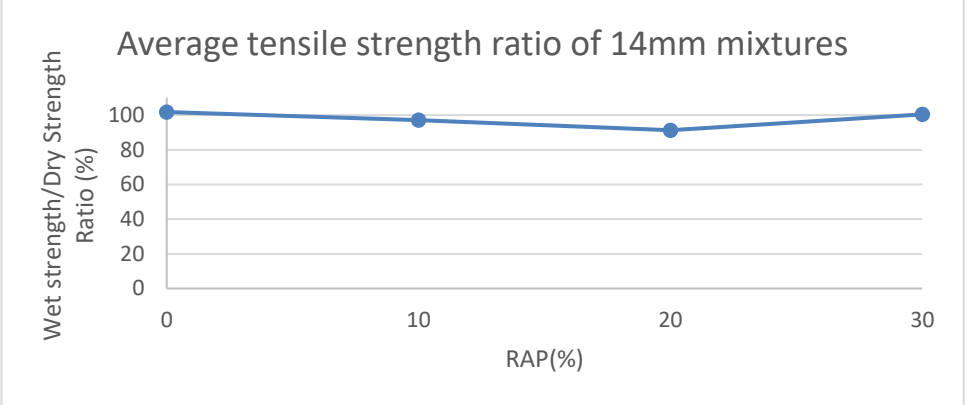

Figure 4-18 Average TSR of 14 mm mixtures versus RAP content

Based on Figure 4-16, the tensile strengths of unconditioned samples increased continuously from 0 to 20% RAP inclusion. However, adding an extra 10% did not significantly change the strength.

For the conditioned samples (partially saturated with water and then F-T conditioned), the strengths were almost the same as their unconditioned counterparts. The only difference seen was with the DG14R20 samples, which showed a small reduction in tensile strength.

The TSR in Figure 4-18 demonstrates that irrespective of the percentage of RAP in the mixture, the TSR values of DG14R0, DG14R10 and DG14R30 were almost 100%; therefore, moisture conditioning had no considerable effect on them. The only effect was observed in DG14R20 that showed a TSR value of 91%, which is still a sign of good performance of the mixture.

4.2.5.2 The 20 mm mixtures

The tensile strength of unconditioned (dry) and conditioned (wet) 20 mm mixtures are presented in Figure 4-19 and Figure 4-20, respectively. Moreover, the TSRs of the same samples are shown in Figure 4-21.

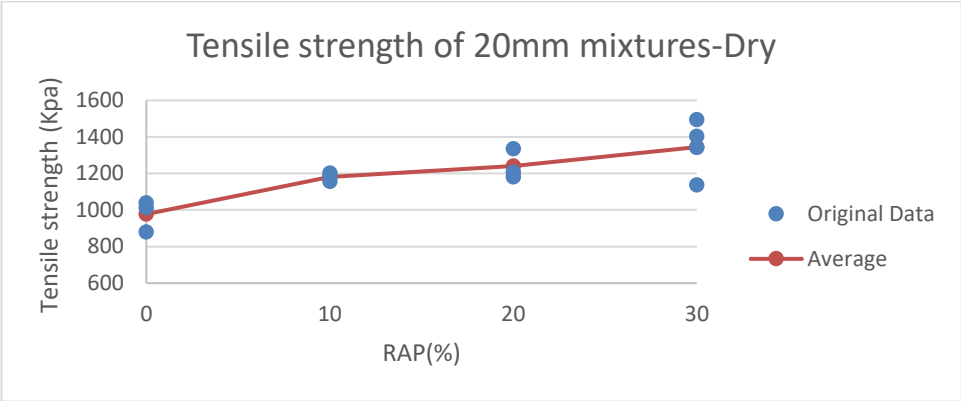

Figure 4-19 Tensile strength of unconditioned (dry) 20 mm mixtures versus RAP content

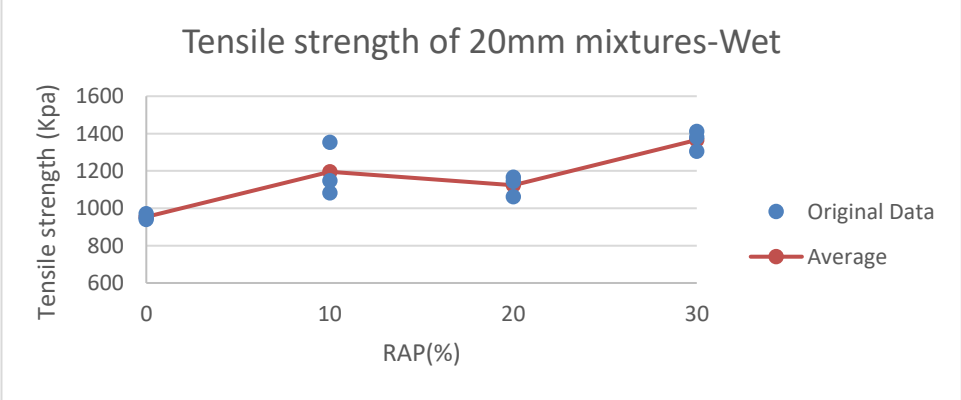

Figure 4-20 Tensile strength of conditioned (wet) 20 mm mixtures versus RAP content

According to Figure 4-19, the tensile strengths of unconditioned samples increased with increasing percentages of RAP in the mixture. Although an increasing trend was also observed for conditioned samples in Figure 4-20 as well, the tensile strength for this group of samples showed a slight decrease in the DG20R20 mixture than in the DG20R10 mixture, before increasing again when 30% RAP was added to the mixture.

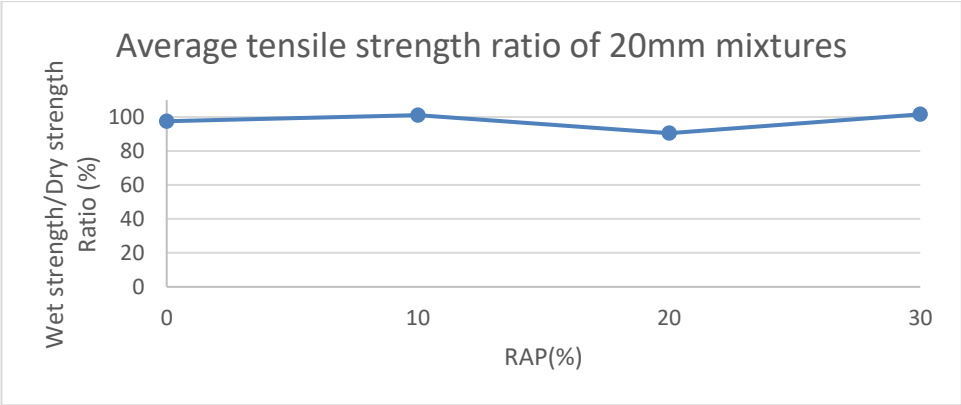

Figure 4-21 Average TSR of the 20 mm mixtures versus RAP content

Because the tensile strengths of the samples did not change meaningfully after conditioning, the TSRs for all the samples were very close to 100%, with the lowest value for the TSR measured in the DG20R20 mixtures at 90%. Therefore, these samples were not affected significantly by facing moisture and a F-T cycle.

4.2.5.3 Comparison of 14 mm and 20 mm mixtures

In Figure 4-22 and Figure 4-23, the average tensile strength of 14 and 20 mm mixtures in unconditioned (dry) and conditioned (wet) situations, respectively, are compared.

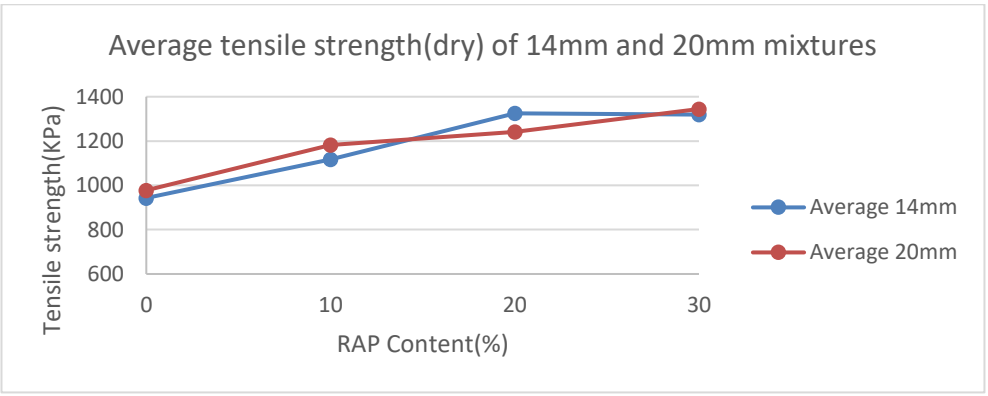

Figure 4-22 Comparison of average tensile strength of unconditioned (dry) 14 and 20 mm mixtures versus RAP content

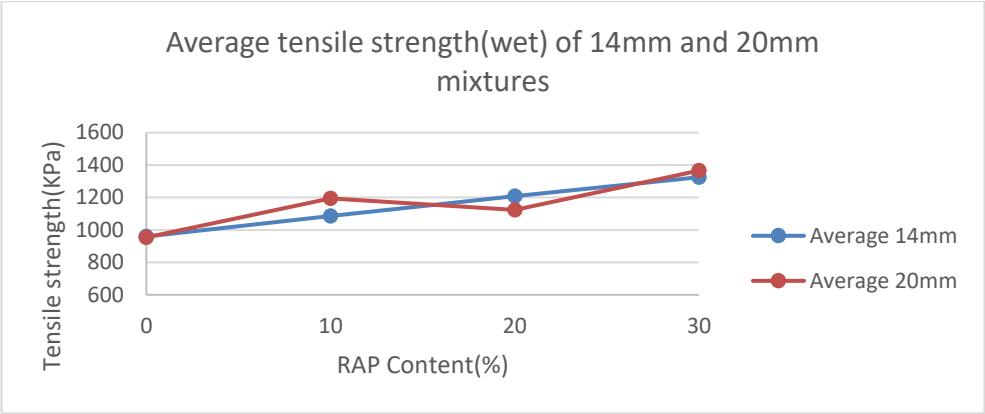

Figure 4-23 Comparison of average tensile strength of conditioned (wet) 14 and 20 mm mixtures versus RAP content

The tensile strengths of both the 14 and 20 mm mixtures were considerably close to each other and follow the same trend for the different percentages of RAP irrespective of whether the samples were conditioned or not. Therefore, the tensile strength of all the control mixtures (no RAP) whether conditioned or unconditioned or even 14 mm or 20 mm was between 943 and 977 KPa. Tensile strength increases by increasing the percentage of RAP in the mixture and when there is 30% RAP in the mixtures the tensile strength of all conditioned or unconditioned samples irrespective of what their nominal size was between 1320 and 1366 KPa.

This supports the hypothesis that the nominal maximum size of the aggregates has little effect on the tensile strength of the samples, which might be caused by the high level of air void and tension failure mode of the samples. Therefore, air voids are considerably high in these samples, which make the contact between aggregates less effective, especially in tension mode. Furthermore, when the sample is in tension, the binder role is crucial and might dominant the role of aggregates.

Moreover, conditioning the samples did not change the tensile strength of the sample dramatically. This can be seen more clearly in Figure 4-24 which shows the TSR of conditioned samples to unconditioned samples.

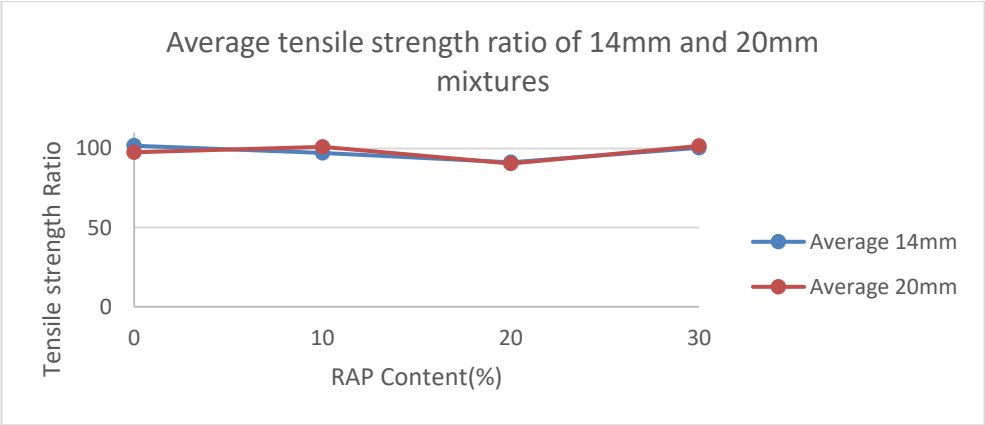

Figure 4-24 Comparison of average TSR of 14 and 20 mm mixtures versus RAP content

According to Figure 4-24, it can be concluded that all samples demonstrated relatively good performance when facing moisture conditioning. The lowest TSR value seen was approximately 90%, which was for mixtures with 20% RAP for both 14 and 20 mm mixtures.

4.2.6 Fatigue life

The performances of beam samples under repetitive bending were evaluated to evaluate their fatigue life according to the method explained in section 3.4.6.5

4.2.6.1 The 14 mm mixtures

The flexural stiffness of the beam samples versus the number of cycles of loading for the 14 mm mixtures are presented in Figure 4-25, Figure 4-26, Figure 4-27 and Figure 4-28 for DG14R0, DG14R10, DG14R20 and DG14R30 mixtures, respectively.

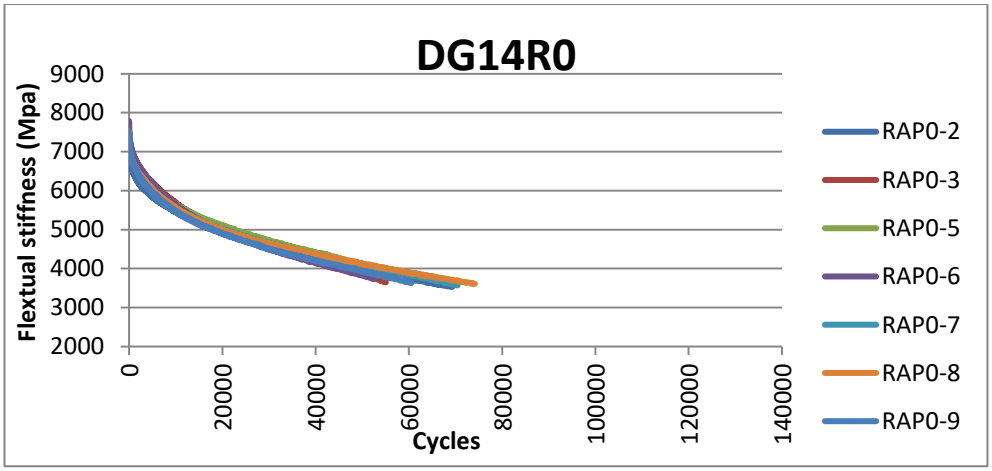

Figure 4-25Flexural stiffness versus the number of cycles for DG14R0 mixture samples

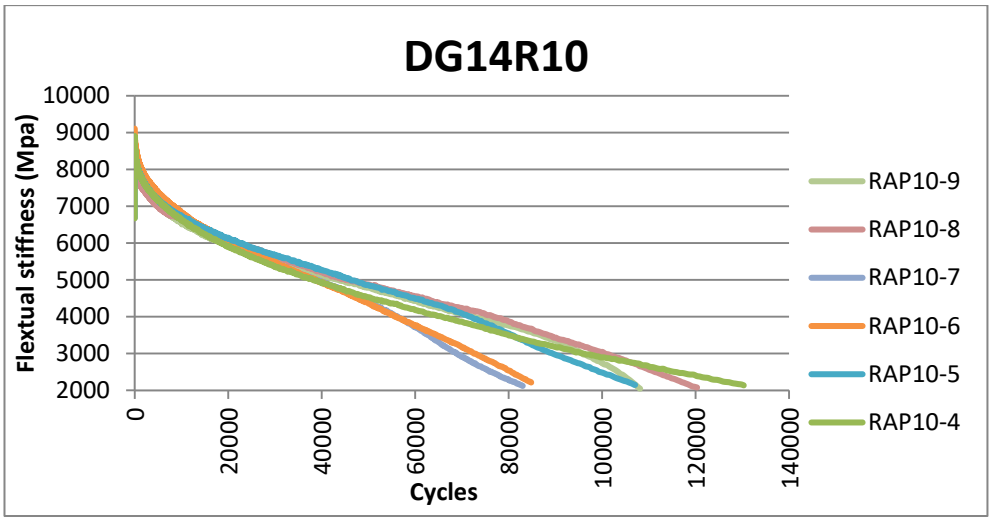

Figure 4-26 Flexural stiffness versus the number of cycles for DG14R10 mixture samples

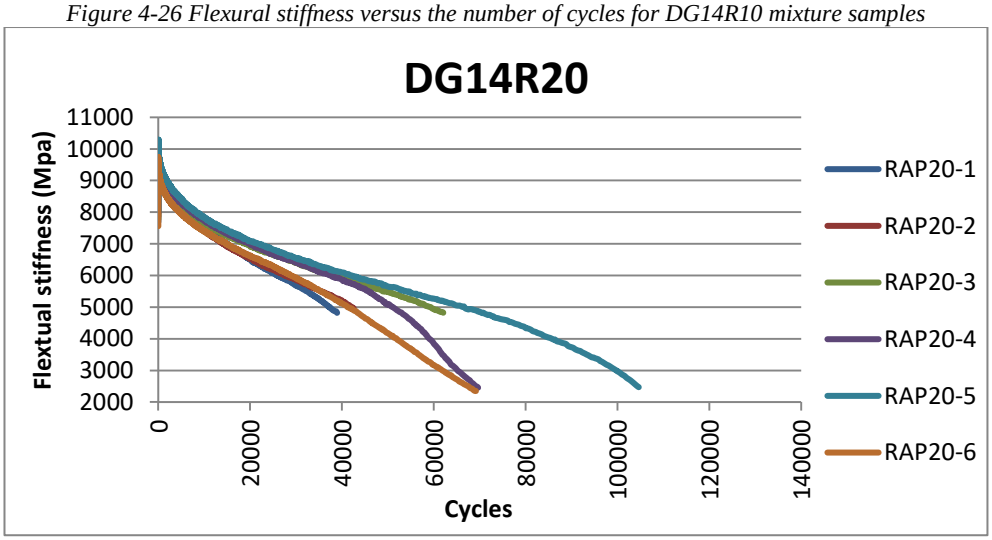

Figure 4-27 Flexural stiffness versus the number of cycles for DG14R20 mixture samples

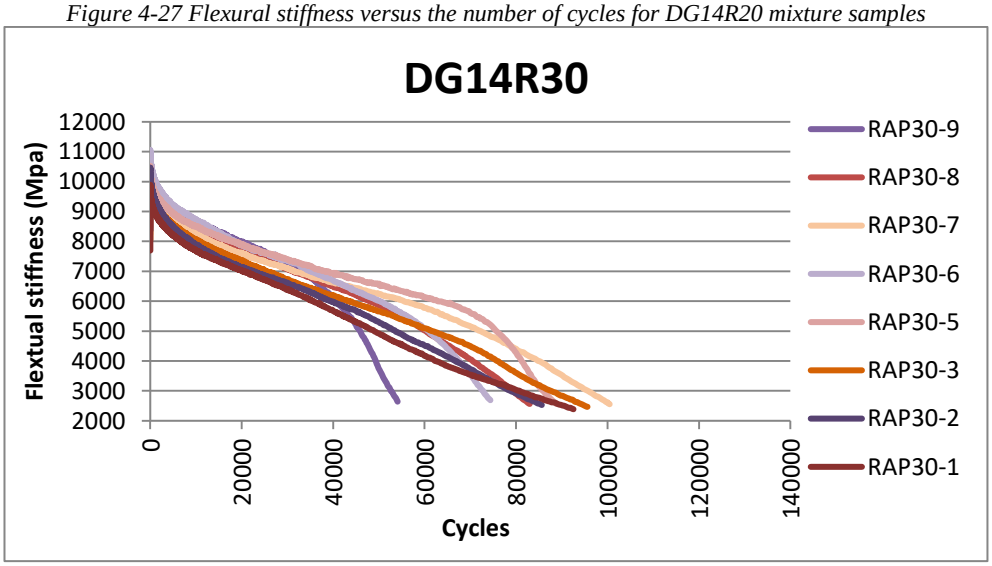

Figure 4-28 Flexural stiffness versus the number of cycles for DG14R30 mixture samples

The test was terminated when the samples reached 25% of their own initial stiffness with the exception of the DG14R0 mixture and three samples of the

DG14R20 mixture, which were terminated at 50% of their initial stiffness. To investigate the data from the beams, several parameters were extracted from the Figure 4-25 to Figure 4-28 , including the initial flexural stiffness, flexural stiffness at 50% of initial stiffness, flexural stiffness at 25% of initial stiffness, phase angle (initial, at 50% reduction of stiffness and at 25% of initial stiffness), cycles to half the stiffness and cycles to quarter of the stiffness.

The initial flexural stiffness, flexural stiffness at 50% of initial stiffness and flexural stiffness at 25% of initial stiffness of the 14 mm mixtures are plotted versus their RAP content in Figure 4-29, Figure 4-30 and Figure 4-31, respectively.

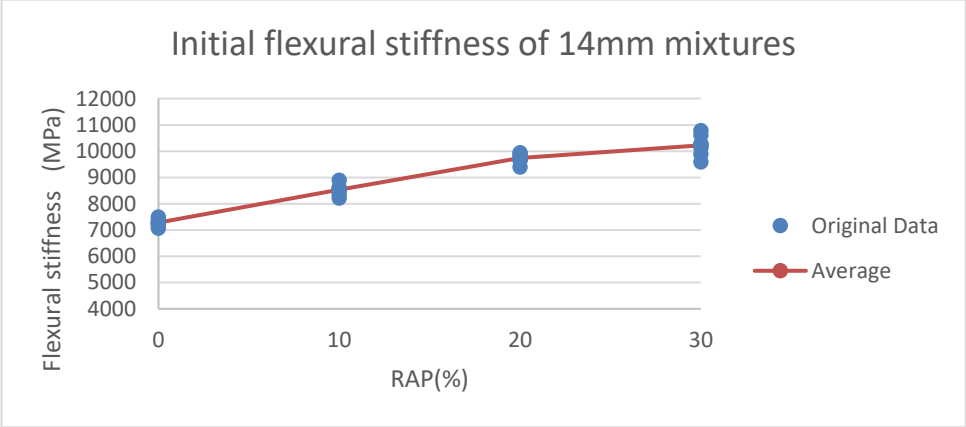

Figure 4-29 Initial flexural stiffness of 14 mm mixtures versus RAP content

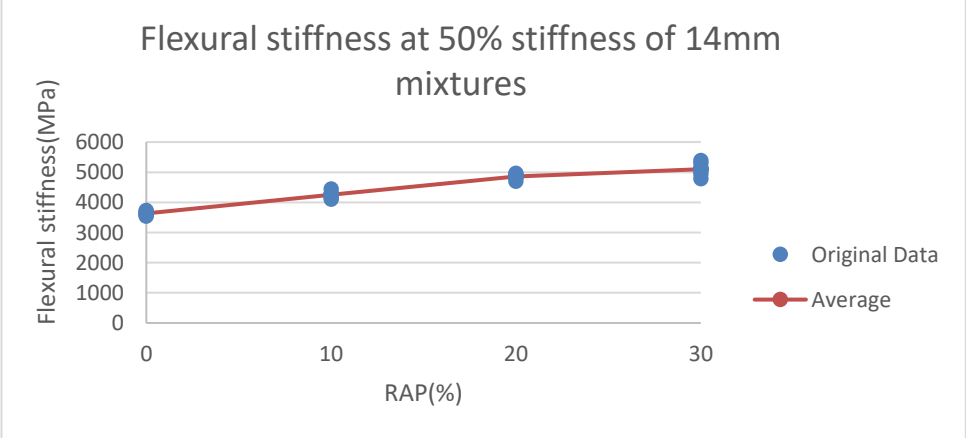

Figure 4-30 Flexural stiffness at 50% of initial flexural stiffness of 14 mm mixtures versus RAP content

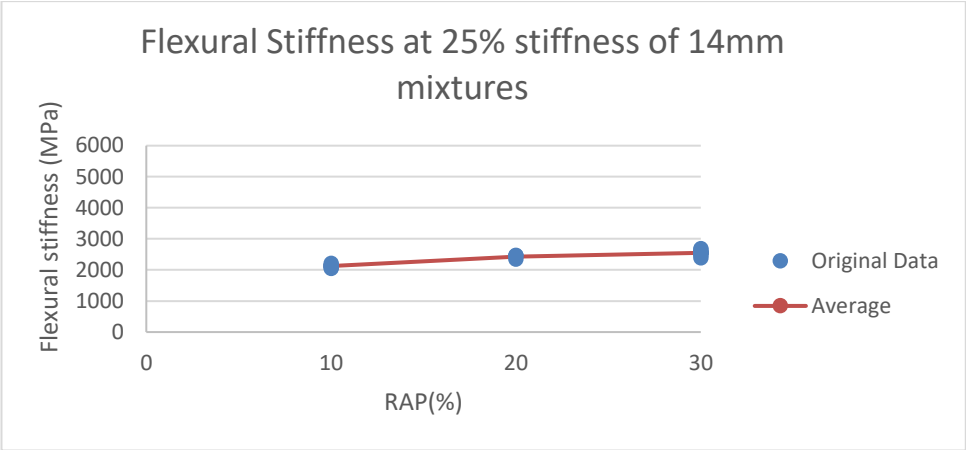

Figure 4-31 Flexural stiffness at 25% of initial flexural stiffness of 14 mm mixtures versus RAP content

Based on the results presented in Figure 4-29, Figure 4-30 and Figure 4-31, the percentage of RAP in the mixture had a significant effect on the flexural stiffness of the samples. The greater the percentage of RAP in the mixture, the higher the value measured for flexural stiffness However, the increase in flexural stiffness is not linear in regards to the amount of RAP in the mixture. To illustrate this, linear and nonlinear regression models for initial flexural stiffness of these mixtures were built based on the original data from the experiments and presented in Table 4-6.

Table 4-6 Regression model of initial flexural stiffness relationship with RAP content for 14 mm mixtures

Regression model	Equation (y = initial flexural stiffness, x = RAP %)	R^2
Linear	$y = 99.147x + 7433.4$	0.9299
2nd order polynomial	$y = -1.9039x^2 + 156.96x + 7253.4$	0.9548
Exponential	$y = 7453.7e^{0.0113x}$	0.9236

As Table 4-6 shows, the initial flexural stiffness values have a better fit with the 2nd order polynomial than with the other models, including linear regression model.

The phase angle (initial, at 50% reduction of stiffness and at 25% of initial stiffness) of the 14 mm mixtures are plotted versus their RAP content in Figure 4-32.

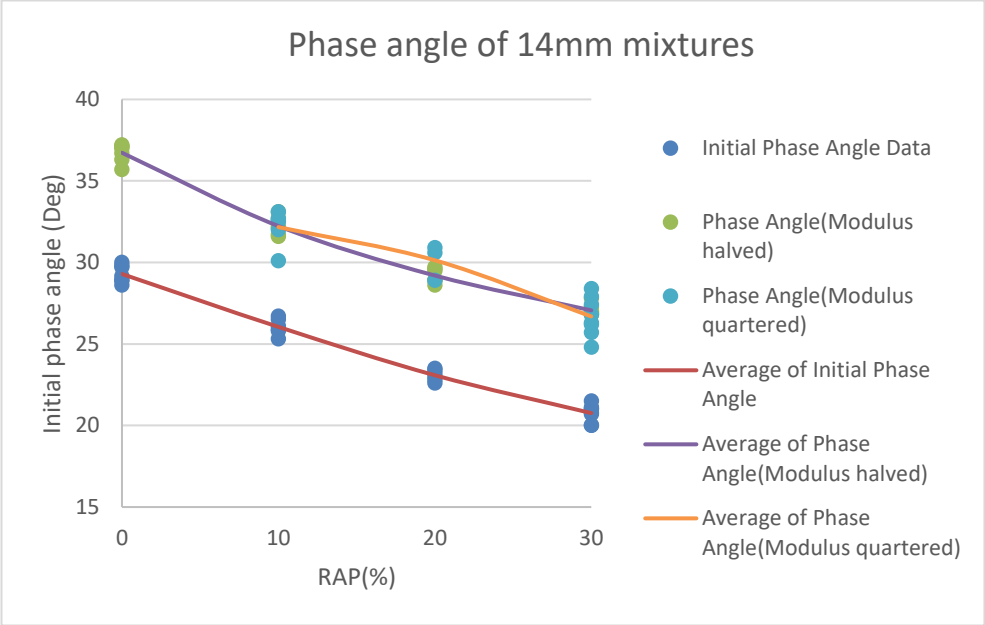

Figure 4-32 Phase angle of 14 mm mixtures versus RAP content

Figure 4-32 illustrates how the phase angles decrease by increasing the percentage of RAP in the mixture, which suggests that the aged binder from the RAP is not only stiffer than the virgin binder, but is also more elastic. Furthermore, the phase angle of the sample increases when it loses its stiffness owing to repetitive loads. The cause of this phenomenon is probably the propagation of micro cracks, which can delay the load transferral in the microstructure of the beams and change the phase angle.

The cycles to half the stiffness and cycles to quarter the stiffness in the 14 mm mixtures are plotted versus their RAP content in Figure 4-33 and Figure 4-34, respectively.

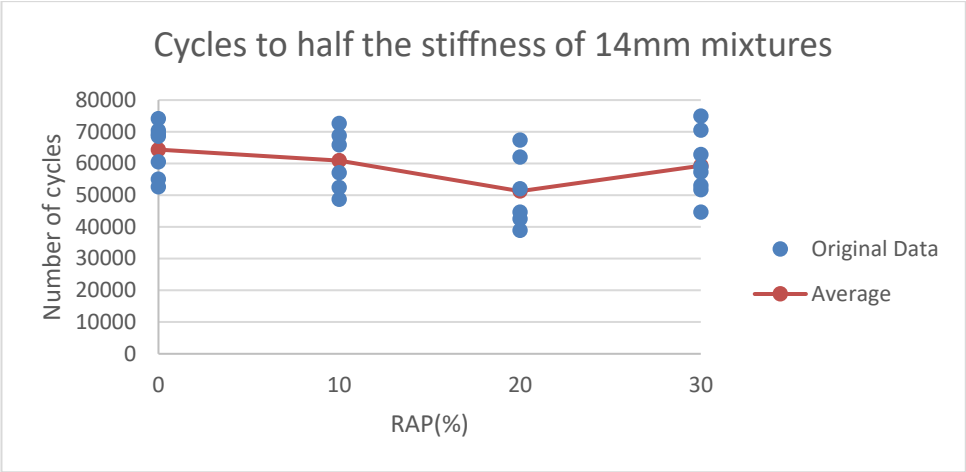

Figure 4-33Number of cycles to halve the flexural stiffness of 14 mm mixtures versus RAP content

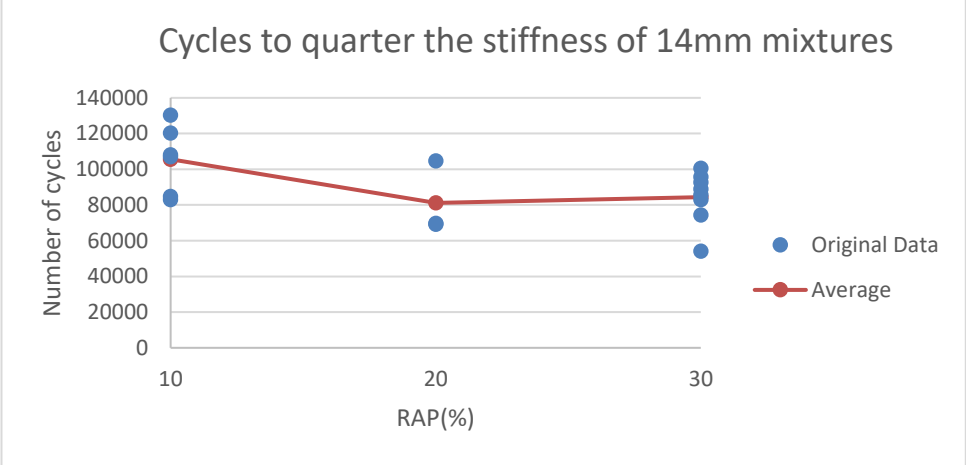

Figure 4-34Number of cycles to quarter the flexural stiffness in 14 mm mixtures versus RAP content

As Figure 4-33 shows, the RAP content of the mixtures did not affect the number of cycles that halve the stiffness of the samples dramatically. The average value only decreased slightly from 60000 when no RAP was in the mixture, to 57103 and 52078 cycles for 10% and 20% RAP, respectively. However, this parameter increased again when the RAP content increased to 30% and reached almost the same value as for the 0 or 10% RAP mixture. Furthermore, this difference is small in comparison to the large discrepancies between results of different samples for the same mixture.

Almost the same story is shown in Figure 4-34 and the number of cycles it takes to quarter the flexural stiffness of the samples. There is no data available for the DG14R0 mixture and less data is available for DG14R20 due to

experimental difficulties; however, the rest of the data shows similar trends to Figure 4-33 (50% reduction).

4.2.6.2 The 20 mm mixtures

The flexural stiffness of the beam samples versus the number of cycles of loading for 20 mm mixtures are presented in Figure 4-35, Figure 4-36, Figure 4-37 and Figure 4-38 for DG14R0, DG14R10, DG14R20 and DG14R30 mixtures, respectively.

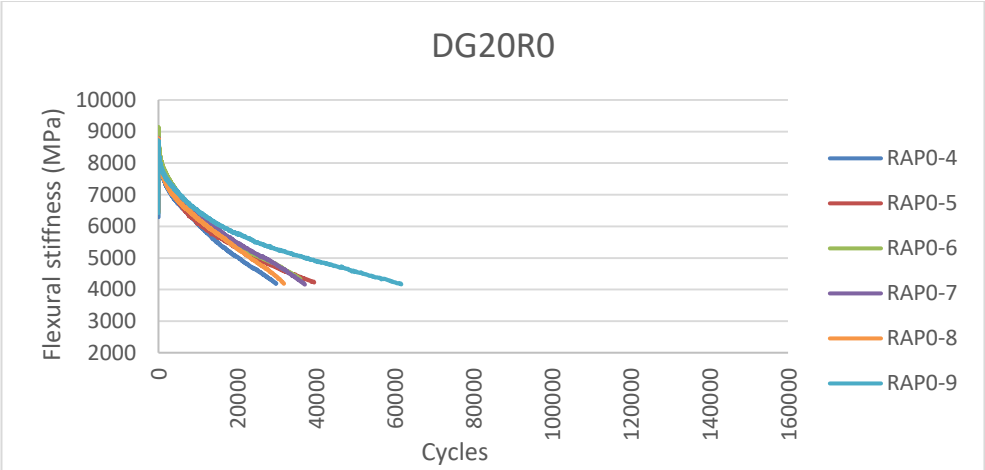

Figure 4-35 Flexural stiffness versus the number of cycles for DG20R0 mixture samples

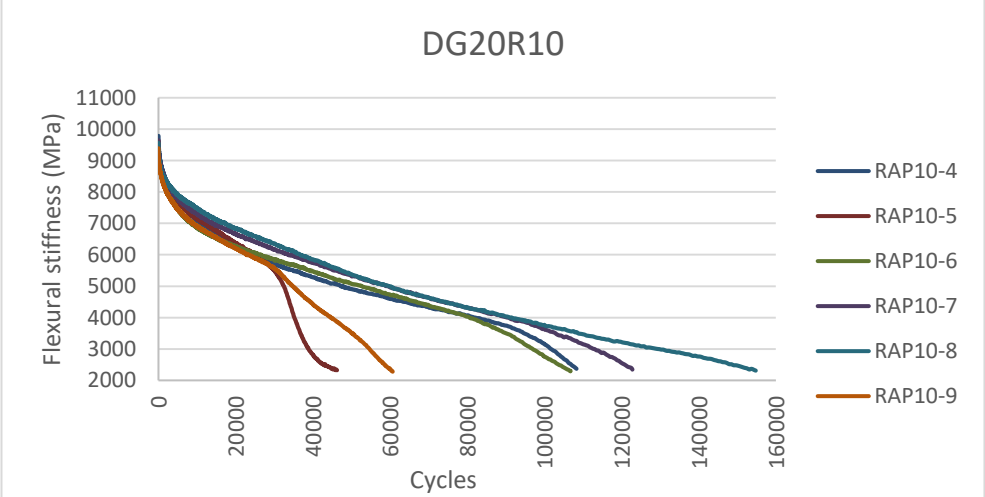

Figure 4-36 Flexural stiffness versus the number of cycles for DG20R10 mixture samples

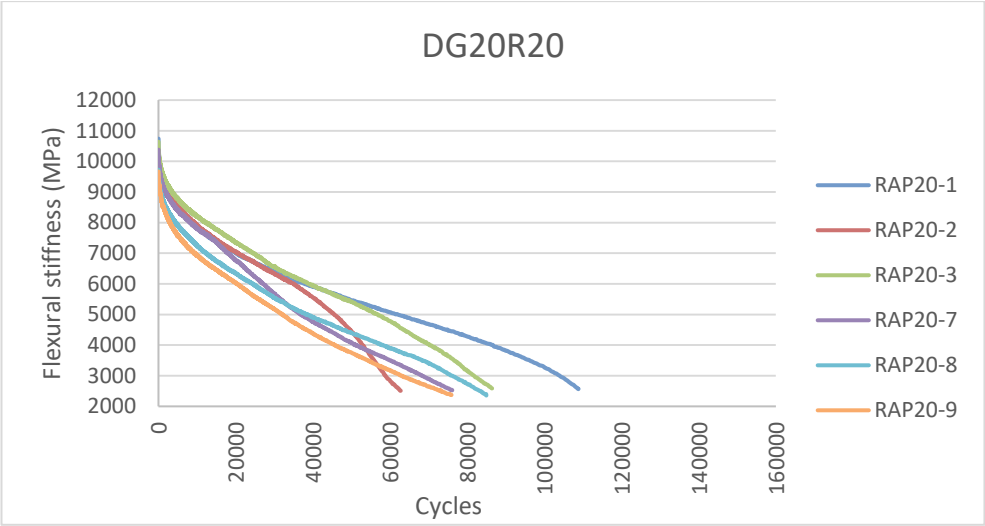

Figure 4-37 Flexural stiffness versus the number of cycles for DG20R20 mixture samples

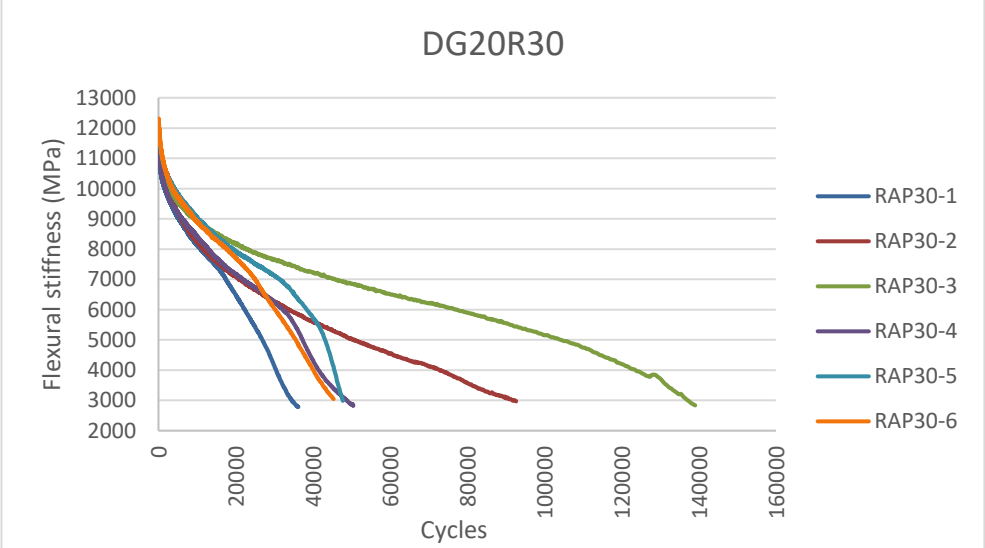

Figure 4-38 Flexural stiffness versus the number of cycles for DG20R30 mixture samples

The test was terminated when the samples reached 25% of their own initial stiffness with the exception of DG14R0 mixture samples that were terminated at 50% of their initial stiffness. The same parameters as those utilised in the 14 mm mixtures to investigate the data from the beams were extracted and discussed below.

The initial flexural stiffness, flexural stiffness at 50% of initial stiffness, flexural stiffness at 25% of initial stiffness of the 20 mm mixtures are plotted versus their RAP content in Figure 4-39, Figure 4-40 and Figure 4-41, respectively.

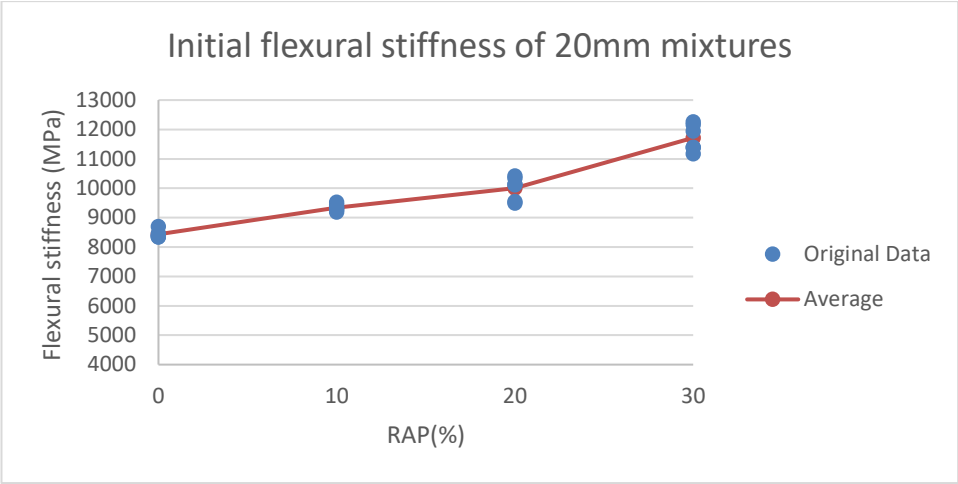

Figure 4-39 Initial flexural stiffness in 20 mm mixtures versus RAP content

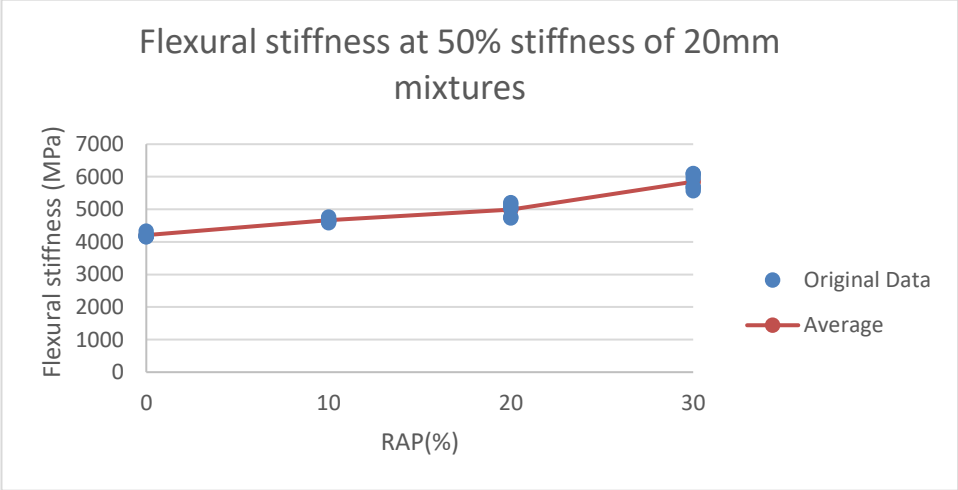

Figure 4-40 Flexural stiffness at 50% of initial flexural stiffness in 20 mm mixtures versus RAP content

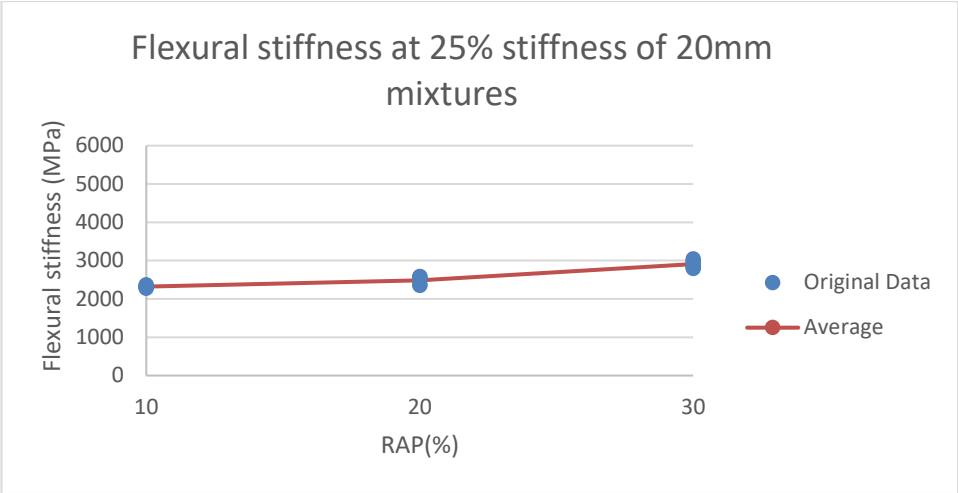

Figure 4-41 Flexural stiffness at 25% of initial flexural stiffness in 20 mm mixtures versus RAP content

From the figures, the percentage of RAP in the mixtures had a significant effect on the flexural stiffness of the samples. The higher the RAP percentage in the mixture, the higher was the measured value for flexural stiffness. However, this increase in the flexural stiffness did not appear linear with regards to the amount of RAP in the mixture. To illustrate this, the linear and nonlinear regression model for initial flexural stiffness of these mixtures were built based on the original data from the experiments and are presented in Table 4-7.

Table 4-7 Regression model of initial flexural stiffness relationship with RAP content for 20 mm mixtures

Regression Model	Equation (y = initial flexural stiffness, x = RAP %)	R^2
Linear	$y = 105.08x + 8298.9$	0.9048
2nd order polynomial	$y = 2.0046x^2 + 44.944x + 8499.4$	0.9312
Exponential	$y = 8369.5e^{0.0105x}$	0.9245

As Table 4-7 shows, the initial flexural stiffness values have a better fit with the 2nd order polynomial rather than with the other models, including linear

regression model, which was the same result as that seen in the 14 mm mixtures.

The phase angle (initial, at 50% reduction of stiffness and at 25% of initial stiffness) of the 20 mm mixtures are plotted versus their RAP content in Figure 4-42.

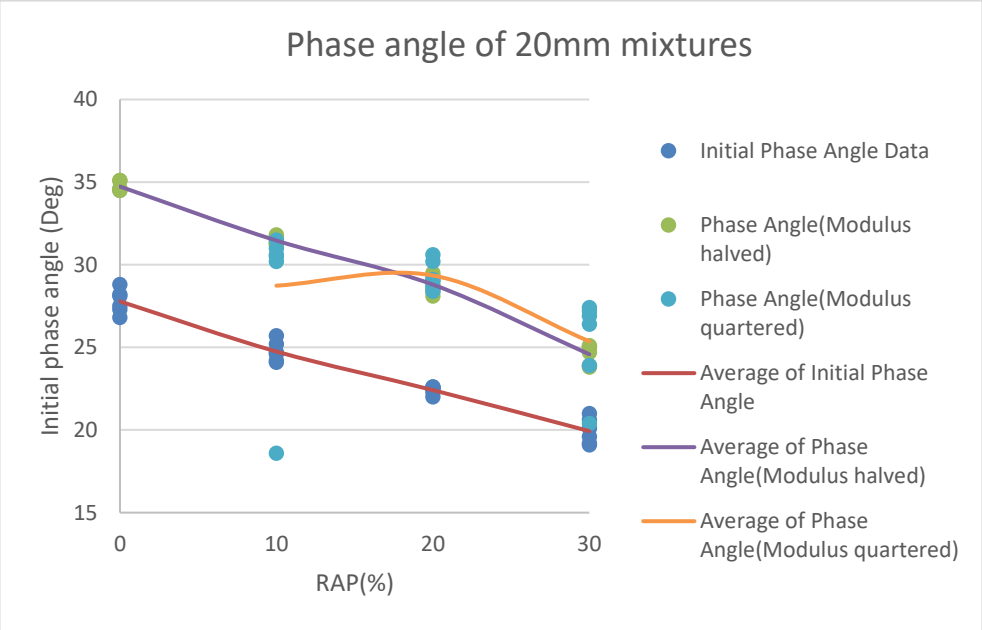

Figure 4-42 Phase angle of 20 mm mixtures versus RAP content

Figure 4-42 shows how the phase angle of 20mm mixtures, had the similar trend as 14mm mixtures. One of the values in the DG20R10 sample for the phase angle when the modulus was quartered from its initial value was much smaller than the other values for the same situation and mixture, which is the reason why the trend line between the average values for this parameter shows an unexpected trend. This discrepancy is probably caused because of experimental errors.

The cycles to half the stiffness and cycles to quarter the stiffness of the 20 mm mixtures are plotted versus their RAP content in Figure 4-43 and Figure 4-44, respectively.

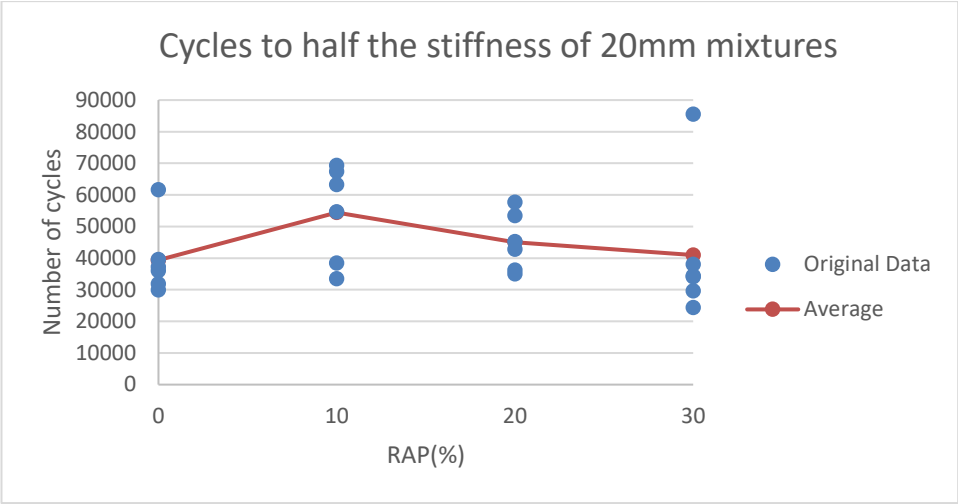

Figure 4-43 Number of cycles to halve the flexural stiffness of 20 mm mixtures versus RAP content

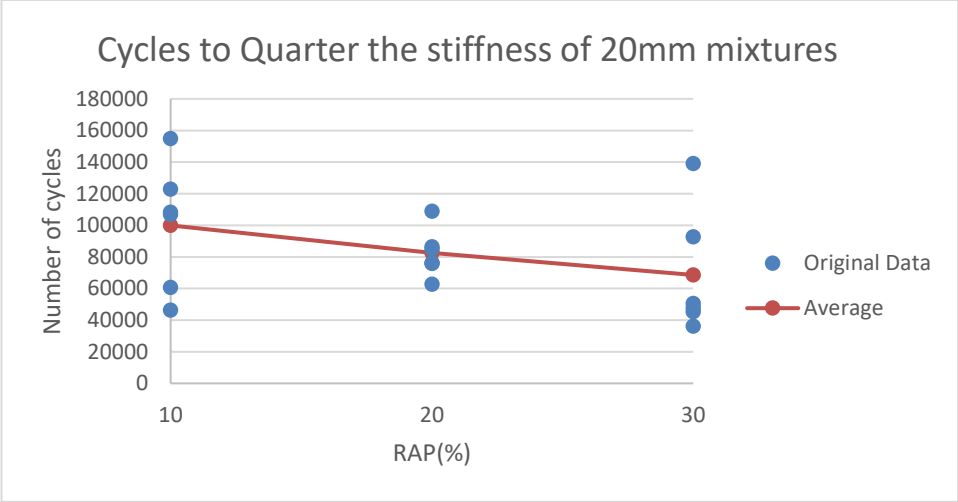

Figure 4-44 Number of cycles to quarter the flexural stiffness for 20 mm mixtures versus RAP content

As Figure 4-43 illustrates, the RAP content of the mixtures did not dramatically affect the number of cycles that halve the stiffness of the samples. The average value increased slightly from 39385 cycles when no RAP was in the mixture to 54425 cycles when there was 10% RAP in the mixture, which was followed by a decreasing trend with addition of more RAP to the mixture. For example, the number of cycles for 20% and 30% RAP were 45056 and 41002 respectively. The number of cycles to halve the initial stiffness for the mixtures with 30% RAP was similar to the results of the control mixture containing no RAP.

Almost the same story can be seen in Figure 4-44 that shows the number of cycles it takes to quarter the flexural stiffness of the samples. There was no

data available for DG20R0 due to experimental difficulties, but the remainder of the data shows a similar decreasing trend as that seen in Figure 4-43 (50% reduction).

4.2.6.3 Comparison of 14 mm and 20 mm mixtures

In Figure 4-45, Figure 4-46 and Figure 4-47 the average initial flexural stiffness, the cycles to halve/quarter the flexural stiffness and phase angle of 14 and 20 mm mixtures are compared, respectively.

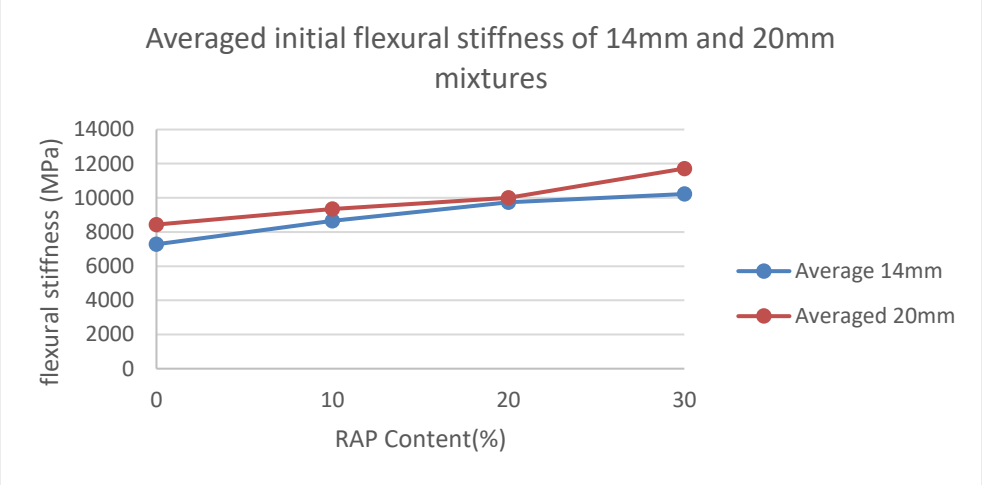

Figure 4-45 Comparison of average initial flexural stiffness of 14 and 20 mm mixtures versus RAP content

According to Figure 4-45, the 20 mm mixtures had a higher stiffness irrespective of how much RAP was added to the mixture. However, this difference was not significant, especially when the RAP percentage was between 10 and 20% (only 680 and 272 MPa difference, respectively). The gap between the 20 mm mixtures and the 14 mm mixtures is more pronounced at 0 and 30% RAP (1152 and 1494 MPa, respectively).

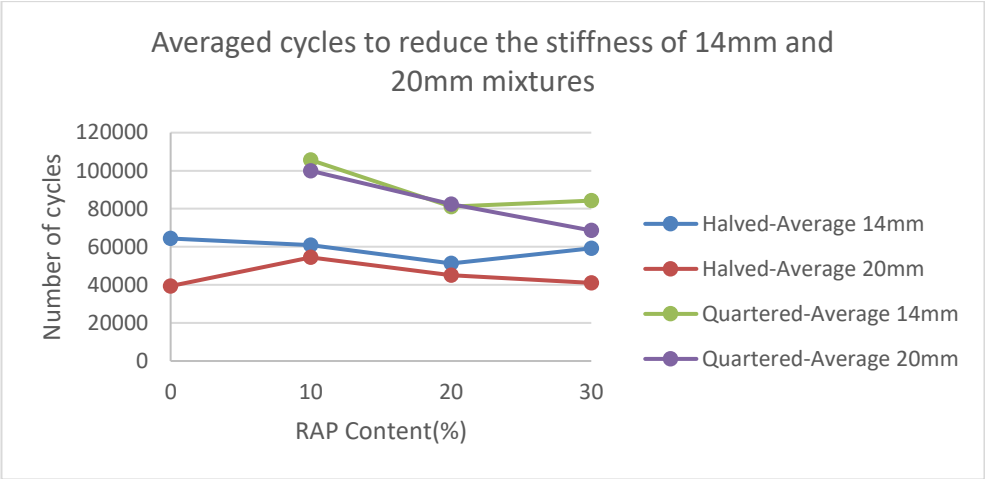

Figure 4-46 Comparison of the average number of cycles to reduce the flexural stiffness to 50% and 25% of its initial value for 14 and 20 mm mixtures versus RAP content

Based on Figure 4-46, the 14 mm mixtures show a slightly better performance in the number of cycles they can tolerate to reach half or a quarter of their initial stiffness on average. In mixtures with no RAP or 30% RAP, there was a considerable difference (approximately 20000 cycles) between the number of cycles in the 14 and 20 mm mixtures. However, these differences are much less for the mixtures that have 10 and 20% RAP. A similar pattern is seen for the number of cycles it takes to quarter the flexural stiffness of the samples.

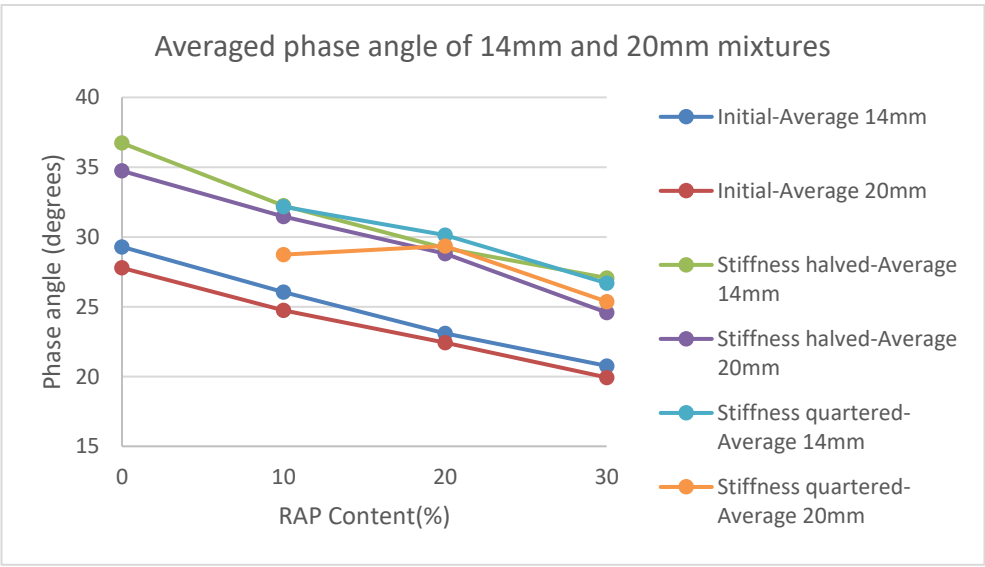

Figure 4-47 Comparison of the average number of phase angles at the beginning of the test, 50% and 75% reduction of flexural stiffness for 14 and 20 mm mixtures versus RAP content

With respect to Figure 4-47, the average initial phase angle in samples of the 14 mm mixtures were always slightly higher (the maximum difference is

under 3 degrees) than their 20 mm counterparts, even though the trend for both of them cause by RAP inclusion is almost identical.

4.2.7 Complex modulus

The performance of cylindrical samples under compressive loading were evaluated to determine their dynamic modulus and phase angle at different temperatures and loading frequencies according to the method explained in section 3.4.6.2.

4.2.7.1 The 14 mm mixtures

In the following subsections, the effect of temperature and RAP content will be studied based on the results from the dynamic modulus and phase angle tests of the 14 mm mixtures for different loading frequencies, including 0.1, 1 and 10 Hz.

4.2.7.1.1 Temperature effect

The change in dynamic modulus and phase angle of the samples owing to the temperature and frequency are shown for each mixture separately in Figure 4-48 to Figure 4-55.

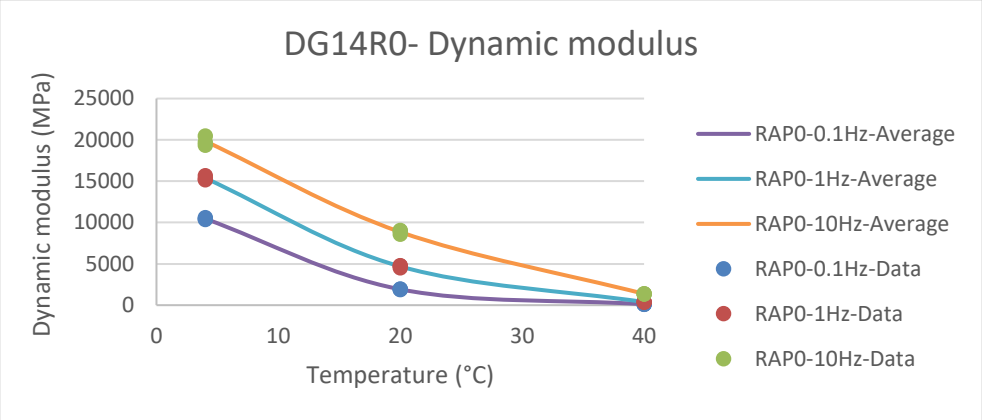

Figure 4-48 Dynamic modulus of DG14R0 mixture versus temperature

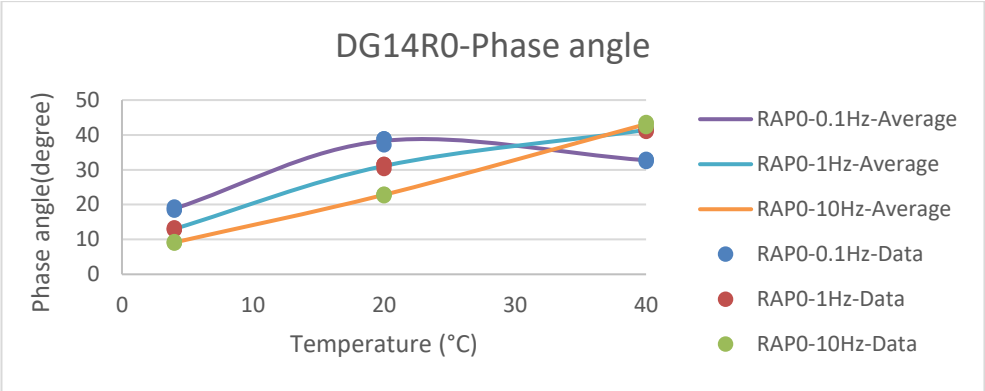

Figure 4-49 Phase angle of DG14R0 mixture versus temperature

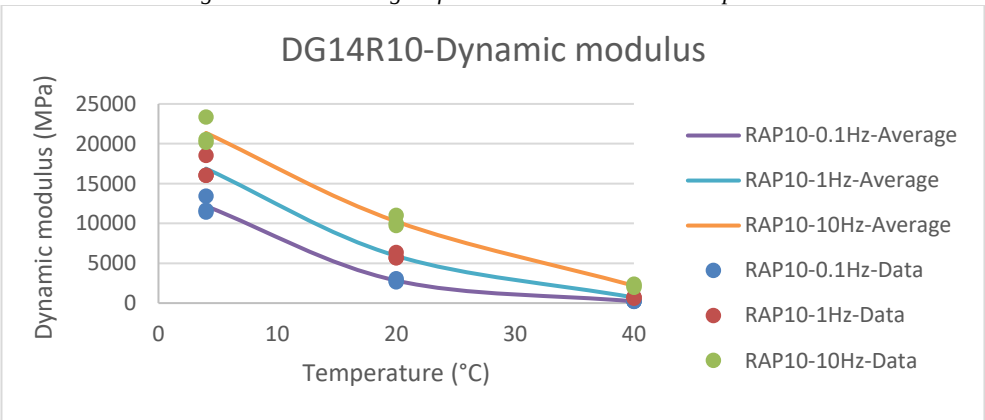

Figure 4-50 Dynamic modulus of DG14R10 mixture versus temperature

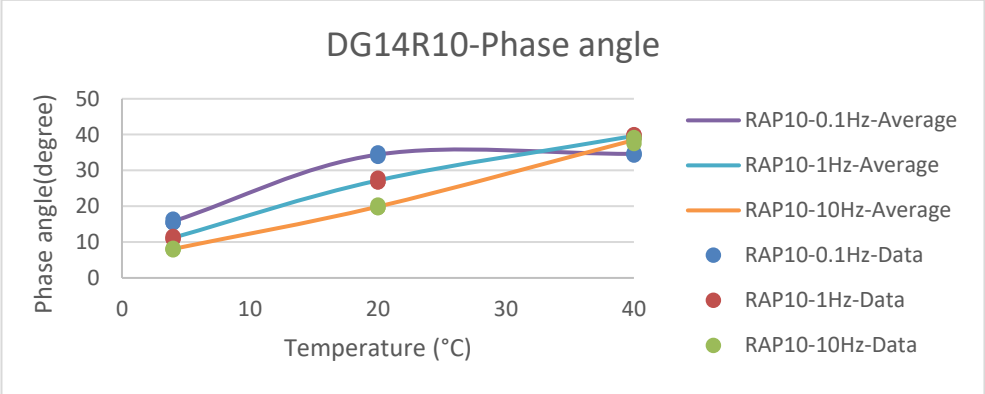

Figure 4-51 Phase angle of DG14R10 mixture versus temperature

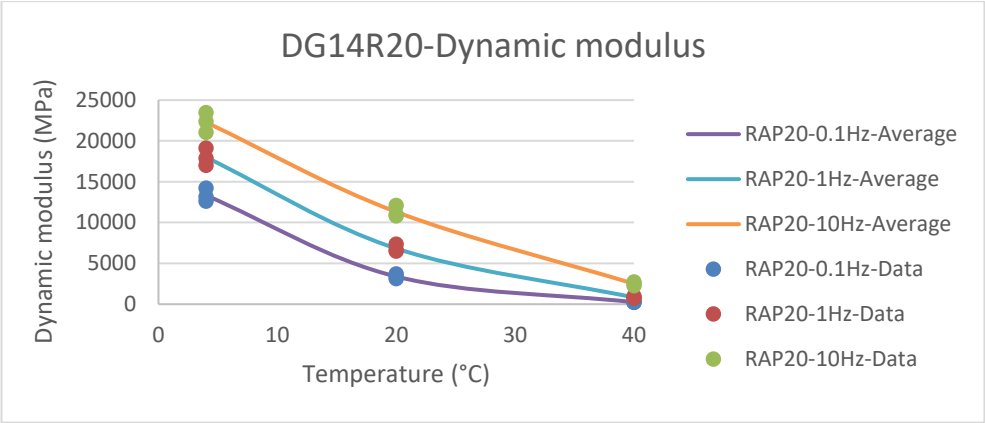

Figure 4-52 Dynamic modulus of DG14R20 mixture versus temperature

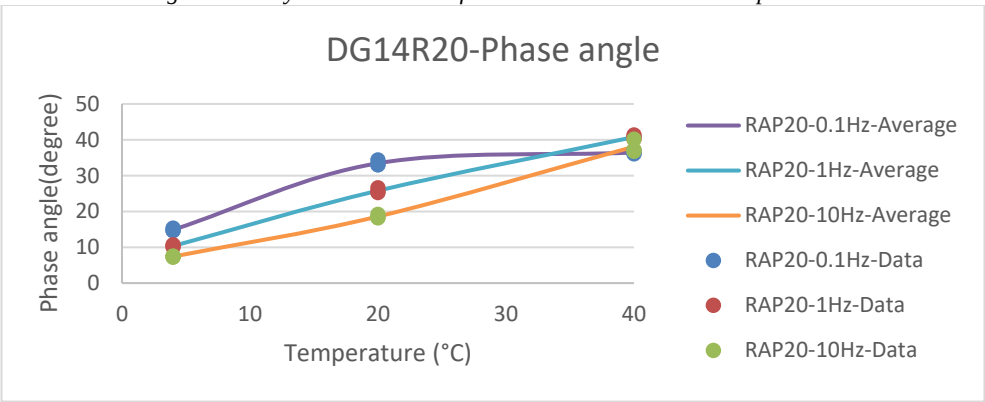

Figure 4-53 Phase angle of DG14R20 mixture versus temperature

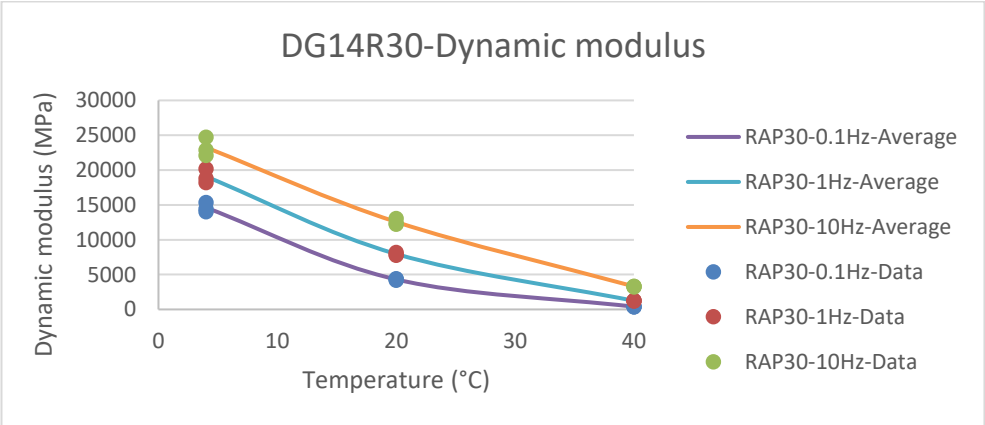

Figure 4-54 Dynamic modulus of DG14R30 mixture versus temperature

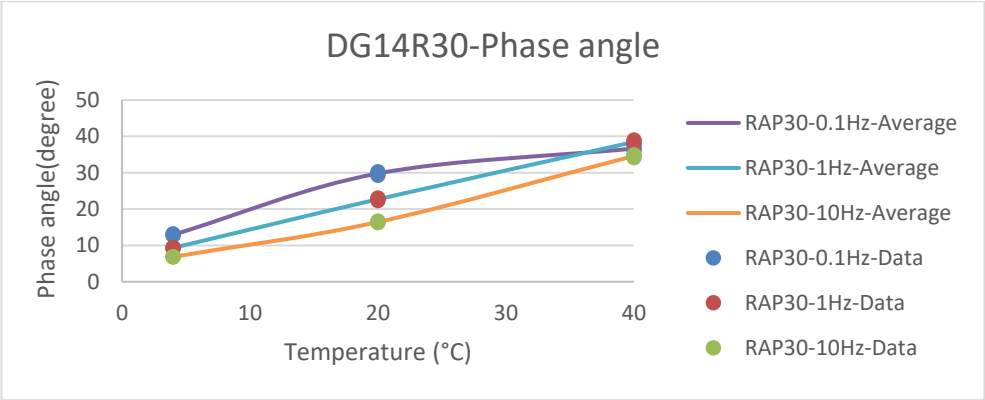

Figure 4-55 Phase angle of DG14R30 mixture versus temperature

According to these figures, it can be seen that temperature significantly changed both the dynamic modulus and phase angle. As expected, the mixtures showed higher dynamic modulus for higher frequencies than for lower ones. Furthermore, the rate of change of dynamic modulus is more noticeable in the lower loading frequencies than in the higher loading frequencies for all mixtures. For example, the average dynamic modulus of DG14R30 mixture at 4 °C was 23246 and 14614 MPa for 10 Hz and 0.1 Hz loading frequency, respectively, while at 40 °C these were 3306 and 394 MPa, respectively.

Regarding the phase angle, the phase angles were generally higher at lower loading frequencies and increased with increasing temperature. However, the phase angle measurement at 40 °C and the lowest loading frequency (0.1 Hz) did not follow the same trend as the other points. Even though it was expected that the phase angle would be greater in lower frequencies at the same temperature, the results reveal this contradiction. For instance, the average phase angle of DG14R30 mixture at 40 °C was 34, 38 and 36 degrees for 10, 1 and 0.1 Hz frequency, respectively.

4.2.7.1.2 RAP content effect

The change of dynamic modulus and phase angle of the samples owing to the RAP content and frequency are shown at each temperature studied in Figure 4-56 to Figure 4-61.

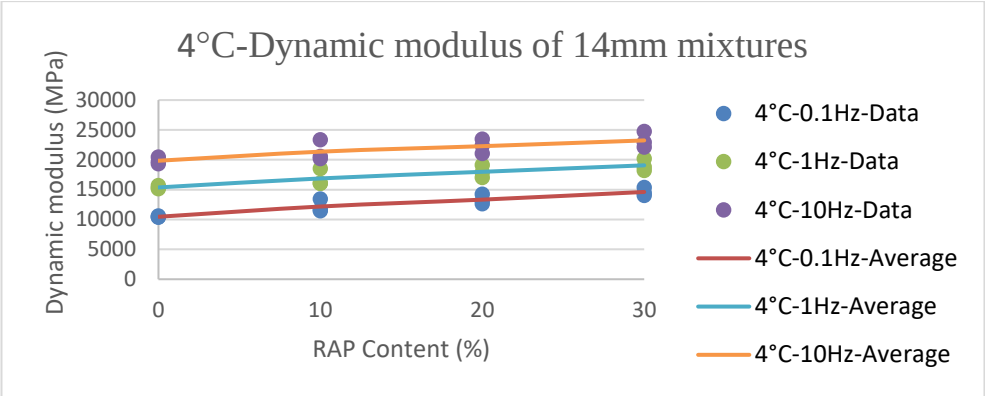

Figure 4-56 Dynamic modulus of 14 mm mixtures versus RAP content at 4 °C

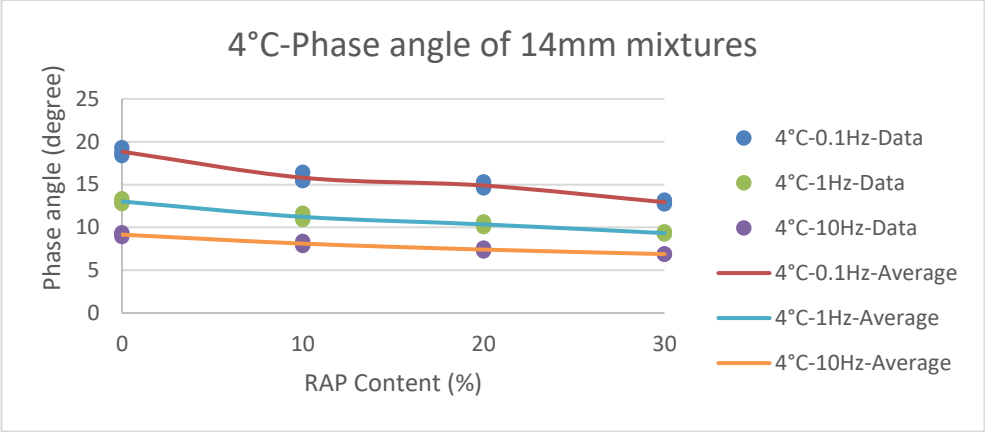

Figure 4-57 Phase angle of 14 mm mixtures versus RAP content at 4 °C

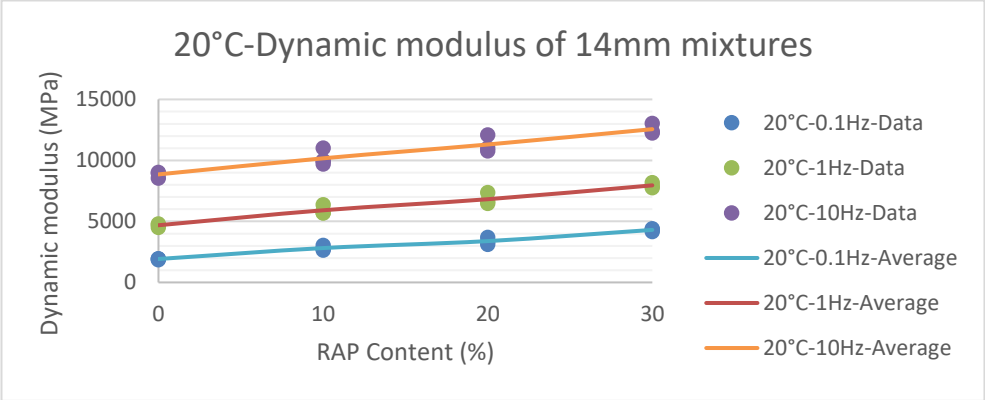

Figure 4-58 Dynamic modulus of 14 mm mixtures versus RAP content at 20 °C

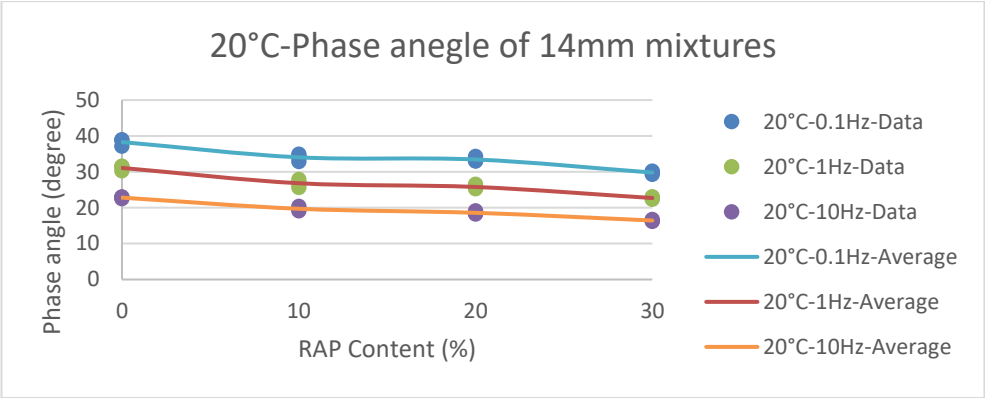

Figure 4-59 Phase angle of 14 mm mixtures versus RAP content at 20 °C

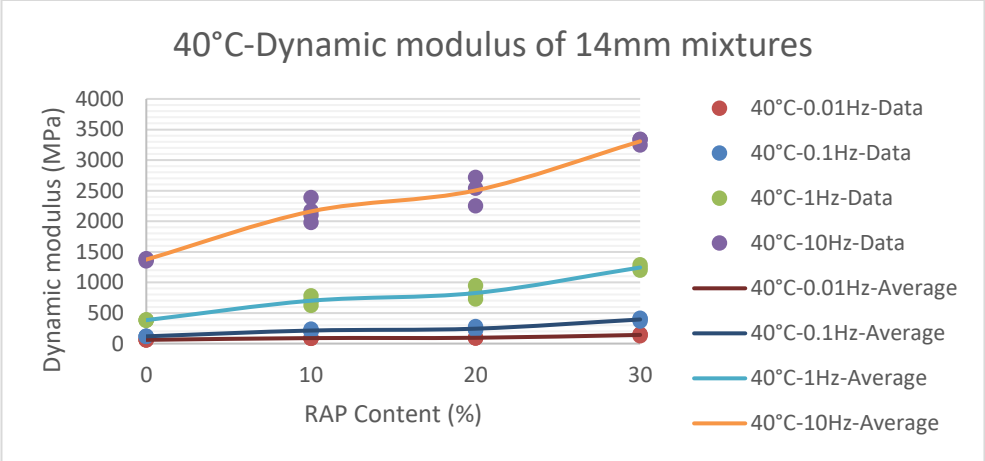

Figure 4-60 Dynamic modulus of 14 mm mixtures versus RAP content at 40 °C

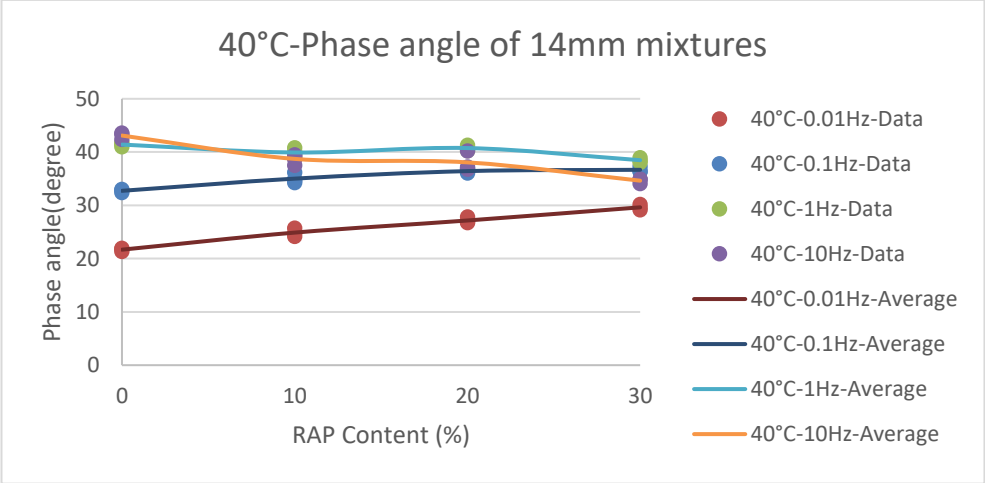

Figure 4-61 Phase angle of 14 mm mixtures versus RAP content at 40 °C

The dynamic modulus of the mixtures at all temperatures increased with the addition of RAP in the mixture or loading with higher frequencies.

Moreover, the phase angle at 4 and 20 °C decreased with greater percentages of RAP in the mixture. Surprisingly, at 40 °C this trend was only true for the highest loading frequency (10 Hz) while at other loading frequencies the trend

increased with respect to the RAP content. It was observed that adding RAP affected the phase angle differently at low temperatures (4 and 20 °C) than at high temperature (40 °C). At low temperatures (4 and 20 °C) or in a high-frequency (10 Hz) at 40 °C, the mixture becomes more elastic by decreasing the phase angle, while at high temperature (40 °C) and lower loading frequencies (1, 0.1 and 0.01 Hz) the mixture becomes more viscous by increasing the phase angle.

4.2.7.2 The 20 mm mixtures

The effect of temperature and RAP content on the results of the dynamic modulus and phase angle tests in the 20 mm mixtures for different loading frequencies, including 0.1, 1 and 10 Hz are discussed in the following subsections.

4.2.7.2.1 Temperature effect

The change in the dynamic modulus and phase angle of the samples owing to the temperature and frequency are shown for each mixture separately in Figure 4-62 to Figure 4-69.

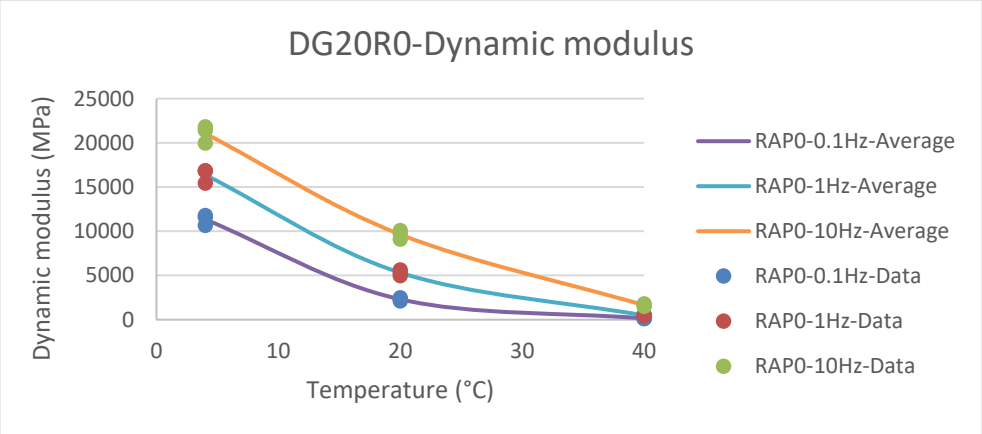

Figure 4-62 Dynamic modulus of DG20R0 mixture versus temperature

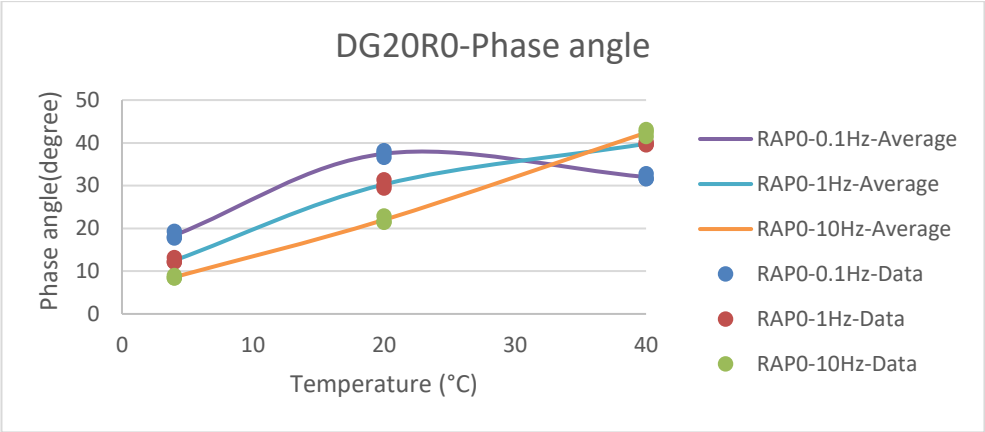

Figure 4-63 Phase angle of DG20R0 mixture versus temperature

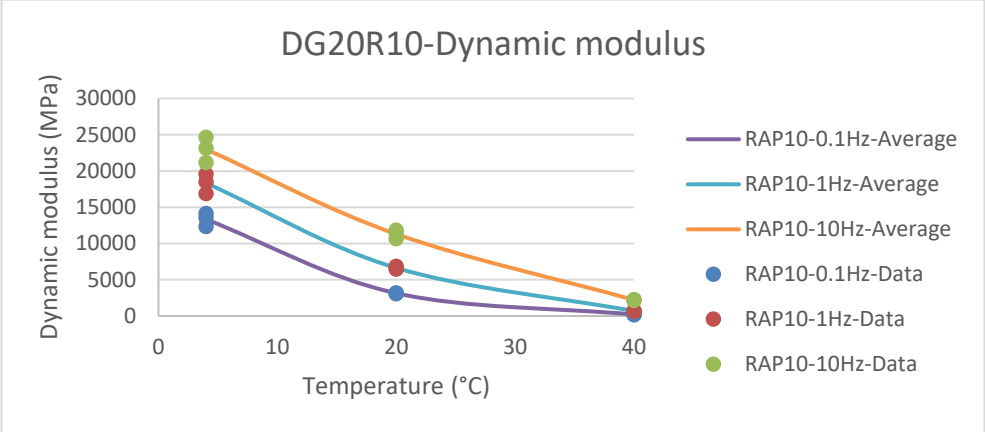

Figure 4-64 Dynamic modulus of DG20R10 mixture versus temperature

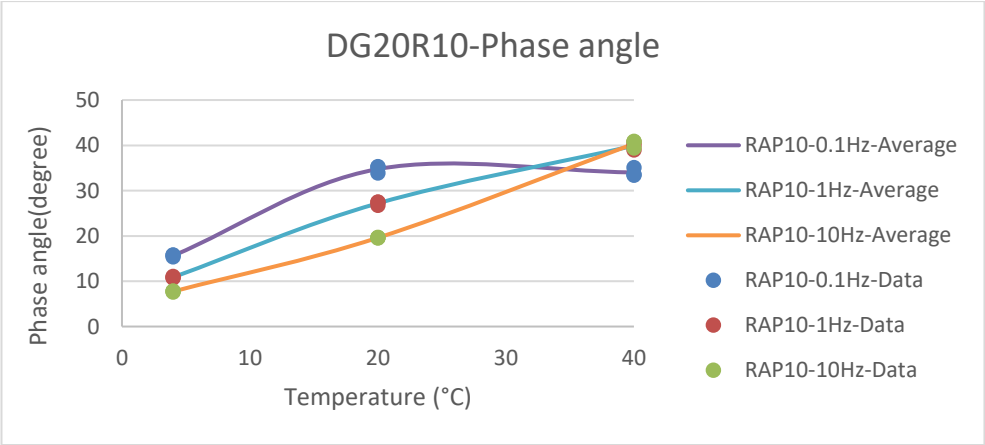

Figure 4-65 Phase angle of DG20R10 mixture versus temperature

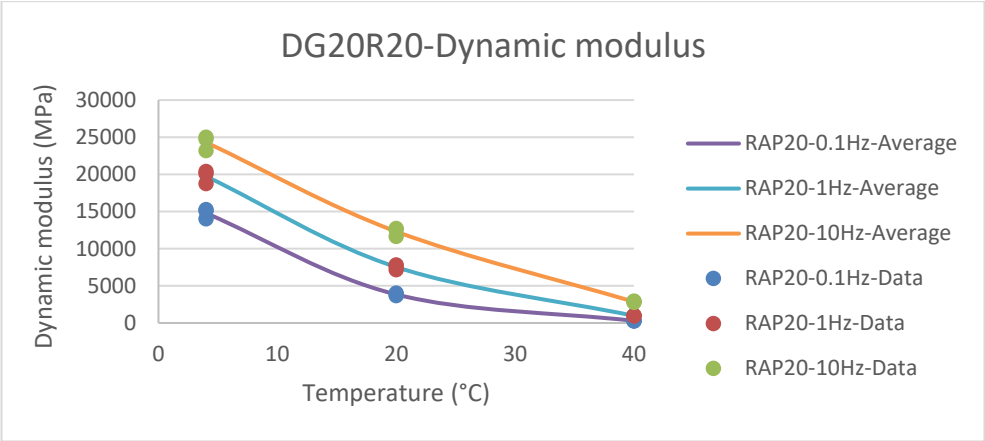

Figure 4-66 Dynamic modulus of DG20R0 mixture versus temperature

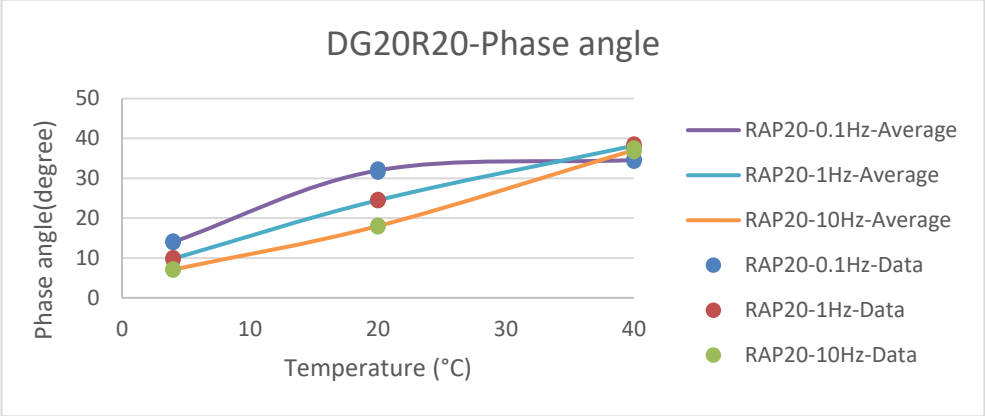

Figure 4-67 Phase angle of DG20R20 mixture versus temperature

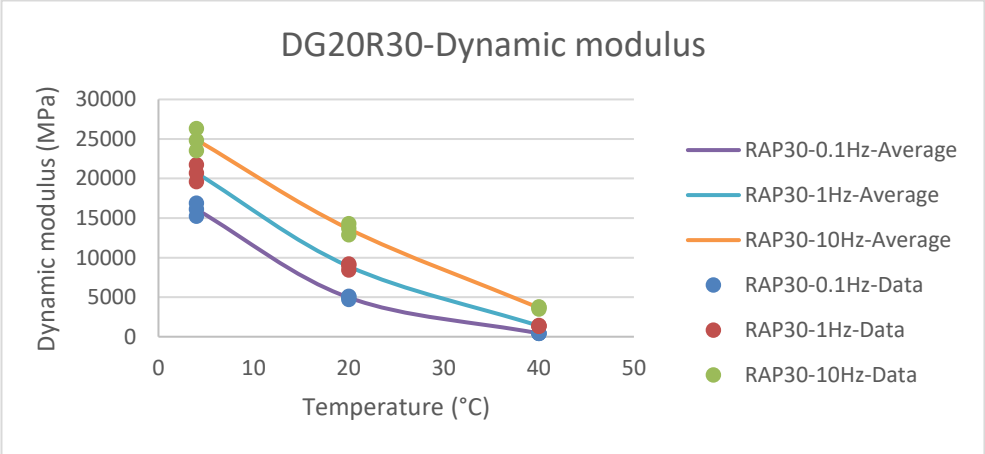

Figure 4-68 Dynamic modulus of DG20R30 mixture versus temperature

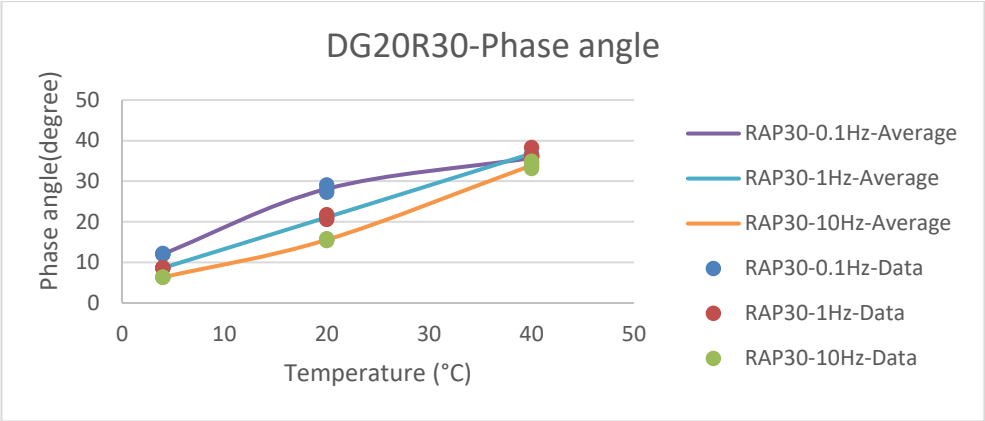

Figure 4-69 Phase angle of DG20R30 mixture versus temperature

According to these figures, temperature noticeably changed both the dynamic modulus and phase angle. As expected, the mixtures showed higher dynamic modulus for higher frequencies than the lower ones. Furthermore, the rates of change in the dynamic modulus are more noticeable in lower loading frequencies than in higher loading frequencies for all the mixtures, which is similar to the 14 mm mixtures.

Regarding the phase angle, these were generally higher at lower loading frequencies and increased with increasing temperature. However, the phase angle measurement at 40 °C and the lowest loading frequency (0.1 Hz) did not follow the same trend as the other points. Even though it is expected that the phase angle should be greater in lower frequencies at the same temperature, the results reveal a contradiction, which was also observed in the 14 mm mixtures.

4.2.7.2.2 RAP content effect

The change in the dynamic modulus and phase angle of the samples owing to the RAP content and frequency are shown separately at each temperature studied in Figure 4-70 to Figure 4-75.

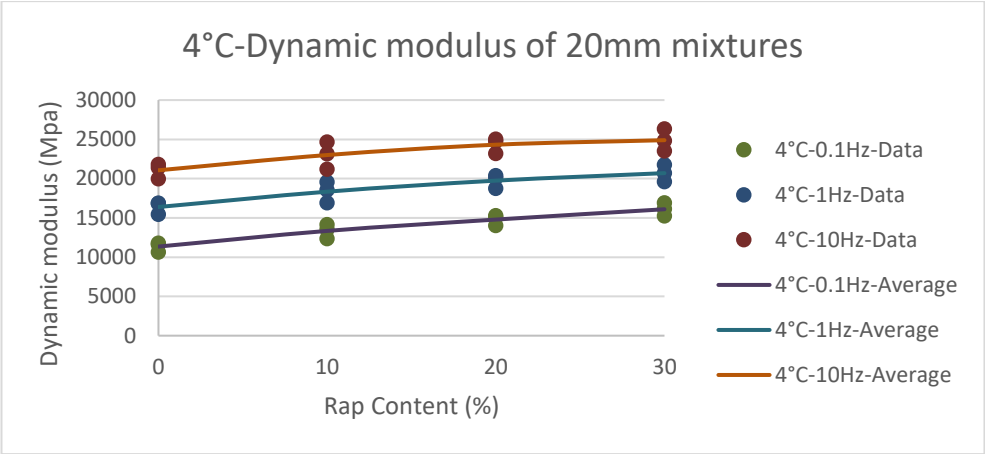

Figure 4-70 Dynamic modulus of 20 mm mixtures versus RAP content at 4 °C

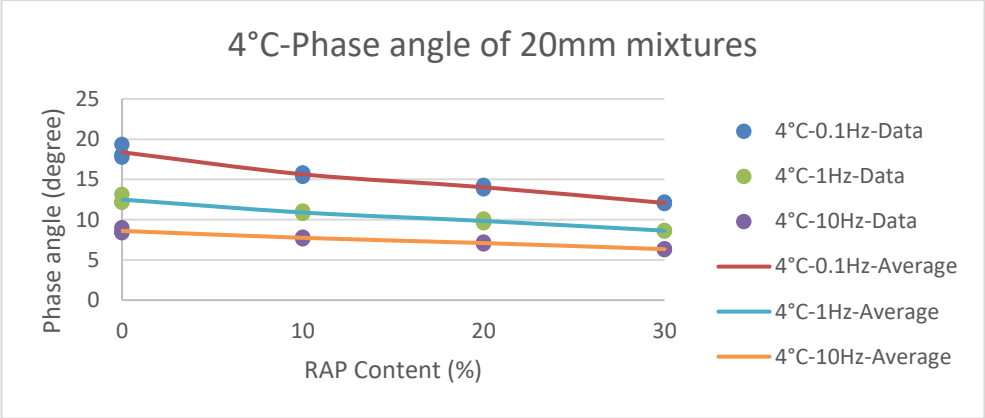

Figure 4-71 Phase angle of 20 mm mixtures versus RAP content at 4 °C

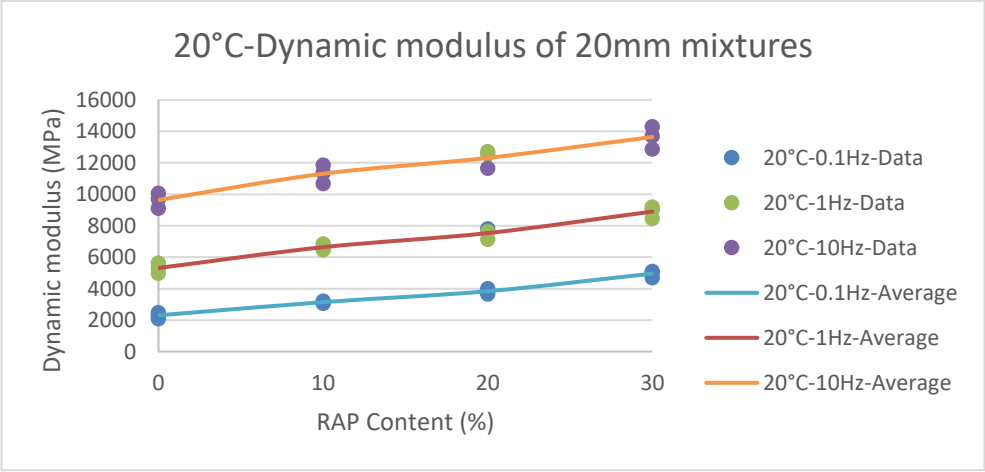

Figure 4-72 Dynamic modulus of 20 mm mixtures versus RAP content at 20 °C

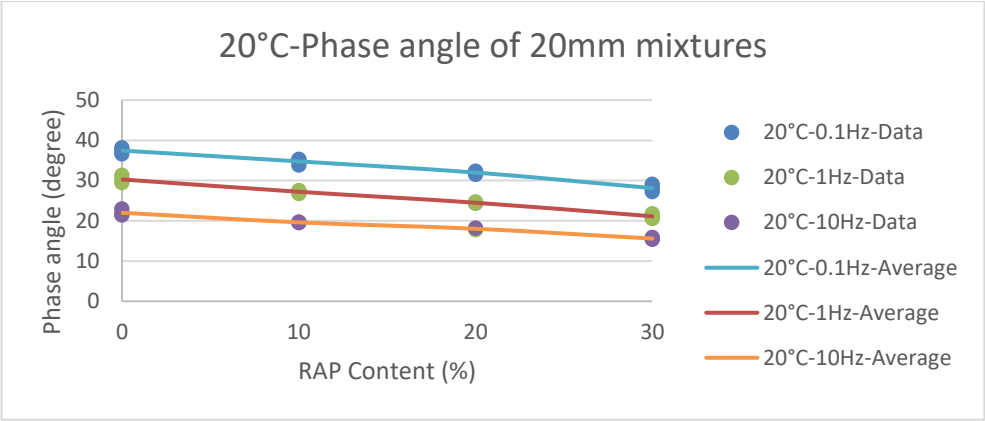

Figure 4-73 Phase angle of 20 mm mixtures versus RAP content at 20 °C

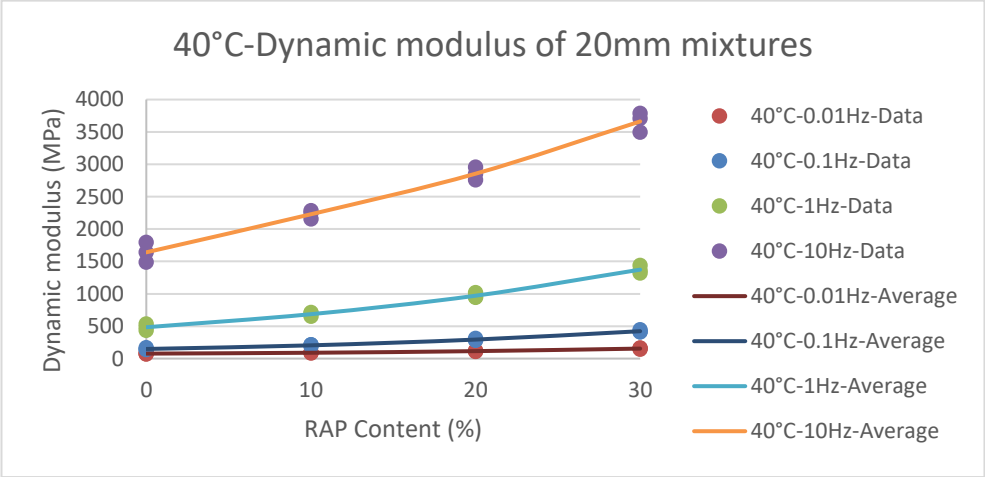

Figure 4-74 Dynamic modulus of 20 mm mixtures versus RAP content at 40 °C

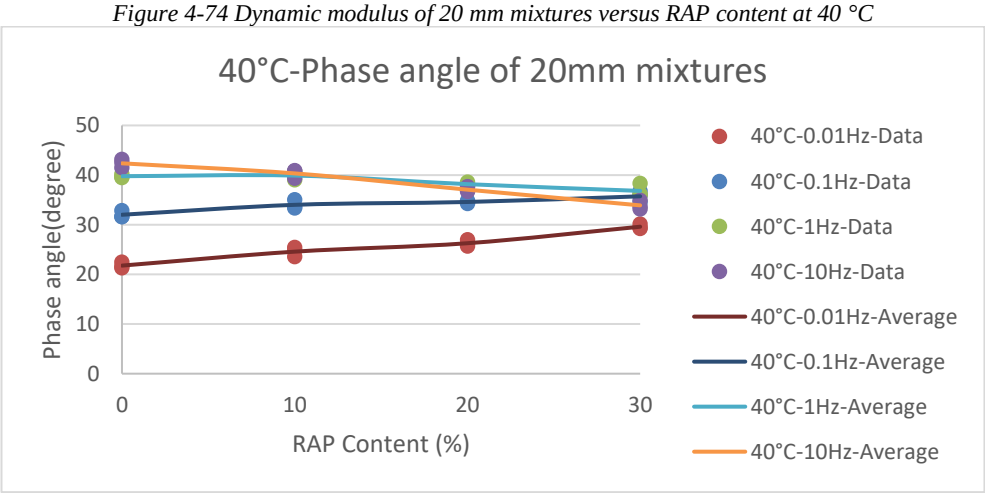

Figure 4-75 Phase angle of 20 mm mixtures versus RAP content at 40 °C

As anticipated, the dynamic modulus of the mixtures at all temperatures increased owing to the addition of RAP in the mixture or loading with higher frequencies.

Similar to the 14 mm mixtures, the phase angle at 4 and 20 °C decreased with greater percentages of RAP in the mixture. However, at 40 °C this trend was only true for the highest loading frequency (10 Hz), while at other loading frequencies the trend increased with respect to RAP content.

4.2.8 Master curve of dynamic modulus and phase angle

In this section, the master curve for the dynamic modulus and phase angle of all the mixtures is produced based on the method explained in section 3.4.6.2.1 and the results from the complex modulus tests of asphalt mixtures available in section 4.2.7.1.

4.2.8.1 The 14 mm mixtures

The dynamic modulus and phase angle master curves for all of the 14 mm mixtures were constructed and are illustrated in Figure 4-76 to Figure 4-83. The reference temperature used while constructing these master curves was 20 °C.

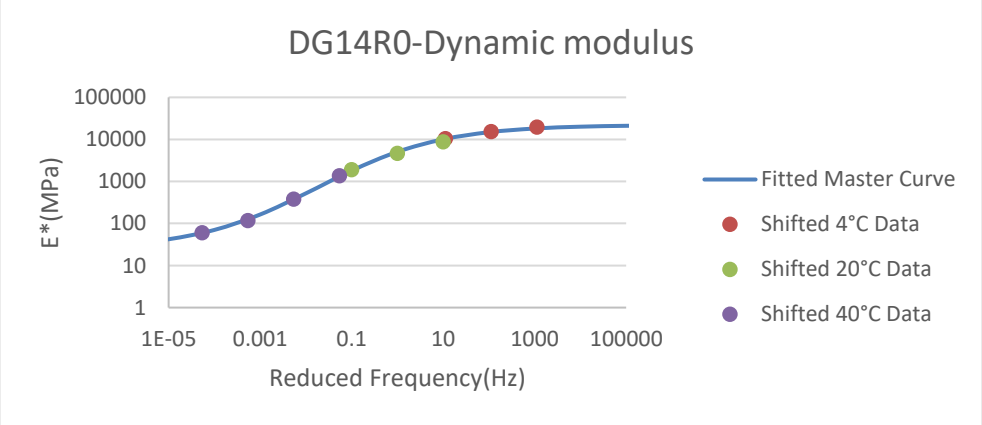

Figure 4-76 Dynamic modulus master curve of DG14R0 mixture at 20 °C reference temperature

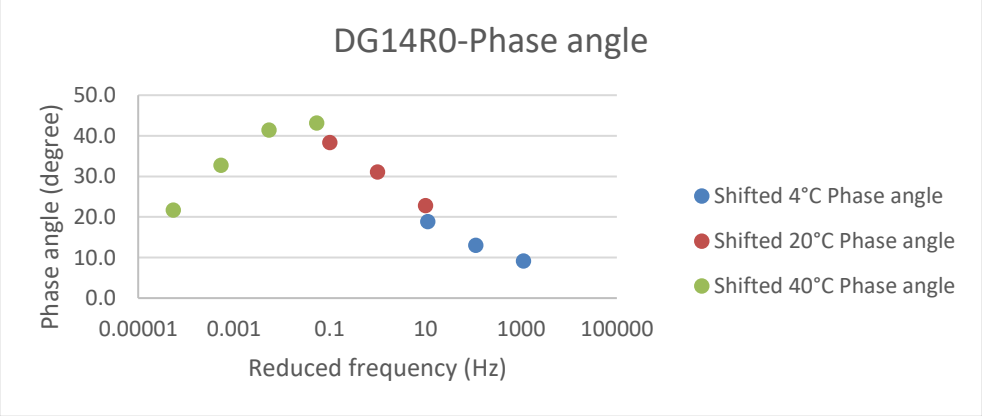

Figure 4-77 Shifted phase angle of DG14R0 mixture at 20 °C reference temperature

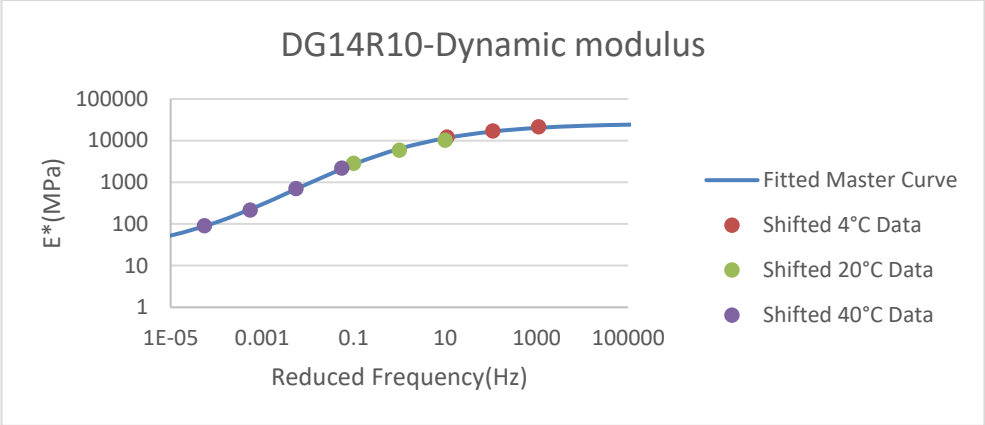

Figure 4-78 Dynamic modulus master curve of DG14R10 mixture at 20 °C reference temperature

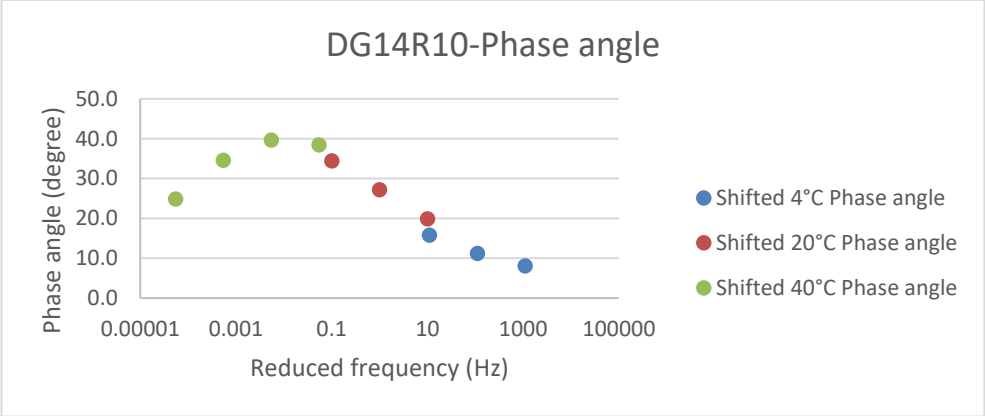

Figure 4-79 Shifted phase angle of DG14R10 mixture at 20 °C reference temperature

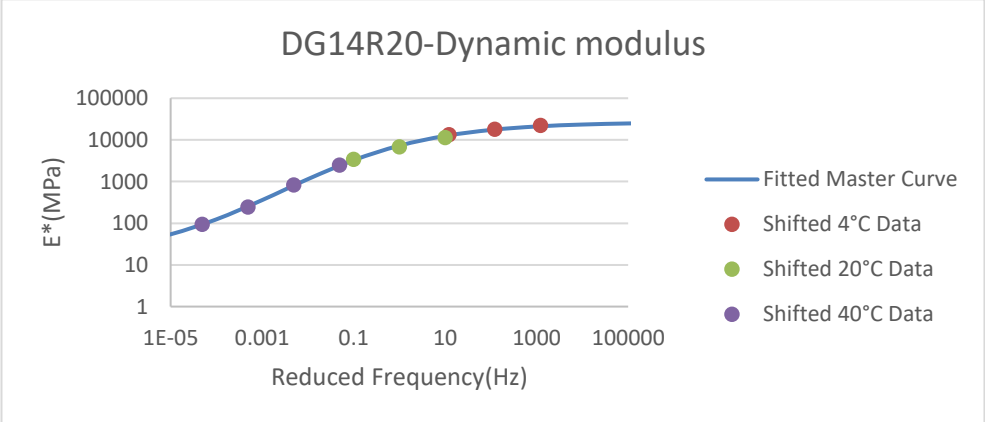

Figure 4-80 Dynamic modulus master curve of DG14R20 mixture at 20 °C reference temperature

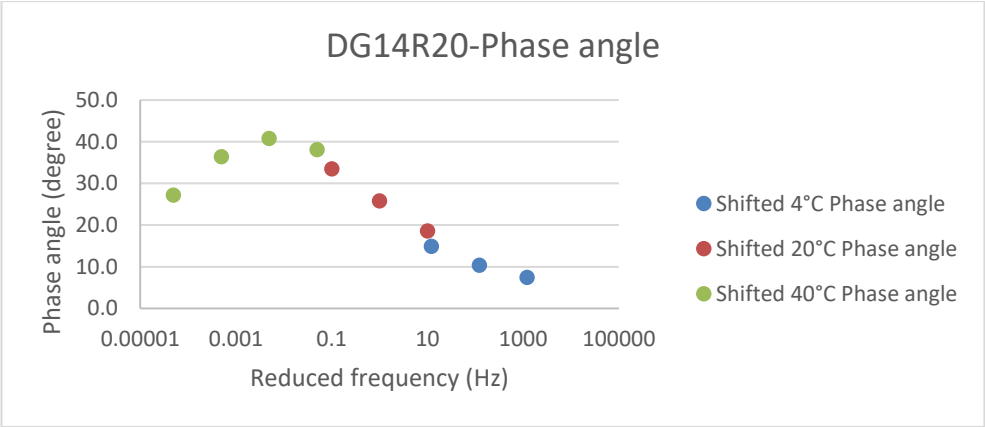

Figure 4-81 Shifted phase angle of DG14R20 mixture at 20 °C reference temperature

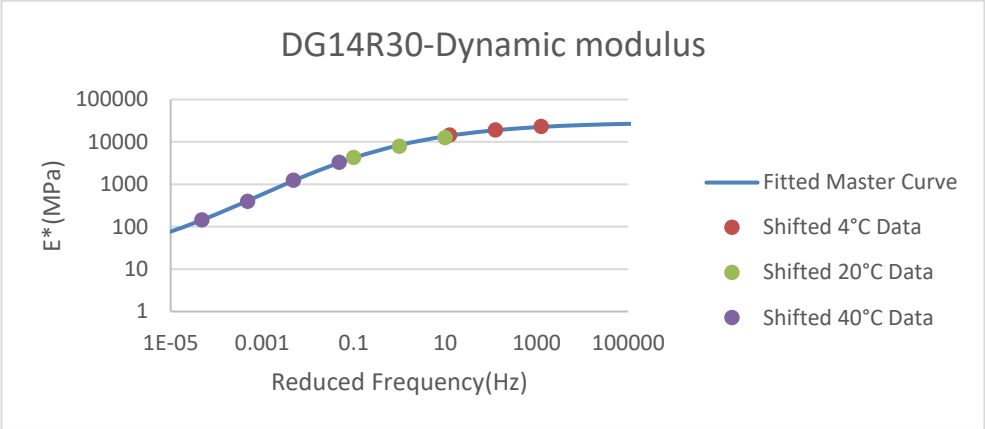

Figure 4-82 Dynamic modulus master curve of DG14R30 mixture at 20 °C reference temperature

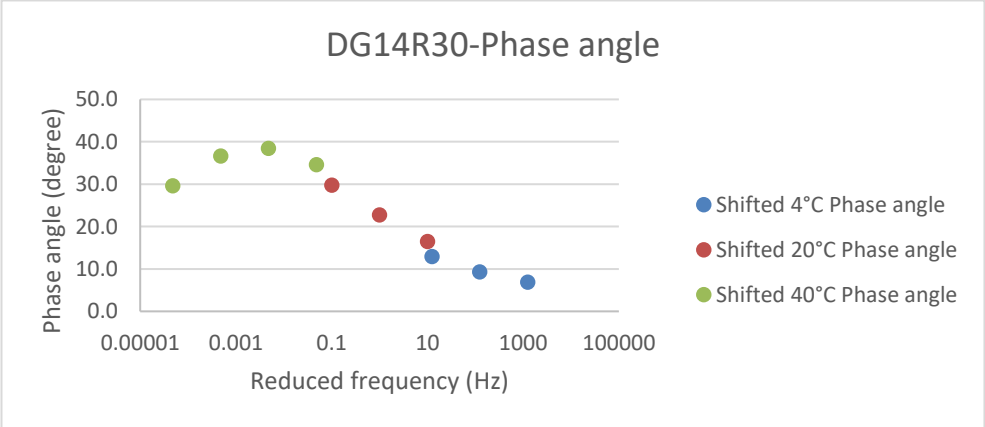

Figure 4-83 Shifted phase angle of DG14R30 mixture at 20 °C reference temperature

To determine how the RAP affected the performance of the mixtures, all the master curves for the 14 mm mixtures are shown on the same graph in Figure 4-84. The data related to this graph is also shown in Table 4-8 for fine comparison that is difficult using only the graph as it is a log-log graph.

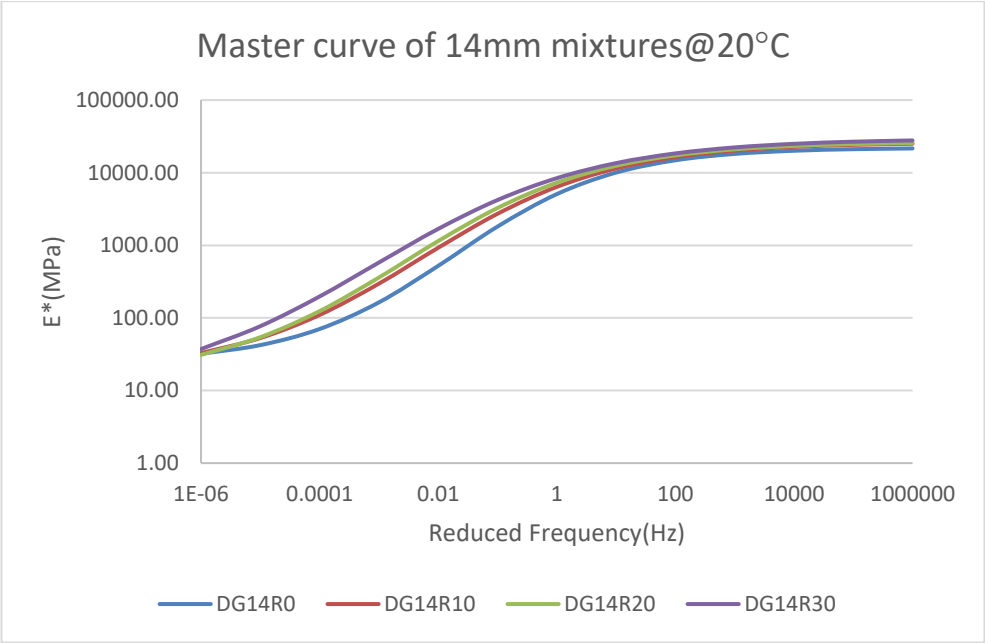

Figure 4-84 Comparison of dynamic modulus master curves of 14 mm mixtures at 20 °C reference temperature

Table 4-8 Dynamic modulus master curve data in the14 mm mixtures at 20 °C reference temperature

Ref Temp: 20 °C	E* (MPa)			
Reduced Frequency (Hz)	DG14R0	DG14R10	DG14R20	DG14R30
1000000	21567.52	25012.07	25622.24	27794.81
100000	21068.06	24167.23	24805.47	26719.96
10000	20063.31	22677.23	23375.67	24978.51
1000	18140.77	20183.56	20989.33	22285.94
100	14811.74	16380.41	17327.59	18431.20
10	10037.26	11424.05	12453.55	13548.48
1	5069.80	6374.77	7271.21	8403.99
0.1	1810.06	2716.61	3262.39	4201.45
0.01	521.10	924.24	1144.48	1682.92
0.001	163.54	296.33	359.57	579.23
0.0001	70.34	109.82	123.97	197.18
0.00001	42.20	52.79	54.26	76.85
0.000001	32.04	32.78	30.98	37.21

As illustrated in Figure 4-84, at 20 °C the presence of RAP increased the dynamic modulus over the whole range of frequencies evaluated. However,

it should be noted that the dynamic modulus of the mixtures becomes less sensitive to the RAP content at high loading frequencies while it is still sensitive to the existence of the RAP. For example, based on Table 4-8 Dynamic modulus master curve data in the14 mm mixtures at 20 °C reference temperature even at the highest frequency (100000 Hz) there is a considerable jump in dynamic modulus between DG14R0 and DG14R10 (approximately 12%), while the difference between the other mixtures with higher percentages of RAP is minimal and less than 7%.

In the middle range of frequencies, the gap between the results increases except for the DG14R10 and DG14R20 mixtures, implying that there is a minimal change in dynamic modulus behaviour of the mixture when the RAP content is between 10 and 20%.

Under very low loading frequencies, the dynamic modulus of all the mixtures become close to one another and they pass each other, i.e. in the 0.000001 Hz frequency, the dynamic modulus of mixtures with 0, 10 and 20% RAP is almost the same, and only the dynamic modulus for DG14R30 is greater than 20% than the others.

To evaluate the performance of the mixtures in lower and higher temperatures, the master curves of the same mixtures were constructed with the reference temperatures equal to 4 and 40 °C. Figure 4-85 and Table 4-9 show the graph and data related to the master curve at 4 °C, while Figure 4-86 and Table 4-10 illustrate the graph and data related to the master curve at 40 °C. The shifted original data and fitted master curve for each individual mixture at 4 °C is provided in Appendix IV, while the same for the 40 °C reference temperature can be found in Appendix V.

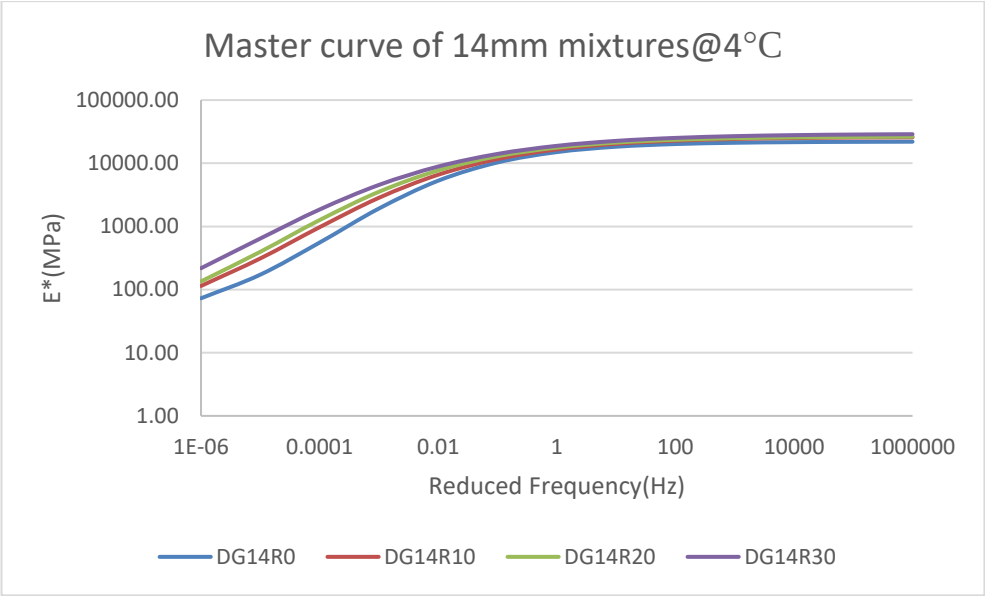

Figure 4-85 Comparison of dynamic modulus master curves of 14 mm mixtures at 4 °C reference temperature

Table 4-9 Dynamic modulus master curve data in the 14 mm mixtures at 4 °C reference temperature

Ref Temp: 4 °C	E* (MPa)			
Reduced Frequency (Hz)	DG14R0	DG14R10	DG14R20	DG14R30
1000000	21925.14	25737.10	26326.87	28839.53
100000	21813.33	25491.53	26090.95	28477.91
10000	21579.99	25038.51	25660.19	27864.74
1000	21098.53	24215.37	24884.37	26841.07
100	20128.16	22761.11	23521.73	25176.64
10	18264.67	20319.74	21234.54	22588.24
1	15015.42	16576.47	17691.20	18848.14
0.1	10296.94	11655.52	12901.10	14042.32
0.01	5289.69	6576.93	7688.21	8872.67
0.001	1919.09	2835.95	3530.33	4533.07
0.0001	554.75	971.74	1259.85	1851.21
0.00001	172.13	310.96	396.38	642.96
0.000001	72.74	114.13	134.61	217.61

At 4 °C, the master curve is slightly shifted to the left-hand side, with the majority of features remaining the same as the master curve at 20 °C. However, because the curve is shifted, the dynamic modulus converges at

lower frequencies than in the 20 °C master curve, while at very low frequencies the values of dynamic modulus are not becoming close to each other and are quite different in the different mixtures with varying RAP content.

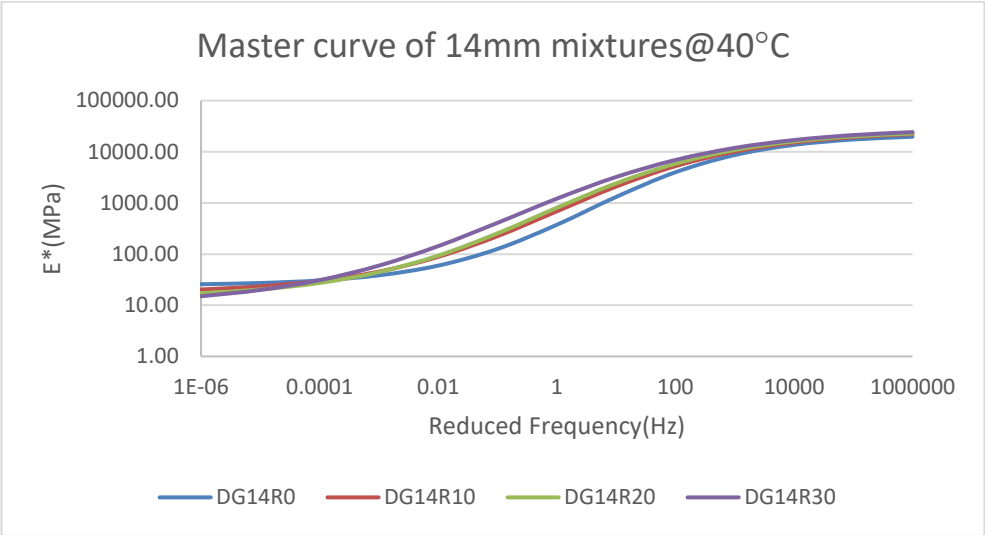

Figure 4-86 Comparison of dynamic modulus master curves of 14 mm mixtures at 40 °C reference temperature

Table 4-10 Dynamic modulus master curve data in14 mm mixtures at 40 °C reference temperature

Ref Temp: 40 °C	E* (MPa)			
Reduced Frequency (Hz)	DG14R0	DG14R10	DG14R20	DG14R30
1000000	19658.80	22137.73	22761.42	24239.94
100000	17403.19	19321.77	20009.39	21191.03
10000	13650.20	15170.05	15937.03	16968.51
1000	8639.26	10049.22	10828.02	11886.68
100	3975.34	5236.79	5853.65	6911.15
10	1309.85	2084.36	2418.15	3212.08
1	373.89	684.43	804.05	1211.76
0.1	125.94	223.87	254.42	408.50
0.01	59.56	88.29	93.44	143.19
0.001	38.48	45.56	44.47	59.52
0.0001	30.56	29.95	27.32	30.99
0.00001	27.23	23.40	20.35	19.90
0.000001	25.74	20.36	17.17	14.99

At 40 °C, the master curve is shifted to the right-hand side; therefore, the convergence of the dynamic modulus occurs only at very high frequencies. At this temperature it can be seen that at approximately 0.0001 Hz, the graphs of mixtures cross over each other. Therefore, in contrast to previous observations at lower temperatures, in frequencies less than 0.0001 Hz the higher the RAP content, the lower the dynamic modulus is.

The details of parameters to construct the master curves are presented in Table 4-11.

Table 4-11 Master curve construction details of 14 mm mixtures at different temperature references

Mixture	Reference Temperature (°C)	δ	β	γ	α	C	SSE
DG14R0	20	1.3883	-1.2895	-0.7458	2.9548	1.0413E+04	6.8678E-04
DG14R10	20	1.2371	-1.4357	-0.6298	3.1782	1.0383E+04	4.2891E-04
DG14R20	20	1.1441	-1.5731	-0.6180	3.2811	1.0593E+04	3.2943E-04
DG14R30	20	0.9915	-1.6864	-0.5494	3.4762	1.0643E+04	2.0366E-04
DG14R0	4	1.3885	-2.8186	-0.7459	2.9544	1.0413E+04	6.8678E-04
DG14R10	4	1.2373	-2.7232	-0.6299	3.1780	1.0383E+04	4.2891E-04
DG14R20	4	1.1451	-2.8626	-0.6183	3.2798	1.0592E+04	3.2943E-04
DG14R30	4	0.9924	-2.8378	-0.5495	3.4751	1.0643E+04	2.0366E-04
DG14R0	40	1.3883	0.4018	-0.7457	2.9548	1.0413E+04	6.8678E-04
DG14R10	40	1.2370	-0.0115	-0.6298	3.1783	1.0384E+04	4.2891E-04
DG14R20	40	1.1442	-0.1473	-0.6180	3.2810	1.0593E+04	3.2943E-04
DG14R30	40	0.9917	-0.4128	-0.5494	3.4760	1.0643E+04	2.0366E-04

4.2.8.2 The 20 mm mixtures

The dynamic modulus and phase angle master curve for all the 20 mm mixtures were constructed and illustrated in Figure 4-87 to Figure 4-94. The reference temperature used while constructing these master curves was 20 °C.

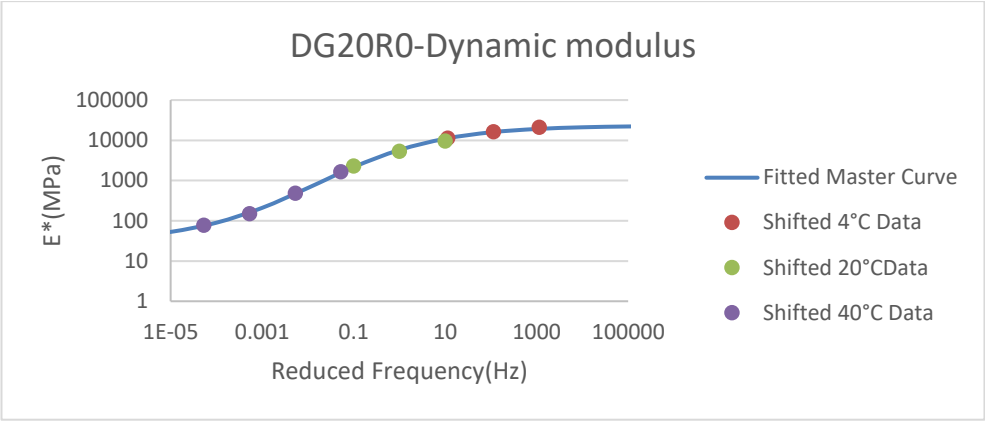

Figure 4-87 Dynamic modulus master curve of DG20R0 mixture at 20 °C reference temperature

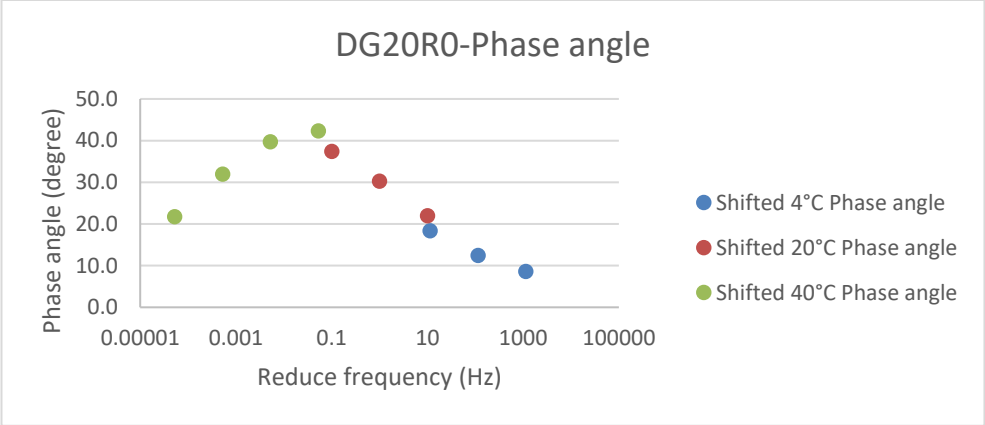

Figure 4-88 Shifted phase angle of DG20R0 mixture at 20 °C reference temperature

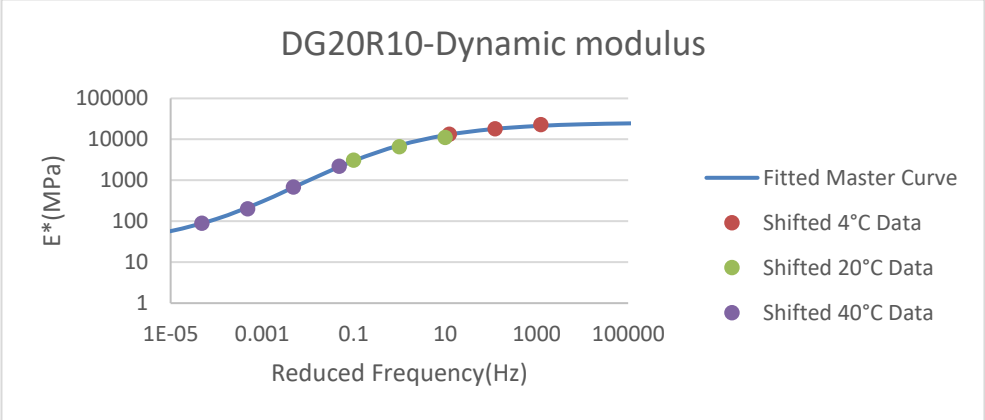

Figure 4-89 Dynamic modulus master curve of DG20R10 mixture at 20 °C reference temperature

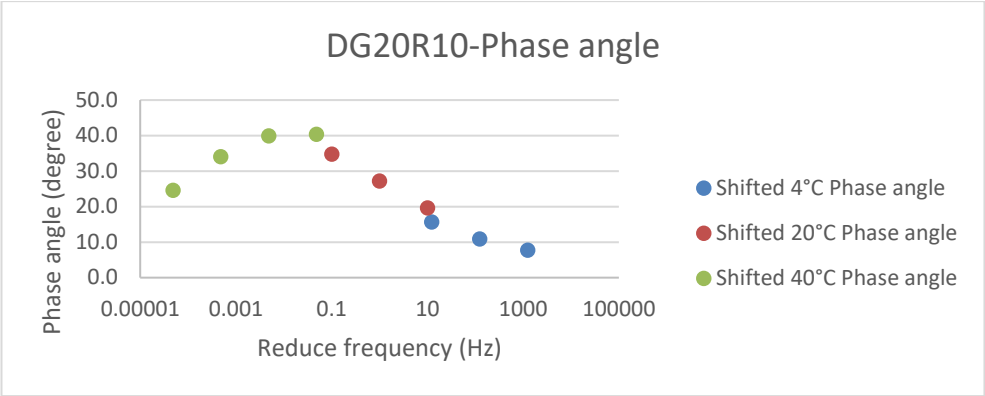

Figure 4-90 Shifted phase angle of DG20R10 mixture at 20 °C reference temperature

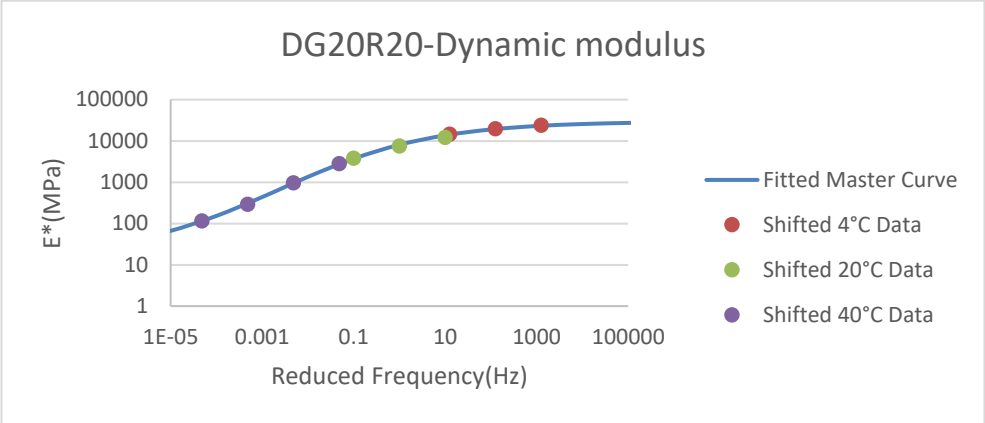

Figure 4-91 Dynamic modulus master curve of DG20R20 mixture at 20 °C reference temperature

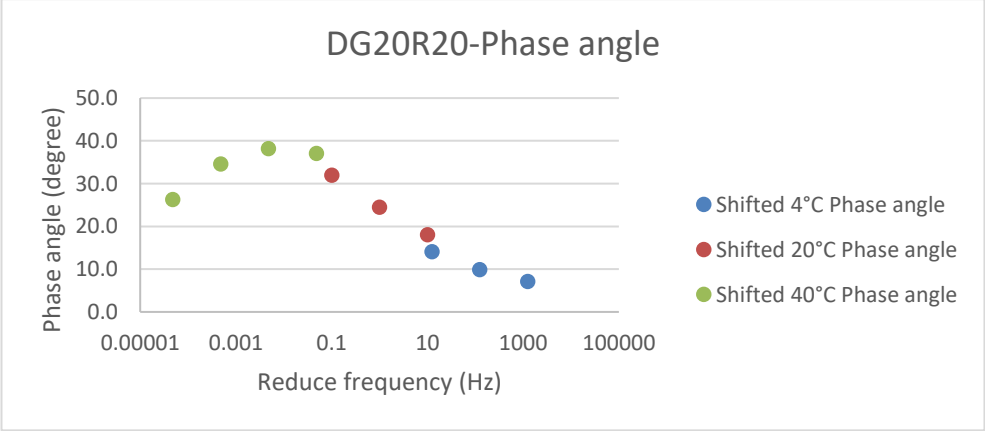

Figure 4-92 Shifted phase angle of DG20R20 mixture at 20 °C reference temperature

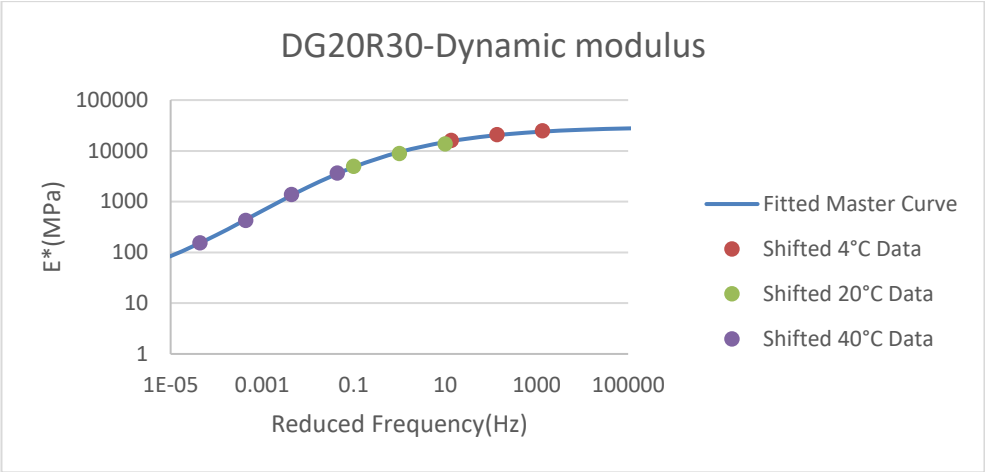

Figure 4-93 Dynamic modulus master curve of DG20R30 mixture at 20 °C reference temperature

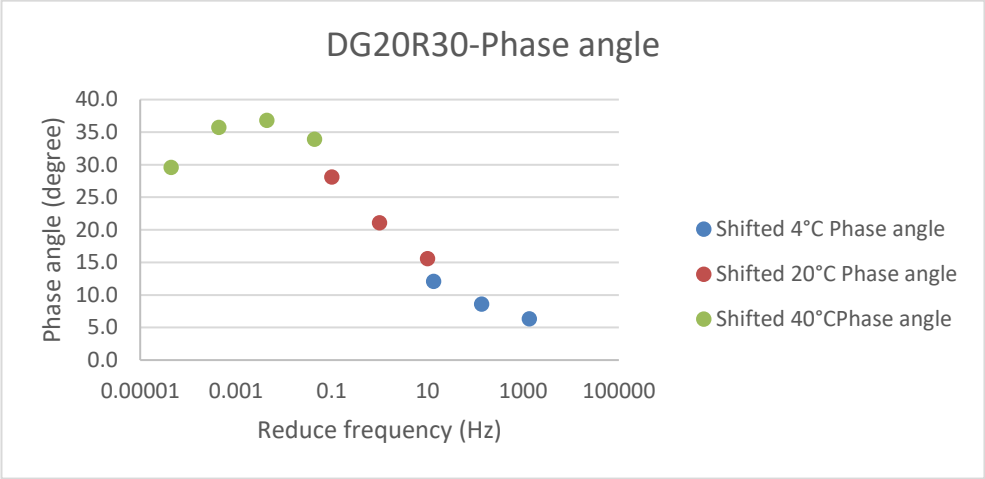

Figure 4-94 Shifted phase angle of DG20R30 mixture at 20 °C reference temperature

To determine how the RAP affected the performance of the mixtures, all the master curves for the 20 mm mixtures were drawn on the same graph in Figure 4-95. The data regarding this graph is also shown in Table 4-12 for fine comparison, which is difficult using only the graph as it is a log-log graph.

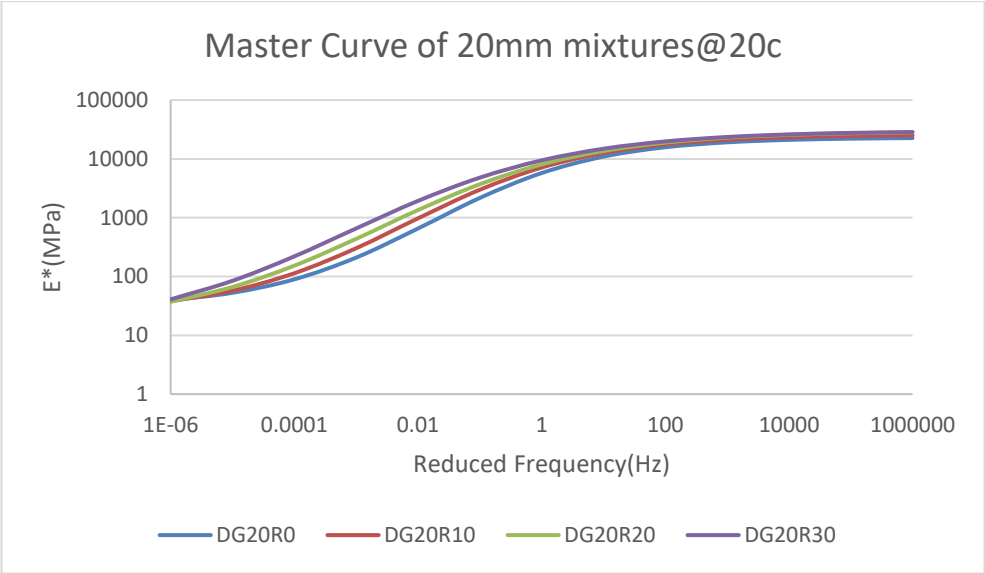

Figure 4-95 Comparison of dynamic modulus master curves of 20 mm mixtures at 20 °C reference temperature

Table 4-12 Dynamic modulus master curve data in the 20 mm mixtures at 20 °C reference temperature

Ref Temp: 20 °C	Asphalt Mixture Type			
Reduced Frequency (Hz)	DG20R0	DG20R10	DG20R20	DG20R30
1000000	22600.96	25168.23	28238.09	28621.26
100000	22089.94	24530.68	27285.47	27669.70
10000	21070.66	23331.56	25648.42	26086.57
1000	19132.74	21177.28	22967.68	23562.77
100	15781.62	17626.18	18929.91	19818.46
10	10931.25	12610.30	13638.14	14877.28
1	5745.20	7124.79	8053.98	9435.18
0.1	2166.49	2986.51	3704.15	4797.58
0.01	654.70	974.25	1346.39	1929.50
0.001	209.57	302.67	436.93	656.86
0.0001	89.55	113.58	152.77	219.67
0.00001	52.89	57.44	66.43	84.57
0.000001	39.60	37.93	37.26	40.90

Regarding Figure 4-95, at 20 °C the occurrence of RAP increased the dynamic modulus over the whole range of frequencies evaluated. However, the dynamic modulus of the mixtures becomes less sensitive to the RAP content at higher loading frequencies than at lower frequencies. In contrast to the 14 mm mixtures where the dynamic modulus had a jump only in the 10 % RAP mixture, the 20 mm mixtures demonstrated that this change in dynamic modulus was present until 20% RAP. However, there was no significant difference in dynamic modulus between DG20R20 and DG20R30 in high frequencies, e.g., the dynamic modulus differences at 1000 Hz between DG20R0 and DG20R10 and between DG20R10 and DG20R20 were 9 and 7%, respectively, while the difference between DG20R20 and DG20R30 was only 2%.

In the middle range of frequencies, the gap between the results increases with no exception in contrast to the 14 mm mixtures where the mixtures with 10 and 20% RAP were very close.

Similar to the 14 mm mixtures, in very low loading frequencies the dynamic modulus of all the mixtures becomes close to one another and they pass each other, i.e., at the 0.000001 Hz frequency, the dynamic modulus of mixtures with 0, 10 and 20% RAP are almost identical and only the dynamic modulus of the DG20R30 mixture is 10% greater than the others.

To evaluate the performance of the mixtures in lower and higher temperatures, master curves of the same mixtures were also constructed with the reference temperature equal to 4 and 40 °C. Figure 4-96 and Table 4-13 shows the graph and data related to the master curve at 4 °C, while Figure 4-97 and Table 4-14 illustrate the graph and data related to the master curve at 40 °C. The shifted original data and fitted master curve for each individual mixture at 4 °C is provided in Appendix VI while the same for the 40 °C reference temperature can be found in Appendix V.

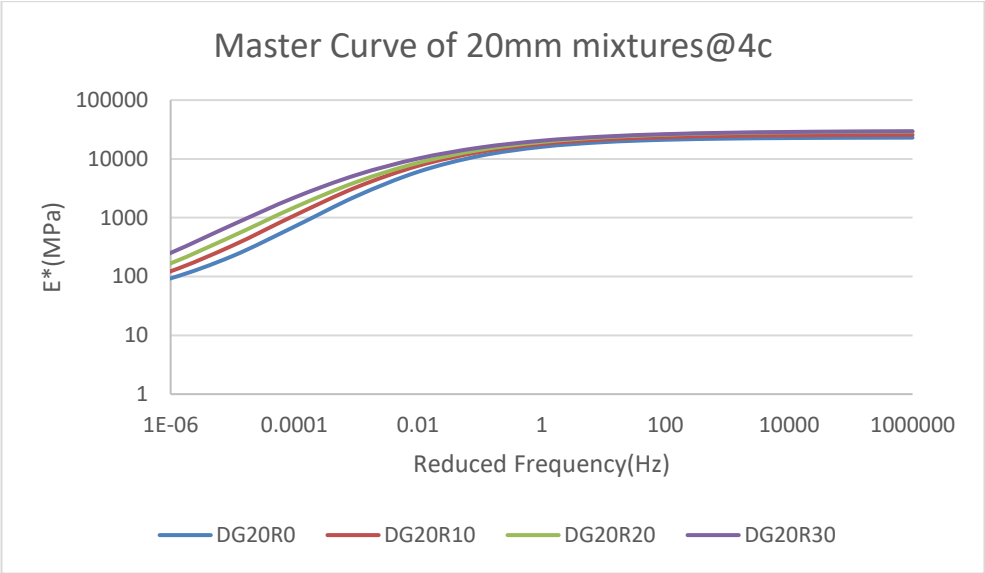

Figure 4-96 Comparison of dynamic modulus master curves of 20 mm mixtures at 4 °C reference temperature

Table 4-13 Dynamic modulus master curve data in the 20 mm mixtures at 4 °C reference temperature

Ref Temp: 4 °C	Asphalt Mixture Type			
Reduced Frequency (Hz)	DG20R0	DG20R10	DG20R20	DG20R30
1000000	25510.06	27758.20	31016.82	31048.00
100000	25284.09	27493.04	30596.75	30631.77
10000	24856.22	27009.73	29883.36	29943.87
1000	24058.24	26141.57	28692.12	28824.18
100	22612.26	24623.18	26759.43	27047.15
10	20129.14	22092.32	23772.40	24341.82
1	16261.03	18216.35	19511.12	20491.20
0.1	11168.74	13071.58	14159.53	15560.30
0.01	6034.50	7621.07	8610.33	10172.99
0.001	2454.52	3420.30	4189.56	5461.02
0.0001	803.89	1205.26	1627.60	2350.20
0.00001	258.40	382.50	545.75	838.33
0.000001	100.66	133.71	183.18	275.53

At 4 °C, the master curve is slightly shifted to the left-hand side; therefore, the majority of the features remained the same as those in the master curve at 20 °C. However, as the curve is shifted, the dynamic modulus converge at lower frequencies in comparison with the 20 °C master curve, while at very

low frequencies the values of dynamic modulus are not getting close to each other and they are quite different for the different mixtures containing varying RAP content.

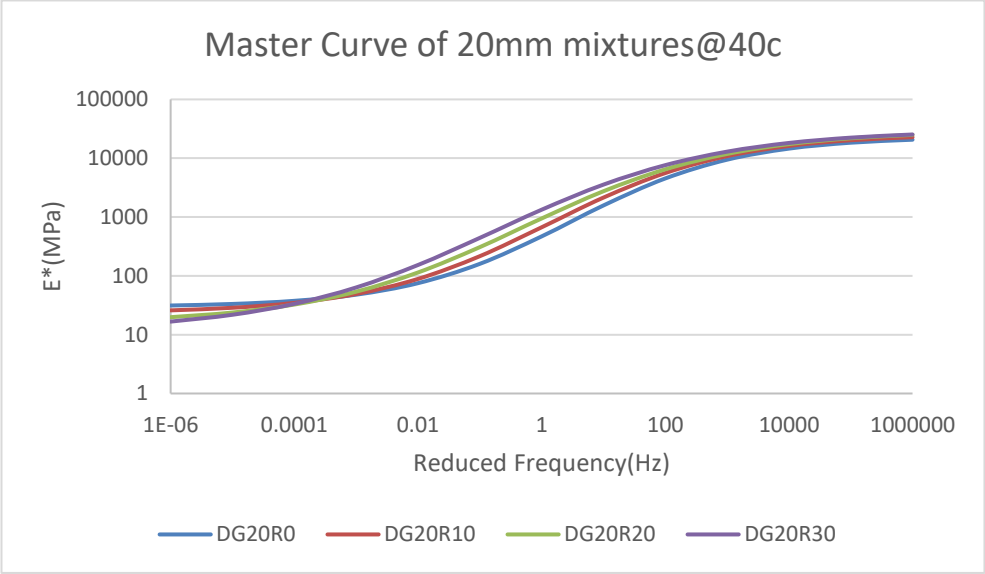

Figure 4-97 Comparison of dynamic modulus master curves of 20 mm mixtures at 40 °C reference temperature

Table 4-14 Dynamic modulus master curve data in the 20 mm mixtures at 40 °C reference temperature

Ref Temp: 40°C	Asphalt Mixture Type			
Reduced Frequency (Hz)	DG20R0	DG20R10	DG20R20	DG20R30
1000000	21678.33	23525.23	25438.00	25672.53
100000	18617.18	20359.47	21830.60	22338.67
10000	14140.14	15801.04	16965.91	17842.97
1000	8825.02	10324.14	11360.09	12538.32
100	4214.06	5309.98	6213.13	7380.45
10	1532.74	2094.75	2694.19	3502.73
1	483.63	684.48	958.77	1345.78
0.1	165.63	222.39	315.10	450.93
0.01	72.83	86.55	112.10	150.71
0.001	42.35	43.87	48.59	57.54
0.0001	30.66	28.34	26.56	27.10
0.00001	25.59	21.82	17.78	15.84
0.000001	23.20	18.80	13.81	11.07

At 40 °C, the master curve is shifted to the right-hand side; therefore, the convergence of the dynamic modulus occurs only at very high frequencies. Similar to the 14 mm mixtures, at this temperature it can be seen that at approximately 0.0001 Hz, the graphs of mixtures cross each other. Therefore, in contrast with previous observations, in frequencies less than 0.001 Hz the higher the RAP content, the lower the dynamic modulus is.

The details of parameters to construct the master curves can be found in Table 4-15.

Table 4-15 Master curve construction details of 20 mm mixtures at different temperature references

Mixture	Reference Temperature(°C)	δ	β	γ	α	C	SSE
DG20R0	20	1.4712	-1.3319	-0.7360	2.8921	1.05E+04	7.26E-04
DG20R10	20	1.3667	-1.4913	-0.6804	3.0457	1.06E+04	4.57E-04
DG20R20	20	1.1953	-1.5716	-0.6023	3.2737	1.06E+04	3.48E-04
DG20R30	20	1.0573	-1.7611	-0.5672	3.4188	1.08E+04	2.54E-04
DG20R0	4	1.3181	-2.6730	-0.6551	3.0928	1.07E+04	6.60E-03
DG20R10	4	1.4713	-2.8477	-0.7362	2.8919	1.05E+04	7.26E-04
DG20R20	4	1.3671	-2.9158	-0.6806	3.0452	1.06E+04	4.57E-04
DG20R30	4	1.1959	-2.8337	-0.6025	3.2731	1.06E+04	3.48E-04
DG20R0	40	1.0579	-2.9698	-0.5674	3.4180	1.08E+04	2.54E-04
DG20R10	40	1.4711	0.3447	-0.7360	2.8922	1.05E+04	7.26E-04
DG20R20	40	1.3665	0.0842	-0.6803	3.0459	1.06E+04	4.57E-04
DG20R30	40	1.1952	-0.1755	-0.6023	3.2740	1.06E+04	3.48E-04

4.2.8.3 Comparison of 14 and 20 mm mixtures

In this section, the effect of the nominal size of aggregates on dynamic modulus of the samples were studied by comparing the dynamic modulus of mixtures with the same amount of RAP but different nominal aggregate size in Figure 4-98 to Figure 4-101. As the diagrams are logarithmic it is difficult to study the minor differences between mixtures; therefore, the same data

with the normalised differences is also presented in Table 4-16. This comparison is only made using master curves with a reference temperature of 20 °C.

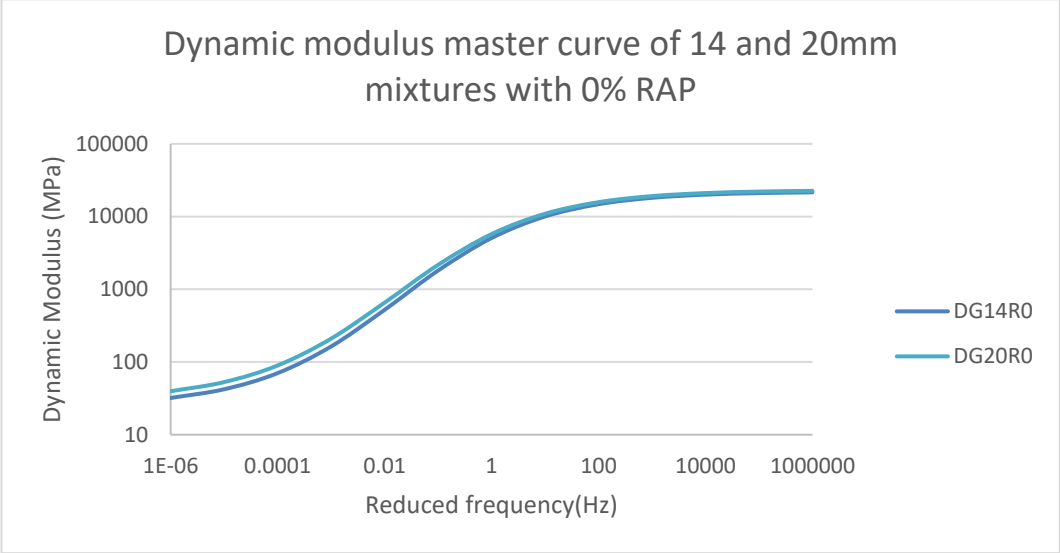

Figure 4-98 Comparison of dynamic modulus master curve of 14 and 20 mm mixtures at 20 °C reference temperature with 0% RAP

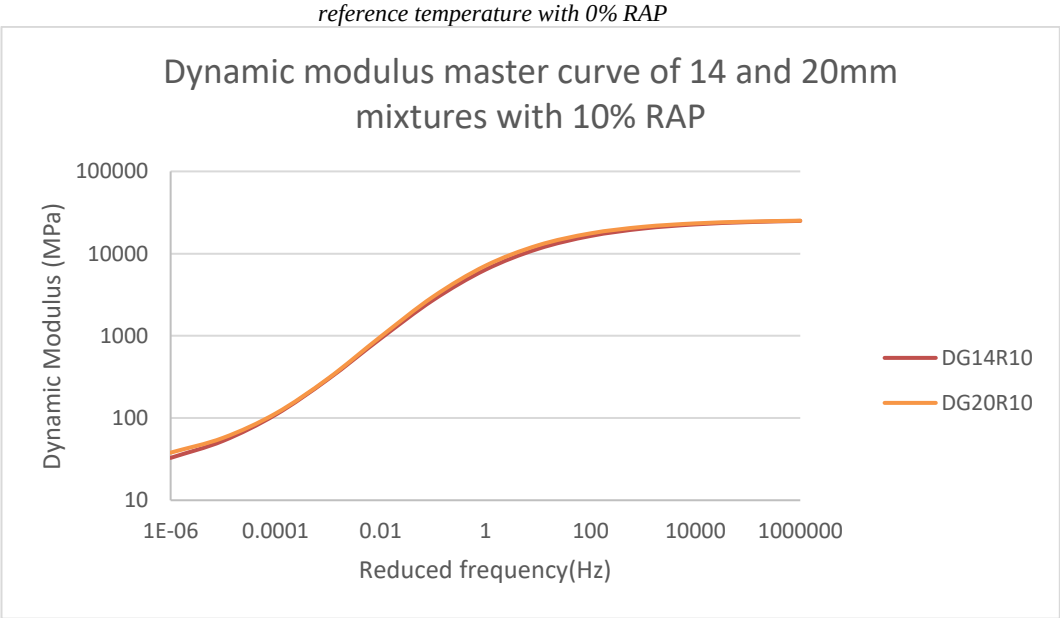

Figure 4-99 Comparison of dynamic modulus master curve of 14 and 20 mm mixtures at 20 °C reference temperature with 10% RAP

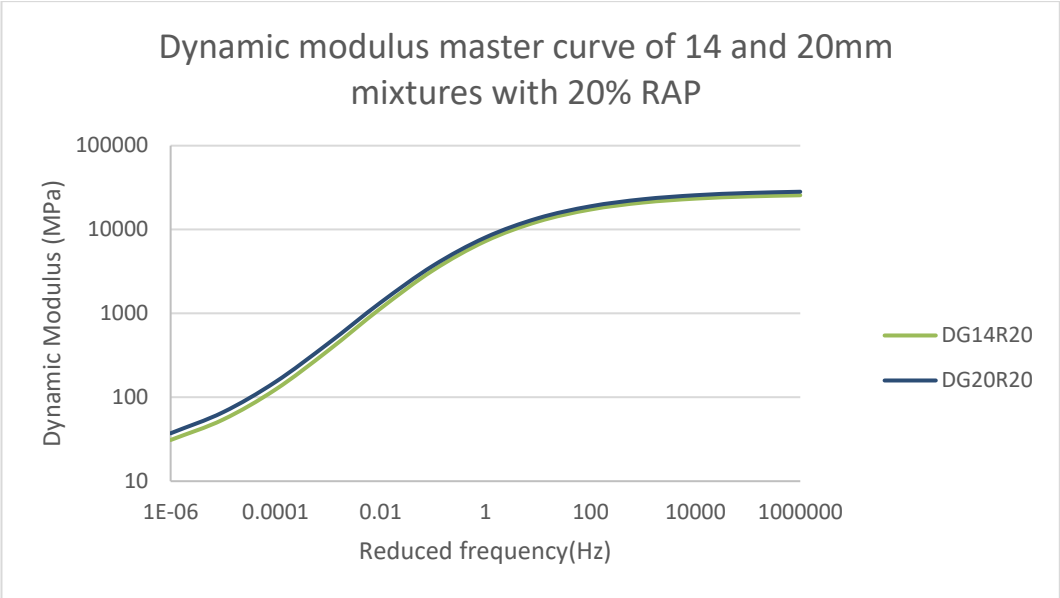

Figure 4-100 Comparison of dynamic modulus master curve of 14 and 20 mm mixtures at 20 °C reference temperature with 20% RAP

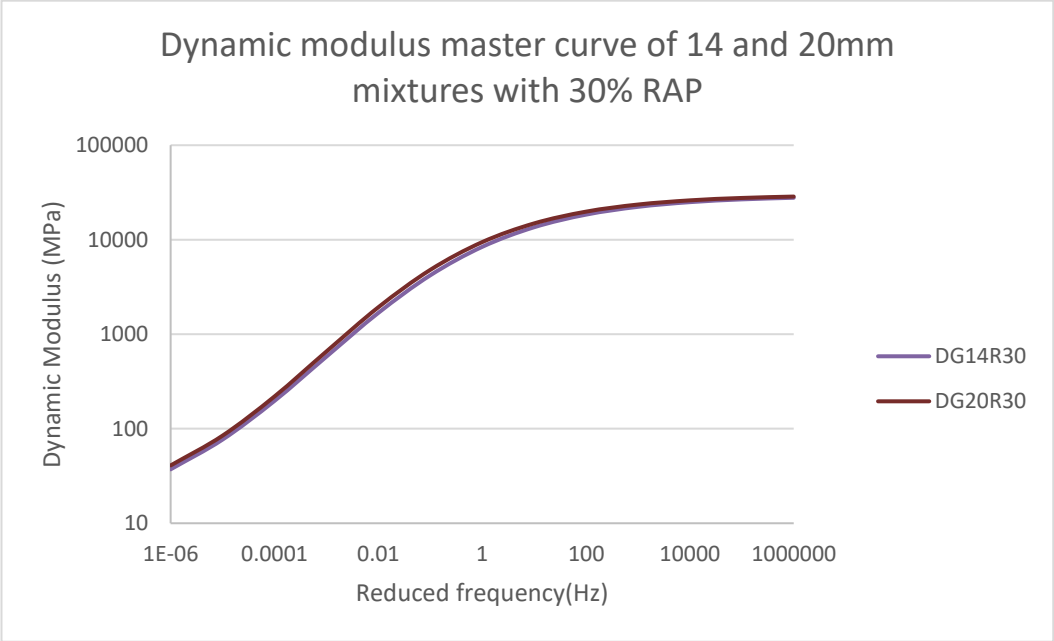

Figure 4-101 Comparison of dynamic modulus master curve of 14 and 20 mm mixtures at 20 °C reference temperature with 30% RAP

Table 4-16 Comparison of dynamic modulus master curve data of 14 and 20 mm mixtures at 20 °C reference temperature

	Dynamic Modulus (MPa)											
	0% RAP			10% RAP			20% RAP			30% RAP		
Reduced Frequency (Hz)	DG14R0	DG20R0	Difference (%)	DG14R10	DG20R10	Difference (%)	DG14R20	DG20R20	Difference (%)	DG14R30	DG20R30	Difference (%)
1000000	21568	22601	5	25012	25168	1	25622	28238	10	27795	28621	3
100000	21068	22090	5	24167	24531	2	24805	27285	10	26720	27670	4
10000	20063	21071	5	22677	23332	3	23376	25648	10	24979	26087	4
1000	18141	19133	5	20184	21177	5	20989	22968	9	22286	23563	6
100	14812	15782	7	16380	17626	8	17328	18930	9	18431	19818	8
10	10037	10931	9	11424	12610	10	12454	13638	10	13548	14877	10
1	5070	5745	13	6375	7125	12	7271	8054	11	8404	9435	12
0.1	1810	2166	20	2717	2987	10	3262	3704	14	4201	4798	14
0.01	521	655	26	924	974	5	1144	1346	18	1683	1930	15
0.001	164	210	28	296	303	2	360	437	22	579	657	13
0.0001	70	90	27	110	114	3	124	153	23	197	220	11
0.00001	42	53	25	53	57	9	54	66	22	77	85	10
0.000001	32	40	24	33	38	16	31	37	20	37	41	10

Regarding the previous figures in this section, it is observed that generally the 20 mm mixtures have a higher dynamic modulus in all the spectrum of frequencies studied.

However, the gap between the dynamic modulus of the 14 and 20 mm mixtures was not constant. In high frequencies (≥ 10 Hz) the difference was 10% or less for all groups of mixtures. However, in lower frequencies (< 10 Hz) the mixtures with 10% RAP demonstrated the least difference. Mixtures with 30% RAP had slightly greater difference (maximum difference 15%). However, mixtures with no RAP or 20% revealed considerable difference at low frequencies (approximately 20–30%).

4.3 Binder performance results

In this section, the properties and performance of the studied binders are evaluated using dynamic shear rheometer (complex modulus test) and penetration test.

4.3.1 Binder complex modulus test

The performance of binder samples under repetitive loading cycles was evaluated to determine their complex modulus and phase angle at different temperatures and loading frequencies according to the method explained in section 3.3.4.4. In the following subsections, the procedure of this experiment is verified from different aspects. Then, the results are presented, analysed and discussed. The master curves of the binders are constructed to compare the results more conveniently. Finally, the binders are graded using critical high temperature and viscosity as explained in section 3.3.4.4.2.1 and 3.3.4.4.2.2.

4.3.1.1 Verification of laboratory procedures of binder testing

4.3.1.1.1 Effect of plate size on the results of the DSR test

As explained before, the size of the plate used for testing the binder samples needed to be changed based on the test temperature or stiffness of the binder, e.g., for the majority of binders, the 25 mm plate was used for the tests at 40 °C or higher while the 8 mm plate was used for lower temperatures. The reason behind the change of plate size is the capability of the apparatus used for the test. The larger the plate, the larger the torque required to oscillate the sample. Therefore, it might not be feasible to use a large plate for very stiff binders or at low temperatures, because having a huge motor on the DSR apparatus is not feasible just for these cases. However, using small plates has its own issues. If a small plate is used with a very soft binder or at hot temperatures, the required torque is very small. Therefore, it might be difficult to control or monitor the machine accurately as other factors such as noise distortion or data acquisition system resolution might become an issue. Therefore, for different scenarios different sizes of plates were required to perform the DSR test and a wide range of temperatures were investigated.

To ensure that the results from the different plates were compatible, a series of tests were performed. In these tests, both plates were used in the same test on the same binder at the same temperature and conditions. The temperature was chosen so that the machine was capable of carrying out the test in that binder on both size plates.

In the present study, the complex modulus of two types of binder, virgin C320 and RTFO aged C320 binder, were tested at 40 °C under a load that produces 1% strain. The test was performed at different loading frequencies from 0.1 to 10 Hz. The test was repeated at least two times for each condition per plate size. The results of tests on virgin C320 binder are presented for both plates in Figure 4-102 while the results for RTFO aged C320 binder is shown in Figure 4-103.

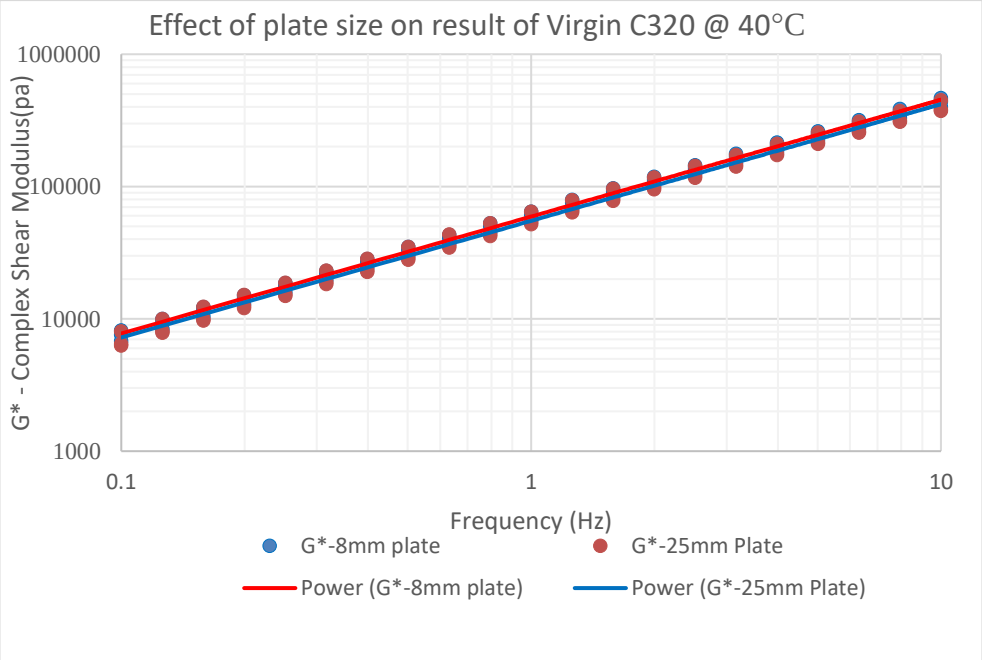

Figure 4-102 The effect of plate size on G of virgin C320 binder at 40 °C*

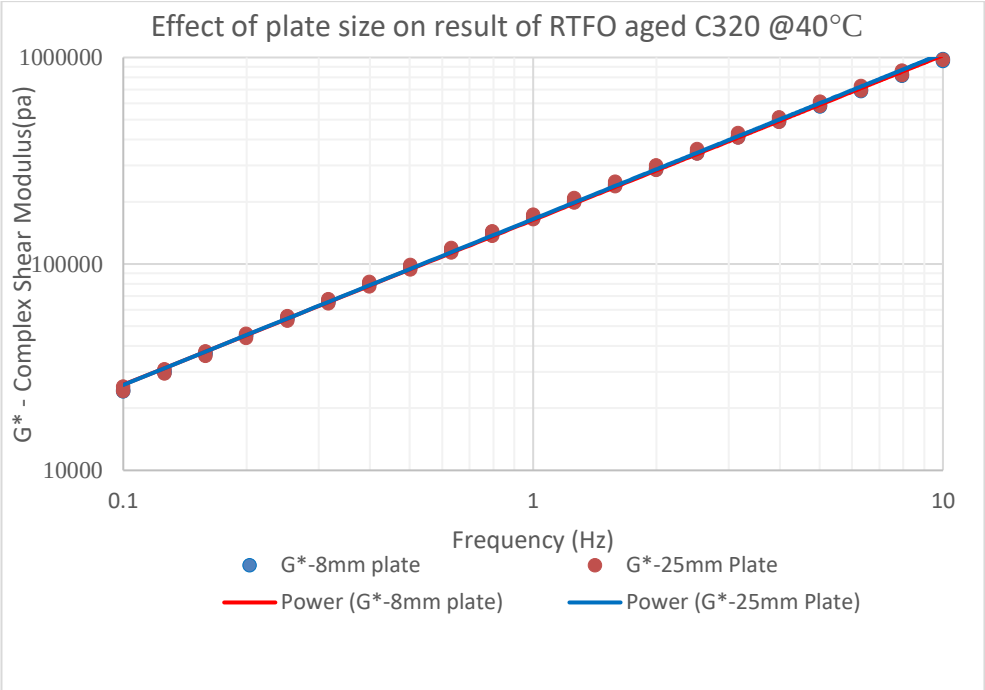

Figure 4-103 The effect of plate size on G of RTFO aged C320 binder at 40 °C*

As the results show, there is no considerable difference between the results of tests with different plates. Therefore the results of different plates can be combined together to investigate the performance of the binders across a wider range of temperatures.

4.3.1.1.2 Linear behaviour verification of binder

When performing the complex modulus test on the binders, the binder behaviour should be in its linear region. Therefore, the results should not be affected by the amount of strain applied to the sample. This is also one of the conditions for utilising the time-temperature superposition theory as explained in section 2.4. To determine the linear region of each binder and ensure the test results are valid, samples from each binder source were taken and tested at different temperatures and strain levels while the loading frequency remained constant (10 rad/s). Figure 4-104 to Figure 4-111 show the results for different binders. The tests were performed at 5, 15, 40 and 70 °C for all binders while the RAP binder was also tested at 60 °C.

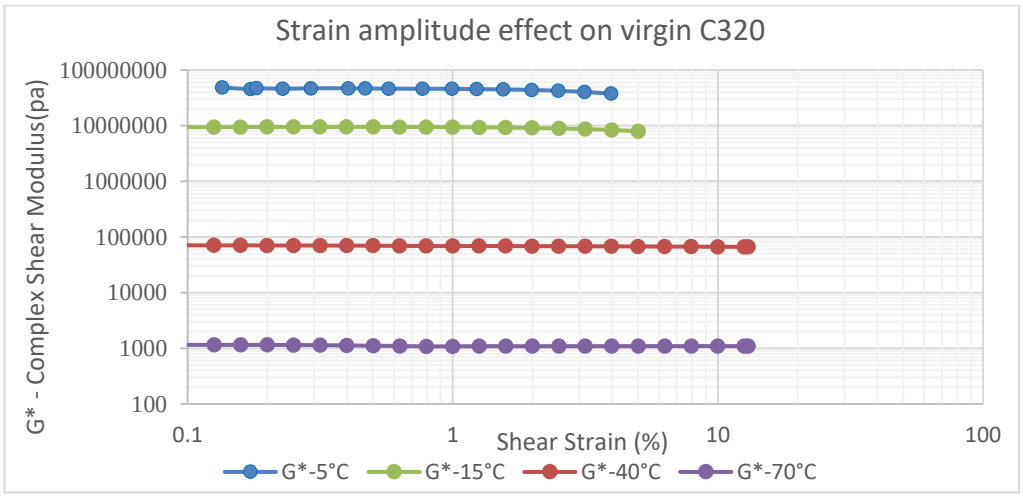

Figure 4-104 Strain amplitude effect on G of virgin C320 binder at 5, 15, 40 and 70 °C*

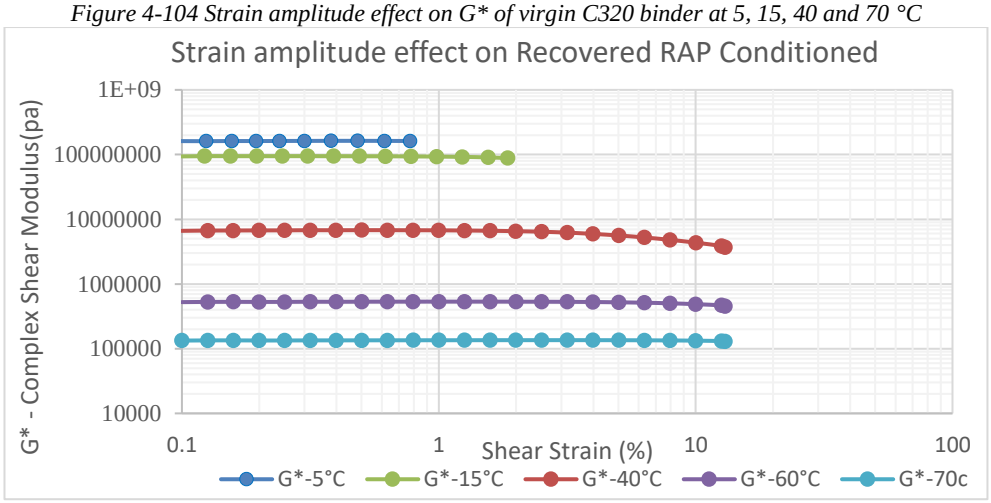

Figure 4-105 Strain amplitude effect on G of recovered conditioned RAP binder at 5, 15, 40, 60 and 70 °C*

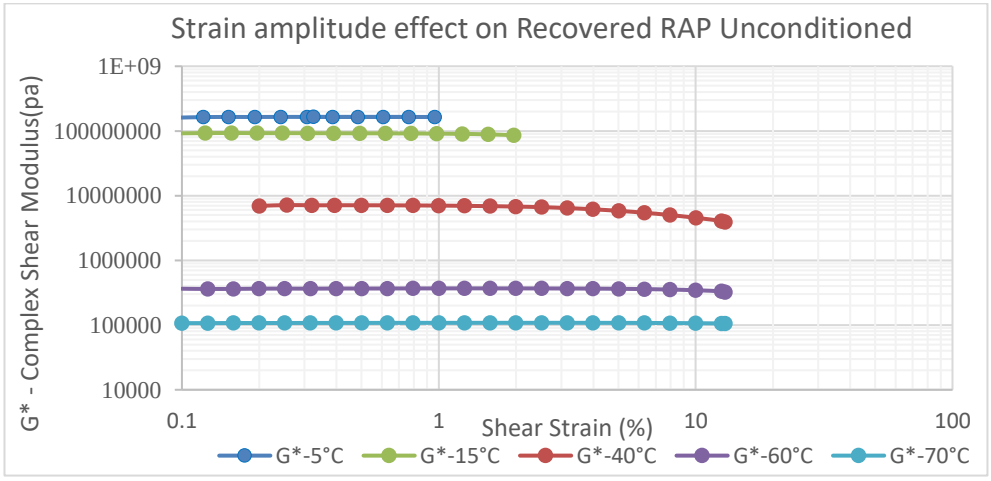

Figure 4-106 Strain amplitude effect on G of recovered unconditioned RAP binder at 5, 15, 40, 60 and 70 °C*

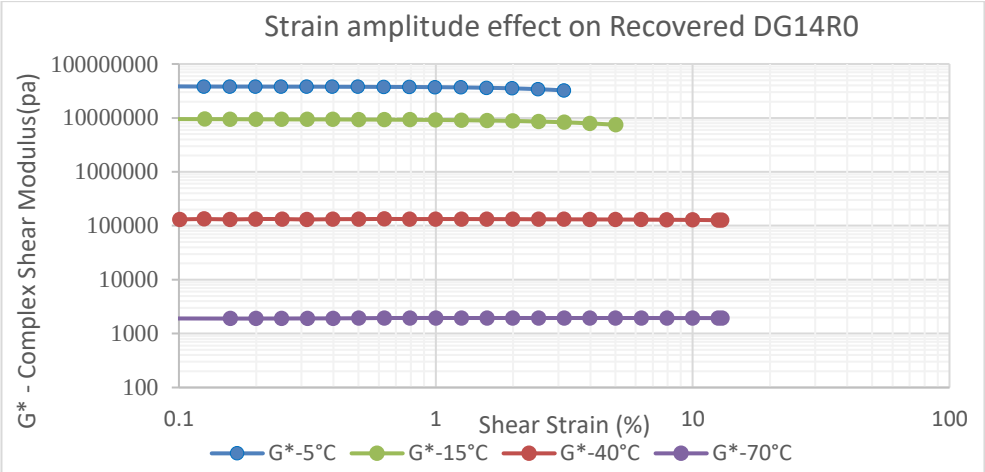

Figure 4-107 Strain amplitude effect on G of recovered DG14R0 binder at 5, 15, 40 and 70 °C*

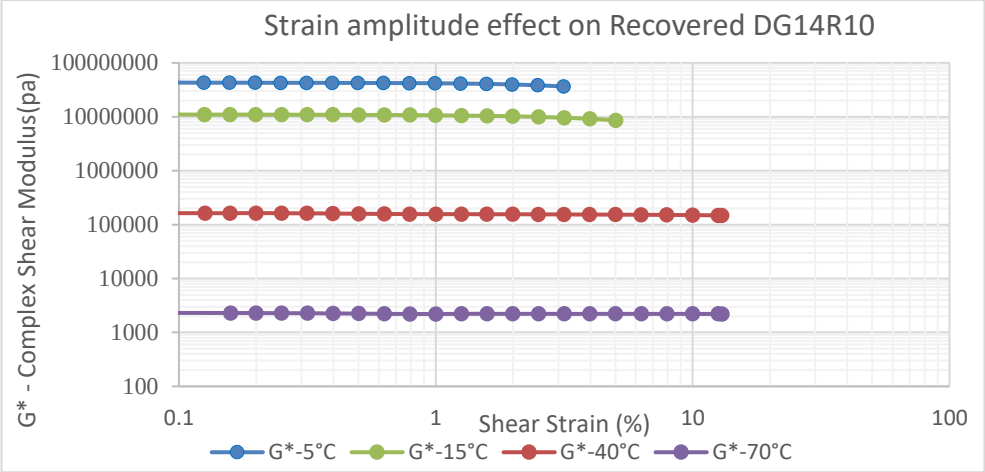

Figure 4-108 Strain amplitude effect on G of recovered DG14R10 binder at 5, 15, 40 and 70 °C*

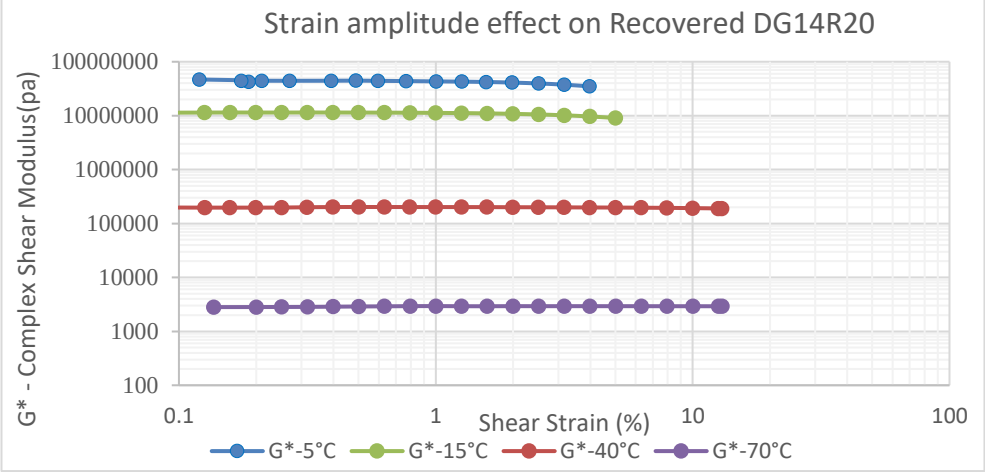

Figure 4-109 Strain amplitude effect on G of recovered DG14R20 binder at 5, 15, 40 and 70 °C*

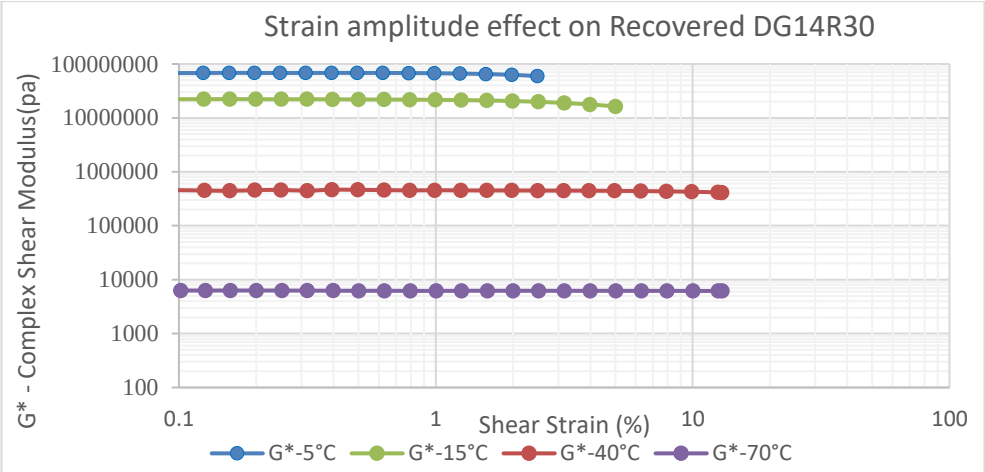

Figure 4-110 Strain amplitude effect on G of recovered DG14R30 binder at 5, 15, 40 and 70 °C*

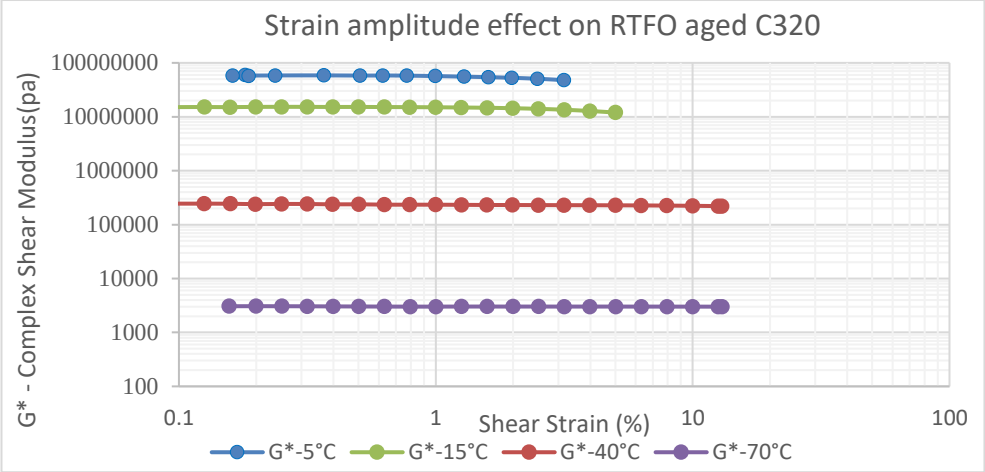

Figure 4-111 Strain amplitude effect on G of RTFO aged C320 binder at 5, 15, 40 and 70 °C*

Based on the results illustrated in this section, it can be verified that the strain level chosen in this study (1%) is well within the linear region of all the binders over a wide range of temperatures. Therefore, the results are reliable and usable. This also verifies that the data using the 1% strain level can be used in constructing the master curves of the binders using time-temperature superposition theorem.

4.3.1.1.3 Validity of recovery procedure

One of the concerns in the present study was that recovering the binder from the mixture might affect its properties. If this occurred, the results of the tests on the recovered binders would not reflect the properties of the binder in the mixture, i.e., the recovered binder properties could not be related to the performance of the mixture they were recovered from.

To verify how the recovery procedure might affect the binder results, two samples were taken from the same source of C320 binder. One sample was tested directly using a DSR apparatus to determine its complex modulus at 20, 40 and 60 °C under different loading frequencies between 0.1 to 10 Hz. Another sample was first dissolved by adding enough toluene as a solvent, and the solution was then treated as an outcome liquid from extraction centrifuge during binder recovery procedure as explained in section 3.3.4.2. The solution was placed under the centrifuging and distillation process to separate the binder from the solution again, and the sample was then tested in a similar way as the first sample was tested. The results of the complex modulus of both samples are illustrated in Figure 4-112.

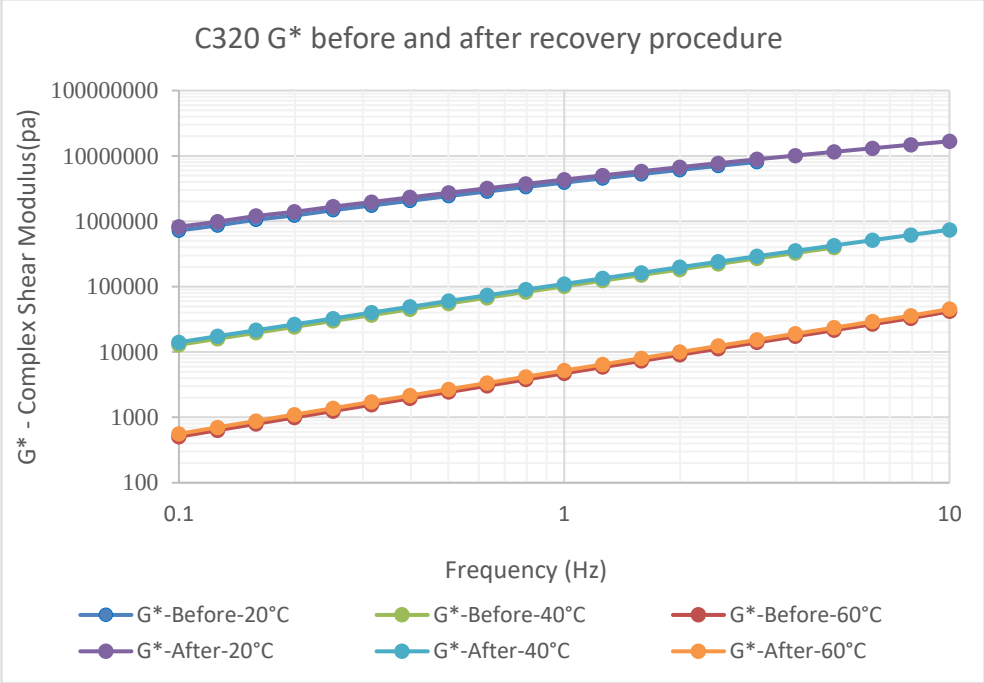

Figure 4-112 Effect of recovery procedure on G of C320 binder versus frequency*

It is obvious that the recovery procedure did not have a significant effect on the rheological properties of the samples. Therefore, the recovered binders can present the binders that are actually in the mixture they are recovered from.

4.3.1.2 Complex modulus test results

The complex modulus and phase angle of binder samples from different sources were measured using dynamic shear rheometer apparatus according to the method explained in section 3.3.4.4. For each source, at least two

samples were tested. For the recovered binders, as recovery process had been performed twice per mixture already, two samples per each recovered binder were then tested (total of four samples) with the exception of DG14R20 that had only recovered one, therefore, only two samples were tested from this mixture.

The tests were performed on different loading frequencies (0.1 to 10 Hz) and temperatures including 5, 20, 30, 40, 50, 60 and 70 °C for all samples. However, the samples recovered from RAP were not tested at 5 °C as they were very stiff and the machine utilised for the tests had overheating problems during the tests. Instead, the RAP samples were tested at 80 °C as well as other temperatures.

The complex modulus results of all the samples and their average values are presented in Figure 4-113 to Figure 4-120 for the different types of binders utilised in the present study. Moreover, the phase angle results and the average phase angles of the sample with the same conditions are illustrated in Figure 4-121 to Figure 4-128 for all the binder sources.

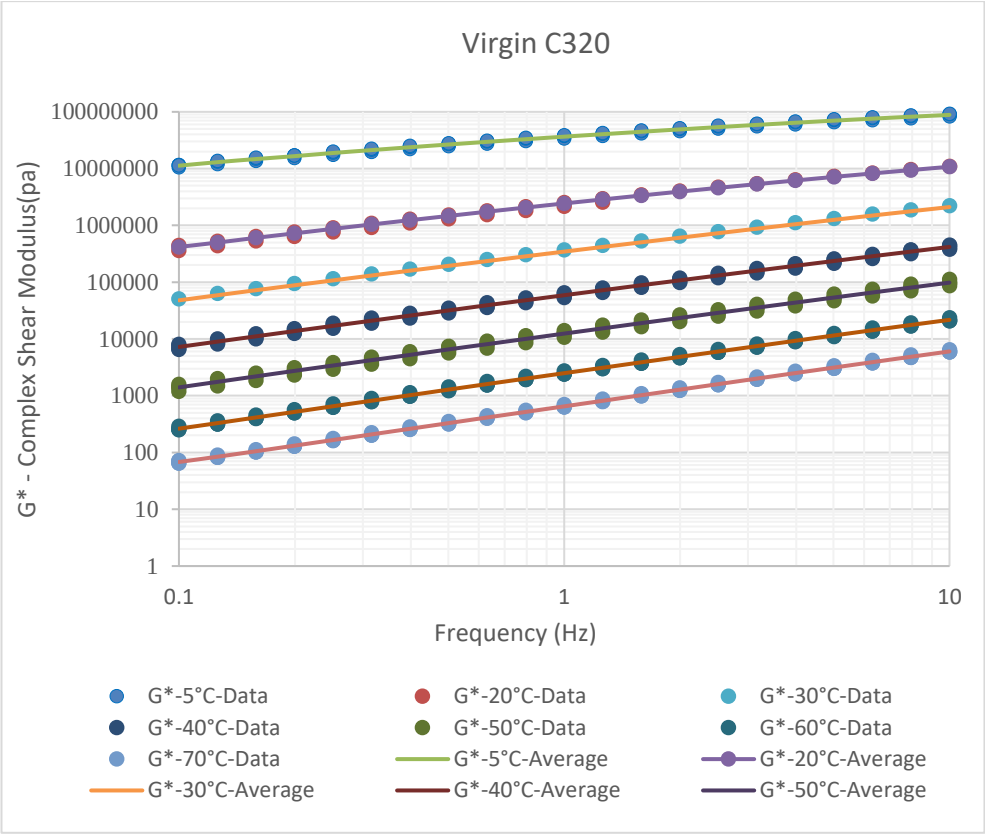

Figure 4-113 Complex shear modulus results of virgin C320 binder at 5, 20, 30, 40, 50, 60 and 70 °C versus frequency

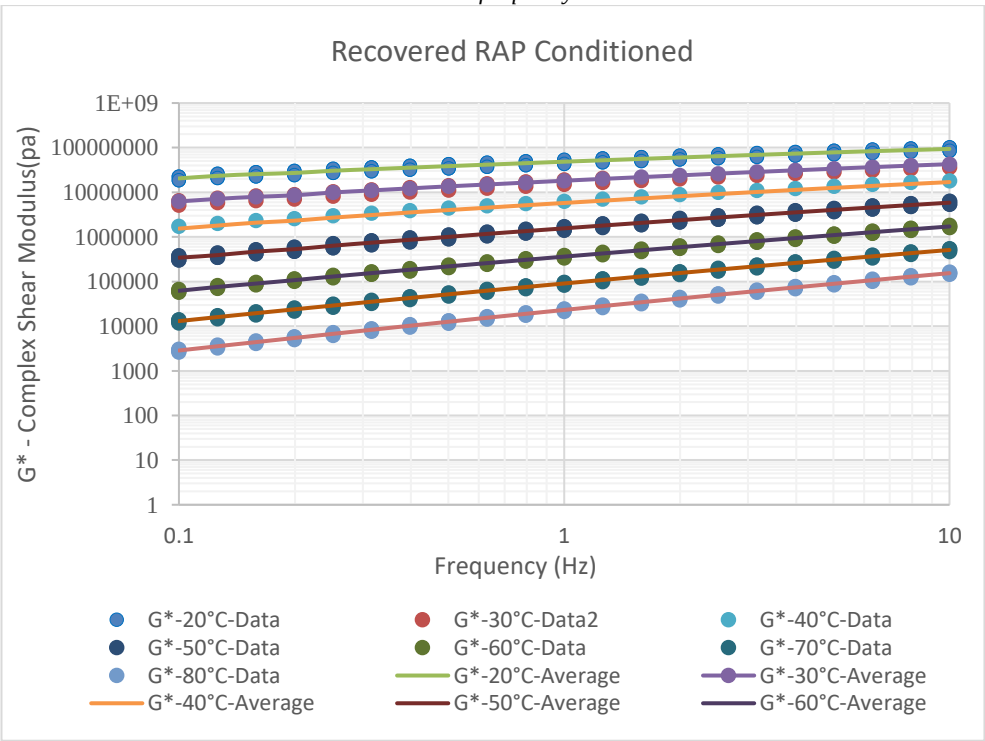

Figure 4-114 Complex shear modulus results of recovered conditioned RAP binder at 20,30, 40, 50, 60, 70 and 80 °C versus frequency

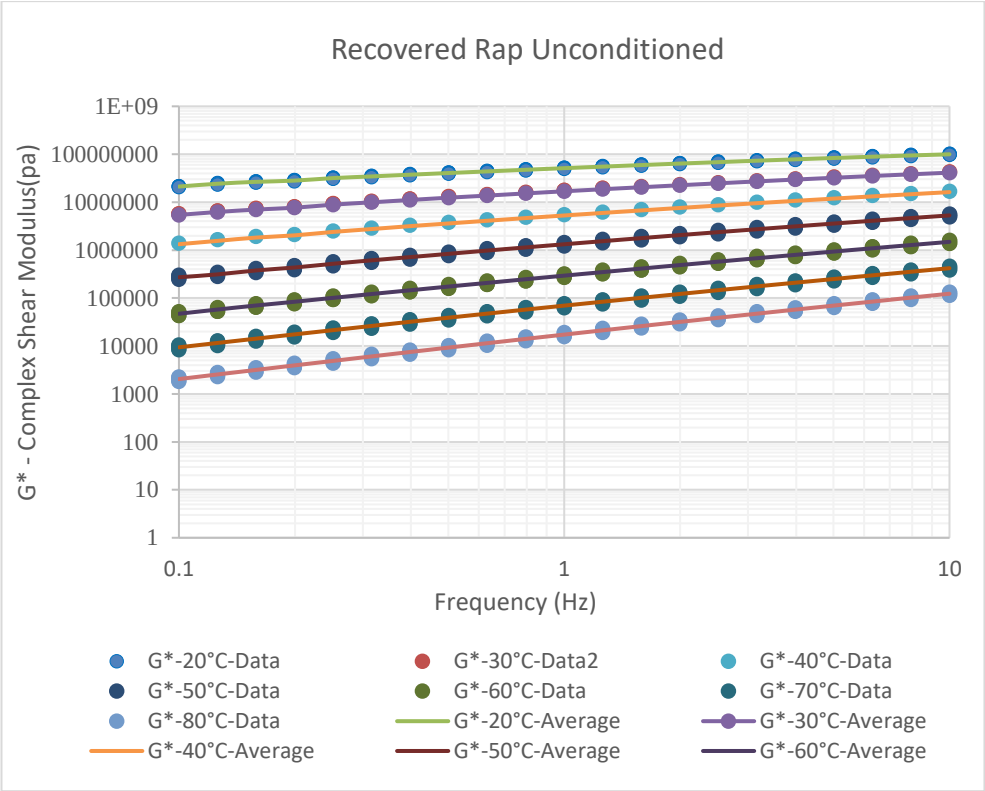

Figure 4-115 Complex shear modulus results of recovered unconditioned RAP binder at 20, 30, 40, 50, 60, 70 and 80 °C versus frequency

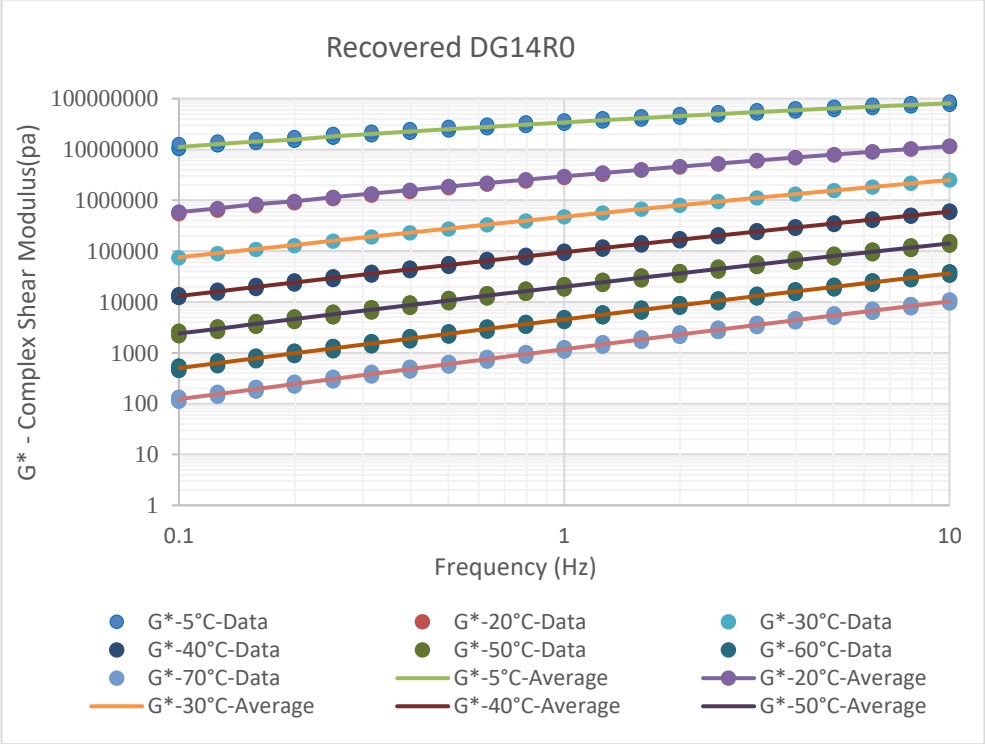

Figure 4-116 Complex shear modulus results of recovered binder from DG14R0 mixture at 5, 20, 30, 40, 50, 60 and 70 °C versus frequency

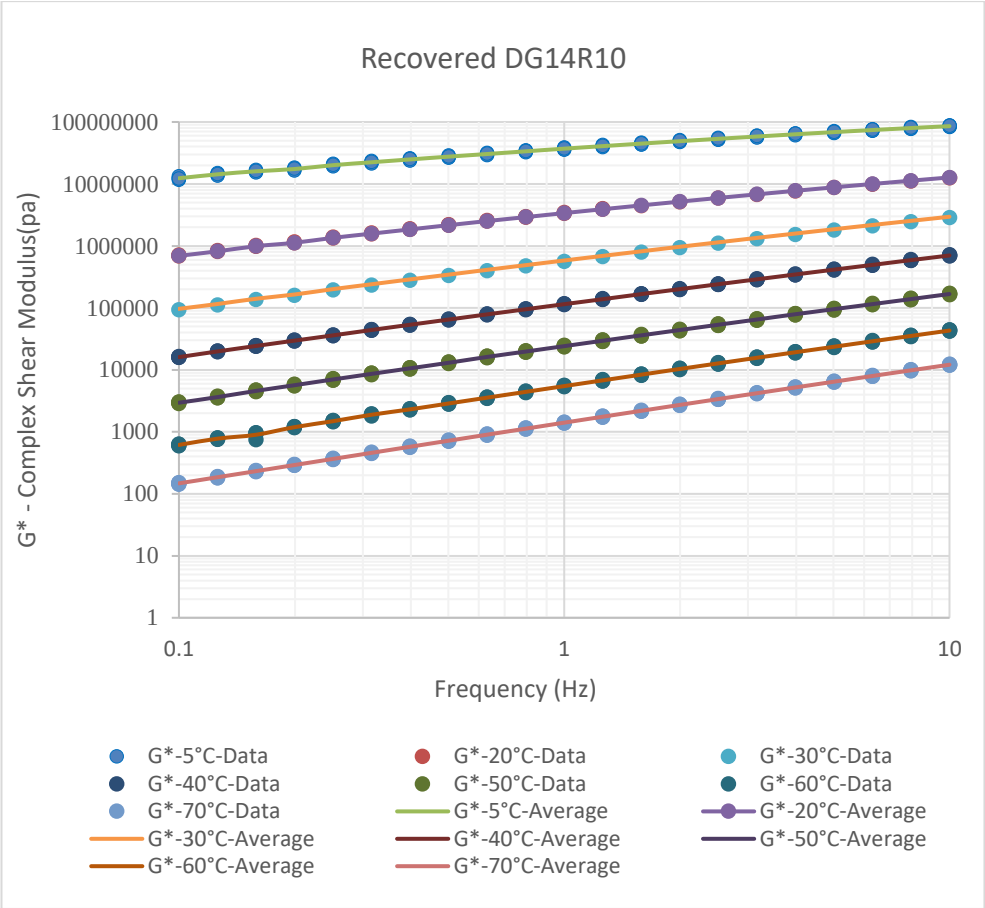

Figure 4-117 Complex shear modulus results of recovered binder from DG14R10 mixture at 5, 20, 30, 40, 50, 60 and 70 °C versus frequency

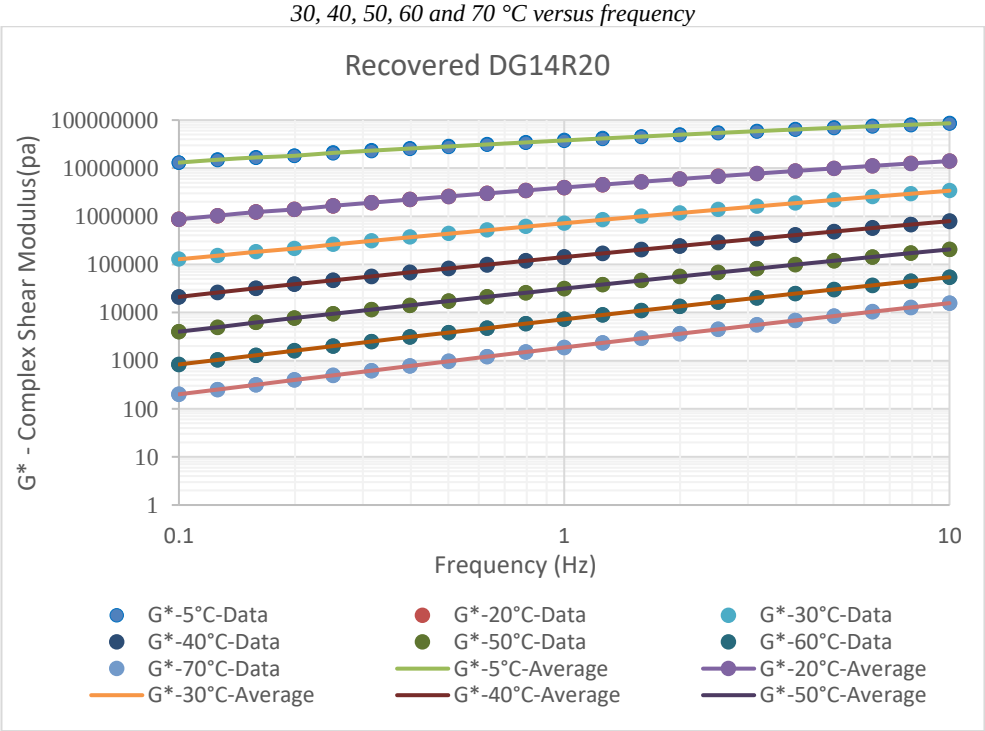

Figure 4-118 Complex shear modulus results of recovered binder from DG14R20 mixture at 5, 20, 30, 40, 50, 60 and 70 °C versus frequency

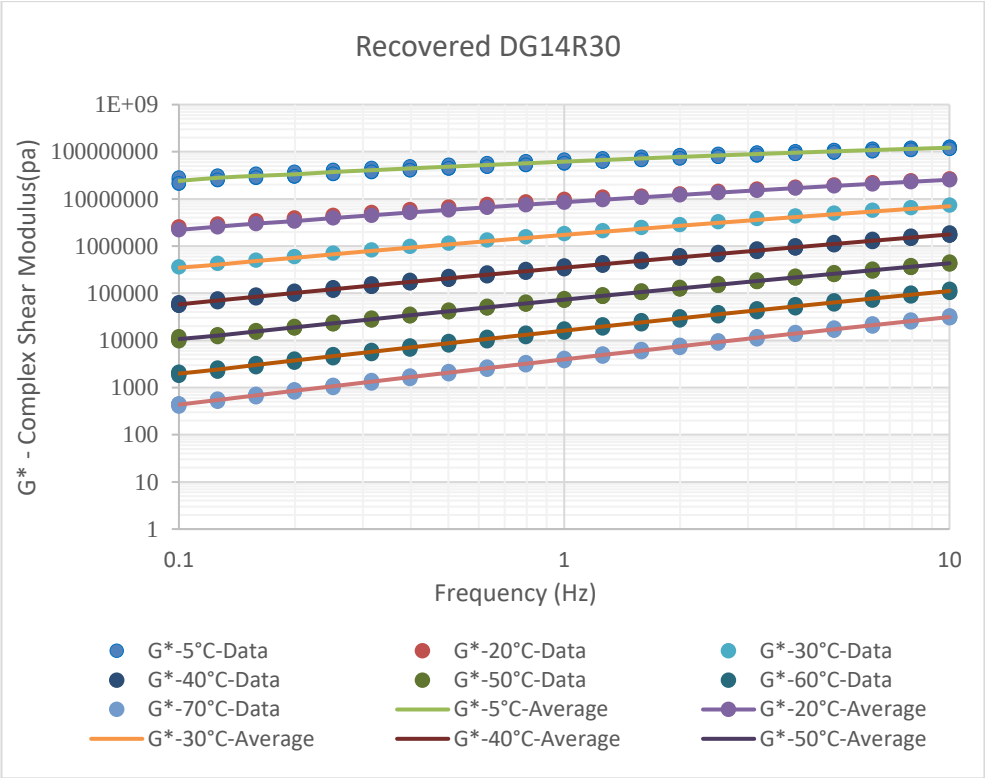

Figure 4-119 Complex shear modulus results of recovered binder from DG14R30 mixture at 5, 20, 30, 40, 50, 60 and 70 °C versus frequency

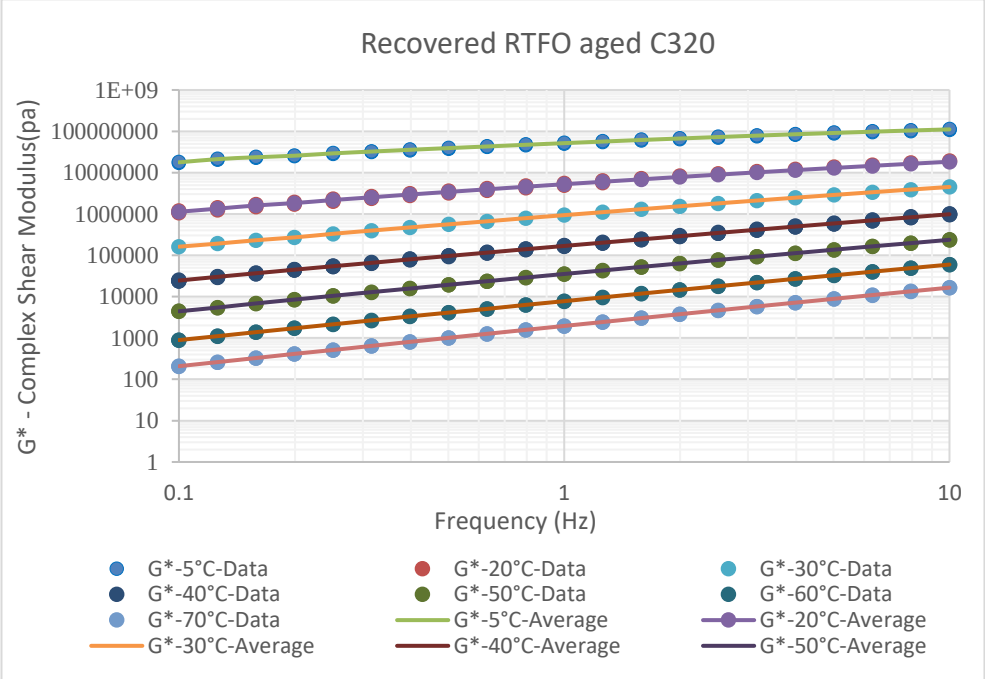

Figure 4-120 Complex shear modulus results of RTFO aged C320 binder at 5, 20, 30, 40, 50, 60 and 70 °C versus frequency

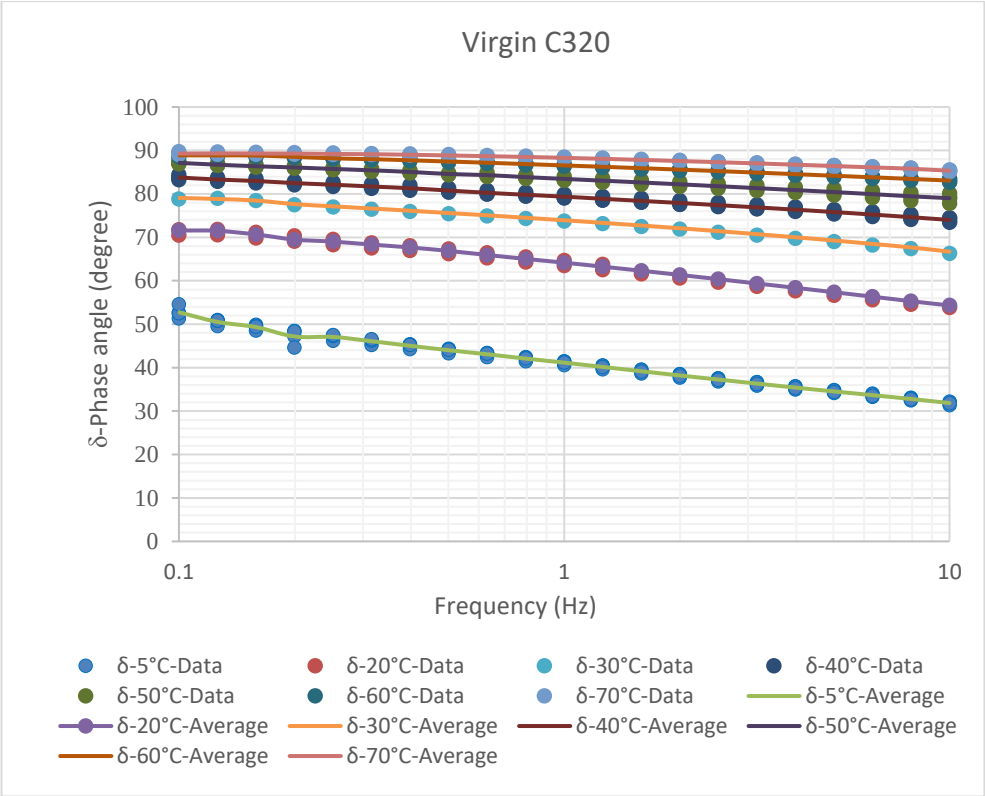

Figure 4-121 Phase angle results of virgin C320 binder at 5, 20, 30, 40, 50, 60 and 70 °C versus frequency

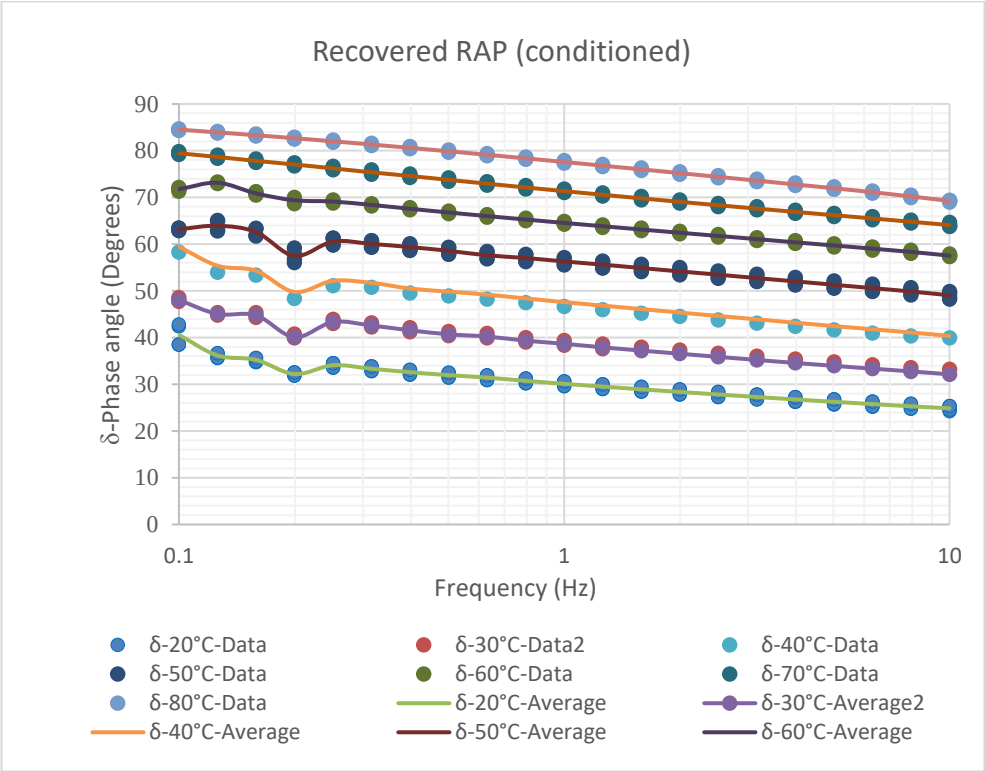

Figure 4-122 Phase angle results of recovered conditioned RAP binder at 20, 30, 40, 50, 60, 70 and 80 °C versus frequency

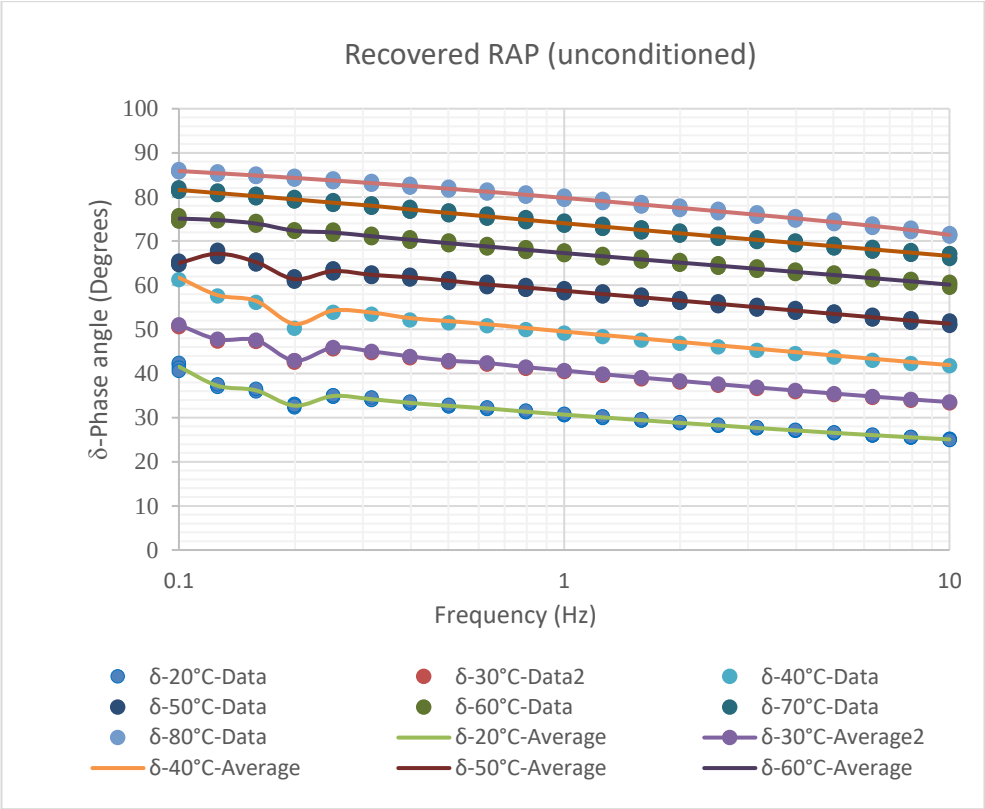

Figure 4-123 Phase angle results of recovered unconditioned RAP binder at 20, 30, 40, 50, 60, 70 and 80 °C versus frequency

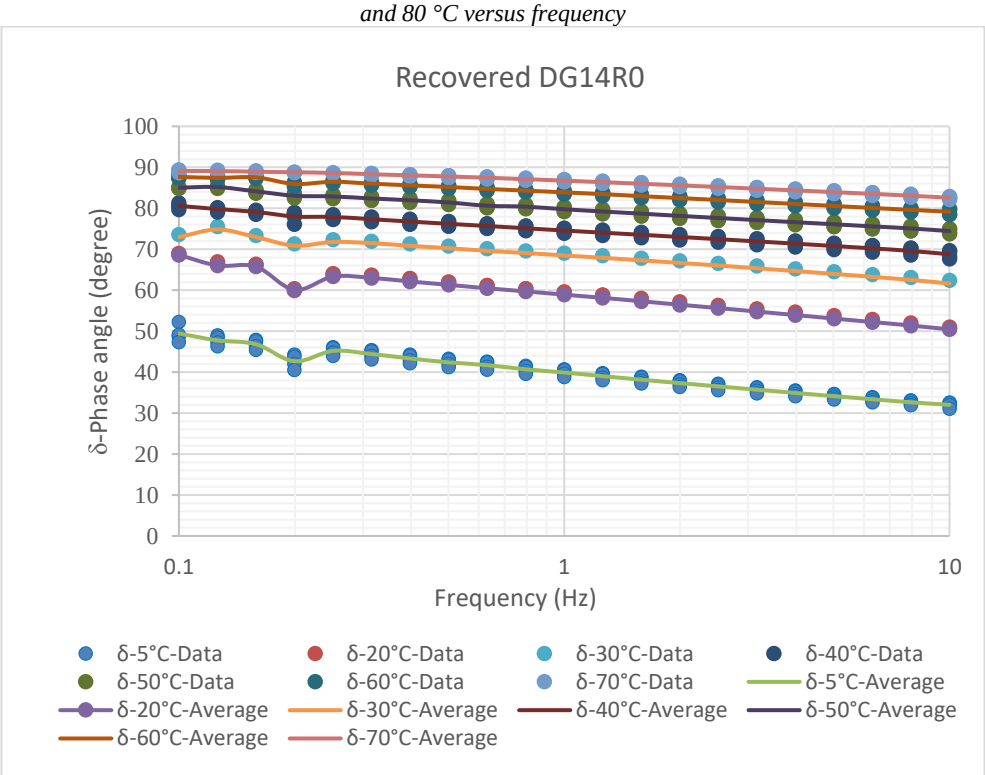

Figure 4-124 Phase angle results of recovered binder from DG14R0 mixture at 5, 20, 30, 40, 50, 60 and 70 °C versus frequency

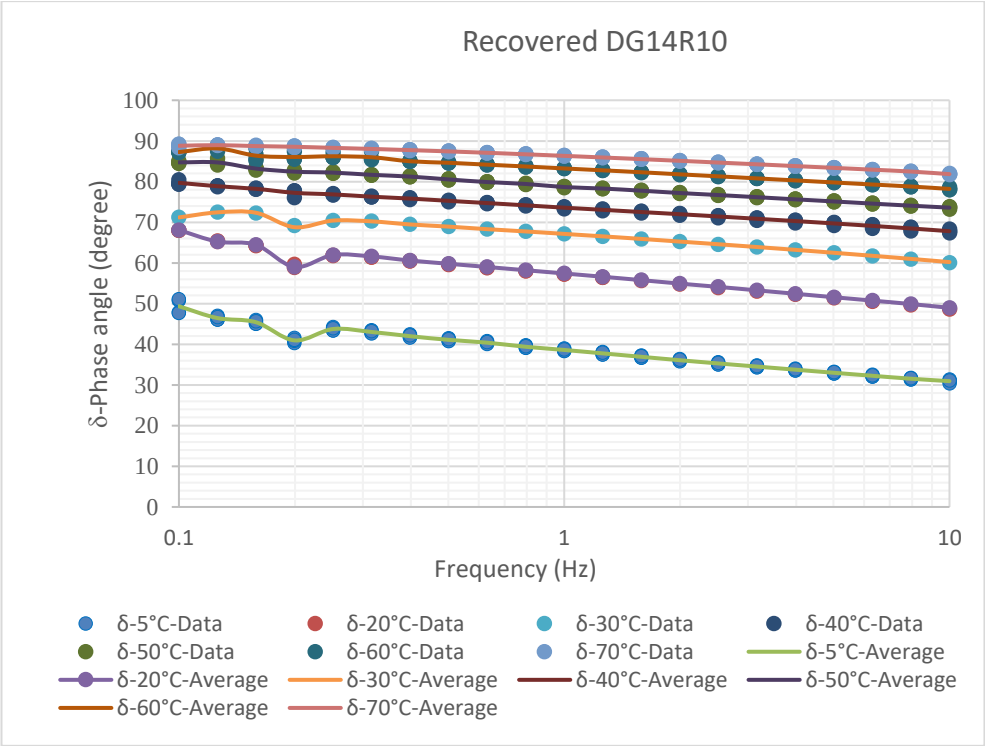

Figure 4-125 Phase angle results of recovered binder from DG14R10 mixture at 5, 20, 30, 40, 50, 60 and 70 °C versus frequency

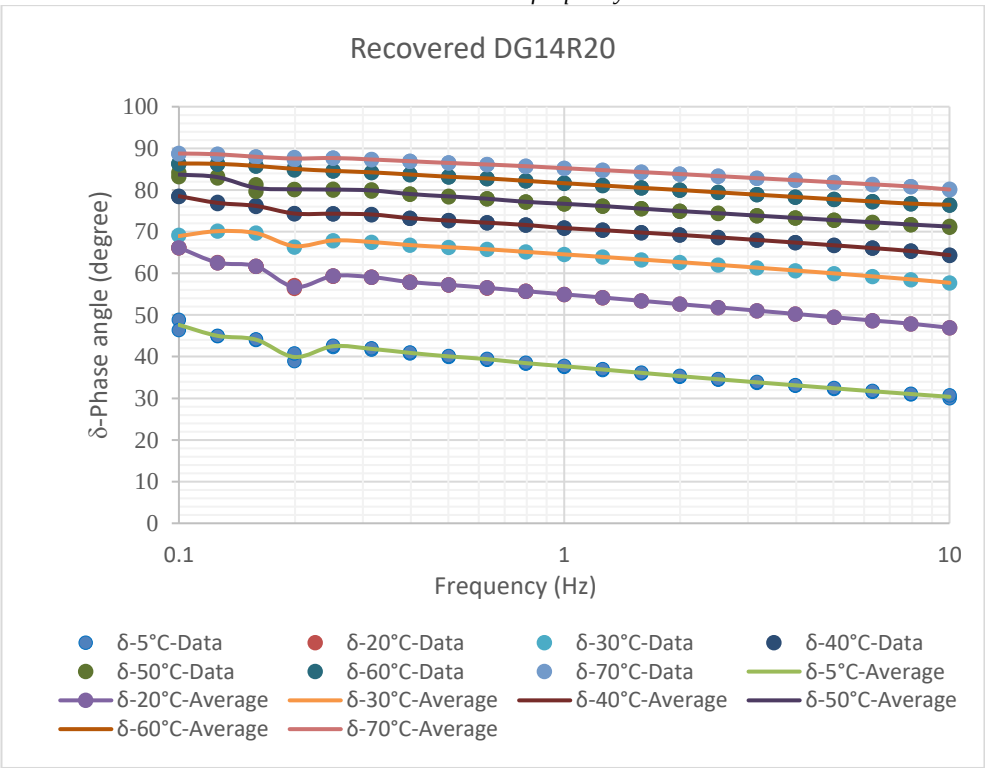

Figure 4-126 Phase angle results of recovered binder from DG14R20 mixture at 5, 20, 30, 40, 50, 60 and 70 °C versus frequency

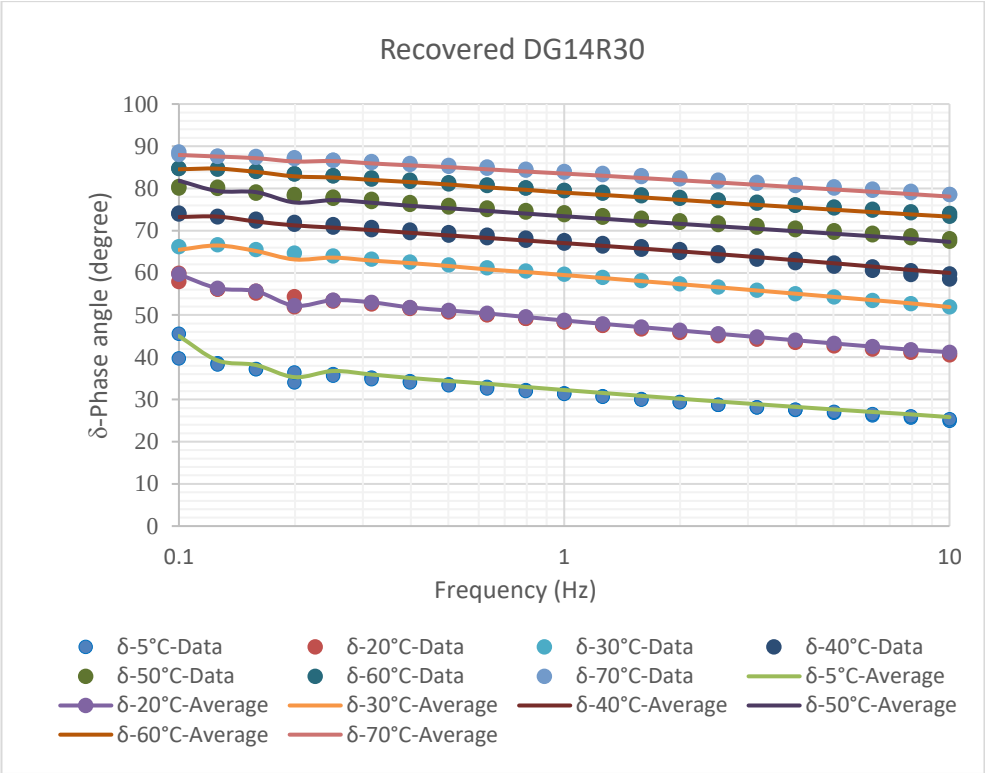

Figure 4-127 Phase angle results of recovered binder from DG14R30 mixture at 5, 20, 30, 40, 50, 60 and 70 °C versus frequency

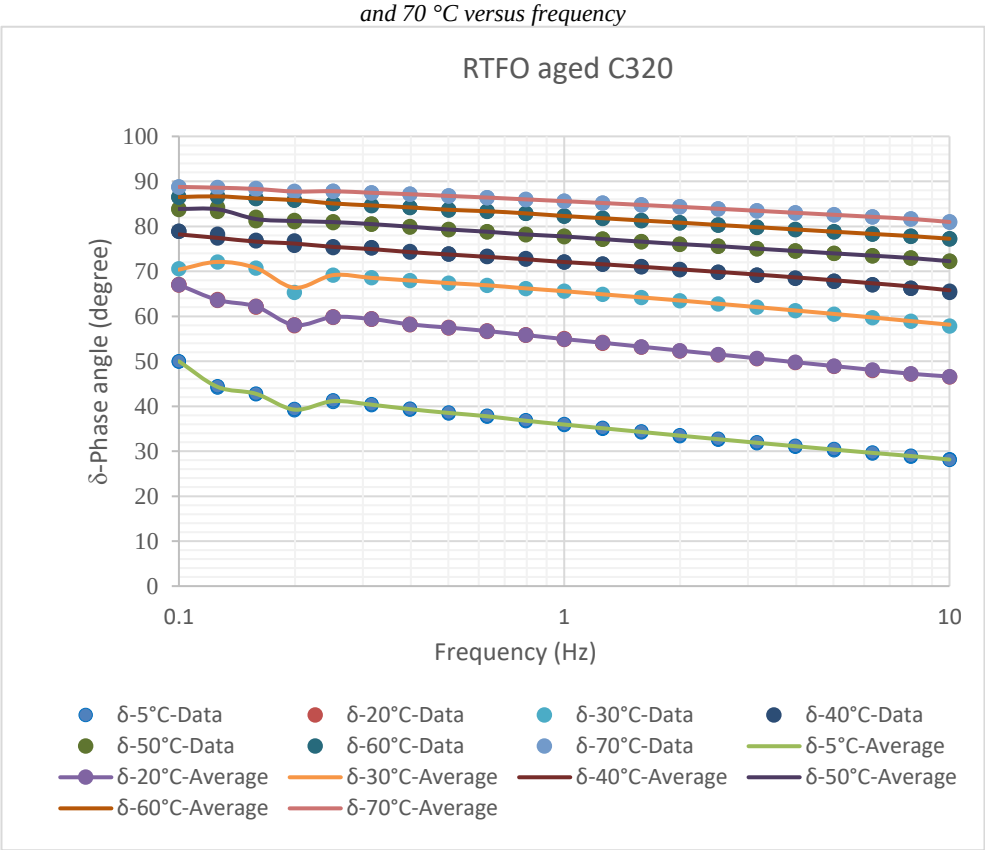

Figure 4-128 Phase angle results of RTFO aged C320 binder at 5, 20, 30, 40, 50, 60 and 70°C versus frequency

As anticipated, Figure 4-113 to Figure 4-120 demonstrated that the complex modulus of all the binders increased when the loading frequency increased

from 0.1 to 10 Hz. Moreover, the complex modulus was noticeably affected by the temperature, i.e., it decreases when the temperature increases and vice versa.

Moreover, Figure 4-121 to Figure 4-128 also illustrate that phase angle of all binders have a decreasing trend with loading frequency, decreasing when the loading frequency increases. Furthermore, it can be seen that the higher the temperature is, the higher the phase angle that was measured. At the low frequencies (lower than 0.3 Hz), some inconsistencies can be observed with the rest of the trend, which is likely caused by the machine struggling to oscillate at these frequencies as it appears it only occur at lower temperatures or for stiffer binders.

4.3.1.3 Master curve of binders

In this section, the master curves of the binders are constructed and the binders performances over a wide range of frequencies are compared to each other using their master curves.

To construct the master curves of dynamic modulus, the procedure explained in section 2.4 was followed and the results illustrated in Figure 4-129 to Figure 4-136 for the different types of binders. In addition, the shifted phase angles of the binders are illustrated in Figure 4-137 to Figure 4-144. The temperature reference for these master curves was 60 °C.

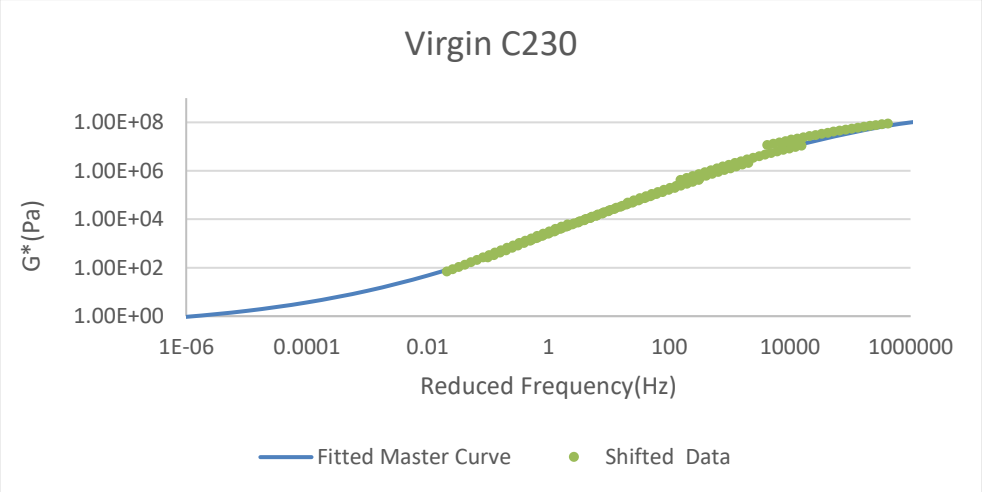

Figure 4-129 G master curve of virgin C320 binder and its shifted data at 60 °C reference temperature versus reduced frequency*

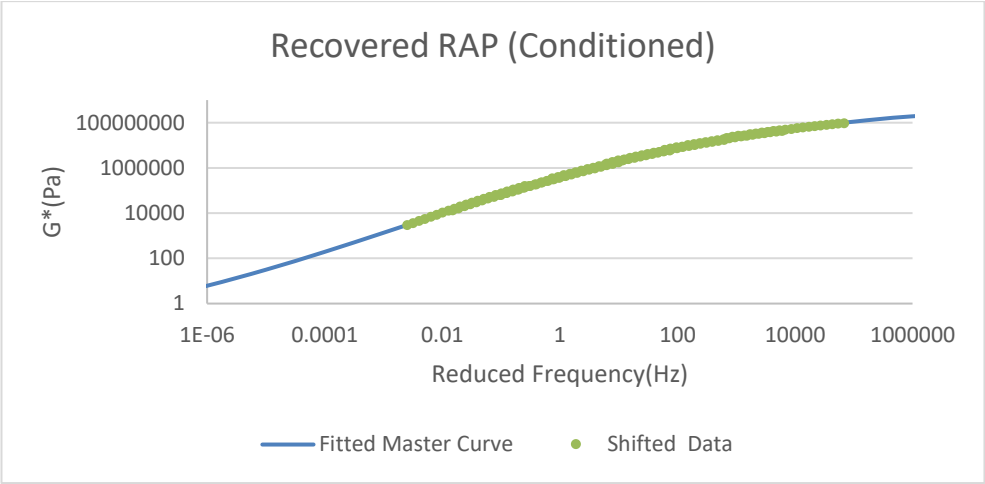

Figure 4-130 G master curve of recovered conditioned RAP binder and its shifted data at 60 °C reference temperature versus reduced frequency*

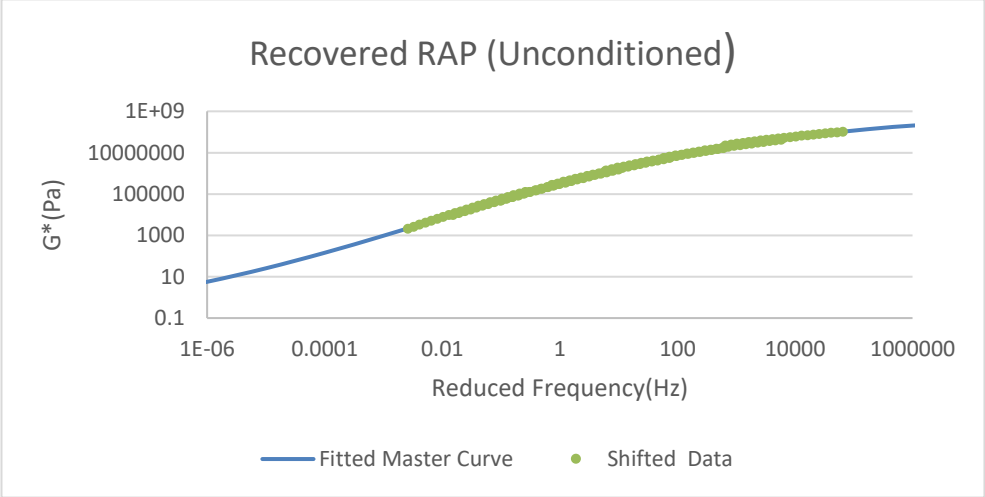

Figure 4-131 G master curve of recovered unconditioned RAP binder and its shifted data at 60 °C reference temperature versus reduced frequency*

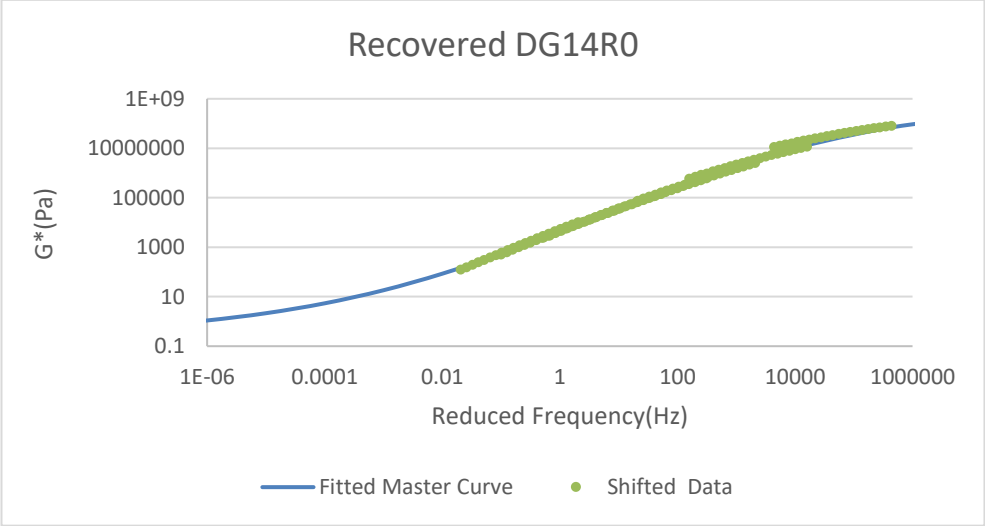

Figure 4-132 G master curve of recovered binder from DG14R0 and its shifted data at 60 °C reference temperature versus reduced frequency*

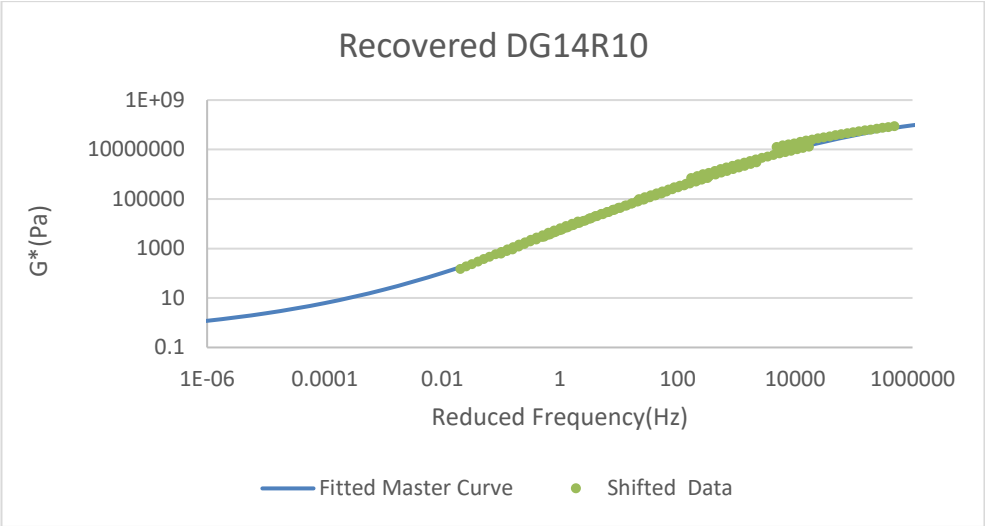

Figure 4-133 G master curve of recovered binder from DG14R10 and its shifted data at 60 °C reference temperature versus reduced frequency*

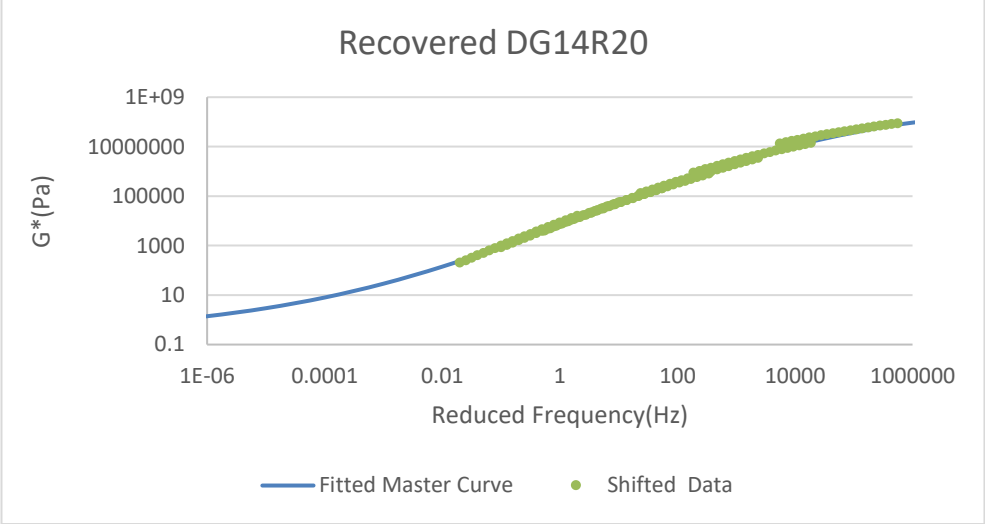

Figure 4-134 G master curve of recovered binder from DG14R20 and its shifted data at 60 °C reference temperature versus reduced frequency*

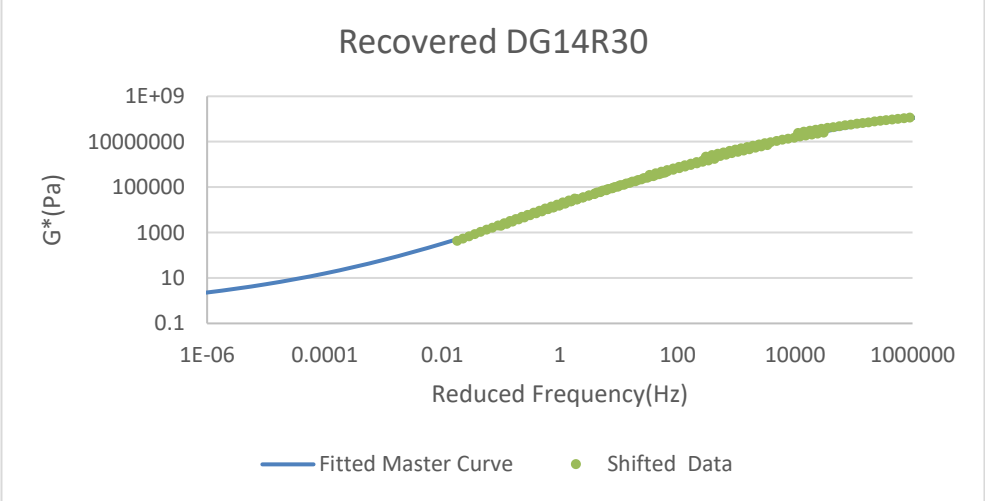

Figure 4-135 G master curve of recovered binder from DG14R30 and its shifted data at 60 °C reference temperature versus reduced frequency*

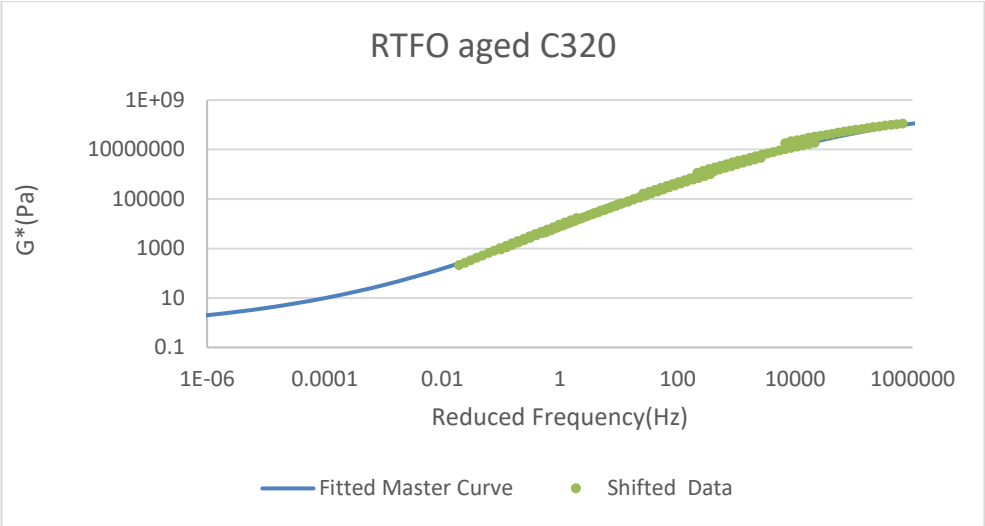

Figure 4-136 G master curve of RTFO aged C320 and its shifted data at 60 °C reference temperature versus reduced frequency*

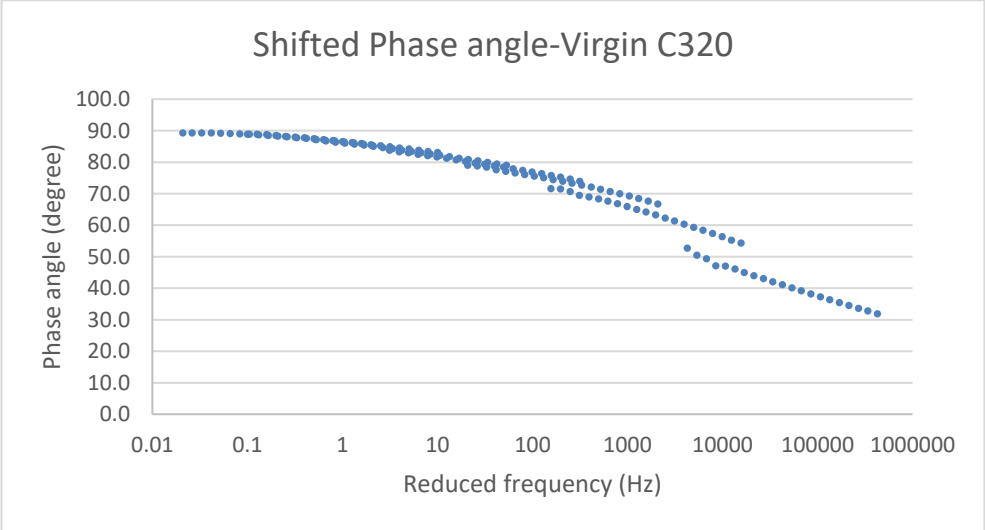

Figure 4-137 Shifted phase angle of virgin C320 binder versus reduced frequency

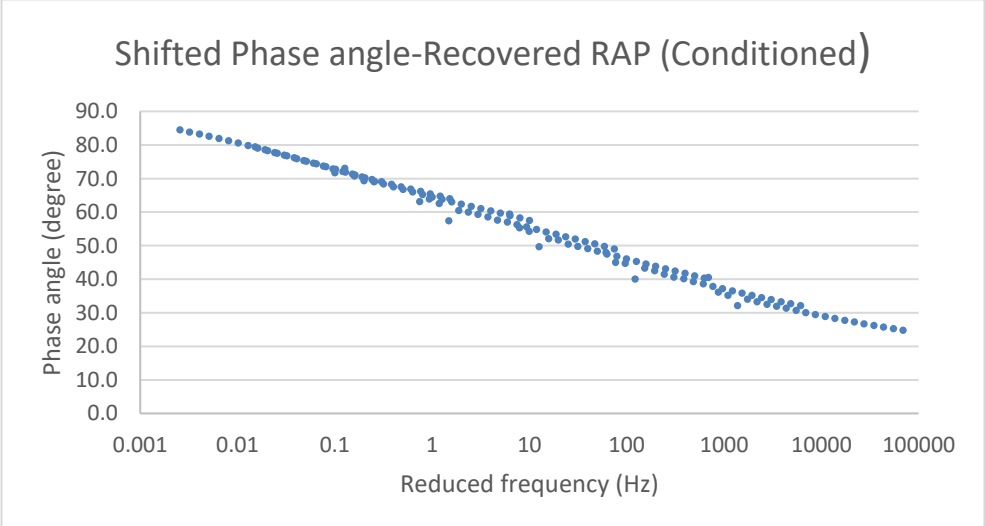

Figure 4-138 Shifted phase angle of recovered conditioned RAP binder versus reduced frequency

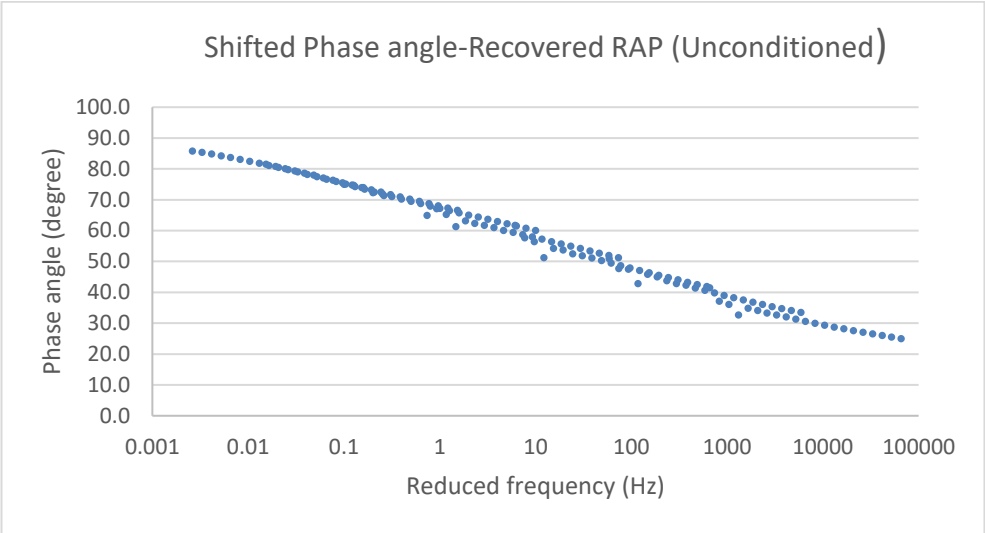

Figure 4-139 Shifted phase angle of recovered unconditioned RAP binder versus reduced frequency

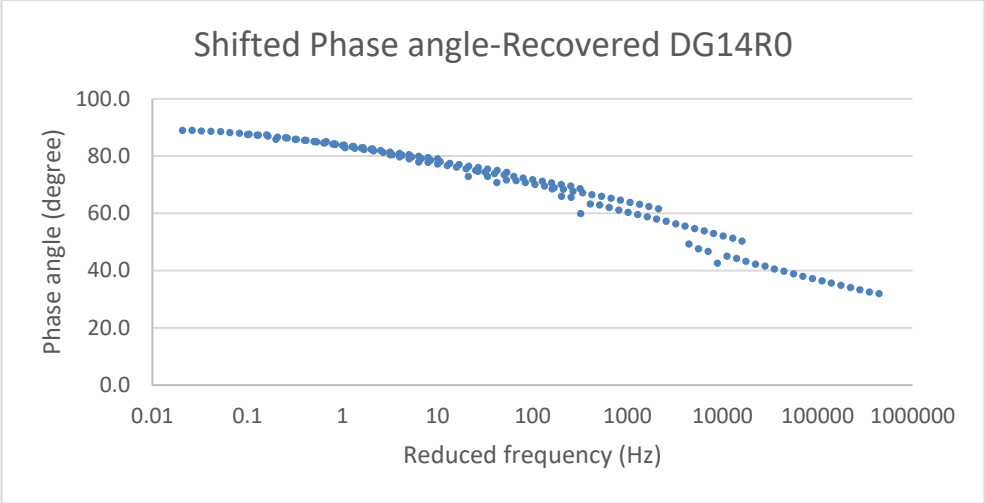

Figure 4-140 Shifted phase angle of recovered binder from DG14R0 mixture versus reduced frequency

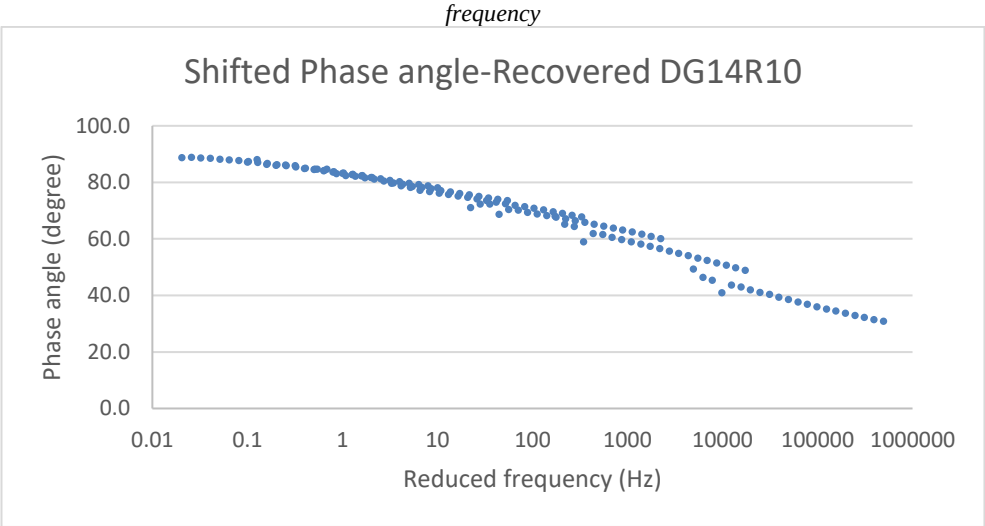

Figure 4-141 Shifted phase angle of recovered binder from DG14R10 mixture versus reduced frequency

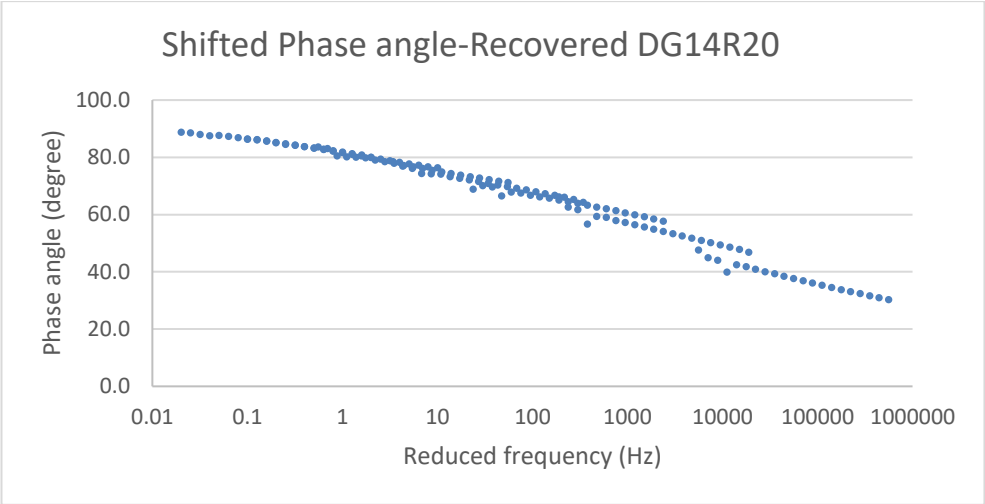

Figure 4-142 Shifted phase angle of recovered binder from DG14R20 mixture versus reduced frequency

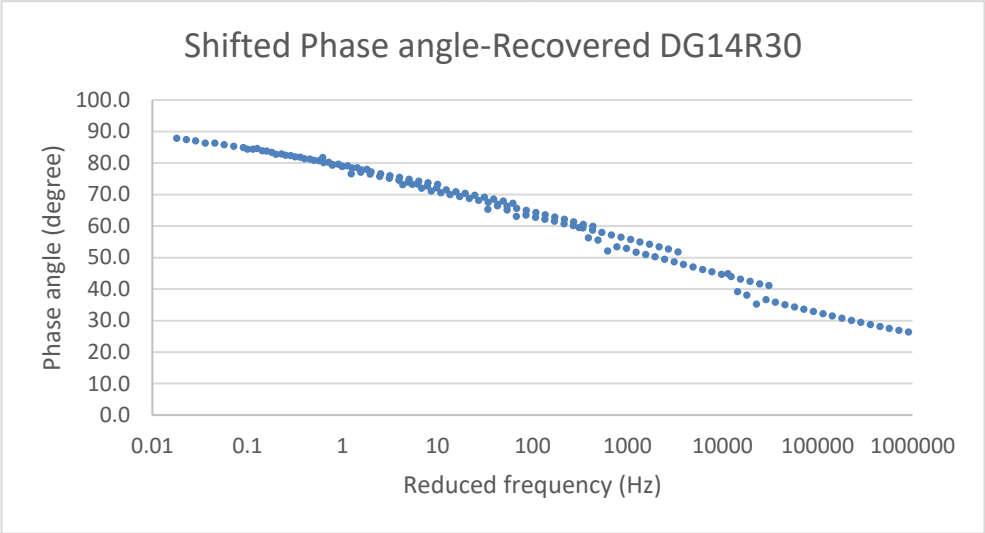

Figure 4-4-143 Shifted phase angle of recovered binder from DG14R30 mixture versus reduced frequency

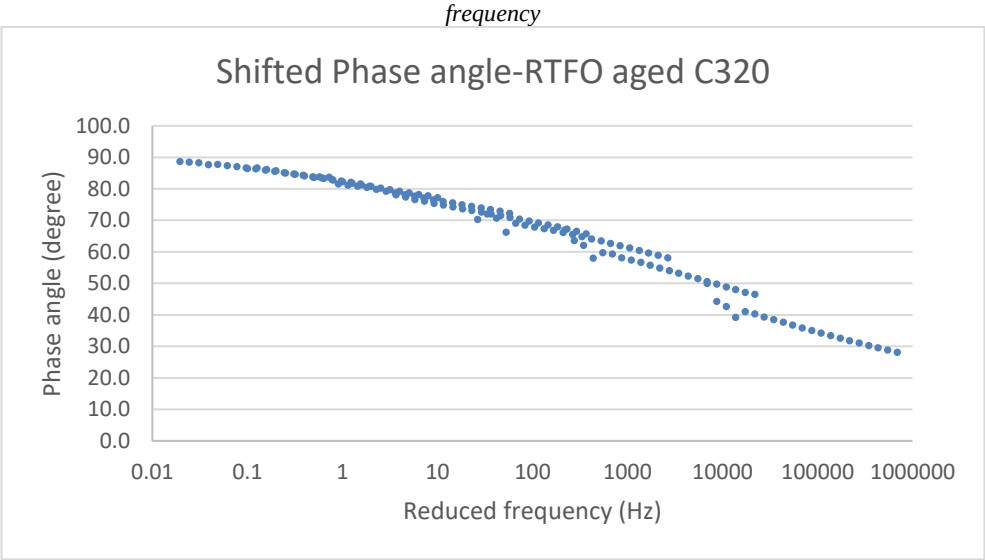

Figure 4-144 Shifted phase angle of RTFO aged C320 binder versus reduced frequency

To determine the difference in performance of the binders more clearly at 60 °C, all the binder master curves were drawn on the same graph in Figure 4-145. The data regarding this graph is also shown in Table 4-17 for fine comparison, which is difficult using only the graph as it is a log-log graph. Moreover, the shifted phase angles of the binders are compared in Figure 4-146.

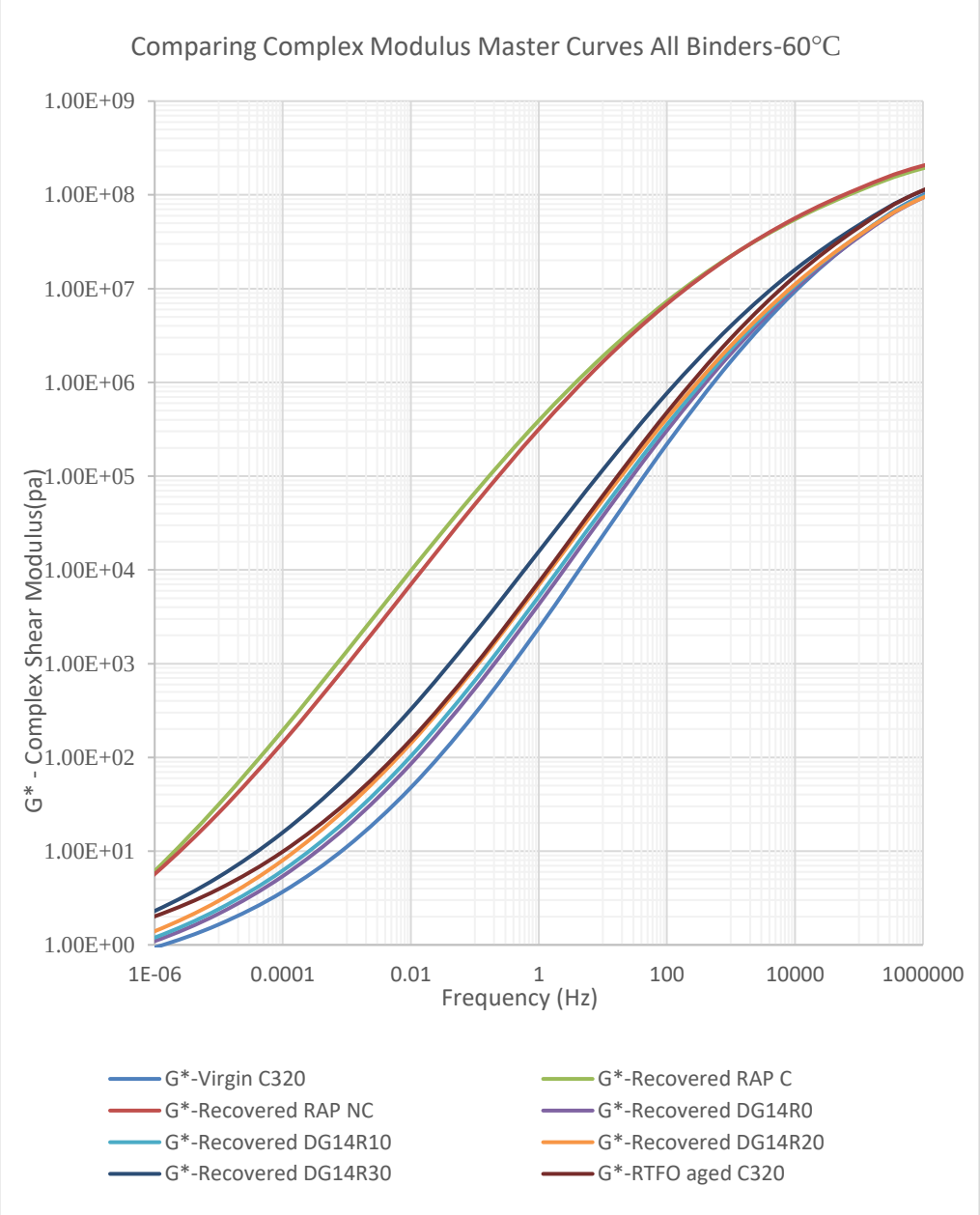

Figure 4-145 Comparing G master curves of all binders at 60 °C versus reduced frequency*

Table 4-17 Comparing G master curve details of all binders at 60 °C at different reduced frequencies*

Frequency (Hz)	G*-Virgin C320(MPa)	G*-Recovered RAP-C(MPa)	G*-Recovered RAP NC(MPa)	G*-Recovered DG14R0(MPa)	G*-Recovered DG14R10(MPa)	G*-Recovered DG14R20(MPa)	G*-Recovered DG14R30(MPa)	G*-RTFO aged(MPa)
1.00E+09	4.89E+08	5.07E+08	5.37E+08	4.54E+08	4.54E+08	4.39E+08	4.57E+08	4.86E+08
1.00E+08	3.44E+08	4.00E+08	4.26E+08	3.17E+08	3.18E+08	3.07E+08	3.29E+08	3.49E+08
1.00E+06	9.94E+07	1.92E+08	2.05E+08	9.33E+07	9.57E+07	9.35E+07	1.11E+08	1.12E+08
1.00E+05	3.61E+07	1.11E+08	1.17E+08	3.55E+07	3.71E+07	3.70E+07	4.77E+07	4.50E+07
1.00E+04	9.33E+06	5.47E+07	5.64E+07	9.97E+06	1.07E+07	1.11E+07	1.59E+07	1.35E+07
1.00E+03	1.68E+06	2.23E+07	2.21E+07	2.03E+06	2.25E+06	2.46E+06	4.00E+06	2.95E+06
1.00E+02	2.19E+05	7.30E+06	6.85E+06	3.06E+05	3.52E+05	4.12E+05	7.65E+05	4.77E+05
1.00E+01	2.32E+04	1.90E+06	1.66E+06	3.75E+04	4.45E+04	5.58E+04	1.17E+05	6.19E+04
1.00E+00	2.40E+03	3.92E+05	3.17E+05	4.29E+03	5.20E+03	6.90E+03	1.57E+04	7.41E+03
1.00E-01	2.91E+02	6.63E+04	4.99E+04	5.39E+02	6.57E+02	9.00E+02	2.11E+03	9.57E+02
1.00E-02	4.75E+01	9.75E+03	6.99E+03	8.51E+01	1.03E+02	1.41E+02	3.24E+02	1.54E+02
1.00E-03	1.11E+01	1.35E+03	9.62E+02	1.82E+01	2.15E+01	2.89E+01	6.24E+01	3.32E+01
1.00E-04	3.68E+00	1.94E+02	1.44E+02	5.40E+00	6.21E+00	7.99E+00	1.58E+01	9.87E+00
1.00E-05	1.65E+00	3.15E+01	2.56E+01	2.15E+00	2.41E+00	2.95E+00	5.31E+00	3.94E+00
1.00E-06	9.37E-01	6.14E+00	5.69E+00	1.10E+00	1.20E+00	1.40E+00	2.30E+00	2.01E+00
1.00E-07	6.33E-01	1.50E+00	1.62E+00	6.76E-01	7.23E-01	8.09E-01	1.23E+00	1.25E+00
1.00E-08	4.85E-01	4.62E-01	5.88E-01	4.82E-01	5.06E-01	5.47E-01	7.81E-01	8.91E-01

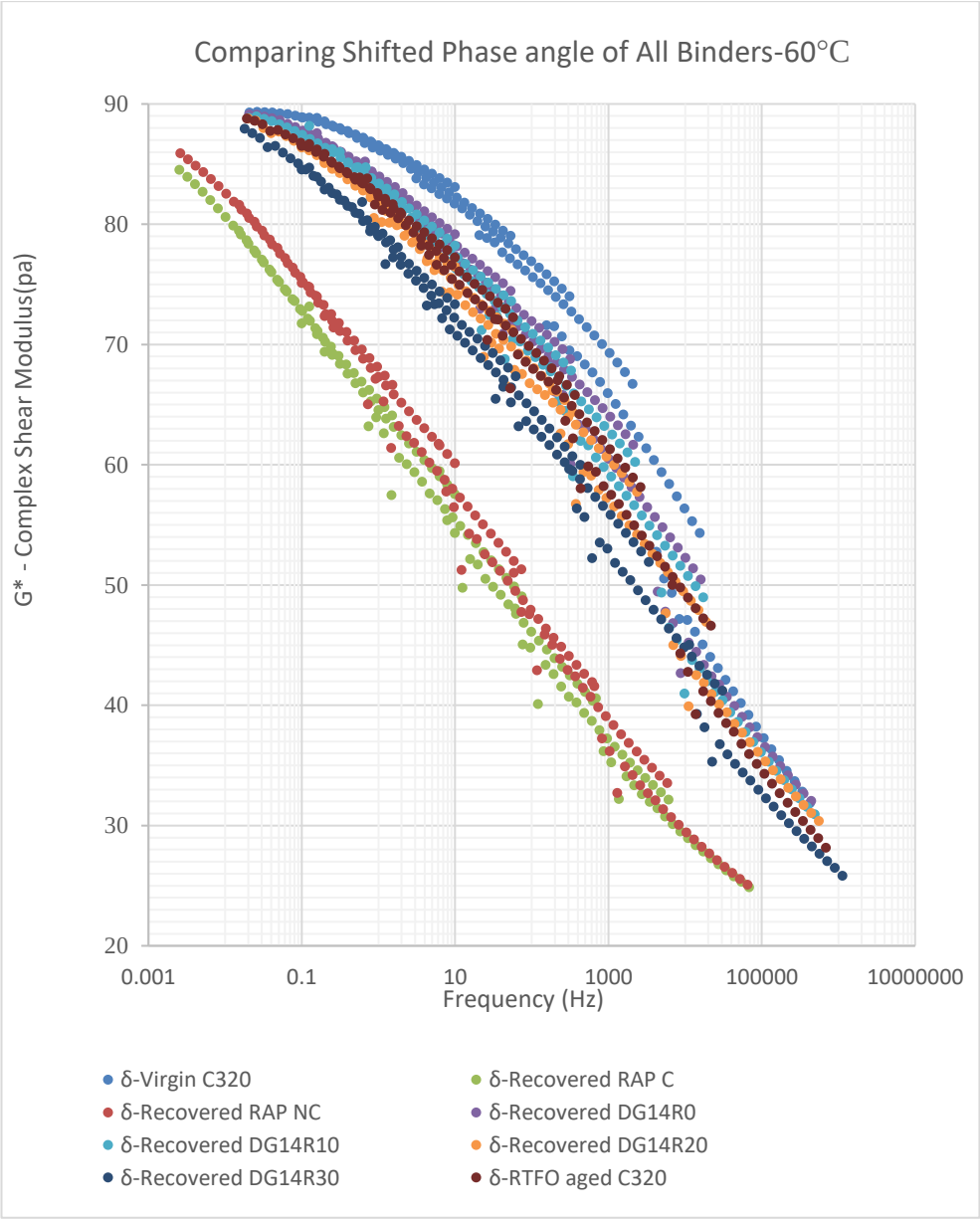

Figure 4-146 Shifted phase angle of all binders at 60 °C reference temperature versus reduced frequency

As Figure 4-145 shows, at low frequencies the complex modulus of the binders becomes close to each other at both ends of the frequency range and in between they are more distinguishable.

As expected, the virgin binder had the lowest complex modulus over the shown range of frequencies, while the recovered binder from the control and DG14R10 mixture had almost the same values of complex modulus over these ranges of frequencies, i.e., 10% RAP in the mixture had no effect on the complex modulus of the binder. Recovered binder from DG14R20 had a higher complex modulus than previously mentioned binders, while the RTFO

aged binder had very similar but slightly higher values than DG14R20 did. This demonstrates that the RTFO aging binder had a similar effect on the binder as the 20% inclusion of RAP in the present study. The recovered binder from DG14R30 mixture had a considerable higher complex modulus than all previously mentioned binders and is the last one to become close to the other recovered binders at high frequencies.

Moreover, the recovered RAP binders had higher complex modulus than the rest of the binders at all frequencies studied. However, at normal frequencies (lower than 1000 Hz) the conditioned RAP showed slightly higher complex modulus than the unconditioned recovered RAP. Furthermore, at higher frequencies than 1000 Hz, this order was changed and the conditioned RAP binder showed less complex modulus than the unconditioned recovered RAP binder.

According to Figure 4-146, the higher the content of aged binder, the lower the shifted phase lag observed, i.e., the conditioned recovered RAP binder generally has the lowest phase angle that is followed by unconditioned recovered RAP. At the next level, the same trend by a huge gap was followed by the recovered DG14R30 and other binders. Finally, the virgin C320 binder showed the highest phase lag in the frequencies studied. The recovered RAP binders had a considerable distance to complete viscous behaviour (90 degrees phase angle) even at a low shifted frequency while this distance is less considerable with other binders. Figure 4-146 also showed that phase lag decreases with increasing loading frequency.

To compare the behaviour of the binders at a lower temperature (20 °C), the master curves of all the binders were constructed at 20 °C (Figure 4-147). The graph of each master curve and the shifted original data can be found in Appendix VIII.

The data regarding this graph is also shown in Table 4-18 for fine comparison, which is difficult using only the graph as it is a log-log graph. Moreover, the shifted phase angles of the binders are compared in Figure 4-148.

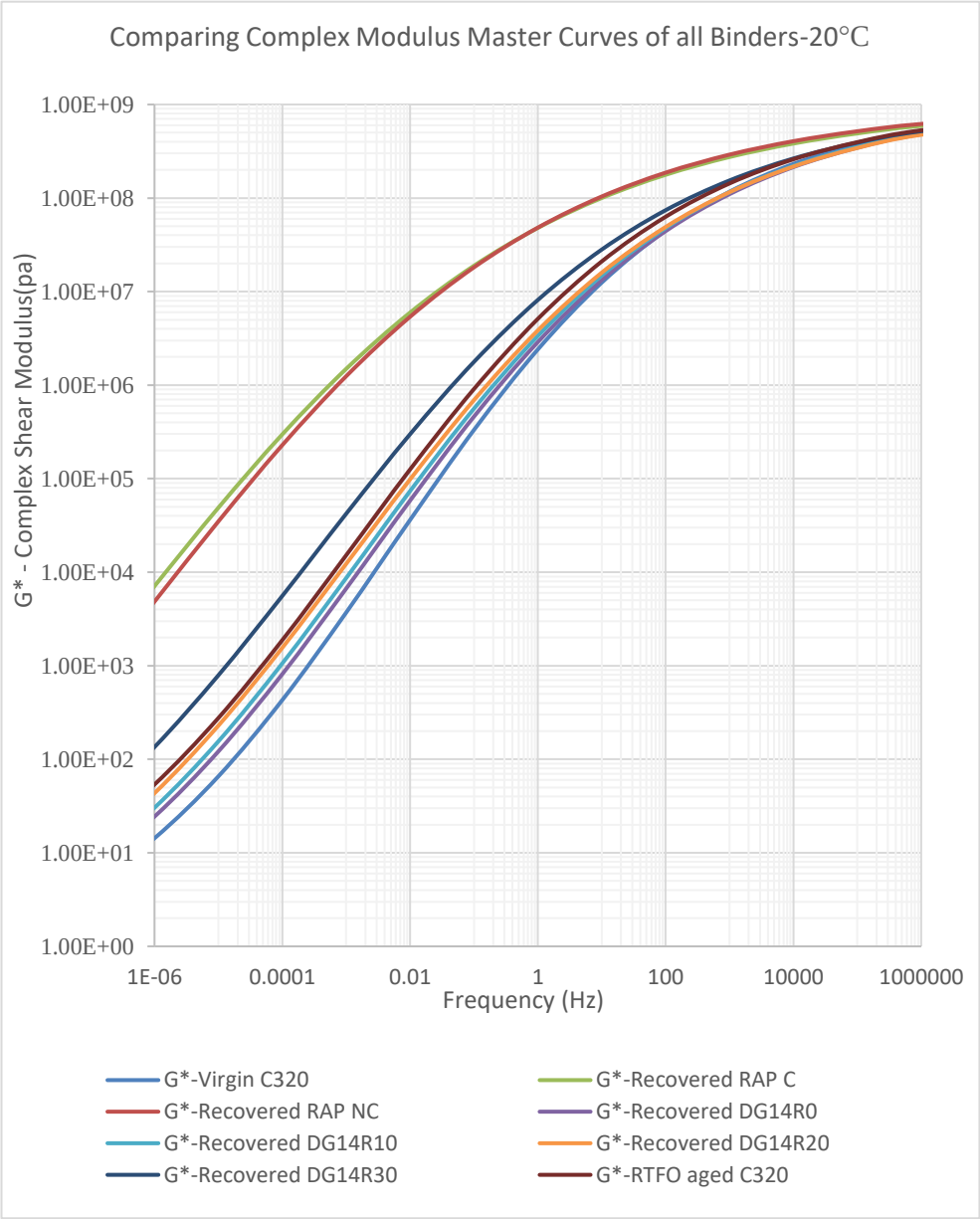

Figure 4-147 Comparing G master curves of all binders at 20 °C versus reduced frequency*

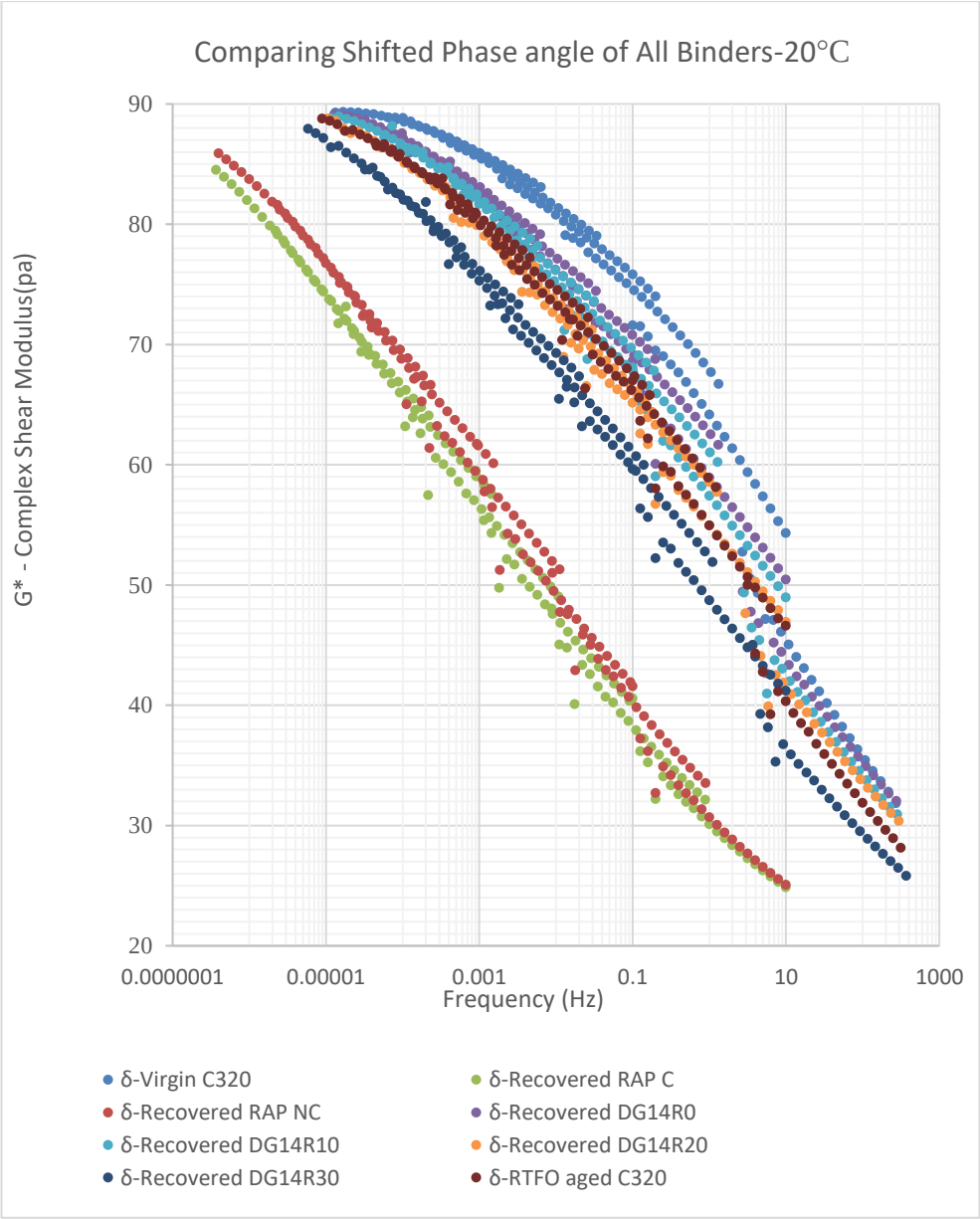

Figure 4-148 Shifted phase angle of all binders at 20 °C reference temperature versus reduced frequency

Table 4-18 Comparing G master curve details of all binders at 20 °C at different reduced frequencies*

Frequency (Hz)	G*-Virgin C320(MPa)	G*-Recovered RAP-C(MPa)	G*-Recovered RAP NC(MPa)	G*-Recovered DG14R0(MPa)	G*-Recovered DG14R10(MPa)	G*-Recovered DG14R20(MPa)	G*-Recovered DG14R30(MPa)	G*-RTFO aged(MPa)
1.00E+09	8.24E+08	8.10E+08	8.34E+08	7.94E+08	7.94E+08	7.82E+08	8.00E+08	8.21E+08
1.00E+08	7.47E+08	7.51E+08	7.78E+08	7.12E+08	7.13E+08	7.00E+08	7.26E+08	7.47E+08
1.00E+06	5.16E+08	5.91E+08	6.20E+08	4.81E+08	4.86E+08	4.75E+08	5.18E+08	5.31E+08
1.00E+05	3.73E+08	4.90E+08	5.18E+08	3.45E+08	3.50E+08	3.43E+08	3.92E+08	3.96E+08
1.00E+04	2.31E+08	3.82E+08	4.05E+08	2.14E+08	2.20E+08	2.17E+08	2.65E+08	2.60E+08
1.00E+03	1.17E+08	2.75E+08	2.91E+08	1.10E+08	1.15E+08	1.15E+08	1.54E+08	1.43E+08
1.00E+02	4.50E+07	1.77E+08	1.87E+08	4.43E+07	4.77E+07	4.91E+07	7.41E+07	6.30E+07
1.00E+01	1.25E+07	1.00E+08	1.04E+08	1.33E+07	1.48E+07	1.59E+07	2.81E+07	2.10E+07
1.00E+00	2.41E+06	4.79E+07	4.83E+07	2.89E+06	3.36E+06	3.84E+06	8.13E+06	5.11E+06
1.00E-01	3.32E+05	1.89E+07	1.82E+07	4.61E+05	5.60E+05	6.91E+05	1.77E+06	9.09E+05
1.00E-02	3.62E+04	5.97E+06	5.38E+06	5.83E+04	7.37E+04	9.82E+04	2.99E+05	1.25E+05
1.00E-03	3.70E+03	1.49E+06	1.24E+06	6.68E+03	8.65E+03	1.23E+04	4.21E+04	1.52E+04
1.00E-04	4.30E+02	2.97E+05	2.28E+05	8.13E+02	1.06E+03	1.56E+03	5.58E+03	1.88E+03
1.00E-05	6.57E+01	4.90E+04	3.50E+04	1.21E+02	1.56E+02	2.29E+02	7.91E+02	2.76E+02
1.00E-06	1.43E+01	7.09E+03	4.85E+03	2.44E+01	3.03E+01	4.34E+01	1.35E+02	5.37E+01
1.00E-07	4.45E+00	9.82E+02	6.72E+02	6.76E+00	8.12E+00	1.10E+01	2.98E+01	1.44E+01
1.00E-08	1.89E+00	1.43E+02	1.03E+02	2.54E+00	2.94E+00	3.78E+00	8.75E+00	5.22E+00

As Figure 4-147 shows, the master curve of the binders at 20 °C is very similar to the master curves at 60 °C but shifted to the left (lower frequencies). Therefore, the trends and order of the complex modulus of different binders are the same as explained before regarding Figure 4-145, e.g. the recovered RAP binders had the highest complex modulus while the virgin C320 binder had the lowest one.

Moreover, the complex modulus curves of the RAP binders cross each other at lower frequencies than the master curves at 60 °C, i.e., the recovered RAP binders have an intersection at a point between 0.1 and 1 Hz. This change of order is not hugely effective as the graphs are very close to each other anyway.

Regarding the shifted phase angle at 20 °C as Figure 4-148 shows, a similar trend in Figure 4-146 for shifted phase angle at 60 °C can be observed because these curves are almost identical, merely shifted to the left (lower

frequencies). Therefore, the higher the content of the aged binder, the lower the shifted phase lag observed. Figure 4-148 also shows that, by increasing the loading frequency, the behaviour of the binder becomes more elastic.

The details of parameters to construct the master curves in this section can be found in Table 4-19.

Table 4-19 Master curve construction details for all the binders at 20 and 60 °C reference temperatures

Binder	Reference Temperature (°C)	δ	β	γ	α	C	SSE
Virgin Binder	60	-0.5457	0.3586	-0.4168	9.5457	7,800.90	5.0321E-02
Recovered RAP	60	-2.1067	-0.8153	-0.3097	11.1067	9,374.94	2.9086E-03
Recovered RAP	60	-1.6085	-0.7088	-0.3263	10.6085	9,322.21	3.8870E-03
Recovered DG14R0	60	-0.6393	0.2284	-0.3919	9.6393	7,829.10	3.4706E-02
Recovered DG14R10	60	-0.6389	0.1934	-0.3881	9.6389	7,908.14	3.0198E-02
Recovered DG14R20	60	-0.6563	0.1381	-0.3773	9.6563	7,999.83	2.6255E-02
Recovered DG14R30	60	-0.5864	0.0046	-0.3675	9.5864	8,519.81	1.5174E-02
RTFO	60	-0.3672	0.1914	-0.3951	9.3672	8,152.51	2.7008E-02
Virgin Binder	20	-0.5451	-0.9727	-0.4169	9.5451	7,800.70	5.0321E-02
Recovered RAP	20	-2.1091	-2.0043	-0.3097	11.1091	9,374.00	2.9086E-03
Recovered RAP	20	-1.6063	-1.9542	-0.3264	10.6063	9,320.94	3.8870E-03
Recovered DG14R0	20	-0.6390	-1.0279	-0.3920	9.6390	7,828.78	3.4706E-02
Recovered DG14R10	20	-0.6384	-1.0631	-0.3881	9.6384	7,907.73	3.0198E-02
Recovered DG14R20	20	-0.6563	-1.0979	-0.3774	9.6563	7,999.58	2.6255E-02
Recovered DG14R30	20	-0.5852	-1.2773	-0.3676	9.5852	8,519.37	1.5174E-02
RTFO	20	-0.3669	-1.1273	-0.3951	9.3669	8,152.44	2.7008E-02

4.3.1.4 Superpave grading of binders

Two samples per binder were collected and these samples were tested according to the method explained in 3.3.4.4.2.1 for both assumptions of

being aged in RTFO and being virgin. The results of the tests are presented in Table 4-20. The results for each sample can be found in Appendix XI.

Table 4-20 Critical high-temperature test results for two different scenarios

Binder	Temperature of Scenario 1 (G*/Sin(δ)=1kpa)	Temperature of Scenario 2 (G*/Sin(δ)=2.2kpa)
RAP conditioned	106.6	99.75
RAP unconditioned	103.95	97.35
C320	71.2	64.43
RTFO	79.3	72.8
Recovered D14R10	76.6	70
Recovered D14R20	79.2	72.7
Recovered D14R30	84.6	77.9
Recovered DG14R0	75.25	69.05

To interpret the results and determine the high temperatures, in the present study the recovered binders from the asphalt mixtures were collected from the conditioned mixtures because these present better the binder in the asphalt samples being tested. However, as these binders were conditioned, their temperature in scenario 2 can be interpreted as their high temperature. This assumption is similar to the assumption in (Bonaquist, 2008) that assumes the conditioning of the mixture in the oven has a similar effect on the binder as aging the binder in RTFO oven does. For the recovered RAP, a minimum of two temperatures (the temperature taken from the test on unconditioned RAP in scenario 1 and the temperature taken from the test on conditioned RAP in scenario 2 were considered. For the virgin binder, the minimum temperature when virgin binder treated in scenario 1 and the temperature which RTFO aged virgin binder treated in scenario 2, can be used. For the virgin binder, there is another option that is to use recovered binder from the conditioned mixture instead of the RTFO aged binder. The results of the high temperatures based on assumptions explained in this paragraph are illustrated in Table 4-21.

Table 4-21 Critical high-temperature results

Source	Superpave High Temperature (°C)
RAP	99.75
C320	71.2 (69.05 if recovered from DG14R0 is considered as RTFO)
Recovered DG14R10	70
Recovered DG14R20	72.7
Recovered DG14R30	77.9

Based on the temperatures in Table 4-21, it can be observed that adding 10% RAP does not affect the temperature considerably and the temperature was still close to the temperature of the C320 binder. Similarly, having 20% RAP in the mixture changed the temperature but not significantly. Assuming that one grade difference in Superpave methodology is 6 °C, even adding 20 % RAP does not change the grade of virgin binder. However, adding further RAP changed the temperature more effectively (greater than 6 °C), which implies that the grading of the binder has changed. Therefore, to maintain the binder in its designated grade, a softer virgin binder might be required to be added to soften the blend. These findings are compatible with the changes that some state transportation services made to raise the level of the RAP to 20 or 25% that can be used without changing the binder grade (Copeland, 2011).

4.3.1.5 Binders grading based on complex viscosity at 60 °C

To grade the binders based on complex viscosity, the approach as explained in 3.3.4.4.2.2 was followed. Although in this study the strain level in the majority of cases was considered to be 1%, it is still correct to use the same measurements because the binders are in their linear region and are not sensitive to the strain level as explained in section 3.3.4.4.3.2. Moreover, in the present study, the tests were performed using a frequency sweep sequence in the DSR machine and the frequencies studies were between 0.1 and 10 Hz with 10 intervals in the logarithmic scale. Therefore, there is no measurement that was performed exactly on 1 rad/s (0.159155 Hz). The closest frequencies to 1 rad/s are 0.1585 Hz (0.995 rad/s) and 0.1995 Hz (1.253 rad/s). Therefore, the viscosities of binders were interpolated for the exact 1 rad/s frequency using the nearest frequencies. After averaging the results of samples, the obtained viscosities from the experiment and their calculated log values are presented in Table 4-22.

Table 4-22 Complex viscosity results on all binders at 60 °C and 1 rad/s loading frequency

Source of Binder	Measure viscosity (Pa.s)	Log Viscosity (Log Pa.s)
DG14R0	784.778	2.89
DG14R10	903.074	2.95
DG14R20	1298.548	3.11
DG14R30	3036.601	3.48
RTFO aged virgin binder	1389.383	3.14
Conditioned RAP	90605.412	4.95

According to Table 2-6, the recovered binder from DG14R0 is graded as C320 binder. However, the DG14R10 can be graded as both C320 and C600 binder. The binder recovered from DG14R20 is graded as C600 binder while the binder sourced from DG14R30 mixture is stiffer even than C600 binder.

Therefore, it can be concluded that 10% RAP did not change the binder grading, while having 20% RAP stiffened the binder by one grade.

4.3.2 Penetration test results

The penetration test was performed three times on prepared samples from each source according to the method explained in section 3.3.4.3. The average results are shown in Table 4-23 and Figure 4-149. The results for each sample can be found in Appendix XII.

Table 4-23 Results of penetration test for all the binders (100 g, 5 s)

Source	Penetration Number
RAP conditioned	4.6
RAP unconditioned	5.3
C320	57
RTFO	29
Recovered from DG14R10	39
Recovered from DG14R20	31.6
Recovered from DG14R30	23
Recovered from DG14R0	35.3

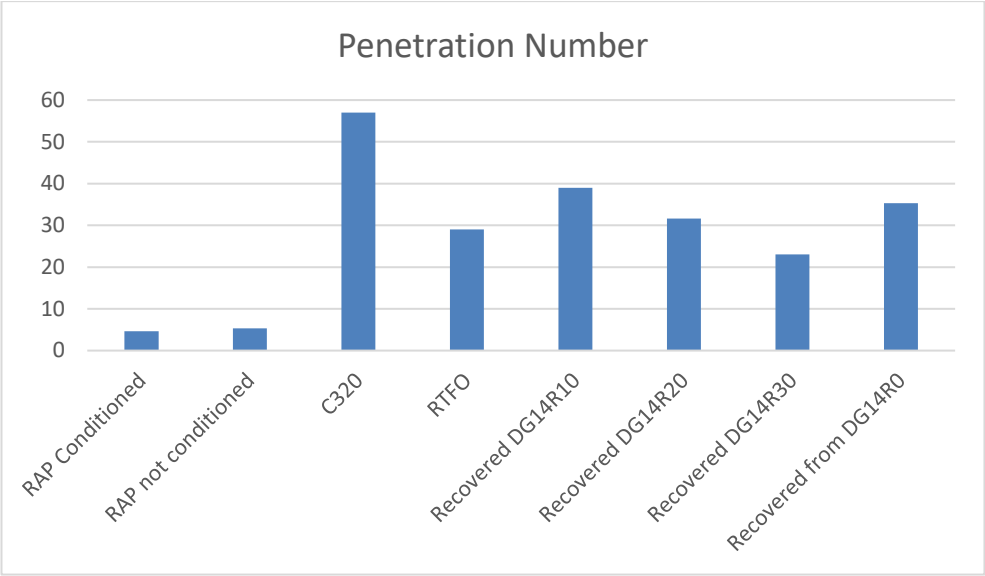

Figure 4-149Comparison of results of penetration test for all binders (100 g, 5 s)

Regarding the penetration number of the binders provided in Table 4-23, it can be seen that there is only a small fraction difference between conditioned and unconditioned RAP binder. Both of these binders are very stiff, so, their penetration numbers are very small. In contrast, the C320 is the softest binder in the present study and has the highest penetration number, which is greater than 10 times that of the RAP binders. According to the recovered binders from asphalt mixtures, the greater the percentage of RAP in the mixture, the lower the penetration number is. Another important feature is that the penetration number of the RTFO aged virgin binder is lower than the recovered conditioned virgin binder from DG14R0 as well as the recovered DG14R10 and DG14R20. Therefore, the binder from RTFO was only softer than the 100% RAP and the mixture with 30% RAP.

4.4 Binder RTFO aging versus mixture oven conditioning

To simulate the short aging that occurs after mixing of the asphalt mixture until the mixture is laid on the pavement, the mixture was retained in an oven for a specific time at a specific temperature after the mixing process. There is a common assumption that the RTFO aging binder has a similar effect on the binder as conditioning the mixture in the oven after mixing procedure does (Bonaquist, 2008).

In this section, this assumption is evaluated to determine to what extent this is correct. To do so, the results of the penetration test (Figure 4-150) and master curve of complex modulus tests at 60 °C (Figure 4-151) of the virgin, RTFO aged binder and recovered conditioned C320 binder forming the mixture were compared to each other.

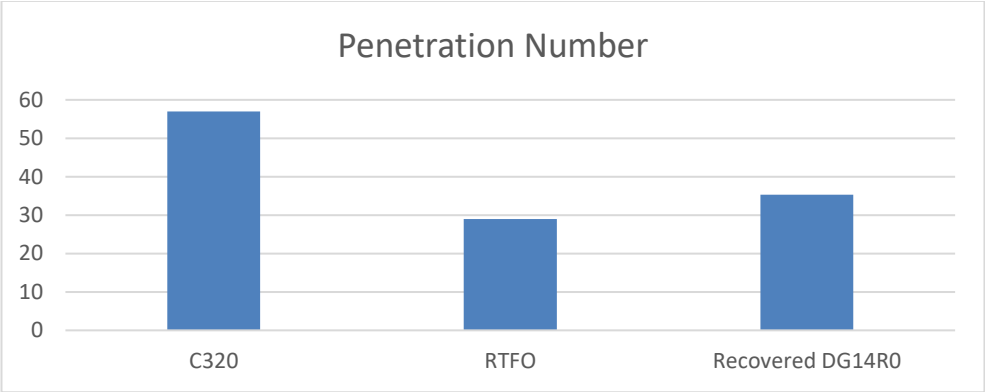

Figure 4-150 Effect of RTFO aging and oven conditioning of mixture on the penetration number of C320 binder

From Figure 4-150, it is obvious that although conditioning the mixture in the oven aged the binder significantly and reduced its penetration number from 57 to 35.3 units, its penetration number is still considerably higher than the results of the RTFO aged binder at 29 units.

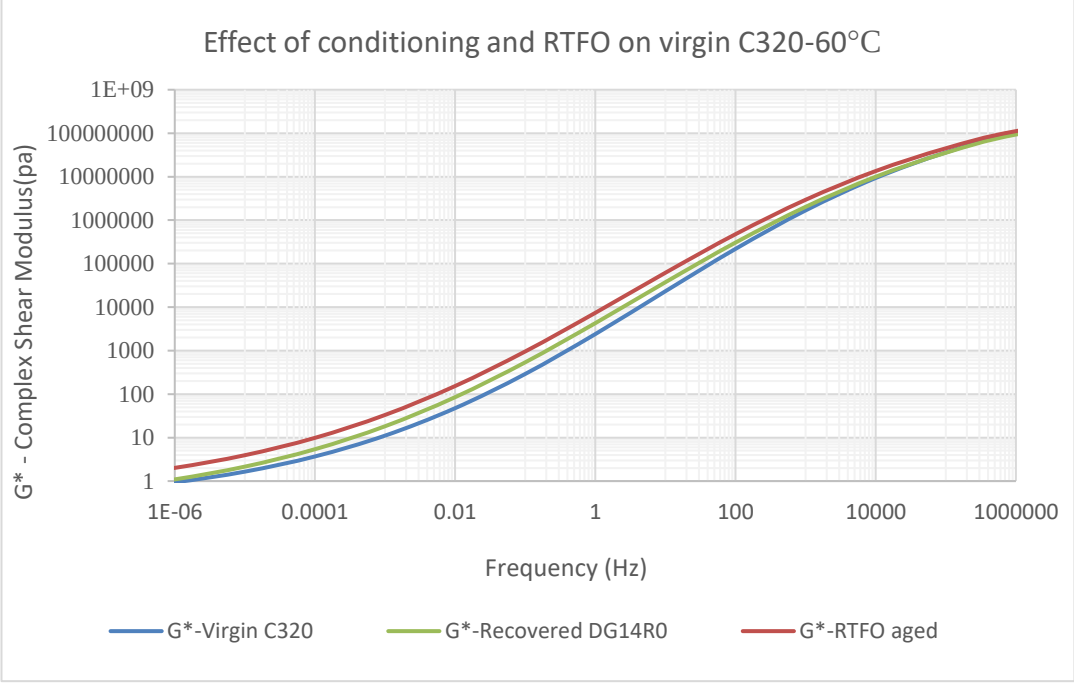

Figure 4-151 Effect of RTFO aging and oven conditioning of mixture on the G master curve of C320 binder at 60 °C reference temperature*

As Figure 4-151 shows, although the recovered conditioned binder from DG14R0 mixture had a significantly higher complex modulus than the virgin C320 binder for the majority of frequencies, in very low or very high frequencies its complex modulus gets close to being the same as the virgin binder. However, the RTFO aged binder had a substantially higher complex modulus than the recovered conditioned binder from the mixture and maintained its distance for almost all over the frequency spectrum except at the very end.

Based on these results it can be concluded that RTFO aging is harsher than conditioning the mixture in the oven.

4.5 The evaluation of binders blend properties prediction methods

As explained in section 2.2.3, there are different approaches for predicting the grade/properties of the binder in an asphalt mixture containing RAP material. In this section, the different methods utilised to estimate the grade/properties of a blend of RAP and virgin binder are evaluated by comparing their estimations to actual values measured from the recovered binders from mixtures. These approaches include blending chart for critical hot temperature, penetration blending equation and Chevron equation. Moreover, conditioning of the RAP and virgin binders to achieve better results are discussed.

To estimate the grade/property of the binder in the mixture based on the properties of the RAP and virgin binder, the ratio of the RAP and virgin binder to the total binder should be known. The definition of the RAP content is the ratio of the weight of the RAP material to the total weight of the mixture; therefore, the ratio of the RAP binder to the total binder is different than the RAP content. The ratio of RAP and virgin binder also depends on the binder content of the RAP and the whole mixture. So, the ratio of the RAP binder contribution to the total binder in the studied mixtures is presented in Table 4-24.

Table 4-24 Participation of RAP and virgin binder in the total mixture and binder

	% of binder by weight of total mixture		% RAP binder contribution in total binder
Mixture	From virgin C320	From RAP	
DG14R0	4.7	0	0
DG14R10	4.29	0.41	8.72
DG14R20	3.88	0.82	17.45
DG14R30	3.47	1.23	26.17

4.5.1 Critical hot temperature blending chart

In this section, the actual critical hot temperature of the recovered binders with 10, 20 and 30 % RAP are compared with their estimated critical high temperature using the blending chart of the critical high temperature of RAP binder and virgin binder. The actual reading for the critical high temperature of all the studied binders in this section is presented in Table 4-20 in section 4.5.1.

To draw the blending chart, two different scenarios were considered for the data of the RAP and virgin binders conditioning level. First, as the definition in the Superpave states, the conditioning is considered to be RTFO aging. Second, the conditioning is considered to be conditioning of the binder in the mixture. Therefore, the binder needs to be recovered after conditioning the mixture in the oven. The data of the RTFO aged binder is not available, so the blending chart was drawn considering only the high temperature of the unconditioned RAP for the first scenario. The blending charts for these scenarios and the actual data are shown in Figure 4-152. In addition, the calculated and measured values for the same points are shown in Table 4-25.

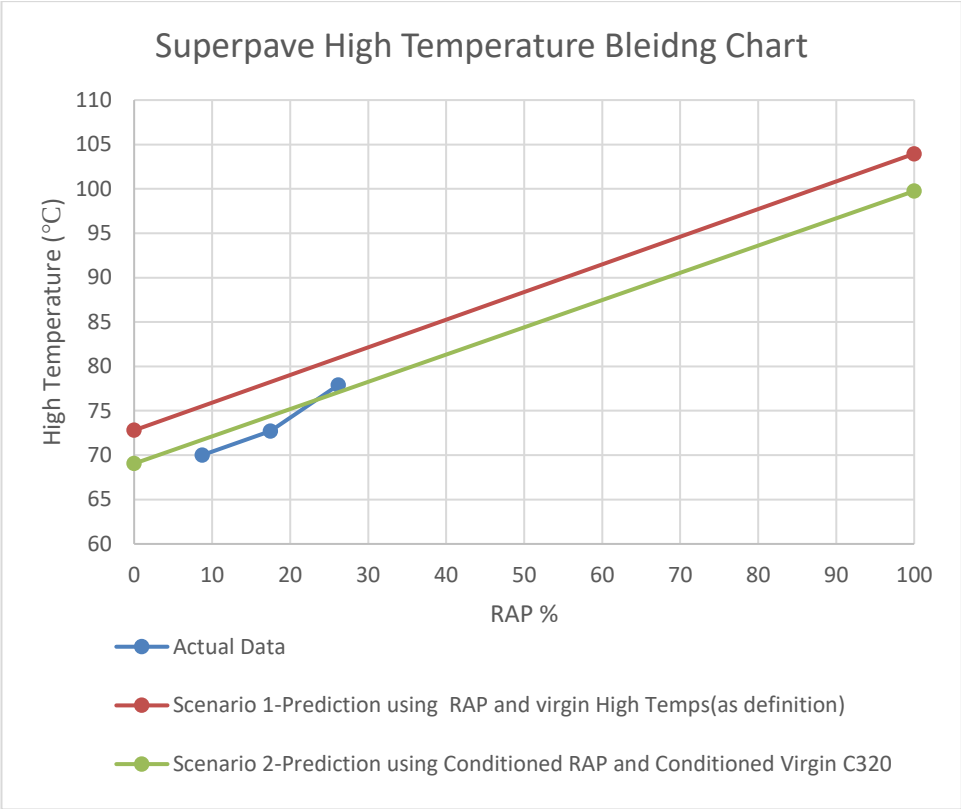

Figure 4-152 Critical high temperature blending chart in two different scenarios for input parameters

Table 4-25 The accuracy of critical high temperature blending chart in two different scenarios for input parameters

		Scenario 1		Scenario 2	
Binder	Measured (°C)	Estimated (°C)	Error (%)	Estimated (°C)	Error (%)
DG14R10	70	75.5	7.9	71.7	2.4
DG14R20	72.7	78.2	11.8	74.4	6.2
DG14R30	77.9	81	15.6	77	10

According to Figure 4-152, it can be concluded that using scenario two, i.e. the oven conditioned binder, leads to relatively accurate results in comparison to the method in scenario one, even though scenario one is recommended by (McDaniel et al., 2000) for using RTFO aged RAP for this purpose. Regarding Table 4-25, the estimation error increases with the increase of RAP content in both scenarios; however, for scenarios two it is equal or less than 10% in all situations while for the scenario one it was mostly over 10%. Even though the data of the RTFO aged RAP binder was not available in the present study, the result is not expected to change dramatically because, as Figure

4-152 shows, a minor change in the high temperature of the RAP in scenario one does not improve the accuracy of this method significantly.

The slopes of the blending chart in both scenarios were similar to the slope of the measured high temperature between binders recovered from DG14R10 and DG14R20. However, there was a sudden discrepancy for the binder recovered from the DG14R30 mixture.

The reason behind the discovery that scenario two was more precise in the present study might be the fact that conditioning in the RTFO oven was found to be harsher than conditioning in the oven.

4.5.2 Penetration blending equation evaluation

In this section, the penetration number of the binders recovered from DG14R10, DG14R20 and DG14R30 are estimated for different scenarios based on the penetration number of RAP and virgin binder and compared with the actual measured values. In the first scenario, the penetration number of virgin and RAP binder were measured when they were unconditioned, whereas in the second scenario, the recovered binders from the oven conditioned mixture were used to measure their penetration number. In the third scenario, the RTFO aged virgin binder and recovered binder from the oven conditioned RAP were examined. The recovered binder from the conditioned RAP was used in the third scenario because the RTFO aged binder for the RAP was not available. Figure 4-153 shows the estimated blend chart for different scenarios in addition to the actual data obtained from the experiment. In addition, the exact values of the measured and estimated penetration number and errors in different situations are presented in Table 4-26.

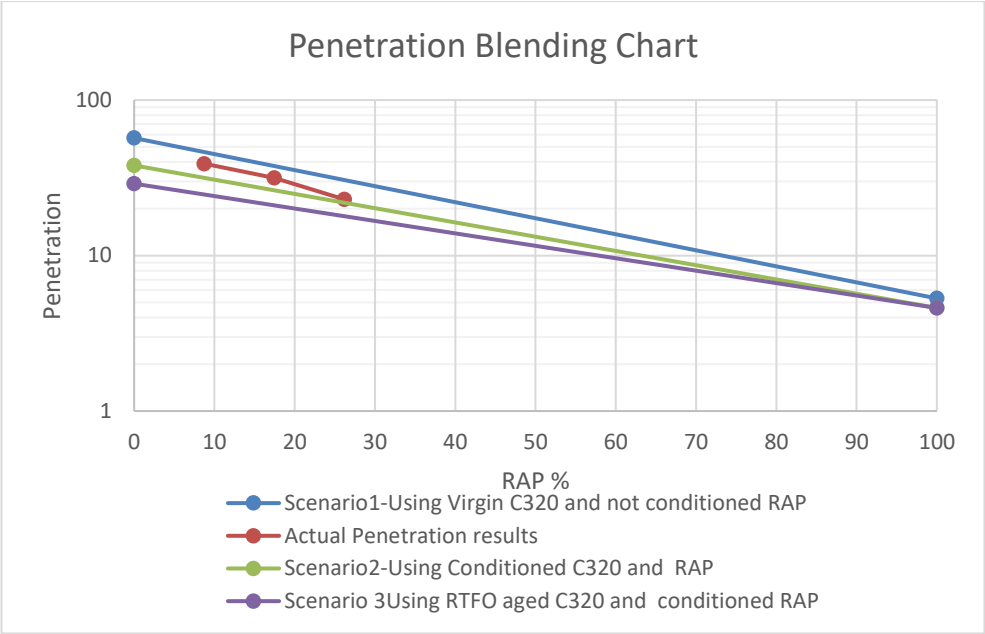

Figure 4-153 Binder blending chart based on penetration number equation for blended binders

Table 4-26 The accuracy of binder blending chart based on penetration number equation for blended binders

		Scenario 1		Scenario 2		Scenario 2	
Binder	Measured (Pu)	Estimated (Pu)	Error (%)	Estimated (Pu)	Error (%)	Estimated (Pu)	Error (%)
DG14R10	39	46.3	18.8	31.6	-18.9	24.7	-36.7
DG14R20	31.6	37.6	19.2	26.3	-16.8	21	-33.4
DG14R30	23	30.6	33.1	21.9	-4.9	17.9	-22.1

Based on Figure 4-153, it can be concluded that scenario two estimated the penetration number more accurately than the other scenarios and maintained the error under 20% for all the studied points. However, the first and third scenarios were not very accurate. Even if the RTFO aged RAP was used in scenario three, it would probably worsen the accuracy, as the RTFO aged RAP is expected to be stiffer than the oven conditioned RAP and, as seen in the figure, it increases the gap between the graph of the third scenario and the actual experimented data.

The slopes of the blending chart in all scenarios were similar to the slope of the measured penetration number between binders recovered from DG14R10 and DG14R20. However, there was a sudden discrepancy for the binder recovered from the DG14R30 mixture.

4.5.3 Chevron equation evaluation

As explained in section 2.2.3.3, the Chevron equation can be used to estimate the viscosity of the blend of RAP and virgin binder. This method has also been suggested in AGPT-T193 standard (Austroads, 2015b). Based on the AGPT-T193 standard, the complex viscosity of the binder is required to be measured according to AGPT-T192 standard (Austroads, 2015a) and then used to predict the complex viscosity of the blended binder. The complex viscosities of the binders are presented in section 4.3.1.5 and these are to be used for evaluation of the Chevron equation.

For estimation of the viscosity of the recovered binders from DG14R10, DG14R20 and DG14R30, two scenarios were considered for the level of aging of the RAP and virgin binder. In the first scenario, the recovered binders from the oven conditioned mixture were used to measure their complex viscosity. In the second scenario, the RTFO aged virgin binder and recovered binder from the oven conditioned RAP was used in the experiment. The recovered binder from conditioned RAP was used in the second scenario as the RTFO aged binder for the RAP was not available.

Figure 4-154 shows the estimated blend chart for the different scenarios as well as the actual data obtained from the experiment. In addition, the exact value of the measured and estimated complex viscosities and their error in the different scenarios are presented in Table 4-27.

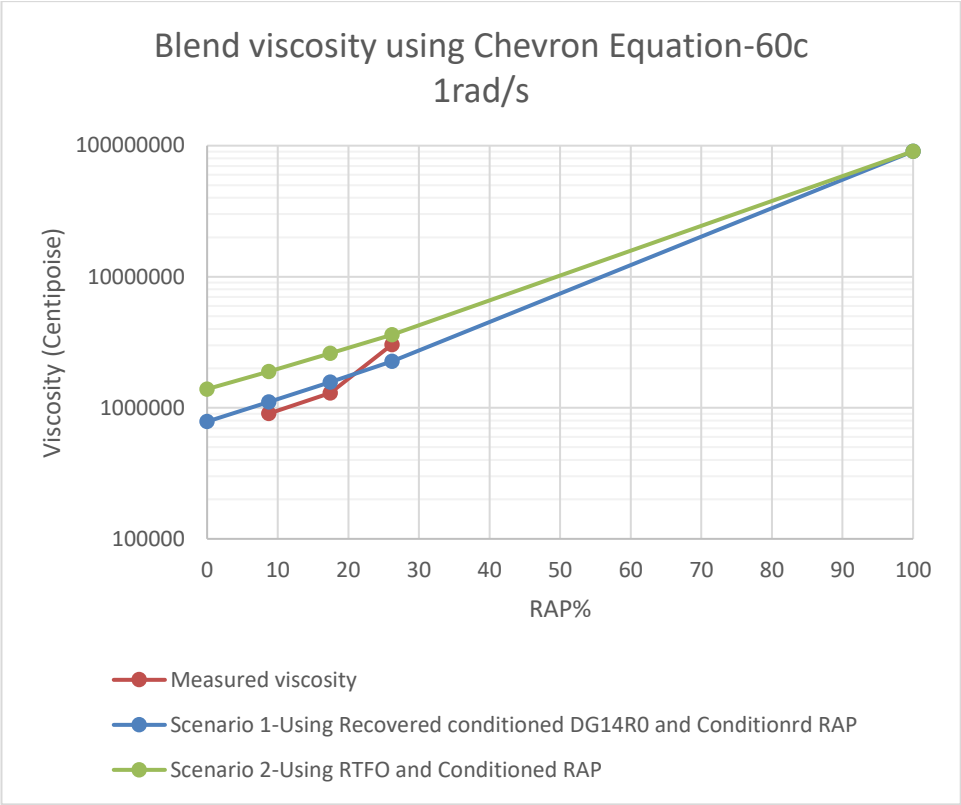

Figure 4-154 Blending chart based on Chevron equation for complex viscosity of blended binders at 60 °C and 1rad/s loading frequency

Table 4-27 The accuracy of blending chart based on Chevron equation for complex viscosity of blended binders at 60 °C and 1rad/s loading frequency

		Scenario 1		Scenario 2	
Binder	Measured (cP)	Estimated (cP)	Error (%)	Estimated (cP)	Error (%)
DG14R10	903074	1104521	22.3	1891336	109.4
DG14R20	1298548	1573325	21.1	2599317	100.2
DG14R20	3036601	2267714	-25.3	3605433	18.7

As Figure 4-154 and Table 4-27 illustrate, the first scenario predicts the actual viscosity better than the second scenario. Although the error of the first scenario is between 20 and 30%, the error of the second scenario is significantly higher, being greater than 100% at several points. The slope of the blending chart in scenario one is similar to the slope of the measured viscosity between binders recovered from DG14R10 and DG14R20. However, there was a sudden discrepancy for the binder recovered from the DG14R30 mixture.

Even though the RTFO aged RAP was used in scenario two, it would probably worsen the accuracy of this scenario, as the RTFO aged RAP is expected to be stiffer than the oven conditioned RAP and, as can be seen in the figure, it increases the gap between the graph of the second scenario blending chart and the actual experimental data.

An advantage of the Chevron equation is that it can be easily used at temperatures other than 60 °C, which has been suggested by (Austroads, 2015a) if the complex viscosity data is available at other temperatures. To illustrate this availability, the blending chart and actual data as well as to their exact value and error of experimental results are shown in Figure 4-155 and Table 4-28.

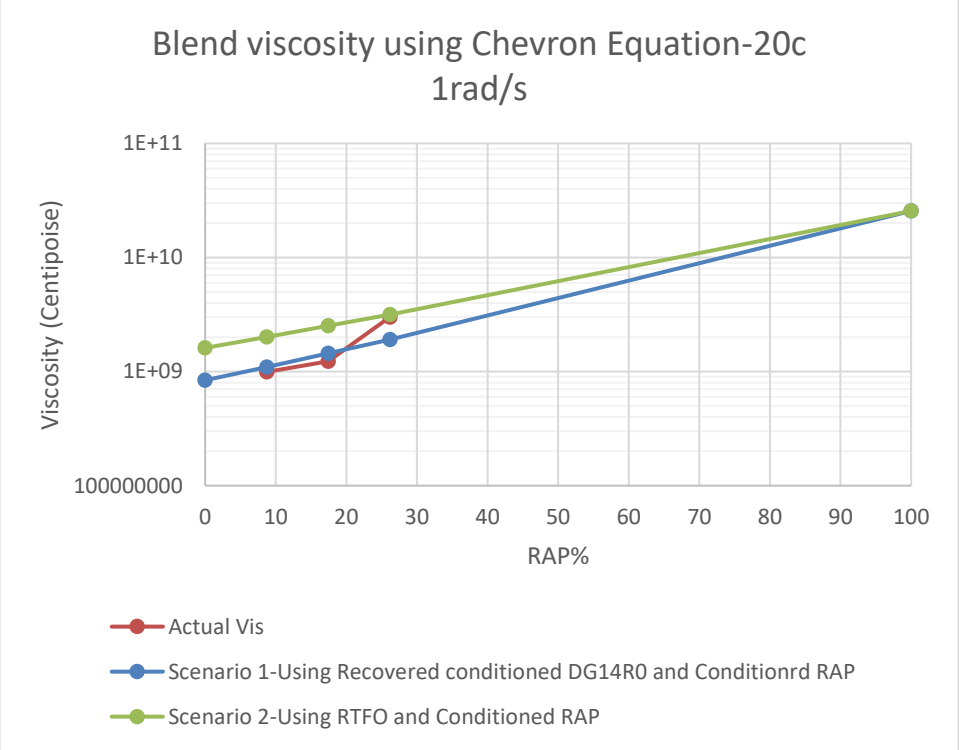

Figure 4-155 Blending chart based on Chevron equation for complex viscosity of blended binders at 20 °C and 1rad/s loading frequency

Table 4-28 The accuracy of blending chart based on Chevron equation for complex viscosity of blended binders at 20 °C and 1rad/s loading frequency

		Scenario 1		Scenario 2	
Binder	Measured (cP)	Estimated (cP)	Error (%)	Estimated (cP)	Error (%)
DG14R10	992701727	1097166663	10.5	2010670142	102.5
DG14R20	1230055875	1441742376	17.2	2517954184	104.7
DG14R20	3005650075	1904246228	-36.6	3163767057	5.3

It can be seen that at 20 °C, the accuracy of scenario one is improved significantly for the binders recovered from mixtures with 10 and 20% RAP, although it becomes less accurate for the binder recovered from the DG14R30 mixture. At this temperature, scenario two can predict the binder viscosity of the DG14R30 mixture with considerable accuracy while it has dramatic errors for other binders.

4.5.4 Comparison of blend properties prediction methods

In this section, the accuracy of the three blending binder properties prediction methods (i.e. critical hot temperature, penetration blending equation, and Chevron equation) are compared, with the level of error of these methods presented in Table 4-29. The conditioned RAP and conditioned virgin binder were used as input parameters for these methods to generate the data in this table as these parameters generated better results in general according to previous sections.

Table 4-29 Accuracy of investigated blending binder properties prediction methods

Binder	Critical hot temperature error (%)	Penetration equation error (%)	Chevron equation error (%)
DG14R10	2.4	-18.9	22.3
DG14R20	6.2	-16.8	21.1
DG14R30	10	-4.9	-25.3

It is obvious from the results presented in Table 4-29 that the critical hot temperature blending chart led to the least error percentage. Although the error level of the Chevron equation appears to be greater than the penetration equation, the Chevron equation predicts the viscosity while the penetration equation predicts the penetration number. Therefore, the values of errors cannot be compared directly. The penetration equation has a power relationship to the viscosity of the binder, e.g. an equation suggested by the Texas Department of Transportation (2014) is equation (4-1) below, which is for penetration numbers below 54:

$$\mu = \frac{1.559719\times10^{9}\times\ln\left(\frac{0.0275}{3.94\times10^{-6}\times P + 0.000075}\right)}{P^{2}} \qquad (4\text{-}1),$$

where, μ is the viscosity of poise and P is the penetration number. If the inputs and outputs of penetration equation are converted to viscosities using equation (4-1), the results and error levels of the same data points presented in Table 4-29 are as shown in Table 4-30.

Table 4-30 Accuracy of penetration equation based on viscosity of the binder

	Measured		Predicted		
Binder	Penetration number	Converted to viscosity (Pa.s)	Penetration number	Converted to viscosity (Pa.s)	Error based on viscosity values (%)
DG14R10	39	491163	31.6	769442	-56
DG14R20	31.6	769442	26.3	1135738	-47
DG14R30	23	1507309	21.9	1671154	-10

According to Table 4-30, it is obvious that the error levels of the penetration equation are much greater than the Chevron equation.

Consequently, it can be concluded that between the Chevron equation and penetration equation, the Chevron equation has the advantage not only because it produces more accurate results, but also because it is more practical and needs less amount of material to be recovered for the test. The critical hot temperature blending chart and Chevron equation are both based on the same data obtained from the DSR machine; therefore, both can be used in different situations based on a parameter of the blend required. In Australia, where the binders are classified based on their viscosity, the Chevron equation is recommended.

4.6 Mixture and binder performance correlation

In this section, the properties of the asphalt mixtures are compared with the parameters extracted from the binder properties. The mixture properties investigated in this section include complex modulus, rutting resistance and four-points bending fatigue life.

4.6.1 Complex modulus

The complex modulus master curves obtained from cylindrical samples using an AMPT machine were compared with master curves of the binders that are used in the asphalt mixtures. The master curves of the mixtures and binders are presented in Figure 4-156 and Figure 4-157. The temperature reference for all the master curves in this section is 20 °C.

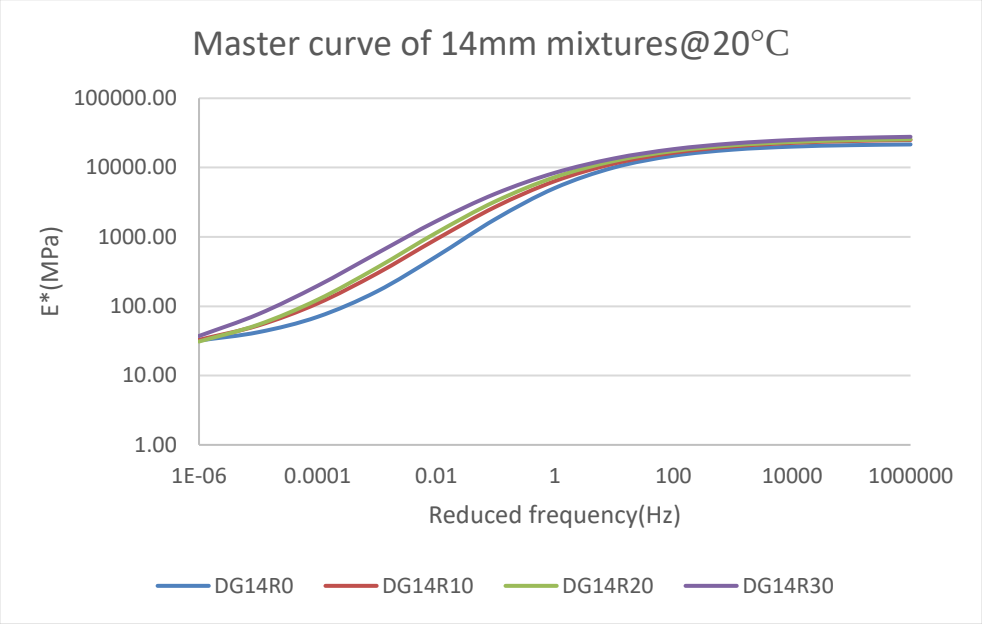

Figure 4-156 Dynamic modulus master curves of 14 mm mixtures at 20 °C reference temperature versus reduced frequency

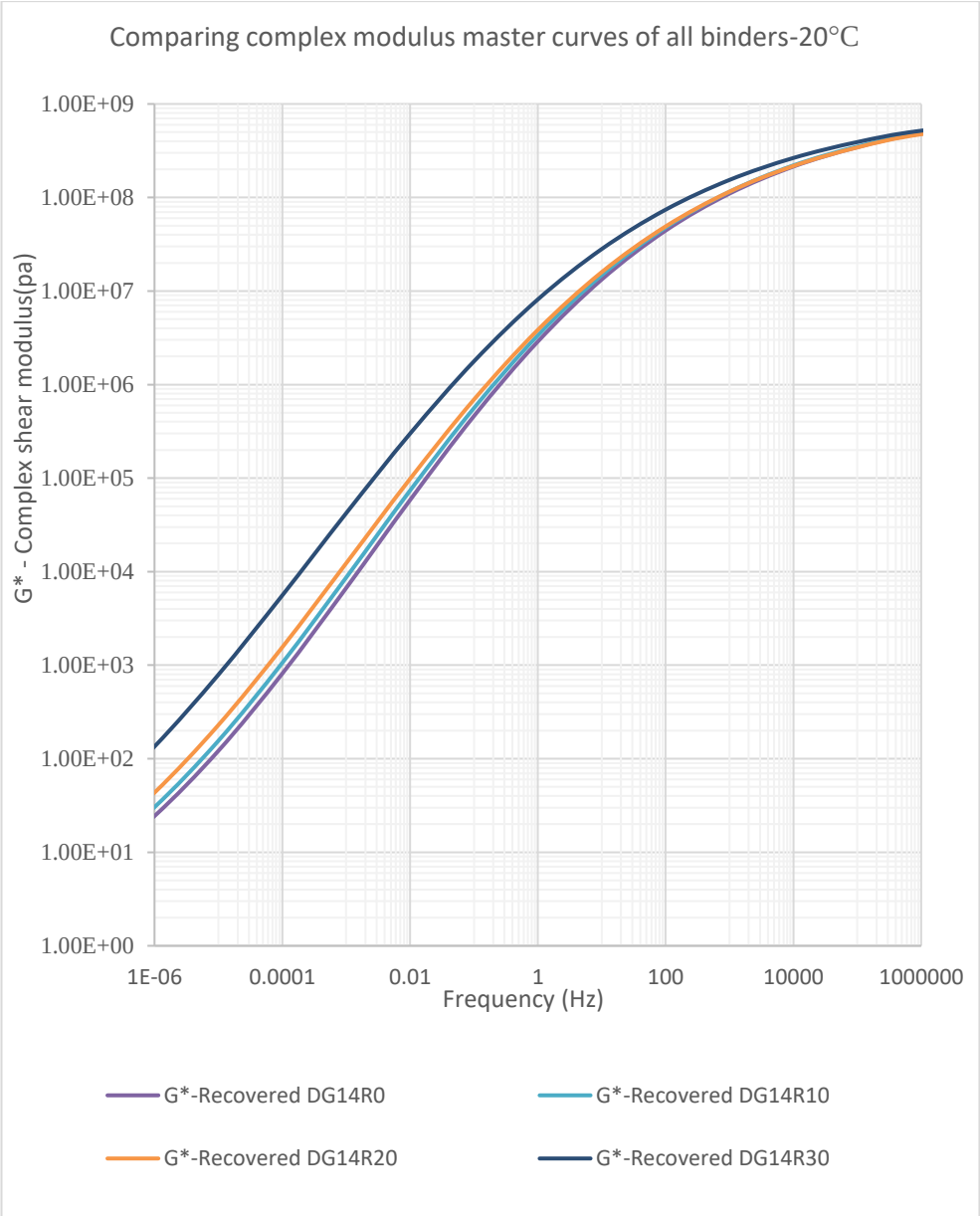

Figure 4-157 Complex modulus master curves of recovered binders from 14 mm mixtures at 20 °C reference temperature versus reduced frequency

By comparing both figures, it was concluded that the ranking of the complex modulus of the binders and asphalt mixtures had the same order owing to their RAP content. In both cases, the complex modulus of the control mixture had the lowest value.

The dynamic modulus of DG14R10 and DG14R20 mixtures were very close in complex modulus values while DG14R0 and DG14R30 had a considerable gap between themselves and the other two. However, in the binder complex modulus master curves, the values of recovered binders from DG14R0,

DG14R10 and DG14R20 were at the same level, while the recovered binder from DG14R30 was significant different to the other binders.

Therefore, there was a considerable increase in the complex modulus of both binder and asphalt mixtures in the 30% RAP mixture than in the other mixtures with less RAP content. However, the effect of 10% RAP in the mixture was more detectable in the performance of mixture than in the binder.

4.6.2 Rutting resistance

In this section, the effect of RAP on resistance of the mixture to rutting that is estimated by measuring the rutting depth under the wheel tracking device was compared with the rut factor of the binder, 1/(G*/sin(δ)) as introduced in section 2.2.3.1. This parameter obtained from the DSR test on the binders recovered from the same mixtures at 60 °C and frequency of 10 rad/S. The G*/sin(δ) has been suggested by (Prithvi S Kandhal & Foo, 1997) as an indicator of rutting sensitivity so that lower values show higher vulnerability of the binder for rutting failure.

Figure 4-158 and Figure 4-159 present the rut depth of the asphalt mixtures and 1/(G*/Sin(δ)) with respect to the RAP content, respectively.

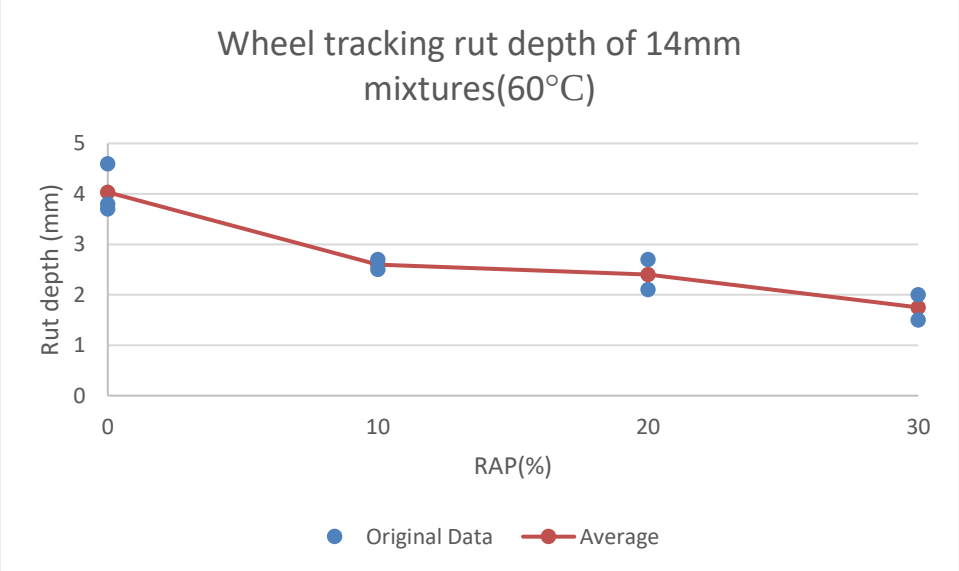

Figure 4-158 Rut depth of 14 mm mixtures at 60 °C versus RAP content

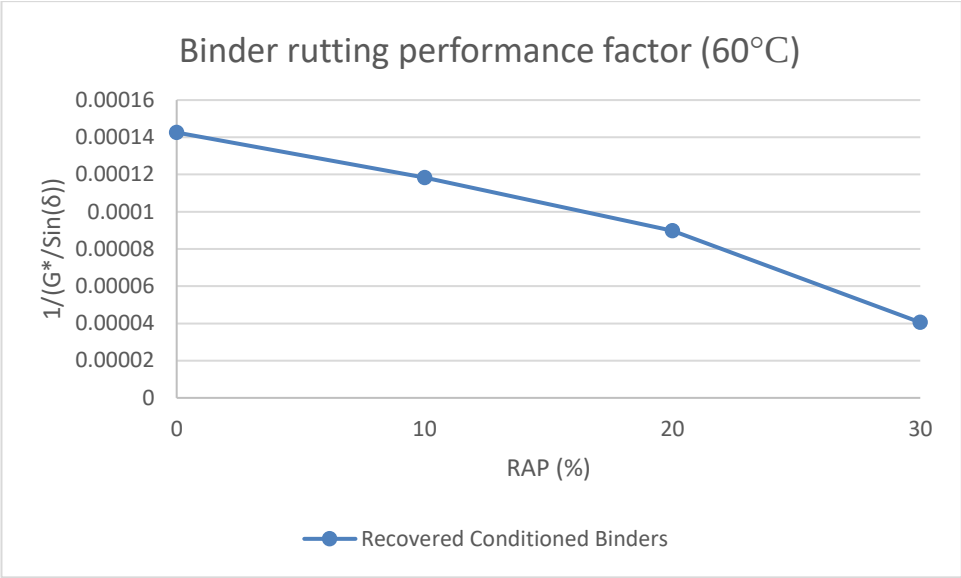

Figure 4-159 Binder rutting performance factor (1/(G/sin(δ))) for recovered binders from 14 mm mixtures at 60 °C against RAP content*

As these figures indicate the 1/(G*/sin(δ)) parameter predicted the decreasing trend of rut depth with respect to RAP content successfully. However, the mixtures' rutting depth did not change significantly between 10 and 20%, while the decreasing trend of the binders was consistent.

4.6.3 Four-points bending beam fatigue life test

In this section, three parameters will be checked (initial flexural stiffness, phase angle and number of cycles to halve the flexural stiffness) to determine how their trends can be predicted using several of the binder properties. The trend of changes in these parameters owing to RAP content was compared with the same trend of G*, phase angle and 1/(G*.Sin(δ)) parameters from the binder, which as explained in section 2.2.3.1 was suggested as an indicator of binders performance due to fatigue in Superpave method. All of these parameters were measured at 20 °C and loading frequency of 10 rad/s.

4.6.3.1 Initial flexural stiffness

The trend of changes of initial flexural stiffness owing to RAP content were compared with the same trend of G* from recovered binders from the same mixtures measured at 20 °C and loading frequency of 10 rad/s.

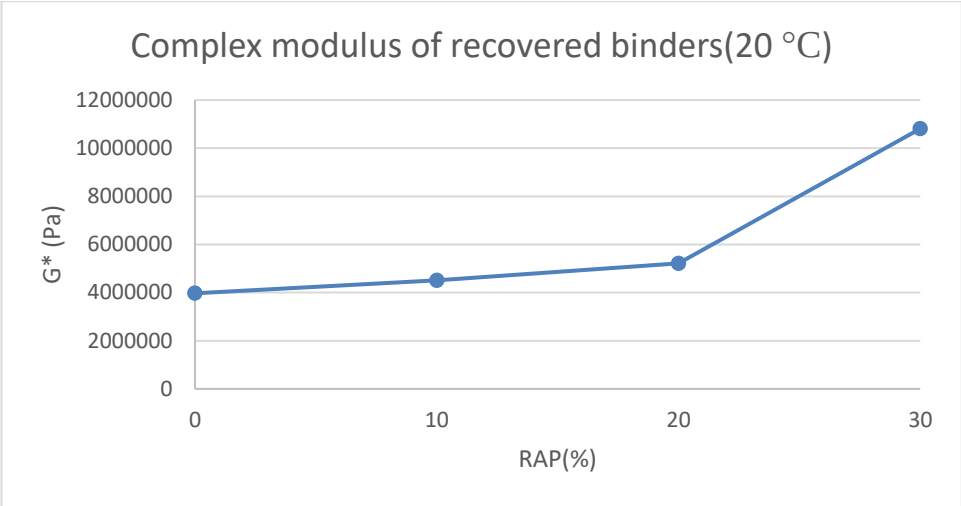

Figure 4-160 Complex modulus of recovered binders from 14 mm mixtures at 20 °C versus RAP content

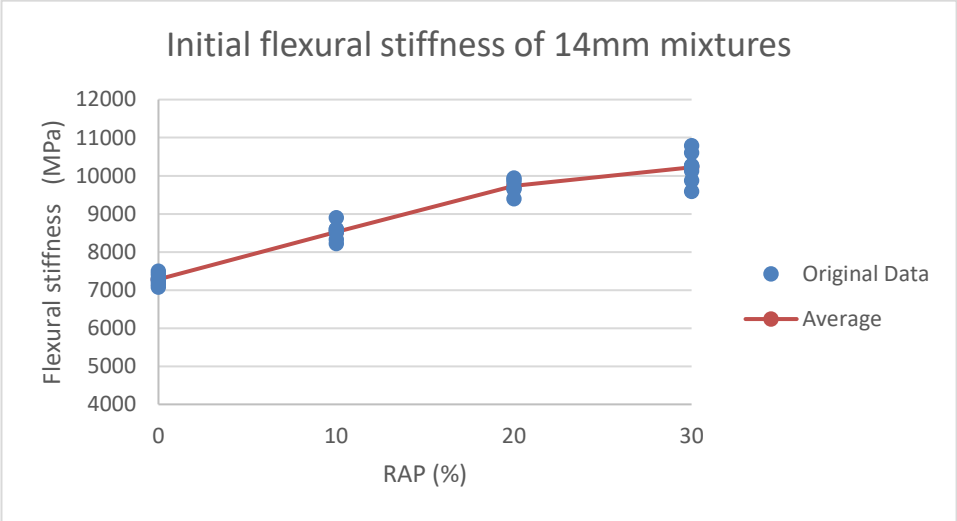

Figure 4-161 Initial flexural stiffness of 14 mm mixtures versus RAP content

Based on Figure 4-160 and Figure 4-161, the G* of the binders show an increasing trend as the initial flexural stiffness of the four-point bending beam samples. Surprisingly, the slope of changes in both figures was constant until 20% RAP. However, between 20 and 30 % RAP, in the G* graph of binders, there was a sudden increase in the slope while in the flexural stiffness graph, the slope decreased within the same range.

4.6.3.2 Initial phase angle

The trend of changes of initial phase angle owing to RAP content was compared with the same trend of phase angle from recovered binders from the same mixtures measured at 20 °C and loading frequency of 10 rad/s in Figure 4-162 and Figure 4-163, respectively

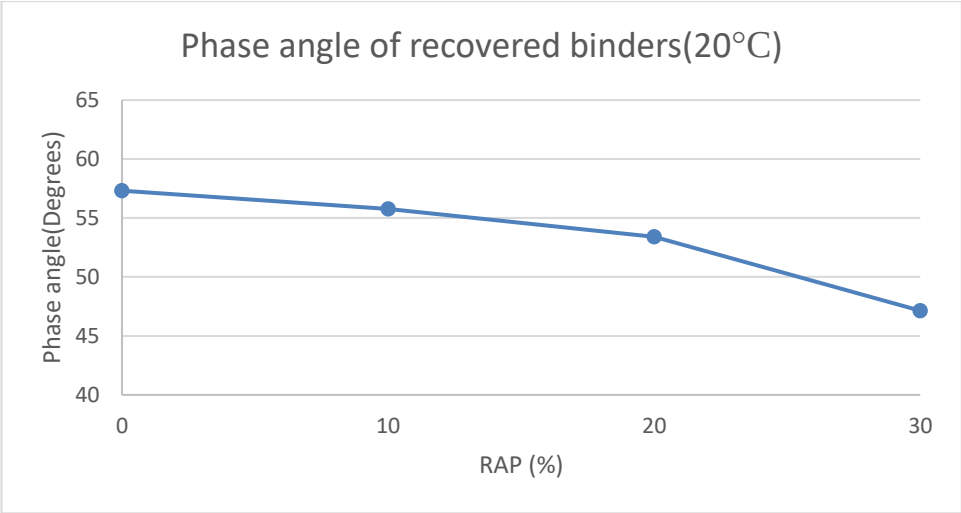

Figure 4-162 Phase angle of recovered binders from 14 mm mixtures at 20 °C versus RAP content

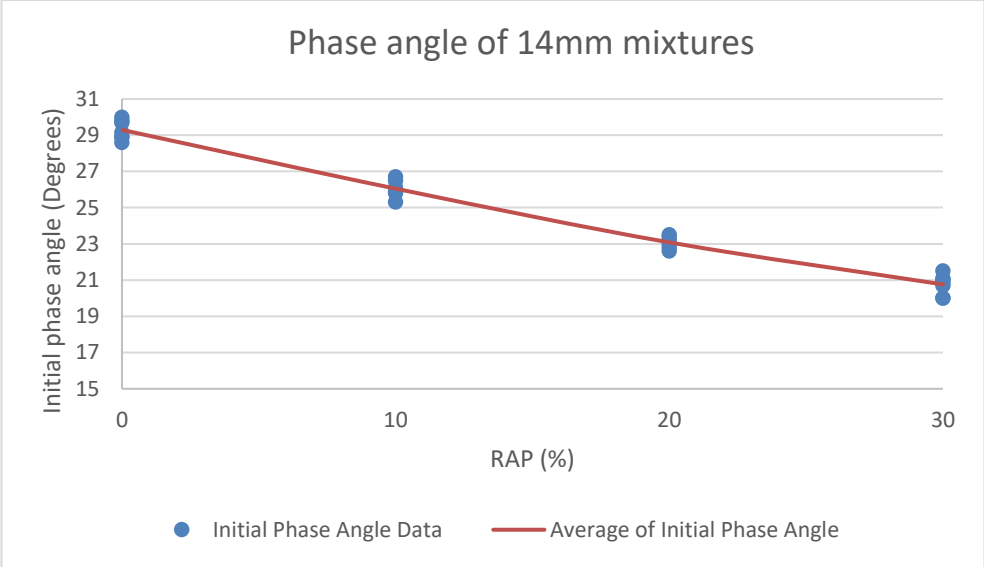

Figure 4-163 Initial phase angle of 14 mm mixtures versus RAP content

Measured phase angle from the recovered binders and four-point bending beam samples have a decreasing trend with respect to RAP percentage in the mixtures, although phase angles measured from the binders are much higher than phase angles from the four-point beam samples. One reason for this difference is the effect of aggregates on the phase angle, which makes the mixture more elastic than the binders.

Another important feature between these two figures is that the phase angle of the binders presented a sudden decrease after 20% RAP; however, such a decrease cannot be seen in the phase angle measured from the four-point bending beam samples.

4.6.3.3 Fatigue life

The trend of changes of number of cycles to halve the flexural stiffness owing to RAP content were compared with the same trend of 1/(G*.Sin(δ)) parameter from the recovered binders from the same mixtures measured at 20 °C and loading frequency of 10 rad/s in Figure 4-164 and Figure 4-165. The G*.sin(δ) was suggested by(Prithvi S Kandhal & Foo, 1997) as an indicator of fatigue life of an asphalt binder so that lower values reveal less vulnerability of binder under fatigue failure.

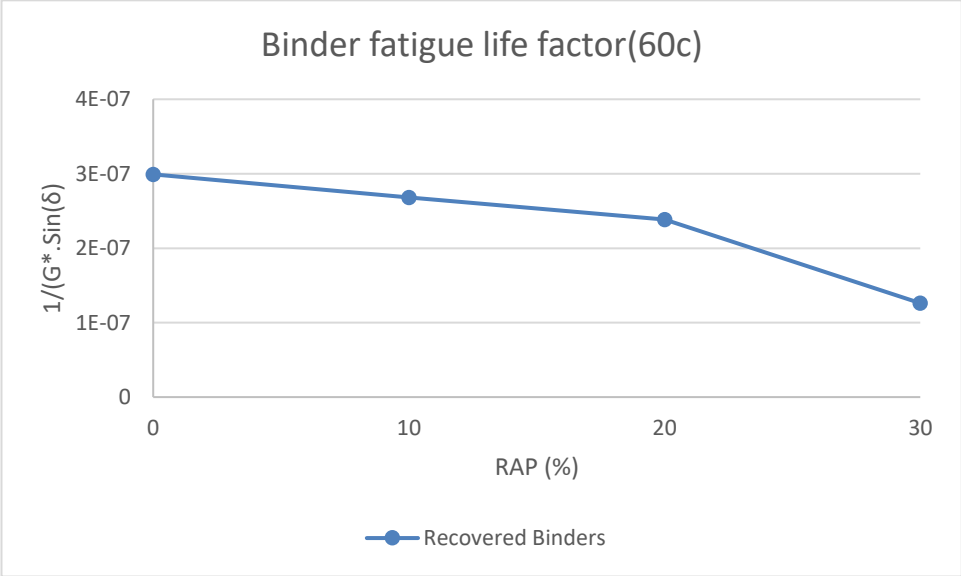

Figure 4-164 Binder fatigue life factor (1/(G.sin(δ))) for recovered binders from 14 mm mixtures at 60 °C versus RAP content*

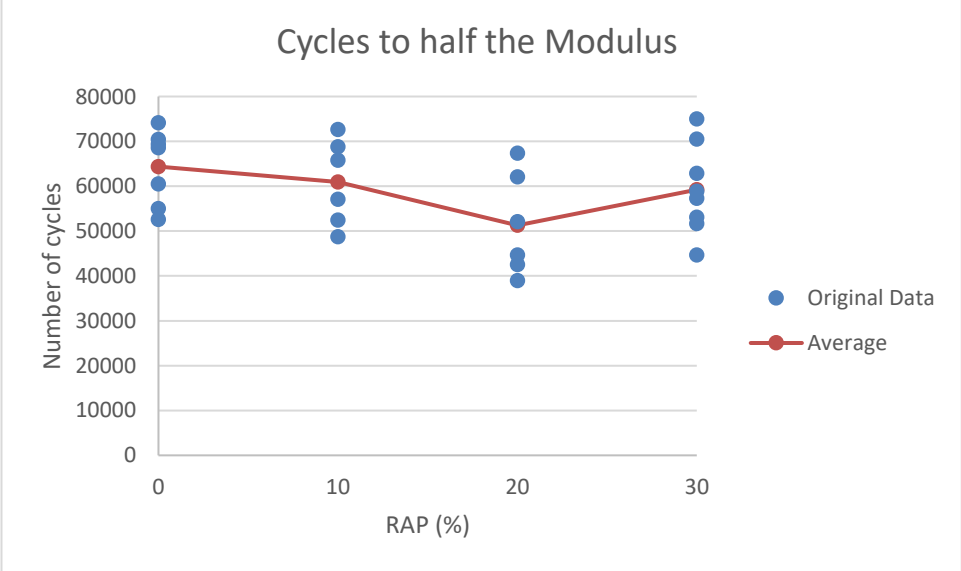

Figure 4-165 Number of cycles to halve the initial flexural stiffness for 14 mm mixtures versus RAP content

By comparing the graph of the 1/(G*.sin(δ)) parameter measured from recovered binders with the number of cycles taken to halve the stiffness of the four-point bending beams, a decreasing trend was seen until 20% RAP in the mixture; however, 30% RAP showed an improvement in the number of cycles at the same time as there was a sudden decrease in the fatigue life indicator measured from recovered binders. In addition, the differences between the numbers of cycles between the mixtures were not significant, which is in the range of discrepancies that could be seen between different samples. Therefore, it can be concluded that the RAP in the present study has not affected the number of cycles taken to halve the flexural stiffness meaningfully, but also the binder indicator suggested by (Prithvi S Kandhal & Foo, 1997) is not a reliable factor and did not match with the results of beam samples in this study.

4.7 Dynamic modulus prediction models evaluation and modification

In this section, several of the dynamic modulus prediction models introduced in section 2.3.1 are evaluated by comparing the measured dynamic modulus values from the experiment with the predicted values. The prediction models under evaluation are the Hirsch and Al-Khateeb model. The Hirsch model was chosen because of its strong documentation in the literature and popularity while the Al-Khateeb model was selected because of its simplicity and lower number of input parameters. Both these models are based on an experimentally obtained relationship between the binder properties (obtained through binder complex modulus test) and several of the mixture properties. After the evaluation, these models were modified to correspond better to the data obtained from the present study.

4.7.1 Evaluation

To evaluate the prediction models, 150 data points that were obtained during the present study from performing the complex modulus test on all 14 mm asphalt mixtures and a 20 mm control mixture at different temperatures (4, 20 and 40 °C) were compared with the outcome of the Hirsch and Al-Khateeb model under the same conditions. The reason that all the 20 mm mixtures

were not considered is that the recovered binder properties were not available for 20 mm mixtures and only the control mixture with no RAP had the binder properties available.

One of the tools utilised to compare the results was the normalised error between the measured and predicted value. This error is calculated as equation (4-2) shows below:

$$Error\ (\%) = \frac{Measured\ Value - Predicted\ Value}{Measured\ Value} \times 100 \qquad (4\text{-}2)$$

4.7.1.1 Hirsch model

As explained in section 2.3.1, the input parameters of the Hirsch model are the binder's dynamic shear modulus, the percentage of voids in mineral aggregates (VMA) and the percentage of voids filled with asphalt (VFA) as shown in equation (4-3), equation (4-4) and equation (4-5) below:

$$|E^*|_m = P_c\left[4200000\left(1-\frac{VMA}{100}\right)+3|G^*|_b\left(\frac{VFA\times VMA}{10000}\right)\right]+\frac{(1-P_c)}{\frac{\left(1-\frac{VMA}{100}\right)}{4200000}+\frac{VMA}{3|G^*|_b(VFA)}} \qquad (4\text{-}3),$$

$$P_c = \frac{\left(20+3|G^*|_b(VFA)/(VMA)\right)^{0.58}}{650+\left(3|G^*|_b(VFA)/(VMA)\right)^{0.58}} \qquad (4\text{-}4),$$

$$\varphi = -21(logP_c)^2 - 55logP_c \qquad (4\text{-}5),$$

where, P_c is aggregate contact volume, $E^*|_m$ is the dynamic modulus of HMA (psi) and Φ is the phase angle of HMA.

To determine the input parameters, for each specimen that was tested for its dynamic modulus, the value of VMA was calculated based on equation (3-10) and VFA was calculated based on equation (4-6) according to (Main Roads Western Australia, 2012) for each sample.

$$VFA = \frac{\rho_{bulk}\times BIT\%}{\rho_{Bit}\times VMA} \qquad (4\text{-}6),$$

where, ρ_{bulk} is the bulk density of the sample according to section 3.4.6, VMA is the percentage voids in mineral aggregate of the sample, BIT% is the percentage of bitumen in the mixture and ρ_{bit} is the density of bitumen (t/m^3) at 25 °C, which in this study is considered to be 1.03 t/m^3.

Furthermore, for determining the binder properties related input parameters of each specimen, the properties of the recovered binder from the same type of mixture was taken into account. The average value of the binder's complex modulus (G*) and phase angle (ϕ) obtained via the DSR test on the recovered binder for each type of mixture at the loading frequencies similar to the mixture complex test loading frequencies according to Table 3-32 were used as other input parameters for this model. To predict the dynamic modulus of the samples at different temperatures, the binder properties at equal temperature is used. For predicting the dynamic modulus of the samples at 20 or 40 °C, the average G* and ϕ of the recovered binder from the same mixture are tested at 20 or 40 °C with similar loading frequencies as the test under AMPT machine. However, to predict the dynamic modulus of the samples at 4 °C, there is no measurement available for the binders at 4 °C and the closest temperature that the DSR test has been performed at is 5 °C. To obtain the binder properties at 4 °C, the master curve of the G* and phase angle of the binder was constructed at 4 °C reference temperature based on the data available for each type of recovered binders and used for this purpose. These master curves can be found in Appendix IX. Although the all the binders were tested at 40 °C, the minimum loading frequency in the tests was 0.1 Hz. Therefore, the binder properties at 40 °C and 0.01 Hz loading frequency were obtained via the master curve constructed for each binder with 40 °C temperature reference as well. The details of these master curves are provided in Appendix X.

Figure 4-166 and Figure 4-167 shows the accuracy of the Hirsch model, for all data points, by comparing the predicted dynamic modulus to the measured values in linear and logarithmic scales, respectively, for both 14 and 20 mm mixtures.

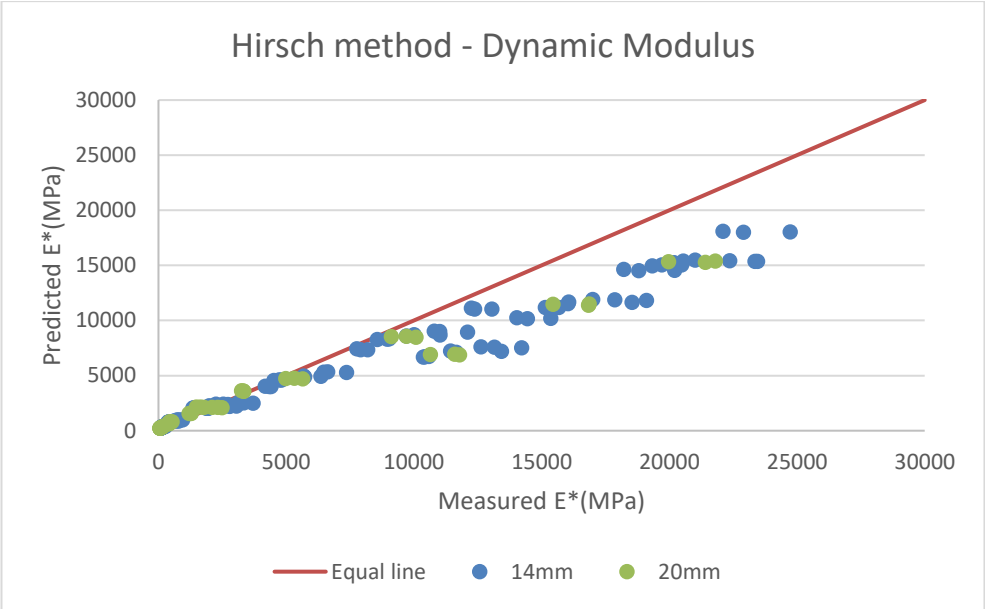

Figure 4-166 Dynamic modulus prediction accuracy of Hirsch model versus measured E (linear scale)*

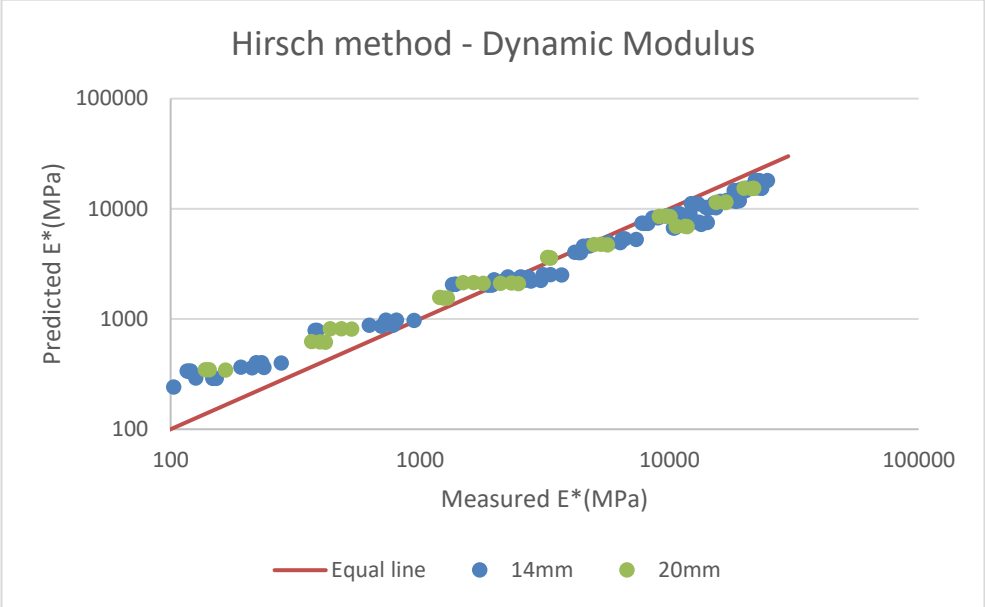

Figure 4-167 Dynamic modulus prediction accuracy of Hirsch model against measured E (logarithmic scale)*

As observed from Figure 4-166 and Figure 4-167, the Hirsch model overestimated the dynamic modulus of the samples having less than approximately 2000 MPa; however, it underestimated the results of the samples with higher stiffness. Furthermore, the same pattern occurred irrespective of what the nominal size of the asphalt mixture was. The normalised error of the Hirsch model regarding the measured mixture dynamic modulus is presented in Figure 4-168.

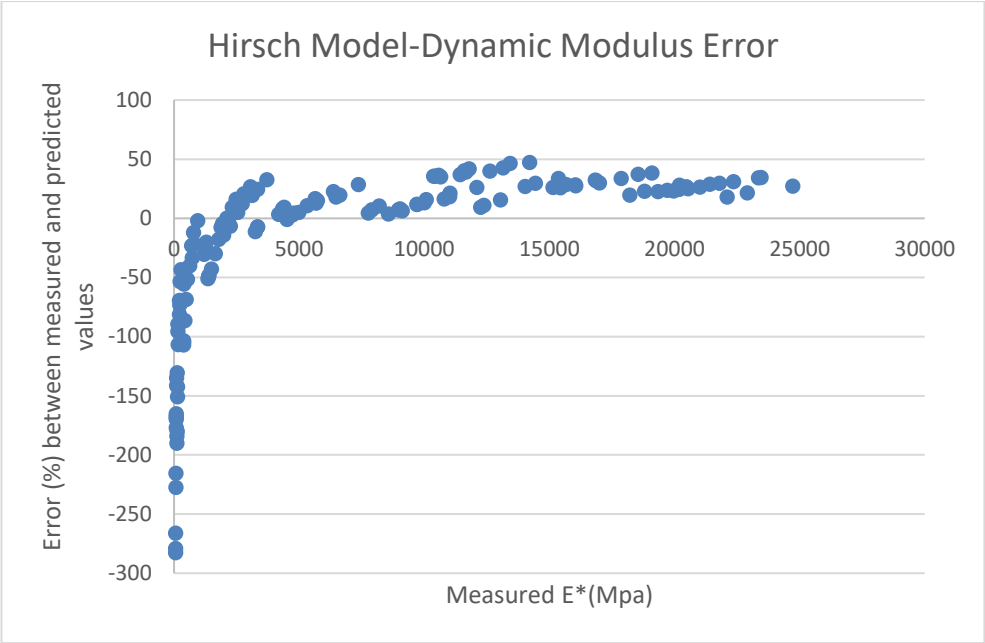

Figure 4-168 Error percentage of Hirsch model in E prediction at different measured E**

Figure 4-168 shows to what extent the Hirsch model was inaccurate. For soft mixtures, the error might reach almost 300%, while for the stiffer mixtures the error can achieve approximately 50% in most cases. Moreover, Figure 4-169 illustrates how accurate the Hirsch model was for predicting the phase angle of each mixture.

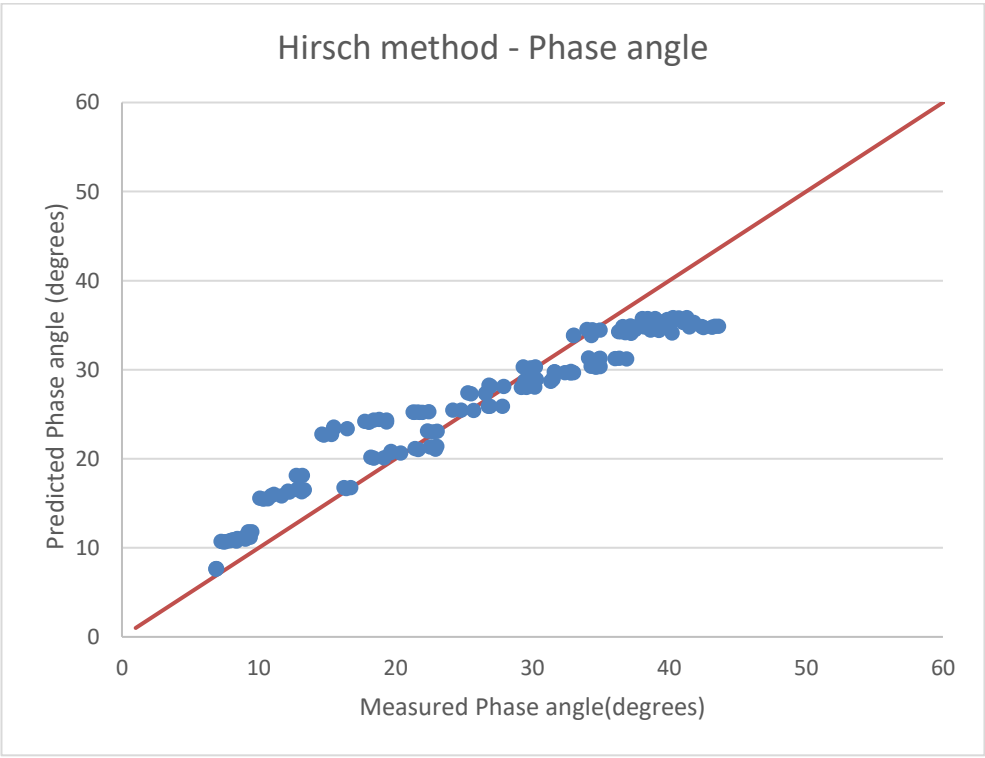

Figure 4-169 Phase angle accuracy of Hirsch model versusmeasured phase angle

The predicted phase angle was generally overestimated when the mixture's phase angle was less than approximately 30 degrees, while it underestimated the phase angle in of the majority of cases for samples that are more viscous. The level of error in the phase angle prediction was calculated using equation (4-2) and is shown in Figure 4-170.

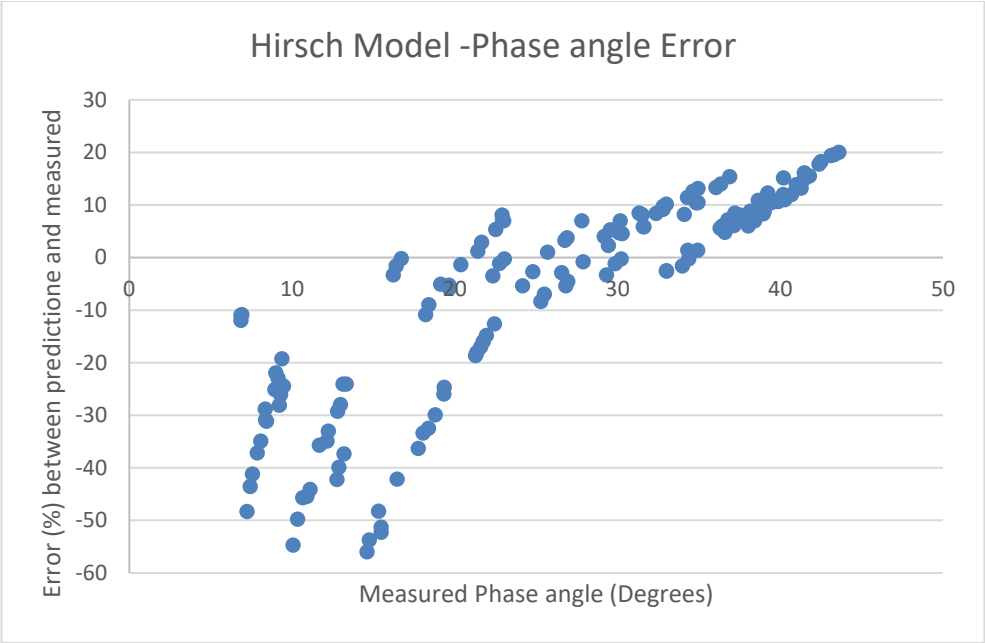

Figure 4-170 Error percentage of Hirsch model at phase angle prediction at different measured phase angle

The phase angle overestimation of this model reached almost 60% for the samples that had approximately 14 degrees phase angle, while the underestimation was mostly less than 20% for more viscous materials according to Figure 4-170.

4.7.1.2 Al-Khateeb model

As introduced in section 2.3.1, this model is based on the law of mixtures for composite materials and only has three input parameters, of which one is usually considered a constant number. Therefore it can be used when only having two arguments, VMA of the asphalt mixture sample and binders' G* according to equation (4-7):

$$|E^*|_m = 3\left(\frac{100 - VMA}{100}\right)\left(\frac{\left(90 + 10000\frac{|G^*|_b}{VMA}\right)^{0.66}}{1100 + \left(900\frac{|G^*|_b}{VMA}\right)^{0.66}}\right)|G^*|_g \qquad (4\text{-}7),$$

where, E* is the dynamic modulus, VMA is the percentage of voids in mineral aggregates, G* is the binder's complex shear modulus and G^*_g is the glassy modulus of the binder which is usually considered to be 145000 psi (Al-Khateeb et al., 2006)

To determine the input parameters for each specimen that was tested for its dynamic modulus, the value of VMA was calculated based on equation (3-10). In addition, for determining the binder's G* for each specimen, the properties of the recovered binder from the same type of mixture was taken into account. The similar data set of binder and asphalt mixture dynamic modulus properties and asphalt sample's dynamic modulus which used to evaluate Hirsch model (explained in section 4.7.1.1), was used for evaluating the Al-khateeb model. Figure 4-171and Figure 4-172 show the accuracy of the Al-khateeb model for all available 150 data points by comparing the predicted dynamic modulus to the measured values in linear and logarithmic scales, respectively, for both 14 and 20 mm mixtures.

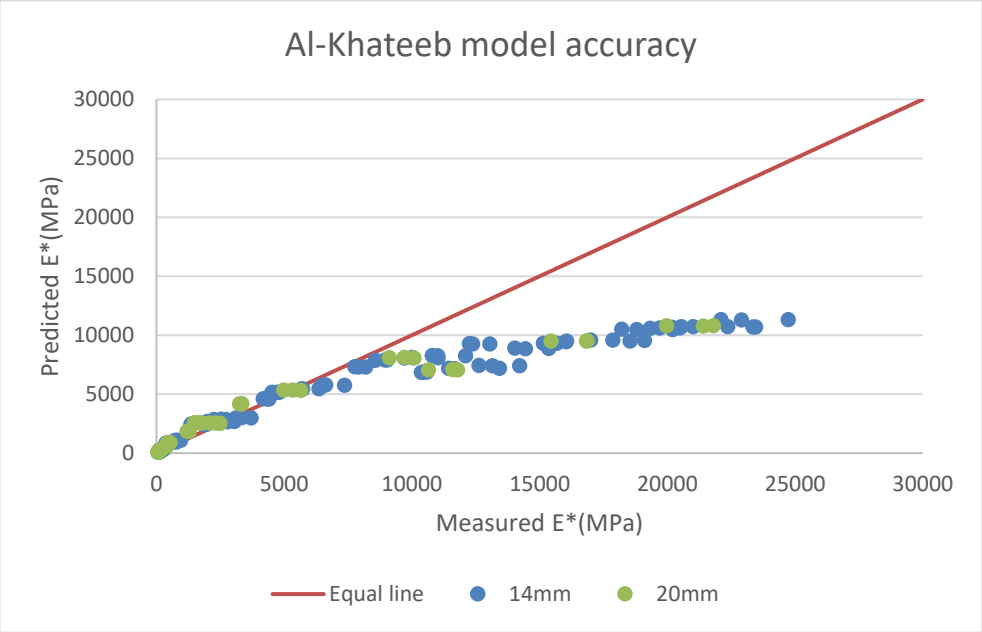

Figure 4-171 Dynamic modulus prediction accuracy of Al-Khateeb model versus measured E (linear scale)*

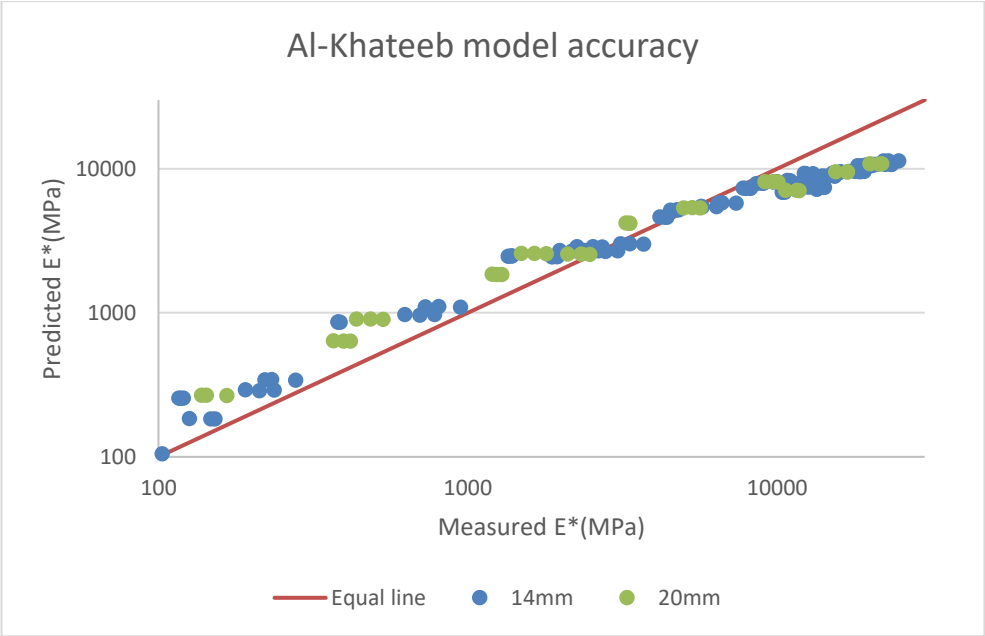

Figure 4-172 Dynamic modulus prediction accuracy of Al-Khateeb model versus measured E (logarithmic scale)*

As observed from Figure 4-171 and Figure 4-172, the Al-Khateeb model overestimated the dynamic modulus of the samples for samples having less than approximately 4000 MPa; however, it underestimated the results of the samples having higher stiffness. Furthermore, the same pattern is true irrespective of what the nominal size of the asphalt mixture was. The error of the Al-Khateeb model regarding the measured mixture dynamic modulus is presented in Figure 4-173. The error percentage was calculated according to equation (4-2).

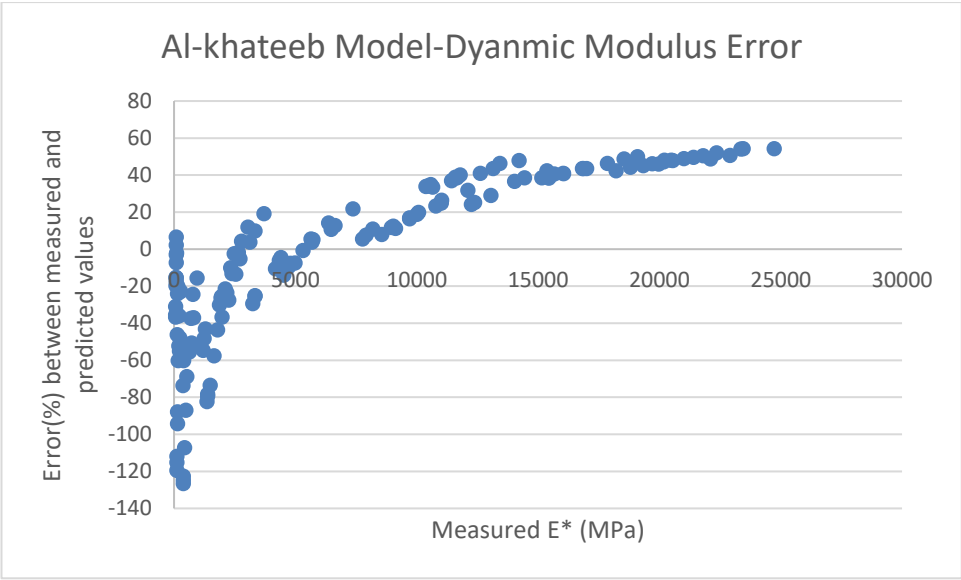

Figure 4-173 Error percentage of Al-Khateeb model in E prediction at different measured E**

Figure 4-173 shows to what extent the Al-Khateeb model was inaccurate. For soft mixtures, the error reached almost 130%,while for the stiffer mixtures the error achieved approximately 50–55% in the majority of cases.

4.7.1.3 Comparison

Figure 4-174 compares the normalised error percentage of both the Hirsch and Al-Khateeb models that were calculated using equation (4-2).

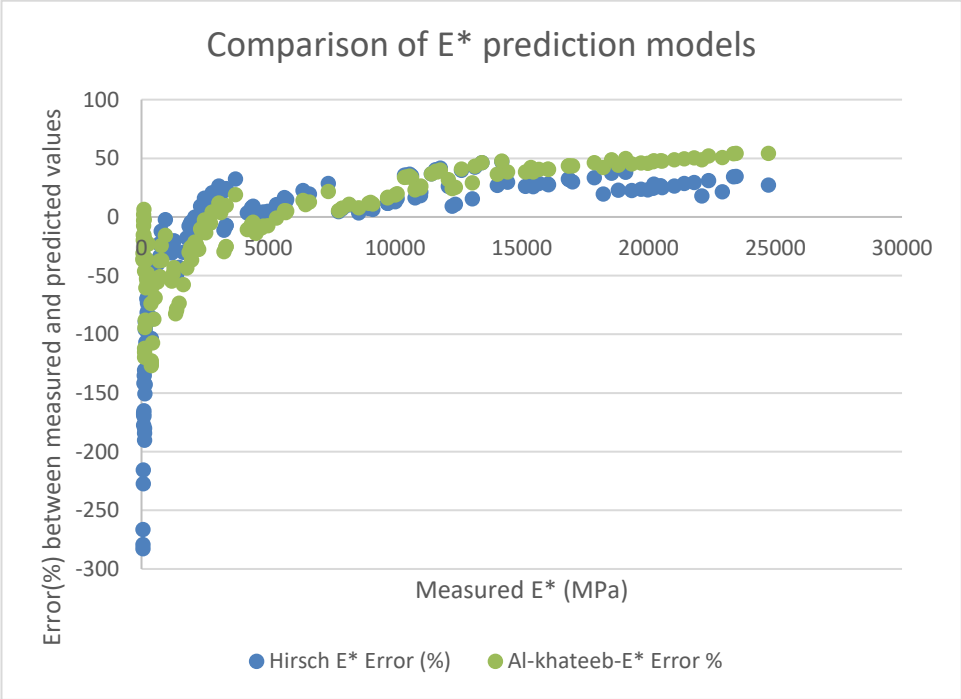

Figure 4-174 Comparison of error percentage of Hirsch and Al-Khateeb model in E prediction at different measured E**

According to this figure, the pattern of overestimation/underestimation for both models was similar. Therefore, at lower dynamic modulus values both models overestimated this value, while at higher values they underestimated this parameter. However, for samples with lower dynamic modulus than approximately 7000 MPa, it appeared that the Al-Khateeb model showed less error than the Hirsch model, while for stiffer samples, the Hirsch model outperforms the Al-Khateeb model.

4.7.2 Model modification

Both of the E* prediction models investigated in the present study experience a large amount of error for most of the investigated samples. One reason that

might have caused the inaccuracy of the models is the fact that these models are calibrated based on mixtures designed based on USA standards, while the mixtures in this study were designed to Western Australian standards. Therefore, it was decided to modify these models based on the 150 data points available from the present study. Although the data available might not be sufficient to calibrate these equations to be utilised for a vast range of mixtures, it is likely a large enough data set to calibrate the 14 and 20mm Western Australian asphalt mixtures with C320 binder and RAP presence till 30%, as the mixtures studied in the present study are typical asphalt mixtures from Western Australia. Only 206 data points were used for finding the coefficient in the Hirsch model (Kim et al., 2011) anyway; therefore, the number of data points in the present study might be sufficient to achieve a reliable model, although further studies are required to prove this assumption.

To modify these models, coefficients of the models were adjusted to minimise the error between the prediction and measured values. To do so, a function was defined as an objective function that can determine how accurate a model is when a set of coefficients are substituted in it. The objective function used in the present study was the SSE as shown in equation (4-8):

$$Objective\ function = \sum_{i=1}^{n} \frac{(V_{m_i} - V_{p_i})^2}{(V_{m_i})^2} \qquad (4\text{-}8),$$

where, n is the number of data points, V_m is the i_{th} measured value and V_p is the i_{th} predicted value. To adjust the coefficients in the model to minimise the objective function, the Solver tool in Microsoft Excel was used.

After modifying both of these models based on the data in the present study, both of the modified models are compared and discussed below.

4.7.2.1 Modified Hirsh model

To modify the Hirsch model, the coefficients in the aggregate contact volume (P_c) and phase angle equation were substituted with parameters going to be adjusted to minimise the models' error as explained in the previous section. These parameters in the P_c and phase angle equations are shown in equation (4-9) and equation (4-10), respectively.

$$P_c = \frac{\left(a + 3\left|G^*\right|_b (VFA)/(VMA)\right)^c}{b + \left(3\left|G^*\right|_b (VFA)/(VMA)\right)^d} \quad (4\text{-}9),$$

$$\varphi = -e \times (logP_c)^2 - f \times logP_c \quad (4\text{-}10),$$

where, a, b, c, d, e and f are the optimisation parameters and the other parameters are as defined previously. The Hirsch model predicts not only the dynamic modulus but also the phase angle, therefore, to minimise the error between model prediction and measured values, three scenarios were followed. In the first scenario, the model was optimised only for achieving the most precise values of E*; therefore, the values of E* used in the objective function were similar to equation (4-8). In the second scenario, the model was optimised for best matching of phase angle and therefore the values of phase angle were used in the objective function. The third scenario was designed to optimise the model for predicting dynamic modulus and phase angle simultaneously by considering the summation of previous objective functions as a new objective function.

The results of the optimisation process are presented in Table 4-31 for all scenarios. In this table, the original parameters and also the SSE of each result regarding dynamic modulus errors, phase angle errors and summation of both is also presented. This table shows that the smaller the value of SSE, the more accurate the prediction for that parameter considering all the data points.

Table 4-31 Results of optimisation on Hirsch model for best matching E, phase angle and both E* and phase angle*

	Optimisation Parameters						SSE		
Optimised for:	a	b	c	d	e	f	E*	ϕ	E* + ϕ
Not optimised (original values)	20	650	0.58	0.58	21	55	86.075	6.9436	93.185
E*	11.4096	2385.42	0.74471	0.73318	21.000	55.000	4.165	44.137	48.303
ϕ	11.6202	2013.89	0.75376	0.76763	19.411	56.616	8.485	1.730	10.216
E* and ϕ	14.3328	3011.82	0.78399	0.79625	18.111	54.718	4.717	1.824	6.541

As Table 4-31 shows, the SSE values of the original parameters were much larger than the SSE values for E*, ϕ and E*+ϕ when the parameters were optimised for each of these goals individually. For example, the SSE value of the original parameters was 93.18 for the total errors of E* and ϕ while the

SSE for the same parameters when the model was optimised for both of them was 6.54. These data shows that the newly obtained values for these parameters enable the model to predict experimental values significantly better than when the original parameters were used. However, if the parameters obtained for a specific goal were used for another purpose, the error might increase significantly, i.e., if the optimised parameters for ϕ were used for the estimation of E*, the results were almost unusable as the SSE vale was huge in comparison to the other situations.

The performance of each set of obtained parameters to predict E* are shown in Figure 4-175, and Figure 4-176 in linear and logarithmic scale, respectively. In addition, the capability to estimate the phase angle of the same set of parameters is depicted in Figure 4-177.

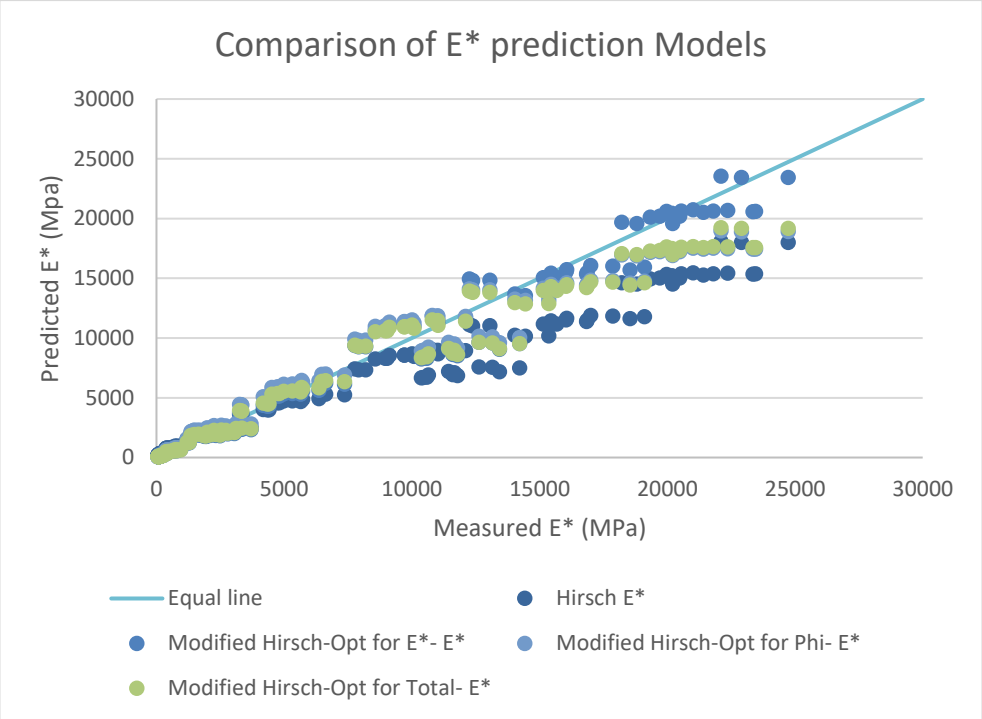

Figure 4-175 Comparison of accuracy of original and modified Hirsch models optimised for best E, δ and both E* and δ fitting for E* prediction versus measured E* values (linear scale)*

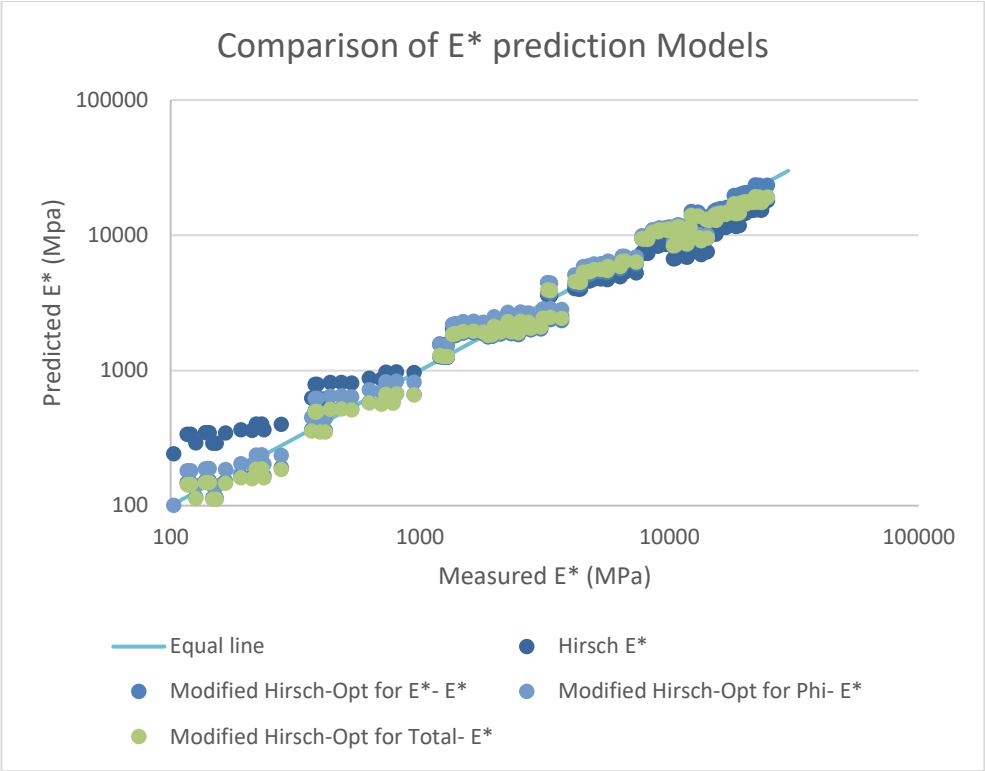

Figure 4-176 Comparison of accuracy of original and modified Hirsch models optimised for best E, δ and both E* and δ fitting for E* prediction versus measured E* values (logarithmic scale)*

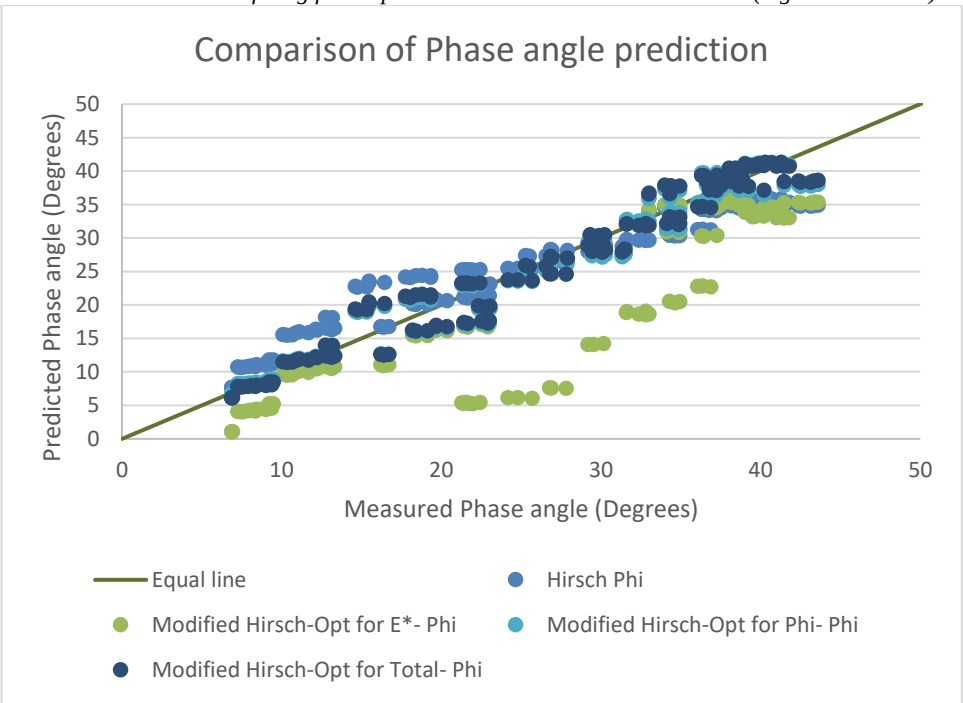

Figure 4-177 Comparison of accuracy of modified Hirsch models optimised for best E, δ and both E* and δ fitting for phase angle prediction versus measured E* values (logarithmic scale)*

As expected, the parameters that were optimised for E* or E* + ϕ performed well while the set of parameters optimised for ϕ performed poorly for predicting E*. Although the accuracy of the sets optimised for E* and E* + ϕ

were similar, for stiffer samples the set of parameters optimised for E* outperforms the other one. For instance, it was obvious that for samples with high measured E* values, the model with the latter set of parameters underestimated the values while the former still performed satisfactorily.

Regarding predicting the phase angle, both sets of parameters optimised for ϕ or summation of ϕ and E* accomplished an acceptable prediction over a range of measured values, while the set optimised specifically for ϕ estimated the values slightly better.

To understand the performance of these sets of model parameters in detail, their normalised error values are plotted against measured values for both E*and ϕ prediction in Figure 4-178 and Figure 4-179, respectively.

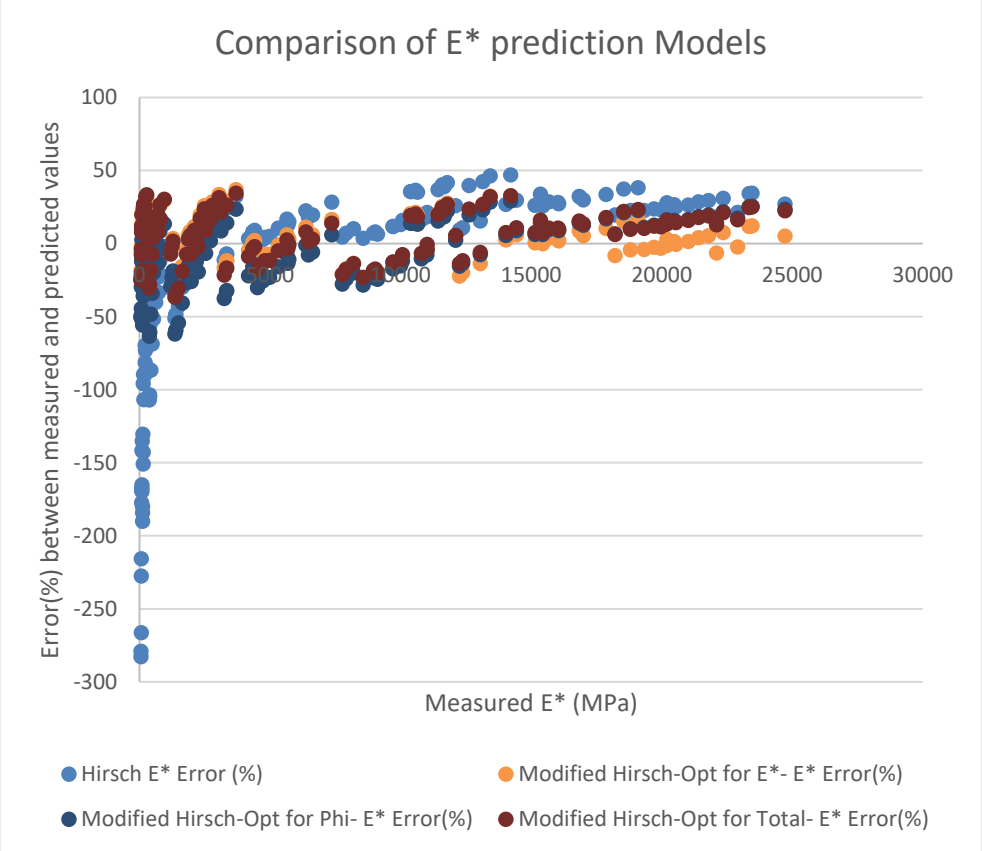

Figure 4-178 Comparison of error percentage of different modified Hirsch models to predict E versus measured E**

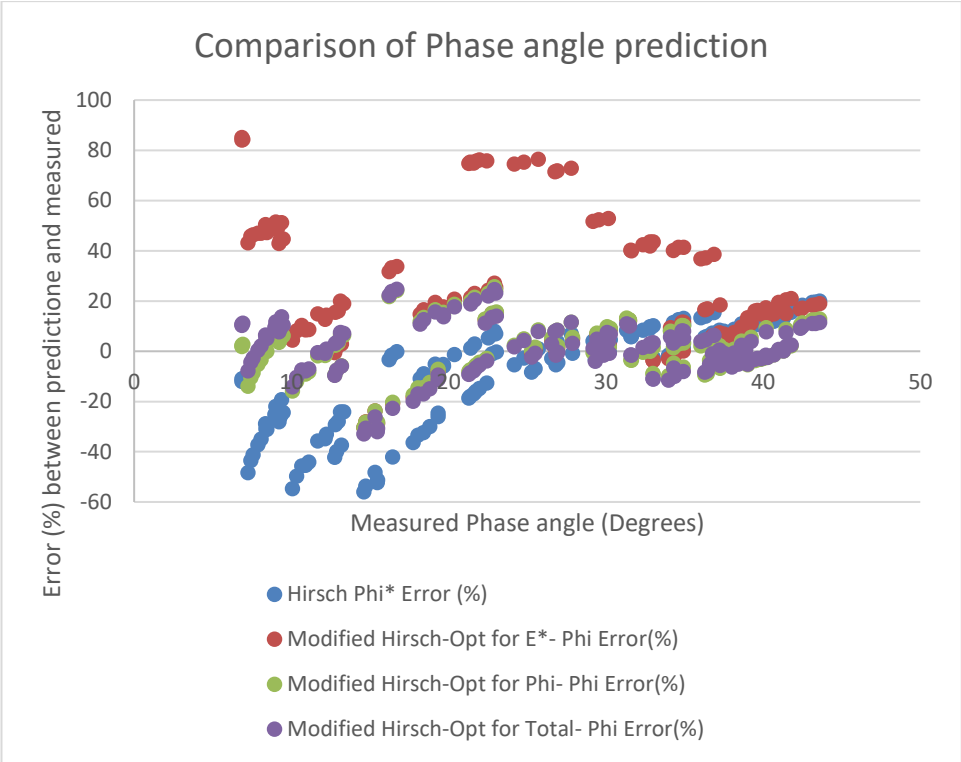

Figure 4-179 Comparison of error percentage of different modified Hirsch models to predict δ versus measured δ

The level of the error for modified models in Figure 4-178 was much lower than the original model in all range of the measured E*. While the error levels of the original model could increase to 50% in underestimation and approximately 300% in overestimation, the range of errors for the other two models shown in the figure were maximum at 40%, while they were less than 20% in a wide range of measured E* values. Although both sets of parameters modified for E* or E* + ϕ illustrate a satisfactory level of error, the set optimised only for E* performed superiorly in comparison to the one optimised for E* + ϕ. The E* + ϕ tended to underestimate the E* value in the higher range of values while the E* set of parameters ensured the model behaved more balanced over the whole range of measured values as well as had slightly smaller level of errors.

Moreover, Figure 4-179 supports the previous findings of prediction of ϕ. The original model showed poor functionality, especially at lower measured phase angles. In addition, the modified Hirsch model that was optimised for E* has difficulty predicting the values of phase angle.

However, the models adjusted for ϕ or E* + ϕ estimated the results in an appropriate way and the level of error was below 25% for the majority of the range of measured phase angles, while the adjusted model for only ϕ revealed a marginally improved performance.

In general, it can be concluded that for estimation of either E* or ϕ, it is rational to use the model that is adjusted for that purpose to minimise the error in prediction as much as possible.

4.7.2.2 Modified Al-Khateeb model

To modify the Al-Khateeb model, the coefficients in the model were substituted with parameters that were going to be adjusted to minimise its error to estimate the dynamic modulus of the samples studied in the present study. These parameters are shown in equation (4-11). The values for G^*_g (assumed to be 145000 psi) and 3 were not substituted with parameters as they are not adjustable factors as explained in (Al-Khateeb et al., 2006).

$$\left|E^*\right|_m = 3\left(\frac{100 - VMA}{100}\right)\left(\frac{\left(a + b\frac{\left|G^*\right|_b}{VMA}\right)^c}{d + \left(e\frac{\left|G^*\right|_b}{VMA}\right)^f}\right)\left|G^*\right|_g \qquad (4\text{-}11),$$

where, a, b, c, d, e and f are the optimisation parameters and the other parameters are as defined before.

The results of the optimisation process are presented in Table 4-32. In this table, the original parameters and also the SSE of each result regarding dynamic modulus errors are presented, with the smaller the value of SSE, the more accurate the prediction for that parameter considering all the data points.

Table 4-32 Results of optimisation of Al-Khateeb model for E prediction*

	Optimisation Parameters						
Model	a	b	c	d	e	f	SSE
Original model	90	10000	0.66	1100	900	0.66	31.27
Modified model	205.6793	3548.2	0.753153	2209.7	253.281	0.719247	4.204

As Table 4-32 shows, the SSE value of the modified model was greatly improved over the SSE value of the original model, i.e., the SSE value of the model before optimisation was 31.27 while after modifications this parameter was reduced to 4.20. The performance of the original and modified Al-Khateeb model is presented in Figure 4-180 and Figure 4-181 in linear and logarithmic scale, respectively.

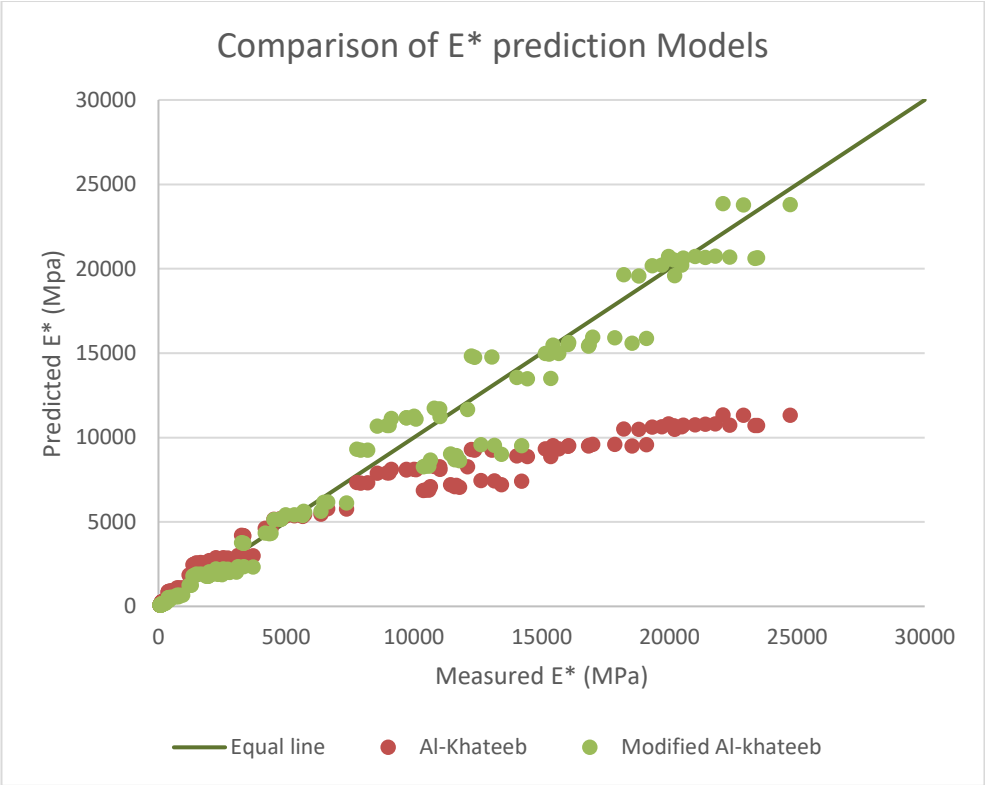

Figure 4-180 Comparison of accuracy of original and modified Al-Khateeb model for E prediction versus measured E* (linear scale)*

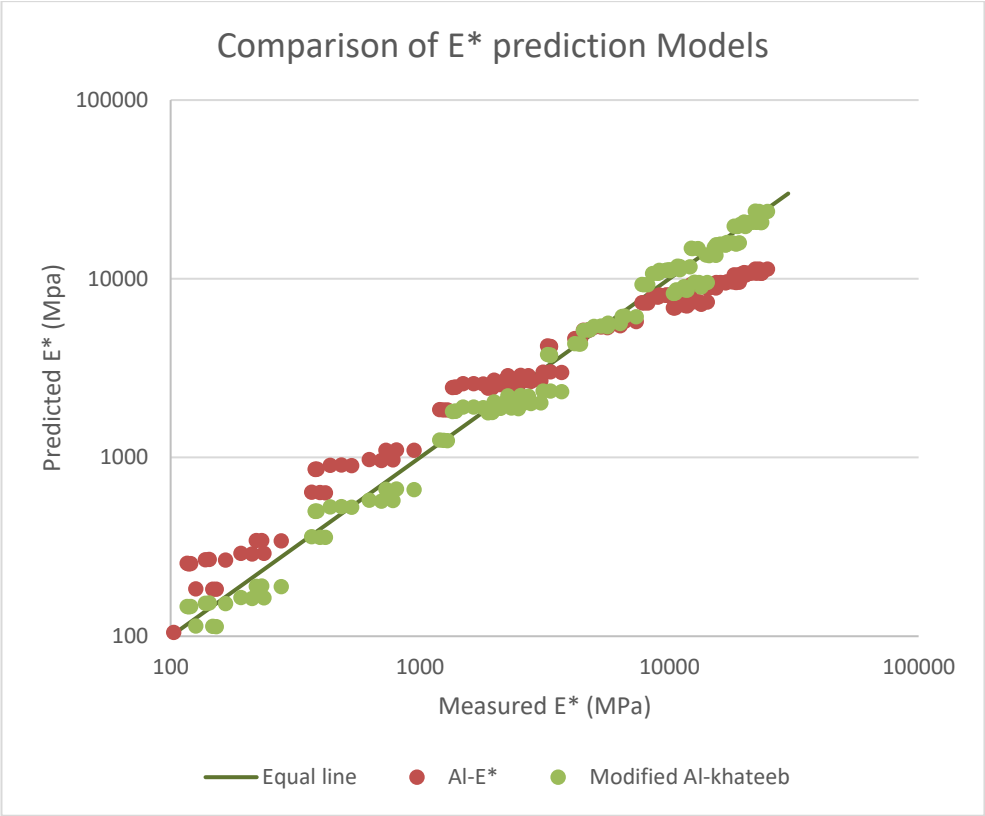

Figure 4-181 Comparison of accuracy of original and modified Al-Khateeb model for E prediction versus measured E* (logarithmic scale)*

As expected owing to a lower value of SSE in the modified model, this model performed satisfactorily in comparison to the original model. This model not only outperforms the original model regarding the level of the errors but it is also better balanced, as the original model tends to underestimate or overestimate in different ranges of measured E* values. To understand the performance of these models in detail, their normalised error in E* prediction are plotted against measured values of E* in Figure 4-182.

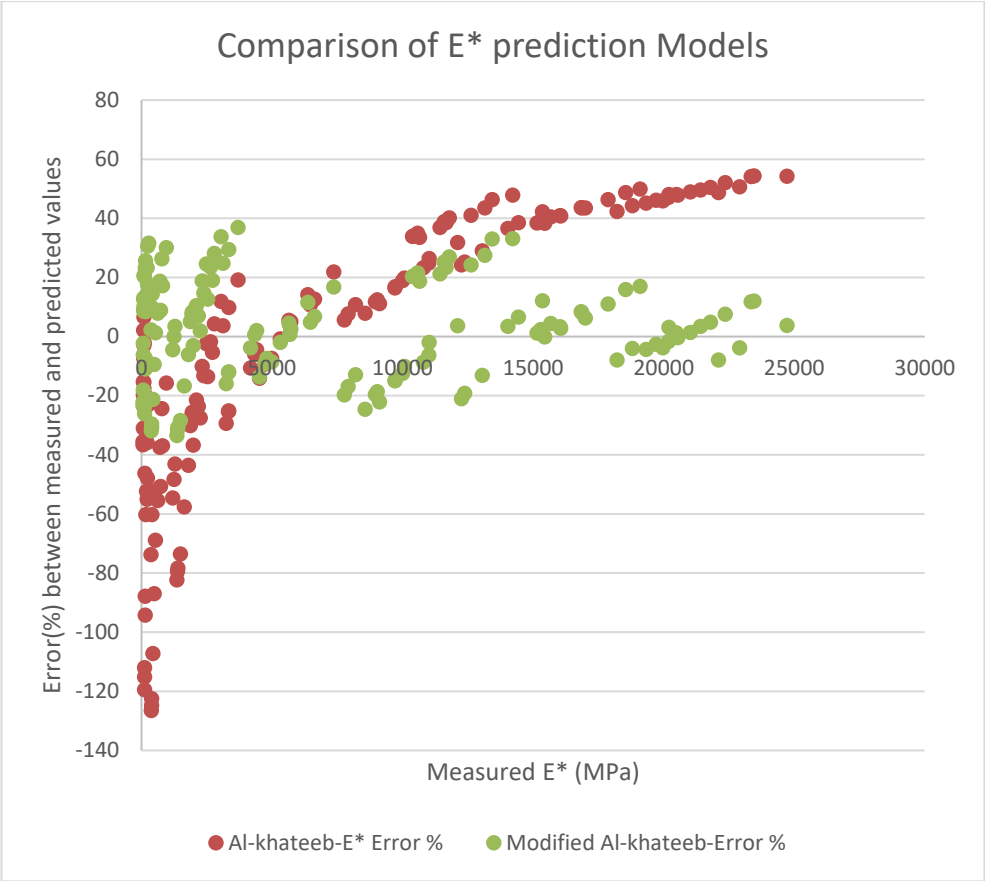

*Figure 4-182 Comparison of error percentage of original and modified Al-Khateeb models to predict E*versus measured E**

The normalised error of the modified error in contrast to the original model was limited to ± 40% and did not tend to underestimate or overestimate the results because it was almost evenly distributed in both positive and negative values. In addition, the range of the errors was very limited in comparison to the original model, e.g., the range of the errors for the original model was between approximately –130% and +60% while for the modified model it was mostly under ±20% and in lower values of measured E*was less than ±40%.

4.7.2.3 Comparison of modified models for E* prediction

In this section, the modified versions of the Hirsch and Al-Khateeb models are compared to each other to determine their capability to predict the E* of the samples. As the performance of the Hirsch model that was optimised for E* prediction was superior to the other optimised version of the same model for E* prediction, in this section the Hirsh model optimised for E* prediction is considered and compared with the modified Al-Khateeb model.

As explained in section 4.7.2.1 and 4.7.2.2, the SSE values of the modified Hirsch and Al-Khateeb models for E* prediction are 4.16 and 4.20, respectively. Therefore, a slightly better performance from the modified Hirsch model was expected. To compare the performance of these models in detail, Figure 4-183 shows the normalised error values for the same measured values of E*.

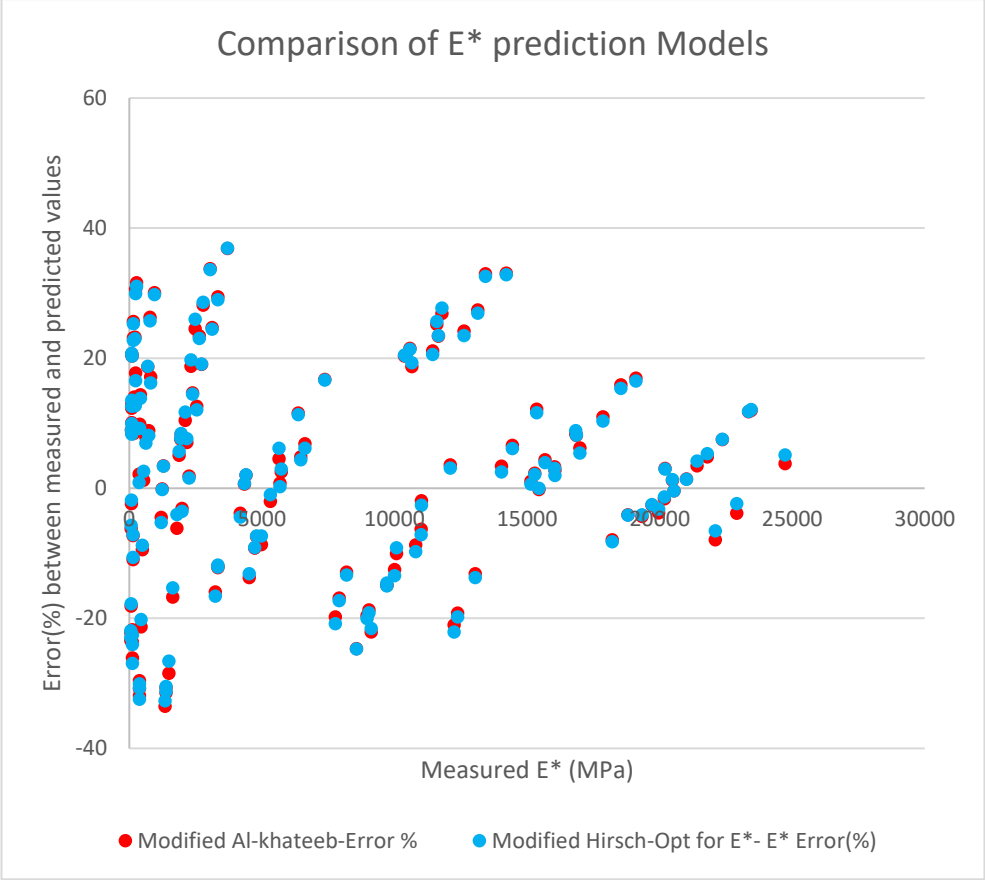

Figure 4-183 Comparison of error percentage of modified Hirsch model (optimised for E) and modified Al-Khateeb model for E* prediction versusmeasured E**

Figure 4-183 shows that the differences between these modified models are very limited and it was difficult to analyse their behaviour only by comparing their normalised error. Consequently, the E* measured values were divided into 100 MPa sections. Then the SSE values of each model were calculated for each 100 MPa window. The difference of this parameter is plotted in Figure 4-184. The difference is determined by subtracting the value of the 100 MPa windows SSE of the modified Hirsch model from the same of the modified Al-Khateeb model; therefore, positive values signify that the error of the Al-Khateeb model was higher than the other model and vice versa.

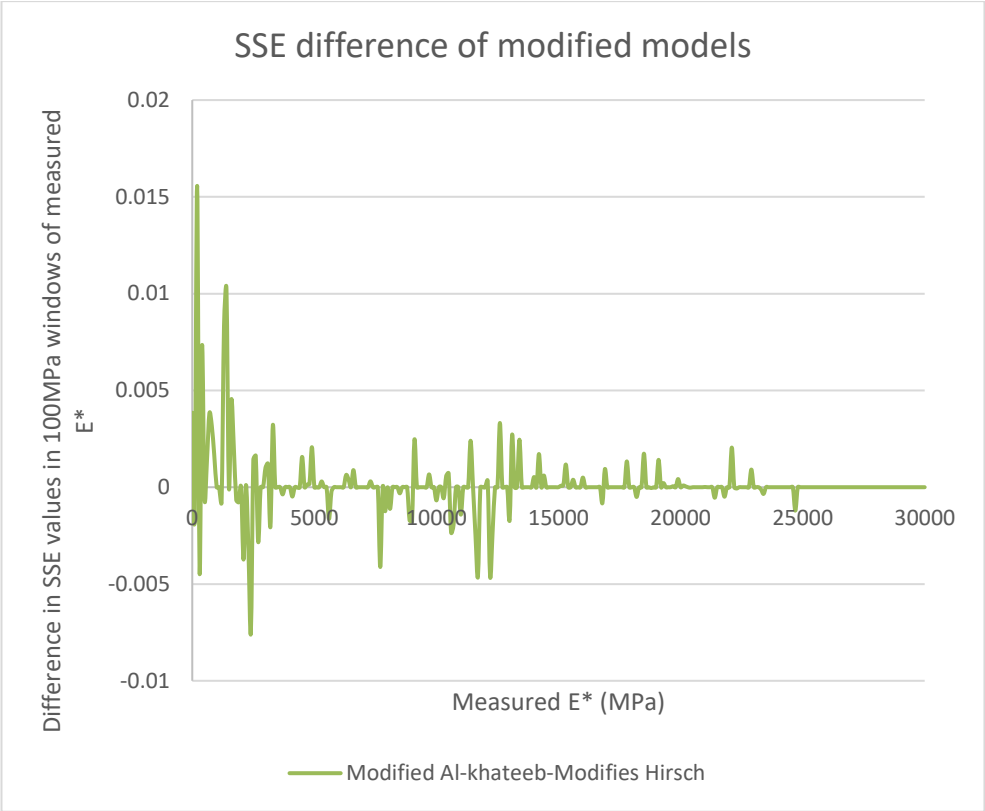

Figure 4-184 Summation of square error difference of modified Al-Khateeb and modified Hirsch model (optimised for E) in 100 MPa segments versus measured E**

Figure 4-184 shows that the positive values were dominant in most of the range of the measured E*. Therefore, in the majority of situations, the modified Hirsch model produced more accurate results in comparison to the modified Al-Khateeb model. Although there were several limited regions that the Hirsch model performed slightly worse, the magnitudes of these errors were not significant. These finding support the hypothesis that the modified Hirsch model, which is optimised only for E*, predicts the E* more precisely.

4.8 Applicability of common approaches in other regions to Western Australian mixtures

Based on the results of the present study, the approach suggested based on mixtures from other regions, such as the USA, are not completely applicable to Australian mixtures. For example, the E* prediction models that originated based on USA mixtures did not perform satisfactorily for the mixtures in the present study. In addition, the RAP did not affect the fatigue life significantly, which is contrary to several other studies in other regions. As discussed earlier, the reasons behind these differences might be the difference in the

sources of ingredients and their characteristics, different binder grading systems, different conditioning procedures, the existence of hydrated lime in the mixture and different specifications and design methods required by domestic authorities. Therefore, further research is required to understand the performance of mixtures containing RAP in Western Australia that has been partially covered in the present study.

5 Conclusions and recommendations

In the present study, two typical asphalt mixtures from Western Australia, 14 and 20 mm dense-grade asphalt with C320 binder, were investigated. These mixtures were then redesigned to contain 0, 10, 20 and 30% RAP by weight of the total mixture. Consequently, eight different mixtures were studied. The RAP material and all other ingredients utilised in the research was taken from an asphalt plant in Western Australia to simulate the field process as much as possible. These materials were then characterised and asphalt samples from these mixtures were produced and assessed to determine how their performance was affected by the presence of RAP. This assessment also helped evaluate the current limits on RAP usage in Western Australia. Currently in Western Australia, the RAP cannot be used in the surface layer and its use is limited to only 10% in the intermediate course layer. Moreover, the binders in the present study, virgin C320 binder, RTFO aged virgin binder and recovered binders from the RAP material and mixtures were investigated to understand how the RAP influences binder properties. The assumption that the presence of the RTFO aging binder and conditioning the mixture in the oven after mixing has similar influences on the binder were also examined. The mixture performances were compared with several properties of their binders to verify whether there is any correlation between them. Different approaches to predict the properties of blended virgin and RAP binder were assessed. Finally, the ability of two asphalt mixture dynamic modulus prediction models were investigated to determine how they can predict the complex modulus parameters of the mixtures in the present study and then several modifications were performed on them to improve their estimations.

In the following subsections, the summary of findings for each individual component of this research is presented.

5.1 Asphalt mixtures performance investigation

The asphalt mixtures in the present study were examined in different aspects including Marshal stability and flow, resilient modulus, rutting resistance using wheel tracker test, moisture susceptibility using TSR comparisons between moisture conditioned and unconditioned samples, fatigue life using

four- points bending beam, and complex modulus test to determine the dynamic modulus and phase angle of the mixture at different frequencies and temperatures. The effect of RAP content in each test is explained below.

5.1.1 Marshal stability and flow

Both the 14 and 20 mm mixtures demonstrated an increasing trend in Marshal stability and flow, although the 14 mm mixtures' was not a continuous rise and it fell slightly between 20 and 30% RAP inclusion. All the mixtures passed the requirements based on the standard specifications followed. However, the higher values and continuous trend of the Marshal flow for the 20 mm mixtures suggests that by adding higher percentages of RAP in the 20 mm mixtures, the maximum 4 mm Marshal flow might be unachievable.

5.1.2 Resilient modulus

As expected, all the mixtures showed an increase in resilient modulus by having higher percentages of RAP included in the mixture, although the slope of increase was higher for the 20 mm mixtures than for the 14 mm mixtures. This might come from the fact that 14mm mixture have higher binder content and stiffer binder is more effective on the behaviour of whole mixture. However, this study suggests further research to understand this behaviour.

5.1.3 Rutting resistance

The 14 mm mixtures' rutting resistance improved noticeably by having higher percentages of RAP in the mixture. For instance, the rut depth in wheel tracking test became less than half in the 30% RAP mixture. However, the RAP inclusion did not have the same influence on the 20 mm mixtures. In fact, it decreased the rut resistance by slightly increasing the rut depth in the test.

5.1.4 Moisture susceptibility

The moisture susceptibility was tested according to the TSR method, where the tensile strengths of all the samples were measured before and after moisture conditioning. Generally it was discovered that the higher the percentage of RAP in the mixture, the higher the tensile strength irrespective of whether the mixture was conditioned or not. Consequently, no change was

observed through having RAP in the mixtures and all the mixtures showed remarkable TSR results.

5.1.5 Fatigue life

The fatigue lives of the mixtures were examined using the four-point bending beam test. Although initial flexural stiffness increased by increasing the amount of RAP in the mixture, the phase angle decreased. Surprisingly, even though mixtures with higher RAP content showed higher flexural stiffness, no meaningful trend was seen in the number of cycles taken to halve the stiffness of the samples according to the RAP content. This finding suggests that the RAP had no effect on the fatigue life of the samples according to the method that was followed in the present study. The same trend was observed in both 14 and 20 mm mixtures. The minimal effect of RAP on the fatigue life of the samples in this study, might come from the low fatigue life of the samples, even with no RAP in the testing conditions in this study. Therefore, further study is recommended to investigate this issue.

5.1.6 Complex modulus

The cylindrical samples of the mixtures were created and tested at different frequencies and temperatures. To compare the results more conveniently, the master curves of the performance of each mixture were constructed based on the average measured values. At the majority of frequencies, the higher the amount of RAP, the higher the dynamic modulus. Furthermore, at higher frequencies the difference became less sensitive to the percentage of RAP content. For 14 mm mixtures, 10 and 20% RAP content performed very closely while 30% RAP increased the dynamic modulus significantly. Regarding 20 mm mixtures, the differences in dynamic modulus of the samples with different RAP content was more distinguishable and had a considerable difference between the performances of the mixtures. Moreover, at high temperatures (40 °C) and very low frequencies, the master curves of all mixtures crossed each other; therefore, the ranking of the binders owing to the magnitude of dynamic modulus was reversed. However, it should be noted that this effect might be because of less accurate test results at high temperatures, because experimental errors, such as separation of the LVDTs

from sample, etc. might affect the results more significantly at higher temperatures. Therefore, more research is suggested to study this behaviour.

5.2 Binder properties investigation

In the present study, different types of binders were studied. These binders included virgin C320 binder, RTFO aged virgin C320, conditioned and unconditioned recovered binder from RAP and recovered binder from all the 14 mm mixtures. These binders were placed under two tests. The main test was performed using a DSR machine to determine their complex modulus properties at different temperatures and frequencies. This machine also helped determine the high critical temperature of the binders. The second test was a determination of their penetration number, using a penetrometer. Moreover, to verify the ineffectiveness of recovery procedure on the properties of binders, a binder was tested before and after recovery. The following analyses were then performed on the results from these tests.

5.2.1 Effect of Binder Recovery process on binder properties

In the present study, the complex modulus of a binder tested before and after recovery procedure occurred. No significant changes were discovered, which verifies that using a recovered binder from the mixtures in the present study was able to represent the binder in the mixture.

5.2.2 Effect of RAP in binders complex modulus results

A master curve was constructed for each type of binder to make it easier to compare their performance. As the results showed, the higher the RAP content, the higher the complex modulus of the binder was. In addition, in the majority of situations, the existence of RAP caused the binders to behave more elastic and therefore had smaller phase angles. However, at 40 °C and low frequencies (0.01, 0.1 and 1 Hz) of loading, the phase increased by having more RAP in the mixture. Another important point is that the master curves revealed that 10% RAP did not affect the complex modulus of the binder effectively. In addition, having 20% RAP in the mixture produced similar results as the result of the binder that experienced the RTFO aging procedure. However, the 30% RAP showed a significant increase in complex modulus of a binder.

5.2.3 Is RTFO aging and mixture oven conditioning equivalent?

Using the data from the binder analysis, the assumption that RTFO aging affects the binder in a similar manner to the oven conditioning of the asphalt mixture was examined. Based on the literature, both methods are used to simulate the aging that occurs after production of asphalt mixtures until it is paved. If both these solutions are simulating the same phenomenon, it was expected that both of them produce the same result. However, in the present study the complex modulus of the RTFO aged binder and binder recovered from a conditioned mixture were compared and it was discovered that the RTFO aging technique aged the binder more severely than the mixture in the oven. In fact, the effect that RTFO aging had on the binder was comparable with the influence that 20% of RAP in the mixture had.

5.2.4 Binder blending equations

The present study also evaluated three different approaches to estimate the properties of a blended binder in mixtures containing RAP. These methods were critical high temperature blending chart, penetration blending equation and Chevron equation as suggested in Austroad specifications. To evaluate these methods, the properties of virgin binder and RAP binder were utilised by each method to estimate the properties of the blend of binders in the asphalt mixtures. Then, the estimated property was compared with the actual property of that blend. Different scenarios were designed to determine the effect of the level of aging of virgin and RAP binder in the accuracy of these methods. Among these scenarios, the one that utilised the conditioned virgin and RAP binder appeared to produce better results in comparison to RTFO aged or virgin binders. One reason for this achievement might be the fact that the data which the results of these blending methods were compared to, were the results of binders recovered from conditioned mixtures. In addition, the error of the penetration equation was found to be very high. This equation requires a large amount of recovered material for the test, which makes it impractical because such a recovery process is time consuming and expensive. Therefore, the Chevron equation and critical high-temperature blending chart were recommended. Considering that in Australia the viscosity of the binders is

used for categorisation purposes, the Chevron equation is the preferred method in Western Australia.

5.3 Binder and asphalt mixture correlation

5.3.1 Mixture performance ranking based on binder properties

In the present study, the mixtures performances were compared with several parameters obtained from their recovered binder to see if there was any correlation between them. The mixture parameters that were investigated include complex modulus, rut depth and fatigue life. These parameters form mixtures that were compared with complex modulus, 1/(G*/sin(δ)) and 1/(G*.Sin(δ)) parameters from the recovered binders. The results revealed that the complex modulus of the mixtures increases as the complex modulus of the binders increases. With regards to rut depth, both parameters decreased owing to a higher amount of RAP and correlated with each other approximately well. In fatigue life comparison, although the binder's fatigue factor changed significantly, no meaningful trend was seen in the number of cycles to halve the flexural stiffness of the samples. This was observed even though the samples' initial flexural stiffness correlated well with the change of G* of the binders according to the RAP content.

The binder is not the only important factor in the mixture, with aggregates important also. Therefore, different aggregate conditions might dominate the influence of binders, so judgment cannot be based only on the condition of the binder. For example, if a binder's 1/(G*/sin(δ)) property in the 14 mm mixtures was compared with the rut depth in the 20 mm mixtures, no meaningful change in rut depth was seen while the binder rutting factor changed significantly. Even though the binder's 1/(G*/sin(δ)) property of only 14 mm mixtures were obtained, the same result for the 20 mm mixtures was expected to be close to their 14 mm counterparts as the RAP binder participation was only slightly different.

5.3.2 E* prediction based on binder properties

Two methods for E* prediction of asphalt mixtures were evaluated and modified in the present study based on 150 data points obtained from tests performed on all 14 mm mixtures with or without RAP and 20 mm control mixture containing no RAP. These methods were the Hirsch and Al-Khateeb models. Both these models use basic asphalt mixtures, i.e., samples in addition to binder properties, to estimate the dynamic modulus or phase angle of the sample. The Hirsch model can predict both dynamic modulus and phase angle of the sample, while the Al-Khateeb model only predicts the dynamic modulus of the asphalt mixture sample. Both of these models performed poorly and had a tendency to overestimate the dynamic modulus of samples with low measured E* while they underestimated the same parameter for the samples with high measured dynamic modulus. Consequently, these models were modified to fit the results obtained in the present study. As the Hirsch model was able to predict both dynamic modulus and phase angle, three scenarios were followed to modify this model: optimising for dynamic modulus, phase angle and both dynamic modulus and phase angle. The present study found that the modified Hirsch model for dynamic modulus performed best for dynamic modulus prediction among all the models. The modified Al-Khateeb model behaved slightly worse in the dynamic modulus prediction even though the results were very similar to the Hirsch model and was much better than original models. Furthermore, to predict the phase angle of the samples, the modified Hirsch model for phase angle estimated the results accurately. Therefore, the modified Hirsch models optimised only for predicting dynamic modulus or phase angle to estimate these parameters are recommended based on the results from this study.

5.4 Limit on RAP percentage

One of the goals of is the present study was to verify whether the limits currently upheld in Western Australia works are satisfactory. To do so, the performance of the mixtures and binders were investigated to determine whether the inclusion of RAP affects the features of asphalt mixtures negatively; therefore, it should be limited.

The performance of the mixtures improved for many aspects including resilient modulus, rutting resistance and complex modulus by increasing the amount of RAP in the mixture. Several features were not affected meaningfully by the existence of RAP material in the mixture, such as moisture susceptibility and fatigue life. Although the rutting resistance of the 14 mm mixtures was improved by having RAP in the mixture, the resistance of the 20 mm mixtures did not change dramatically. However, it appears that adding percentages of RAP to the mixture increases the Marshal flow, which has a high limit. Mixtures containing 30% RAP caused this parameter to become very close to its higher limit and having more RAP in the mixture might disqualify the mixture based on Western Australia requirements, although all the mixtures in the present study passed those requirements.

If the grade of the binder is considered to limit the RAP content, the present study indicated that 10% RAP in the mixture did not change the grade of the binder while 20% RAP did change it by one grade according to viscosities at 60 °C. However, using the Superpave methodology, which are used in the USA, even 20% RAP had no effect on grading of the binder as it changed its critical high temperature less than 6 °C, yet having 30% RAP increased the critical high temperature by more than 6 °C and consequently changed the binder grade. Therefore, the percentage of RAP that had no effect on binder grading depended on the grading system. As the present study is based on Western Australian standards, 10% RAP can be used without changing the binder's grade, which is in agreement with the limits in the specifications for using RAP in Western Australia.

In general, only by considering the performance of the mixtures in this study, RAP content can be increased to 30% with no negative impacts, although it might change the binder grading. However, only the laboratory obtained features in the present study were considered in this conclusion and the concerns in the field and production or other factors are not included.

5.5 Recommendations

As explained before, the characteristics of mixtures containing RAP in other regions apart from Australia are not completely applicable to Western

Australian mixtures. Therefore, a vast research program is required to investigate and evaluate the different approaches for seeking the best option possible depending on the region of interest. Although the present study attempted to cover this gap partially, there is still a need for further study. Consequently, it is recommended to continue further investigations by using a greater number of samples, mixtures, material sources and test conditions for characterising mixtures containing RAP with a wider range of RAP content. Moreover, different sources of RAP need to be investigated. A comprehensive study on the in-field performance of the mixtures containing RAP including fatigue and rutting resistance evaluation is recommended, which can be completed using different types of instrumentation in the field. In addition, the feasibility of production of the mixtures with RAP in the local asphalt plant needs to be studied. RAP characterisation and handling might be difficult for asphalt plants; therefore, further investigation should occur to discover procedures to characterise and handle RAP in asphalt plants that are both affordable and easy to apply.

6 References

AASHTO. (2007). *Determining Dynamic Modulus of Hot Mix Asphalt*

AASHTO. (2008). *Mechanistic-Empirical Pavement Design Guide - A Manual of Practice (Interim Edition)*

AASHTO. (2013). *Specification For Superpave Volumetric Mix Design*

Al-Khateeb, G., Shenoy, A., Gibson, N., & Harman, T. (2006). A New Simplistic Model for Dynamic Modulus Predictions of Asphalt Paving Mixtures. *AAPT, 75E*

Al-Qadi, I. L., Carpenter, S. H., Roberts, G. L., Hasan Ozer, Aurangzeb, Q., Elseifi, M. A., & Trepanier, J. (2009). *Determination of Usable Residual Asphalt Binder in RAP* (FHWA-ICT-09-031). I. C. f. Transportation.

Al-Qadi, I. L., Elseifi, M. A., & Carpenter, S. H. (2007). *Reclaimed Asphalt Pavement – A Literature Review* (FHWA-ICT-07-001).

Asphalt-Institute. (1981). *Asphalt Hot-Mix Recycling (MS-20)*

Association, A. A. P. (2000). *National Asphalt Specification*

ASTM. (2008). *Standard Test Method for Determining the Rheological Properties of Asphalt Binder Using a Dynamic Shear Rheometer* doi:10.1520/d7175-08

Australian Standard. (1993a). *Determination of penetration*

Australian standard. (1993b). *Specification for test sieves*

Australian Standard. (2012). *Sampling—Aggregates*

Australian/New Zealand Standard. (2013). *Determination of the resilient modulus of asphalt-indirect tensile method*

Australian/New Zealand Standard. (2014). *Sample preperation-mixing, quartering and conditioning of asphalt in the labpratory*

Australian/New Zealand Standard. (2015). *Determination of the effect of heat and air on a moving film of bitumen (rolling thin film oven (RTFO) test)*

Austroads. (2005). *Sample Preparation– Compaction Of Asphalt Slabs Suitable For Characterisation*

Austroads. (2006a). *Deformation Resistance Of Asphalt Mixtures By The Wheel Tracking Test*

Austroads. (2006b). *Fatigu life of compacted bitminous mixes subject to repeated flexural bending*

Austroads. (2007a). *Part 4B: Asphalt*

Austroads. (2007b). *Stripping Potential Of Asphalt – Tensile Strength Ratio*

Austroads. (2008). *Part 4F: Bituminous Binders*

Austroads. (2015a). *Characterisation of the Viscosity of Reclaimed Asphalt Pavement (RAP) Binder Using the Dynamic Shear Rheometer (DSR)*

Austroads. (2015b). *Design of bituminous binder blends to a specified viscosity value*

Baburamani, P. (1999). *Asphalt fatigue life prediction models- a literature review*.

Baghaee Moghaddam, T., Rehan Karim, M., & Abdelaziz, M. (2011). A review on fatigue and rutting performance of asphalt mixes. *Scientific Research and Essays, 6*, 670-682. http://dx.doi.org/10.5897/SRE10.946

Bennert, T. (2012). *Advanced Characterization Testing of RAP Mixtures Designed and Produced Using a "RAP Binder Contribution Percentage"*. New York State Department of Transportation (NYSDOT).

Bonaquist, R. (2008). *Report 614 Refining the Simple Performance Tester for Use in Routine Practice NCHRP 9-29*.

CHAFFIN, J. M. (1996). *Characterization of asphalt recycling agents and evaluation of recycled asphalt binder aging properties.* Doctor of Philosophy Texas A&M University

Clyne, T. R., Li, X., Marasteanu, M. O., & Skok, E. L. (2003). *Dynamic And Resilient Modulus Of Mn/Dot Asphalt Mixtures*.

Colbert, B., & You, Z. (2012). The determination of mechanical performance of laboratory produced hot mix asphalt mixtures using controlled RAP and virgin aggregate size fractions. *Construction and Building Materials, 26*(1), 655-662. http://dx.doi.org/10.1016/j.conbuildmat.2011.06.068

Copeland, A. (2011). *Reclaimed Asphalt Pavement in Asphalt-State of Practice* (FHWA-HRT-11-021).

Denneman, E. (2013). *AP-T248-13 Improved Design Procedures for Asphalt Pavements: Pavement Temperature and Load Frequency Estimation*. Austroad.

Denneman, E., Dias, M., Malone, S., Choi, Y., Woodall, E., & Urquhart, R. (2013). *AP-T245-13 Maximising the Re-use of Reclaimed Asphalt Pavement: Binder Blend Characterisation*. Austroads.

Diefenderfer, S. D., Diefenderfer, B. K., & Apeagyei, A. K. (2011). Rutting Resistance of Asphalt Concrete Mixtures That Contain Recycled Asphalt Pavement. *Transportation Research Record: Journal of the Transportation Research Board, 2208*(-1), 9-16. http://dx.doi.org/10.3141/2208-02

Doyle, J. D. (2011). *Characterization of reclaimed asphalt and performance based evaluation of its use in recycled mixtures.* Doctor of Philosophy Mississippi State University

Farrar, M., Sui, C., Salmans, S., & Qin, Q. (2015). *Determining the Low-Temperature Rheological Properties of Asphalt Binder Using a Dynamic Shear Rheometer (DSR)*. Western Research Institute:

Fontes, L. P. T. L., Trichês, G., Pais, J. C., & Pereira, P. A. A. (2010). Evaluating permanent deformation in asphalt rubber mixtures. *Construction and Building Materials, 24*(7), 1193-1200. http://dx.doi.org/10.1016/j.conbuildmat.2009.12.021

Gallivan, V. L. (2014). *Rationale for Revising AAHTO M 323 Table 2* [Meeting Report]. http://www.asphaltpavement.org.

Ghabchi, R., Singh, D., & Zaman, M. (2014). Evaluation of moisture susceptibility of asphalt mixes containing RAP and different types of aggregates and asphalt binders using the surface free energy method. *Construction and Building Materials, 73*, 479-489. http://dx.doi.org/10.1016/j.conbuildmat.2014.09.042

Gillespie, H. M. (1992). *The History of Hot Mix Asphalt-A Century of Progress*: NAPA.

Glover, C. J., Martin, A. E., Chowdhury, A., Han, R., Prapaitrakul, N., Jin, X., & Lawrence, J. *Evaluation Of Binder Aging And Its Influence In*

Aging Of Hot Mix Asphalt Concrete: Literature Review And Experimental Design (FHWA/TX-08/0-6009-1). Federal Highway Administration (FHWA).

Hajj, E. Y., Sebaaly, P. E., & Shrestha, R. (2009). Laboratory Evaluation of Mixes Containing Recycled Asphalt Pavement (RAP). *Road Materials and Pavement Design, 10*(3), 495-517. http://dx.doi.org/10.1080/14680629.2009.9690211

Hansen, K. R., & Copeland, A. (2013). *Annual Asphalt Pavement Industry Survey on Recycled Materials and Warm-Mix Asphalt Usage: 2009–2012*.

Harrigan, E. T. (2001). *RESEARCH RESULTS DIGEST-Recommended Use of Reclaimed Asphalt Pavement in the Superpave Mix Design Method: Guidelines* (253).

Hassan, R. A., & Tran, B. T. (2011). Performance of Hot-Mix Asphalt Containing Recycled Asphalt Pavement. *Transportation Research Record: Journal of the Transportation Research Board, 2205*, 121-129. http://dx.doi.org/10.3141/2205-16

Huang, B., Shu, X., & Vukosavljevic, D. (2011). Laboratory Investigation of Cracking Resistance of Hot-Mix Asphalt Field Mixtures Containing Screened Reclaimed Asphalt Pavement. *Journal of Materials in Civil Engineering, 23*(11), 1535-1543. http://dx.doi.org/10.1061/(asce)mt.1943-5533.0000223

IPC Global. (2015). AUSTRACK -Accelerated Pavement Tester

Iranian National Standardization Organization. (2013). *Hot Mix Asphalt Recycling – Code of Practice*

JUNG, S. H. *The effects of asphalt binder oxidation on hot mix asphalt concrete mixture rheology and fatigue performance.* Doctor of Philosophy Texas A&M University

Kandhal, P. S., & Foo, K. Y. (1997). Designing Recycled Hot Mix Asphalt using Superpave Technology. *ASTM SPecial Technical Publication, 1322*

Kandhal, P. S., & Mallick, R. B. (1997). *Pavement Recycling Guidelines for State and Local Governments Participant's Reference Book* (FHWA-SA-98-042).

Kim, Y. R., Underwood, B., Sakhaei Far, M., Jackson, N., & Puccinell, J. (2011). *LTPP Computed Parameter: Dynamic Modulus*.

Kodippily, S., Holleran, G., Holleran, I., Wilson, D., & Henning, T. F. (2014). Laboratory performance of recycled asphalt pavement mixes: The New Zealand experience. *Road & Transport Research: A Journal of Australian and New Zealand Research and Practice, 23*(3)

Lee, H. S., Kim, S., & Choubane, B. (2011). *Construction Of Dynamic Modulus Master Curves Using Resilient Modulus and Creep Test Data* (FL/DOT/SMO/11-544).

Lee, J., Denneman, E., & Choi, Y. (2015). *AP-T286-15 Maximising the Re-use of Reclaimed Asphalt Pavement - Outcomes of Year Two: RAP Mix Design* (AP-T286-15). Austroads.

Li, J., Zofka, A., & Yut, I. (2012). Evaluation of dynamic modulus of typical asphalt mixtures in Northeast US Region. *Road Materials and Pavement Design, 13*(2), 249-265. http://dx.doi.org/10.1080/14680629.2012.666641

LI, Q., Xiao, D. X., Wang, K. C. P., Hall, K. D., & Qiu, Y. (2011). Mechanistic-empirical pavement design guide (MEPDG): a bird's-eye view. *Journal of Modern Transportation, 19* http://dx.doi.org/10.3969/j.issn.2095-087X.2011.02.007

Liske, T., Kass, S., Barton, M., Sebaaly, P. E., Hajj, E. Y., & Loria, L. (2011). Performance Evaluation of Asphalt Mixtures with High Recycled Asphalt Pavement Content. *Transportation Research Record: Journal of the Transportation Research Board, 2208*(-1), 72-81. http://dx.doi.org/10.3141/2208-10

Loria-Salazar, L. G. (2011). *Evaluation of New and Existing Test Methods to Assess Recycled Asphalt Pavement Properties for Mix Design*. Doctor of Philosophy University of Nevada, Reno

Main Roads Western Australia. (2010). *Engineering Road Note 9-Procedure For The Design Of Flexible Pavements*

Main Roads Western Australia. (2011a). *Asphalt Mix Design*

Main Roads Western Australia. (2011b). *Bitumen Content And Particle Size Distribution Of Asphalt And Stabilised Soil: Centrifuge Method*

Main Roads Western Australia. (2011c). *Maximum Density Of Asphalt - Rice Method*

Main Roads Western Australia. (2011d). *Specification 510- Full Depth Asphalt Pavement*

Main Roads Western Australia. (2012). *Bulk Density And Void Content Of Asphalt*

Main Roads Western Australia. (2013). *Specification 504- Asphalt Wearing Course*

Main Roads Western Australia. (2014). *Specification 510 Asphalt Intermediate Course*

Main Roads Western Australia. (2015). *Specification 504 Asphalt Wearing Course*

Main Roads Western Australia. (2016). *Stability And Flow Of Asphalt: Marshall Method*

McDaniel, R. S., & Anderson, R. M. (2001). *NCHRP Report 452-Recommended Use of Reclaimed Asphalt Pavement in the Superpave Mix Design Method: Technician's Manual*.

McDaniel, R. S., & Shah, A. (2003). Use of Reclaimed Asphalt Pavement (RAP) Under Superpave Specifications *Journnal of Association of Asphalt Paving Technologists(AAPT),*

McDaniel, R. S., Soleymani, H., Anderson, R. M., Turner, P., & Peterson, R. (2000). *Recommended Use of Reclaimed Asphalt Pavement in the Superpave Mix Design Method- Project D9-12: Contractors final report*.

Medani, T. O., & Huurman, M. *Constructing the Stiffness Master Curves for Asphaltic Mixes*. D. U. o. Technology.

Missouri Highway And Transportation Department. (1982). *Evaluation Of A Recycled Asphaltic Concrete Pavement* (39). Federal Highway Administration (FHWA).

National Asphalt Pavement Association (NAPA). (2007). *Recycling Hot-Mix Asphalt Pavements*.

National Asphalt Pavement Association (NAPA). (2009). *How to increase RAP usage and ensure pavement performance* [Brochure].

Neumann, P. M., & Somasundaraswaran, K. (2014). Evaluation Of Strength Characteristics Of Recycled Asphalt Pavement Materials*26th ARRB Conference held in Sydney, NSW*: Australian Road Research Board (ARRB).

Newcomb, D. E., Brown, E. R., & A.Epps, J. (2007). *Designing HMA mixtures with high rap content-A practical guide*: National Asphalt Pavement Association (NAPA).

NSAI. (2006). *I.S. EN 13108-1:2006-BITUMINOUS MIXTURES - MATERIAL SPECIFICATIONS - PART 1: ASPHALT CONCRETE*

NSAI. (2013). *EN12697-3-2013-Bituminous mixtures - Test methods for hot mix asphalt - Part 3: Bitumen recovery: Rotary evaporator*

Oliver, J., & Luke, R. (2004). *AP-R256-04 Changes to the Austroads Mix Design Procedure to incorporate Recycled Asphalt*. Austroad.

Pereira, P. A. A., Oliveira, J. R. M., & Picado-Santos, L. G. (2004). Mechanical Characterisation of Hot Mix Recycled Materials. *International Journal of Pavement Engineering, 5*(4), 211-220. http://dx.doi.org/10.1080/10298430412331333668

Petersen, J. C., Robertson, R. E., Branthaver, J. F., Harnsberger, P. M., Duvall, J. J., KIM, S. S., . . . Bahia, H. U. (1994). *SHRP A-367: Binder Characterization and evaluation-Vol1*.

Petersen, J. C., Robertson, R. E., Branthaver, J. F., Harnsberger, P. M., Duvall, J. J., KIM, S. S., . . . Glover, C. J. (1994). *SHRP A-370: Binder Characterization and evaluation-Vol4*.

Pradyumna, T. A., Mittal, A., & Jain, P. K. (2013). Characterization of Reclaimed Asphalt Pavement (RAP) for Use in Bituminous Road Construction. *Procedia - Social and Behavioral Sciences, 104*, 1149-1157. http://dx.doi.org/10.1016/j.sbspro.2013.11.211

Qin, Q., Schabron, J. F., Boysen, R. B., & Farrar, M. J. (2014). Field aging effect on chemistry and rheology of asphalt binders and rheological predictions for field aging. *Fuel, 121*, 86-94. http://dx.doi.org/10.1016/j.fuel.2013.12.040

Read, J., & Whiteoak, D. (2003). Shell Bitumen Handbook (5th Edition). (ICE Publishing).

Rebbechi, J. (2006). *AP-T66-06-Asphalt Recycling*. Austroads.

Schramm, G. (1998). *A practical approach to rheology and rhometry* (2nd ed.). Germany: Gebrueder HAAKE GmbH.

Shahadan, Z., Hamzah, M. O., Yahya, A. S., & Jamshidi, A. (2013). Evaluation of the dynamic modulus of asphalt mixture incorporating reclaimed. *Indian Journal of Engineering & Materials Sciences 20*, 376-384.

Shen, J., Amirkhanian, S., & Tang, B. (2007). Effects of rejuvenator on performance-based properties of rejuvenated asphalt binder and mixtures. *Construction and Building Materials, 21*(5), 958-964. http://dx.doi.org/10.1016/j.conbuildmat.2006.03.006

Shen, S., Airey, G. D., Carpenter, S. H., & Huang, H. (2006). A Dissipated Energy Approach to Fatigue Evaluation. *Road Materials and Pavement Design, 7*(1), 47-69. http://dx.doi.org/10.1080/14680629.2006.9690026

SHRP. (1994). *Superior Performing Asphalt Pavements (Superpave)'. The Product of the SHRP Asphalt Research Program*

Shu, X., Huang, B., & Vukosavljevic, D. (2008). Laboratory evaluation of fatigue characteristics of recycled asphalt mixture. *Construction and Building Materials, 22*(7), 1323-1330. http://dx.doi.org/10.1016/j.conbuildmat.2007.04.019

Silva, H. M. R. D., Oliveira, J. R. M., & Jesus, C. M. G. (2012). Are totally recycled hot mix asphalts a sustainable alternative for road paving? *Resources, Conservation and Recycling, 60*, 38-48. http://dx.doi.org/10.1016/j.resconrec.2011.11.013

Solaimanian, M., Harvey, J., Tahmoressi, M., & Tandon, V. (2003). Test Methods to Predict Moisture Sensitivity of Hot-Mix Asphalt Pavements*Transportation Research Board National Seminar. San Diego, California, held in*

Sondag, M. S., Chadbourn, B. A., & Drescher, A. (2002). *Investigation Of Recycled Asphalt Pavement (RAP) Mixtures* (MN/RC – 2002-15). M. D. o. Transportation.

Su, K., Hachiya, Y., & Maekawa, R. (2009). Study on recycled asphalt concrete for use in surface course in airport pavement. *Resources, Conservation and Recycling, 54*(1), 37-44. http://dx.doi.org/10.1016/j.resconrec.2009.06.003

Sullivan, J. (1996). *Pavement Recycling Executive Summary And Report* (FHWA-SA-95-060).

Tarbox, S., & Daniel, J. S. (2012). Effects of Long-Term Oven Aging on Reclaimed Asphalt Pavement Mixtures. *Transportation Research Record: Journal of the Transportation Research Board, 2294*(-1), 1-15. http://dx.doi.org/10.3141/2294-01

Texas Department of Transportation. (2014). *Calculating Viscosty from Penetration* (Tex-535-C).

Timm, D. H., & Robbins, M. M. (2011). Evaluation of Dynamic Modulus Predictive Equations for Southeastern United States Asphalt Mixtures. *Transportation Research Record: Journal of the Transportation Research Board, 2210*(-1), 122-129. http://dx.doi.org/10.3141/2210-14

West, R., Willis, J. R., & Marasteanu, M. (2013). *Improved Mix Design, Evaluation, and Materials Management Practices for Hot Mix Asphalt with High Reclaimed Asphalt Pavement Content* (752).

Widyatmoko, I. (2008). Mechanistic-empirical mixture design for hot mix asphalt pavement recycling. *Construction and Building Materials, 22*(2), 77-87. http://dx.doi.org/10.1016/j.conbuildmat.2006.05.041

Witczak, M. (2005). *NCHRP 547- Simple Performance Tests: Summary of Recommended Methods and Database*.

Yousefdoost, S., Vuong, B., Rickards, I., Armstrong, P., & Sullivan, B. (2013). Evaluation of Dynamic Modulus Predictive Models for Typical Australian Asphalt Mixes*15th APAA International Flexible Pavement Conference, held in Brisbane, Australia,*

Yusoff, N. I. M., Chailleux, E., & Airey, G. D. (2011). A Comparative Study of the Influence of Shift Factor Equations on Master Curve Construction. *International Journal of Pavement Research and Technology, 4*(6)

Yusoff, N. I. M., Jakarni, F. M., Nguyen, V. H., Hainin, M. R., & Airey, G. D. (2013). Modelling the rheological properties of bituminous binders

using mathematical equations. *Construction and Building Materials*, *40*, 174-188. http://dx.doi.org/10.1016/j.conbuildmat.2012.09.105

Every reasonable effort has been made to acknowledge the owners of copyright material. I would be pleased to hear from any copyright owner who has been omitted or incorrectly acknowledged.

Appendices

Appendix I. Results of sieve analysis for stockpiles

	%Pass from sieves for each stockpile (S1= Sample 1, S2=Sample2)													
	Dust		5 mm		7 mm (i)		7 mm (ii)		10mm		14 mm		20 mm	
Sieve Size(mm)	S1*	S2*	S1*	S2*	S1*	S2*	S1*	S2*	S1*	S2*	S1*	S2*	S1*	S2*
26.5	100	100	100	100	100	100	100	100	100	100	100	100	100	100
19.0	100	100	100	100	100	100	100	100	100	100	100	100	97.0	94.7
13.2	100	100	100	100	100	100	100	100	100	100	88.8	88.6	32.5	32.3
9.5	100	100.0	100	100	100	99.0	100	100	80.7	82.9	15.1	14.9	7.9	8.2
6.7	100	100.0	100	100	85.7	86.8	87	88.7	13.4	17.2	2.2	2.4	4.3	4.2
4.8	99.8	99.6	86.4	86.6	23.2	25.8	28.1	30.3	1.9	3.2	1.5	1.5	3.2	3.2
2.4	78.2	78.8	19.5	19.2	1.6	2.7	5.3	4.5	1.3	1.8	1.3	1.3	2.6	2.4
1.2	53.1	54.1	8.7	8.7	0.8	1.5	3.5	2.4	1.2	1.7	1.3	1.3	2.3	2.1
0.6	35.7	36.9	6.1	6.2	0.7	1.2	2.8	1.6	1.2	1.5	1.2	1.2	2.1	1.9
0.3	23.6	24.5	5.0	5.1	0.6	1.1	2.4	1.1	1.1	1.4	1.0	1.0	1.9	1.7
0.2	14.6	15.3	4.1	4.1	0.6	0.9	2.1	0.8	1.0	1.2	0.9	0.9	1.6	1.4
0.1	9.7	10.2	3.1	3.1	0.5	0.8	1.7	0.4	0.8	1.0	0.7	0.7	1.3	1.1

Appendix II. Result of binder content and sieve analysis for RAP

	% Pass	
Sieve Size(mm)	Sampe1	Sample2
26.5	100.0	100.0
19.0	100.0	100.0
13.2	100.0	99.7
9.50	93.8	93.8
6.70	77.9	76.7
4.75	61.8	61.4
2.36	41.6	40.0
1.18	32.1	30.6
0.600	25.2	24.0
0.300	17.0	16.4
0.150	9.9	9.8
0.075	6.3	6.2

Binder Content	**4.10**	**4.0**

Appendix III. Result of binder content and particle size distribution verification for each mixture

DG14R0

DG14R0						
	Result 1	Result 2	Average	Target	Variance	Tolerance
Bitumen Content	4.67	4.57	4.62	4.70	-0.08	0.10

	%Pass					
Sieve(mm)	Result 1	Result 2	Average	Target	Variance	Tolerance
26.50	100.00	100.00	100.00	100.00	0.00	2.00
19.00	100.00	100.00	100.00	100.00	0.00	2.00
13.20	97.40	98.30	97.85	98.28	-0.43	2.00
9.50	84.60	83.00	83.80	83.86	-0.06	2.00
6.70	68.70	67.90	68.30	68.39	-0.09	2.00
4.75	54.70	54.40	54.55	54.03	0.52	2.00
2.36	36.90	36.50	36.70	35.86	0.84	2.00
1.18	24.68	24.50	24.59	24.11	0.48	1.00
0.60	17.09	17.01	17.05	16.37	0.68	1.00
0.30	11.70	11.63	11.67	10.96	0.70	1.00
0.15	7.13	7.09	7.11	6.88	0.23	1.00
0.08	4.78	4.74	4.76	4.48	0.28	0.50

DG14R10

DG14R10						
	Result 1	Result 2	Average	Target	Variance	Tolerance
Bitumen Content(%)	4.71	4.73	4.72	4.70	0.02	0.10

	%Pass					
Sieve(mm)	Result 1	Result 2	Average	Target	Variance	Tolerance
26.50	100.00	100.00	100.00	100.00	0.00	2.00
19.00	100.00	100.00	100.00	100.00	0.00	2.00
13.20	97.45	97.69	97.57	98.28	-0.71	2.00
9.50	83.05	86.84	84.95	83.86	1.09	2.00
6.70	66.32	72.22	69.27	68.39	0.88	2.00
4.75	52.87	57.07	54.97	54.03	0.93	2.00
2.36	36.14	38.01	37.07	35.86	1.21	2.00
1.18	24.74	25.37	25.05	24.11	0.94	1.00
0.60	17.15	17.45	17.30	16.37	0.93	1.00
0.30	11.70	11.89	11.79	10.96	0.83	1.00
0.15	7.30	7.38	7.34	6.88	0.46	1.00
0.08	3.86	4.75	4.31	4.48	-0.17	0.50

DG14R20

DG14R20						
	Result 1	Result 2	Average	Target	Variance	Tolerance
Bitumen Content(%)	4.67	4.68	4.68	4.70	-0.03	0.10

	% Pass					
Sieve(mm)	Result 1	Result 2	Average	Target	Variance	Tolerance
26.50	100.00	100.00	100.00	100.00	0.00	2.00
19.00	100.00	100.00	100.00	100.00	0.00	2.00
13.20	98.50	98.40	98.45	98.28	0.17	2.00
9.50	83.56	84.50	84.03	83.86	0.17	2.00
6.70	68.09	69.30	68.69	68.39	0.30	2.00
4.75	53.83	55.00	54.41	54.03	0.38	2.00
2.36	35.66	36.20	35.93	35.86	0.07	2.00
1.18	24.51	24.40	24.45	24.11	0.34	1.00
0.60	16.99	17.00	17.00	16.37	0.62	1.00
0.30	11.58	11.60	11.59	10.96	0.63	1.00
0.15	7.34	7.30	7.32	6.88	0.44	1.00
0.08	4.80	4.90	4.85	4.48	0.37	0.50

DG14R30

DG14R30						
	Result 1	Result 2	Average	Target	Variance	Tolerance
Bitumen Content(%)	4.64	4.78	4.71	4.70	0.01	0.10

	% Pass					
Sieve(mm)	Result 1	Result 2	Average	Target	Variance	Tolerance
26.50	100.00	100.00	100.00	100.00	0.00	2.00
19.00	100.00	100.00	100.00	100.00	0.00	2.00
13.20	97.80	98.60	98.20	98.28	-0.08	2.00
9.50	79.80	85.70	82.75	83.86	-1.11	2.00
6.70	63.80	71.20	67.50	68.39	-0.89	2.00
4.75	50.50	56.00	53.25	54.03	-0.78	2.00
2.36	33.70	36.80	35.25	35.86	-0.61	2.00
1.18	23.22	25.09	24.16	24.11	0.04	1.00
0.60	16.06	17.45	16.76	16.37	0.38	1.00
0.30	10.87	11.92	11.40	10.96	0.43	1.00
0.15	6.84	7.66	7.25	6.88	0.37	1.00
0.08	4.66	5.32	4.99	4.48	0.51	0.50

DG20R0

DG20R0						
	Result 1	Result 2	Average	Target	Variance	Tolerance
Bitumen Content(%)	4.30		4.30	4.30	0.00	0.10

	% Pass					
Sieve(mm)	Result 1	Result 2	Average	Target	Variance	Tolerance
26.50	100.00		100.00	100.00	0.00	2.00
19.00	99.50		99.50	99.00	0.50	2.00
13.20	80.30		80.30	82.00	-1.70	2.00
9.50	69.70		69.70	71.00	-1.30	2.00
6.70	54.20		54.20	55.00	-0.80	2.00
4.75	43.70		43.70	45.00	-1.30	2.00
2.36	32.30		32.30	33.00	-0.70	2.00
1.18	22.50		22.50	23.00	-0.50	1.00
0.60	16.93		16.93	17.00	-0.07	1.00
0.30	12.04		12.04	12.00	0.04	1.00
0.15	8.07		8.07	8.50	-0.43	1.00
0.08	4.73		4.73	4.50	0.23	0.50

DG20R10

DG20R10						
	Result 1	Result 2	Average	Target	Variance	Tolerance
Bitumen Content(%)	4.27	4.25	4.26	4.30	-0.04	0.10

	% Pass					
Sieve(mm)	Result 1	Result 2	Average	Target	Variance	Tolerance
26.50	100.00	100.00	100.00	100.00	0.00	2.00
19.00	98.20	98.70	98.45	99.00	-0.55	2.00
13.20	79.30	83.10	81.20	82.00	-0.80	2.00
9.50	70.80	73.20	72.00	71.00	1.00	2.00
6.70	56.70	54.80	55.75	55.00	0.75	2.00
4.75	47.10	44.40	45.75	45.00	0.75	2.00
2.36	34.20	32.60	33.40	33.00	0.40	2.00
1.18	23.18	22.64	22.91	23.00	-0.09	1.00
0.60	17.19	16.88	17.04	17.00	0.04	1.00
0.30	12.22	12.00	12.11	12.00	0.11	1.00
0.15	8.17	8.07	8.12	8.50	-0.38	1.00
0.08	4.97	4.88	4.93	4.50	0.43	0.50

DG20R20

DG20R20						
	Result 1	Result 2	Average	Target	Variance	Tolerance
Bitumen Content(%)	4.10	4.33	4.22	4.30	-0.09	0.10

	% Pass					
Sieve(mm)	Result 1	Result 2	Average	Target	Variance	Tolerance
26.50	100.00	100.00	100.00	100.00	0.00	2.00
19.00	99.40	99.37	99.38	99.00	0.38	2.00
13.20	78.00	83.73	80.87	82.00	-1.13	2.00
9.50	68.70	75.19	71.95	71.00	0.95	2.00
6.70	51.30	59.00	55.15	55.00	0.15	2.00
4.75	41.80	49.13	45.47	45.00	0.47	2.00
2.36	31.10	35.55	33.33	33.00	0.33	2.00
1.18	21.68	24.13	22.91	23.00	-0.09	1.00
0.60	16.07	17.73	16.90	17.00	-0.10	1.00
0.30	11.53	12.68	12.11	12.00	0.11	1.00
0.15	7.98	8.74	8.36	8.50	-0.14	1.00
0.08	4.80	5.10	4.95	4.50	0.45	0.50

DG20R30

DG20R30						
	Result 1	Result 2	Average	Target	Variance	Tolerance
Bitumen Content(%)	4.31	4.20	4.26	4.30	-0.04	0.10

	% Pass					
Sieve(mm)	Result 1	Result 2	Average	Target	Variance	Tolerance
26.50	100.00	100.00	100.00	100.00	0.00	2.00
19.00	98.90	99.20	99.05	99.00	0.05	2.00
13.20	84.93	76.24	80.59	82.00	-1.41	2.00
9.50	74.89	67.40	71.15	71.00	0.15	2.00
6.70	59.27	53.07	56.17	55.00	1.17	2.00
4.75	48.24	43.49	45.87	45.00	0.87	2.00
2.36	34.29	31.77	33.03	33.00	0.03	2.00
1.18	23.24	21.84	22.54	23.00	-0.46	1.00
0.60	17.09	16.15	16.62	17.00	-0.38	1.00
0.30	12.14	11.57	11.85	12.00	-0.15	1.00
0.15	8.35	8.02	8.18	8.50	-0.32	1.00
0.08	5.00	4.90	4.95	4.50	0.45	0.50

Appendix IV. Master curves for 14 mm mixtures at 4°C

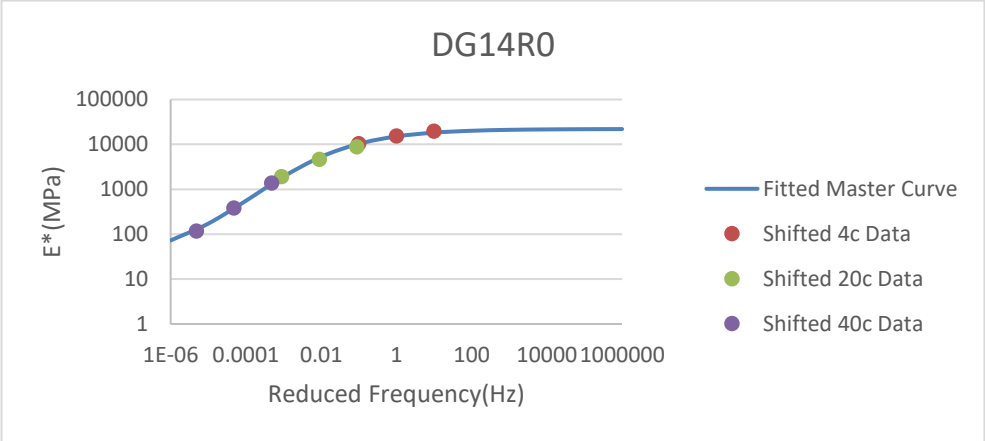

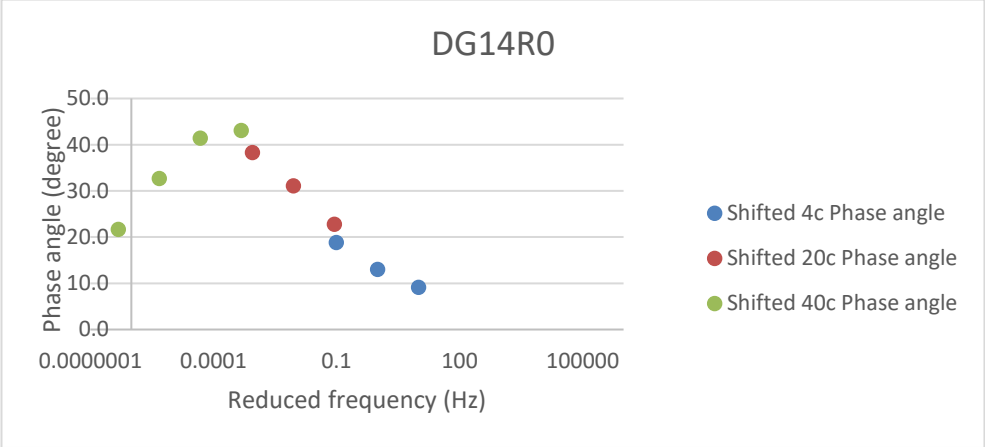

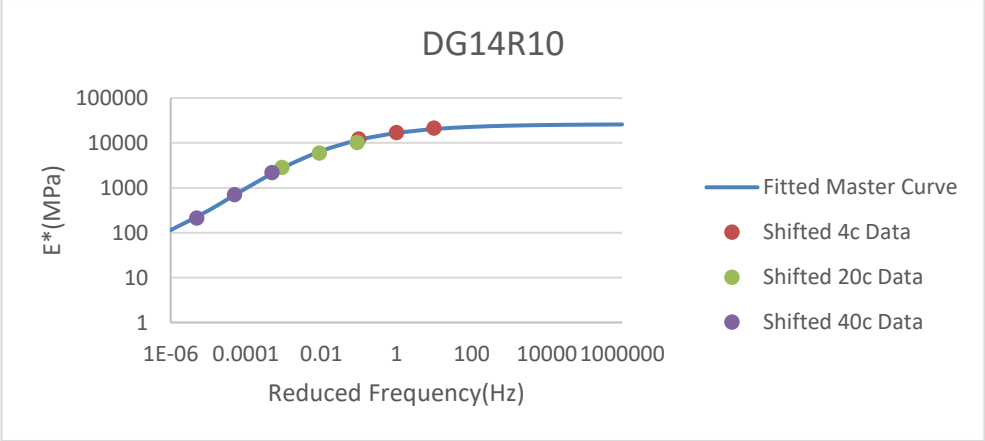

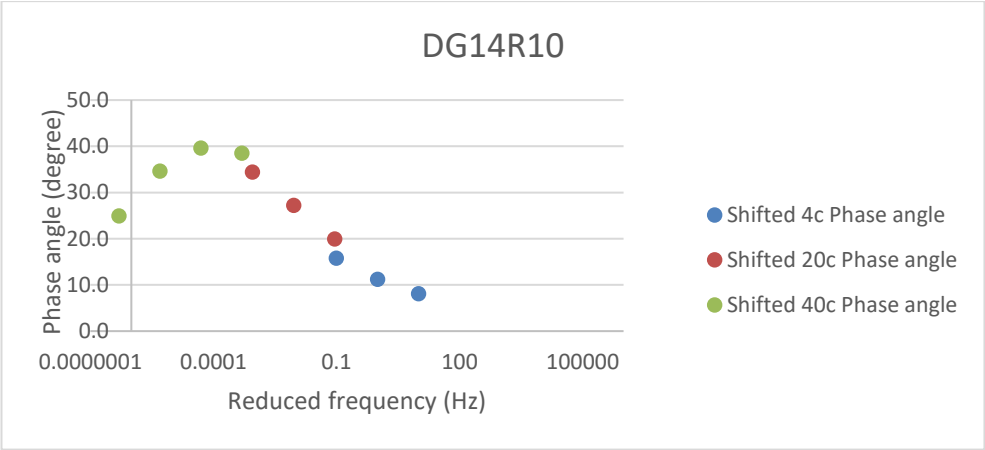
DG14R10
Phase angle (degree)
50.0
40.0
30.0
20.0
10.0
0.0
0.0000001
0.0001
0.1
100
100000
Reduced frequency (Hz)
Shifted 4c Phase angle
Shifted 20c Phase angle
Shifted 40c Phase angle

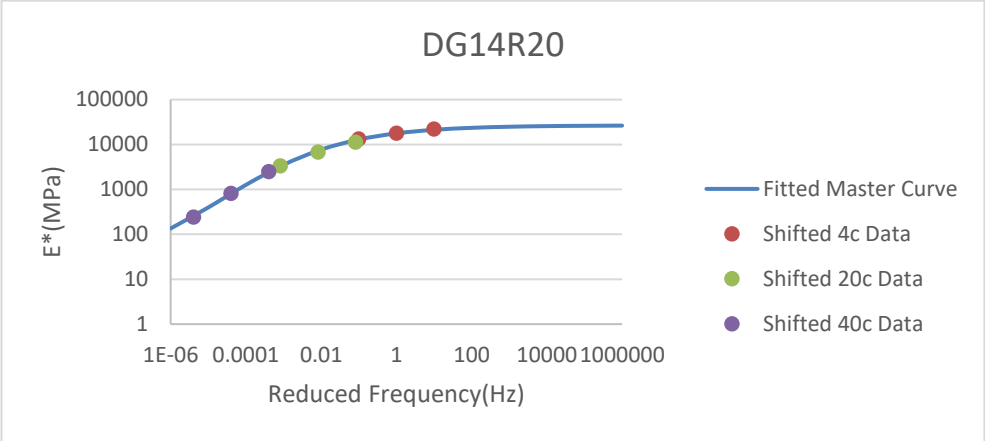
DG14R20
E*(MPa)
100000
10000
1000
100
10
1
1E-06
0.0001
0.01
1
100
10000
1000000
Reduced Frequency(Hz)
Fitted Master Curve
Shifted 4c Data
Shifted 20c Data
Shifted 40c Data

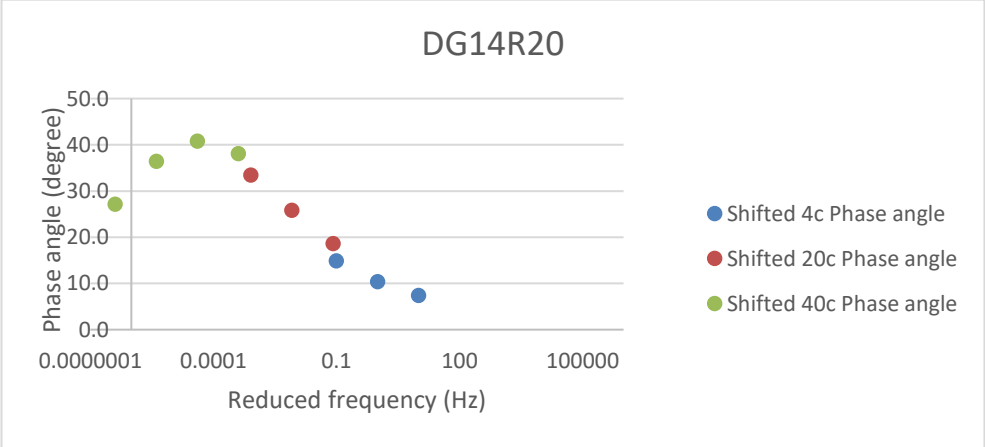
DG14R20
Phase angle (degree)
50.0
40.0
30.0
20.0
10.0
0.0
0.0000001
0.0001
0.1
100
100000
Reduced frequency (Hz)
Shifted 4c Phase angle
Shifted 20c Phase angle
Shifted 40c Phase angle

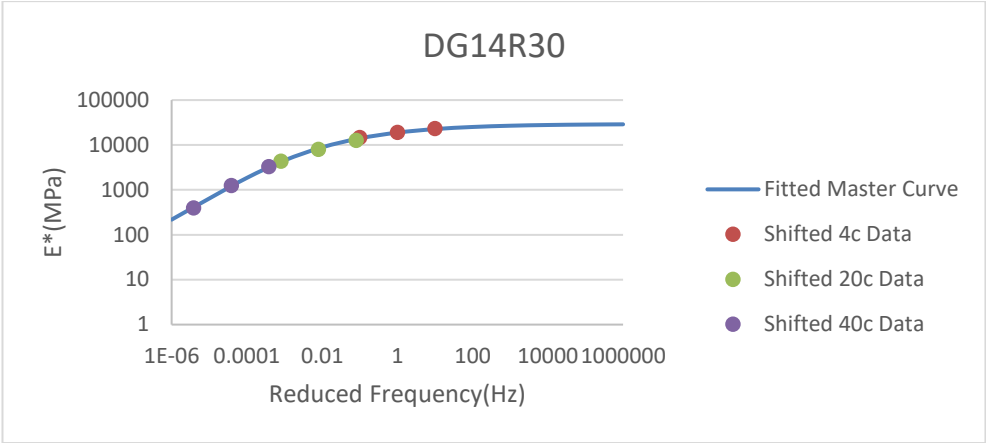
DG14R30
100000
10000
1000
100
10
1
E*(MPa)
1E-06
0.0001
0.01
1
100
10000
1000000
Reduced Frequency(Hz)
Fitted Master Curve
Shifted 4c Data
Shifted 20c Data
Shifted 40c Data

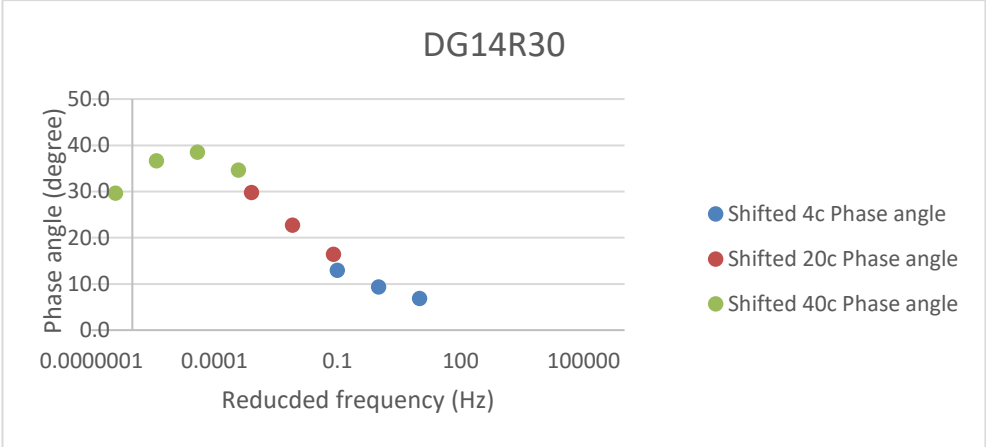
DG14R30
50.0
40.0
30.0
20.0
10.0
0.0
Phase angle (degree)
0.0000001
0.0001
0.1
100
100000
Reducded frequency (Hz)
Shifted 4c Phase angle
Shifted 20c Phase angle
Shifted 40c Phase angle

Appendix V. Master curves for 14 mm mixtures at 40°C

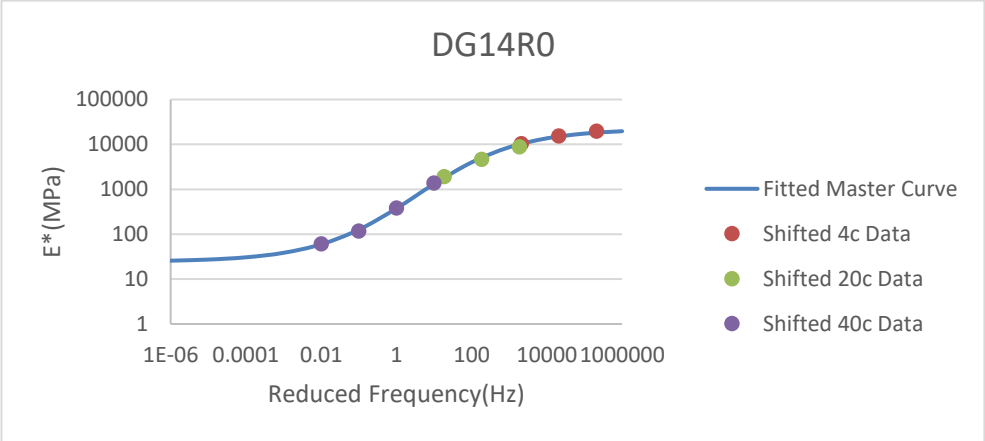

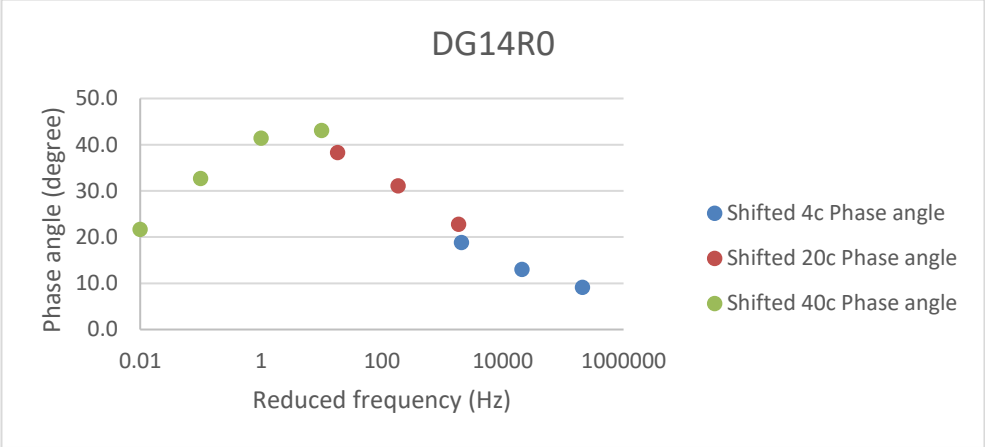

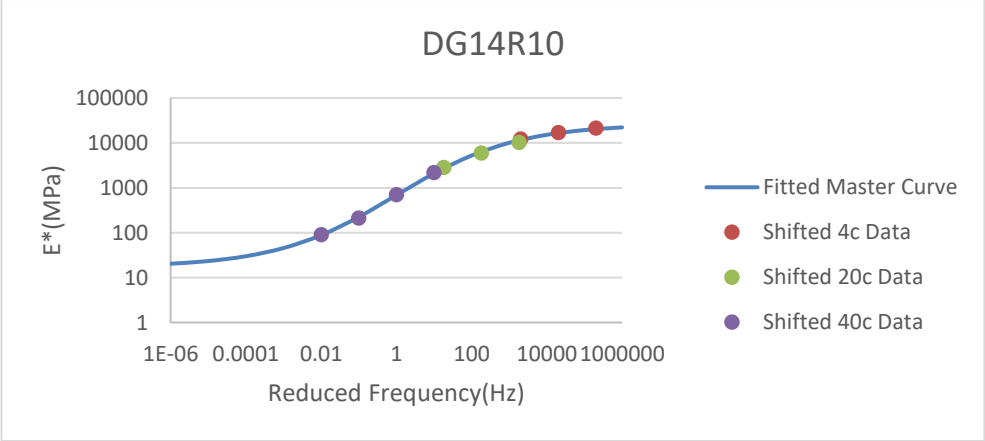

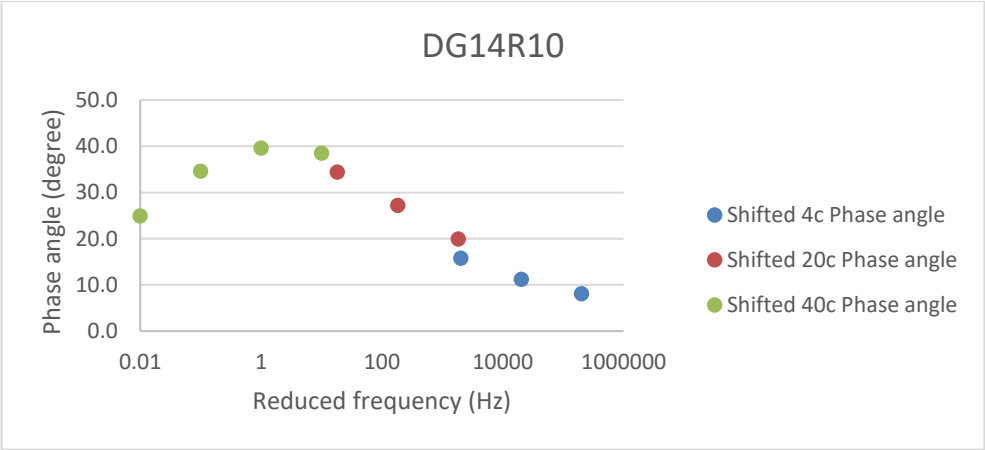
DG14R10
Phase angle (degree)
50.0
40.0
30.0
20.0
10.0
0.0
0.01
1
100
10000
1000000
Reduced frequency (Hz)
Shifted 4c Phase angle
Shifted 20c Phase angle
Shifted 40c Phase angle

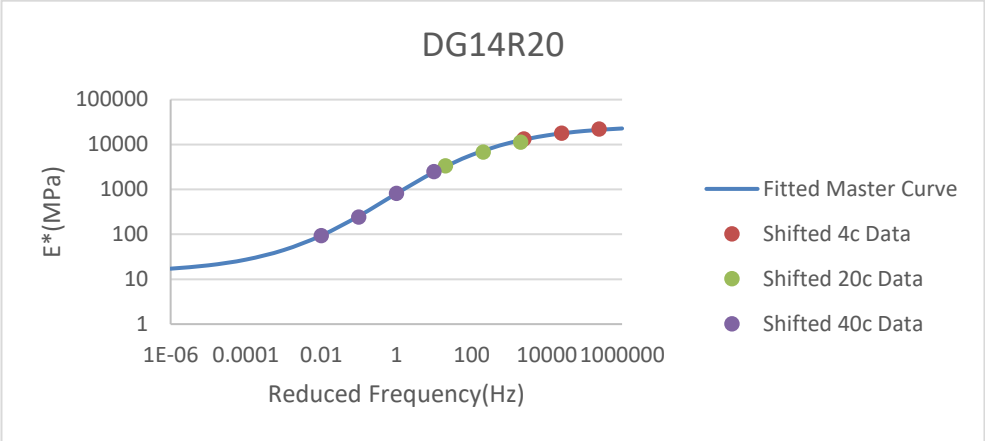
DG14R20
E*(MPa)
100000
10000
1000
100
10
1
1E-06
0.0001
0.01
1
100
10000
1000000
Reduced Frequency(Hz)
Fitted Master Curve
Shifted 4c Data
Shifted 20c Data
Shifted 40c Data

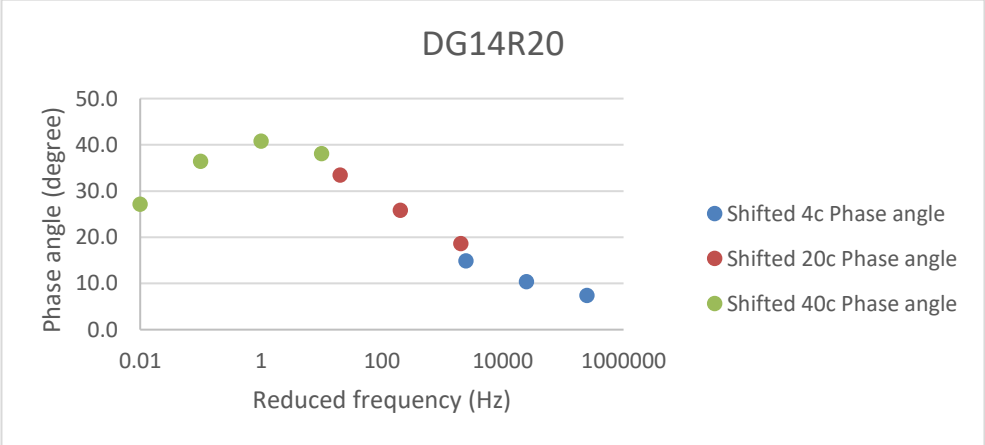
DG14R20
Phase angle (degree)
50.0
40.0
30.0
20.0
10.0
0.0
0.01
1
100
10000
1000000
Reduced frequency (Hz)
Shifted 4c Phase angle
Shifted 20c Phase angle
Shifted 40c Phase angle

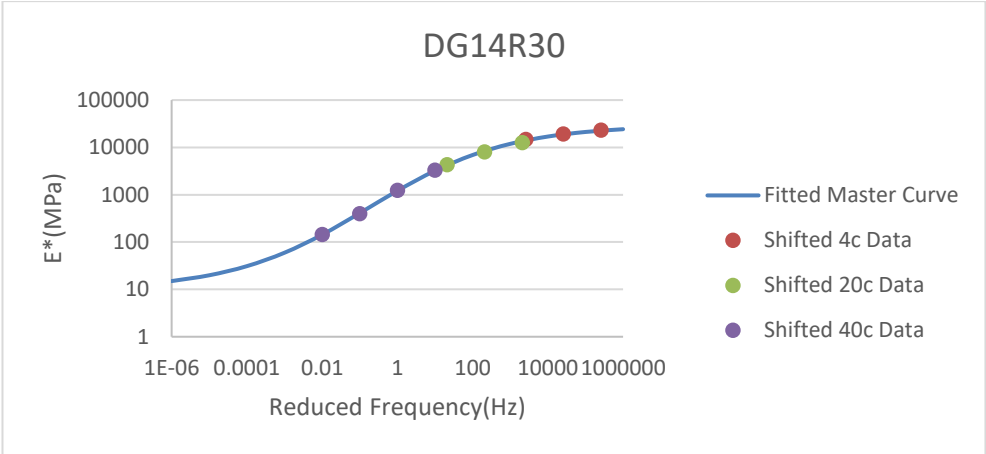
DG14R30
100000
10000
1000
100
10
1
E*(MPa)
1E-06
0.0001
0.01
1
100
10000
1000000
Reduced Frequency(Hz)
Fitted Master Curve
Shifted 4c Data
Shifted 20c Data
Shifted 40c Data

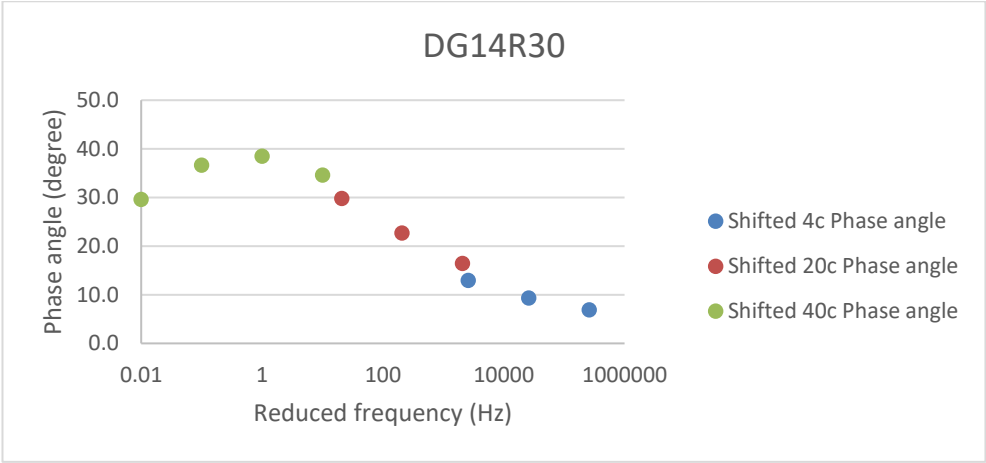
DG14R30
50.0
40.0
30.0
20.0
10.0
0.0
Phase angle (degree)
0.01
1
100
10000
1000000
Reduced frequency (Hz)
Shifted 4c Phase angle
Shifted 20c Phase angle
Shifted 40c Phase angle

Appendix VI. Master curves for 20 mm mixtures at 4°C

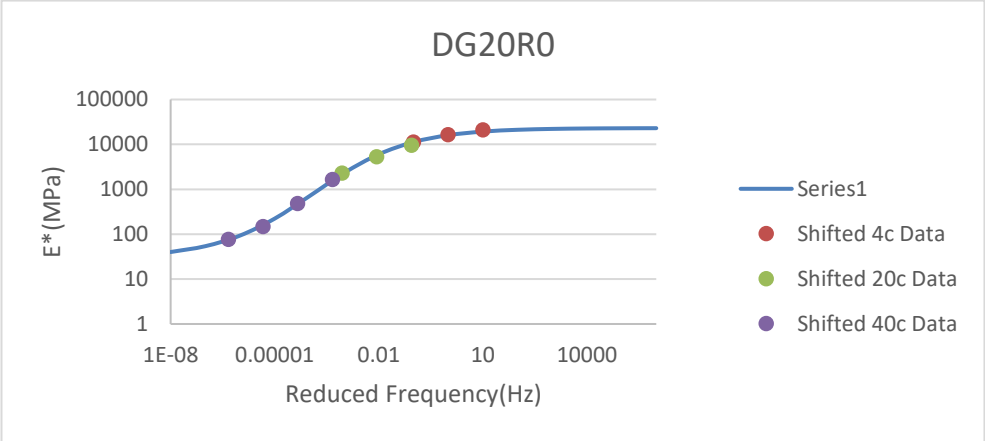

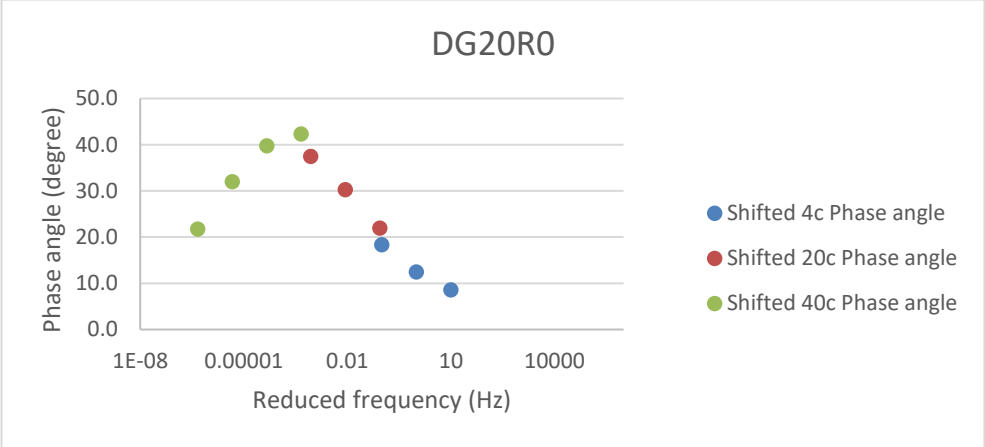

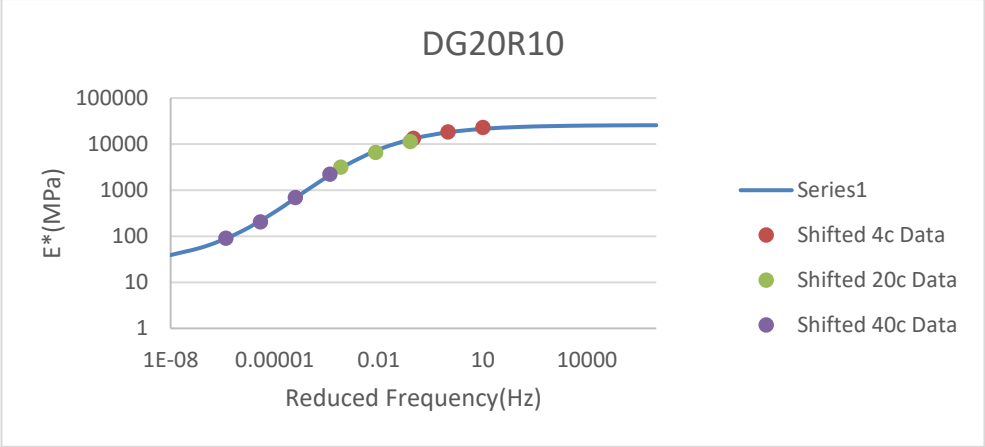

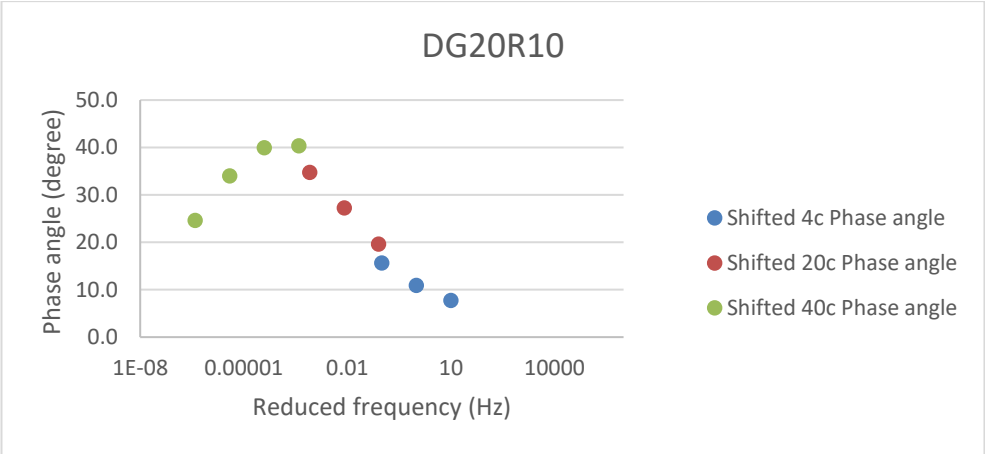
DG20R10
Phase angle (degree)
50.0
40.0
30.0
20.0
10.0
0.0
1E-08
0.00001
0.01
10
10000
Reduced frequency (Hz)
Shifted 4c Phase angle
Shifted 20c Phase angle
Shifted 40c Phase angle

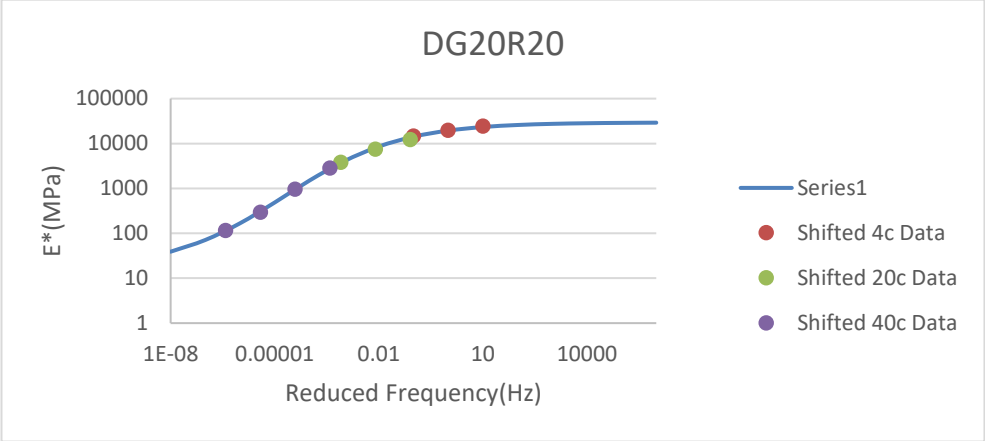
DG20R20
E*(MPa)
100000
10000
1000
100
10
1
1E-08
0.00001
0.01
10
10000
Reduced Frequency(Hz)
Series1
Shifted 4c Data
Shifted 20c Data
Shifted 40c Data

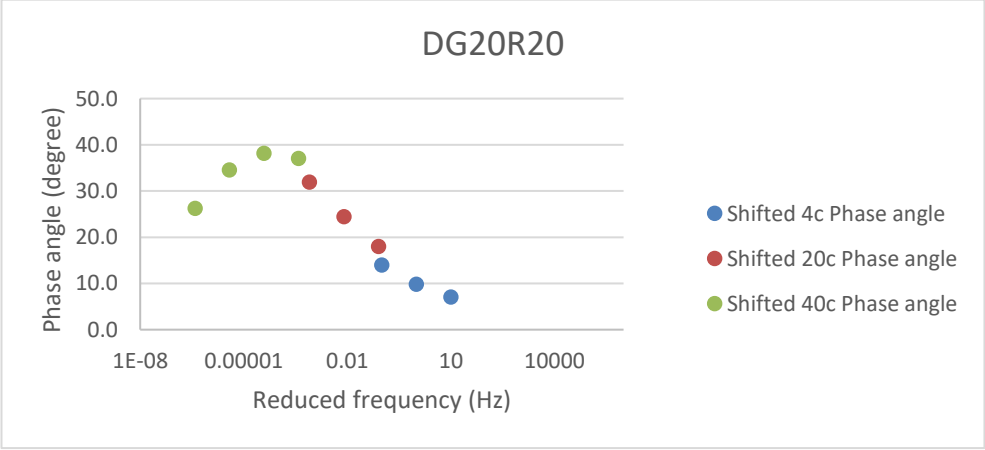
DG20R20
Phase angle (degree)
50.0
40.0
30.0
20.0
10.0
0.0
1E-08
0.00001
0.01
10
10000
Reduced frequency (Hz)
Shifted 4c Phase angle
Shifted 20c Phase angle
Shifted 40c Phase angle

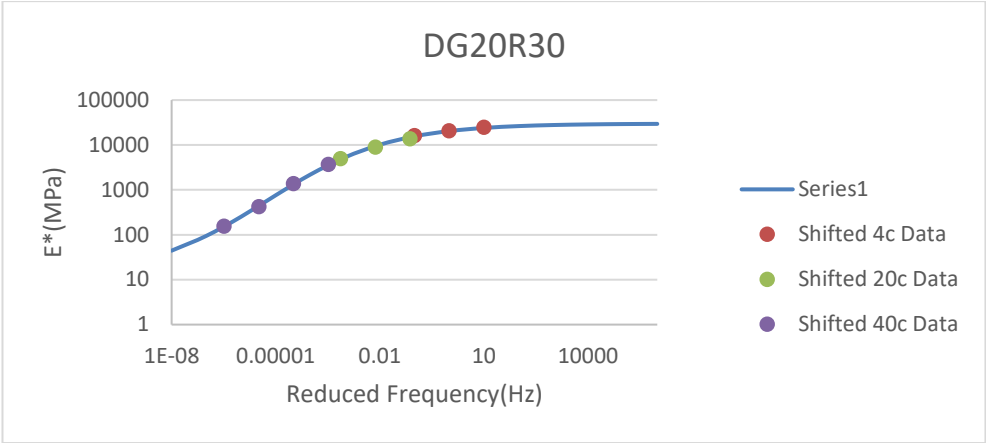
DG20R30
100000
10000
1000
100
10
1
E*(MPa)
1E-08
0.00001
0.01
10
10000
Reduced Frequency(Hz)
Series1
Shifted 4c Data
Shifted 20c Data
Shifted 40c Data

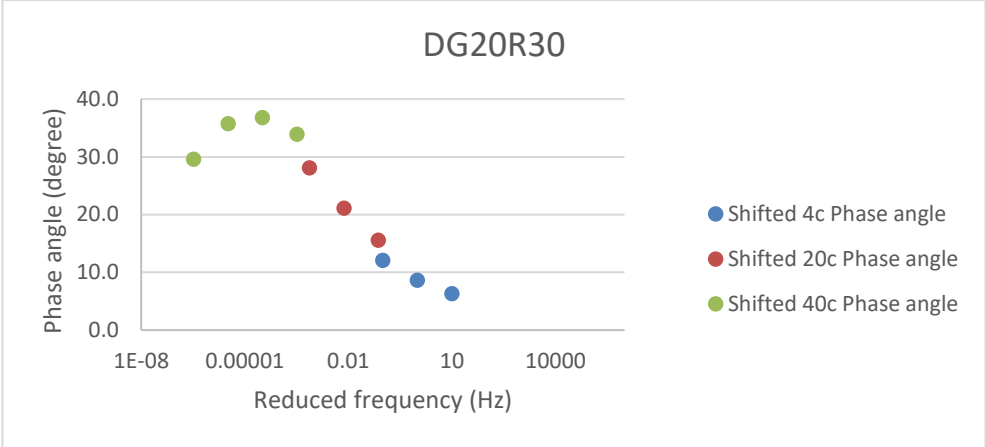
DG20R30
40.0
30.0
20.0
10.0
0.0
Phase angle (degree)
1E-08
0.00001
0.01
10
10000
Reduced frequency (Hz)
Shifted 4c Phase angle
Shifted 20c Phase angle
Shifted 40c Phase angle

Appendix VII. Master curves for 20 mm mixtures at 40°C

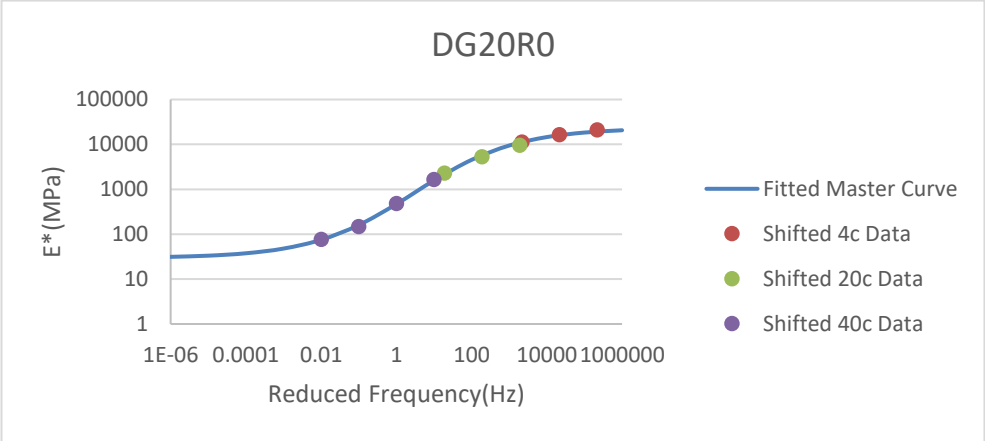

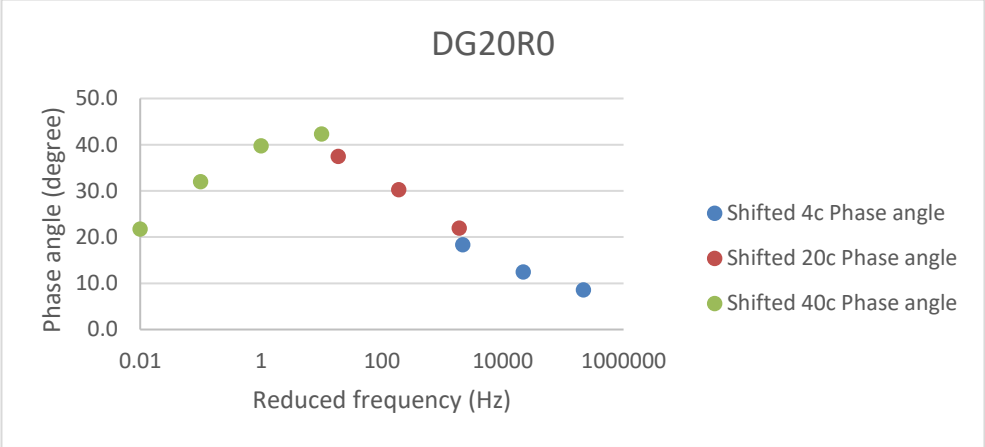

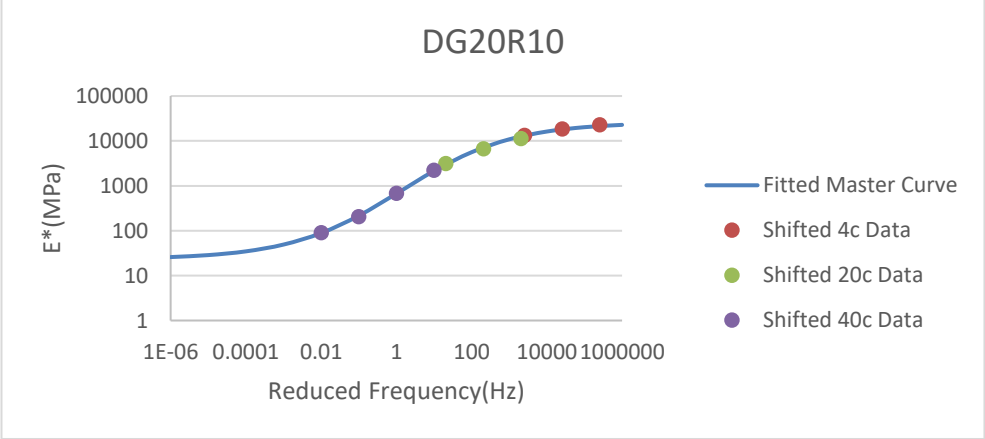

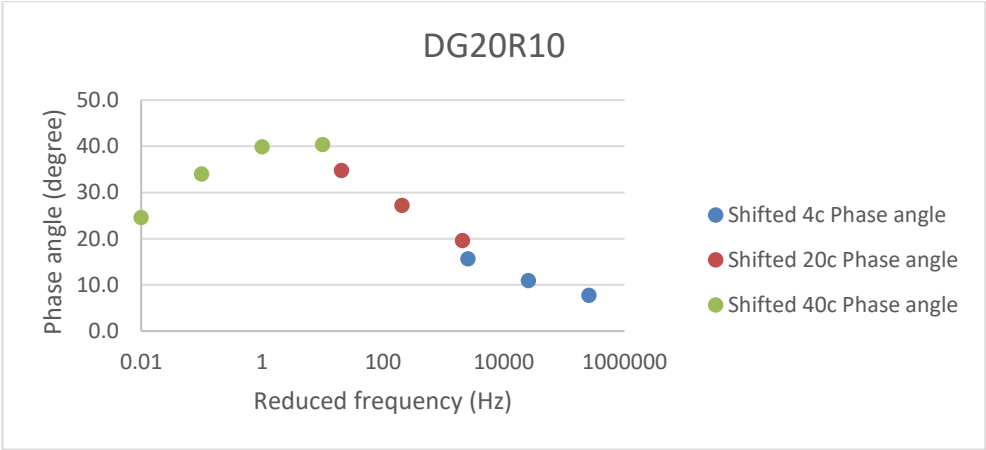
DG20R10
Phase angle (degree)
50.0
40.0
30.0
20.0
10.0
0.0
0.01
1
100
10000
1000000
Reduced frequency (Hz)
Shifted 4c Phase angle
Shifted 20c Phase angle
Shifted 40c Phase angle

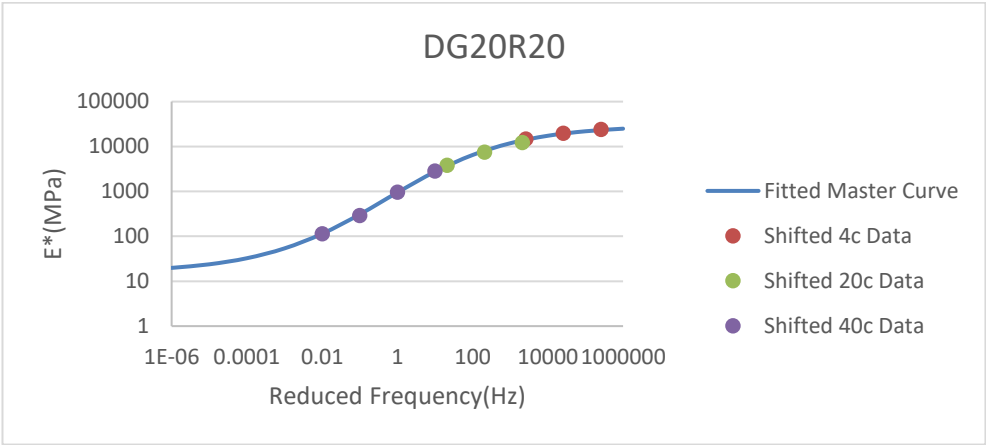
DG20R20
E*(MPa)
100000
10000
1000
100
10
1
1E-06
0.0001
0.01
1
100
10000
1000000
Reduced Frequency(Hz)
Fitted Master Curve
Shifted 4c Data
Shifted 20c Data
Shifted 40c Data

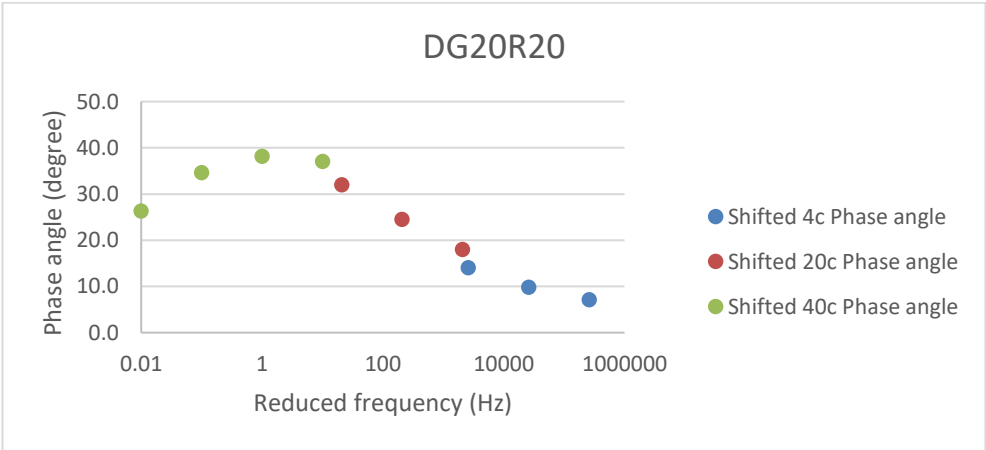
DG20R20
Phase angle (degree)
50.0
40.0
30.0
20.0
10.0
0.0
0.01
1
100
10000
1000000
Reduced frequency (Hz)
Shifted 4c Phase angle
Shifted 20c Phase angle
Shifted 40c Phase angle

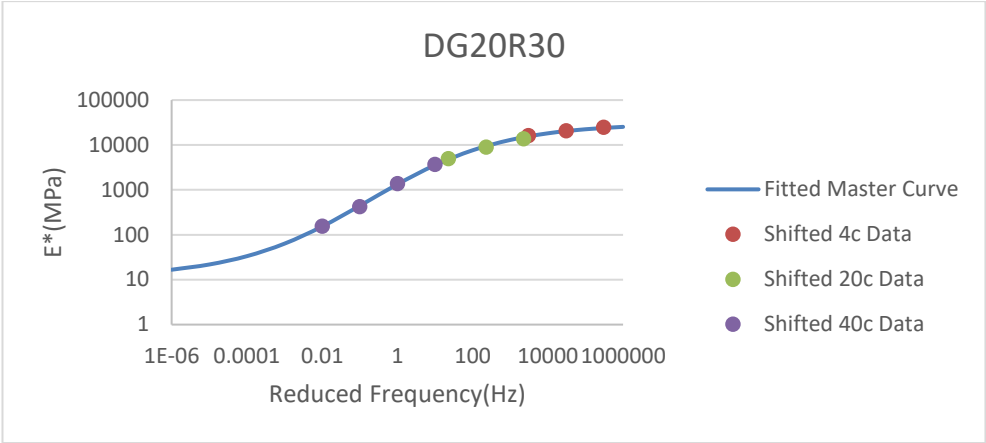
DG20R30
100000
10000
1000
100
10
1
E*(MPa)
1E-06
0.0001
0.01
1
100
10000
1000000
Reduced Frequency(Hz)
Fitted Master Curve
Shifted 4c Data
Shifted 20c Data
Shifted 40c Data

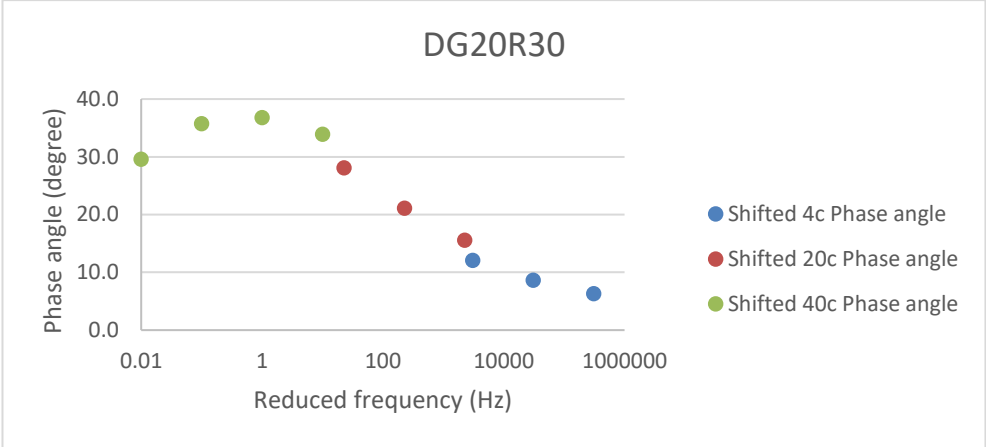
DG20R30
40.0
30.0
20.0
10.0
0.0
Phase angle (degree)
0.01
1
100
10000
1000000
Reduced frequency (Hz)
Shifted 4c Phase angle
Shifted 20c Phase angle
Shifted 40c Phase angle

Appendix VIII. Master curves for binders at 20°C

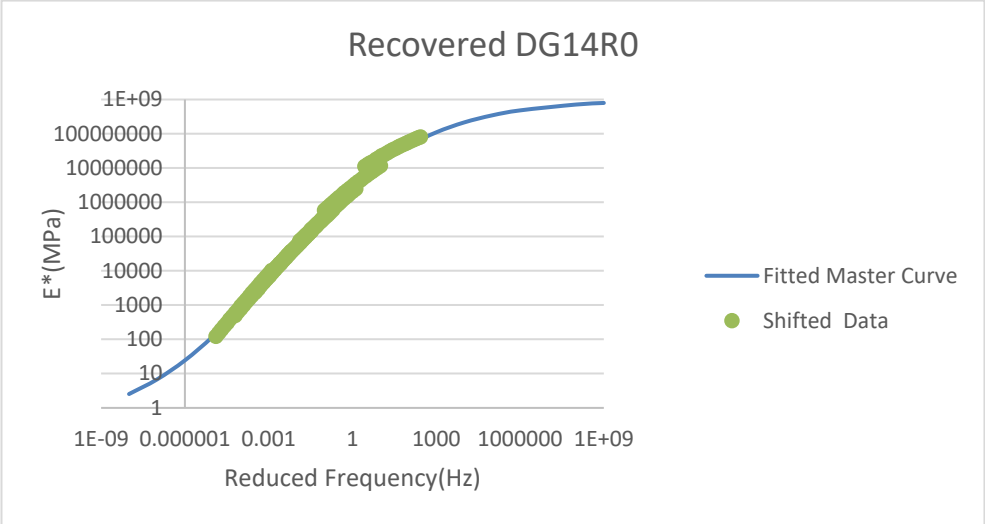

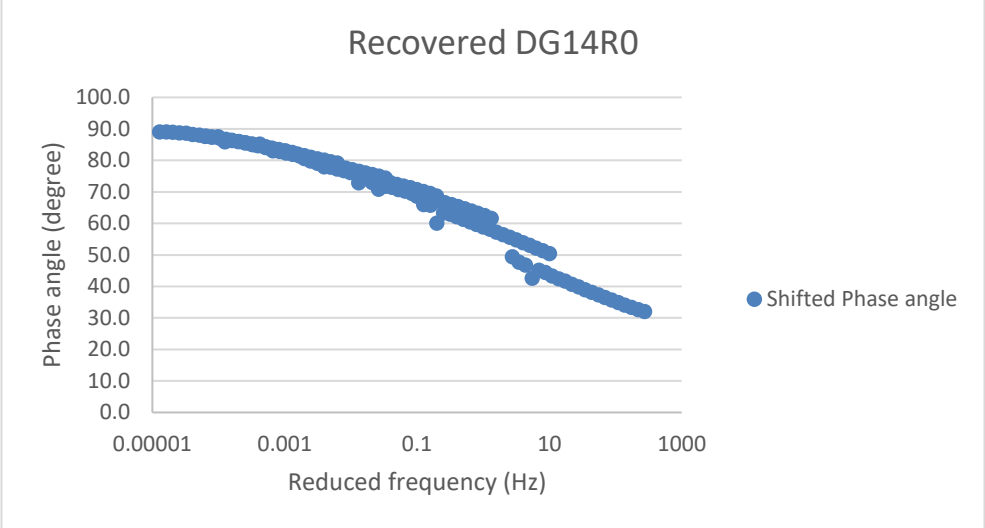

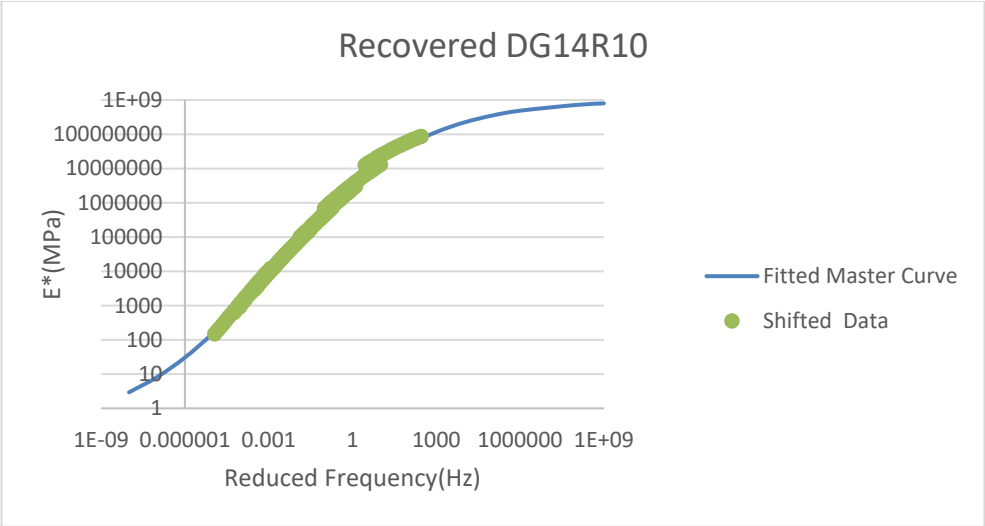

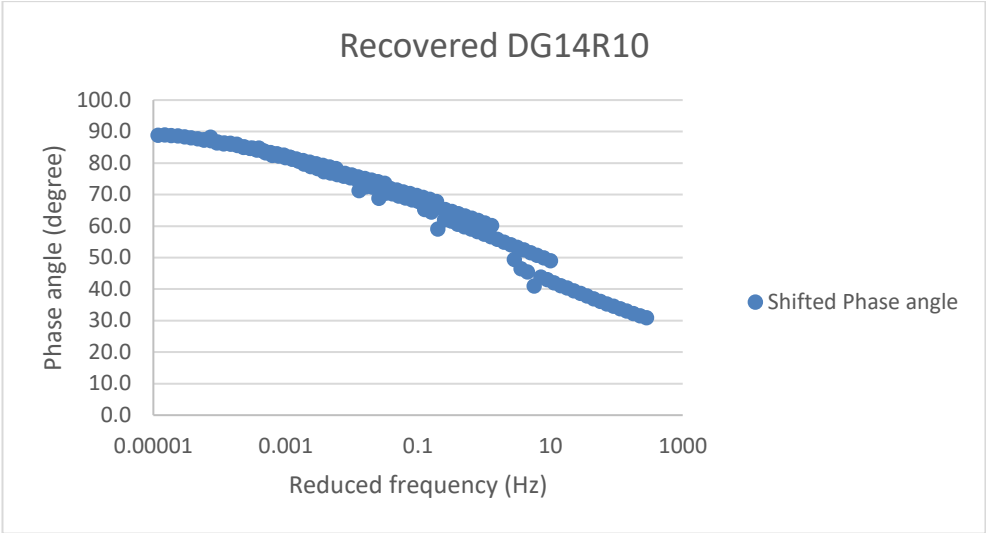
Recovered DG14R10
Phase angle (degree)
100.0
90.0
80.0
70.0
60.0
50.0
40.0
30.0
20.0
10.0
0.0
0.00001
0.001
0.1
10
1000
Reduced frequency (Hz)
Shifted Phase angle

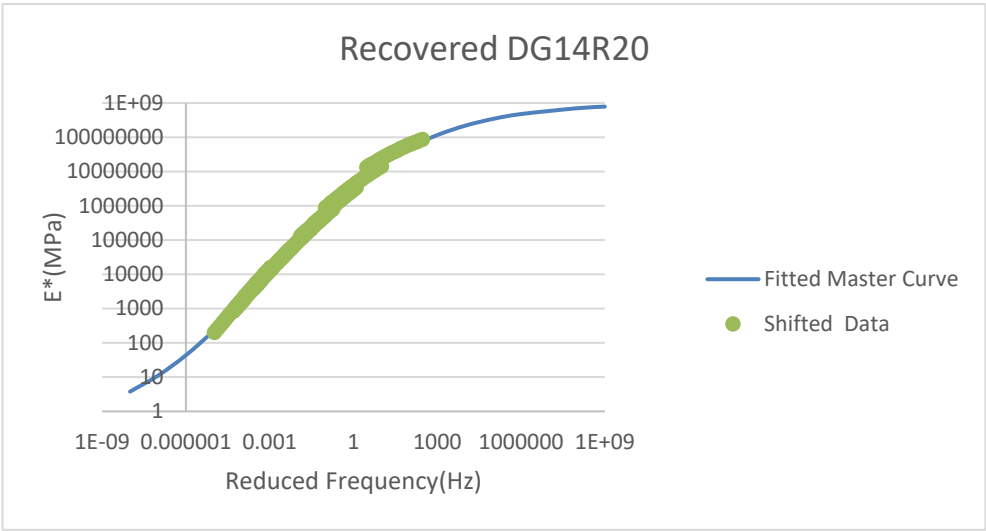
Recovered DG14R20
E*(MPa)
1E+09
100000000
10000000
1000000
100000
10000
1000
100
10
1
1E-09
0.000001
0.001
1
1000
1000000
1E+09
Reduced Frequency(Hz)
Fitted Master Curve
Shifted Data

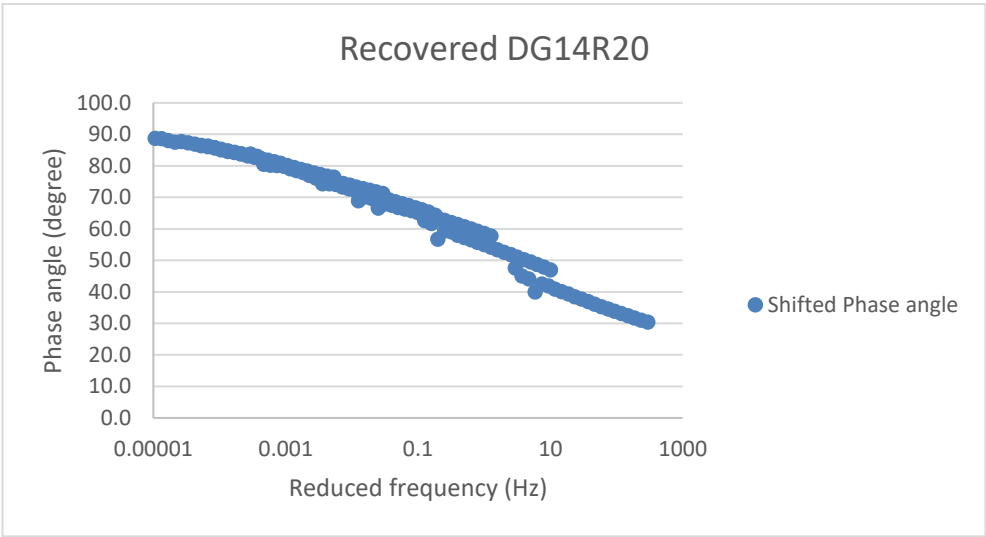
Recovered DG14R20
Phase angle (degree)
100.0
90.0
80.0
70.0
60.0
50.0
40.0
30.0
20.0
10.0
0.0
0.00001
0.001
0.1
10
1000
Reduced frequency (Hz)
Shifted Phase angle

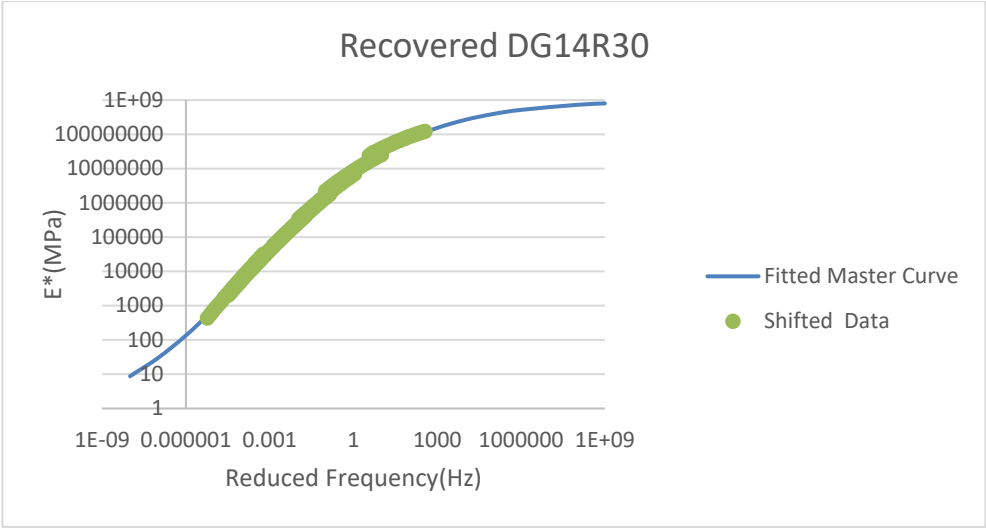
Recovered DG14R30
1E+09
100000000
10000000
1000000
100000
10000
1000
100
10
1
E*(MPa)
1E-09 0.000001 0.001 1 1000 1000000 1E+09
Reduced Frequency(Hz)
Fitted Master Curve
Shifted Data

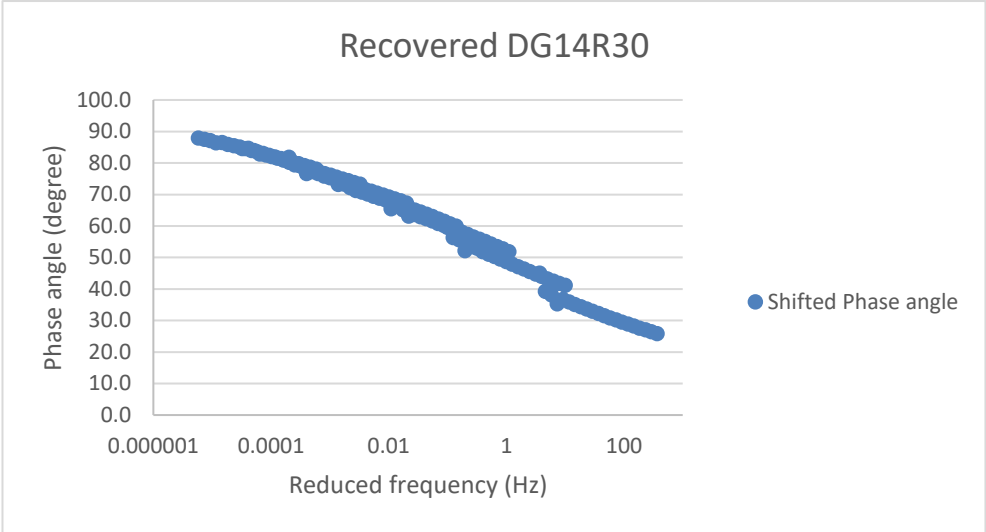
Recovered DG14R30
100.0
90.0
80.0
70.0
60.0
50.0
40.0
30.0
20.0
10.0
0.0
Phase angle (degree)
0.000001 0.0001 0.01 1 100
Reduced frequency (Hz)
Shifted Phase angle

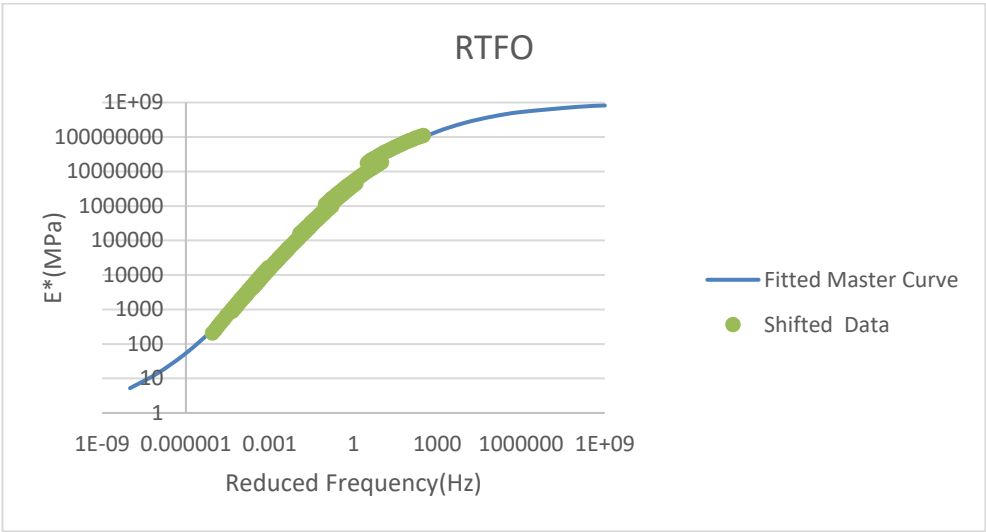
RTFO
1E+09
100000000
10000000
1000000
100000
10000
1000
100
10
1
E*(MPa)
1E-09 0.000001 0.001 1 1000 1000000 1E+09
Reduced Frequency(Hz)
Fitted Master Curve
Shifted Data

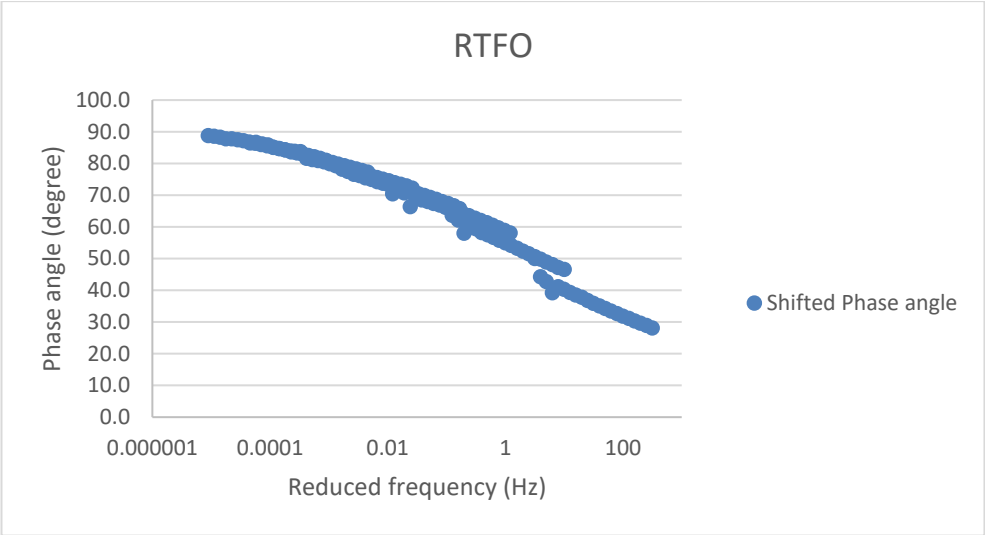
RTFO
100.0
90.0
80.0
70.0
60.0
50.0
40.0
30.0
20.0
10.0
0.0
Phase angle (degree)
0.000001
0.0001
0.01
1
100
Reduced frequency (Hz)
Shifted Phase angle

Appendix IX. Master curves for binders at 4°C

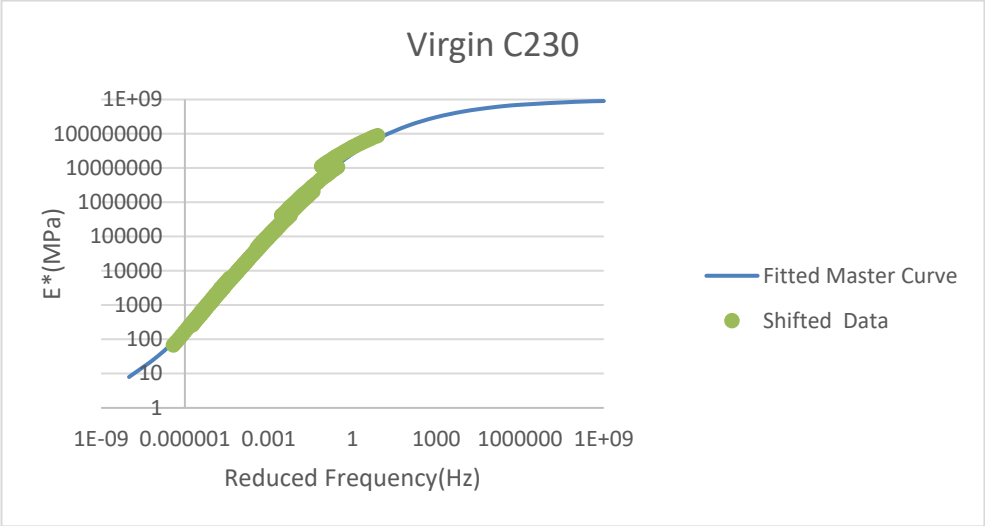

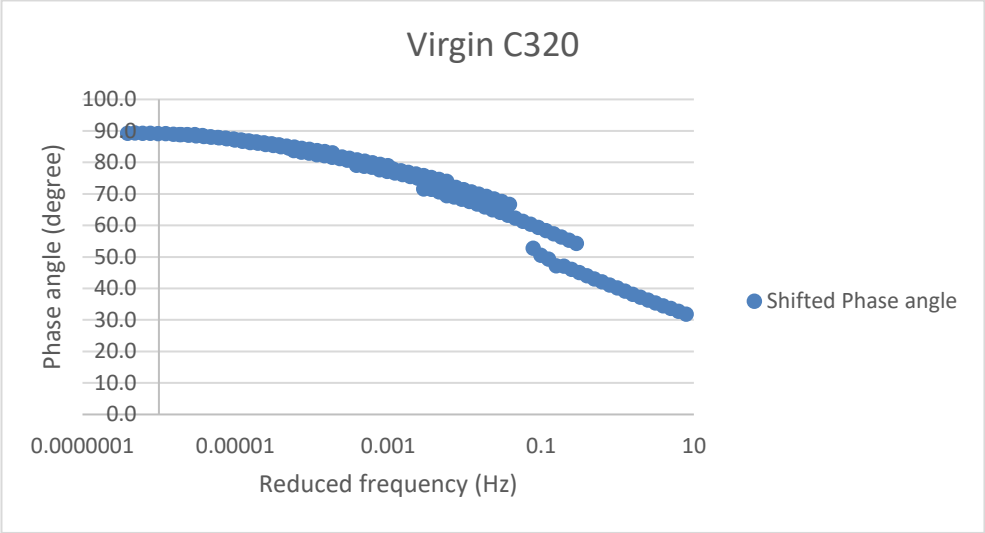

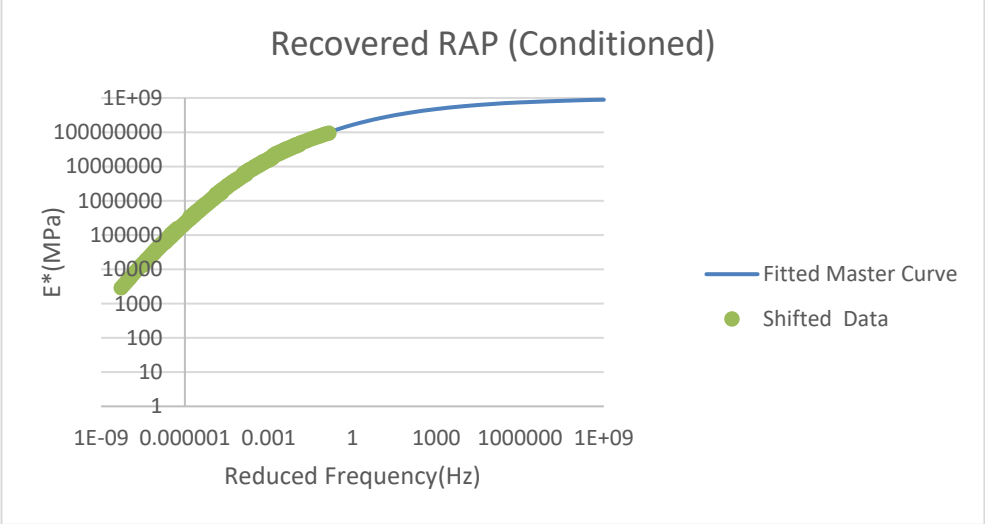

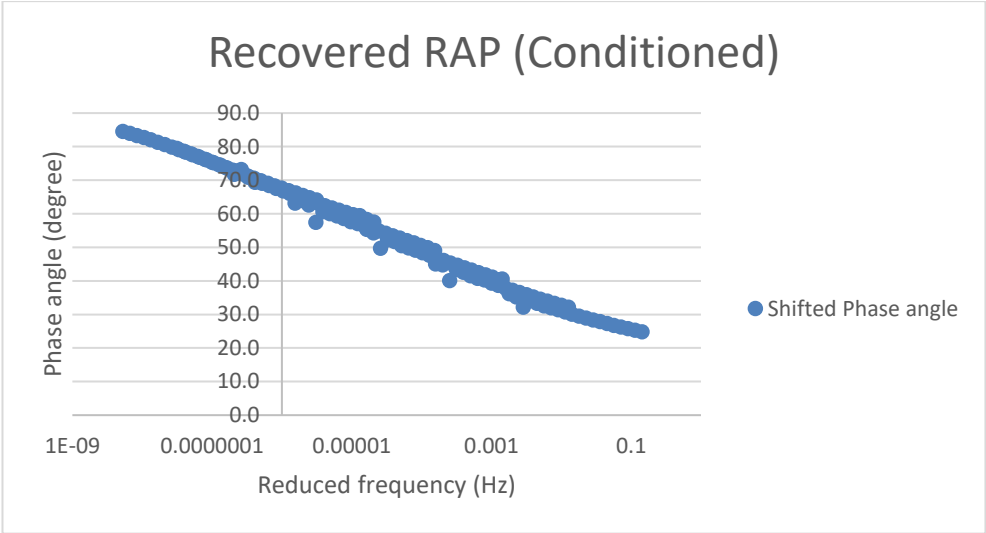
Recovered RAP (Conditioned)
Phase angle (degree)
90.0
80.0
70.0
60.0
50.0
40.0
30.0
20.0
10.0
0.0
1E-09
0.0000001
0.00001
0.001
0.1
Reduced frequency (Hz)
Shifted Phase angle

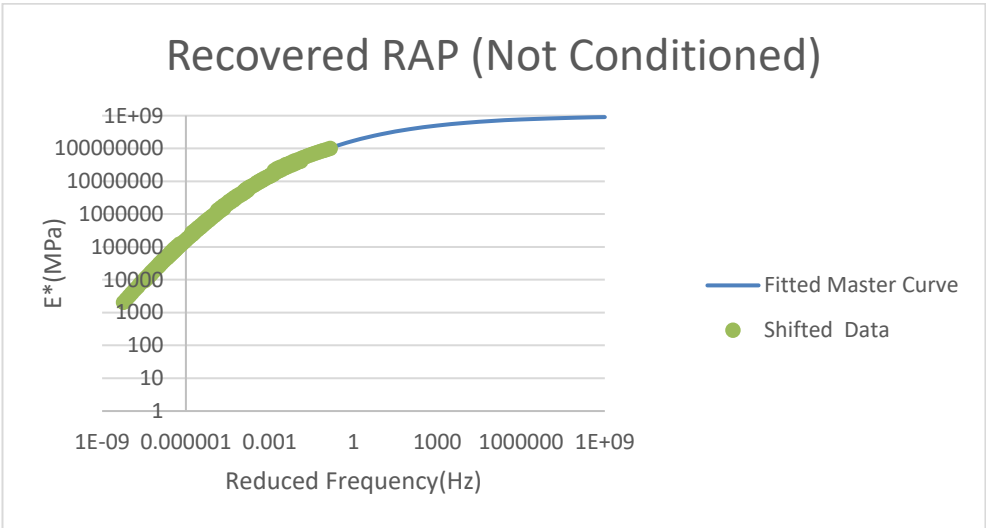
Recovered RAP (Not Conditioned)
E*(MPa)
1E+09
100000000
10000000
1000000
100000
10000
1000
100
10
1
1E-09
0.000001
0.001
1
1000
1000000
1E+09
Reduced Frequency(Hz)
Fitted Master Curve
Shifted Data

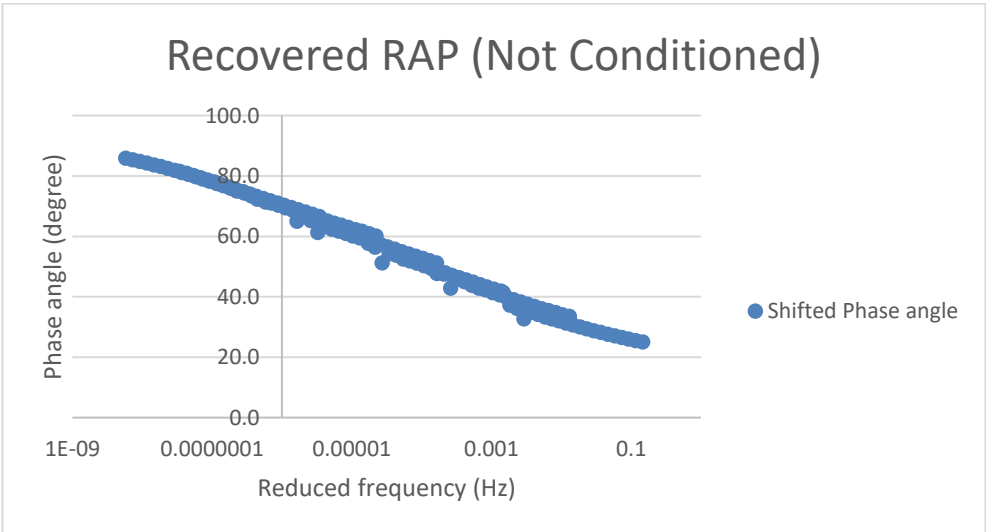
Recovered RAP (Not Conditioned)
Phase angle (degree)
100.0
80.0
60.0
40.0
20.0
0.0
1E-09
0.0000001
0.00001
0.001
0.1
Reduced frequency (Hz)
Shifted Phase angle

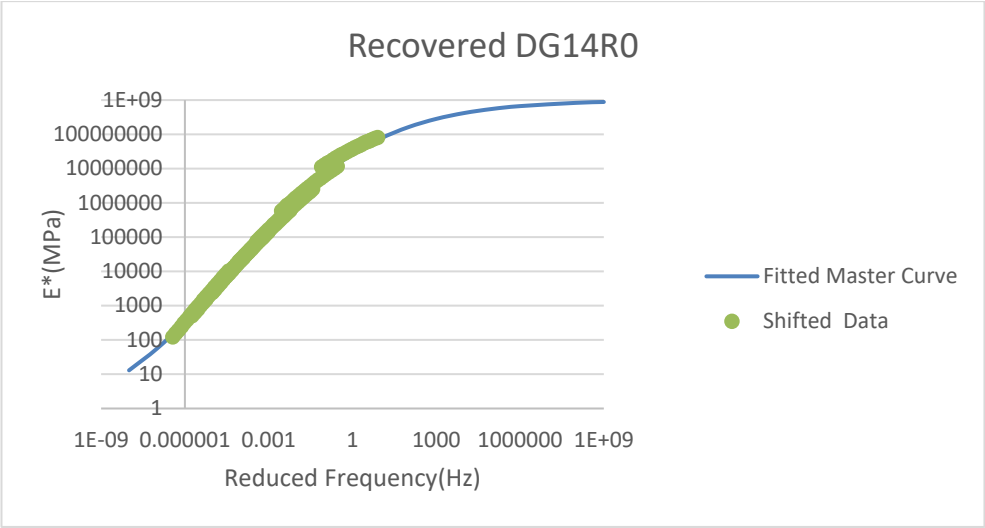
Recovered DG14R0
1E+09
100000000
10000000
1000000
100000
10000
1000
100
10
1
E*(MPa)
1E-09 0.000001 0.001 1 1000 1000000 1E+09
Reduced Frequency(Hz)
Fitted Master Curve
Shifted Data

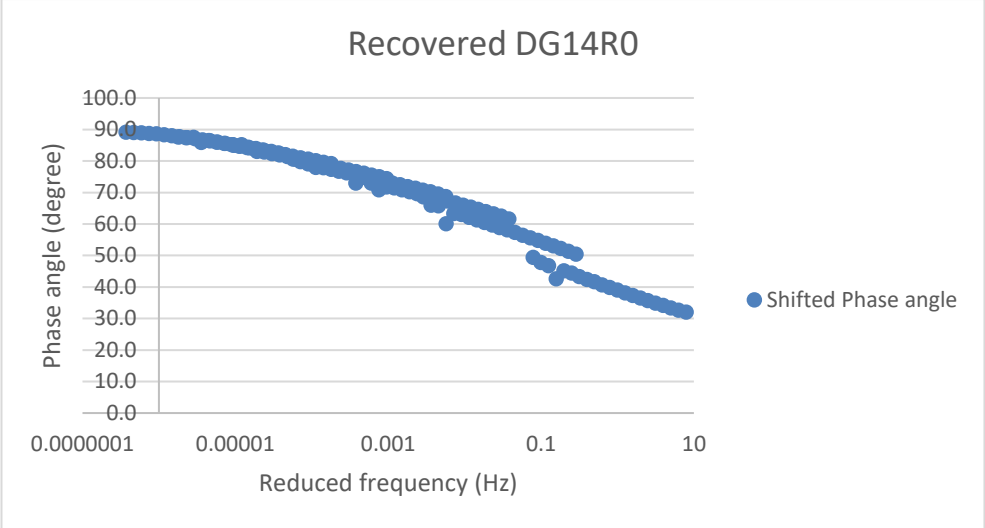
Recovered DG14R0
100.0
90.0
80.0
70.0
60.0
50.0
40.0
30.0
20.0
10.0
0.0
Phase angle (degree)
0.0000001 0.00001 0.001 0.1 10
Reduced frequency (Hz)
Shifted Phase angle

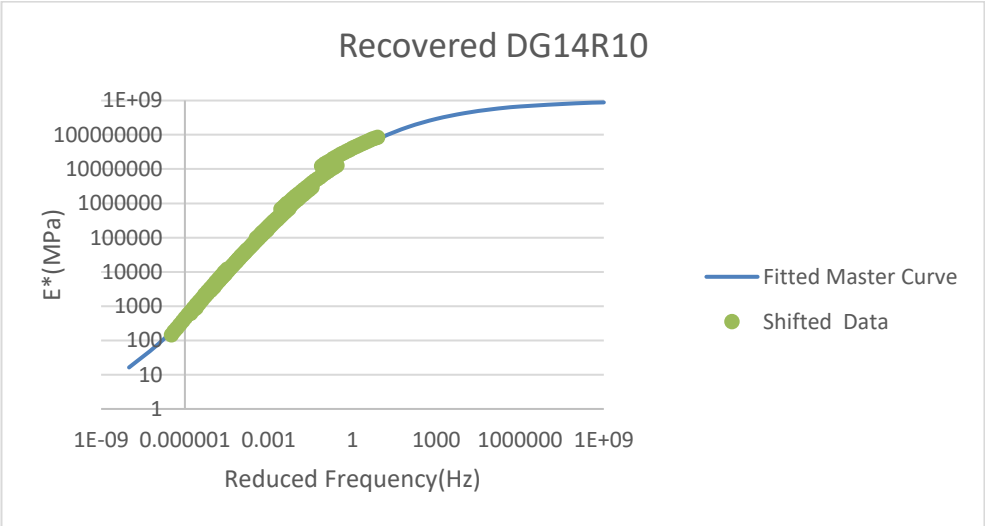
Recovered DG14R10
1E+09
100000000
10000000
1000000
100000
10000
1000
100
10
1
E*(MPa)
1E-09 0.000001 0.001 1 1000 1000000 1E+09
Reduced Frequency(Hz)
Fitted Master Curve
Shifted Data

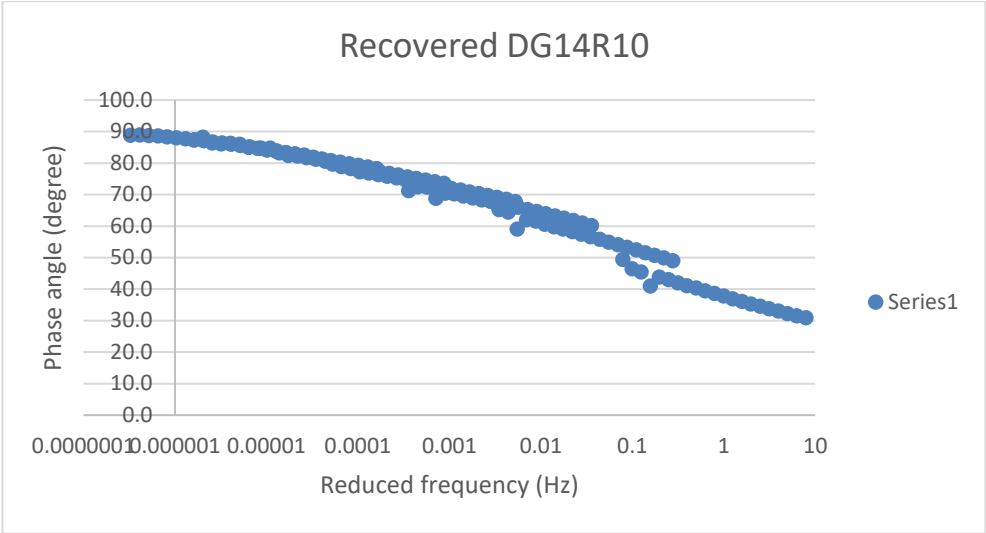
Recovered DG14R10
Phase angle (degree)
100.0
90.0
80.0
70.0
60.0
50.0
40.0
30.0
20.0
10.0
0.0
0.0000001
0.000001
0.00001
0.0001
0.001
0.01
0.1
1
10
Reduced frequency (Hz)
Series1

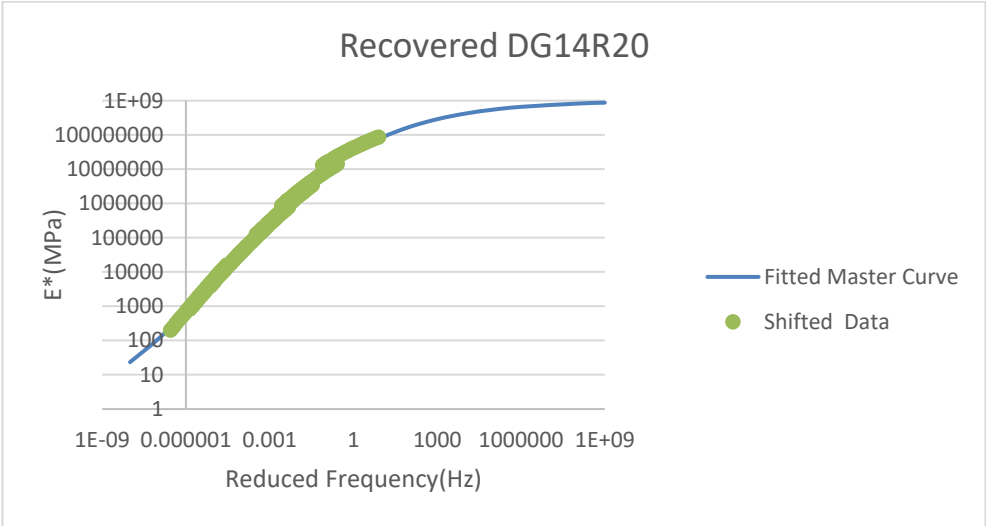
Recovered DG14R20
E*(MPa)
1E+09
100000000
10000000
1000000
100000
10000
1000
100
10
1
1E-09
0.000001
0.001
1
1000
1000000
1E+09
Reduced Frequency(Hz)
Fitted Master Curve
Shifted Data

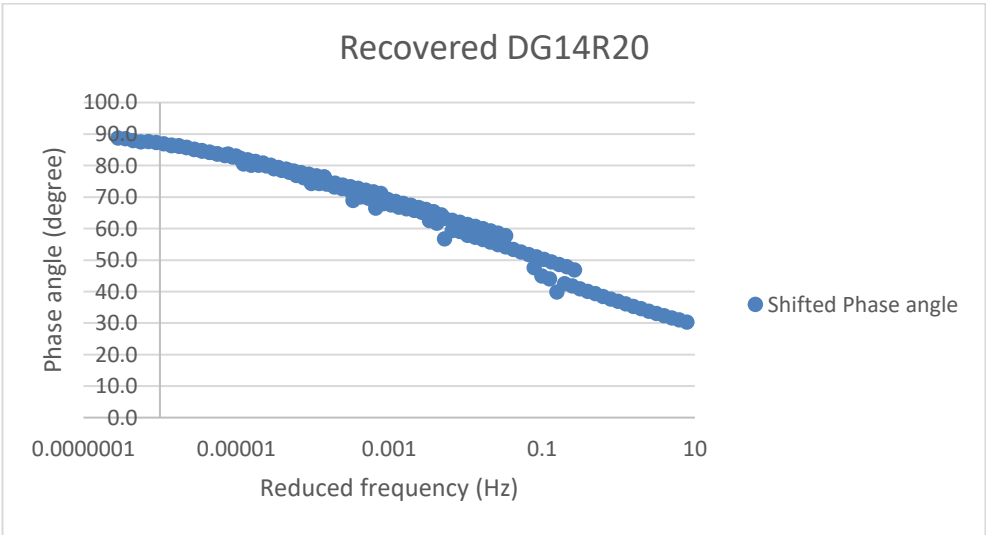
Recovered DG14R20
Phase angle (degree)
100.0
90.0
80.0
70.0
60.0
50.0
40.0
30.0
20.0
10.0
0.0
0.0000001
0.00001
0.001
0.1
10
Reduced frequency (Hz)
Shifted Phase angle

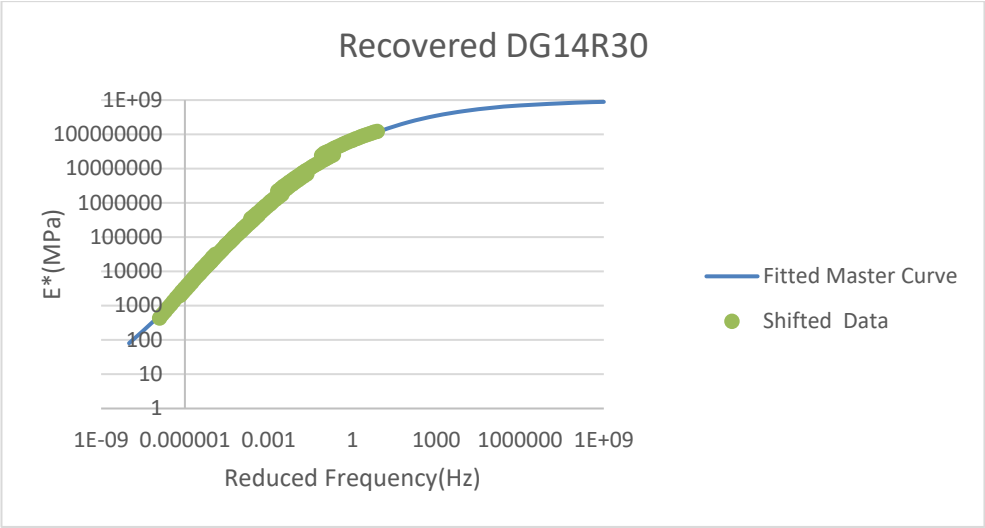
Recovered DG14R30
1E+09
100000000
10000000
1000000
100000
10000
1000
100
10
1
E*(MPa)
1E-09 0.000001 0.001 1 1000 1000000 1E+09
Reduced Frequency(Hz)
Fitted Master Curve
Shifted Data

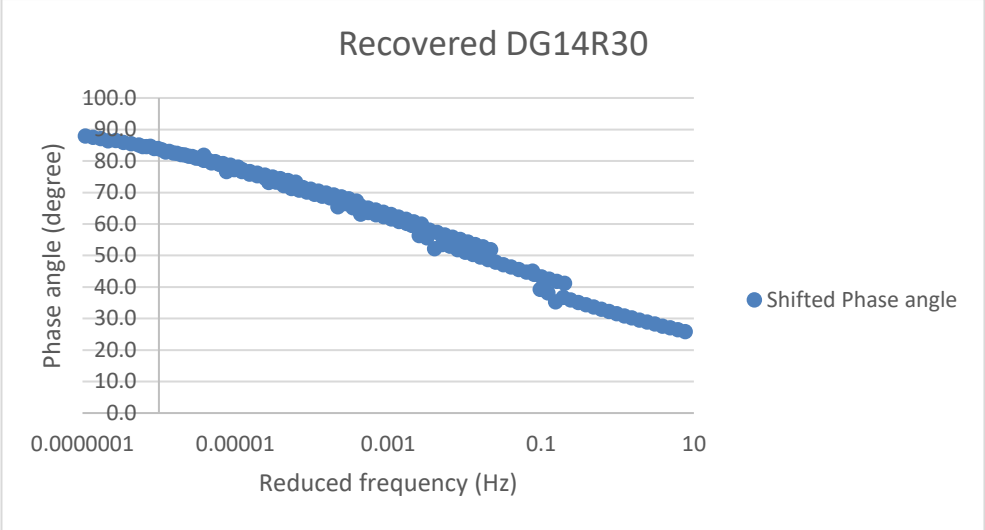
Recovered DG14R30
100.0
90.0
80.0
70.0
60.0
50.0
40.0
30.0
20.0
10.0
0.0
Phase angle (degree)
0.0000001 0.00001 0.001 0.1 10
Reduced frequency (Hz)
Shifted Phase angle

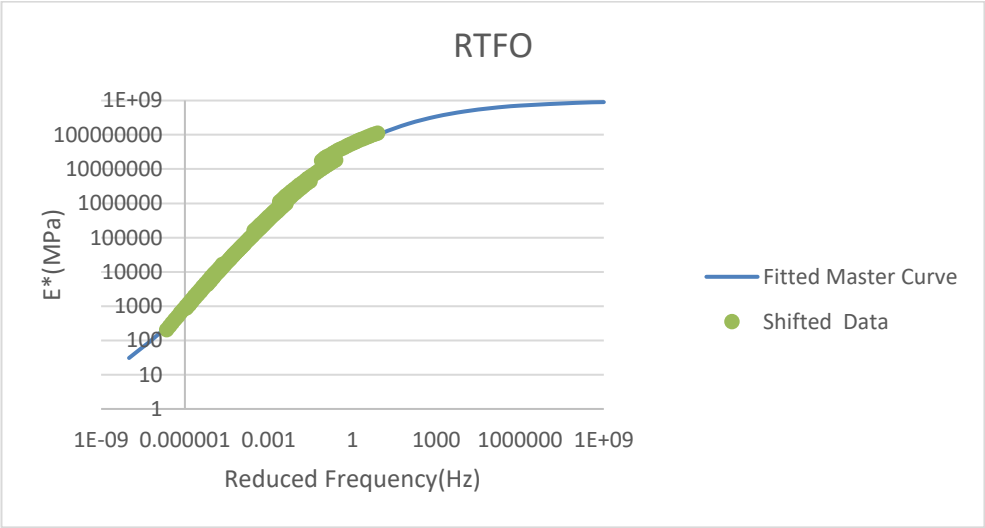
RTFO
1E+09
100000000
10000000
1000000
100000
10000
1000
100
10
1
E*(MPa)
1E-09 0.000001 0.001 1 1000 1000000 1E+09
Reduced Frequency(Hz)
Fitted Master Curve
Shifted Data

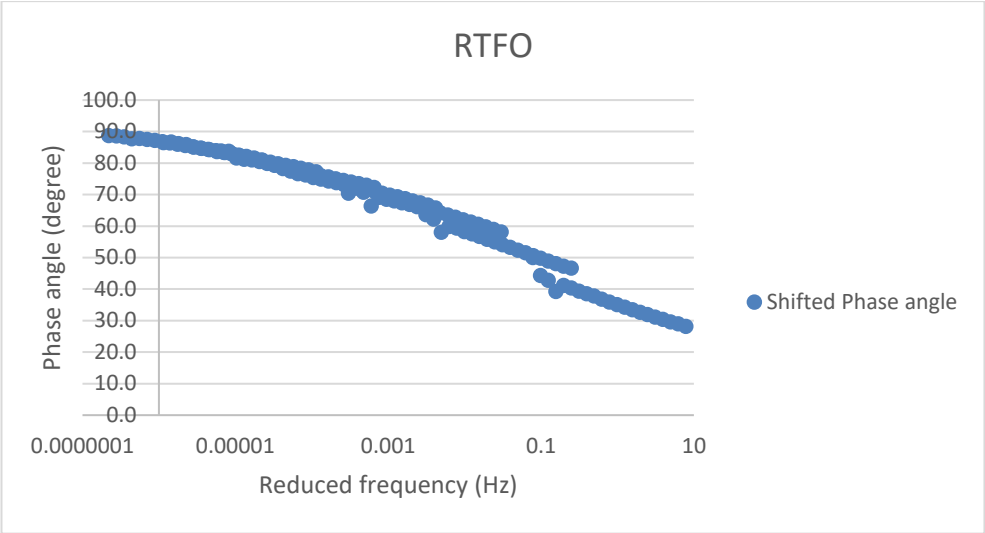
RTFO
100.0
90.0
80.0
70.0
60.0
50.0
40.0
30.0
20.0
10.0
0.0
Phase angle (degree)
0.0000001
0.00001
0.001
0.1
10
Reduced frequency (Hz)
Shifted Phase angle

Appendix X. Master curves for binders at 40°C

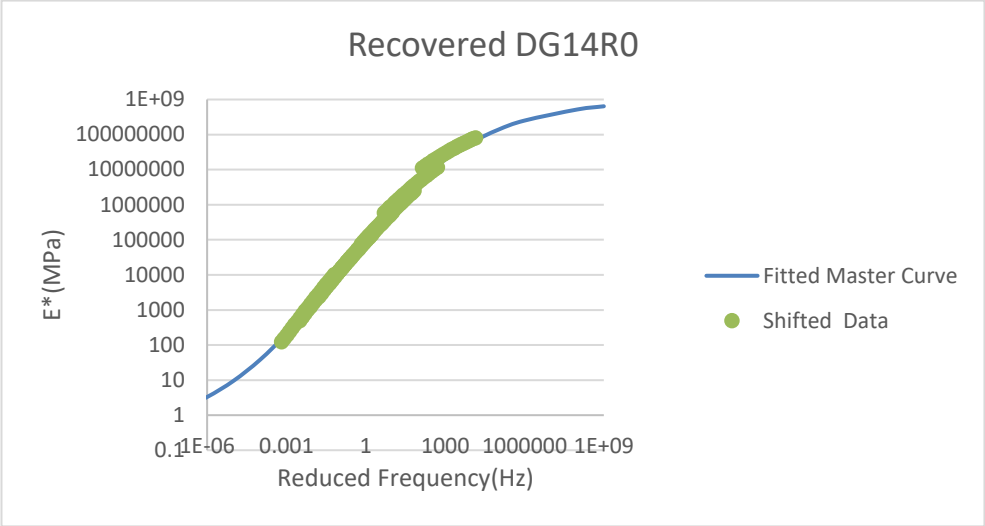

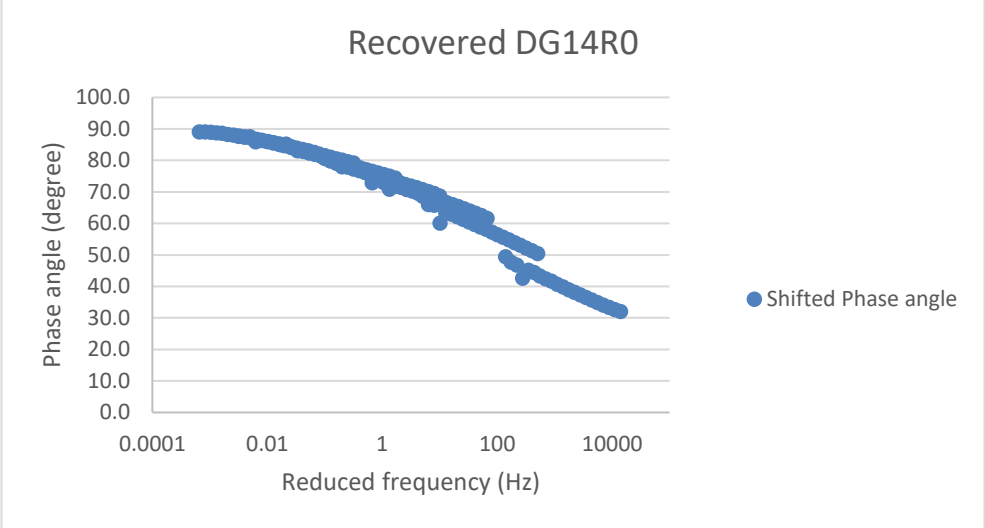

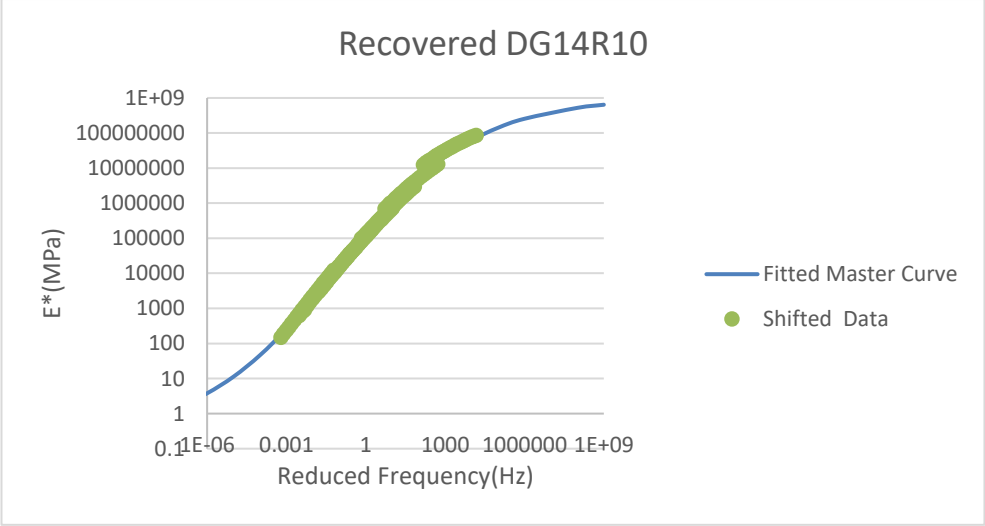

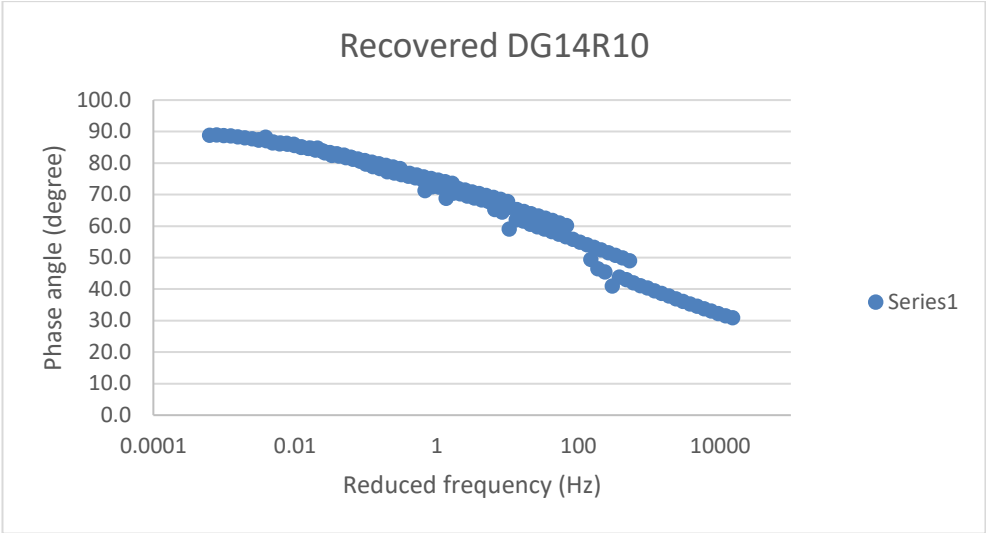
Recovered DG14R10
Phase angle (degree)
100.0
90.0
80.0
70.0
60.0
50.0
40.0
30.0
20.0
10.0
0.0
0.0001
0.01
1
100
10000
Reduced frequency (Hz)
Series1

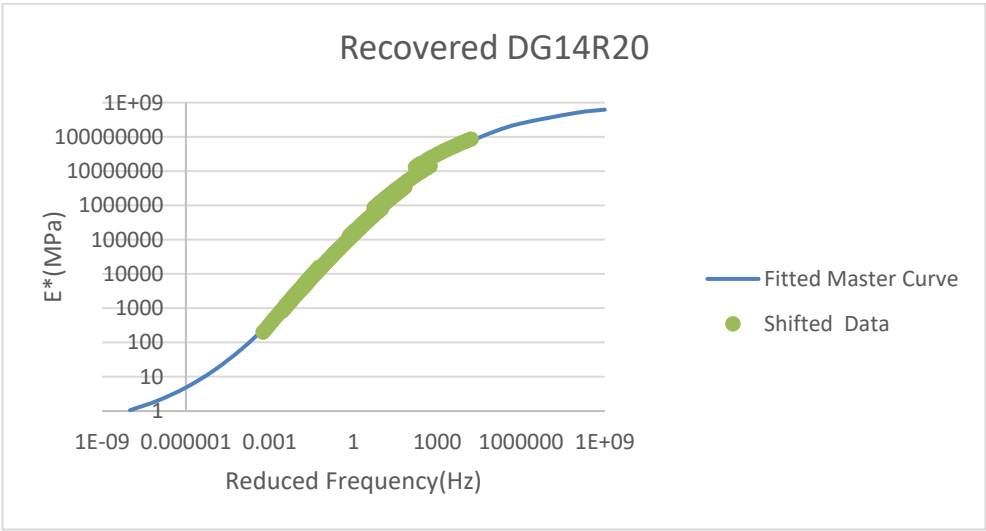
Recovered DG14R20
E*(MPa)
1E+09
100000000
10000000
1000000
100000
10000
1000
100
10
1
1E-09
0.000001
0.001
1
1000
1000000
1E+09
Reduced Frequency(Hz)
Fitted Master Curve
Shifted Data

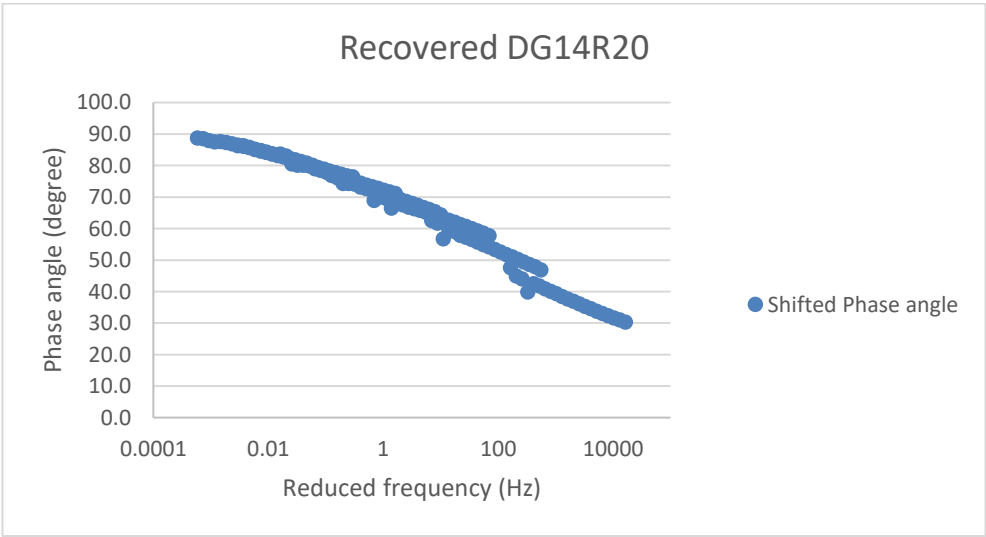
Recovered DG14R20
Phase angle (degree)
100.0
90.0
80.0
70.0
60.0
50.0
40.0
30.0
20.0
10.0
0.0
0.0001
0.01
1
100
10000
Reduced frequency (Hz)
Shifted Phase angle

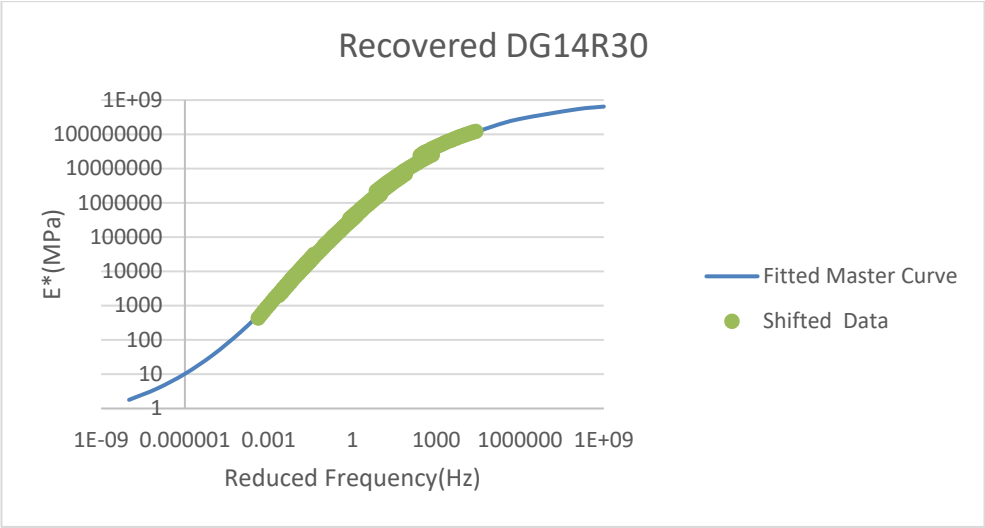
Recovered DG14R30
1E+09
100000000
10000000
1000000
100000
10000
1000
100
10
1
E*(MPa)
1E-09 0.000001 0.001 1 1000 1000000 1E+09
Reduced Frequency(Hz)
Fitted Master Curve
Shifted Data

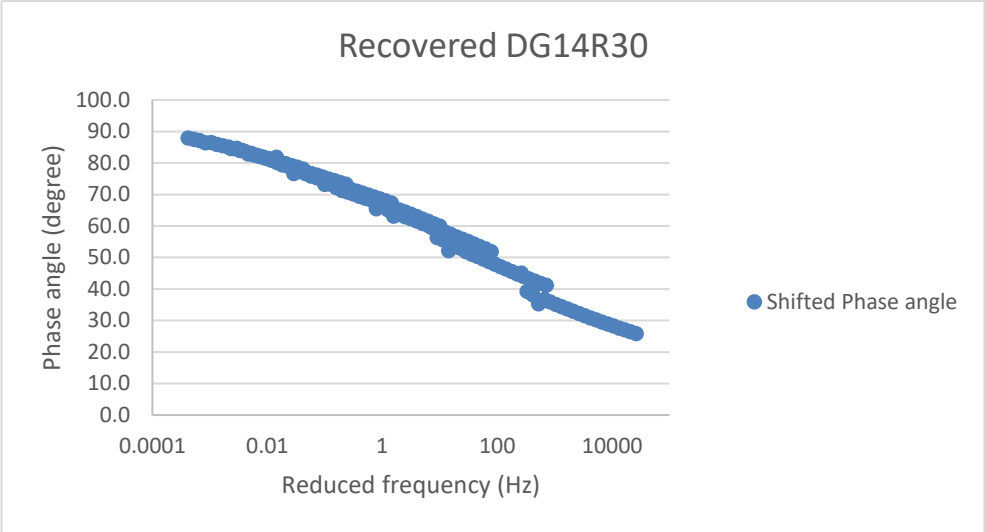
Recovered DG14R30
100.0
90.0
80.0
70.0
60.0
50.0
40.0
30.0
20.0
10.0
0.0
Phase angle (degree)
0.0001 0.01 1 100 10000
Reduced frequency (Hz)
Shifted Phase angle

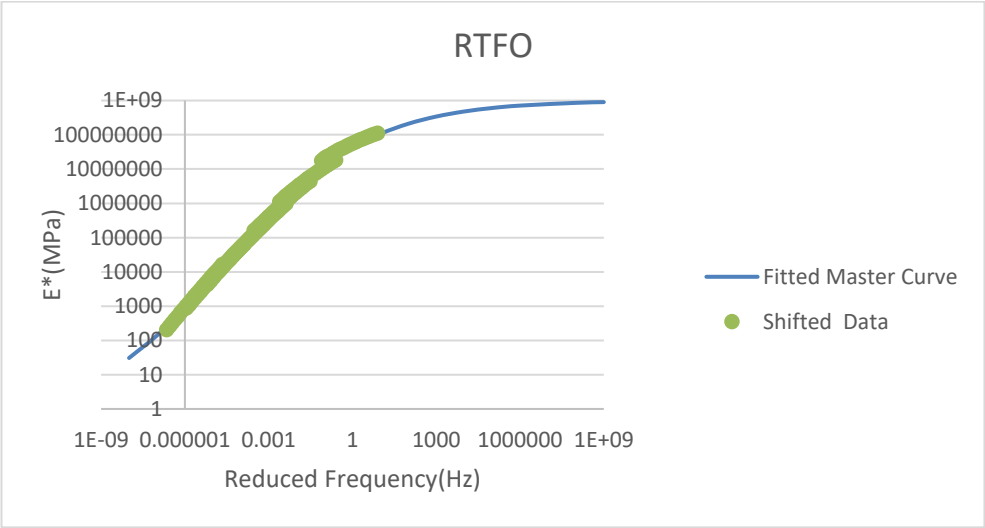
RTFO
1E+09
100000000
10000000
1000000
100000
10000
1000
100
10
1
E*(MPa)
1E-09 0.000001 0.001 1 1000 1000000 1E+09
Reduced Frequency(Hz)
Fitted Master Curve
Shifted Data

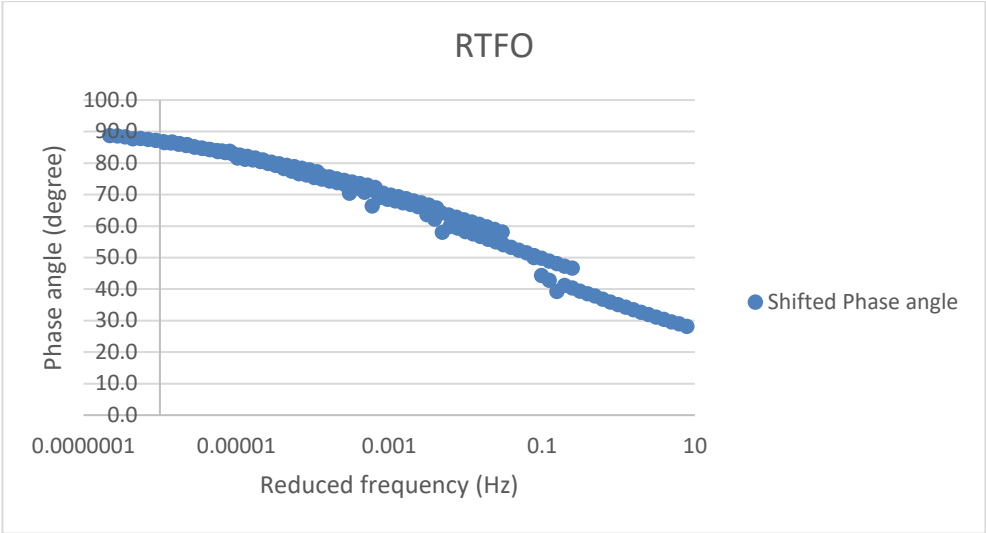
RTFO
100.0
90.0
80.0
70.0
60.0
50.0
40.0
30.0
20.0
10.0
0.0
Phase angle (degree)
0.0000001
0.00001
0.001
0.1
10
Reduced frequency (Hz)
Shifted Phase angle

Appendix XI. Binders' critical high-temperature test results

	Scenario1 Temperature (°C) (treated as OB)		Scenario2 Temperature(°C) (treated as RTFO)	
Binder Source	Sample 1	Sample2	Sample 1	Sample2
RAP Conditioned	107.3	105.9	100.4	99.1
RAP un conditioned	104.7	103.2	98.1	96.6
C320	71.2		64.43	
RTFO	79.3		72.8	
R10	76.6		70	
R20	79.2		72.7	
R30	84.6		77.9	
R0	75.6	74.9	69.4	68.7

Appendix XII. Binders' penetration test results

	Penetration number		
Binder Source	Test1	Test2	Test3
RAP Conditioned	4	5	5
RAP not conditioned	5	5	6
C320	56	57	58
RTFO	29	29	29
R10	39	38	40
R20	31	32	32
R30	24	22	23
R0	37	38	39